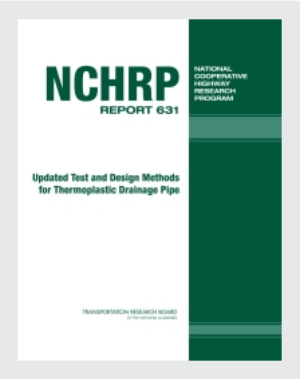

Updated Test and Design Methods for Thermoplastic Drainage Pipe

DETAILS

287 pages | | PAPERBACK
ISBN 978-0-309-11776-0 | DOI 10.17226/23045

AUTHORS

NATIONAL COOPERATIVE HIGHWAY RESEARCH PROGRAM

NCHRP REPORT 631

Updated Test and Design Methods for Thermoplastic Drainage Pipe

T.J. McGrath
SIMPSON GUMPERTZ & HEGER INC.
Waltham, MA

I.D. Moore
QUEEN'S UNIVERSITY
Kingston, ON

G.Y. Hsuan
DREXEL UNIVERSITY
Philadelphia, PA

Subject Areas
Bridges, Other Structures, and Hydraulics and Hydrology • Soils, Geology, and Foundations • Materials and Construction

Research sponsored by the American Association of State Highway and Transportation Officials
in cooperation with the Federal Highway Administration

TRANSPORTATION RESEARCH BOARD

WASHINGTON, D.C.
2009
www.TRB.org

NATIONAL COOPERATIVE HIGHWAY RESEARCH PROGRAM

Systematic, well-designed research provides the most effective approach to the solution of many problems facing highway administrators and engineers. Often, highway problems are of local interest and can best be studied by highway departments individually or in cooperation with their state universities and others. However, the accelerating growth of highway transportation develops increasingly complex problems of wide interest to highway authorities. These problems are best studied through a coordinated program of cooperative research.

In recognition of these needs, the highway administrators of the American Association of State Highway and Transportation Officials initiated in 1962 an objective national highway research program employing modern scientific techniques. This program is supported on a continuing basis by funds from participating member states of the Association and it receives the full cooperation and support of the Federal Highway Administration, United States Department of Transportation.

The Transportation Research Board of the National Academies was requested by the Association to administer the research program because of the Board's recognized objectivity and understanding of modern research practices. The Board is uniquely suited for this purpose as it maintains an extensive committee structure from which authorities on any highway transportation subject may be drawn; it possesses avenues of communications and cooperation with federal, state and local governmental agencies, universities, and industry; its relationship to the National Research Council is an insurance of objectivity; it maintains a full-time research correlation staff of specialists in highway transportation matters to bring the findings of research directly to those who are in a position to use them.

The program is developed on the basis of research needs identified by chief administrators of the highway and transportation departments and by committees of AASHTO. Each year, specific areas of research needs to be included in the program are proposed to the National Research Council and the Board by the American Association of State Highway and Transportation Officials. Research projects to fulfill these needs are defined by the Board, and qualified research agencies are selected from those that have submitted proposals. Administration and surveillance of research contracts are the responsibilities of the National Research Council and the Transportation Research Board.

The needs for highway research are many, and the National Cooperative Highway Research Program can make significant contributions to the solution of highway transportation problems of mutual concern to many responsible groups. The program, however, is intended to complement rather than to substitute for or duplicate other highway research programs.

NCHRP REPORT 631

Project 4-26
ISSN 0077-5614
ISBN: 978-0-309-11776-0
Library of Congress Control Number 2009902317

COPYRIGHT PERMISSION

NOTICE

The project that is the subject of this report was a part of the National Cooperative Highway Research Program conducted by the Transportation Research Board with the approval of the Governing Board of the National Research Council. Such approval reflects the Governing Board's judgment that the program concerned is of national importance and appropriate with respect to both the purposes and resources of the National Research Council.

The members of the technical committee selected to monitor this project and to review this report were chosen for recognized scholarly competence and with due consideration for the balance of disciplines appropriate to the project. The opinions and conclusions expressed or implied are those of the research agency that performed the research, and, while they have been accepted as appropriate by the technical committee, they are not necessarily those of the Transportation Research Board, the National Research Council, the American Association of State Highway and Transportation Officials, or the Federal Highway Administration, U.S. Department of Transportation.

Each report is reviewed and accepted for publication by the technical committee according to procedures established and monitored by the Transportation Research Board Executive Committee and the Governing Board of the National Research Council.

The Transportation Research Board of the National Academies, the National Research Council, the Federal Highway Administration, the American Association of State Highway and Transportation Officials, and the individual states participating in the National Cooperative Highway Research Program do not endorse products or manufacturers. Trade or manufacturers' names appear herein solely because they are considered essential to the object of this report.

Published reports of the

NATIONAL COOPERATIVE HIGHWAY RESEARCH PROGRAM

are available from:

Transportation Research Board
Business Office
500 Fifth Street, NW
Washington, DC 20001

and can be ordered through the Internet at:

http://www.national-academies.org/trb/bookstore

Printed in the United States of America

THE NATIONAL ACADEMIES

Advisers to the Nation on Science, Engineering, and Medicine

The **National Academy of Sciences** is a private, nonprofit, self-perpetuating society of distinguished scholars engaged in scientific and engineering research, dedicated to the furtherance of science and technology and to their use for the general welfare. On the authority of the charter granted to it by the Congress in 1863, the Academy has a mandate that requires it to advise the federal government on scientific and technical matters. Dr. Ralph J. Cicerone is president of the National Academy of Sciences.

The **National Academy of Engineering** was established in 1964, under the charter of the National Academy of Sciences, as a parallel organization of outstanding engineers. It is autonomous in its administration and in the selection of its members, sharing with the National Academy of Sciences the responsibility for advising the federal government. The National Academy of Engineering also sponsors engineering programs aimed at meeting national needs, encourages education and research, and recognizes the superior achievements of engineers. Dr. Charles M. Vest is president of the National Academy of Engineering.

The **Institute of Medicine** was established in 1970 by the National Academy of Sciences to secure the services of eminent members of appropriate professions in the examination of policy matters pertaining to the health of the public. The Institute acts under the responsibility given to the National Academy of Sciences by its congressional charter to be an adviser to the federal government and, on its own initiative, to identify issues of medical care, research, and education. Dr. Harvey V. Fineberg is president of the Institute of Medicine.

The **National Research Council** was organized by the National Academy of Sciences in 1916 to associate the broad community of science and technology with the Academy's purposes of furthering knowledge and advising the federal government. Functioning in accordance with general policies determined by the Academy, the Council has become the principal operating agency of both the National Academy of Sciences and the National Academy of Engineering in providing services to the government, the public, and the scientific and engineering communities. The Council is administered jointly by both the Academies and the Institute of Medicine. Dr. Ralph J. Cicerone and Dr. Charles M. Vest are chair and vice chair, respectively, of the National Research Council.

The **Transportation Research Board** is one of six major divisions of the National Research Council. The mission of the Transportation Research Board is to provide leadership in transportation innovation and progress through research and information exchange, conducted within a setting that is objective, interdisciplinary, and multimodal. The Board's varied activities annually engage about 7,000 engineers, scientists, and other transportation researchers and practitioners from the public and private sectors and academia, all of whom contribute their expertise in the public interest. The program is supported by state transportation departments, federal agencies including the component administrations of the U.S. Department of Transportation, and other organizations and individuals interested in the development of transportation. **www.TRB.org**

www.national-academies.org

CRP STAFF FOR NCHRP REPORT 631

Christopher W. Jenks, *Director, Cooperative Research Programs*
Crawford F. Jencks, *Deputy Director, Cooperative Research Programs*
Edward T. Harrigan, *Senior Program Officer*
Eileen P. Delaney, *Director of Publications*
Hilary Freer, *Senior Editor*
Natassja Linzau, *Editor*

NCHRP PROJECT 4-26 PANEL
Field of Materials and Construction—Area of General Materials

Donald J. Flemming, *URS Corporation, Minneapolis, MN* (Chair)
James A. Barna, *E. L. Robinson Engineering Company, Dublin, OH*
R. Scott Christie, *Pennsylvania DOT, Harrisburg, PA*
James B. Goddard, *Advanced Drainage Systems, Inc., Hilliard, OH*
Cecil L. Jones, *North Carolina DOT, Raleigh, NC*
Michael G. Katona, *Gig Harbor, WA*
James C. Schluter, *Contech Construction Products, Inc., West Chester, OH*
G. P. Jayaprakash, *TRB Liaison*

AUTHOR ACKNOWLEDGMENTS

The work report was a collaborative effort of Simpson Gumpertz & Heger Inc. (SGH), University of Western Ontario, and Drexel University. The successful completion of the project required the input and assistance of many, including research agency staff, manufacturers, and DOTs.

The departments of transportation of the states of Florida, North Carolina, and Pennsylvania; and manufacturers Advanced Drainage Systems and Hancor Inc. conducted round-robin stub compression tests to assist in developing the test standard.

Advanced Drainage Systems, Hancor Inc., JM Pipe, KWH, and Big "O" provided pipe to the project for the various tests that were conducted.

Benjamin Schafer and Jesse Beaver made major contributions for SGH, as did the laboratory staff that conducted extensive tests.

Ashutosh Dhar conducted soil cell tests and numerical analyses at the University of Western Ontario.

FOREWORD

By Edward T. Harrigan
Staff Officer
Transportation Research Board

This report contains the findings of research performed to develop a recommended load and resistance factor design (LRFD) specification for thermoplastic pipe used in culverts and drainage systems for highway structures. The report details the research performed and includes a recommended LRFD design specification, a quality assurance specification for manufactured thermoplastic pipe, and the results of supporting analyses. Thus, the report will be of immediate interest to bridge and structural design engineers and materials engineers in state highway agencies, as well as to thermoplastic pipe suppliers.

The current "Soil-Thermoplastic Pipe Interaction System" design procedure in the AASHTO Bridge Specifications dates from the early 1980s and is based on the design procedure for corrugated metal pipe. As such, the procedure relies on ring compression limits although this mode of failure may not occur in thermoplastic pipe either in practice or in research. At the same time, the procedure ignores other relevant performance limits, such as deflection and wall profile stability, and does not account for the time-dependent nature of thermoplastic materials. Taken together, these shortcomings may either limit the cost-effective application of thermoplastic pipe products or lead to designs that are not conservative or may be susceptible to unexpected failure modes. There is a need to expand the LRFD specifications to better accommodate the distinct material properties and performance of thermoplastic pipe in culvert and drainage system applications.

This research had two objectives. The first was to develop a recommended LRFD specification for thermoplastic pipe used in culvert and drainage systems that is clearer and simpler than the present design procedure and that accounts for performance and failure criteria derived from soil-structure interaction and the time-dependent properties of thermoplastic pipe. The second objective was to develop the necessary construction and quality assurance specifications to help ensure that manufactured and installed thermoplastic pipe complies with the requirements of the LRFD design method.

The research effort included mechanical testing to evaluate the tension and compression behavior of polyvinyl chloride (PVC) and high–density polyethylene (HDPE) thermoplastic resins. This testing showed that the same compression strain limit can be used for both filled and unfilled PVC resins, leading to a substantial increase in the allowed burial depth of pipe manufactured with filled PVC resin. Extensive stub compression tests were also conducted; their results were used to develop a recommended AASHTO test method for stub compression and a procedure for using results of the stub compression test to compute compression strength. Structural performance of profile-wall pipe was evaluated through a series of soil-structure interaction tests and 2-D and 3-D finite element modeling; the results were used to help develop guidelines for comprehensive analysis of thermoplastic pipe

installations. Extensive testing was done to evaluate stress crack resistance (SCR) of HDPE in profile pipe using the notched constant ligament stress (NCLS) test; this work demonstrated the need to evaluate the SCR of the finished pipe for design purposes. Finally, the results of the experimental work and the modeling were used to develop a simplified design method for thermoplastic pipe in most design conditions; suggested design, construction, and quality assurance specifications; and the necessary material test methods.

The research was performed by Simpson Gumpertz & Heger Inc. The report fully documents the research leading to the recommended specifications and test methods. The recommendations are under consideration for possible adoption by the AASHTO Highway Subcommittee on Bridges and Structures and Subcommittee on Materials.

CONTENTS

SUMMARY

Updated Test and Design Methods for Thermoplastic Drainage Pipe

This report presents the work, findings, and recommendations of a project to update design, construction, and quality assurance/quality control (QA/QC) protocols for thermoplastic culvert pipe. Project tasks have included tests on raw materials and manufactured pipe as well as extensive computer modeling and pipe interaction tests.

Mechanical tests evaluated tension and compression behavior of polyvinyl chloride (PVC) and high-density polyethylene (HDPE) thermoplastic resins. The tests demonstrated that, in engineering stress, the strength and modulus determined in a compression test are higher than when determined by tension tests. One key finding is that filled PVC resins can use the same compression strain limit as unfilled resins. This substantially increases the burial depths for pipe manufactured with filled PVC resin.

Extensive stub compression tests were conducted. These included extensive tests by the research agencies and round-robin testing by participating laboratories to correlate test results with the calculated compression strength based on local buckling. Test results were used to develop a draft AASHTO specification for the stub compression test and to provide a procedure for using the stub compression test result to compute the compression strength as an alternate to the calculation procedure. Overall, compression strain limits should be set to fixed values for each type of thermoplastic, rather than the current method of using the strain at yield assuming linear behavior.

Structural performance of profile wall pipe was evaluated through a series of soil-structure interaction tests conducted in soil cells and through two- and three-dimensional (2D and 3D) finite element modeling. Tests included hoop compression tests (in which a pipe is surrounded by a ring of soil and compressed axisymmetrically) and biaxial cell tests (in which a pipe is subjected to forces representative of in-ground conditions). These tests have demonstrated local buckling behavior of profile wall pipe and validate the proposals for the simplified design method. Tests and analysis were conducted to evaluate the effects of poor haunch support on bending strains and to support recommendations for the shape factor parameter used in the simplified design method. Overall, the modeling and testing demonstrate a complex stress field in profile wall pipe under earth load further complicated by the occurrence of local buckling. This suggests that even though overall tension stresses in pipe are small or nonexistent when the pipe is installed properly, AASHTO should continue to maintain a minimum tension required strength for resins to ensure that local stresses do not result in long-term failures.

The computer modeling and tests were also used to assist in developing guidelines for comprehensive analysis of thermoplastic pipe installations. In particular, these guidelines provide a more precise method for computing the buckling capacity of thermoplastic pipe relative to the simplified method provided in the draft design specifications. These guidelines will assist designers for unusual projects where computer modeling can be used to provide more cost-effective designs.

A simplified design method was developed for thermoplastic pipe that should be suitable for evaluating thermoplastic pipe for most design conditions. The design method is drawn largely from prior

methods, but provides enhancements where necessary. The load factor for earth load is reduced to the same values as rigid pipe; however, to preserve the traditional safety for thermoplastic pipe installations, an "installation factor" is incorporated into the design method. Designers are allowed to reduce the installation factor if specific guidelines for monitoring installation quality are met. This will allow substantial increases in depths of fill, the feasibility of which has been demonstrated in full-scale field testing. Earth loads are calculated using the current AASHTO method, which considers the low hoop stiffness of thermoplastic pipe and the load reduction resulting from that low stiffness. Material modulus values for a 75-year design period have been added. Most pipe designs are controlled by compression capacity. For profile wall pipe, the compression capacity is most often controlled by local buckling of the profile elements. Design for local buckling is largely unchanged except that the compression capacity of a pipe determined through the stub compression test can be used in lieu of the capacity calculated with the design equations. Guidelines for computing bending strain have been improved with the addition of better guidance for the shape factor, which considers non-elliptical deformation due to non-uniform bedding. Tests and computer modeling have shown that the low hoop stiffness of profile wall HDPE can result in reduced bending strains relative to pipe with higher hoop stiffness. Provisions are added to estimate the expected field deflection; however, this is presented as a reasonability check for selecting appropriate backfill and compaction levels. Contractor field control is ultimately responsible for limiting deflection under construction.

Extensive testing was performed to evaluate slow crack growth resistance (SCR) of HDPE used in profile wall pipe. The notched constant ligament stress (NCLS) test is the primary tool to evaluate SCR. Tests included pipe manufactured from 100% virgin resin and with virgin resin +10% and +20% regrind. Regrind is reprocessed waste material from the manufacturer's own production. The tests demonstrate the need to evaluate SCR based on the finished pipe, as the addition of carbon black and the manufacturing process can have a significant effect on the NCLS failure time. An NCLS failure time for pipe specimens removed from the liner of profile wall pipe is recommended at 18 h. This will require virgin resins to have a failure time of approximately 33 h. Testing the finished pipe will reward manufacturers who have good processes, as the necessary NCLS of the virgin resin can be lower.

Material testing also included evaluation of the oxidation induction time (OIT), which measures the quantity of antioxidants present in a polymer. The testing found widely varying results for the various materials tested. The work conducted in this study was preliminary in nature and no firm recommendation is made at this time; however, a study in Florida has recommended an OIT time of 25 min for 75-year design life.

Several changes are recommended to the AASHTO product standards for HDPE and PVC culverts. The following are the most significant changes proposed:

- Modification of the crosshead speed for the parallel plate test to 2% per min for pipe larger than 600 mm (24 in.) in diameter. This will speed up the test and produce a slightly higher stiffness that is more representative of pipe behavior during construction. Required minimum pipe stiffnesses have been increased slightly so that the products produced will be essentially the same as under the current standards.
- Inclusion of a stub compression test to evaluate the compression strength of profile wall pipe. There is no test for this strength parameter at the current time, yet the performance of profile wall pipe depends greatly on the compression strength.
- Inclusion of a strength limit for PVC pipes in the parallel plate test. This provision requires reaching 30% deflection without loss of load. A similar provision is currently included in the HDPE product standard.
- Addition of the new SCR test on finished HDPE pipe.

- Addition of recordkeeping provisions.
- Addition of the heat reversion test to the PVC standard as a better test to evaluate extrusion quality.

Complete draft design and construction specifications are provided for design of thermoplastic culvert pipe. These include the changes proposed for the simplified design method. For construction, emphasis is placed on post-construction inspection to confirm that deflection levels are within specified limits, and line and grade and joints are all as specified.

CHAPTER 1

Introduction and Research Approach

Thermoplastic pipe design in bridge specifications was first adopted in the AASHTO standard specifications in the 1980s, and was largely based on the corrugated metal pipe design procedure. The current procedure focused on ring compression stresses computed from the weight of soil directly over the pipe and did not address deflection or bending. Research since that time, as demonstrated in Appendix A, has shown several behaviors in thermoplastic pipe that warrant a different approach. Earth loads can be greatly reduced due to low pipe hoop stiffness, especially with profile wall HDPE; however, capacity of this type of pipe can be reduced from the full compression strength times the cross-sectional area by the occurrence of local buckling in the thin flat elements that make up the profile. Field experience has shown that deflection of thermoplastic pipe can be high if construction procedures are not controlled; thus, deflection checks during design should be considered. The time-dependent nature of thermoplastic materials is also largely ignored or misinterpreted within the design procedure. In many cases, the current specifications tend to limit the cost-effective application of thermoplastic culvert products. In other instances, designs may not be conservative and may be susceptible to unexpected failure modes.

In addition to design issues, thermoplastic pipes do not have standardized wall profiles, are made from raw materials with a wide variety of actual properties, and the manufacturing process can have a significant effect on the properties of the finished product. All of this means that tests on the finished product are very important in ascertaining that a given product is suitable for use as drainage pipe. Thus, with more than 40 states currently using some type of thermoplastic drainage pipe, and with the pipe becoming available in ever larger sizes, this project was initiated to improve product standards for thermoplastic pipe. The project was divided into the following three phases:

- **Phase 1**—Tasks 1 through 4 involved assessing current practice, identifying perceived shortcomings of current practice, completing a design proposal for local buckling of profile wall pipe, assessing appropriate performance limits of thermoplastic pipe, and updating the detailed work plan to address perceived needs.
- **Phase 2**—Tasks 5 through 8 involved the development of comprehensive and simplified design procedures and a QA/QC procedure for thermoplastic pipe.
- **Phase 3**—Tasks 9 through 11 included verification and calibration of the design methods and preparation of proposed revisions to AASHTO product and design specifications.

The research agencies are Simpson Gumpertz & Heger Inc. (SGH), the University of Western Ontario (UWO), and Drexel University.

Note that AASHTO currently uses customary English units for the *AASHTO LRFD Bridge Specifications* and International System (SI) units for product specifications. Both unit systems are used in this report.

CHAPTER 2

Findings

The project work is presented in the following three primary areas:

- Pipe-soil interaction—Several investigations were conducted into the behavior of thermoplastic pipe in soil. These investigations are classified into two broad areas: studies of the complexities of the 3D behavior of profile wall pipe and general studies of the pipe-soil interaction of thermoplastic pipe. These investigations, carried out by soil cell studies and computer modeling, studied and validated aspects of pipe-soil interaction behavior for inclusion in a simplified design procedure and provided guidance for comprehensive analyses of thermoplastic pipe.
- Design—Design work focused on findings related to designing thermoplastic pipe to carry earth, live, and water loads. These findings include investigations of stress-strain behavior of thermoplastic materials, the compression behavior of pipe, evaluation of procedures to use a simple stub compression test as an alternate to the current local buckling calculation to determine pipe compression capacity, and selection of procedures for use in the simplified design procedure proposed for inclusion in the *AASHTO LRFD Bridge Design Specifications* (AASHTO 2007a).
- QA/QC—This section presents investigations of the properties of thermoplastic resins and pipe not embedded in soil. These tests and investigations contributed proposed changes to the product specifications for thermoplastic culvert pipe.

This chapter presents the major findings and support information on each of these subjects. Additional details are presented in the appendices.

Studies of Pipe-Soil Interaction

2D Behavior of Thermoplastic Pipe—Testing and Computer Modeling

The 2D behavior of thermoplastic pipe was investigated through tests and computer modeling. Details are provided in Appendix C.1. Tests were conducted in a laboratory biaxial soil cell on corrugated 24-in. inside diameter pipe manufactured with high-density polyethylene (HDPE) and 24-in. inside diameter standing rib pipe manufactured with polyvinyl chloride (PVC) (Figure 1).

The development and details of the 6.6 × 6.6 ft biaxial soil cell are reported in Brachman et al. (2000). The pipes were embedded in poorly graded sand compacted to approximately 85% of maximum standard Proctor density. Instrumentation included strain gages (see Figure 1 for locations) deflection gages, and soil pressure cells. Subsequently, finite element models of the tests were developed to investigate the ability of 2D modeling to capture the overall pipe behavior. Methods used to estimate the soil modulus are described in Appendix C.1 and include both linear and non-linear behavior. Deflection data are compared with the model predictions in Figure 2. Strain data are compared with model predictions in Figure 3 for the invert of the PVC pipe. Comparisons at other locations, and for the HDPE pipe, were similar (Appendix C.1). Overall, the computer models were found to provide reasonable estimates of the pipe behavior.

After the computer models were validated, they were extended to investigate the effect of variable haunch support. A soft haunch zone was selected and the modulus of the backfill material in this zone (E_h) was varied from 1% to 100% of the general backfill (E_s). The crest and valley strain in an HDPE pipe is shown in Figure 4, which also shows the haunch zone used in the computer model.

Figure 4 shows that at a ratio of $E_s/E_h = 10$, the peak strains are approximately 50% higher than in the uniform case, and when $E_s/E_h = 100$, the peak strains are more than double the uniform case. The test results were also used to investigate suggested procedures for the simplified design method, as discussed later.

Effects of Compaction and Burial Conditions

The effects of backfill compaction and variable haunch support were further investigated with another series of six

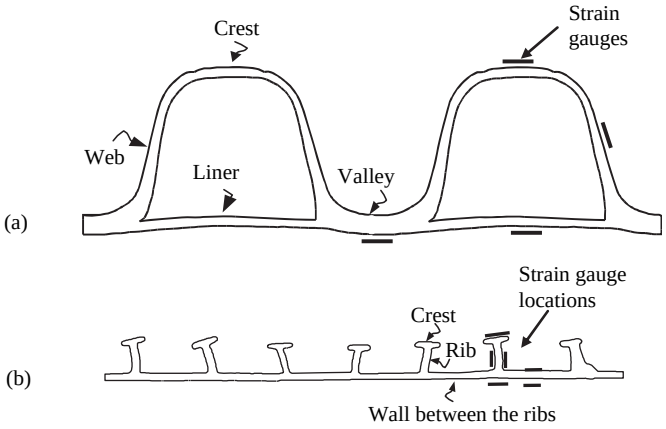

Figure 1. Pipe profiles and strain gage locations: (a) lined corrugated HDPE pipe; (b) ribbed PVC profile.

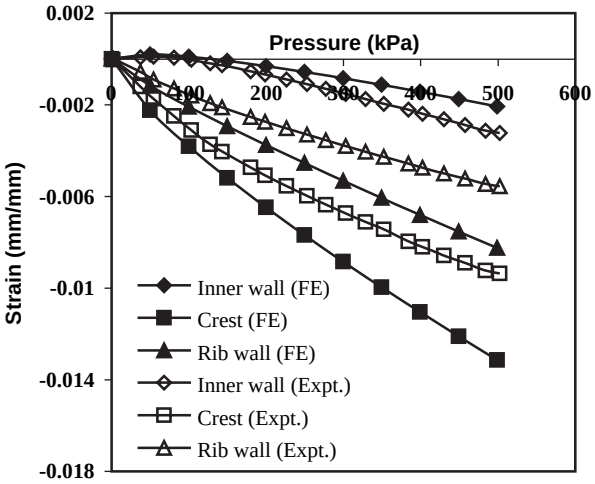

Figure 3. Comparison of strains at invert of PVC pipe.

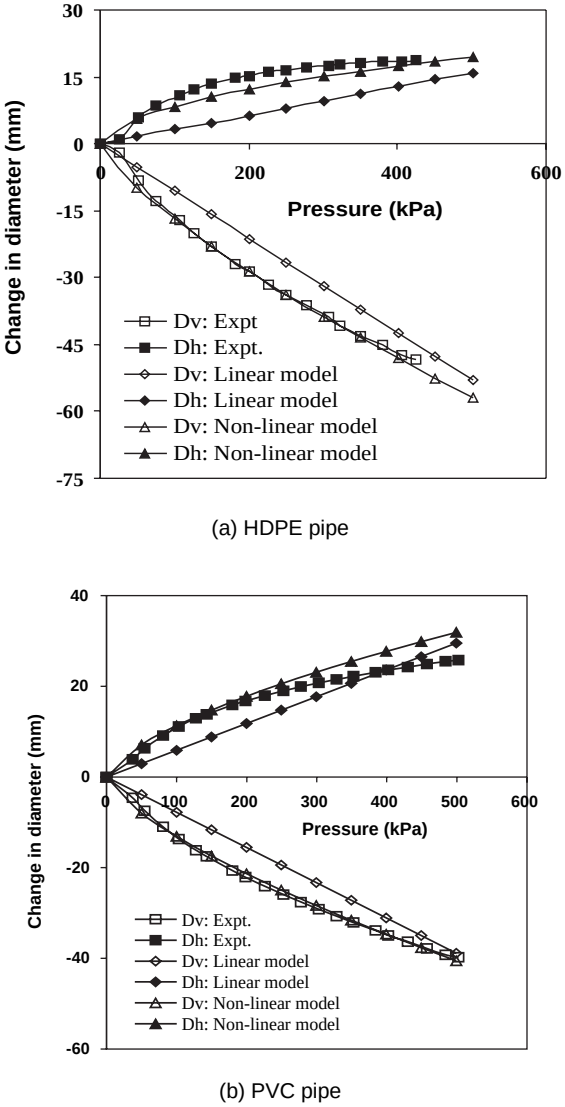

Figure 2. Comparison of measured deflection data with computer model.

tests in the biaxial test cell on 600-mm diameter corrugated HDPE and corrugated PVC pipe. The tests and results are presented in detail in Appendix C.4. Test variables are summarized in Table 1.

Deflections and strains from the tests are summarized in Table 2 and Table 3, respectively. As expected, the lowest deflections occur in the GW backfill material (Tests 5 and 6). Of particular note is the ratio of vertical to horizontal deflections in Table 2. This ratio is higher for the HDPE pipes because of the low circumferential stiffness (modulus of elasticity times

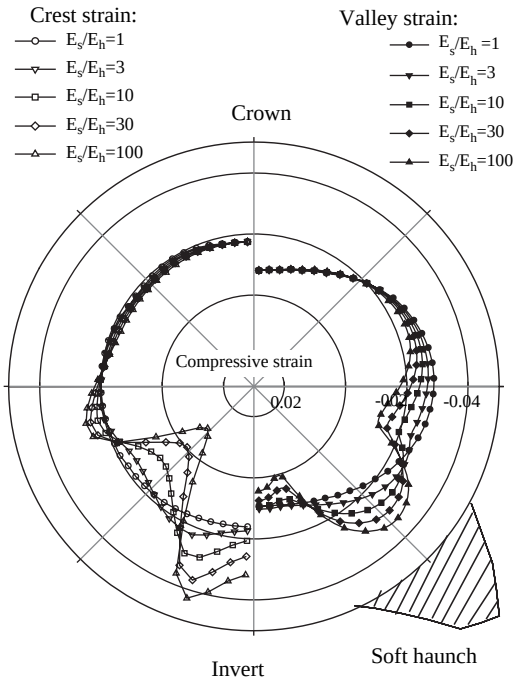

Figure 4. Strains in HDPE pipe due to variable haunch support.

Table 1. Test variables for study of effects of compaction and haunch support.

Test	Description*	Type of Pipe	Method of Compaction
T1	SP-HDPE-PT	HDPE	Vibratory plate tamper
T2	SP-HDPE-R	HDPE	Rammer
T3	SP-HDPE-SB	HDPE	Stiff base with a loose haunch, compacted above springline
T4	SP-PVC-SB	PVC	Stiff base with a loose haunch, compacted above springline
T5	GW-HDPE-PT	HDPE	Vibratory plate tamper
T6	GW-PVC-PT	PVC	Vibratory plate tamper

*Note: SP = poorly graded sand; GW = well-graded gravel; HDPE = high-density polyethylene; PVC = polyvinyl chloride; PT = vibratory plate tamper; R = Rammer; and SB = stiff base/loose haunch.

wall area over pipe radius: EA/R) of these pipes. This is discussed further under the simplified design method. The low circumferential stiffness causes the pipe to shorten circumferentially due to hoop compression stresses in addition to relative deflection due to bending. Circumferential shortening increases the vertical deflection and decreases the horizontal deflection—hence the high ratios. The deflections in all of the tests are well below typical field limiting deflections, which for AASHTO are 5%, and are quite low given the magnitude of applied vertical stress, which is equivalent to about 34 ft of fill. Strains are similarly low relative to typical strain limits.

Although the highest strains might be expected in the tests with soft haunches (T3 and T4), this was not the case for the PVC pipe, where Test T6 had a higher strain than Test T4. However, in Test T6, the peak strain occurred at the left springline while the other tests showed the peak strain at or near the invert. This could be the result of backfill compaction near the pipe. Note that Test T6 also had the lowest vertical deflection.

The application of the results to the simplified design method is presented in a later section.

Studies of Complex Behavior of Profile Wall Pipe

Profile wall pipe makes effective use of material by relying on two behaviors that can be considered second order. The first can be characterized as circumferential shortening. By virtue of low cross-sectional area and low long-term modulus, a polyethylene pipe circumference shortens sufficiently to reduce the interface contact pressures and cause load to flow around the pipe rather than through it (i.e., increase the arching effect). This behavior can reduce the load on the pipe significantly. Achieving this behavior requires installation of the pipe in stiff soil capable of carrying the extra load with minimal compression strain (soil compression negates the effect). This behavior was incorporated into AASHTO design procedures for thermoplastic pipe in 2000 based on the work of McGrath (1998a, 1999).

The second type of second-order behavior is the consideration of local buckling. Although metal pipes are designed to carry the full yield stress prior to buckling, thermoplastic pipe will undergo local buckling at a stress lower than the full yield

Table 2. Vertical and horizontal deflections at an applied pressure of 29 psi.

Test	Description	DD_v (%)	DD_h (%)	DD_v/DD_h
T1	SP-HDPE-PT	-0.9%	0.1%	-8.5
T2	SP-HDPE-R	-0.8%	0.0%	-4.4
T3	SP-HDPE-SB	-2.1%	0.5%	-4.1
T4	SP-PVC-SB	-1.2%	0.7%	-1.8
T5	GW-HDPE-PT	-0.6%	0.2%	-3.1
T6	GW-PVC-PT	-0.1%	0.2%	-0.5

Table 3. Measured maximum circumferential compression strains on the valley interior at applied pressure of 29 psi.

Test	Description	$e_{c\text{-}max}$ (%)	Location (degrees from rt. springline - ccw)
T1	SP-HDPE-PT	-0.5	-90
T2	SP-HDPE-R	-0.4	-90
T3	SP-HDPE-SB	-1.0	-90
T4	SP-PVC-SB	-0.3	-90
T5	GW-HDPE-PT	-0.4	-83
T6	GW-PVC-PT	-0.4	180

strength of the pipe wall material. However, the theory developed by Winter (1946) for light gage metal sections shows substantial post-buckling capacity of a section. Use of this capacity increases the depth to which some profile wall thermoplastic pipe may be buried. McGrath and Sagan (2000) adapted this theory for the AASHTO specifications; however, validation of the methods was not complete and the procedure has been found cumbersome for calculation. This section presents additional investigation to address that issue.

Liner Buckling

Liner buckling is characterized by the development of circumferential waves in the liner element of a corrugated pipe. Hashash and Selig (1990) conducted a deep burial field test that experienced liner buckling, and Selig et al. (1994) demonstrated that laboratory testing can be used to investigate liner buckling behavior. In this project, tests were conducted to investigate this liner buckling through biaxial tests, which simulate in-ground behavior directly, and axisymmetric tests, which simulate pure compression behavior in pipe with low deflections. The tests are described in detail in Appendix C.3. The profiles of the tested pipe are shown in Figure 5. The pipes in Figure 5a and Figure 5b are the predominant profiles used for thermoplastic culvert pipe and were tested in the axisymmetric test. All four pipes were tested in biaxial compression.

The axisymmetric test embeds a vertical pipe specimen in a ring of soil and applies uniform radial compression stress to the outer periphery of the soil. The development of liner buckling in this test is demonstrated in Figure 6.

Liner buckling could also be observed in the data from the tests in the biaxial cell test, as shown in Figure 7. The nonlinear strain development in the liner, shown in Figure 7b, indicates that buckling takes place at a compression strain of about 0.8%.

Overall, the liner buckling strains for each profile type are presented in Table 4. The data demonstrate the significance of the ratio of the liner width (W) to thickness (t). Most liners with a ratio of about 20 to 25 buckle at about 1% strain while the box profile with a liner width to thickness ratio of 10.4 buckles at a strain of about 2.4%. This is consistent with the local buckling theory presented later. Also significant is the demonstration that local buckling of the liner, which occurs at about 0.8% strain, does not represent a limit state for pipe wall compression capacity, as the test was conducted to more than 3% strain without a compression failure (Figure 7).

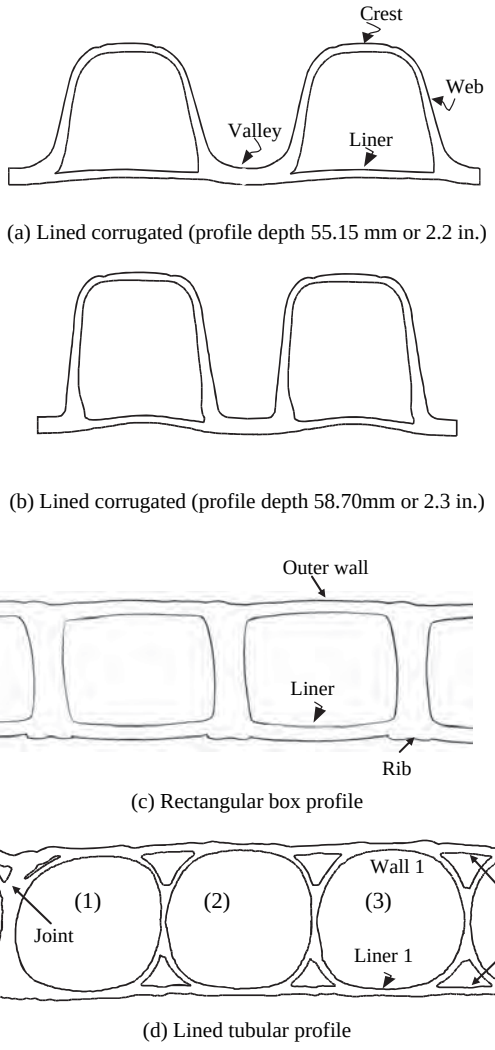

(a) Lined corrugated (profile depth 55.15 mm or 2.2 in.)

(b) Lined corrugated (profile depth 58.70mm or 2.3 in.)

(c) Rectangular box profile

(d) Lined tubular profile

Figure 5. Pipes tested for liner buckling behavior.

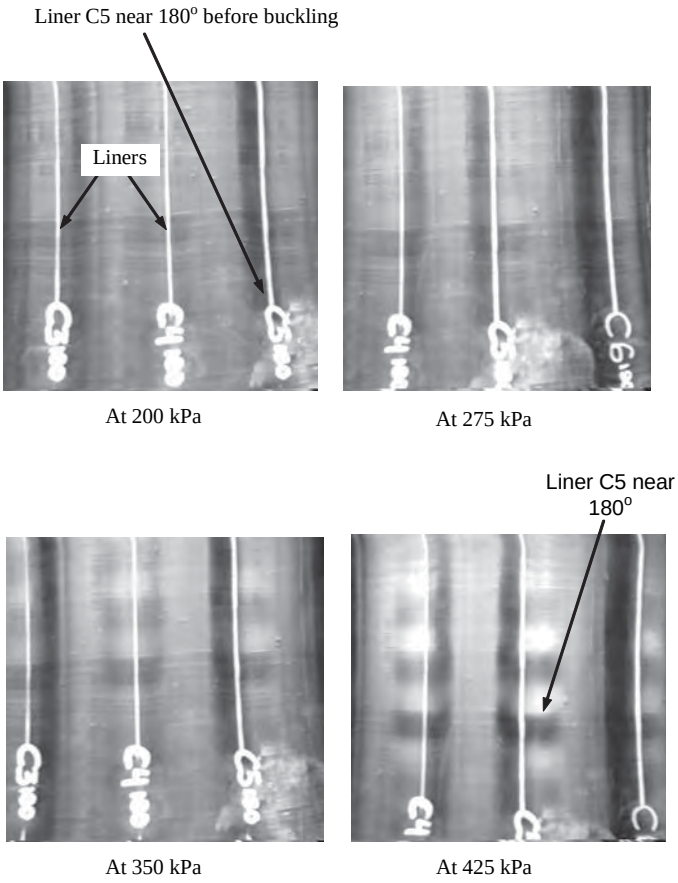

Figure 6. Development of local buckling in profile wall pipe. (Note: 1 psi = 6.89 kPa.)

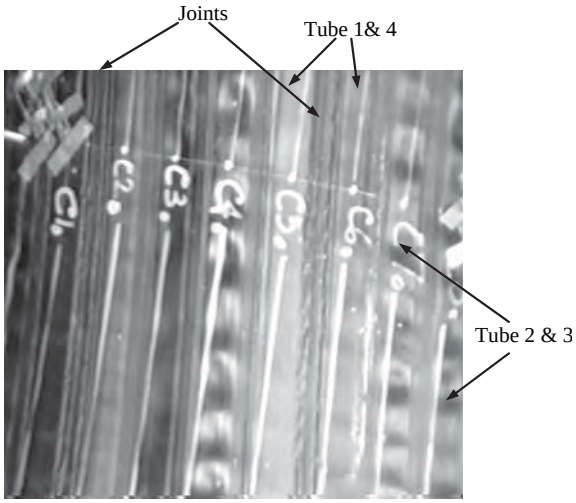

(a) Observation of liner buckling, Test DH

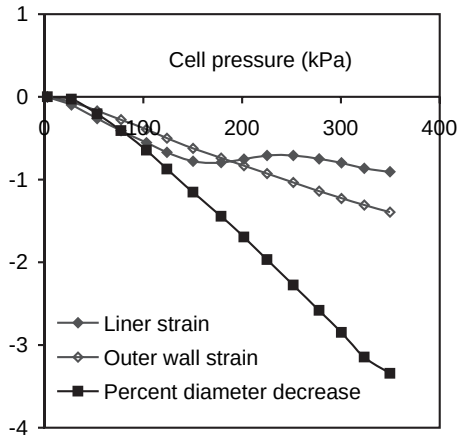

(b) Non-linear liner strain due to local buckling, 1 psi = 6.89 kPa

Figure 7. Liner buckling in biaxial cell test.

Local Bending in Profile Wall Pipe

Finite element analysis by Moore and Hu (1995) demonstrated that longitudinal tensile strains exist in profile wall pipe subject to hoop compression. Local bending in corrugated pipe liners was further investigated with computer modeling presented in Appendix C.2. Pipe liners are not directly loaded by the soil surrounding the pipe. Stress is applied to the liner only at the edges where it attaches to the corrugation, which deforms under earth and other applied loads. As a result, when the corrugation is compressed, the liner compresses at the edges but not at the center. This is demonstrated in Figure 8, which shows that as the pipe corrugation moves toward the pipe center under compression, the center of the liner remains nearer the original radius, creating longitudinal bending. The liner hoop strains that result from this

Table 4. Summary of liner buckling strains.

Test Type	Pipe	*W* (mm)	*t* (mm)	W/t	Buckling Strain (%)
Biaxial	Lined corrugated	62.0	2.46	25.2	0.76
		50.0	2.36	21.1	1.05
Hoop	Lined corrugated	62.0	2.46	25.2	0.85
		62.0	2.46	25.2	1.1
		50.0	2.36	21.1	1.2
	Box profile	46.0	4.42	10.4	2.4
	Tubular profile	43.5	2.21	19.8	0.80

Note: 1 in. = 25.4 mm.

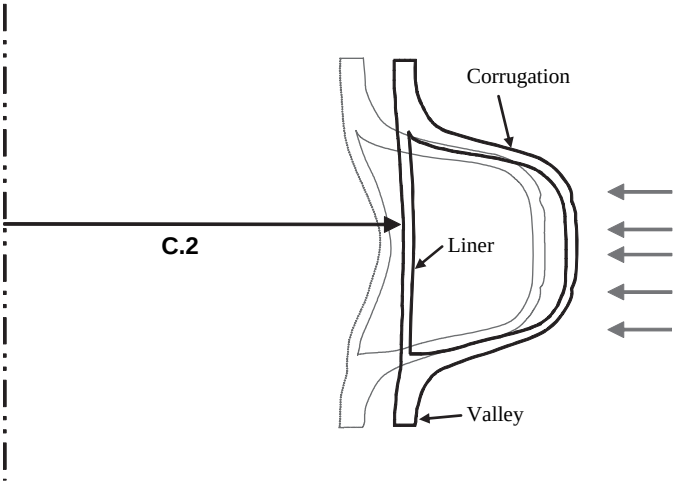

Figure 8. Mechanism of liner bending.

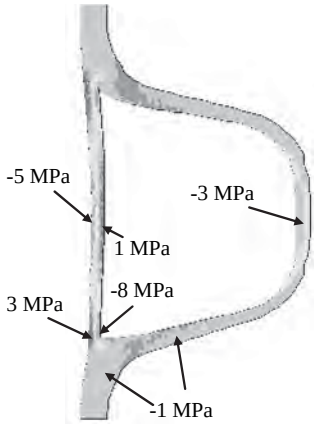

Figure 10. Longitudinal stresses in corrugated profile. (Note: 145 psi = 1 MPa.)

behavior are shown in Figure 9, and the axial stresses are shown in Figure 10.

The stresses shown in Figure 10 are for the short-test period relative to the life of a pipe in the ground and would reduce over time due to relaxation. However, the hoop stresses are significant in magnitude and indicate that resin quality must be maintained to ensure that secondary stresses that are not directly considered in design will not result in cracking during the culvert service life.

3D Behavior of Profile Wall Pipe

Further analysis of the pipe tests was conducted using axisymmetric models for the axisymmetric cell and a Fourier method to investigate behavior in the biaxial test cell. These models were fully 3D and investigated local stresses in detail. The analyses are described in Appendix C.5.

Generally, the analyses demonstrate that 3D behavior can be effectively modeled to investigate behaviors not captured in two dimensions. Of note is behavior of the box and honeycomb profiles. Figure 11 shows the hoop strains in the box profile under a 44 psi (300 kPa) radial pressure. The figure shows a gradient in the hoop strain of about 20% from one side to the other. Thus, as only one side is in contact with the soil, differential stresses develop to carry the load. This behavior was not seen in the corrugated profiles, which are loaded both at the crest and at the valley.

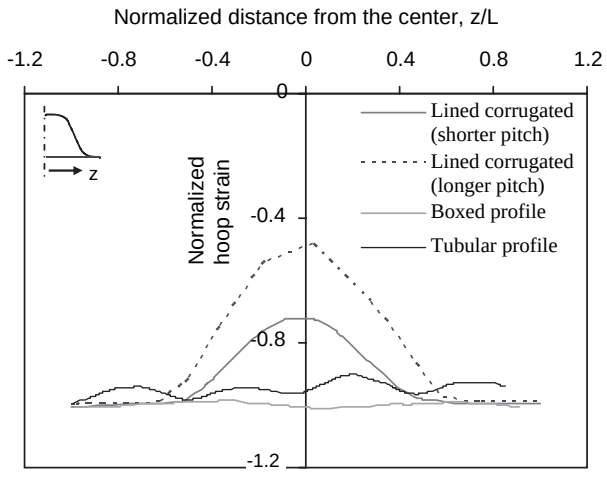

Figure 9. Comparison of average liner hoop strains (%) by profile type.

Design

Material Tension and Compression Behavior

Material tests were conducted with the objectives of investigating: relative behavior in compression and tension of PVC and HDPE resins used for thermoplastic culvert pipes, and strain limits for compression behavior of PVC and polyethylene (PE) pipes (Appendix B.1).

The tests were conducted on reground pipe resin supplied by pipe manufacturers. The PVC samples included both filled and unfilled resins. Results indicate the following:

- Previous assumptions about the compression behavior of PE appear to be appropriate; *NCHRP Report 438* (McGrath and Sagan 2000) concluded that a 4% compression strain limit is appropriate for PE and the figures show this is the point where the stress strain curves deviate significantly to non-linear behavior; this is consistent with the compression behavior previously reported by Zhang and Moore (1998).
- The PVC filled and unfilled resins show the known difference in tension strength; however, the compression strengths of these resins are approximately equal, indicating that fillers that disrupt the flow of tensile stresses through the polymer transfer compression stresses quite well, much like aggregate in concrete. This is shown in Figure 12, where a sig-

Figure 11. Hoop stresses in box profile at 44 psi (300 KPa) radial pressure.

nificant deviation from linear behavior occurs at about 2.5% strain for both filled and unfilled resins. This suggests a constant limiting compression strain for approved PVC resins, rather than the current strain limit based on modulus and tensile strength.

- For both PE and PVC, the modulus and strength are higher in compression relative to tension when calculated in engineering units (neglecting Poisson effect).

Compression Behavior of Profile Wall Pipe

A significant effort in this project was devoted to investigating the behavior of profile wall pipe in compression. Objectives of this work were to develop a standard to evaluate the compression strength of pipe as a quality control test and to provide a standard procedure to determine the compressive strength of a pipe wall through testing, rather than through the local buckling calculations in the current LRFD specifications.

The bulk of the investigation consisted of stub compression testing of pipe specimens. The stub compression test was developed by McGrath and Sagan (2000) as a means of validating the local buckling design procedures in the current LRFD specification. The test consists of compressing a short circumferential section of pipe at a slow rate. The peak load

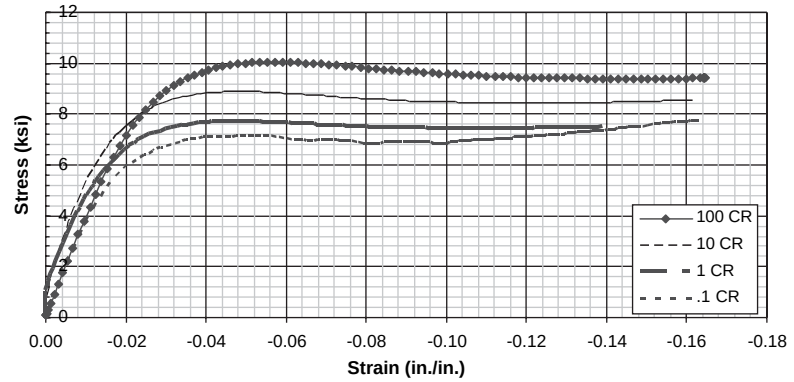

(a) Unfilled resin

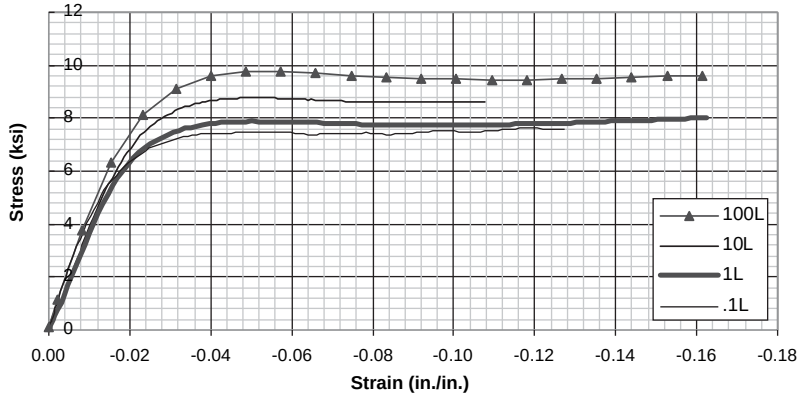

(b) Filled resin

Figure 12. Stress-strain curves for PVC in compression.

Figure 13. Corrugated PVC pipe in stub compression test.

is the primary test result, but the strain at peak load is also of interest. The specimen chord length is about 1.5 times the depth of the corrugation, a length that minimizes the bending due to the specimen curvature but is long enough to permit buckling in the corrugation elements as shown in Figure 13 and Figure 14 for PVC and HDPE pipe respectively. The HDPE pipes, which have a relatively low modulus of elasticity and thin elements, have a substantial post buckling capacity. The PVC pipes, which have a higher modulus of elasticity and thicker elements, are stressed almost to their material compressive strength prior to the onset of buckling. These behaviors are consistent with theory.

The basis of the stub compression test and local buckling design procedure is to determine the overall section capacity while allowing individual elements of a profile provided to buckle. This procedure was developed by Winter (1946) and was long used to design light-gage steel sections. The Winter procedure consists of idealizing a profile into a series of flat plate elements and determining the quantity of cross-sectional

Figure 14. Corrugated HDPE pipe in stub compression test.

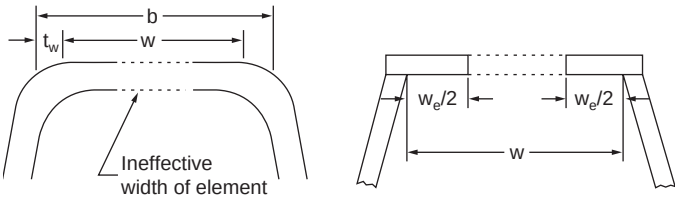

Figure 15. Illustration of element effective area for local buckling calculations.

area in the center portion of flat elements rendered ineffective due to buckling. The corners of the profile, where two elements meet, provide out-of-plane bracing and prevent buckling; however, as the load on the section increases, the ineffective area increases; the load on these ineffective areas is transferred to the remaining effective area (i.e., the corners). Capacity is reached when the corners are stressed to the material strength. This is demonstrated in Figure 15.

The local buckling calculations use the following equations:

$$b_{eff} = \rho w \qquad \text{(Eq. 1)}$$

$$\lambda = \frac{w/t}{\sqrt{k/\varepsilon_y}} \qquad \text{(Eq. 2)}$$

$$\text{if} \quad \lambda \le 0.673 \quad \text{then} \quad \rho = 1$$

$$\text{if} \quad \lambda > 0.673 \quad \text{then} \quad \rho = (1 - 0.22/\lambda)/\lambda$$

where:

b_{eff} = effective width of the element
b = gross width of the element
w = clear width of the element, computed based on the idealized section (see Figure 15)
k = plate buckling coefficient (k = 4 for elements supported on both sides, k = 0.43 for one side support—such a standing rib)
ε_y = limiting compressive strain of the material (set in the design specifications)
ρ = effective width reduction factor
λ = slenderness of the element

Round-Robin Testing to Develop Stub Compression Test Standard

Preliminary testing described in Appendix B was conducted to develop a draft test specification. During this testing and in discussion with other laboratories, the test end conditions were changed from pinned-fixed as recommended by McGrath and Sagan (2000) to fixed-fixed. This change produces somewhat more moment in the ends of the specimens, which is undesirable, but allows more laboratories to conduct the test without modifying existing equipment. Sub-

Table 5. Round-robin results, Round 1, all specimens.

Peak Load, lb/in.				Strain at Peak Load, %			
Sample	Average	St. Dev.	COV, %	Sample	Average	St. Dev.	COV, %
24A	724	55.8	7.7	24A	7.2	1.1	14.7
24C	881	81.0	9.2	24C	8.7	1.6	18.2
42B	946	57.9	6.1	42B	5.4	0.8	14.8
42C	994	93.1	9.4	42C	6.0	0.7	12.0

sequently, two rounds of inter-laboratory tests were conducted to evaluate precision and repeatability. Round 1 consisted of testing specimens prepared in the laboratory of Simpson Gumpertz & Heger Inc. This round investigated the repeatability of the test with specimens prepared in a consistent manner. In Round 2, each laboratory prepared its own specimens from pipe samples provided to it. The results of the tests are presented in Table 5 and Table 6 for Rounds 1 and 2, respectively.

The tables show a consistent coefficient of variation for the load of less than 10%. The coefficient of variation for the strain is somewhat higher; however, this was expected due to variability in sample preparation. Also, only the load is to be used in design or as a quality control limit. Examination of the data also showed that the test results varied consistently with the position of the pipe around the circumference. This is demonstrated in Figure 16, in which the normalized peak loads are plotted versus position around the pipe.

With the successful completion of the round-robin tests and data evaluation, the final recommended test standard was developed (Appendix G).

Use of Stub Compression Test in Design

Further evaluation of the stub compression data demonstrated that the test could be used to determine the compression capacity of the pipe to be used in design. One aspect of this determination is to consider the effect of time. Examination of Equations 1 and 2 shows that the effective width, and hence the buckling capacity of a section, is a function of the strain in an element of a profile. Since the apparent modulus of thermoplastics under sustained load decreases with time (Appendices A and B), it follows that pipe compression strain will increase with time and the strength will decrease with time. Thus, for design, the strength from a short-term test must be adjusted to reflect the time period under consideration. Knowledge of the modulus of elasticity versus time addresses this issue. AASHTO specifications currently provide values for the short-term (initial) and 50-year modulus of elasticity of PVC and HDPE materials. This allows computing strength for these periods. Modulus values for 75-year design periods are presented later and proposed for inclusion in AASHTO specifications.

Stub compression capacity from the various tests was compared to the compression capacity calculated in accordance with the simplified design procedure (Appendix B). These calculations indicated that for polyethylene, the long-term capacity calculated very closely to 30% of the short-term stub compression capacity for HDPE, and about 60% of capacity for PVC. The standard deviation is about 0.03%.

Simplified Design Method

A simplified design method for thermoplastic pipe, like simplified design for all buried pipes, must be conservative to account for the many unknowns of ground conditions and installation procedures. Unless there is good information available on in situ soils and there is an expectation of good quality control during construction, there is little benefit to be derived from comprehensive analyses. When such information and quality control will be exercised, generally on large projects with deep fills or other cost implications, finite element analyses can be used to study the influence of the various loading parameters to achieve economical designs. Guidelines for comprehensive analyses of thermoplastic pipes are provided in Appendix D.

The simplified design method is largely assembled from previously available procedures for evaluating flexible thermoplastic culverts. The development and validation of the method is presented in the appendices and Chapter 3. This section presents the findings of studies instituted to evaluate the various elements of the procedures.

Table 6. Round-robin results, Round 2, all specimens.

Peak Load, lb/in.				Strain at Peak Load, %			
Sample	Average	St. Dev.	COV, %	Sample	Average	St. Dev.	COV, %
24A	719	65.3	9.2	24A	6.7	1.3	20.0
24C	889	73.1	8.2	24C	8.1	1.3	16.2
42B	947	77.0	8.1	42B	5.7	0.9	15.6
42C	994	57.7	5.8	42C	6.0	0.4	6.2
24D	1991	118.6	6.0	24D	5.3	0.6	10.7

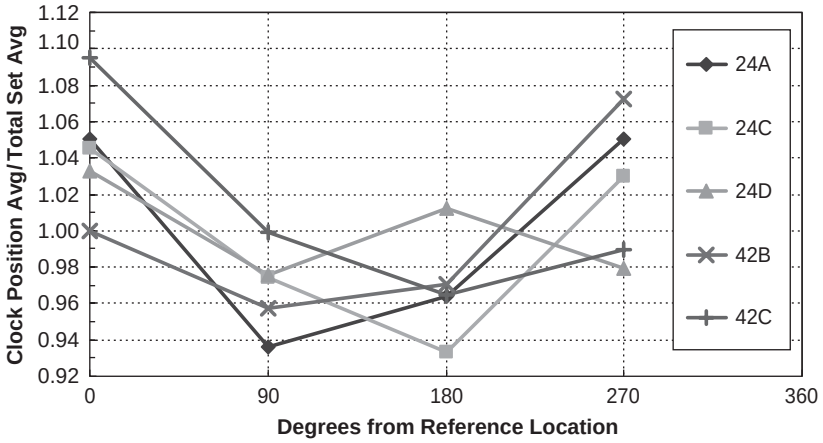

Figure 16. Variation in stub compression capacity around pipe circumference.

Design Criteria for Thermoplastic Pipe

Simplified or comprehensive design methods for thermoplastic pipe use the same limiting strength criteria to evaluate performance. These include compression thrust strain, combined bending and thrust strain, and general buckling.

Compression Thrust Strain. Compressive thrust results from earth, live, and external hydrostatic loads. Strain limits are set based on performance of pipe materials in compression tests. Thrust capacity of profile wall thermoplastic pipe is local buckling. This design procedure was developed by McGrath and Sagan (2000) and previously adopted by AASHTO. As originally adopted, the compression strain limit was based on the strain at yield assuming linear behavior and the initial modulus of elasticity. Work on this project presented above and in Appendix B shows that a fixed strain limit is more appropriate. For HDPE pipe, the compressive strain limit is set at 4.1%, and for PVC, the limit is set at 2.6%.

Combined Strain. Combined strain adds the bending strain that results from deflection to the thrust strain. Due to the stability of profiled wall pipe in the parallel plate test, combined compression strain is allowed to be 50% larger than thrust strain alone. Combined tension strain should be small or nonexistent in properly installed thermoplastic culvert pipe. However, analysis of local stresses not addressed in the proposed simplified design method (Appendix C.4 and as discussed above) shows that tensile stresses are likely due to local buckling and complex profile geometry. Except for the work on stress crack resistance of HDPE, this project has not investigated tensile strain limits but recommends that the criteria in the current *AASHTO LRFD Bridge Specifications* be preserved.

General Buckling. A pipe wall must have sufficient stiffness to remain stable under compression loads. Currently, AASHTO evaluates buckling in thermoplastic pipe using a "Winkler" model based on a spring supported tube. Work by Moore (1990) has shown that a model based on continuous pipe support (i.e., continuum model), which better represents in-ground pipes, provides better predictions. The continuum model places more emphasis on soil support than pipe stiffness relative to the Winkler model. The continuum model is recommended for use by AASHTO.

Deflection. The only service criterion for thermoplastic pipe is deflection. A deflection limit is easily checked in the field after construction and provides a good tool for enforcement of installation specifications. In the past, AASHTO established a service limit of a 5% reduction in vertical diameter. The actual service limit on thermoplastic pipe will be variable; however, a single value is retained here to simplify enforcement and as recognition that good construction practices will result in deflections less than 5%. In evaluating installations where deflections have exceeded 5%, the actual service deflection limit may be calculated and used.

The simplified design method was evaluated using soil box tests and computer modeling. The soil box tests were conducted to provide data under controlled conditions against which to compare calculated values from computer finite element modeling and the proposed simplified design method. Details of the testing and analysis are provided in Appendix C. The profiles evaluated included profile wall HDPE and standing rib PVC, which are shown in Figure 1. The pipes were monitored for deflection and strain. One finding of the analyses is that the proposed soil modulus values appear to be conservative. There are two primary reasons for this, as follow:

1. The constrained soil modulus table in AASHTO compresses all suitable backfill soils into three very broad groups. Of necessity, the properties of a soil group must

represent the lower-quality soils included in that group. The soils used in the testing conducted in this project were not the highest quality possible, but were not representative of the lower-quality soils allowed in their groups.

2. McGrath (1998b) developed the constrained soil properties in AASHTO from the hyperbolic models used to develop the concrete pipe direct design method in AASHTO. The properties were developed by Selig (1988); however, Selig (1990) presented a second set of hyperbolic properties for plastic pipe design that produced constrained moduli about two times the values derived from the 1988 properties. McGrath (1998b) examined both sets of properties and compared them with Howard's (1977) E' values, which have historically been used in simplified deflection predictions with the Spangler equation. Howard's E' values were back-calculated from field-installed pipe and thus represent typical field variations as well as soil behavior. McGrath concluded that the lower stiffness properties from Selig (1988), which correlated reasonably well with Howard's E' values, were more reasonable for design by providing some consideration of real world variability. McGrath concluded that the higher stiffness soil properties in Selig (1990) could be appropriate for design if proper field control was exercised.

Thermoplastic Materials Studies

Studies were carried out to investigate various properties of HDPE resins that could affect long-term material performance. The primary focus of this program was on the effect of regrind materials on general properties and on SCR in particular. A second purpose was to evaluate the oxidative induction time, a measure of the long-term stability of a resin. Details of the entire program are provided in Appendix F.

Twenty-four specimens of corrugated HDPE pipe were tested along with a sample of pure resin from which the pipe was manufactured. The range of variables is summarized in Table 7. Tests were conducted on pure resin (resin plaque, RP), ground pipe (pipe plaque, PP; this removes residual stresses due to manufacturing), and from sections of pipe (pipe liner, PL). Tests evaluated resin density, melt index, carbon black, oxidative induction time, and slow crack growth through the notched constant ligament stress (NCLS) test.

Table 7. HDPE corrugated pipe samples for material studies.

Company	Pipe Diameter (in.)	Regrind (%)	Carbon Black (Estimated) (%)
I	24, 36, 48, 60	0 to 20	2 - 2.5
II	24, 36, 48, 60	0 to 20	2 - 2.5
III	24, 30	0 to 20	2 - 2.5
IV	24	0	2 - 2.5
V	24, 36	0 to 20	2 - 2.5

*Pure resin type varied also.

Effect of Carbon Black

For a majority of the resins, the addition of carbon black with carrier resin decreased the SCR of the resin as shown by the NCLS failure times for 100% resin samples. Table 8 demonstrates this effect in the ratio of the PP/RP failure times. The reduction factors range from 0.50 to 0.99. For pipes I-36″ (representing pipe manufacturer and pipe diameter) and III-30″, the failure time of a pipe specimen was slightly higher than the corresponding resin specimen.

Effect of Manufacturing Process

The effect of the manufacturing processing on SCR is obtained by comparing the NCLS failure times of pipe liner specimens with the corresponding pipe plaque specimens (Table 9). In each set of pipe samples, which includes 0%, 10%, and 20% regrind quantities, the pipe-liner-to-pipe-plaque (PL/PP) ratio is relatively similar, since these pipes were produced from the same machine. However, the processing effects vary significantly from machine to machine. The average reduction factors range from 0.44 to 0.91. Examination of Table 9 for variations by diameter shows no discernible trend. For pipes with diameters of 36 in. and 48 in., the reduction factors are very similar regardless of the manufacturer, while large differences are observed for pipes with diameters of 24 in. and 60 in.

Table 8. Ratios of failure times for 100% resin specimens.

Pipe	Pipe Plaque/ Resin Plaque
I-24"	0.89
I-36"	1.05
I-48"	0.74
I-60"	0.50
II-24"	0.81
II-36"	0.99
II-48"	0.87
II-60"	0.77
III-24"	0.96
III-30"	1.16
V-24"	0.73
V-36"	0.70
Average	**0.85**
Standard Deviation	0.18
Coefficient of Variation	0.21

Table 9. Effect of pipe manufacturing processing on SCR.

Pipe	NCTL Ratio PL/PP 100% Virgin	NCTL Ratio PL/PP 10% Regrind	NCTL Ratio PL/PP 20% Regrind	Average Ratio Value
I-24"	0.80	0.91	0.88	0.87
I-36"	0.71	0.73	0.78	0.74
I-48"	0.44	NA	NA	0.44
I-60"	0.64	NA	NA	0.64
II-24"	0.60	0.62	0.58	0.60
II-36"	0.74	NA	NA	0.74
II-48"	0.65	0.45	0.47	0.52
II-60"	0.91	NA	NA	0.91
III-24"	0.60	NA	NA	0.60
III-30"	0.63	NA	0.57	0.60
IV-24"	NA	NA	0.54	0.54
V-24"	0.49	0.47	0.48	0.48
V-36"	0.55	NA	NA	0.55
Average				**0.63**
Standard Deviation				0.14
Coefficient of Variation				0.22

NA = Not available

Combined Effect of Carbon Black and Pipe Processing

The combined effect of carbon black and manufacturing process on SCR of the resin is reflected by the ratio of NCLS failure times between the pipe liner and resin plaque specimens. As expected, the reduction factors, shown in Table 10, are greater than carbon black alone, ranging from 0.32 to 0.74.

Effects of Regrind Materials

The effects of regrind materials on the SCR were evaluated on both pipe plaque and pipe liner materials, as shown in Table 11. For the same pipe sample, the ratio values are relatively similar between plaque and liner, except for Sample II-48″. However, large differences are detected among pipes. The uncertainty is the type of regrind being added to these pipes. For II-24 in. and II-48 in. pipes, the regrind material enhances the SCR of the pipes more than 50%, as indicated in the data obtained from the pipe plaques. Such a large increase suggests that the regrind materials used in these two pipes probably came from materials with different SCR properties (i.e., not the same regrind material from the corresponding pipe containing 100% virgin resin). This hypothesis seems consistent with the melt index (MI) results of these two pipes since the pipes containing regrind have lower MI values than pipes without regrind. The high carbon black content in the 20% regrind material may contribute to the high ratio value of 1.17 for III-30 in. pipe.

Nevertheless, assuming the same regrind material is used in each case, increasing the regrind fraction from 10% to 20% does not show significant change in the SCR.

Table 10. Combined effect of carbon black and manufacturing process.

Pipe	Pipe Liner/ Resin Plaque
I-24"	0.71
I-36"	0.74
I-48"	0.33
I-60"	0.32
II-24"	0.49
II-36"	0.72
II-48"	0.57
II-60"	0.70
III-24"	0.57
III-30"	0.73
V-24"	0.35
V-36"	0.38
Average	0.55
Standard Deviation	0.17
Coefficient of Variation	0.31

Oxidation Resistance Evaluation

The long-term oxidation resistance of the corrugated pipe was assessed using the oxidative induction time (OIT) test according to ASTM D 3895. The OIT tests were performed on both the resin and finished pipe. A higher OIT value indicates a greater amount of remaining antioxidants. Table 12 shows the average OIT values of resins and pipes and reveals a large variation. In addition, the pipe processing does not seem to decrease the amount of antioxidants in all 12 tested samples, since 7 of the 12 samples exhibit a P/R ratio value

Table 11. Effect of regrind materials on SCR by comparing NCLS failure times.

Pipe	Pipe Plaque Ratio 10%/0% Ratio	Pipe Plaque Ratio 20%/0% Ratio
I-24"	0.72	0.67
I-36"	0.93	1.04
II-24"	1.52	1.59
II-48"	1.65	1.55
III-30"	NA	1.17
V-24"	0.87	0.92
Average	**1.15**	
Pipe	**Pipe Liner Ratio**	
	10%/0% Ratio	**20%/0% Ratio**
I-24"	0.82	0.74
I-36"	0.96	1.16
II-24"	1.57	1.52
II-48"	1.13	1.11
III-30"	NA	1.01
V-24"	0.84	0.89
Average	**1.07**	

Table 12. OIT value between resin and pipe without regrind.

Pipe	OIT (min.)		OIT Ratio Pipe/Resin
	Resin	Pipe	
I-24"	17.4	24.3	1.40
I-36"	66.3	44.6	0.67
I-48"	16.3	24.6	1.51
I-60"	15.4	10.4	0.68
II-24"	28.2	30.7	1.09
II-36"	26.3	25.9	0.98
II-48"	19.8	23.1	1.17
II-60"	39.9	34.2	0.86
III-24"	12.9	24.5	1.90
III-30"	25.7	30.5	1.19
V-24"	11.1	8.3	0.75
V-36"	7.5	8.8	1.17

Table 13. Effect of regrind material in OIT value.

OIT Test on Pipe					
Pipe	OIT (min.)			Ratio	
	0% Regrind	10% Regrind	20% Regrind	10%/0% Ratio	20%/0% Ratio
I-24"	24.3	18.6	21.3	0.77	0.88
I-36"	44.6	42.9	39.9	0.96	0.89
II-24"	30.7	30.4	28.5	0.99	0.93
II-48"	23.1	26.6	27.1	1.15	1.17
III-30"	30.5	NA	33.7	NA	1.10
V-24"	8.3	7.9	8.6	0.95	1.04

greater than 1.0. (Note that the ASTM standard indicates the repeatability of the test being ±5% for HDPE material with OIT value of 163 min.)

Antioxidants can be introduced to the pipe in two ways. One is from the virgin resin, and the other is from the master batch of carbon black with carrier resin. If antioxidants are included in the virgin resin only, the OIT value of the finished pipe should be lower than the corresponding resin, since some of the antioxidants are consumed during pipe manufacture. For example, Pipe I-36 may fall into this case. On the other hand, if antioxidants are added to the virgin resin as well as in the carbon black master batch, the OIT of the finished pipe should exhibit a higher OIT value than the corresponding resin. Five of the 12 samples exhibited a 10% higher OIT value in the finished pipe than in the corresponding resin.

Due to the uncertainty in the properties of the carbon black master batch, the oxidation resistance of the pipe should be evaluated instead of the virgin resin.

The effects of regrind materials on OIT are shown in Table 13. In general, varying the quantity of regrind in the range of 0% to 20% does not significantly change the OIT. The only exception is Pipe I-24 with 10% regrind.

Recommendations based on the material tests are discussed in Chapter 3.

CHAPTER 3

Interpretation, Appraisal, and Application

Pipe-Soil Interaction and Pipe Design

Numerous researchers have investigated the behavior of buried thermoplastic pipe with widely varying results. Although researchers consistently report good performance in controlled field tests, there are also a significant number of reports of high deflection and poor performance in actual installations, in spite of good construction specifications. Researchers, and the findings of this project, also consistently report that available simplified design models and computer finite element simulations of buried thermoplastic pipe installations provide reasonable estimates of in-ground behavior. The findings that must be drawn from this experience include:

- Thermoplastic pipes provide good performance when installed according to good construction procedures.
- Current simplified design techniques are adequate to predict behavior for typical installation conditions.
- Computer modeling with finite element methods can be used to design thermoplastic pipe installations for unusual conditions or when sufficient field control is used to ensure full compliance with proper specifications.
- Thermoplastic pipe, at the stiffnesses used for culverts, can be very sensitive to proper construction procedures; thus, proper construction is vital to good performance of thermoplastic culvert pipe.

These conclusions lead to design recommendations that largely make use of existing methods, with enhancements based on the findings of this project. Further, we conclude that control of construction procedures is imperative and that the critical construction control is implementation of post-construction inspections to evaluate changes in pipe diameter and any other anomalies in the installed pipe. In this chapter, we present the key elements of a simplified design method for thermoplastic culvert pipe, providing the basis for the recommendations. Guidelines for comprehensive design of thermoplastic pipe using finite element methods are presented in Appendix D. Proposed design and construction specifications are provided in Appendices H and I, respectively.

Design of Thermoplastic Culvert Pipe

This section discusses the design features to address the critical limit states.

Load Factors

Earth load factors for buried flexible culverts have traditionally been set at about 2.0, while the earth load factors for rigid culverts are set at 1.3. These values were both established prior to the incorporation of thermoplastic culverts in AASHTO specifications. One concern that might have caused this variation was that flexible culverts are subject to high deflections when not installed properly. High deflections remain possible in flexible culverts; however, as noted above, numerous researchers have shown that, when properly installed, thermoplastic pipes provide good performance at very significant depths. The most notable of these is a 24-in. diameter culvert pipe installed in Pennsylvania under approximately 100 ft of fill (Hashash and Selig 1990) and an Ohio study where a variety of PVC and HDPE pipes were installed under 40 ft (Sargand et al. 2002) of fill. To allow designers to take advantage of the expected good performance when good field control is exercised, the proposed design method reduces the earth load factor for thermoplastic pipe to 1.3, but introduces an installation factor that is multiplied by the load factor. For most installations, the installation factor will be set to 1.5, which provides a total safety of 1.95, equal to current specifications. However, for special installations where detailed construction controls are implemented, designers may reduce the installation factor to values as low as 1.0. Construction controls are detailed in Appendix I, and include monitoring of backfill

materials, compaction levels during construction, and of deflection during sidefilling, backfilling, and after construction.

No changes are proposed for live load factors for thermoplastic culverts.

Limit States

No changes are proposed to the current AASHTO limit states. Strength limit states include wall area, buckling, and flexibility limit. The one service limit state is deflection. The limit state for wall area includes an evaluation of local buckling for profile wall pipe, modified based on findings of this study.

Design Periods

AASHTO specifications currently provide the modulus of elasticity for "initial" and 50-year design periods. The initial values are those derived from the material qualification tests and represent very short loading periods. The 50-year values were provided by industry. Although the specific testing used to develop the 50-year values is not available, they are considered reasonable and have been in use for many years. Since AASHTO now asks for a design life of 75 years for bridges, a similar standard should be applied to thermoplastic pipe and appropriate modulus values should be provided. Papers presenting long-term stiffnesses of HDPE and PVC pipes are discussed in Appendix A. These tests were conducted by monitoring load over time while holding a pipe at a fixed deflection in a parallel type apparatus. For both materials, the tests indicate that the 75-year and even 100-year moduli are only slightly reduced from the 50-year values, which is logical, as the modulus decreases on a logarithmic basis. Based on these tests, estimates of the modulus of elasticity for longer design periods are presented in Table 14.

These values are recommended for AASHTO specifications until such time as more definitive data become available.

Loads

Thermoplastic pipe and corrugated HDPE pipe, in particular, have a low cross-sectional area and a low long-term modulus of elasticity. McGrath (1999) demonstrated that these features combine to give pipe such a low hoop stiffness that the long-term loads can be greatly reduced from the weight of the soil prism directly over the pipe, which has been the traditional load used for flexible culverts. A design method based on this behavior was adopted by AASHTO and is proposed for continued use in the simplified design method. The key feature in this method is to compute a vertical arching factor (VAF) based on the hoop stiffness of the pipe. In broad terms, the method consists of computing a hoop stiffness factor, S_H, which is the ratio of the soil stiffness to the pipe hoop stiffness, and then using that parameter to compute the VAF. The design approach is provided in general terms here and as a full design equation in Appendices E and H.

$$S_H = M_s/(EA/R) \quad \text{(Eq. 3)}$$

$$\text{VAF} = 0.76 - 0.71[(S_H - 1.17)/(S_H + 2.92)] \quad \text{(Eq. 4)}$$

$$W_E = \text{VAF}(P_{sp}) \quad \text{(Eq. 5)}$$

where:

- S_H = hoop stiffness factor, ratio of soil stiffness to pipe hoop stiffness
- M_s = soil constrained modulus, used to represent the soil stiffness, psi
- E = pipe material modulus of elasticity, psi
- A = pipe wall area per unit length, in.^{2}/ft
- R = radius to centroid of pipe wall, in.
- VAF = vertical arching factor, multiplied times soil prism load to determine design earth load
- W_E = design earth load on pipe, lb/ft
- P_{sp} = soil prism load, lb/ft

This load computation can be quite sensitive to the soil stiffness at the sides of the pipe, which can be quite variable without good field control; thus, a resistance factor is introduced in the proposed design equation to reduce the possibility of underestimating the earth load. The pipe material modulus should represent the length of loading—for earth load, this will be the long-term modulus, to represent the permanent nature of earth loads.

Table 14. Long-term design values for modulus of elasticity, ksi.

Material	Current 50-Year Modulus in AASHTO	Proposed Long-Term Modulus Values	
		75-Year	100-Year
Profile PE pipe (ASTM D3350, 34433C)	20.0	19	18
Other PE materials, including corrugated	22.0	21	20
PVC 12454C	140.0	137	136
PVC 12364C	158.4	156	154

No proposed changes are recommended here for calculating live load on thermoplastic pipe. *NCHRP Project 15-29: Design Specification for Live Load Distribution to Buried Structures* is nearing completion with recommendations on this subject.

Because of the low cross-sectional area of some thermoplastic pipes, external hydrostatic load can be a significant load if the groundwater levels are above the top of the pipe; thus, water load must be considered in design. There has been some debate on the appropriate load factor for this load. One argument is that it should be 1.0, as there is no uncertainty in the density of water. The counterargument is that there is often considerable uncertainty in the level of groundwater as it cycles with seasonal and longer-term cycles in weather and rainfall. A design factor of 1.3 is used to address this uncertainty, although it is not specifically called a load factor. This continues current AASHTO practice.

Capacity

Compression Capacity

Pipe capacity in compression, which addresses the wall area limit state, is determined by the design long-term yield strength of the pipe material and the cross-sectional area and, for some profile wall pipe, by the local buckling capacity of the elements of the pipe wall. The local buckling capacity of a profile wall pipe is based on the "effective width" concept first proposed by Winter (1946) and implemented by AASHTO. However, the design method has proved cumbersome in practice and this project has developed an alternative method to determine the compression capacity of a pipe. Using this alternate, the pipe capacity is determined from the stub compression test, development of which is discussed in Appendix B, with a proposed test standard provided in Appendix G.

Combined Bending and Compression

Bending in the pipe wall due to pipe deflection under load can induce significant tension and compression strains. Design for tension strain is in accordance with current AASHTO practice. The same tension strain limits are imposed; however, design limits for compression strain are set at fixed values, which is a change from prior practice. This change is prompted by PVC resins. Culverts manufactured from PVC use filled and unfilled resins which have different tensile moduli and tensile strengths. Since prior AASHTO practice determined strain limits as the ratio of strength to modulus, the different tensile properties led to different strain limits. Testing reported in Appendix B demonstrates that the compression behavior of filled and unfilled PVC resins is very similar and there is no justification for using different compression strain limits. Under tension, fillers create stress concentrations as load flows around the individual particles. In compression, load flows through the filler particles and no stress concentration effect is created.

Determination of bending strain is based on the assumption that the pipe will be deflected to the allowable limit, set at 5% for all types of thermoplastic pipe. Strain is based on a simple shape factor equation as follows:

$$\varepsilon_b = D_f\left(\Delta/D\right)\left(c/R\right) \qquad \text{(Eq. 6)}$$

where:

ε_b = bending strain, in./in.
D_f = shape factor, discussed below
Δ = change in vertical pipe diameter due to bending, in.
D = diameter to centroid of pipe wall, in.
c = distance from centroid of pipe wall to extreme fiber, in.
R = radius to centroid of pipe wall, in.

Deflection in thermoplastic pipe can result from bending deformation or from circumferential shortening due to thrust. Equation 6 provides an empirical means to estimate the bending strain. The key to using Equation 6 is the shape factor. A shape factor of 3.0 is about the minimum possible for design, indicating that pipe is deforming into an elliptical shape. A pipe tested in the parallel plate test has a shape factor of about 4.27. At first, this seems like a high value; however, in the parallel plate test, the top and bottom of the pipe deform equally, while in the ground pipe, distortion is often irregular. A case in point is a pipe set on hard flat bedding with poor haunch support. In this condition, the top surrounded by backfill might deform as an ellipse while the bottom might deform as if in a parallel plate test. Thus, the overall deflection might be reduced from the parallel plate test while the strain in the pipe wall is the same as in a parallel plate test. The strain factor in this case would be more than 4.27.

In current AASHTO practice, the shape factor is taken from the American Water Works Association's *Fiberglass Pipe Design Manual* (AWWA 2005). Computer modeling and soil box tests reported and discussed in Appendix C indicate that for a large unsupported haunch area (Figure 17), shape factors have values greater than 10 for PVC and HDPE pipe; however, these values are likely too high for design primarily because the zone of unsupported haunch was quite large and would represent an extremely poor installation—beyond what should be considered for typical design. On the other extreme, testing and analysis of properly installed pipe, reported in Appendix C.5, indicate that the shape factors could be as low as the ideal value of 3.0, although these values were for reasonably well-installed pipes.

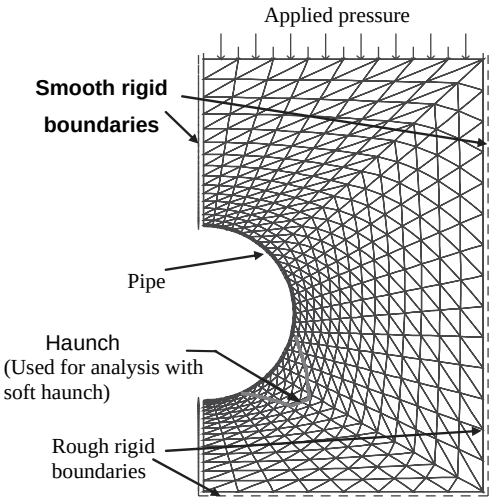

Figure 17. Large unsupported haunch evaluated in computer model.

The conclusions to be drawn from this are that the approximate values for the shape factor currently drawn from AWWA, ranging from 3.5 to 8.0 are reasonable, except that the shape factors for HDPE are lower than for PVC due to the low hoop stiffness, which reduces the thrust that drives the distortion. This, in turn, leads to the recommendation to allow a reduction in the shape factor for PE pipe as proposed in the draft design specifications in Appendix H. A reduction of 1.0 is selected as being reasonably conservative.

General Buckling

Since AASHTO introduced design for thermoplastic pipe into the *Bridge Design Specifications,* the equation for general buckling has been of the following form:

$$f_{cr} \sim \left(M_s * \frac{EI}{R^3} \right)^{0.5} \qquad \text{(Eq. 7)}$$

where:

f_{cr} = critical buckling stress, psi
M_s = soil constrained modulus, psi
E = modulus of elasticity of pipe material (modulus for the specified design life), psi
I = moment of inertia of pipe wall, in.^{4}/in.
R = radius of pipe wall, in.

Equation 7 is based on the Winkler model of a pipe supported by springs at discreet locations. More recent work by Moore (1990), based on continuous soil support, concludes that a different form of equation, as follows, best captures buckling behavior:

$$f_{cr} \sim (M_s)^{\frac{2}{3}} (EI)^{\frac{1}{3}} \qquad \text{(Eq. 8)}$$

This change in form results in soil support having a greater influence on buckling capacity than the pipe stiffness, which is consistent with field experience.

In design, the factored thrust must be less than the critical buckling stress.

Material Properties

Testing reported in Chapter 2 was conducted to evaluate suitable tests for slow crack growth resistance (SCR) of virgin resin and finished pipes. The key manufacturing variables of interest are the effects of carbon black, the quantity of regrind material, and the effect of the manufacturing process itself. Properties determined included density, melt index (MI), notched constant ligament stress (NCLS) failure time, and oxidation induction time (OIT). These are discussed in detail in Appendix F. The impact on the proposed testing and test limits to evaluate SCR are discussed here.

Focusing on the SCR, Table 15 summarizes the ratios of NCLS failure times for resin plaques, pipe plaques, and pipe liners. These ratios demonstrate the effect of carbon

Table 15. Ratios of failure times from resin plaques (RP), pipe plaques (PP), and pipe liners (PL).

Manufacturer – Diameter	Pure Resin (%)	NCLS Test		
		PP/RP Ratio	PL/PP Ratio	PL/RP Ratio
I-24“	100%	0.89	0.80	0.71
	90%	0.64	0.91	0.58
	80%	0.59	0.88	0.52
I-36”	100%	1.05	0.71	0.74
	90%	0.98	0.73	0.72
	80%	1.10	0.78	0.86
I-48”	100%	0.74	0.44	0.33
I-60”	100%	0.50	0.64	0.32
II-24”	100%	0.81	0.60	0.49
	90%	1.22	0.62	0.76
	80%	1.28	0.58	0.74
II-36”	100%	0.99	0.73	0.72
II-48”	100%	0.87	0.65	0.57
	90%	1.44	0.45	0.64
	80%	1.35	0.47	0.63
II-60”	100%	0.77	0.91	0.70
III-24”	100%	0.96	0.60	0.57
III-30”	100%	1.16	0.63	0.73
	80%	1.35	0.57	0.78
IV-24”	95%	0.82	NA	NA
	75%	0.65	0.54	0.78
V-24”	100%	0.73	0.49	0.35
	90%	0.63	0.47	0.30
	80%	0.67	0.48	0.32
V-36”	100%	0.70	0.55	0.38
Average		**0.92**	**0.63**	**0.59**
Standard Deviation		**0.27**	**0.15**	**0.18**

black (PP/RP), the manufacturing effect (PL/PP), and the combined effect (PL/RP). The effect of the various quantities of regrind can be evaluated by comparing ratios within a group of samples. These effects are discussed in the following paragraphs.

For the SCR property, the addition of carbon black decreases the resistance of the pure resin by an average factor of 0.85 (Table 8), although the effect of regrind is variable, likely as a function of the SCR of the added regrind material (Table 11). These effects are shown graphically in Figure 18, which shows that regrind content between 10% and 20% does not significantly affect the SCR properties. Note that regrind materials are limited to materials generated from a manufacturer's own production, and properties of regrind material are required to meet the same cell classification as new material. In current practice, no tests are conducted to determine whether the properties were changed during the manufacture. Proposed modifications to the product standard for HDPE pipe (Appendix J) recommend incorporation of a finished product test to address this in the future.

The combined effect of adding 2% to 3% carbon black and up to 20% regrind material on the SCR of virgin resins is evaluated by examining all 25 PP/PR values. As shown in Table 15, the overall average of the PP/RP ratio is 0.92. Figure 19 shows the standard deviation for each specimen, along with the overall mean and 95% confidence intervals (details of the calculation are presented in Appendix F). The 95% single-side confidence interval of the mean is from 0.72 to 1.06.

NCHRP Report 429 (Hsuan and McGrath 1999) recommended from an investigation of 19 field-cracked pipes that the appropriate required failure time for a pipe plaque should be 24 h. This was adopted as the AASHTO requirement for

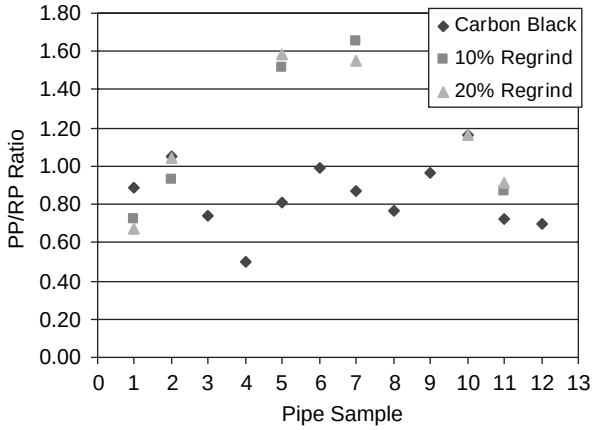

Figure 18. Effects of carbon black and regrind on the SCR of virgin resin.

resin plaques (AASHTO 2007b). The broader evaluation made in this study suggests a more conservative approach, increasing the 24-h limit by a factor based on the 95% lower confidence limit of the PP/RP ratio of 0.72. The new recommended failure time is 24 h/0.72 = 33 h for virgin resin prior to the addition of carbon black.

Another issue is the acceptable NCLS failure time for a pipe liner, which will reflect the effects of carbon black, manufacturing process, and any other additives to the virgin resin. The manufacturing process can affect the SCR of the virgin resin significantly due to residual stress and introducing polymer orientation. The processing effects are identified by comparing the failure time of the pipe liner to the corresponding pipe plaque. Figure 20 compares the reduction factors caused by the addition of carbon black (PP/RP) and

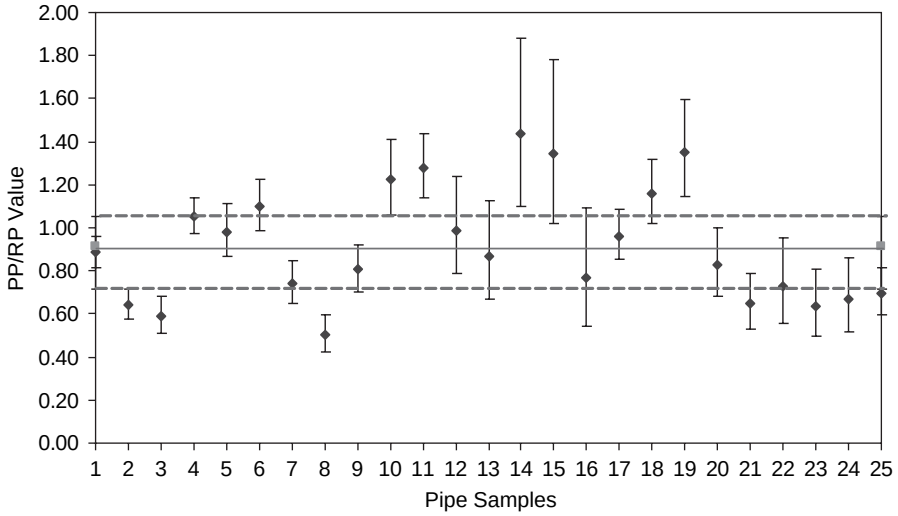

Figure 19. PP/RP values together with the 95% confidence interval.

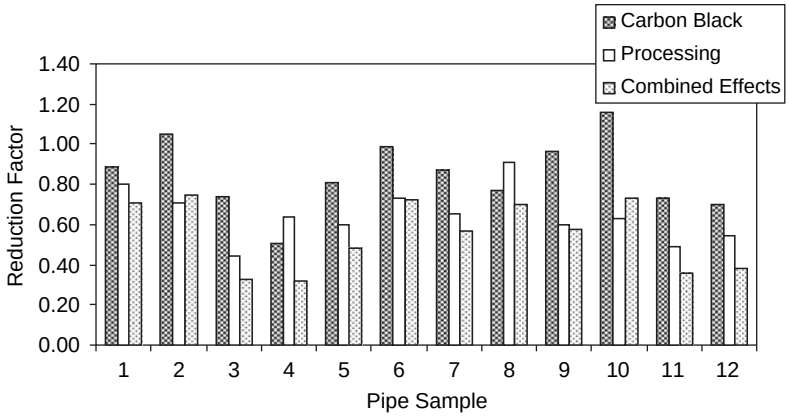

Figure 20. Influence factors on pipes made from 100% virgin resin.

the pipe processing (PL/PP) with the combined effects (PL/RP) for pipes made from 100% virgin resins. Except for Samples 4 and 8 (I-60 in. and II-60 in.), the processing effect has a greater influence on the combined effect than does the carbon black.

The reduction factor of manufacturing processing is evaluated by comparing the failure time of the pipe liner to the corresponding pipe plaque. The average combined reduction factor is 0.63, as shown in the PL/PP column of Table 15. Figure 21 shows the ratios, the standard deviation for each dataset, and the 95% confidence interval. The 95% confidence interval of the mean is from 0.55 to 0.76. Again, using the 24-h recommendation from *NCHRP Report 429,* a conservative approach is to establish an NCLS failure time from pipe samples that include additives and manufacturing effects. Using the upper 95% confidence limit, the recommended time is 24 h * 0.76 = 18 h.

The OIT test was used to assess the amount of antioxidants in each of the pipe resins and finished pipes. A large variation is observed among tested materials. The OIT values range from 7.5 to 66.3 min for virgin resins and from 8.8 to 44.6 for finished pipes containing no regrind material (Appendix F). Five of the 12 pipes showed OIT values higher than the corresponding virgin resins, suggesting that the resin used to make up the carbon black master batch influences the OIT value. On the other hand, the regrind materials have no significant effect on the OIT value; less than 10% reduction in the OIT value is obtained after the addition of regrind. Due to the unknown impact of the carbon black master batch, the OIT test should be performed

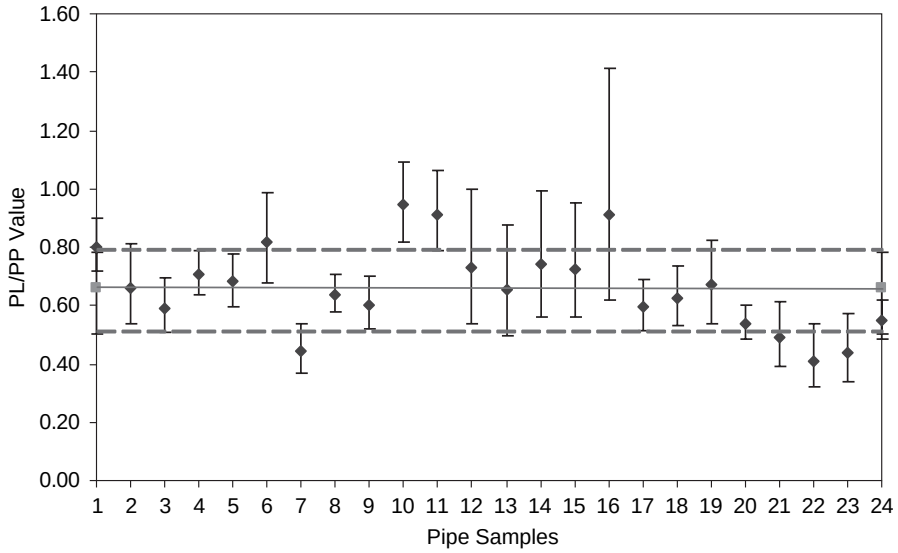

Figure 21. PL/PP values together with the 95% confidence interval.

on the finished pipe instead of the virgin resin. Although the focus of this part of the project does not include establishing the appropriate OIT value for corrugated HDPE pipes due to the long required testing time, the Florida Department of Transportation (FDOT) did set a minimum OIT value of 25 min for 100-year design life. This value was developed based on aging data obtained from HDPE geomembranes. AASHTO should consider this in future work.

Proposed Specification Failure Times for NCLS Test

In summary, three specified values are proposed to evaluate the SCR of the corrugated HDPE pipes, as follows:

1. Minimum average failure time of virgin resin should be 33 h.
2. Minimum average failure time of a pipe plaque should be 24 h.
3. Minimum average failure time of the pipe liner should be 18 h.

Appendix J recommends that AASHTO incorporate only the pipe liner test to qualify products. The 33-h test can be used by manufacturers for guidance in selecting virgin resins, but each manufacturer's combination of additives and processing effect will be different and will require a specific evaluation.

Material Standards

A QA/QC protocol for thermoplastic culvert pipe must establish that the finished product meets the product specifications and will provide good service for the intended life of the product when used in accordance with the manufacturer's guidelines. This requires that the product be manufactured from suitable raw materials and that the finished product have the necessary quantities of materials, geometry, strength, and durability.

Current PE Pipe Practice

The primary AASHTO specification for thermoplastic PE pipe is *Standard Specification M294* (AASHTO 2007b). Product controls include the following:

Raw Materials

Raw materials are specified through a cell classification system that identifies and sets limits on parameters deemed important for strength, stiffness, processing, and durability. This system is used for most plastic pipe products, whether the applications are pressure or gravity flow, or sanitary, storm, or culvert applications. PE culvert pipe has an additional parameter for slow crack growth that replaces older provisions within the cell class system for environmental stress crack resistance. These parameters were revised in 2000 based on the recommendations of *NCHRP Report 429* (Hsuan and McGrath 1999), and no new recommendations are being developed under this project.

Finished Product

The finished product is currently evaluated for strength, stiffness, and durability. Current tests include dimensions, pipe stiffness, flattening (strength), environmental stress cracking, and brittleness (impact).

The flattening test requires loading to 20% deflection with no loss of load, cracking, or local buckling. Thus, this is a test of the pipe strength in bending.

The parallel plate test is conducted with a constant cross head speed of 0.5 in./min. Table 16 summarizes the testing time and strain levels when the parallel plate test is conducted on several pipes to 5% deflection.

Table 16 raises the following two issues:

- At a crosshead speed of 0.05 in. per min, it takes a long time to conduct the test for large-diameter pipe, especially since

Table 16. Strain and strain rate in parallel plate test at 5% deflection.

Diameter (in.)	Corrugation Style	Stiffness (lb/in./in.)	Maximum Bending Strains		Time to 5% Deflection (min)	Maximum Tension Strain Rate* (%/min)
			Tens. (%)	Compr. (%)		
18	Corr. PE	53.8	1.3	-2.1	1.94	0.65
24	Corr. PE	77.4	1.7	-2.2	2.60	0.67
36	Corr. PE	31.2	1.0	-1.8	3.79	0.27
36	Corr. PE	59.1	1.3	-2.1	3.86	0.35
48	Corr. PE	18.2	0.9	-1.4	5.07	0.18
48	Honeycomb PE	14.9	1.0	-1.0	5.07	0.21
24	Corr. PVC	86.5	0.8	-1.0	2.44	0.34

*Based on a load rate of 0.5 in./min.
Source: *NCHRP Report 438* (McGrath and Sagan 2000).

it must be conducted to 20% deflection for HDPE pipe. No benefit is achieved with this slow test time.
- The strain rate decreases significantly for the larger diameter pipes. Since the effective modulus of elasticity of the pipe decreases with slower strain rates, the test evaluates each size of pipe at a different modulus. This is not desirable.

To address both of these issues, it is proposed to increase the test speed of thermoplastic pipe from 0.5 in./min to the faster of 0.5 in./min or 2% of the nominal inside diameter/minute. This change will set the strain rate to be approximately the same for all pipe over 24 in. in diameter and will reduce the time to test a 60-in. diameter pipe from about 25 min to about 11 min. Since the test will be conducted at a higher rate, the apparent stiffness of these pipes will increase. Table 17 provides increased minimum pipe stiffnesses using the higher test rate to preserve the same pipe stiffness as currently required.

The proposed change is based on a simplified review of apparent modulus versus time. Selig et al. (1994) proposed the following simplified modulus based on time:

$$E_p = 96{,}000t^{-0.0859} \quad \text{(Eq. 9)}$$

where:

E_p = modulus of elasticity of PE, psi
t = elapsed time, min

This expression gives a modulus of elasticity of 82,000 psi for a test lasting 6 min (the current time for a 60-in. [1500 mm] pipe to reach 5% deflection) and a modulus of 88,000 psi for a test lasting 2.6 min (the reduced time for a 60-in. pipe to reach 5% deflection when deflected at 2% per minute). Thus the apparent stiffness would be about 8% higher for a 60-in. diameter pipe under the proposed test rate. To account for this higher modulus, the proposed pipe stiffnesses range from unchanged for 24-in. diameter pipe up to about 10% higher for 60-in. diameter pipe.

Table 17. Recommended modification to pipe stiffness to account for increased test speed.

Pipe Diameter (in.)	Pipe Stiffness (kPa)	
	Current	Proposed
30	195	200
36	150	155
42	140	145
48	125	135
54	110	120
60	95	105

Note: No change is proposed for smaller diameters.

PVC Pipe

PVC pipe used by AASHTO is most commonly specified by *Standard Specification M304* (AASHTO 2001). The most recent edition was approved in 1994 and reapproved in 1997. Requirements include the following:

Raw Materials

As with PE, raw materials for PVC pipe are specified through a cell classification system that identifies and sets limits on parameters deemed important for strength, stiffness, processing, and durability. Two cell classes are allowed for PVC pipe; one has a lower modulus and higher strength, while the other has a higher modulus and a lower strength. The latter properties result from the inclusion of fillers.

Finished Product

Current tests for finished PVC pipe include dimensions, pipe stiffness, flattening (splitting, cracking, rib separation), impact, and acetone immersion.

Although the pipe stiffness standards are the same for PE and PVC (i.e., stiffness determined at 5% deflection after loading at 0.5 in./min), the flattening test is quite different. For PVC pipe, the flattening test requires loading to 60% deflection with no cracking, splitting, breaking, or separation of the seams, but the load on the pipe can decrease during the test. Thus, for PVC, the flattening test evaluates material strength more than pipe strength. *Standard Specification M304* (AASHTO 2001) has no equivalent to the slow crack growth or environmental stress crack tests for PE. PVC does have the acetone immersion test to evaluate whether the PVC is properly fused (rebonded after passing around extrusion spiders during manufacture).

Some PVC pipe specifications (*ASTM F949* for profile wall sewer pipe) include a heat reversion test (ASTM 2006). This test exposes pipe specimens to 180°C for 30 min and reveals incomplete exsiccation and the presence of stress, infused areas, or contamination. It is our understanding that this is a more demanding test of extrusion quality than the acetone immersion test (although *ASTM F949* includes both tests). We recommend inclusion of the heat reversion test in AASHTO standards for PVC pipe.

Both PVC and PE have parallel plate test requirements for flattening, but as noted previously, the test is used for different purposes. PVC should have an equivalent to the PE test requiring a certain deflection capacity without loss

of load. The PE test limit for this is currently set at 20%, based on the performance of current profiles. The trend toward optimizing profile performance has shown that this limit could be increased to about 30%, mostly by redistributing material within the profile to move the neutral axis toward the mid-depth of the profile. PVC profiles are not as deep as PE, but PE has a higher strain limit. Overall, we recommend that a limit of 20% be applied to PVC as it is to PE.

All Thermoplastic Pipe

Manufacturers must be able to document the quality of resin used for any particular pipe through the records of all materials used for blending resins for production. Recommendations for quality control of materials include requirements that manufacturers keep records of the following:

- Resin manufacturer's data sheets and certification that the base resin meets cell class requirements of the product specification,
- Manufacturer's data sheets and quantities for all additives, and
- Test results to demonstrate that if resins of two different cell classifications are blended, the resulting mixture meets the requirements of the specified cell class.

It is not clear from current practice whether all manufacturers can trace the source shipment of resin based on current pipe markings. This is desirable and should be implemented.

In general, resin properties should be specified as determined from finished pipes to ensure that all additive and manufacturing effects are considered.

CHAPTER 4

Conclusions

This report presents the findings and conclusions of extensive studies of the materials used to manufacture thermoplastic culvert pipes, the behavior of complex profile wall pipe, soil culvert interaction of thermoplastic pipe, and design methods for thermoplastic pipes. Pipes considered included profile wall HDPE and PVC. Many profiles were tested and analyzed.

Soil cell studies included axisymmetric loading and biaxial loading. Tests monitored soil stresses and pipe deflections and strains. Most test results were then investigated with finite element modeling to test whether our understanding of thermoplastic pipe behavior was adequate to create accurate numerical models and to validate design predictions from the proposed simplified methods. The tests demonstrated the following:

- Well-installed thermoplastic pipe has low stresses and deflections; pipe installed with poor haunch support shows much higher bending stresses depending on the size and stiffness of the regions of poor support.
- Liner buckling in axisymmetric tests can be predicted using the plate buckling equation developed by Winter (1946).
- Complex profile geometry produces secondary bending in various elements of the profile that can produce tension stresses, even in properly installed pipes. These secondary stresses are not considered in design and must be addressed through the selection of resins with good stress crack resistance.
- Profiles with a closed outer surface, such as the box profile, develop higher compression stresses on the outside than on the inside surface.
- Pipe behavior in tests can be effectively modeled with finite element analysis.
- Finite element analyses can be implemented with varying degrees of sophistication, with non-linear soil and material models, but tests and finite element analyses validate the proposal for a simplified design method.

Material tests to compare tension and compression behavior of PE and PVC showed that tension moduli can be used to represent compression behavior and tension strength forms a lower bound for compression strength. In particular, filled PVC resins have a higher compressive strength that should be considered in design.

Stub compression tests were conducted to validate the current AASHTO design procedure for local buckling effects, to develop a standard quality control test for pipe compression strength, and to evaluate how the test strength can be used in design as an alternate to conducting the local buckling calculations. Round-robin tests in private, DOT, and manufacturer laboratories showed good repeatability.

Slow crack growth resistance of HDPE was studied on virgin resins and on pipe manufactured with virgin resin and 10% and 20% regrind material. All pipe had about 2% carbon black. Slow crack growth resistance is affected both by carbon black and by the manufacturing process. This demonstrates that pipe qualification tests for SCR must be conducted on specimens cut from finished pipe and not remolded. Tests on oxidation induction time, which quantifies remaining antioxidants in pipe, show widely variable results.

A simplified design approach was developed and is presented in draft design specifications. The proposed method largely draws on prior design procedures with some modifications.

- The load factor for earth load is reduced from 1.95 to 1.30 to provide consistency with other types of culverts. An installation factor of 1.50 is introduced to bring new designs to the same level of safety as past designs; however, a designer can reduce the installation factor to as low as 1.00 if stringent controls on construction practices are introduced.
- Deflection design is incorporated to generally evaluate type of backfill and density. Responsibility for control of deflection in the field is assigned clearly to the contractor, as construction procedures have more influence on final deflection than do the design. Deflection is calculated using

the Spangler formula (Spangler 1941) with a term added to consider hoop compression.
- Earth loads for thrust are calculated using the arching factor that considers soil and pipe hoop stiffness. This can reduce load substantially relative to the soil prism load. This method was already adopted by AASHTO during the course of this project.
- Local buckling calculations, adopted by AASHTO during the course of this project, are included, but the compressive strength from the stub compression test can be incorporated into the design method as an alternate.
- General buckling calculations are changed from a spring-supported model to a continuum model that better represents in-ground pipe response.

Construction specifications are proposed for thermoplastic pipe. These place an emphasis on post-construction inspection.

Changes are proposed to pipe product standards. The crosshead speed of the parallel plate test is increased to minimize test time and to provide a constant strain rate for all size diameters. A slow crack growth test is proposed for the liner of a finished PE pipe. Average failure time for this test is set at 18 h. The stub compression test could be incorporated as a standard quality control test or added to the periodic tests conducted as part of the NTPEP program. A heat reversion test is incorporated into PVC pipe standards as a better evaluation of extrusion quality, and a strength limit has been added to the PVC standard to ensure a minimum deflection level without loss of load.

References

AASHTO M304-01 Standard Specification for Poly(Vinyl Chloride) (PVC) Profile Wall Drain Pipe and Fittings Based on Controlled Inside Diameter, AASHTO, Washington, D.C., 2001.

AASHTO LRFD Bridge Design Specifications, 4th ed., AASHTO, Washington, D.C., 2007a.

AASHTO M294-07 Standard Specification for Corrugated Polyethylene Pipe, AASHTO, Washington, D.C., 2007b.

ASTM F1057-87 Standard Practice for Estimating the Quality of Extruded Poly (Vinyl Chloride) (PVC) Pipe by the Heat Reversion Technique, American Society for Testing and Materials, West Conshohocken, PA, 2005.

ASTM F949-06a Standard Specification for Poly(Vinyl Chloride) (PVC) Corrugated Sewer Pipe with a Smooth Interior and Fittings, American Society for Testing and Materials, West Conshohocken, PA, 2006.

AWWA Fiberglass Pipe Design Manual, 2nd ed., American Water Works Association, Denver, CO, 2005.

Brachman, R. W. I., Moore, I. D., and Rowe, R. K. "The Design of a Laboratory Facility for Evaluating the Structural Response of Small Diameter Buried Pipes," *Canadian Geotechnical Journal,* Vol. 37, No. 2, 2000, pp. 281–295.

Hashash, N. and Selig, E. T., "Analysis of the Performance of a Buried High Density Polyethylene Pipe," *Structural Performance of Flexible Pipe,* Sergand, Mitchell, and Hurd eds., Balkema, Rotterdam, Netherlands, 1990.

Howard, A. K., "Modulus of Soil Reaction Values for Buried Flexible Pipe," *ASCE Journal of the Geotechnical Engineering Division,* Vol. 103, No. GT1, 1977.

Hsuan, Y. G., and McGrath, T. J., *NCHRP Report 429: HDPE Pipe: Recommended Material Specifications and Design Requirements,* Transportation Research Board, Washington, D.C., 1999.

McGrath, T. J., *Design Method for Flexible Pipe,* a report prepared for the Polyethylene Pipe Design Task Group of the AASHTO Flexible Culvert Liaison Committee, Simpson Gumpertz & Heger Inc., Arlington, MA, 1998a.

McGrath, T. J., "Replacing E' with the Constrained Modulus in Buried Pipe Design," in *Pipelines in the Constructed Environment,* J. P. Castronovo and J. A. Clark, eds., American Society of Civil Engineers, Reston, VA, 1998b.

McGrath, T. J., "Calculating Loads on Buried Culverts Based on Pipe Hoop Stiffness," *Transportation Research Record 1656,* Transportation Research Board, Washington, D.C., 1999.

McGrath, T. J., and Sagan, V. E., *NCHRP Report 438: LRFD Specification for Plastic Pipe and Culverts,* Transportation Research Board, Washington, D.C., 2000.

Moore, I. D., "Three-Dimensional Response of Elastic Tubes," *International Journal of Solids and Structures,* Vol. 26, No. 4, 1990.

Moore, I. D. and Hu, F., "Response of Profiled High-Density Polyethylene Pipe in Hoop Compression," *Transportation Research Record 1514,* Transportation Research Board, Washington, D.C., 1995.

Sargand, S. M., Hazen, G. A., Masada, T., Schehl, D. J., Moran, A., and Altarawneh, B., *Field Verification of Structural Performance of Thermoplastic Pipe Under Deep Fill Conditions, Final Report,* Ohio Research Institute for Transportation and the Environment, Ohio University, Athens, 2002.

Selig, E. T., "Soil Properties for Design of Buried Pipelines," *Proceedings, Pipeline Infrastructure Conference,* American Society of Civil Engineers, Boston, MA, 1988.

Selig, E., "Soil Properties for Plastic Pipe Installations," *Buried Plastic Pipe Technology,* ASTM STP 1093, G. S. Buczala and M. J. Cassady, eds., American Society of Civil Engineers, West Conshohocken, PA, 1990.

Selig, E. T., DiFrancesco, L. C. and McGrath, T. J., "Laboratory Test of Buried Pipe in Hoop Compression," in *Buried Plastic Pipe Technology,* 2nd Vol., Special Technical Publication 1222, D. Eckstein, ed., American Society of Civil Engineers, West Conshohocken, PA, 1994.

Spangler, M. G., "Structural Design of Flexible Pipe Culverts," *Iowa Engineering Experiment Station Bulletin 153,* Iowa State University, Ames, 1941.

Winter, G. "Strength of Thin Steel Compression Flanges," *Transactions,* American Society of Civil Engineers, Vol. 112, 1946.

Zhang, C. and Moore, I. D. "Nonlinear Finite Element Analysis for Thermoplastic Pipes," *Transportation Research Record 1624,* Transportation Research Board, Washington, D.C., 1998, pp. 225–230.

APPENDIX A

Literature Review

CONTENTS

A.1 Introduction

Structural design of buried thermoplastic pipe requires the design of a pipe-soil-interaction system. Experience and the technical literature make it clear that installation and proper compaction of the embedment soil is the first priority for the successful performance of such a system. Nonetheless, success and failure are ultimately judged by the behavior of the pipe, not the soil, and thus the limit states of the pipe must be assessed in a manner similar to the limit states of any structural member. Current practice, as presented in U.S. and European codes as well as newly proposed methods, is presented to provide a summary of available methods for the design of buried thermoplastic pipe.

The summary begins with current U.S. practice, followed by a brief discussion of European design methods. These initial presentations serve to introduce the overall subject matter, which should make it easier to assimilate the later information. Buried thermoplastic pipe design is then examined in more detail in the following key areas:

- Soil properties,
- Limit states,
- Serviceability, and
- Testing.

In each case, current practice in the United States and Europe is examined to understand and compare methods that are already in general use. This is followed by discussion of proposed methods for use in design. The focus throughout is on an introduction of methods either used in design or directly proposed for design. For detailed presentation and derivation of the identified methods, references to the source material are provided.

The goal of this review is not to provide a complete history of flexible pipe design, but rather to bring out the methods, issues, and ideas that need to be examined in the development of a new design method for thermoplastic pipe.

A.1.1 Current U.S. Practice

The standard code of practice for the design of thermoplastic pipe in the United States is *AASHTO LRFD Bridge Design Specifications* (AASHTO 2007) Article 12.12, "Thermoplastic Pipes." Design of thermoplastic pipe by AASHTO Article 12.12 explicitly considers the following:

- Pure thrust with consideration of local buckling,
- Global buckling (Winkler model),
- Minimum spacing between adjacent pipe and minimum cover, and
- Short- and long-term material properties.

No guidance is provided on the calculation of the allowable and ultimate deflections, local buckling capacity, or buckling under low cover heights.

Although not developed for design of thermoplastic pipe, the American Water Works Association's *AWWA Manual of Water Supply Practices M45 Fiberglass Pipe Design* (1996) is well regarded for flexible pipe design. The manual provides procedures to calculate and check deflections, strains (or stresses), and buckling. The soil prism load with no arching (VAF = 1.0) is assumed, and Marston trench load reductions are not used. Soil stiffness is calculated based on the soil class and the installed condition, and considers the influence of native soils in the trench wall. Deflections are calculated using Spangler's equation and compared against a limiting value of 5% (Spangler 1941). Strain demands are calculated using the shape factor (D_f) approach and compared to limiting values. Buckling is checked using a Winkler model as calibrated by Glascock and Cagle (1984). No guidance is provided for local buckling phenomena or for buckling under low cover heights.

A.1.2 Current European Practice

Over the last 16 years, the European Committee for Standardization (CEN), the European standards group, has been in the process of generating a unified standard for buried pipe design. Though no consensus has been reached, much information has been gathered on the relative assumptions employed in the various national methods. In particular, a significant amount of attention has been paid to the calculation of the deflection of rigid and flexible pipe.

CEN (European Committee for Standardization 1999b) provides information summarizing the codes for buried pipe design from Austria, Belgium, Denmark, France, Germany, the Netherlands, Norway, Spain, Sweden, Switzerland, and the United Kingdom.

European pipe design is, in general, more unified than the design of pipe in the United States. In most countries a single pipe specification (often a binding national code) covers the structural design of all buried pipe, regardless of pipe material. In many of the codes, specific material standards are referenced for relevant values such as material modulus, long-term properties, etc.; however, the safety factors for the various limit states (deflection, strain, buckling) are defined by the code and may or may not be material dependent.

In the following detailed examination of soil properties and limit states, both current U.S. and European practice are examined to demonstrate significant features and differences.

A.2 Soil Properties

A.2.1 Current Codes of Practice

Soil properties for use in design exhibit significant variation for all of the codes, both European and U.S. Soil stiffness, E_{soil} (E′ in the modified Spangler deflection equation), a crucial parameter for flexible pipe, varies from simple prescribed values (e.g., France) to detailed determination (e.g., Germany). Typical U.S. practice is somewhere between these extremes.

In European design, E_{soil} may be dependent on the following:

- Soil group (from as few as three to as many as seven different soil groups);
- Installation method (e.g., up to four different methods may be prescribed);
- Verification of properties (higher values may be used if some "verification" is performed);
- Density (some codes give soil stiffness as a function of Proctor density, other codes simply give stiffness values for compacted and uncompacted soils, and still other codes tie Proctor density to the selected soil group and installation method);
- Vertical pressure of the soil (the Austrian code provides an expression to increase the soil stiffness as a function of the amount of vertical load, i.e., burial depth); and
- Deflection and load concentration calculation (in some codes, the basic value of E_{soil} may be modified further to include such effects as native soils, groundwater subsidence, long-term stiffness values, and variation in stiffness along the pipe).

Other soil parameters such as the friction angle, Φ_{soil}, and unit weight, γ_{soil}, are generally assigned based on a soil group. The value of Φ_{soil} used in Marston trench load calculations is sometimes reduced from the basic soil group value as a function of the installation method. The vertical to horizontal soil pressure ratio, K, is typically taken as 0.5, but some codes decrease this to as little as 0.2 depending on the relative ratio of pipe to soil stiffness and the soil group. None of the codes gives any guidance on a rational selection for the Poisson's ratio, ν_{soil}, of the soil.

Soil stiffness values from French, German, and U.S. practice, summarized in Tables A-1 to A-3, show significant variation in design values of soil stiffness. This may be partially explained by different calculation methods and the ultimate use of the soil stiffness. For instance, the French method provides minimum stiffness values, while the German method provides mean values for use in calculation of forces but uses two-thirds of the reported soil stiffness for deflection calculations. Also note that the various deflection equations presented in Section A.3.2.1 use different coefficients as a multiple for the E_{soil} term.

A.2.2 Additional Proposals

Soil properties for use in flexible pipe design generally evolved from consideration of Spangler's (1941) deflection expression and Watkins' and Spangler's (1958) modification to express the soil stiffness as an elastic-modulus-type parameter, E′ (E_{soil} in the previous discussion is typically referred to as E′), rather than a subgrade-modulus-type parameter (with units of lb/cu in. as originally developed by Spangler.

Table A-1. Soil stiffness as prescribed in the French code.

Soil Group	Backfill Density		
	Noncompacted E_{soil} (MPa*)	Compacted and Inspected E_{soil} (MPa)	Compacted, Inspected, and Verified E_{soil} (MPa)
1	0.7	2.0	5.0
2	0.6	1.2	3.0
3	0.5	1.0	2.5
4	< 0.3	0.6	0.6

*1 MPa = 145 psi

Table A-2. Soil stiffness as prescribed in the German (ATV) code.*

Soil Group	Backfill/Bedding Condition					
	A1/B1		A2 and A3/B2 and B3		A4/B4	
	D_{pr} (%)†	E_{soil} (MPa‡)	D_{pr} (%)	E_{soil} (MPa)	D_{pr} (%)	E_{soil} (MPa)
1	95	16	90	6.0	97	23
2	95	8.0	90	3.0	97	11
3	92	3.0	90	2.0	95	5.0
4	92	2.0	90	1.5	–	–

*Actual soil stiffness used in calculations is further modified by factors that include native soil, trench width, groundwater subsidence, etc. Deflection calculations use two-thirds of the values.
†D_{pr} = % of maximum Proctor density
‡1 MPa = 145 psi

Table A-3. Soil stiffness as prescribed in *AWWA M45* (1996).*

Soil Group	Backfill Density			
	Dumped (E_{soil} [MPa†])	Slight D_{pr} < 85% (E_{soil} [MPa])	Moderate 85% < D_{pr} < 95% (E_{soil} [MPa])	High D_{pr} > 95% (E_{soil} [MPa])
SC1	6.9	20.7	20.7	20.7
SC2	1.4	6.9	13.8	20.7
SC3	0.69	2.8	6.9	13.8
SC4	0.34	1.4	2.8	6.9
SC5	NR	NR	NR	NR

*The AWWA values are those recommended by Howard (1977).
†1 MPa = 145 psi, D_{pr} = % of maximum Proctor density
NR = not recommended.

Howard (1977) presented E′ values calibrated for use in design and to a large extent these have been accepted into U.S. practice. Later, Howard (1996) presented slightly modified values for E′. Hartley and Duncan (1987), using finite element analysis, proposed design values for E′ that varied with confining pressure.

The "correct" values for E′ are a topic of debate, and the discussion is complicated by the connection between E′ and deflection prediction. Attempts have been regularly made to back-calculate E′ from experimental values using Spangler's deflection expression. Back-calculated E′ values, however, are inconsistent at best because of the large number of unknowns in Spangler's expression (Moser 1997a). In addition to the unknowns, the determination of E′ is further complicated since E′ is not a true soil parameter.

McGrath (1998a, 1998b) has proposed replacing E′ with a true elastic parameter—the one-dimensional (1D) modulus, M_s. Replacing E′ with M_s is justified by the following:

1. Researchers agree that E′ is closely related to M_s.
2. Precision of deflection prediction is low and an approximate relationship between E′ and M_s is acceptable.
3. Accepted elasticity solutions of buried pipe problems use M_s (Burns and Richard 1964).

The 1D modulus, M_s, can be determined directly via experiment or analytically from the hyperbolic soil model (McGrath 1998a, McGrath 1998b). The stiffness increases with depth of fill, as it does in 1D tests and in the hyperbolic soil model. The hyperbolic soil model is used in the finite element programs CANDE and SPIDA and was the soil model used to develop the accepted SIDD installations for reinforced concrete pipe. M_s values based on the Standard Installation Direct Design (SIDD) hyperbolic soil model agree well with the traditional Howard E′ values (note: AASHTO adopted these values since the start of this project) at moderate depths of fill. McGrath has suggested the values in Table A-4 for use of M_s in practice.

A.3 Limit States

A.3.1 Thrust-Soil Load and VAF

Failure of thermoplastic pipe due to large thrust demands is an accepted limit state in AASHTO. Experience and analysis demonstrate that determination of the thrust demand that reaches the pipe requires consideration of the pipe and soil stiffness. The thrust demand may be expressed in terms of the soil prism load (weight of the soil directly above the pipe) and a vertical arching factor (VAF) as

$$T = VAF\, W_{sp}/2$$

$$W_{sp} = \gamma_s\left(H + 0.11D_o\right)D_o$$

where VAF is the vertical arching factor, T is the thrust demand, W_{sp} is the soil prism load, γ_s is the soil unit weight, D_o

Table A-4. Suggested design values for constrained soil modulus, M_s.

Stress Level* (kPa)	Soil Type and Compaction Condition (MPa)									
	SW100	SW95	SW90	SW85	ML95	ML90	ML85	CL95	CL90	CL85
7	16.2	13.8	8.8	3.2	9.8	4.6	2.5	3.7	1.8	0.9
35	23.8	17.9	10.3	3.6	11.5	5.1	2.7	4.3	2.2	1.2
69	29.0	20.7	11.2	3.9	12.2	5.2	2.8	4.8	2.4	1.4
138	37.9	23.8	12.4	4.5	13.0	5.4	3.0	5.1	2.7	1.6
275	51.7	29.3	14.5	5.7	14.4	6.2	3.5	5.6	3.2	2.0
413	64.1	34.5	17.2	6.9	15.9	7.1	4.1	6.2	3.6	2.4

*Free field vertical effective soil stress, $\gamma_s H$
1 MPa=145 psi
Source: McGrath, T.J., "Replacing E' with the Constrained Modulus in Buried Pipe Design," in *Pipelines in the Constructed Environment*, J.P. Castronovo and J.A. Clark, eds., ASCE, San Diego, CA, 1998, p 38.

is the outside diameter of the pipe, and H is the depth of fill above the pipe.

There are two design bases for reducing the VAF to values less than 1.0. The Marston trench load theory takes advantage of the development of shear stresses between the native soil and the trench wall to reduce the load on pipe. This approach is used in some design codes, but not in most U.S. codes for flexible pipe. Consideration of circumferential shortening can also reduce the load on the pipe. This approach has been proven for corrugated steel structural plate pipe where keyhole slotted joints have been successfully used to reduce load. Recent work has shown that some thermoplastic pipe has low circumferential stiffness and can also take advantage of this behavior. These approaches to design are discussed below.

A.3.1.1 Current Codes of Practice

Calculation of the vertical soil load on the pipe is a fundamental first step in the European codes. Table A-5 presents a summary of the calculation method for vertical loads in flexible pipe. Several of the national codes allow the vertical load to be less than the soil prism load (i.e., VAF may be less than 1.0).

Codes that allow VAF < 1.0 in flexible pipe have some unique features worthy of note.

In applying the Marston trench load theory, the following should be noted:

- Soil parameters in the Marston trench load equations are tied to prescribed installation methods; if these methods are not used, the reduction is not available.
- Sloped trench walls are explicitly considered.
- Stepped trench walls are explicitly considered.
- In some codes, simplified expressions are used in place of the Marston theory.

For the reduction in vertical load due to the relative stiffness of the pipe and soil, two methods are generally used:

- The German ATV method, or a variation thereof, which is a relatively complicated series of expressions, relating the soil stiffness and the pipe bending stiffness; and
- Simple specified reductions as a function of pipe material.

A.3.1.2 Theories for Thrust Load

A.3.1.2.1 Marston Trench Load. In U.S. practice, the Marston trench load is generally applied only to rigid pipe, with flexible pipe being designed for the embankment condition. The theoretical basis for the trench load is the soil friction at the trench walls that is indifferent to the type of pipe buried below. Thus, some have argued for the extension of the Marston trench loads in flexible pipe design in the United States (Schrock 1993). The application of the Marston trench load has occurred in several European codes.

A.3.1.2.2 Circumferential Shortening and Thrust Demands. Field observations and testing indicate that under soil load, thermoplastic pipes undergo significant circumferential shortening (Moser 1997b, Hashash and Selig 1990). No design method accounted for this shortening at the start of this project. Circumferential shortening can decrease the amount of load experienced by a pipe and was the motivation for the use of slotted keyholes in corrugated metal pipe (Katona and Akl 1987). Proper calculation of the thrust demand in thermoplastic pipes requires consideration of this phenomenon.

As discussed in McGrath (1999), the large amount of circumferential shortening can be readily understood by examining the pipe hoop stiffness:

$$PS_H = EA/R$$

Table A-5. Calculation of vertical soil load on flexible pipe.

Country	How Is It Determined that a Pipe Is "Flexible"?	Can the Marston Trench Load Reduction Be Applied?	Can the Load Be Reduced Further Due to the Relative Stiffness of the Pipe versus the Soil?	VAF
Austria	Relative Stiffness*	No	No	1.0
Belgium	Relative Stiffness*	Yes	Yes	**≤ 1.0**
Denmark	N/A	N/A	N/A	1.0
France	Relative Stiffness*	No	No	1.0
Germany	Relative Stiffness*	Yes	Yes	**≤ 1.0**
Netherlands	Relative Stiffness*	Yes	Yes	**≤ 1.0**
Norway	N/A	No	No	≥ 1.0
Sweden	By Material	No	Yes	**≤ 1.0**
United Kingdom	By Material	No	No	1.0
United States†	By Material	No	No	1.0

*Relative stiffness is calculated by a variety of methods, but is generally based on the ratio of soil stiffness to pipe flexural stiffness (based on EI/r^3).
†*AWWA M45* (1996) is selected here for comparison to U.S. practice for flexible pipe design.

where E is the pipe material modulus, A is the pipe cross-section area per unit length, and R is the radius of the pipe. PS_H represents the circumferential shortening under a unit of external pressure. Reinforced concrete, corrugated metal, clay, and other traditional pipe materials have pipe-hoop-stiffness values on the order of 500 to 5,000 MPa, while profile-wall polyethylene pipes under long-term loading may have values as low as 3.5 MPa (McGrath 1999). Thus, profile-wall thermoplastic pipes may experience substantially more circumferential shortening under earth load than pipes made of traditional materials.

McGrath (1999) went on to show that the prediction of earth load in the Burns and Richards (1964) elasticity solution can be reduced to a simplified form based solely on the ratio of the soil stiffness (represented by the constrained soil modulus, M_s) to the pipe hoop stiffness. This ratio is called the hoop stiffness factor:

$$S_H = M_s / PS_H$$

McGrath (1999) presented best-fit solutions for the VAF using the no-slip and full-slip interface:

$$\text{No Slip:} \quad VAF = 1.06 - 0.96(S_H - 0.7)/(S_H + 1.75)$$

$$\text{Full Slip:} \quad VAF = 0.76 - 0.71(S_H - 0.7)/(S_H + 1.75)$$

Additional verification work performed by McGrath (1998a) using CANDE and the hyperbolic soil model indicates that a good design value for the VAF is:

$$\text{Design:} \quad VAF = 0.76 - 0.71(S_H - 1.17)/(S_H + 2.92)$$

The McGrath proposal was balloted and adopted by AASHTO for incorporation into the LRFD bridge design specifications at the June 2000 meetings.

The debate over the correct VAF to use in design is complicated by the potential role of VAF in predicting both the thrust and the vertical load for deflection. Moser (1997a) has argued that VAF should be taken as one (i.e., the prism load), because under long-term settlement, deflections will approach those predicted by the full prism load. At the same time, however, his tests show large circumferential shortening in thermoplastic pipe which is indicative of significant reductions in the thrust experienced (VAF < 1).

McGrath (1998a) provides an explanation of why VAF may be less than one for purposes of thrust, but using VAF = 1 appears to produce accurate designs for prediction of deflection. He notes that the input for the Burns and Richard deflection and thrust prediction equations is the soil prism load, which yields a VAF that is a function of the hoop stiffness factor and a deflection that is very similar to the Spangler formula (this is discussed further in the section on deflections). This leads to the suggestion that a design model should apply the soil prism load (or more generally the free field geostatic pressure) as input to a pipe-soil model, which then resolves thrust and deflection based on appropriate treatment of the system interaction. In other words, the load is applied to the pipe-soil system, which then leads to thrust and deflection responses.

A.3.1.3 Thrust Capacity (and Limiting Strain)

Thrust capacity of thermoplastic pipe is limited by either excessive deformation of the material, similar to "yielding" in conventional materials (in compression, this yielding is generally manifested as crimping, or inelastic buckling), or buckling, either in local or global modes. Buckling is treated separately in this discussion of limit states.

In current U.S. practice (AASHTO), the thrust capacity due to "yielding" is assessed based on stress limits based on short- and long-term tensile strengths. Tensile strengths have been used for compression as well as tension for lack of suitable data to assess performance in compression.

For strain-rate-dependent thermoplastic pipe (e.g., PE or PVC), a compressive strain limit or allowable strain would provide a more direct means of controlling "yielding." Compressive strain limits have been approximated from AASHTO Section 18 based on the prescribed modulus and allowable stress (McGrath and Sagan 2000):

- HDPE: short term, 2.8% to 3.8% strain; long-term, 4.1% to 5.6% strain.
- PVC: short term, 1.4% to 1.7% strain; long term, 1.7% to 2.6% strain.

Comparisons with stub compressions tests indicate that these may be reasonable limiting strains (McGrath and Sagan 2000).

Compression tests by Zhang and Moore (1997c) show the significant rate dependence of HDPE properties. For strain rates between 10^{-1}/sec to 10^{-5}/sec, the stress-strain curves essentially plateau (yield) beyond 8% strain. McGrath and Sagan (2000) also provide calculations demonstrating that compressive strains in a parallel plate test at 20% deflection for HDPE pipe range from 4.27% to 8.9% strain at the crown.

A.3.2 Deflection

Deflection was not currently recognized as a limit state in AASHTO at the start of this project. The *AWWA Manual of Water Supply Practices M45* (1996) for fiberglass pipe and all of the European codes do consider deflection limits. Deflection itself is not a direct limit state, but the phenomena associated with large deflection, high strain demands, yielding, buckling, and serviceability problems, etc., all may be more appropriately considered limit states. Since deflection is the behavior most

easily inspected in the field, however, it is typically considered a limit state by itself.

A.3.2.1 Current Codes of Practice

All of the codes that explicitly treat flexible pipe use one of the model pressure distributions shown in Figure A-1. Most of the European codes that explicitly treat flexible pipe use some variation of Molin's model shown in (Figure A-1b, see, e.g., Molin 1985). The French, however, use a model based on the work of Gerbault (1995) as shown in Figure A-1c.

Calculations for the vertical and horizontal pressures (q_v, q_h, q_h^*) differ significantly from country to country (e.g., see the VAF discussion previously). Further, the extent to which the idealizations used in Figure A-1 control the deflections and demands (stresses and strains) also depends on the code.

All of the deflection expressions used in current practice can be characterized into a form similar to Spangler's formula, as follows:

$$\text{deflection} = \frac{\text{soil load}}{\text{pipe stiffness} + \text{soil stiffness}} \qquad \text{(Eq. A.1)}$$

Ignoring deflection lag, assuming uniform (180°) bedding, and assuming that horizontal deformation is equal to the vertical deformation, Spangler's expression for deflection may be expressed as

$$\frac{\Delta_v}{D} = \frac{0.083 q_v}{8 S_R + 0.061 E_{soil}} \left(\text{Spangler}\right) \qquad \text{(Eq. A.2)}$$

where:

Δ_v is the vertical diameter change
D is the diameter
$S_R = EI/D^3$

This is the same formula used in the *AWWA Manual of Water Supply Practices M45* (1996). Assuming the same E_{soil}, the Swedish method for flexible pipe, which is based on Molin's (1971) model, predicts one-half of the Spangler value for flexible pipe in good soil as follows:

$$\frac{\Delta_v}{D} = \frac{0.083 q_v}{16 S_R + 0.122 E_{soil}} \left(\begin{array}{l}\text{simplified version}\\ \text{of Molin as used}\\ \text{in Sweden}\end{array}\right) \qquad \text{(Eq. A.3)}$$

Molin's model, however, does apply the same soil properties; thus, direct comparison of the methods is complicated. Note that the Swedish method also includes several additive empirical factors that increase the deflection prediction for installation and bedding (Molin 1985). The deflection prediction of Gerbault's method (used by the French) may also be expressed in a form similar to Spangler. For uniform bedding, Poisson's ratio of soil = 0.3, no hydrostatic pressure, and K (the ratio of horizontal to vertical soil pressure) equal to 0.5, the deflection is

$$\frac{\Delta_v}{D} = \frac{0.083 q_v}{16 S_R + 2 \cdot 0.122 E_{soil}} \left(\begin{array}{l}\text{Gerbault's expression}\\ \text{used in France}\end{array}\right) \qquad \text{(Eq. A.4)}$$

Under the same assumptions, the German (ATV) prediction takes the following form:

$$\frac{\Delta_v}{D} = \frac{0.083 \left(q_v - q_h\right)}{8 S_R + 0.064 E_{soil}} \left(\begin{array}{l}\text{after Molin, as used}\\ \text{in Germany}\end{array}\right) \qquad \text{(Eq. A.5)}$$

The form is similar to Spangler, but the actual calculation is complicated by the dependence of q_v and q_h dependence on pipe stiffness, soil stiffness, installation methods, etc. Further, two-thirds of E_{soil} is used for deflection calculations. If the pipe is very flexible and placed in very stiff soil, q_v will be relieved and q_h will be increased, resulting in deflection predictions even lower than those in the Swedish formula. In more-typical

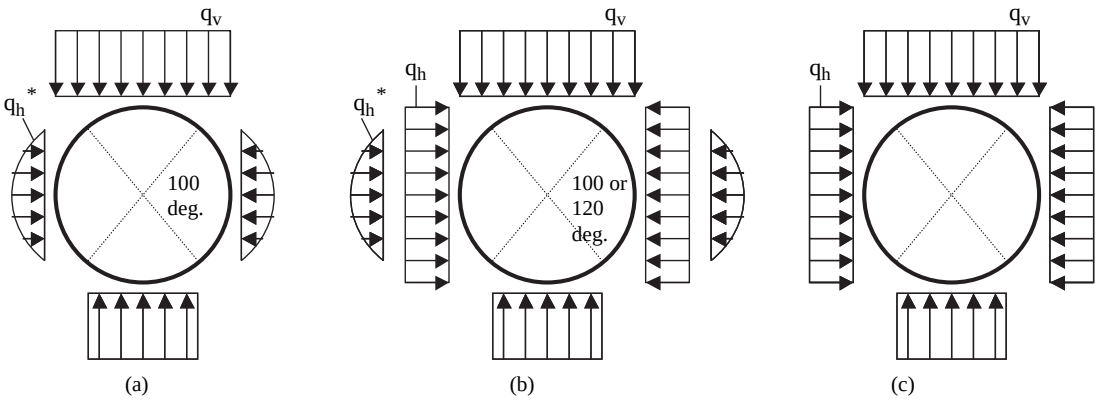

Note: q_v, q_h, and q_h* are not equal in the various models.

Figure A-1. Basic load distribution for (a) Spangler's model (b) Molin's model or variations thereof and (c) Gerbault's model.

cases, however, predicted deflection will lie between the Swedish formula and Spangler (for the same E_{soil}). In addition to all of these complications, the code in the Netherlands also adds an additional term for deflection due to $q_{lh}^{\star}$.

Although the various deflection formulas appear different, and predict deflections that may differ by a factor of two or more, the terms driving the expressions are all quite similar overall. Thus, there is agreement on the important variables to be considered in design.

Additional considerations for the deflection calculation that the standards address include the addition of empirical installation factors that add from 0% to 2% deflection depending on installation methods, and the addition of empirical bedding factors that add from 1% to 5% deflection.

How the time dependence of the soil (and the pipe material if relevant) is handled is also of interest. The deflection lag factor on the Spangler expression is used in several European codes with values ranging from 1.5 to 2.0. Other European codes suggest using long-term soil modulus values. For pipe materials that creep, some codes consider the creep of the pipe for deflection calculations, and some do not. The Swedish code provides clear guidance—the short-term modulus can be used for all pipe deflection calculations unless the backfill is a cohesive soil, in which case the long-term modulus ($0.25E_o$ for HDPE and $0.4E_o$ for PVC) must be used.

A.3.2.2 Additional Proposals

The Spangler expression for deflection of flexible pipe has been criticized. A sample of the criticisms includes the following:

- Negative E′ values readily occur in design problems (Prevost 1990, Faragher, Rogers and Fleming 1998).
- The equation overestimates deflection for stiffer pipe and underestimates deflection for flexible pipe (Schluter and Capossela 1998).
- Deflections only agree for horizontal deformation (Prevost and Kienow 1985).
- The equation cannot account for deflections observed in testing in which horizontal and vertical deflections are markedly different (Moser 1997a).
- It does not account for circumferential shortening (McGrath 1998a).

Since soil plays such a significant role in design, some researchers assert that the Spangler expression should be abandoned and that focus should be placed exclusively on soil design (Watkins 1990; Prevost and Kienow 1994; Prevost 1990).

Determination of the load to be used for deflection calculation in Spangler's expression is a topic of some discussion. Some European codes allow VAF <1 in deflection determinations, while others do not. Moser (1997a) has argued that the prism load will occur eventually, so either use full prism load and ignore deflection lag factors, or use VAF less than 1 and include deflection lag factors. Comparison between the elasticity solution of Burns and Richard and the Spangler expression sheds significant light on this issue.

McGrath (1998a) showed that for pipe with high hoop stiffness Spangler's expression and the Burns and Richard elasticity solution are essentially identical. Moser (1997a) also provides several examples where the Spangler and the Burns and Richard solutions yield similar results. For the Burns and Richard solution, the full soil prism load is the demand on the pipe-soil system and is used to determine the deflections. The implication of the similarity of the two methods is that Spangler's expression is not an expression for the deformation of the pipe alone; it is an expression for the deformation of the pipe-soil system, a system that is loaded by the full soil load regardless of the amount of arching that occurs around the pipe. This fact would also seem to decouple deflection lag factor issues as well. As McGrath (1998a) proposes, the full soil load should be used for deflection determination and deflection lag factors should be applied in addition to this as deemed appropriate by the expected settlement. The only possible reduction in the load for deflection determination would be Marston trench load effects, since this reduces the load on the entire pipe-soil system.

Some European codes (notably from Sweden) empirically add additional deflections above the deflection calculated via Spangler (or similar) expression. These factors account for additional deflections due to installation and bedding details. Additive empirical factors for deflection have been proposed for U.S. practice as well (Greenwood and Lang 1990; Petroff 1995; Chambers, McGrath and Heger 1980). The proposed deflection factors are motivated by the large variability in pipe deflections and the observation that Spangler's expression generally matches the mean response (McGrath and Chambers 1981). Petroff's (1995) proposal provides a means for approximating the expected variability in the response and for predicting a deflection that reflects a desired confidence level in the results.

In addition to additive factors, Howard (1996) suggests using a factor applied directly to the soil modulus in the denominator of the deflection expression. Values for the factor vary from 0.5 for dumped fine-grained soils to 1.0 for compacted coarse-grained soils.

Field observations and testing indicate that under soil load, thermoplastic pipes undergo significant circumferential shortening (Moser 1997b, Hashash and Selig 1990). McGrath (1998a) studied alternatives to Spangler's expression using the Burns and Richards elasticity solution and presented an expression for deflection that accounts for circumferential shortening. The expression is presented in terms of the bending

stiffness factor ($S_B = M_s R^3/EI$) and the hoop stiffness factor ($S_H = M_s R^3/EI$):

$$\frac{\Delta_v}{D} = \frac{q_v}{M_s}\left(\frac{S_H}{1+0.57S_H}\right) + \frac{q_v}{M_s}\left(\frac{D_l K S_B}{1+0.061S_B}\right) \qquad \text{(Eq. A.6)}$$

Substituting in the definitions for the bending stiffness factor and the hoop stiffness factor, the solution can be presented in more conventional terms:

$$\frac{\Delta_v}{D} = \left(\frac{q_v}{\frac{EA}{R}+0.57M_s}\right) + \left(\frac{D_l K q_v}{\frac{EI}{R^3}+0.061M_s}\right) \qquad \text{(Eq. A.7)}$$

The estimated deflection is the traditional Spangler expression with E′ replaced by the 1D soil modulus, M_s, together with an additional deflection due to circumferential shortening. McGrath (1998a) reports good agreement with Burns and Richards elasticity solution, but further verification has not yet been performed.

A.3.2.3 Proposed Deflection Limits

Deflection limits are put in place to achieve a variety of safety goals, including: limiting strain demands, prevention of local or general buckling, and prevention of serviceability problems such as joint leakage. A variety of limits have been suggested.

Initially, for metal pipe, deflections were often limited to 5% change in diameter on the basis that reverse curvature and collapse were observed at about 20% deflection and that a factor of safety of 4.0 was considered desirable. Others suggest measuring successful field installations with large deformation and applying a factor of safety with respect to these installations, with suggested design values in the 8% to 10% deflection range for HDPE and PVC (Miles and Schrock 1998). Others have suggested abandoning deflection limits altogether (Prevost and Kienow 1994). Moser (1997a) has noted that local buckling will not be readily controlled by global deflection limits.

Typical proposed deflection limits as a percentage of the inside diameter are as follows:

- 10%—ultimate limit (Miles and Schrock 1998);
- 8%—design limit (Miles and Schrock 1998);
- 8%—CEN draft document on plastic pipe standards (CEN 1991b, 1991a, 1992, 1997, 1999a, and 1999b);
- 6%—German ATV code;
- 6%—after 12 months, UK Water Research Centre (reported by Rogers et al. 1995);
- 5%—of the inside diameter after construction (Rogers et al. 1995);
- 5%—to limit global buckling (Prevost and Kienow 1994, Prevost 1990); and
- Variable—to limit local buckling, the limiting deflection decreases as the depth of fill increases (McGrath and Sagan 2000).

A.3.3 Flexure-Stress/Strain Demands

Current AASHTO specifications for thermoplastic pipe limit total tension strain (combined hoop compression and flexure), but place no other limits on flexural performance. High bending strain demands are the result of excessive deformation (deflection) and may lead to local buckling or rupture/fracture of the thermoplastic material.

A.3.3.1 Current Codes of Practice

The European codes that explicitly treat flexible pipe all limit stress or strain demand. Available CEN documentation (CEN 1991a, 1991b, 1992, 1997, 1999a, and 1999b) does not provide guidance on allowable values for stress or strain, since the specifications generally defer to material-specific standards for these limits.

The calculation of the demands follows one of two basic procedures: (1) based on the pressure distributions of Figure A-1, statics are applied to determine the bending moment at critical pipe locations, and this is converted to stress or strain, or (2) based on the estimated deflection and a shape factor, the strain demand is calculated directly. Austria, Belgium, France, Germany, and the Netherlands follow methods consistent with the first approach (1), while Sweden, the United Kingdom, and the United States (AWWA 1996) follow the second approach (2).

For Method 1, coefficients are provided for the moment and thrust around a plain pipe (as a function of bedding angle etc.). These demands are converted into stress using the following formula

$$\sigma = \frac{P}{A} + \alpha\frac{My}{I} \qquad \text{(Eq. A.8)}$$

where P is the thrust, A the area, M the moment, y the distance to the extreme fiber, I the moment of inertia, and α a correction to account for the curvature of the pipe. For nonstandard cross-sections (corrugated profiles, etc.) in which coefficients are not given for P and M, the forces must be determined via a model of the pipe loaded with the appropriate distribution from Figure A-1. The calculations assume that the only stress or strain demands of interest develop directly from the applied loads that are explicitly considered in design. Thrust and bending are both implicitly considered in this approach.

The strain demand of Method 2 may be expressed as

$$\varepsilon_b = D_f \frac{\Delta_v}{D}\frac{c}{R} \qquad \text{(Eq. A.9)}$$

where D_f is the shape factor, c is the distance to the extreme fiber, and R is the radius. The Swedish code notes that a D_f of 3.0 corresponds to elliptical deformation and suggests the use of $D_f = 6.0$. Based on the work of Turkopp, Torp, and Carlstrom (1985), the *AWWA Manual of Water Supply Practices M45* (1996) provides a set of shape factors that range from 3.3 to 8.0 as a function of the pipe stiffness and the relative energy required to compact the backfill. The shape factor approach is intrinsically different from method 1, since D_f attempts to account for local random deformations that occur during installation in addition to deformation occurring directly from the considered applied loads. The shape factor approach primarily addresses strains developing due to bending, not thrust.

A.3.3.2 Stress/Strain Limits

Stress and strain limits currently used in practice or proposed for HDPE and PVC are shown in the following display:

HDPE
Short-Term Allowable Stress
- 21 MPa—AASHTO Section 18
- 30 MPa—ATV (Germany)

Long-Term (50-Year) Allowable Stress
- 6.2 to 9.9 MPa—AASHTO Section 18
- 14.4 MPa—ATV (Germany)

Strain Limits
- 5%—AASHTO Article 12
- 5%—If slow crack growth resistance is good (Mruk 1990, 1998)
- 5%—Based on 50-year life under constant stress and free creep, Janson (1985a)
- 4%—Schrock (1993)

PVC
Short-Term Allowable Stress
- 41 to 48 MPa—AASHTO Section 18
- 90 MPa—ATV (Germany)

Long-Term (50-Year) Allowable Stress
- 18 to 25.5 MPa—AASHTO Section 18
- 50 MPa—ATV (Germany)

Strain Limits
- 3.5 to 5%—AASHTO Article 12
- 2.3%—Based on 50-year life under constant stress and free creep, Janson (1985b)
- 2%—Schrock (1993)

All of the presented values are allowable stress or strain values. Tensile specimens of HDPE show nonlinear deformation for even small strains. Beyond 4% to 6% strain, HDPE shows significant nonlinear behavior in a tensile specimen, but yield strains commonly exceed 10% and rupture strains are generally much higher. Typically limiting stress/strain values are actually based on insuring a certain safety factor on long-term resistance to cracking in pressure pipe (Janson 1985a; Mruk 1990, 1998). These types of criteria are not necessarily directly applicable to gravity flow pipe.

A.3.3.3 Modulus of Elasticity

Long-term design criteria for thermoplastics are often related to the modulus of elasticity, which is time dependent. AASHTO provides initial and 50-year values for the modulus of elasticity for PVC and HDPE, although the exact time periods considered for the initial values are not defined. The test basis for the values in the LRFD Bridge Specifications is not clear. The current AASHTO specifications target a 75-year design life for bridges. Modulus values in this time range are desired.

Sharff and DelloRusso (1994) presented data for PVC pipes held under constant deflection in ring-bending for more than two years and computed coefficients to extrapolate the modulus to longer time periods using the viscoelastic model of Horsley. The data show that the 75- and 100-year moduli of elasticity are approximately 98.5% and 97.5% of the 50-year modulus, respectively. Moser, Shupe and Bishop (1990) present data that indicate a similarly small change in PVC modulus from 50 to 100 years. The test pipes were solid-wall PVC pipes held at 5% and 7.5% deflection.

Hashash and Selig (1990) presented the following equation for the modulus of elasticity of HDPE versus time:

$$E = 664\, t^{0.0859} \qquad \text{(Eq. A.10)}$$

where:
E is the modulus of elasticity in MPa and
t is the time in minutes.

This equation predicts moduli values at 50 years that are consistent with the values published in AASHTO specifications. The equation indicates that the 75- and 100-year moduli of elasticity are approximately 97% and 94% of the 50-year modulus respectively. McGrath, Selig, and DiFrancesco (1994) published data, based on ring-bending tests held at constant deflection for more than 2 years, that support these values. The test pipes were held at deflection levels of 5% and 10%.

A.3.4 Combined Thrust and Flexure

Combined compressive thrust and flexure is not widely considered in flexible pipe design. As for flexure demand, two basic methods are used to calculate the demand:

1. The demands come directly from the assumed pressure distribution on the pipe, and thrust and flexure are combined in a classical way ($\sigma = P/A + \alpha My/I$) and compared to an allowable stress.
2. Thrust and flexure demands are calculated separately, e.g., thrust calculations are based on a thrust of $0.5 \times (VAF) \times$ (soil prism load) converted to stress or strain as appropriate, and flexural calculations are based on the shape factor (D_f) approach.

If Method 1 is employed, then combination of thrust and flexure is implicitly considered. If Method 2 is employed, then proper combination and limiting values need to be considered.

McGrath and Sagan (2000) advocate using a strain limit 50% higher than the compressive limit for combined bending and compression based on local buckling criteria. They draw this conclusion from performance of HDPE and PVC pipe in hoop compression and parallel plate tests. This criterion results in combined limiting strains of 6.2% to 8.4% strain for HDPE and of 2.4% to 3.9% strain for PVC.

When considered as separate modes of behavior, thrust and flexure are often checked in some variation of the following form:

$$\frac{\text{thrust demand}}{\text{thrust capacity}} + \frac{\text{flexure demand}}{\text{flexure capacity}} \le 1 \qquad \text{(Eq. A.11)}$$

This may provide a convenient means for checking combined thrust and flexure.

A.3.5 Global Buckling

A.3.5.1 Current Codes of Practice

The German and Swedish standards and both the *AWWA Manual of Water Supply Practices M45* (1996) and AASHTO use some form of the Winkler theory to predict buckling of the pipe, where

$$q_{cr} = \sqrt{32 S_R E_{soil}} \qquad \text{(Eq. A.12)}$$

Current U.S. practice suggests using long-term modulus for both the pipe stiffness (when applicable) and the soil stiffness, but the Swedish standard uses long-term values only for the soil modulus, and thus short-term values for the pipe stiffness.

The U.S. standards add an additional factor to account for water buoyancy. The German and Swedish standards calculate one factor of safety for overall buckling (FS_1) and another for external hydrostatic pressure buckling (FS_2) and then combine them to calculate an overall factor of safety, as follows:

$$FS = \frac{1}{\frac{1}{FS_1} + \frac{1}{FS_2}} \qquad \text{(Eq. A.13)}$$

This expression is quite conservative; for instance, if $FS_1 = FS_2 = 2$, then the resulting factor of safety (FS) is 1.

For weak soil, when $S_R > 0.0275 E_{t,soil}$ (where $E_{t,soil}$ is the tangent modulus of the soil), the Swedish code also checks an additional expression for buckling, where

$$q_{cr} = 24 S_R + \tfrac{2}{3} E_{soil}. \qquad \text{(Eq. A.14)}$$

The Swedish standard suggests using long-term values for pipe and soil stiffness in this formula, using the rationale that in weak soils a form of creep buckling can occur and thus buckling never engages the short-term pipe stiffness. In addition, another expression is presented in the Swedish code for buckling (squaring) under low cover due to traffic load.

The United Kingdom uses continuum-buckling theory, predicting the buckling to occur at

$$q_{cr} = 0.6 S_R^{0.33} E_{soil}^{0.67} \qquad \text{(Eq. A.15)}$$

The factor of safety against buckling is determined by combining the factor of safety for long-term buckling under sustained loads (FS_1) and for short-term buckling under hydrostatic or surcharge loads (FS_2) in the same manner as above. For long-term buckling, the demand is the soil pressure, and the capacity uses the continuum buckling equation with long-term properties of the pipe and soil. For short-term buckling, the demand is the surcharge and hydrostatic pressure and the capacity again uses the continuum buckling equation, but now with short-term properties of pipe and soil. Moore (e.g., Moore and Selig 1990) has also written widely on the continuum buckling theory.

The acceptable factor of safety against buckling ranges from 2.0 to 2.5 in the codes. The German code (ATV) associates a factor of safety of 2.5 with a failure probability of 1 in 100,000 and a factor of safety of 2.0 with a failure probability of 1 in 1,000.

A.3.5.2 Additional Proposals

Prevost and Kienow (1985, 1994) have argued that both the Winkler and Continuum buckling models in current practice are not conservative. They estimate that bulges and flat spots occurring in installation reduce buckling to as little as 10% to 20% of the value for an equivalent elliptic pipe and thus conclude that current models allow weak pipe that may buckle. As an alternative, they argue for a "dynamic buckling model." The model uses the stiffness at 5% deflection and classical fixed ended arch buckling of a segment of the pipe (180°) and ignores any soil contribution. The suggested expression is

$$q_{cr} = \frac{8EI}{\rho^3} \qquad \text{(Eq. A.16)}$$

where ρ is the radius of the curvature of the pipe—and should be updated to include the deformed geometry. This method has not been incorporated into any current design specifications.

A.3.6 Local Buckling

Current practice for local buckling at the start of this project is stated in *AASHTO Standard Specifications for Highway*

Bridges, "manufacturers . . . should demonstrate the adequacy of their pipes against local buckling" (AASHTO 1996, article 18.4.1.7, p. 380). How the manufacturer should ensure this adequacy, or the designer check this limit state, is not provided.

A.3.6.1 Current Work

Checks on local buckling capacity of thermoplastic pipe using classical plate buckling solutions have been suggested by Schluter as early as 1985. Experience in some profile-wall thermoplastic pipe indicates that local buckling may be the first limit state for the pipe. Soil box tests on HDPE pipe also show local buckling to be the first limit state (Moser 1997b). Measurements and analysis of local buckling in pure hoop compression have been performed by Selig, DiFrancesco, and McGrath (1994) and Moore and Laidlaw (1997).

NCHRP Report 438 by McGrath and Sagan (2000) provides guidance on local buckling of thermoplastic pipe. Based on a review of the literature, available test data, and current engineering practice, as well as independent "stub compression" tests, they propose to modify methods currently used for local buckling in cold-formed steel design (American Iron and Steel Institute 1997) for the design of thermoplastic pipe. For the purposes of local buckling calculations, the proposed method assumes that the pipe profile may be idealized as a series of connected uniform flat plates. The elastic buckling strain of each "plate" is calculated using classical plate buckling solutions. Based on an empirical expression, which includes the elastic buckling strain and the "yield" strain, an "effective width" is determined. The effective width is a reduced portion of the pipe that may be assumed to act at the yield strain. Reduced section properties (e.g., the sum of the effective portions equals effective area) are used to assess local buckling. Complete design examples are given in the report.

The proposed method assumes post-buckling capacity exists; this places certain assumptions on the strain capacity of the thermoplastic. The proposed method conservatively ignores contribution from the soil; however, tests show that soil support does influence the results and that further calibration may be required. The proposed procedure was adopted into the *AASHTO LRFD Bridge Design Specifications* (AASHTO 2001) in 2000.

A.4 Serviceability and Other Considerations

A.4.1 Flexibility Factor and Pipe Stiffness

The relationship between the flexibility factor, the traditional stiffness criterion for corrugated metal pipe, and pipe stiffness, the stiffness criterion for plastic pipe, should be properly understood. Both criteria are derived from the equation that relates load and deflection in a parallel plate test, as follows:

$$F = \Delta \frac{EI}{0.149R^3}$$

where F is the applied load, Δ is the change in vertical deflection, I is the moment of inertia of the pipe wall, and R is the radius to the centroid of the pipe wall. The inverse of the flexibility factor is defined as

$$\frac{1}{FF} = \frac{EI}{D^2} = \frac{F}{53.8\Delta/D}$$

while pipe stiffness is defined as

$$PS = \frac{EI}{0.149R^3} = \frac{F}{\Delta}$$

and the two can be related as

$$PS = \frac{53.8}{D}\left(\frac{1}{FF}\right)$$

Thus, the flexibility factor is related to the force required to deflect a pipe 1% of its diameter, while the pipe stiffness is the force required to deflect a pipe one unit (1 mm in SI units and 1 in. in customary U.S. units).

Currently, AASHTO LRFD specifications limit FF to a maximum of 0.54 m/kN (95 in./k) for thermoplastic pipe, while AASHTO material standards limit pipe stiffness to 150 kPa to 345 kPa (22 lbs/in./in. to 50 lbs/in./in.) for PE pipe in AASHTO M294 and 85 kPa to 320 kPa (12 lbs/in./in. to 46 lbs/in./in.) for PVC pipe in AASHTO M304. Comparison of these values is presented in Table A-6. Direct comparison of PS or FF factors across diameters is complicated by the strain rate dependency of thermoplastics.

The FF is a topic of some debate. One argument is that FF provides an important aspect of stiffness; that temperature dependence of the modulus should be considered in its determination; and that lower limits such as those used for steel pipe, 43 in./kip, would ensure more-reliable installation and handling. Alternate arguments are that FF is not useful because it is material dependent and has no rational basis (Prevost and Kienow 1994; Prevost 1990).

A.4.2 Other Suggested Limits

Based on dimensional analysis and soil box testing of pipes used in current practice, Moser (1997b) has suggested a series of geometric limits for thermoplastic profile wall (HDPE) pipe. Moser's proposed limits are presented in Table A-7 along with our interpretation of what the particular limit may be related to.

Table A-6. AASHTO flexibility factors based on pipe stiffnesses required in material specifications.

	M304 (PVC)		M294 (HDPE)	
SI Units				
Diameter (mm)	**PS (kPa)**	**FF (m/kN)**	**PS (kPa)**	**FF (m/kN)**
300	318	0.56	345	0.52
600	165	0.54	235	0.38
900	110	0.54	150	0.40
1,200	83	0.54	125	0.36
1,350	–	–	110	0.36
1,500	–	–	95	0.38
Customary U.S. Units				
Diameter (in.)	**PS (lb/in./in.)**	**FF (in./k)**	**PS (lb/in./in.)**	**FF (in./k)**
12	46.1	98.7	50.0	90.1
24	23.9	95	34.1	66.8
36	16.0	95	18.1	62.8
48	12.0	94.5	16.0	63.4
54	–	–	16.0	63.4
60	–	–	13.8	66.1

Note: AASHTO maximum FF for thermoplastic pipe is 0.54 m/kN (95 in./k)

A.4.3 Longitudinal Effects

Longitudinal effects are not generally considered in current practice for nonpressure pipe. It has been argued, however, that longitudinal effects are of significant importance and may swamp transverse effects (Prevost 1990). Some European codes provide guidance for consideration of longitudinal effects in nonpressure pipe, including longitudinal demands from discontinuous bedding, variability in horizontal soil stiffness along the pipe, and temperature effects.

Further, several European codes provide methods for considering allowable stress for a biaxial stress demand due to both transverse and longitudinal effects. McGrath and Beaver (2005) found that seasonal thermal expansion of contraction of 1,500 mm diameter corrugated HDPE pipe with 300 mm to 600 mm of cover caused pavement cracking.

A.4.4 Thermal Effects

Thermal effects are generally not considered in design of thermoplastic pipe. It has been argued that since the modulus of elasticity of thermoplastic materials is sensitive to temperature, thermal considerations should be made when assessing both serviceability and limit states of thermoplastic pipe (Schluter 1985). Some European codes provide provisions for checking thermal strain demands on pipe, but the codes do not modify the material modulus for temperature effects.

A.5 Pipe Testing Methods

Full-scale tests, particularly under shallow cover, have been conducted and numerous actual constructions have been monitored. These results provide valuable insight into the actual performance of buried pipe, but are not the focus of the testing methods discussed here. Instead, the focus is on simpler tests that may be conducted to assess the structural performance of thermoplastic pipe. The primary pipe test for thermoplastic pipe in current use is the parallel plate test. Due to perceived shortcomings and inherent limitations of the parallel plate test, several other tests have been conducted in recent years and suggested for augmenting, or in some cases replacing, this test. These include a curved beam test, stub compression test, and hoop compression test. In addition to a discussion of these pipe tests, two larger-scale types of tests are also briefly discussed: soil box testing and centrifuge testing.

Table A-7. Suggested dimensional limits.

Dimensional Parameter	Interpretation of the Behavior Being Controlled
$t_{min}/r > 0.005$	Not Certain
$t_{min}/w_{uns} > 0.02$	Local Buckling Limit
$I/r^3 > 4 \times 10^{-5}$	Bending Stiffness Limit
$A/r > 0.2$	Hoop Stiffness Limit
$L_p/r < 0.3$	Transverse Profile Stiffness

Note: where t_{min} is the minimum depth of the overall pipe wall, r is the radius, w_{uns} is the unsupported length of any flat element, I is the moment of inertia, A is the area, and L_p is the period of the profile section

A.5.1 Pipe Tests

A.5.1.1 Parallel Plate Test

The primary pipe test used in current practice is the parallel plate test (ASTM D2412). This test is used to determine the bending stiffness of the pipe at 5% deflection and also to ensure that the peak load capacity and buckling do not occur before some limiting deflection level is reached. AASHTO M294 requires that PE pipe reach a 20% deflection without wall buckling (defined as a loss of load accompanied by reverse curvature), cracking, splitting, or delamination. AASHTO M304 requires that pipe reach a 60% deflection without splitting, cracking, breaking, or separation of ribs or seams but provides no deflection level that the pipe must reach without loss of load. Moore and Zhang (1998) provide a finite element analysis of constant wall thickness thermoplastic pipe in the parallel plate test.

The parallel plate test is conducted at a rate of 0.5 in./min. for all pipe diameters. McGrath and Sagan (2000) present results of the strain demands at 20% deflection for a variety of different HDPE and PVC pipe. The results have been adapted in Table A-8 to show the time to reach 20% deflection and the average strain rate in the test. The stiffness of HDPE and PVC is strain rate dependent; therefore, as currently conducted for thermoplastic pipe, the parallel plate test does not provide a consistent measure of pipe stiffness. Also, the parallel plate test only provides an assessment of bending stiffness and does not expose the pipe cross-section to significant thrust.

A.5.1.2 Compression Cell—Hoop Compression Test

Selig et al. (1994) conducted compression tests of thermoplastic pipe in a hoop compression cell. The cell consists of a stiff outer cylinder lined with an inflatable bladder. Pipe is placed in the cylinder and the space between the pipe and the bladder is filled with soil. The bladder is inflated, resulting in compression of the pipe-soil system. The test approximates the conditions of a pipe under deep burial, where thrust, rather than bending, dominates the response. The exact stress/strain state of the pipe is unknown due to load sharing between the pipe and the soil. Tests of this nature have also been conducted by Li and Donovan (1994) and Moore and Laidlaw (1997).

A.5.1.3 Curved Beam Test

Gabriel and Goddard (1999) have proposed compression testing of an arc of pipe as an alternative to parallel plate testing. The test places a larger percentage of thrust to flexure in the pipe than does the parallel plate test. They propose loading at very short times and allowing relaxation to assess the pipe stiffness. They examine wall stability using this test by monitoring the thickness of the pipe as it changes under deformation. The test requires special end supports to minimize bending effects in the specimen ends, but otherwise may be conducted with standard testing apparatus. Currently, the testing has only been conducted in one laboratory.

A.5.1.4 Stub Compression Test

The "stub compression" test is a common test used to assess local buckling capacity of cold-formed steel members. A short segment of the member is tested in pure compression, and the peak load is used to determine the local buckling capacity—the peak load divided by the yield stress is used as the "effective area" in subsequent calculations. McGrath and Sagan (2000) modified the test for use in assessing local buckling of profile wall thermoplastic pipe. They found that a member consisting of three corrugations, fixed at one end and pinned at the other, and directly bearing on steel end plates provided the most consistent results. This test procedure provides a direct way to assess the local buckling capacity of profile wall thermoplastic pipe under large thrust and small bending demands. Any contribution from soil support is conservatively ignored. McGrath and Sagan (2000) report that local buckling occurred in many sections before the peak load was reached, indicating the existence of post-buckling capacity.

Table A-8. Parallel plate test.

Material	Diameter (mm)	Profile Type	Strain at Crown (%)	Time to 20% Deflection at 12.5 mm/min. (min.)	Average Strain Rate (mm/mm/sec)
PE	460	Corrugated	8.4	7.3	1.93E-02
	610		8.9	9.6	1.54E-02
	910		7.1	14.3	8.26E-03
	910		8.2	14.3	9.54E-03
	1,220		5.7	19.2	4.94E-03
	1,220	Honeycomb	4.2	19.2	3.64E-03
PVC	610	Corrugated	4.2	9.6	7.29E-03

Source: Adapted from McGrath and Sagan 2000.

A.5.2 Soil Box Tests

Soil box testing has been used at Ohio University, University of Massachusetts, University of Western Ontario, Utah State University, the United States Bureau of Reclamation, and numerous other large- or small-scale facilities. This test consists of a rigid or semi-rigid cell holding a pipe embedded in a confined mass of soil. Loads are applied externally. The cell that is largest and has been used the most is that at Utah State. Their test consists of installing pipe in a conventional manner in a large U-shaped steel shell and backfilling with soil. Load is applied to the soil from above using hydraulic jacks which use tension in the steel shell to develop a reaction. No lateral restraint is provided at the ends of the cell. The pipe response is examined under increasing load. Typical test results may be found in Watkins (1990) and Moser (1997a). It has been argued that such a test could be used to provide a complete prescriptive design method (Moser 1997a). Soil box tests on thermoplastic pipe have reported large circumferential shortening, local buckling, and poor agreement with conventional (Spangler 1941) deflection calculations.

A.5.3 Centrifuge Tests

Centrifuge testing is too involved for consideration as a standard pipe test but, like soil box tests, provides a means for learning much about the pipe-soil system under load. Tohda et al. (1990) report centrifuge testing and curves of the soil pressure distribution around a pipe. Flexible pipe shows a pressure distribution on the side that more closely matches the Gerbault or Molin distribution than that of Spangler (see Figure A-1). Centrifuge testing is also used to evaluate quality of soil support, particularly for poor soils with fines and water saturation (Tohda et al. 1995). Others argue, however, that testing is problematic and the methods unaccepted (Moser 1997a).

A.6 Analysis and Testing of Buried Plastic Pipe

A.6.1 Introduction

Since its introduction for use as drainage pipe during the late 1950s, thermoplastic pipe has generally been designed based on the semi-empirical deflection equation developed at Iowa State University. Spangler (1941) developed the equation, commonly known both as the "Iowa Formula" and "Spangler" equation, using assumptions based on his observations during field-loading experiments on corrugated metal pipe culvert. Following modification to incorporate a dimensionally consistent soil "modulus" in 1958, the "Modified Iowa Formula" (Watkins and Spangler 1958) has been widely used for flexible pipe design.

Material properties of thermoplastic are very different from those of metals for which the Iowa equation was developed. The very low hoop stiffness of some thermoplastic pipe causes redistribution of load around the pipe in a manner different from that of metal pipe. Moreover, thermoplastic materials exhibit time, temperature, and strain-rate-dependent mechanical behavior, raising questions regarding the appropriateness of elastic models.

Profile wall thermoplastic pipe came into use during the 1960s in Europe and was introduced into use in North America in the 1970s. A number of different wall profiles are used by manufacturers, and these have some additional design considerations that need to be addressed.

In the past several decades, various projects have been undertaken to improve thermoplastic pipe design and numerous articles have been published on the subject. A number of specialized ASCE, ASTM, and other conferences and symposia have been held. Many of the important design aspects for thermoplastic pipe have been established. This report reviews thermoplastic pipe design, performance prediction methods, and performance limits. Methods of analysis including the finite element method are examined, as are physical test procedures and facilities for examining pipe behavior.

Two relatively recent texts covering pipe testing, analysis, and design are those of Moser (1990) and Janson (2003).

A.6.2 Analysis

A.6.2.1 Closed-Form Solutions for Static Pipe Response

A.6.2.1.1 Ring Only Analysis. Earlier researchers analyzed the behavior of an elastic ring subjected to internal or external pressure. The buried pipe can be thought of as an elastic ring subjected to external pressures from the surrounding soil and the internal fluid pressure. The ring only analysis provides valuable information to understand the behavior of buried pipe.

A.6.2.1.2 Ring Wall Strain. Buried pipes are subjected to localized-circumferential strain in the hoop direction that results from both nonuniform and uniform components of external pressure. The total circumferential strain for gravity flow pipe is made up of ring compression strain, bending strain, and strain due to Poisson's effect.

The ring compression in buried pipe is caused by the uniform components of the geostatic stress. The well-known hoop compression formula is used to calculate the hoop stain due to ring compression, as follows:

$$\varepsilon_c = \frac{PD}{2AE} \qquad \text{(Eq. A.17)}$$

where:

P is the external pressure,
D is the pipe diameter,
A is the wall thickness or area per unit length, and
E is the elastic modulus.

The maximum pipe bending strains were interpreted from the deformed pipe shape by ring bending theory and the theory of elasticity (Roark 1943). The bending strain in a circular inextensible ring deflected by a small amount into an elliptical shape is

$$\varepsilon = 3\left(\frac{d}{D}\right)\left(\frac{\Delta}{D}\right) \qquad \text{(Eq. A.18)}$$

where:

Δ is the change in ring diameter,
d is the distance from the centroidal axis to the extreme fiber, and
D is the pipe diameter.

Naturally, the total strains in a buried pipe are a combination of hoop compression and bending, and these are further complicated by local effects associated with nonuniform soil support and any distortion from elliptical shape that results from construction loads.

A.6.2.1.3 Critical Thrust. The critical buckling load for a circular ring subjected to uniform hydrostatic pressure (first obtained by Levy 1884), is

$$P_{cr} = \frac{3EI}{R^3} \qquad \text{(Eq. A.19)}$$

In the case of plane strain, Timoshenko (1936) has provided the formula for long, thin-walled pipe

$$P_{cr} = \frac{2E}{(1-\nu^2)(S_D)^3} \qquad \text{(Eq. A.20)}$$

where:

S_D is the standard dimension ratio, $S_D = (D_{avg}/t - 1)$,
D is pipe outer diameter, and
t is wall thickness.

A.6.2.1.4 Continuum Modeling. Continuum mechanics principles have been used to develop a number of closed-form solutions for use in buried pipe analysis. Burns and Richard (1964) examined the idealized post-stressed soil structure system subjected to vertical and horizontal pressure, where the horizontal pressure was given by

$$\sigma_h = \left[\frac{\nu_s}{1-\nu_s}\right]\sigma_v \qquad \text{(Eq. A.21)}$$

The analysis presents the interaction of an elastic, circular cylinder embedded in a linearly elastic, isotropic, homogeneous continuum. Hoeg (1968) derived the mathematical formulation for the more generalized case of $\sigma_h = K\sigma_v$. The solutions are limited to the plane strain condition.

Moore (1993, 2000) adopted Hoeg's solution in the analysis of buried circular pipe and culvert. To simplify the interpretation, the two-dimensional (2D) load system was divided into uniform (σ_m) and nonuniform components (σ_d) of pressures (Figure A-2). Distribution of interface radial and shear stress on the external boundary of the pipe was obtained from the elastic analysis as

$$\sigma = \sigma_o + \sigma_2 \cos 2\theta \qquad \text{(Eq. A.22)}$$

$$\tau = \tau_2 \sin 2\theta \qquad \text{(Eq. A.23)}$$

θ, is measured from the vertical axis and where:

$$\sigma_o = A_m \sigma_m \qquad \text{(Eq. A.24)}$$

$$\sigma_2 = A_{d\sigma} \sigma_d \qquad \text{(Eq. A.25)}$$

$$\tau_2 = A_{d\tau} \sigma_d \qquad \text{(Eq. A.26)}$$

A_m, $A_{d\sigma}$, and $A_{d\tau}$ are called arching coefficients and are defined for smooth and fully bonded interface in terms of the soil stiffnesses relative to pipe stiffnesses and the Poisson's ratio.

For the post-stressed pipe, where earth pressure develops after the pipe is placed in the ground, the uniform and nonuniform components of stress are given by:

$$\sigma_m = \frac{\sigma_v + \sigma_h}{2} \qquad \text{(Eq. A.27)}$$

$$\sigma_d = \frac{\sigma_v - \sigma_h}{2} \qquad \text{(Eq. A.28)}$$

Einstein and Schwartz (1979) considered the response of a thin elastic tube inserted in prestressed elastic ground and obtained the closed-form solution.

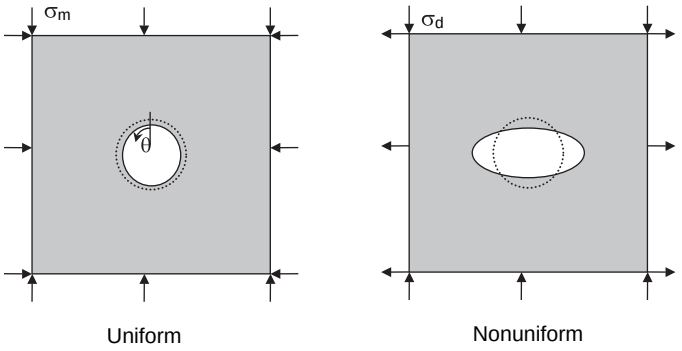

Figure A-2. Uniform and nonuniform deformation on buried pipe (after Moore 1993).

The uniform component of pressure produces a uniform hoop thrust in the pipe wall and uniform diametral strain. The distortional stress component generates a deviatoric component of hoop thrust and out-of-round deflections. The principle of superposition is used to obtain the combined effect. Thus the radial deflection of the pipe is

$$\omega = \omega_o + \omega_2 \cos 2\theta, \qquad \text{(Eq. A.29)}$$

Here, ω_o and ω_2 are deformations due to the uniform and nonuniform component of stresses respectively, and are given by

$$\omega_o = -\frac{\sigma_o R^2}{EA} \qquad \text{(Eq. A.30)}$$

$$\omega_2 = -\frac{(2\sigma_2 - \tau_2)R^4}{18EI} \qquad \text{(Eq. A.31)}$$

Further relationships can be developed for thrusts at crown, N_{cr}, and springline, N_{sp}, in terms of pipe radius, R and harmonic interface stress components (Moore 1993):

$$N_{cr} = \sigma_o R + (\sigma_2/3 - 2\tau_2/3)R \qquad \text{(Eq. A.32)}$$

$$N_{sp} = \sigma_o R - (\sigma_2/3 - 2\tau_2/3)R \qquad \text{(Eq. A.33)}$$

Small deflection elastic analysis is valid for higher pipe diameter/thickness ratio (D/t) (Gumbel and Wilson 1981). Gumbel and Wilson (1981) extended the elastic analysis to make approximate allowance for the second-order distortional effects for pipe with smaller D/t ratios.

The closed-form solutions discussed above are derived using thin shell theory to describe the structural response. However, thermoplastic pipes often have thicker walls. Moore (1985) developed a full elastic solution that is applicable for any thickness pipe. Examination of the thin shell theory with the full elastic solution indicated that the thin shell theory is satisfactory when the thickness to radius ratio $t/R \leq 0.05$ ($DR > 40$). Moore (1985) also obtained rigorous prebuckling and postbuckling solution for buried tubes. He investigated the effects of initial imperfections on the solution.

Chua and Lytton (1987) obtained the linear viscoelastic solution by extending Hoeg's elastic solution. This can be used to characterize the time-dependent behavior of thermoplastic pipe. The "power law" relaxation modulus was used to model the viscous behavior of the pipe material. The compressibility and the flexibility factors of the elastic solution are replaced with the following expressions for the viscoelastic solution:

$$c = \frac{1}{2}\frac{1}{1-\nu}\frac{\left(\frac{1}{2T}\right)^m M_1\Gamma(1-m)\left(\frac{D}{t}\right)}{\left[\left(\frac{1}{2T}\right)^{m_c} E_{c1}\Gamma(1-m)\right]}(1-\nu_c^2) \qquad \text{(Eq. A.34)}$$

$$F = \frac{1}{4}\frac{1-2\nu}{1-\nu}\frac{\left(\frac{1}{2T}\right)^m M_1\Gamma(1-m)\left(\frac{D}{t}\right)^3}{\left[\left(\frac{1}{2T}\right)^{m_c} E_{c1}\Gamma(1-m)\right]}(1-\nu_c^2) \qquad \text{(Eq. A.35)}$$

in which Γ is the gamma function, M_1 is the 1D (constrained) soil modulus, ν is soil Poisson's ratio, E is Young's modulus of the pipe, D is the average pipe diameter, t is the wall thickness, E_{c1} is the initial pipe modulus, m is the exponent of the power law model, and T is time. The subscript "c" is used to represent the elastic pipe parameters in the equation.

Other viscoelastic modeling has been undertaken using Laplace transforms to determine buried pipe response for viscoelastic theories based on conventional rheological (spring and dashpot) elements (Moore 1994b).

A.6.2.2 Finite Element Analysis

All the methods of pipe analysis—empirical, semi-empirical, or closed-form solutions—employ simplified deflection patterns. The final shape of the pipe is an important assumption used in the derivation of the empirical equations. For example, Spangler's deflection equation and Watkins's strain formula assume that the pipe buried in backfill deforms into an approximately elliptical shape. "Squaring" has been reported in some cases, however, particularly in well-compacted backfill (Howard 1972; Howard 1981; Soini 1982; Lang and Howard 1985; Rogers 1988). Rogers (1988) also identified "heart" and "inverted heart" shaped pattern at below and above the springline, respectively, for pipe in well-compacted soil.

The closed-form elasticity solutions are based on the assumption of an infinite, homogeneous, isotropic, and linear elastic ground medium, and of elastic pipe properties. The problem is also idealized as geometrically linear and assumes 2D-plane strain response. Applicability of the analytical solution is strictly limited to deep burial. In reality, the material response is not homogeneous, isotropic, linear, and elastic, nor is the response necessarily 2D.

The finite element method provides a convenient alternative to overcome the simplified deflection approximations associated with analytical and semi-empirical solutions. Furthermore, the finite element method can be used to account for a whole range of nonlinear and time-dependent material (soil and pipe) responses. This analysis is critical too for research and is valuable for design of some high cost structures. Users must be well trained.

A.6.2.2.1 2D Finite Element Analysis of Soil-Structure Interaction. Advanced design approaches based on soil-structure interaction analysis have been in use for flexible metal culverts since the early 1970s (Duncan and Chang 1970; Allgood and Takahashi 1972; Abel, Mark and Richards 1973;

Katona et al. 1974; Duncan 1979). The procedure has been extended further for use in analysis of buried thermoplastic pipes (Chua and Lytton 1987; Hashash and Selig 1990; Moore 1994a,1994b; Zhang and Moore 1997a).

Most analyses incorporate straight-beam-column elements with linear elastic stress-strain relations for the pipe, and continuum elements with the hyperbolic stress-strain constitutive model for the nonlinear behavior of the surrounding soil. Common features include small strain assumptions and 2D plane strain analysis. CANDE, developed by Katona et al. (1974) for FHWA, has been used with some modification, for analysis and design of buried thermoplastic pipe (Brown and Lytton 1984; Katona 1988; Hashash and Selig 1990; Hurd, Sargand, and Masada 1997). The program incorporates linear elastic, incremental elastic, and Hardin's hyperbolic (Hardin 1971) type soil models. Katona and Vittes (1982) added Duncan's hyperbolic soil model (Duncan and Chang 1970), and its extension by Selig was later implemented by Musser (1989). McGrath et al. (1999) used CANDE to model installation effects.

Duncan and his research group (Ozawa and Duncan 1973, Duncan 1979) developed the computer codes SSTIP and NLSSIP at the University of California, Berkeley, for metal culvert design. The programs also make use of the hyperbolic relation to model nonlinear soil behavior. Researchers at the Utah State University at Logan and the University of Massachusetts at Amherst, have been using the programs with slight modification for thermoplastic pipe analysis (Moser 1990, Hashash and Selig 1990). The modified programs are called PIPE and SOILCON, respectively.

A.6.2.2.2 Viscoelastic Analysis Using CANDE. The finite element analysis has been successfully used to simulate short-term soil-pipe interaction. Hashash and Selig (1990) achieved reasonable agreement for their short-term analysis of the deep burial installation of HDPE pipe in Pittsburgh, Pennsylvania (Adam, Muindi, and Selig 1989). McGrath et al. (1999) achieved good agreement modeling installation effects for various compaction and backfill types. Efforts have been made to mimic the long-term pipe behavior using the linear elastic finite element program CANDE. Katona (1988, 1990) implemented reduced material modulus for long-term response in his analysis to develop design guidelines for corrugated polyethylene pipe. Brown and Lytton (1984) adopted a simple power law formulation to account for the reduction of stiffness with time. Based on the analysis of the deep burial installation, Hashash and Selig (1990) concluded that time-dependent models were needed to characterize the long-term pipe responses successfully.

A.6.2.2.3 Linear Viscoelastic Analysis. Adapting the general soil-structure interaction code AFENA (Carter and Balaam 1980), Moore (1994a, 1994b) implemented a linear viscoelastic model based on conventional rheological parameters. Moore and Hu (1996) used that linear viscoelastic finite element analysis to estimate the time-dependent response of thermoplastic pipe subjected to a constant rate of vertical diameter decrease with time. The small deflection (5%) relaxation rheology was found to provide good predictions up to 3% of vertical pipe deflection and the large deflection (10%) rheology yielded better predictions for pipe deflection between 3% to 10%. The linear viscoelastic model was reported to be poor in simulating time-dependent response at large deflections (> 10%).

A.6.2.2.4 Nonlinear Viscoelastic and Viscoplastic Analysis. Nonlinear viscoelastic and viscoplastic models have also been implemented to facilitate the assessment of time-dependent pipe response beyond small deflection limits (Zhang and Moore 1997b, 1997c, 1997d). Stress dependent springs and dashpots were used in the development of the nonlinear viscoelastic model. The viscoplastic model employed inelastic work and inelastic strain-rate dependent material properties. Both material and geometrically nonlinear analysis were performed to analyze the laboratory parallel plate-loading test for plain pipe (Moore and Zhang 1998). While both methods successfully predicted the pipe response at large strain and large deflection, the performance of the viscoplastic model was found to be superior. Zhang and Moore (1998) examined pipe response measured in a hoop compression cell using the nonlinear viscoelastic and the viscoplastic material models. Comparison of the theoretical results to the measured laboratory data showed good correlation between the predictions and the measurements.

A.6.2.2.5 3D Semianalytic Method. Most use of finite element analysis has involved 2D linear and nonlinear investigations of soil-pipe interaction. Moore (1994b) developed a three-dimensional (3D) time-dependent analysis of profiled thermoplastic pipe. Assuming simplified axis-symmetric geometry, a Fourier series was used to model the variations of stress, strain, and deformation around the pipe circumference. Response of the pipe to each Fourier harmonic was determined separately and assembled together using superposition to attain the full pipe response. Moore (1994b) utilized 100 Fourier terms in the 3D analysis of pipe during the laboratory "parallel plate loading" test. When the 3D geometry and viscoelastic material characteristics are represented, finite element estimates of pipe response under parallel plate loading are very close to laboratory measurements. Examinations of the laboratory hoop compression test (Moore and Hu 1995) and biaxial field loading (Moore 1995) have revealed that important 3D stresses develop in profiled pipes that cannot be predicted using conventional 2D analysis.

A.6.2.3 Buckling Solutions

Compressive hoop thrusts in flexible pipe act to reduce the flexural stiffness of the pipe cross-section. If large enough, this compressive thrust can cause the flexible pipe to become elastically unstable. Design against instability is typically undertaken by comparing the hoop thrust that develops at working loads with the critical buckling loads. Rigorous bucking solutions have been developed for buried pipe using "Winkler" and continuum soil models. Moore (1989b) reviewed the relevant literature in detail.

A.6.2.3.1 Elastic Subgrade Model. The elastic subgrade model characterizes the soil support as a series of elastic springs and the pipe as an elastic ring. Buckling analysis using this "Winkler" soil model leads to the uniform critical hoop thrust, N_{cr}, of

$$N_{cr} = 2\left(\frac{EI.k}{R}\right)^{1/2} \qquad \text{(Eq. A.36)}$$

where k is the modulus of subgrade reaction (Stevens 1952; Booy 1957; Flugge 1962; Meyerhof and Baikie 1963; Luscher 1966; Kloppel and Glock 1970; Chelapati and Allgood 1972). Various versions of the theory are employed in the assessment of buckling strength (Carlstrom 1981; Heierli and Yang 1982; Schluter 1985; AWWA 1981). Glascock and Cagle (1984) introduced empirical correction factors to account for the influence of both shallow burial and pore water pressures in the soil. However, the Winkler model neglects the contribution of the shear stiffness of the soil to the buckling resistance, and the determination of spring stiffness is complex, since k is a function of the wavelength of the pipe deformation, the burial depth, and the nonuniform ground support.

A.6.2.3.2 Elastic Continuum Model for Soil. The elastic continuum buckling theory models the soil as an elastic solid and the pipe as an elastic ring.

Solution for Uniform Semi-Infinite Ground Elastic continuum modeling of the ground for pipes deeply buried in an infinitely large soil envelope yields buckling thrust,

$$N_{cr} = 1.2\left(EI\right)^{1/3}\left(\frac{E_s}{1-\nu^2}\right)^{2/3} \qquad \text{(Eq. A.37)}$$

for soil-structure interface that is smooth (Forrestal and Herrmann 1965; Dunes and Butterfield 1971; Cheney 1976; Moore and Booker 1985b). The formula uses linear "multiwave" theory and assumes that the ground resists deformations both into and out from the cavity. Gumbel (1983) pointed out that the resistance of the soil to inward movement is a function of effective stresses in the soil. Therefore, the solution is valid where effective stress does not dwindle to zero, i.e., structural load does not come from fluid pressure. "Single" wave theory governs the buckling capacity in the cases of no inward resistance (Sonntag 1966; Hain 1970; Cheney 1971). An initial compressive prestress develops between pipe and ground where pore water pressures are small, however; and model test data confirms that linear elastic "multiwave" solutions are effective as design tools (Moore, Selig and Haggag 1988).

Moore and Booker (1985a) examined circular pipe stability under nonuniform hoop thrusts. They established that maximum hoop thrust generally controls pipe stability and that conservative designs can result from the comparison of uniform thrust buckling theory with the maximum thrust.

The results of the theoretical solution of buckling are influenced by shallow burial (Somogy et al. 1985). Moore (1987) examined the effect of burial depth on the calculation of critical buckling load. Moore and Selig (1990) introduced a "correction factor" to the continuum buckling solution to account for burial depth and the influence of nonuniform surrounding soil. They also included a "calibration factor" for the inelastic and nonlinear soil response and geometrically nonlinear structural response. Based on comparisons between buckling measurements and predictions, the elastic continuum model has been found to be superior and able to provide rational assessment of backfill geometry (Moore and Selig 1990).

Solution for Nonuniform Ground Moore, Haggag, and Selig (1994) presented a closed-form linear buckling solution for a two-zone solid to account for the effect of the nonuniform elastic modulus on the buckling strength. They considered the stability of circular structures in axisymmetrically nonuniform ground. The stiffness equation relates the interface deformations with the interface tractions for the nonuniform elastic continuum surrounding the cylinder.

$$N_{cr} = l\left(\frac{EI\left(n^2-1\right)}{R^2} + 2G_s R\chi\right) \qquad \text{(Eq. A.38)}$$

Parameters in the equation are pipe modulus E, second moment of area I, shear modulus of soil G_s, harmonic term n, and two other functions, "*l*" and "χ".

The variable *l* accounts for the load behavior on the stability of a cylindrical shell. Moore and Booker (1985b) revealed that the effect of load behavior is insignificant if a reasonable level of soil support exists. Therefore, the case of "constant directional" load behavior was considered in the solution for critical buckling load (Moore, Haggag, and Selig 1994).

Parameter χ quantifies the level of solid resistance to structural deformation, along with the soil modulus G_s. The parameter was defined as a function of envelope width W (Figure A-3) to pipe radius R ratio, (W/R), Poisson's ratios for pipe and soil (ν_c, ν_s), and the harmonic number (n), for smooth and rough pipe interface.

The solution was presented in the form of correction factor, R_h, which expresses the critical hoop thrust relative to the hoop

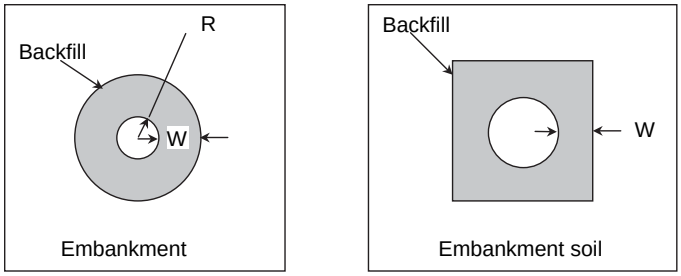

Figure A-3. Geometry of the buried pipe problem (after Moore, Haggag, and Selig 1994).

thrust for pipe deeply buried in uniform infinite large soil envelope. Moore and colleagues (1994) provide R_h values for a range of pipe burial conditions. Values of R_h are also provided for cases where a larger-diameter structure is buried close to the ground,

$h < R$.

A.6.2.3.3 Local Buckling Analysis. Corrugated and profiled wall pipes are composed of thin structural elements that can undergo individual short wave buckling. DiFrancesco (1993) observed ripples in tests on twin wall HDPE pipe subjected to hoop compression. Moore and Hu (1995) demonstrated that these ripples were due to local buckling in the inner wall (liner). Moser (1998) observed the local buckling as the lowest performance limit in some of his tests with profile-wall pipe. The local buckling can be on the liner and on the corrugated walls (sidewall, crown, and valley) (Figure A-4). Liner buckling may affect the hydraulic properties of the pipe, whereas corrugation buckling compromises structural integrity.

In *NCHRP Report 438,* McGrath and Sagan (2000) reviewed the state-of-the-art of local buckling for corrugated polyethylene pipe. The plate buckling equations for metals (Bryan 1891; Winter 1946) were examined for use in estimating the local stability of corrugations (also, Schluter 1985). The Euler formula for thin plate buckling (after Bryan 1891) is

$$\sigma_{cr} = \frac{k\pi^2 E}{12(1-\nu^2)(W/t)^2} \qquad \text{(Eq. A.39)}$$

where σ_{cr} is the critical buckling stress, k is the edge support coefficient, W is the plate width, and t is the plate thickness.

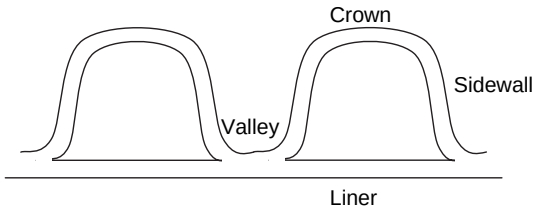

Figure A-4. Structural elements in corrugated pipe (after Moore 1994a).

Winter (1946) proposed an "effective width approach" and set buckling criteria defining a slenderness factor, λ

$$\lambda = \sqrt{\frac{12(1-\nu^2)}{\pi^2 k}}\left(\frac{W}{t}\right)\sqrt{\frac{\sigma_c}{E}} \le 0.673 \qquad \text{(Eq. A.40)}$$

where λ is the slenderness factor and σ_c is the compressive stress on the element.

An "effective width" is then computed as

$$w = \frac{(1-0.22/\lambda)}{\lambda} W \qquad \text{(Eq. A.41)}$$

where *W* is the unsupported width of the element.

Moore and Laidlaw (1997) utilized the stiffened plate model from the ASCE (1984) Structural Plastics Design Manual to examine corrugation buckling. The manual makes use of Bryan's equation for plate buckling, though Moore and Laidlaw (1997) re-expressed the critical buckling criteria in the form of critical hoop strain as follows:

$$\left(\frac{\Delta D}{D}\right)_{cr} = \left(\frac{C_b t}{w}\right)^2 \qquad \text{(Eq. A.42)}$$

where w is the plate width, t is the plate thickness, D is the pipe diameter, ΔD is the diameter decrease, and C_b is the end restraint factor. Recommendations were made for the edge restraint factors, C_b (Table A-9), based on the results of laboratory "Hoop Compression" cell tests. They also proposed design values for C_b based on potential for soil to penetrate the corrugation valley.

Moser (1998) performed extensive "soil box" testing and proposed empirically derived dimensionless geometric parameters to limit corrugation buckling (Table A-10). The limits, however, are subjective to the laboratory loading conditions.

Table A-9. Edge restraint factors for corrugation buckling.

Soil in Valley	C_b Side Wall	C_b Valley	C_b Crown
None	Clamp-free 1	Simple-free 0.6	Simp.-Simp. 1.8
Partial	Clamp-Simp. 2.1	Clamp-free 1	Clamp-Clamp 2.4
Full	Clamp-Clamp 2.4	Clamp-Clamp 2.4	Clamp-Clamp 2.4

Table A-10. Dimensionless geometric parameters to control profile-wall pipe.

Dimensionless Parameter	Possible Value for HDPE
t_{min}/R	≥ 0.005
t_{min}/l_{uns}	≥ 0.02
I/R^3	$\geq 4\times10^{-5}$
A/R^3	≥ 0.02
L_p/R	< 0.3

Note:
t_{min} = minimum thickness of profile element
R = the effective radius of the pipe
l_{uns} = unsupported length (or width)
A = area per unit length of cross section
I = moment of inertia per unit length
L_p = length of the profile section

Moore (1996) derived theoretical relationships for liner buckling using the linear buckling theory for a stiffened cylindrical shell (Moore 1990b). The theory is expressed graphically in terms of critical compressive hoop strain in the liner (Figure A-5). The uniform and nonuniform components of compressive hoop strains on the liner are evaluated using the ring theory discussed earlier in the report (see also Flugge 1962).

$$\varepsilon_u = \left(\frac{\Delta D_v}{D} + \frac{\Delta D_h}{D} \right) \qquad \text{(Eq. A.43)}$$

and

$$\varepsilon_n = \frac{6h}{D}\left(\frac{\Delta D_v}{D} - \frac{\Delta D_h}{D} \right) Cos(2\theta) \qquad \text{(Eq. A.44)}$$

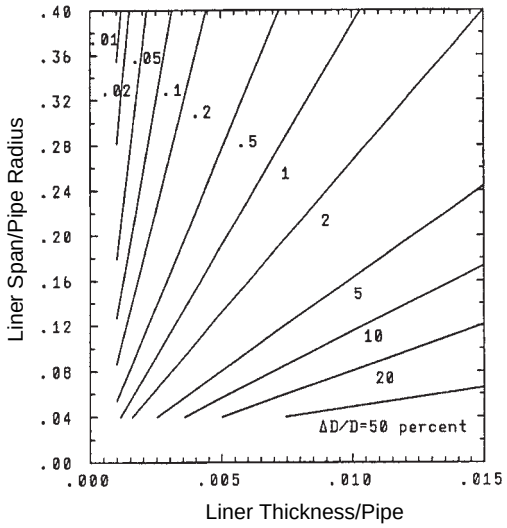

Source: Reprinted from Moore, I.D., *Local Buckling in Profiled HDPE Pipes*, 1996 Annual Conference of the Canadian Society for Civil Engineering (CSCE), Edmonton, AB, Canada, 1996.

Figure A-5. Critical hoop contraction for liners of various thickness and span.

where D is the distance of the internal fiber from the neutral axis, θ is the circumferential position, and ΔD_v and ΔD_h are change in vertical and horizontal diameters, respectively.

Total strain on the liner is assumed equal to $\varepsilon = \varepsilon_u + \varepsilon_n$. Tests on pipes featuring measurement of strains in the liner indicate that these expressions may be very conservative.

A.6.2.4 Constitutive Models

The mechanical response of thermoplastic material can be highly nonlinear, as well as time and temperature dependent. Materials possessing time-dependent properties show creep and relaxation behaviors. The secant modulus concept has been conventionally used, in the form of time-dependent "relaxation modulus," to present nonlinear stress-strain characteristic of the polymer. The secant modulus is defined as

$$E(t) = \frac{\sigma(t)}{\varepsilon(t)} \qquad \text{(Eq. A.45)}$$

and can be defined for a range of load paths (including creep and relaxation). Viscoelastic and viscoplastic models have also been developed to represent the time-dependent behaviors of thermoplastic materials.

A.6.2.4.1 Linear Elastic Approximations Based on "Creep Modulus." Long-term modulus of elasticity has been used to determine long-term pipe performance for thermoplastic pipe. AASHTO (2007), Janson and Molin (1981), and Janson (1985a) defined pseudoelastic values at the time period over which deformations have been sustained. A 50-year design life is generally used for most culvert designs.

AASHTO recommended the values of 758 MPa and 152 MPa for short-term and long-term moduli, respectively, for HDPE pipes. The AASHTO values for PVC pipes are 2,760 MPa and 965 MPa for materials of the ASTM D1784 12454C cell class, and 3,030 MPa and 1,090 MPa for materials of the ASTM D1784 12364C cell class.

Janson and Molin (1981) extrapolated creep modulus to 50 years' loading time (in a Finnish test) and obtained the values of 800 MPa for uPVC and 100 MPa for HDPE. Janson (1985a) also extrapolated pipe relaxation test data and obtained a 50-year modulus for HDPE of 190 MPa.

Kienow and Prevost (1983) derived approximate relations between 50-year values of pipe stiffness and the initial stiffness. They documented that long-term modulus for HDPE is 16% of the initial modulus, whereas the percent value for PVC is 33%.

A.6.2.4.2 Power Law Relationship for Viscoelasticity. A number of researchers have expressed the modulus, at any particular strain level, as a power law relation of time (Janson

1985a and 1985b, Chua 1986, Hashash 1991). The "Power Law" form of the relaxation modulus is given by

$$E(t) = E_\infty + (E_1 - E_\infty)t^{-m} \quad \text{(Eq. A.46)}$$

where E_∞ is the relaxation modulus at very long time, E_1 is the modulus at one unit of time, and m is the rate of decrease of modulus.

Parameters for the power law equation are obtained by conducting relaxation tests and plotting modulus versus time on a log-log scale (Figure A-6). For "E" expressed in MPa and "t" in hours, the parameters as obtained for HDPE from different tests at 5% diametral deflection are shown in Table A-11.

A.6.2.4.3 Linear Viscoelastic Model. Conventional rheology consisting of springs and dashpots can be used to develop a viscoelastic model. Moore (1994b) selected nine-log cycles of time for modeling. One Kelvin element successfully models one-log cycle of time, so nine Kelvin elements and an independent spring element were employed in series for the linear time-dependent response. Viscosity of each element is assumed to increase by a factor of 10 from the first element to the last. The number of independent springs was reduced by assuming that consecutive springs have a constant modular ratio. The linear viscoelastic constitutive relation is therefore given by

$$\dot{\varepsilon} = \dot{\varepsilon}^e + \dot{\varepsilon}^v \quad \text{(Eq. A.47)}$$

$$\dot{\varepsilon}^e = \frac{\dot{\sigma}}{E_o} \quad \text{(Eq. A.48)}$$

$$\dot{\varepsilon}^v = \sum_{i=1}^{9}\left(\frac{\sigma}{E_i\tau_i} - \frac{\dot{\varepsilon}^v}{\tau_i}\right) \quad \text{(Eq. A.49)}$$

where the parameters for the model are

E_o = the independent elastic spring modulus,
E_1 = first Kelvin spring modulus,
η_1 = the first Kelvin dashpot viscosity,
$E_r = E_{i+1}/E_i$ $(i > 0)$ = modular ratio between consecutive springs,
$\eta_i = \eta_1 10^{i-1}$,
$\tau_i = \eta_i/E_i$ = the retardation time.

Moore and Hu (1996) defined two different sets of parameters: (1) "small deflection rheology," which represents the response at small strain, and (2) "large deflection rheology," which attempts to capture the nonlinear pipe response at a larger deflection level. Their linear viscoelastic parameters for HDPE obtained from data provided by DiFranesco, Selig, and McGrath (1994) are given in Table A-12.

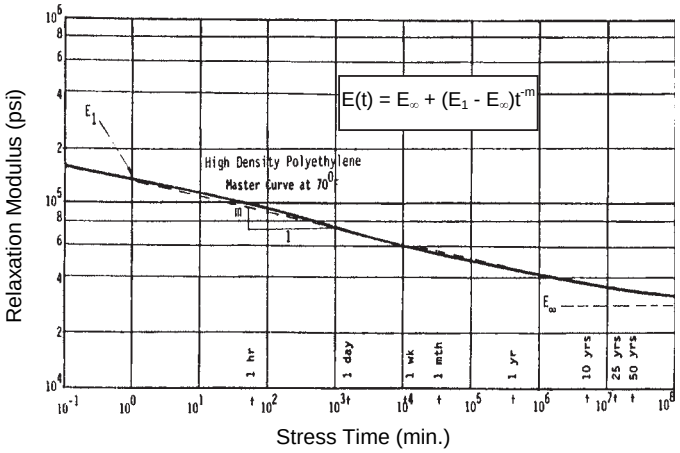

Source: Reprinted from K.M. Chua, "Time-Dependent Interaction of Soil and Flexible Pipe," PhD thesis, Texas A&M University, College Station, 1986.

Figure A-6. Determination of "Power Law" parameters.

Moore and Hu (1996) performed linear viscoelastic finite element analysis to investigate the time-dependent response of HDPE pipe under parallel plate loading. It was suggested that the linear viscoelastic model with "small deflection" parameters provides reasonable prediction at strain levels of up to 0.8%. The "large deflection" rheology was only partially successful at representing material response beyond this strain limit.

A.6.2.4.4 Nonlinear HDPE Viscoelastic Modeling (NVE). Further investigations with the linear viscoelastic model have revealed that the model is poor in predicting pipe response at strain levels beyond 0.8% (Moore and Zhang 1995). Zhang and Moore (1997d) therefore formulated a nonlinear viscoelastic model to overcome the limitations associated with the linear model. Six-log cycles of time were selected for modeling, which induce a combination of one spring and six Kelvin elements in series. Thus, the constitutive relation becomes

$$\dot{\varepsilon} = \dot{\varepsilon}^e + \dot{\varepsilon}^v = \frac{\dot{\sigma}}{E_o} + \sum_{i=1}^{6}\left(\frac{\sigma}{E_i\tau_i} - \frac{\dot{\varepsilon}^v}{\tau_i}\right) \quad \text{(Eq. A.50)}$$

Table A-11. "Power Law" parameters at 5% deflection.

Parameters	Janson (1985a) at 23°C	Chua (1986) at 21°C	Hashash (1991) at 20°C – 32°C
E_∞ (MPa)	0	52.6	0
E_1 (MPa)	520	460	329
m	–0.0795	–0.097786	–0.0859

Table A-12. Parameters for linear viscoelastic model, Moore and Hu (1996.)

Model	E_0 (MPa)	E_1 (MPa)	E_r (MPa)	η_1 (MPa.d)	η_r
S	1,120	3,615.6	0.845	0.503	10
L	1,000	1,066.6	1.17	0.503	10

Solution of the equation is obtained as

$$\varepsilon = \varepsilon^e + \varepsilon^v = \frac{\sigma_n}{E_i} + \sum_{i=1}^{6} \frac{\sigma_n}{E_i}\left\{1 - \exp\left(-\frac{t}{\tau_i}\right)\right\} \qquad \text{(Eq. A.51)}$$

where σ_n is the engineering stress.

To encompass nonlinear behavior, E_o, E_i, and τ_i are defined as functions of stresses. Parameters of the Kelvin elements are related to the values of the first element to reduce the number of material functions, viz.

$$E_i = m^{i-1}E_1 \qquad \text{(Eq. A.52)}$$

$$\tau_i = \sigma^{i-1}\tau_1 \qquad \text{(Eq. A.53)}$$

and $m = 0.635$ and $\alpha = 10.0$.

Then, the remaining stress dependent parameters E_o, E_1, and τ_1 are approximated following curve fitting to the experimental creep data as

$$E_o = a_o \exp\left(-a_1\sigma_n^3\right) \qquad \text{(Eq. A.54)}$$

$$E_1 = b_o + b_1 \exp\left(-\frac{\sigma_n}{b_2}\right) \qquad \text{(Eq. A.55)}$$

$$\tau_1 = c_o \exp\left(c_1 + c_2\sigma_n + c_3\sigma_n^2 - c_4\sigma_n^3\right) \qquad \text{(Eq. A.56)}$$

Zhang and Moore (1997d) provided the values of the material parameters a_i, b_i, c_i for HDPE obtained from one specific pipe product tested under conventional uniaxial compression. Numerical simulation for a variety of other loadings using the new constitutive model and comparison with measured response indicated that the model was capable of predicting time-dependent behavior of HDPE in uniaxial tests, except where there is strain reversal (Zhang and Moore 1997c).

A.6.2.4.5 Viscoplastic HDPE Modeling. Thermoplastic material response includes both viscoelastic and viscoplastic components starting from very small strain. Zhang and Moore (1997d) developed a viscoplastic model of HDPE adapting the unified theory of Bodner and Partom (1975). According to the theory, both the elastic and inelastic deformation occurs at all stages of loading and unloading. Hence, the total stain rate is decomposed into both the elastic and inelastic parts. For the uniaxial case, the total strain rate can be expressed as

$$\dot{\varepsilon} = \dot{\varepsilon}^e + \dot{\varepsilon}^I \qquad \text{(Eq. A.57)}$$

A strain hardening state variable X is introduced to express the inelastic strain rate for HDPE, with strong rate dependent and work hardening properties,

$$\dot{\varepsilon}^p = C\left(\frac{\sigma}{X}\right)^n \qquad (n \geq 1) \qquad \text{(Eq. A.58)}$$

where C is a scalar factor. The state variable X is a function of inelastic work and inelastic strain rate

$$X = X\left(W^I, \dot{\varepsilon}^I\right) \qquad \text{(Eq. A.59)}$$

Here, the inelastic work, $W^p = \int \sigma d\varepsilon^I$

Several approximations, and trial and error and curve fitting to the experimental data, were used to establish effective parameters for inelastic strain. The study yielded

$$C = 0.01$$

$$n = 8.0$$

$$\frac{X_o}{X} = \alpha + \left\{\frac{\beta}{\gamma + W^p}\right\}^{1/2}$$

$$X_o = 1.0$$

$$\gamma = 10^{-4}\,MPa$$

$$\alpha = d_1 \exp\left\{d_2\left(\dot{\varepsilon}^I\right)^{d_3}\right\}$$

The parameters β, d_1, d_2, and d_3 are constants. Zhang and Moore (1997d) obtained model parameters from the conventional test results for HDPE and implemented them in the numerical simulation of different uniaxial compression tests. The viscoplastic model was found to be superior to the nonlinear viscoelastic model in simulating time-dependent HDPE behavior without strain reversal.

Zhang and Moore (1998) extended their uniaxial models to characterize multiaxial stress states and implemented both the NVE and VP forms into their geometrically nonlinear finite element analysis to study pipe response under parallel plate loading and laboratory hoop compression. Good agreement of the analysis was achieved with the laboratory measurements of pipe response.

Zhang and Moore (1999) also undertook work to model other thermoplastic materials [polypropylene and polyvinyl chloride (PVC)].

A.6.3 Pipe-Soil Interaction Testing

A.6.3.1 Pipe and Material Tests

A.6.3.1.1 Uniaxial Tension Test. Properties of thermoplastic materials in tension are typically determined from the uniaxial tension test as specified in ASTM D638. Standard flat

"dog-bone" specimens are tensioned under defined conditions of pretreatment, temperature, humidity, and testing machine speed. The test specimens are inserted and clamped between the two grips so that the long axis of the specimen coincides with the direction of pull through the centerline of the grip assembly. The grips are self-aligning with inner surfaces deeply scored or serrated to prevent slippage of the specimen. Change of the specimen height is measured either by recording the ram position with the help of the displacement transducer in the machine, or preferably using an extensometer over the test section.

A.6.3.1.2 Uniaxial Compression Test. ASTM D695 provides the specifications for standard test method to determine the compressive properties of thermoplastics. The standard test specimen is a right cylinder (or prism) whose length is twice its diameter (or the least dimension). ASTM-suggested standard specimen sizes include 12.7 mm diameter × 25.4 mm height for cylinder and 12.7 mm × 12.7 mm × 25.4 mm for prism. Load is applied through two load platens having flat parallel surfaces held perpendicular to the long axis of the specimen. Thin polytetrafluoroethylene sheets can be used to make the platen-specimen interface smooth (Zhang and Moore 1997c).

The uniaxial tension and compression tests are useful for qualitative characterization and for research and development to model the mechanical behavior of thermoplastic material.

A.6.3.1.3 Parallel Plate Test. The parallel-plate-loading test is a basic quality control test often performed in the laboratory for flexible pipe. ASTM D2412 provides complete specifications for the test method. A short length of pipe is diametrically compressed between two rigid parallel plates (Figure A-7).

The pipe stiffness (PS) is then calculated from the load-deflection data of the test.

$$PS = F/\Delta Y \qquad \text{(Eq. A.60)}$$

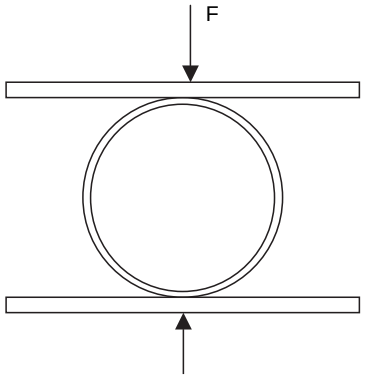

Figure A-7. Parallel plate loading test.

where F is the load and ΔY the change in inside diameter in the direction of load application.

The modulus of elasticity (E) can also be obtained from the parallel plate test, though the test induces a complex 3D pipe response that requires 3D analysis to relate measured response successfully to equivalent 2D parameter such as E (Moore 1994b).

The pipe stiffness is a useful measure for quality assurance/quality control (QA/QC) during manufacturing and may also give some indication of the handling and installation characteristics of the pipe.

A.6.3.1.4 Wall Segment Tests. McGrath and Sagan (2000) devised a simple "axial" compression test for pipe segments to evaluate local wall stability of profile wall thermoplastic pipe. The test specimen, cut from the pipe samples, was compressed between the two end plates of a Universal Testing Machine. The specimen used is a circular arc of the pipe section that includes three cycles of corrugation (Figure A-8). Load, vertical end displacement, and lateral deflection at the center of the specimen are recorded. Different end conditions with neoprene bearing pad, plaster encasement, plywood bracing of crest, and no special bearing have been examined to develop an understanding of the end effects of the tests. They observed local buckling in many sections of the test specimen at loads below the ultimate.

A.6.3.2 Axisymmetric Buried Pipe Tests

Selig, DiFrancesco, and McGrath (1994) developed a test cell to investigate the behavior of buried pipe under hoop compression. Both the hoop-compression and ring-bending stresses are present in a pipe subjected to earth loads. Separate tests for the two stress modes can help identify the pipe performance in each mode. These improve understanding of the soil-pipe system under burial. Parallel-plate loading may be used to evaluate pipe stiffness in ring bending. The devised hoop compression test has provided the ability to examine the performance limits dominated by the hoop stresses. Failure modes that can be reached under hoop compression include circumferential strain, general buckling, and liner and corrugation buckling.

The apparatus consists of a 900-mm diameter cylindrical steel vessel lined with a polymer air bladder. The pipe, instrumented with strain gages and potentiometers, is placed upright and centered in the vessel. A ring of compacted soil is placed in the annulus between the pipe and the bladder. The schematic of the test cell is shown in Figure A-9. The air pressure applied within the bladder offers compressive stress to the pipe through the surrounding soil.

The concept was used in the development of hoop-compression cells at the University of Western Ontario (Moore, Laidlaw, and Brachman 1996). The test facility has

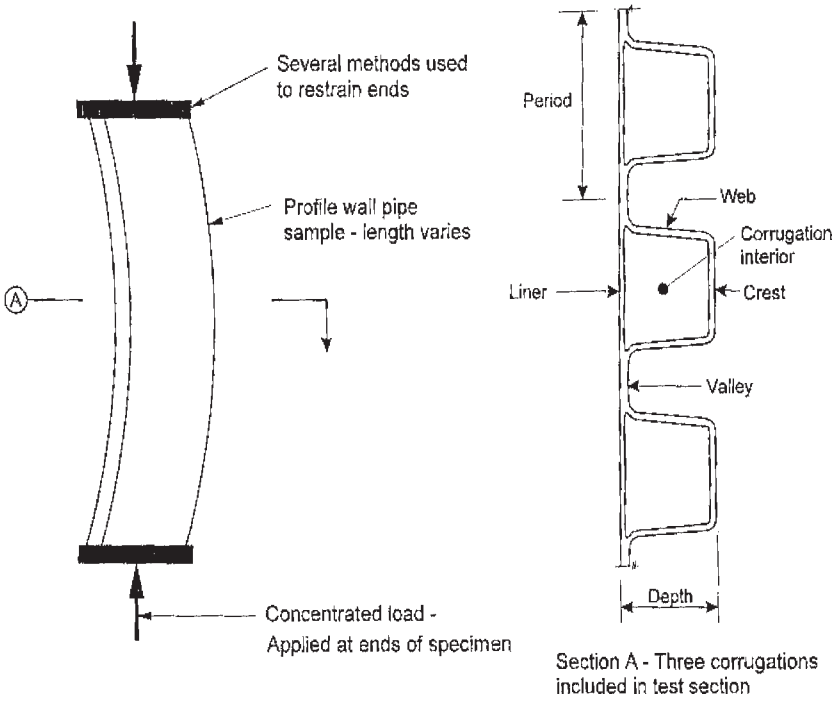

Source: From *NCHRP Report 438: LRFD Specification for Plastic Pipe and Culvert*, Transportation Research Board, Washington D.C., 2000.

Figure A-8. Specimen in the compression test.

the capability of testing several sizes of pipe. Figure A-10 shows the schematic view of the test cell.

A.6.3.3 Multiaxial Buried Pipe Test

A.6.3.3.1 Soil Box Tests. Many researchers have developed and used soil boxes for testing buried pipes and other geotechnical engineering problems in the laboratory. Examples include the facilities at California State University, Sacramento; MIT; the Transportation Research Laboratory at Crowthorne in the United Kingdom; the U.S. Bureau of Reclamation in Denver; and Utah State University. Four specific soil boxes are discussed below in more detail.

The Loughborough University of Technology pipe testing facility comprises a reinforced box as shown in Figure A-11 (Rogers, Fleming, and Talby 1996). The glass panel holds the backfill sand in place and allows the cross section of the pipe to be recorded photographically. The loading is achieved by forcing water into a rubber membrane mounted to the underside of the test box lid. Although the side walls of the test box should be rigid to resemble the zero lateral strain condition, small lateral deflections of the walls were encountered during loading. The test box featured unlubricated sidewalls so that only a portion of the surface load reaches the pipe. Rogers, Fleming, and Talby (1996) used the box to simulate trench installation, since trench walls in practice are rough and also deflect when stressed.

Gaube and Mueller (1981) used a sand box test to determine pipe performance limits (Figure A-12). The sand box is reinforced with steel profiles made up of 5 mm thick sheet. A water-filled car-tire inner bladder is placed on top of the sand surface below the lid of the sand box. The bladder applies surface pressure on the sand and hence on the pipe. Again, the sidewalls were not lubricated, so sidewall friction means that only a portion of the surface pressure reaches the pipe below.

Brachman, Moore, and Rowe (1996) developed a pipe test cell at the University of Western Ontario. The apparatus was designed to model the conditions a buried pipe experiences in the field. The biaxial test cell facilitates examination of pipe response under both the uniform and nonuniform components of earth pressures.

The cell consists of a steel box of dimension 2 m × 2 m × 1.6 m (Figure A-13). The side boundaries are restrained enough to limit deflections so that it represents close to zero-lateral-strain conditions. The rigid lateral boundaries are designed to be far enough away from the pipe to avoid any deviation from the test condition expected in the field. Finite element analysis undertaken during the cell design process indicated that sidewall friction in earlier facilities substantially limits loads from reaching the pipe. Therefore, an extensive side wall treatment was developed involving lubricated polymer sheets to diminish the impact of side friction. Instrumented pipes are placed horizontally at the center and either mid-height or near the base of the cell. The pipe can be backfilled with various soil materials. Uniform vertical pressure is applied at the top of the soil surface by inflating an air bladder placed on the top of the surface below the lid of the box. The cell is designed for vertical soil pressures of up to 1 MPa.

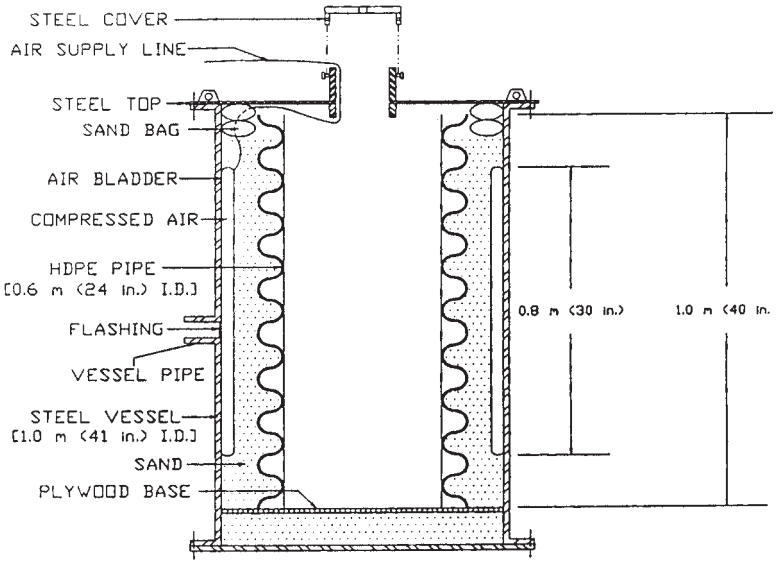

Source: Reprinted, with permission, from *ASTM STP 1222—Buried Plastic Pipe Technology,* 2nd Vol., p. 124, copyright ASTM International, 100 Barr Harbor Drive, West Conshohocken, PA 19428.

Figure A-9. Selig hoop compression cell.

Zoladz, McGrath, and Selig (1996) designed an indoor test facility to investigate pipe installation procedures. The soil box facility can be used to test pipe with outer diameter of approximately 910 mm and trench widths varying from 1.5 to 2.5 times pipe diameter. Figure A-14 illustrates the elements of the test facility. The trench wall stiffness was varied by incorporating foam materials into the wall to model different in situ soil conditions. The pipe and surrounding soil are monitored as the backfill materials are placed and compacted using different degrees of compaction effort. The test plan was to investigate the pipe and soil behavior during installation and backfilling.

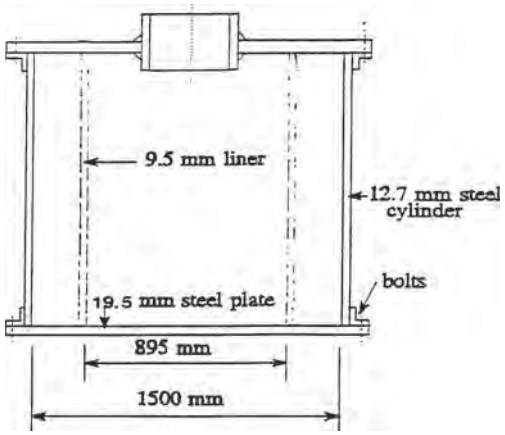

Source: Reprinted from I.D. Moore, T.C. Laidlaw, and R.W.I. Brachman, "Test Cells for Static Pipe Response under Deep Burial," 49th Canadian Geotechnical Conference, St. John's, NF, Canada, 1996.

Figure A-10. Hoop compression cell at UWO.

A.6.3.3.2 Load Frame Testing. A full-scale testing facility was designed and built at Utah State University under the direction of Watkins (Moser 1990, Goddard 1995). A pipe is placed in the cell in a manner similar to field installations. Load is applied at the top soil surface through a series of hydraulic jacks reacting against a load frame until the performance limits are reached. Data thus obtained are directly used in the design of the soil-pipe system.

The test cell at Utah State University is an elliptically shaped vessel made up of steel plate surrounded by reinforced concrete. To date, no analysis has been performed to investigate the impact of the elliptical soil containment system, the sidewall friction, the nonuniform applied vertical forces used at large load levels, and the unrestrained ends of the test facility. Moser et al. (1985) report that the test cell has been calibrated to simulate embankment conditions, and it has subsequently been used to evaluate many different buried pipe products.

The Ohio University cell is a load frame developed for pipe testing (Sargand 1993). Two large hydraulic cylinders acting against a superstructure apply vertical force to a loading platform and thereby to the underlying soil and pipe. The load frame consists of eight W-section steel beams welded together to form a platform of 1.83 m × 2.74 m dimension. The schematic of the test setup is shown in Figure A-15. Pipe backfilled with sand in the test pit is loaded to failure. The test results are used to examine the field performance of pipe. The ultimate load is interpreted as an equivalent height of fill the pipe can sustain. Brachman, Moore, and Rowe (1996) discussed the complex stress state that develops in this facility and procedures needed for test interpretation. Tests in the facility include a study on PVC pipe (Sargand et al. 1995) and 18 tests

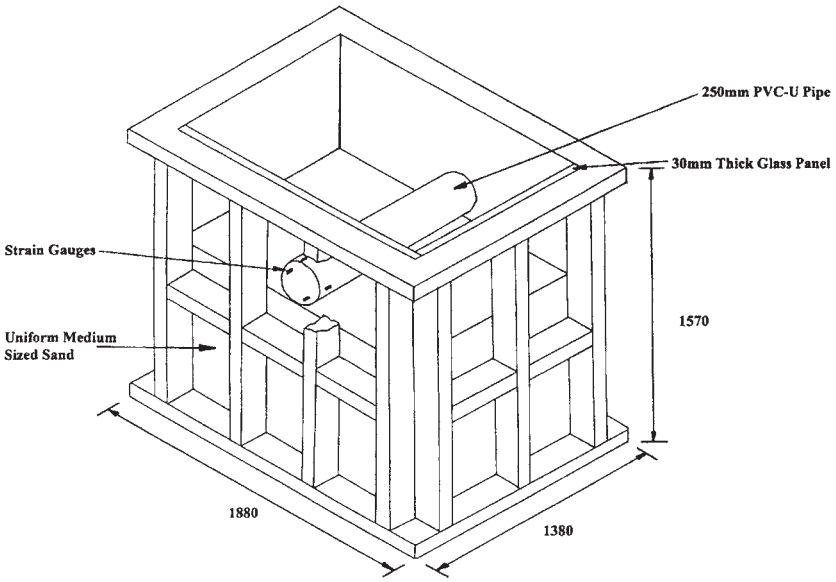

Source: From *Transportation Research Record 1541,* Transportation Research Board, Washington, D.C., 1996, Figure 1, p. 77. Reproduced with permission of TRB.

Figure A-11. Schematic diagram of test cell.

reported in FHWA/OH-98/011 (Sargand, Hazen, and Masada 1998).

A.6.3.4 Field Installations

A.6.3.4.1 Temporary Field Tests. Webb, McGrath, and Selig (1996) carried out full-scale field tests on the campus of the University of Massachusetts at Amherst to investigate the pipe-soil interaction during installation. Different pipes were positioned in test trenches, excavated under undisturbed in situ soil conditions. Observations were made for a variety of backfill materials, trench widths, haunching procedures, and compaction methods. Investigations included pipe shape, pipe strains, interface stresses, soil density, soil strain, and soil pressure. The study demonstrated that the installation condition can have a significant effect on the ultimate response of the pipe. Compaction effort by rammer compactor was reported to be superior to vibrating plate.

A.6.3.4.2 Monitored Field Installations. A test installation of corrugated polyethylene (610 mm diameter) pipe was carried out under high embankment (30.5 m) near Pittsburgh,

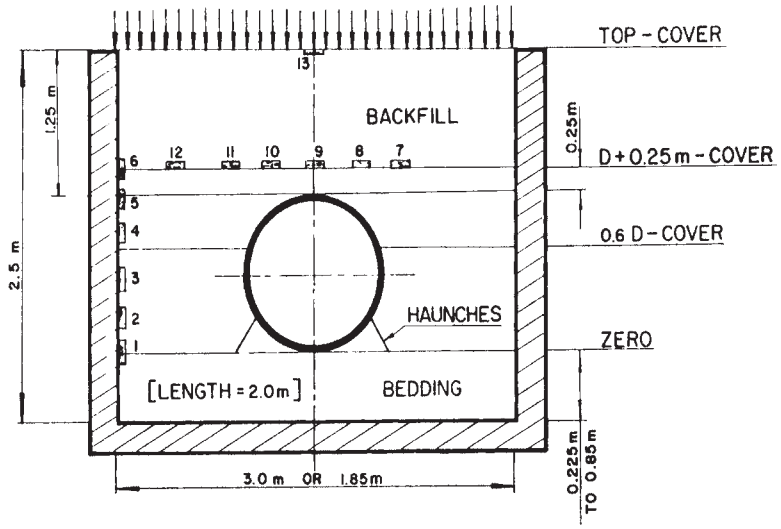

Source: Gaube, E. and Mueller, W., "Twelve Years of Deformation Measurements on Sewer Pipes from Hostalen GM 5010," *International Conference on Underground Plastic Pipes*, American Society of Civil Engineers, New Orleans, LA, 1981. Reprinted with permission from ASCE.

Figure A-12. Sand box test.

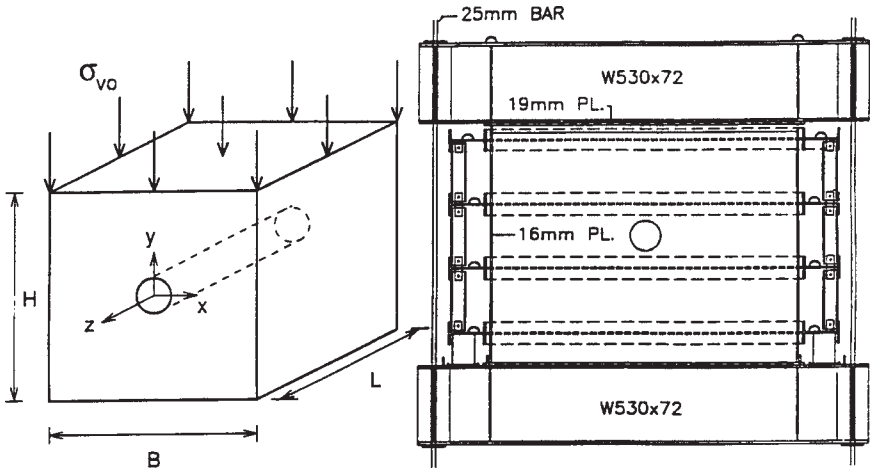

(a) Schematic (b) Elevation

Figure A-13. University of Western Ontario biaxial test cell.

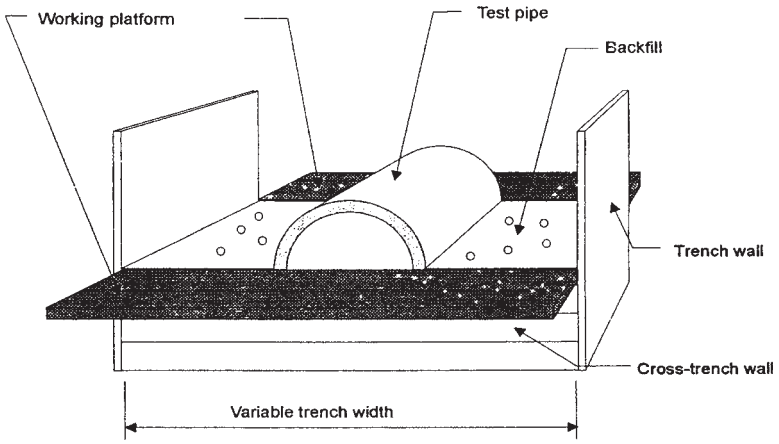

Source: From *Transportation Research Record 1541*, Transportation Research Board, Washington D.C., 1996, p. 87.

Figure A-14. Principal elements of soil box.

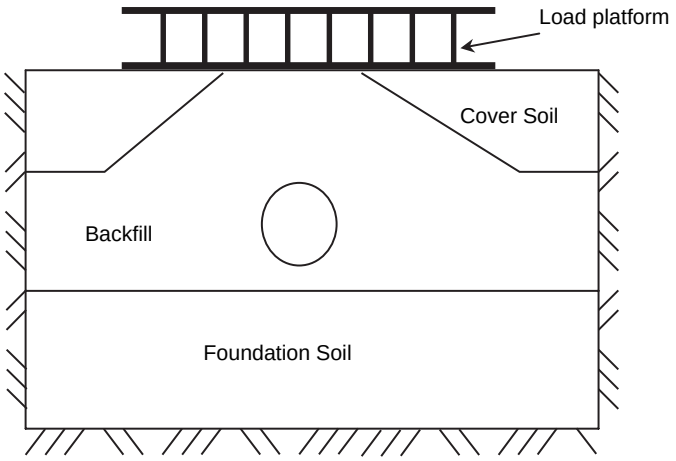

Figure A-15. Setup of Ohio University test facility.

PA (Adam, Muindi, and Selig 1989). Instrumentation measured pipe diameter change, pipe wall strain, vertical soil strain, earth pressures, and the pipe wall temperature. Measurements of short-term loading (during construction) indicated that the increase of horizontal diameter was very small. An average circumferential shortening of 1.2% was observed. Consequently, the contribution of the ring compression was found to dominate the pipe deformation. An earth pressure gauge at the pipe crown indicated much less stress than the free-field overburden pressure (as a result of positive arching under the embankment load). Hashash and Selig (1990) extended the field study. The long-term measurements followed the same trend as the fill height, with only small increases in pipe deformation once embankment construction was completed.

Hurd (1986) inspected field performance of 172 corrugated polyethylene pipe culverts over a four-year period in 21 counties in Ohio. Observations of pipes with different flexibility

factors indicated that the maximum pipe deflections were dependent of flexibility factor, not on the diameter of the pipe. Hurd, Sargand, and Masada (1997) also documented field performance data of honeycombed-HDPE pipe buried under 15.85 m fill at a highway construction site in Ohio. Pipe was instrumented to monitor the pipe strain, earth pressure, and change in horizontal and vertical diameters at mid-length. The installation featured placement of sand over gravel without proper separation. Observation over 386 days showed that the deflection stabilized at values of −10% and +3% for vertical and horizontal pipe deflection, respectively. They also reported localized short-wave deformations. Inner-wall tearing was observed at the springline after placement of 40 ft of fill. Linear elastic solutions and finite element analysis using CANDE-89 were employed to analyze the field performance data. Both analytical methods were partially successful in matching the field performance.

A.7 Quality Assurance/Quality Control Procedures for Thermoplastic Pipe

A.7.1 Introduction

Quality assurance (QA) and quality control (QC), when applied to thermoplastic pipe, are interpreted in many ways, depending on the area of involvement of any specific individual. Parties that will be involved include at least the following:

- Owner (in this case a department of transportation),
- Resin supplier,
- Pipe manufacturer,
- Project designer, and
- Installation contractor.

This project focuses only on a portion of the overall program that would be required to provide proper QA/QC for the complete purchase and installation of thermoplastic pipe, the pipe product itself. A proper QA/QC protocol should provide assurance to a purchaser that the pipe product meets the product standard. This assumes that the product standard includes all relevant testing and guidelines to ensure that a pipe can be reliably designed based on accepted specifications for buried pipe.

A.7.2 Corrugated Polyethylene Pipe Association Proposed Quality Control/Quality Assurance

The Corrugated Polyethylene Pipe Association (CPPA) (1999) has proposed a QA/QC program for consideration to AASHTO. The plan is divided into seven key areas:

1. General,
2. Program requirements,
3. Interface between producer and specifying agency,
4. Sampling and testing procedures,
5. Notification of noncompliant product,
6. Sample identification and record keeping, and
7. Correlation and resolution system.

Each of these seven areas is briefly discussed below.

A.7.2.1 General

The basic CPPA plan places quality control (QC) in the hands of the producer and quality assurance (QA) in the hands of the person specifying the product (the specifying agent). The CPPA proposal states, "It is the intent of this program that acceptance or rejection of product be based on the producer's total quality program" (CPPA 1999).

A.7.2.2 Quality Control/Quality Assurance Program Requirements

The basic requirements of the QA/QC plan are a written QA/QC plan at each plant, approved laboratories, and quality control technicians. The written QA/QC plan of the plant must address responsible personnel; pipe identification; sampling methods; and procedures for QC sample failures, loading, and shipping. The approved laboratory must be able to conduct testing identified in AASHTO M252 and M294.

A.7.2.3 Interface between Producer and Specifying Agency

CPPA proposes that QA/QC is the responsibility of the producer and the monitoring may be completed by the specifying agency to the extent it deems necessary. The specifying agency may require annual registration and certification. Verification of the producer's compliance—which may involve sampling at a producer's facility, review of laboratories, review of technician's qualifications and performance, review of raw materials, and/or inspections—may be scheduled or random. The lot sizes for QC samples are specified. Proper identification and record keeping are required.

The QA/QC plan recognizes that a specifying agency may conduct correlation testing of the producer's material or pipes. Samples collected by the specifying agency from a plant may be tested for the following:

- Density (per ASTM D1505),
- Melt index (per ASTM D1238),
- Pipe stiffness (per ASTM D2412),
- Pipe flattening (per ASTM D2412),

- Brittleness (per ASTM D2444), and
- Joint integrity.

Samples collected by the specifying agency from distribution yards may be tested for the following:

- Brittleness (per ASTM D2444),
- Pipe flexibility (for 10 in. Diameter or smaller AASHTO 252),
- Pipe stiffness (per ASTM D2412), and
- Pipe flattening (per ASTM D2412).

If the specifying agency finds a material or product in noncompliance, additional testing shall be conducted by both the specifying agency and producer. If the agency still finds that the product is noncompliant, then the "resolution system" defined in the final section is undertaken.

A.7.2.4 Sampling and Testing Procedures

This section details steps to be completed by the producer. For every resin lot, the producer must perform the following:

- Density (per ASTM D1505), and
- Melt index (per ASTM D1238).

For each finished pipe, tested once per shift, per diameter, per machine, the producer must perform the following:

- Unit weight, and
- Wall thickness (per ASTM D2122).

All produced pipe must be traceable to the original lot.

If the producer finds noncompliance during testing, then an outside "referee" sample will be conducted. If the "referee" finds the sample in compliance, the sample is deemed acceptable, and the producer resumes normal testing. If the "referee" also finds noncompliance, the producer will investigate to determine the cause of noncompliance. If the cause is attributable to material, sampling, test procedures, or equipment, corrective action may be taken and an additional "referee" sample performed. If the second referee sample indicates compliance, the producer may resume normal testing procedures. If the sample is still in noncompliance, then notification of a noncompliant product should proceed.

A.7.2.5 Notification of Noncompliant Product

If a sample (material or pipe) is determined by the producer not to be in compliance, then notification must be made to the specifying agency and all noncompliant product must be discarded.

A.7.2.6 Sample Identification and Record Keeping

All samples must be properly identified.

A.7.2.7 Correlation and Resolution System

Correlation between producer testing and specifying agency testing will be evaluated to determine the efficacy of the sampling and testing procedures. The resolution system in the CPPA proposal states as follows:

> If any pipe, fitting or coupling, fails to conform with the applicable specification, it may be re-tested to establish conformity. Individual test results will be used to determine conformity. The purchase agreement between the Purchaser and Producer of the product and the requirements of the Specifying Agency will determine the methods utilized to resolve product quality concerns. (CPPA 1999)

A.7.3 North Carolina Department of Transportation Draft HDPE Quality Control/Quality Assurance Plan

The North Carolina Department of Transportation (NCDOT) drew up a draft QC/QA plan in cooperation with the CPPA (North Carolina Department of Transportation 1998). The plan is similar to the CPPA proposal to AASHTO. The plan does indicate that the "referee" samples mentioned in the CPPA proposal will be performed by the DOT. The QA tests to be conducted by the DOT are the same as those listed in the CPPA proposal. Specific QC/QA comparison ranges are given for density, melt index, pipe stiffness, and other tests. If DOT testing is outside of these ranges compared to the producer's test, then an investigation must be performed. The resolution system for disagreements is more clearly outlined in the NCDOT draft plan. During the resolution system, the producer and the DOT take two new samples (twice the number of the original samples). If the samples are in noncompliance with the testing program or the QC/QA comparison ranges, then the DOT may reject them.

A.7.4 Advanced Drainage Systems Quality Control/Quality Assurance Plan

The Advanced Drainage Systems (ADS) QC/QA plan specifically states that AASHTO M252M, AASHTO M294M, and AASHTO MP7 will be used as the quality parameters (Advanced Drainage Systems 1999). The required verification testing via ADS's QA program is as follows:

- Weight (1),
- Material distribution (1),
- Pipe dimensions (1),

- Perforation dimensions (1) (for type "cp"/"sp" only),
- Water inlet area (for type "cp"/"sp" only),
- Pipe stiffness (1),
- Pipe flattening (1),
- Elongation (for type "c"/"cp" only),
- Brittleness (1),
- Environmental stress crack resistance,
- Workmanship (1), and
- Marking (1).

A greater number of tests are required by ADS than in the proposed CPPA QC/QA program. Those tests designated with a "(1)" are tested regularly on production pipe. Identification, process control, and several areas also addressed in the CPPA proposed QC/QA plan are addressed in ADS's plan. The ADS plan specifically requires that each compartment of each railcar of resin be tested for density and melt index.

A.7.5 New Hampshire Department of Transportation Approval Process for Manufacturers of Plastic Pipe

The New Hampshire DOT has a specific approval process (QA plan) for producers of HDPE and PVC pipe. The plan requires the same battery of QC tests required in the CPPA proposal and specifically states that all records must be maintained for a period of five years. The plan does not address additional QA that may be conducted by NHDOT, but rather outlines the QC plan that must be in effect at the producer's plants (New Hampshire Department of Transportation 1997).

A.7.6 Kentucky Department of Transportation Quality Control/Quality Assurance Plan

The Kentucky DOT is currently in the process of finalizing its QC/QA plan for thermoplastic pipe. Discussion with the Kentucky DOT indicates that its efforts to develop a QC/QA plan attempt to address product quality issues as well as installation issues, with the premise that QC/QA for the DOT involves (1) the pipe (producer-DOT QC/QA) and (2) the installation and final adequacy (contractor-DOT-producer QC/QA relationship).

A.7.7 Survey of Installation Quality Control/Quality Assurance Procedures

Amarasiri, Jayawickrama, and Senadheera (1999) report on the current DOT practice for larger diameter HDPE pipe. Based on completed surveys from 32 state DOTs, they report that Georgia, Indiana, Louisiana, North Carolina, Wisconsin, and Wyoming report using mandrel testing. For larger-diameter pipe, mandrel testing is generally not used because access to the pipe is complicated. A large, heavy mandrel must be disassembled and reassembled in the pipe. Thus, Georgia, Indiana, Michigan, New Jersey, North Carolina, and South Carolina allow the use of video cameras to inspect the installation. In a separate document, Minnesota (Minnesota DOT 1998) also requires mandrel testing.

A.7.8 Uni-Bell PVC Performance Specification

Uni-Bell provides a detailed QC/QA plan similar to the CPPA's recent proposal, but examination of Uni-Bell's recommended specifications highlights some QC/QA issues for PVC pipe that are not addressed in the CPPA proposal for HDPE pipe (Uni-Bell 1990). These include the following:

- Joint-integrity testing (per ASTM D3212),
- Impact resistance (per ASTM D2444 and similar to "brittleness" ASTM D2444 for HDPE),
- Air test (no air leak at 3.5 psig for 2 to 5.6 min as a function of diameter),
- Gasket material QC/QA procedures,
- Extrusion quality (per ASTM F1057), and
- Specific guidance on testing of helically wound pipe.

Other tests, dimensions, pipe stiffness and flattening, etc., are similar to those outlined in the CPPA proposal. Even when the test procedures are the same, however, the requirements may be very different for PVC and HDPE.

A.7.9 Fiberglass Pipe Quality Control/Quality Assurance Suggestions

Based on more than 20 years of research and practice experience, Ishai and Lifshitz (1999) recently provided a summary of testing methods required for QA of fiberglass (glass-fiber-reinforced resin, sometimes abbreviated as FRP, GRP, or GFRP) pipes, many of which have diameters as large as several meters. Although many concerns for fiberglass pipe are not the same for thermoplastics, the testing methods may provide guidance on additional QA testing that should be conducted, particularly as the diameters of pipe sizes increase for thermoplastics. The suggested tests for fiberglass pipe are the following:

- Parallel plate test (ASTM D2412),
- Three-point bending test of an arc of pipe (ASTM D790H),
- Three-point bending test of a longitudinal segment of pipe (ASTM D790L),
- Split disk tension test (ASTM D2290),
- Dog-bone tensile test (ASTM D638), and
- Interlaminar shear strength (D2344).

The parallel-plate test is already a standard for thermoplastic pipe. Ishai and Lifshitz argue that for pipe diameters greater

than 800 mm (30 in.), the three-point bending tests of ASTM D790 should be considered for stiffness and strength determination rather than the parallel-plate test. The practicality of testing ever-larger parallel-plate samples has come into question for thermoplastic pipe as well, and D790 may be an alternative already used in practice.

The split disk tension test provides a relatively uniform hoop tension in the pipe and may be more applicable to pressure pipe. The dog-bone tensile test, ASTM D638, is also suggested for common use to assess properties. The interlaminar shear strength test is typically not needed for thermoplastic pipe.

A.7.10 National Transportation Product Evaluation Program

Since the start of this project, an AASHTO National Transportation Product Evaluation Program (NTPEP) has been established to evaluate PE pipe on a regular basis. This program samples pipe at random from manufacturing plants and conducts tests to evaluate compliance with product and material specifications. The program has been very successful and provides an independent check on manufacturing quality.

A.8 References

AASHTO LRFD Bridge Design Specifications, 2nd ed., AASHTO, Washington, D.C., 1998 with 2001 Interim Specifications.

AASHTO LRFD Bridge Design Specifications, 4th ed., AASHTO, Washington, D.C., 2007.

AASHTO Standard Specifications for Highway Bridges, 16th ed., AASHTO, Washington, D.C., 1996.

Abel, J. F., Mark, R., and Richards, R., "Stresses around Flexible Elliptic Pipes," *Journal of the Soil Mechanics and Foundations Division,* Vol. 99, No. SM7, 1973.

Adam, D. N., Muindi, T., and Selig, E. T., "Polyethylene Pipe under High Fill," *Transportation Research Record 1231,* Transportation Research Board, Washington D.C., 1989.

Advanced Drainage Systems, Inc. Quality Control/Assurance Plan, Advanced Drainage Systems, Inc., New Miami, OH, April 1999.

Allgood, J. R. and Takahashi, S. K., "Balanced Design and Finite Element Analysis of Culverts," *Highway Research Record 413,* Highway Research Board, Washington D.C., 1972.

Amarasiri, A., Jayawickrama, P. W., and Senadheera, S. P., "Use of Large Diameter HDPE Pipes in Highway Construction: Current State of Practice," *Proceedings of the Transportation Research Board,* Transportation Research Board, Washington, D.C., 1999.

American Iron and Steel Institute, *Specification for the Design of Cold-Formed Steel Structural Members with Commentary,* American Iron and Steel Institute, Washington, D.C., 1997.

American Society of Civil Engineers, *Structural Plastics Design Manual–ASCE Manual for Practice No. 63,* American Society of Civil Engineers, New York, 1984.

American Water Works Association, *ANSI/AWWA C950-81—AWWA Standard for Glass Fiber Reinforced Thermosetting-Resin Pressure Pipe,* American Water Works Association, Denver, CO, 1981.

American Water Works Association, "Fiberglass Pipe Design," *AWWA Manual of Water Supply Practices M45,* 1st ed., American Water Works Association, Denver, CO, 1996.

ATV 127, *Guidelines for Static Calculation of Drainage Conduits and Pipelines. 2nd ed.,* translated from the German by the James Hardie Co. of Australia, 1988.

Bodner, S. R. and Partom Y., "Constitutive Equations for Elastic-Viscoplastic Strain-Hardening Materials," *Journal of Applied Mechanics,* Vol. 24, 1975.

Booy, C., "Flexible Conduit Studies," Prairie Farm Rehabilitation Administration, Canada Department of Agriculture, Saskatoon, SK, Canada, 1957.

Brachman, R. W. I., Moore, I. D., and Rowe, R. K., "A New Laboratory Facility for Evaluating the Performance of Small Diameter Buried Pipes," *Proceedings of the 1996 Annual Conference of the Canadian Society for Civil Engineering,* Canadian Society for Civil Engineering, Edmonton, Alberta, Canada, 1996.

Brown, F. A. and Lytton, R. L., "Design Criteria for Buried Flexible Pipe," *Pipeline Material and Design,* American Society of Civil Engineers National Convention, San Francisco, CA, 1984.

Bryan, G. H., "On the Stability of a Plane Plate under Thrusts in its Own Plane, with Applications to the Buckling of the Sides of a Ship," *Proceedings of the London Mathematical Society,* Vol. 22, London, 1891.

Burns, J. Q. and Richard, R. M., "Attenuation of Stresses for Buried Cylinders," *Proceedings of Symposium on Soil-Structure Interaction,* University of Arizona, Tucson, 1964.

Carlstrom, B. I., "Structural Design of Underground GRP Pipe," International Conference on Underground Plastic Pipe, American Society of Civil Engineers, New Orleans, LA, 1981.

Carter, J. P. and Balaam, N. P., "AFENA—A General Finite Element Algorithm: Users Manual," School of Civil and Mining Engineering, University of Sydney, Sydney, Australia, 1980.

CEN (European Committee for Standardization), "Comments on DOC 70 E Showing Results of the Calculations Made According to the Calculation Parameters Given in DOC 62 E," CEN/TC 164/165/JWG1 N72E, European Committee for Standardization, Brussels, Belgium, 1991a.

CEN (European Committee for Standardization), "Results on DOC 62 E 'Calculation of Pipes,' " CEN/TC 164/165/JWG1 N70E, European Committee for Standardization, Brussels, Belgium, 1991b.

CEN (European Committee for Standardization), "Proposed General Concept for Searching a 'Unified Calculation Method' for Buried Pipes," CEN/TC 164/165/JWG1 N96E, European Committee for Standardization, Brussels, Belgium, 1992.

CEN (European Committee for Standardization), "Proposed Draft: Plastics Piping System for Non-Pressure Underground Drainage and Sewerage—Structured-Wall Piping Systems of Unplasticized Poly (Vinyl Chloride), (PVC-U), Polypropylene (PP) and Polyethylene (PE), Part 1: Specification and Requirements for Pipes, Fittings and the System," CEN/TC 155 Doc. 155/13 N328, European Committee for Standardization, Brussels, Belgium, 1997.

CEN (European Committee for Standardization), "March 1999 Preliminary Draft, Annex to EN1295-2, Piping Systems—Structural Design of Buried Pipelines (Common CEN Method)," CEN/TC 164/165/JWG1 N214E, European Committee for Standardization, Brussels, Belgium, 1999a.

CEN (European Committee for Standardization), "Structural Design of Buried Pipelines under Various Conditions of Loading—Additional Details about Established Methods," CEN/TC 164/165/JWG1 EN 1295-2, European Committee for Standardization, Brussels, Belgium, 1999b.

Chambers, R. E., McGrath, T. J., and Heger, F. J. *NCHRP Report 225: Plastic Pipe for Subsurface Drainage of Transportation Facilities,* Transportation Research Board, Washington, D.C., 1980.

Chelapati, C. V. and Allgood, J. R., "Buckling of Cylinders in a Confining Medium," *Highway Research Record 413,* Highway Research Board, Washington D.C., 1972.

Cheney, J. A., "Pressure Buckling of Ring Encased in a Cavity," *Journal of Engineering Mechanics,* Vol. 97, No. 2, 1971.

Cheney, J. A., "Buckling of Thin-Walled Cylindrical Shells in Soil," Suppl. Rep. 204, Transport and Road Research Laboratory, Department of the Environment, Crawthorne, Berkshire, United Kingdom, 1976.

Chua, K. M., "Time-Dependent Interaction of Soil and Flexible Pipe," PhD thesis, Texas A&M University, College Station, 1986.

Chua, K. M. and Lytton, R. L., "A New Method of Time-Dependent Analysis for Interaction of Soil and Large Diameter Flexible Pipe," Texas Transportation Institute, Texas A&M University System, *Proceedings of the 66th Annual Meeting of the Transportation Research Board,* Transportation Research Board, Washington D.C., 1987.

Chua, K. M. and Lytton, R. L, "Viscoelastic Approach to Modeling Performance of Buried Pipes," *Journal of Transportation Engineering,* Vol. 115, No. 3, 1989.

Corrugated Polyethylene Pipe Association, *QC/QA Recommendations to AASHTO,* Corrugated Polyethylene Pipe Association, Toledo, OH, June 11, 1999.

DiFrancesco, L. C., "Laboratory Testing of High Density Polyethylene Drainage Pipes," MSc thesis, Department of Civil Engineering, University of Massachusetts, Amherst, 1993.

DiFrancesco, L. C., Selig, E. T., and McGrath, T. J., "Laboratory Testing of High Density Polyethylene Drainage Pipes," *Geotechnical Report No. CPP93-412F,* Department of Civil Engineering, University of Massachusetts, Amherst, 1994.

Duncan, J. M., "Behavior and Design of Long-Span Metal Culverts," *ASCE Journal of the Geotechnical Engineering Division,* Vol. 105, No. GT3, 1979.

Duncan, J. M. and Chang, C-Y, "Nonlinear Analysis of Stress and Strain in Soil," *ASCE Journal of the Soil Mechanics and Foundations Division,* Vol. 96, No. SM5, 1970.

Dunes, C. S. and Butterfield, R., "Flexible Buried Cylinders Part III: Buckling Behavior," *International Journal of Rock Mechanics and Mining Sciences,* Vol. 8, No. 6, 1971.

Einstein, H. H and Schwartz, C. W., "Simplified Analysis for Tunnel Support," *ASCE Journal of Geotechnical Engineering Division,* Vol. 105, GT4, 1979.

Faragher, E., Rogers, C. D. F., and Fleming, P. R., "Laboratory Determination of Soil Stiffness Data for Buried Plastic Pipes," *Transportation Research Record 1624,* Transportation Research Board, Washington, D.C., 1998.

Flugge, W., *Stresses in Shells,* Springer-Verlag, Berlin, Federal Republic of Germany, 1962.

Forrestal, M. J. and Herrmann, G., "Buckling of a Long Cylindrical Shell Surrounded by an Elastic Medium," *International Journal of Solids and Structures,* Vol. 1, 1965.

Gabriel, L. H. and Goddard, J. R., "Curved Beam Stiffness for Thermoplastic Gravity-Flow Drainage Pipes," *Transportation Research Record 1656,* Transportation Research Board, Washington D.C., 1999.

Gaube, E. and Mueller, W., "Twelve Years of Deformation Measurements on Sewer Pipes from Hostalen GM 5010," *International Conference on Underground Plastic Pipes,* American Society of Civil Engineers, New Orleans, LA, 1981.

Gerbault, M., "A Soil-Structure Interactive Model," *Second International Conference on Advances in Underground Pipeline Engineering,* J. K. Jeyepalan and M. Jeyepalan, eds., American Society of Civil Engineers, Bellevue, WA, 1995.

Glascock, B. C. and Cagle, L. L., "Recommended Design Requirements for Elastic Buckling of Buried Flexible Pipe," *Proceedings of the 39th Annual Conference,* Reinforced Plastic/Composites Institute, Society of the Plastic Industry, Inc., Houston, TX, 1984.

Goddard, J. B. A., "A Comparison of the Utah State and Ohio University Soil Cell Tests," *Proceedings of the ORTEC Conference,* Columbus, OH, 1995.

Greenwood, M. E. and Lang, D. C., "Vertical Deflection of Buried Flexible Pipes," *Buried Plastic Pipe Technology,* ASTM STP 1093, G. S. Buczala and M. J. Cassady, eds., American Society for Testing and Materials, West Conshohocken, PA, 1990.

Gumbel, J. E., "Analysis and Design of Buried Flexible Pipes," Ph.D. thesis, University of Surrey, Surrey, England, United Kingdom, 1983.

Gumbel, J. E. and Wilson, J., "Interactive Design of Buried Flexible Pipes—A Fresh Approach from Basic Principle," *Ground Engineering,* Vol. 14, No. 4, 1981.

Hain, H., "Stabilitat von im Boden Eingebetteten Tunnelrorhen mit Kreisformigen Querschnitt [Stability of Soil-Surrounded Tunnel Rings of Circular Cross-Section]," *Strasse Brucke Tunnel,* Vol. 22, Nos. 6 and 8, 1970.

Hardin, B. O., "Characterization and Use of Shear-Stress-Strain Relation for Airfield Subgrade and Base Course Materials," *Technical Report No. AFWL-TR-81-60,* Air Force Weapon Laboratory, Kirtland Air Force Base, NM, July 1971.

Hartley, J. P. and Duncan, J. M., "E′ and Its Variation with Depth," *Journal of Transportation Engineering,* ASCE, Vol. 113, No. 5, 1987.

Hashash, N. M. A., "Design and Analysis of Deeply Buried Polyethylene Drainage Pipes," PhD thesis, Department of Civil Engineering, University of Massachusetts, Amherst, 1991.

Hashash, N. M. A. and Selig, E. T., "Analysis of the Performance of a Buried High Density Polyethylene Pipe," *Structural Performance of Flexible Pipe,* Sergand, Mitchell, and Hurd eds., A. A. Balkema, Rotterdam, Netherlands, 1990.

Heierli, W. and Yang, F. L., "The Static Analysis of Buried Sewer Pipes," *Paper 13, Europipe '82 Conference,* Access Conferences Limited, Basel, Switzerland, 1982.

Hoeg, K., "Stress against Underground Cylinder," *Journal of Soil Mechanics and Foundation Engineering,* Vol. 94, No. SM4, 1968.

Howard, A. K., "Laboratory Load Tests on Buried Flexible Pipe," *Journal of the American Water Works Association,* Vol. 66, No. 9, 1972.

Howard, A. K., "Modulus of Soil Reaction Values for Buried Flexible Pipe," *ASCE Journal of the Geotechnical Engineering Division,* Vol. 103, No. GT1, 1977.

Howard, A. K., "The USBR Equation for Predicting Flexible Pipe Deflection," *International Conference on Underground Plastic Pipe,* American Society of Civil Engineers, New Orleans, LA, 1981.

Howard, A. K., *Pipeline Installation,* Relativity Publishing, Lakewood, CO, 1996.

Hurd, J. O., "Field Performance of Corrugated Polyethylene Pipe Culverts in Ohio," *Transportation Research Record 1087,* Transportation Research Board, Washington D.C., 1986.

Hurd, J. O., Sargand, S. M, and Masada, T., *Performance of Large Diameter HC-HDPE Pipe under Highway Embankment in Ohio,* Paper No. 970894, 76th Annual Meeting, Transportation Research Board, Washington D.C., 1997.

Ishai, O. and Lifshitz, J. M., "Quality Assurance of GFRP Pipes for Seawater Cooling of Power Plants," *Journal of Composites for Construction,* Vol. 3, No. 1, 1999.

Janson, L. E., "Investigation of the Long Term Modulus for Buried Polyethylene Pipes Subjected to Constant Diflection," in *Advances in Underground Pipeline Engineering,* J. K. Jeyapalan, ed., American Society of Civil Engineers, New York, 1985a.

Janson, L. E., "The Relative Strain as a Design Criterion for Buried uPVC Gravity Sewer Pipes," in *Advances in Underground Pipeline Engineering,* J. K. Jeyapalan, ed. American Society of Civil Engineers, New York, 1985b.

Janson, L. E., *Plastics Pipes for Water Supply and Sewage Disposal 4th ed.,* Borealis, Majornas CopyPrint AB, Boras, Sweden, 2003.

Janson, L. E. and Molin, J., "Design and Installation of Underground Plastic Sewer Pipes," International Conference on Underground Plastic Pipes, American Society of Civil Engineers, New Orleans, LA, 1981.

Katona, M. G., *Allowable Fill Heights for Corrugated Polyethylene Pipe,* Paper No. 87-0012, 67th Annual Meeting, Transportation Research Board, Washington D.C., January 1988.

Katona, M. G., "Minimum Cover Heights for Corrugated Plastic Pipe under Vehicle Loading," *Transportation Research Record 1288,* Transportation Research Board, Washington D.C., 1990.

Katona, M. G. et al., "Computer Design and Analysis of Pipe Culvert," *Interim Technical Report 51-040,* FHWA 3-1-1170, U.S. Naval Civil Engineering Laboratory, Port Hueneme, CA, 1974.

Katona, M. G. and Akl, A. Y., "Structural Design of Buried Culverts and Slotted Joints," *Journal of Structural Engineering,* Vol. 113, No. 1, 1987.

Katona, M. G. and Vittes, P. D., "Soil-Structure Analysis and Evaluation of Buried Box-Culvert Designs," *Transportation Research Record 878,* Washington, D.C., Transportation Research Board, 1982, pp. 1–7.

Kienow, K. K. and Prevost, R. C., "Stiff Soils—An Adverse Environment for Low Stiffness Pipe," *Proceedings of the Conference on Pipelines in Adverse Environments II,* San Diego, CA, 1983.

Kloppel, K. and Glock, D., "Theoretische und Experimentelle Untersuchungen zu den Traglastproblem Biegeweichen, in die erde Eingebetter Rohre," Publication No. 10, Institut fur Statik und Stahlbau der Technischen Hochnischen Hochschule, Darmstadt, Federal Republic of Germany, 1970.

Lang, D. C. and Howard, A. K. "Buried Fiberglass Pipe Response to Field Installation Methods," in *Advances in Underground Pipeline Engineering,* American Society of Civil Engineers, New York, 1985.

Levy, M., "Memoire Sur un Nouveau Cas Integrable du Probleme de l'Elastique et l'Une de Ses Applications," *Journal de Math Pure et Applied,* Series 3, Vol. 7, 1884.

Li, H. and Donovan, J. A., *Ring Bending and Hoop Compression Tests on Big 'O' HDPE Pipe,* Department of Civil Engineering, University of Massachusetts, Amherst, 1994.

Luscher, U., "Buckling of Soil-Surrounded Tubes," *Journal of Soil Mechanics and Foundation Engineering,* Vol. 92, No. 6, 1966 (also discussion in Vol. 93, Nos. 2, 3, and 5, 1967, and author's closer on discussion in Vol. 94, No. 4, 1968).

McGrath, T. J., *Design Method for Flexible Pipe,* a report prepared for the Polyethylene Pipe Design Task Group of the AASHTO Flexible Culvert Liaison Committee, Simpson Gumpertz & Heger Inc., Arlington, MA, 1998a.

McGrath, T. J., "Replacing E′ with the Constrained Modulus in Buried Pipe Design," in *Pipelines in the Constructed Environment,* J. P. Castronovo and J. A. Clark, eds., American Society of Civil Engineers, San Diego, CA, 1998b.

McGrath, T. J., "Calculating Loads on Buried Culverts Based on Pipe Hoop Stiffness," *Transportation Research Record 1656,* Transportation Research Board, Washington D.C., July 1999.

McGrath, T. J. and Beaver, J. L., *Performance of Thermoplastic Pipe Under Highway Vehicle Loading,* Research Report to Minnesota DOT, Simpson Gumpertz & Heger Inc., Oakdale, MN, 2005.

McGrath, T. J. and Chambers, R. E., "Field Performance of Buried Plastic Pipe," *Proceedings: Underground Plastic Pipe,* B. J. Schrock, ed., American Society of Civil Engineers, New Orleans, LA, 1981.

McGrath, T. J. and Sagan, V. E., *NCHRP Report 438: LRFD Specification for Plastic Pipe and Culvert,* Transportation Research Board, Washington, D.C., 2000.

McGrath, T. J., Selig, E. T., and DiFrancesco, L. C., *Stiffness of HDPE Pipe in Ring Bending, Buried Plastic Pipe Technology, 2nd. Vol.,* ASTM STP 1222, D. Eckstein, ed., American Society for Testing and Materials, West Conshohocken, PA, 1994.

McGrath, T. J., Selig, E. T., Webb, M. C., and Zoladz, G. V., *Pipe Interaction with the Backfill Envelope,* Publication No. FHWA-RD-98-191, Federal Highway Administration, U.S. Department of Transportation, McLean, VA, June 1999.

Meyerhof, G. G. and Baikie, L. D., "Strength of Steel Culvert Sheets Bearing against Compacted Backfill," *Highway Research Records, No. 30,* Highway Research Board, Washington D.C., 1963.

Miles, R. W. and Schrock, B. J., "Integrated Design Procedure for Flexible Pipe," in *Pipelines in the Constructed Environment,* J. P. Castronovo and J. A. Clark, eds., American Society of Civil Engineers, Reston, VA, 1998.

Minnesota Department of Transportation, *Use of Dual-Wall Corrugated Polyethylene Pipe for Storm Sewer on Trunk Highways,* Technical Memorandum No. 98-24-B-01, Engineering Services Division, Minnesota Department of Transportation, Oakdale, 1998.

Molin, J., "Calculation Principles for Underground Plastic Pipes," *Svenska Vatten-Och Avloppsverksforeningen,* VAV, January 1971, p.16.

Molin, J., "Long Term Deflection of Buried Plastic Sewer Pipes," *Advances in Underground Pipeline Engineering,* American Society of Civil Engineers, New York, 1985.

Moore, I. D., "The Stability of Buried Tubes," PhD thesis, Department of Civil Engineering, The University of Sydney, Sydney, Australia, 1985.

Moore, I. D., "The Elastic Stability of Shallow Buried Tubes," *Geotechnique,* Vol. 37, No. 2, 1987.

Moore, I. D., "Elastic Buckling of Buried Flexible Tubes—A Review of Theory and Experiment," *Journal of Geotechnical Engineering,* Vol. 115, No. 3, 1989a.

Moore, I. D., "Review of Buried Plastic Pipe Design," Research Report 039.05.89, Department of Civil Engineering and Surveying, University of Newcastle, New South Wales, Australia, 1989b.

Moore, I. D., "Influence of Rib Stiffeners on the Buckling Strength of Elastically Supported Tubes," *International Journal of Solids and Structures,* Vol. 26, No. 5/6, 1990a.

Moore, I. D., "Three-Dimensional Response of Elastic Tubes," *International Journal of Solids and Structures,* Vol. 26, No. 4, 1990b.

Moore, I. D., "Structural Design of Profiled Polyethylene Pipe, Part I—Deep Burial," *Geotechnical Research Centre Report, GEOT-8-93,* Faculty of Engineering Science, The University of Western Ontario, London, ON, Canada, 1993.

Moore, I. D., "Local Strain in Corrugated Pipe: Experimental Measurements to Test Numerical Model," *Journal of Testing and Evaluation,* Vol. 22, No. 2, 1994a.

Moore, I. D., "Three Dimensional Time-Dependent Models for Buried HDPE Pipe," *Proceedings of the 8th International Conference on Computer Methods and Advances in Geomechanics,* 2nd Vol., H. J. Siriwardane and M. M. Zaman, eds., A. A. Balkema, Rotterdam, Netherlands, 1994b.

Moore, I. D.,*Three Dimensional Response of Deeply Buried Profiled Polyethylene Pipe,* Paper No. 950822, 74th Annual Meeting, Transportation Research Board, Washington D.C., 1995.

Moore, I. D., *Local Buckling in Profiled HDPE Pipes,* 1996 Annual Conference of the Canadian Society for Civil Engineering, Edmonton, AB, Canada, 1996.

Moore, I. D., "Culverts and Buried Pipelines," in *The Geotechnical and Geoenvironmental Handbook,* R. K. Rowe, ed., Kluwer Academic Publishers, Norwell, MA, 2000.

Moore, I. D. and Booker, J. R., "The Behaviour of Buried Flexible Cylinders under the Influence of Nonuniform Hoop Compression," *International Journal of Solids and Structures,* Vol. 21, No. 9, 1985a.

Moore, I. D. and Booker, J. R., "Simplified Theory for the Behaviour of Buried Flexible Cylinders under the Influence of Uniform Hoop Compression," *International Journal of Solids and Structures,* Vol. 21, No. 9, 1985b.

Moore, I. D., Haggag, A., and Selig, E. T., "Buckling Strength of Flexible Cylinders with Non-Uniform Elastic Support," *International Journal of Solids and Structures,* Vol. 31, No. 22, 1994.

Moore, I. D. and Hu, F., "Response of Profiled High-Density Polyethylene Pipe in Hoop Compression," *Transportation Research Record 1514,* Transportation Research Board, Washington, D.C., 1995.

Moore, I. D. and Hu, F., "Linear Viscoelastic Modelling of Profiled High Density Polyethylene Pipe," *Canadian Journal of Civil Engineering,* Vol. 23, 1996.

Moore, I. D., Laidlaw, T. C., and Brachman, R. W. I., "Test Cells for Static Pipe Response under Deep Burial," 49th Canadian Geotechnical Conference, St. John's, NF, Canada, 1996.

Moore, I. D. and Laidlaw, T. C., "Corrugation Buckling in HDPE Pipes—Measurement and Analysis," No. 970565, *Proceedings of the 76th Annual Meeting of the Transportation Research Board,* Transportation Research Board, Washington D.C., 1997.

Moore, I. D., Selig, E. T., and Haggag, A., *Elastic Buckling Strength of Buried Flexible Culverts,* Transportation Research Board Annual Conference, Session 143, Transportation Research Board, Washington, D.C., 1988.

Moore, I. D. and Selig, E. T., "Use of Continuum Buckling Theory for Evaluation of Buried Plastic Pipe Stability," in *Buried Plastic Pipe Technology,* ASTM STP 1093, G. S. Buczala and M. J. Cassady, eds., American Society for Testing and Materials, West Conshohocken, PA, 1990.

Moore, I. D. and Zhang, C., "Computer Models for Predicting HDPE Pipe Stiffness," *Proceedings of the Annual Conference of the Canadian Society of Civil Engineering,* Ottawa, ON, Canada, 1995.

Moore, I. D. and Zhang, C., "Nonlinear Predictions for HDPE Pipe Response under Parallel Plate Loading," *Journal of Transportation Engineering,* Vol. 124, No. 3, 1998.

Moser, A. P., "Analytical Methods for Predicting Performance of Buried Flexible Pipes," submitted for review to the Transportation Research Board, Washington, D.C., July 29, 1997a.

Moser, A. P., "The Structural Performance of Buried Profile-Wall Pipe and the Influence of Pipe Wall Geometry," submitted for review to the Transportation Research Board, Washington, D.C., July 29, 1997b.

Moser, A. P., *Structural Performance of Buried Profile-Wall High-Density Polyethylene Pipe and Influence of Pipe Wall Geometry,* Paper No. 98-0811, *Transportation Research Record 1624,* Transportation Research Board, Washington, D.C., 1998.

Moser, A. P., *Buried Pipe Design,* McGraw-Hill, Inc., New York, 1990.

Moser, A. P., Bishop, R. R., Shupe, O. K., and Bair, D. R., "Deflection and Strain in Buried FRP Pipes Subjected to Various Installation Conditions," *Transportation Research Record 1008,* Transportation Research Board, Washington, D.C., 1985.

Moser, A. P., Shupe, O. K., and R. R. Bishop, "Is PVC Pipe Strain Limited after All These Years?" in *Buried Plastic Pipe Technology,* ASTM STP 1093, G. S. Buczala and M. J. Cassady, eds., American Society for Testing and Materials, West Conshohocken, PA, 1990.

Mruk, S. A., "The Durability of Polyethylene Piping," in *Buried Plastic Pipe Technology,* ASTM STP 1093, G. S. Buczala and M. J. Cassady, eds., American Society for Testing and Materials, West Conshohocken, PA, 1990.

Mruk, S. A., "More on PE's Long-Term Strain Capacity," private communication with Tim McGrath, 1998.

Musser, S. C., *CANDE-89 User Manual,* Report No. FHWA-RD-89-169, Federal Highway Administration, McLean, VA, 1989.

New Hampshire Department of Transportation, *New Hampshire Department of Transportation Approval Process for Manufacturers of Plastic Pipe,* New Hampshire Department of Transportation, Concord, November 1997.

North Carolina Department of Transportation and Members of the Corrugated Polyethylene Pipe Association, *DRAFT—HDPE Pipe Quality Control/Quality Assurance Program,* North Carolina Department of Transportation, Raleigh, June 1998.

Ozawa, Y. and Duncan, J. M., "ISBILD: A Computer Program for Analysis of Static Stress and Movements in Embankments," geotechnical engineering report, University of California, Berkeley, CA, 1973.

Petroff, L. J., "Installation Technique and Field Performance of HDPE Profile Pipe," *Advances in Underground Pipeline Engineering II,* American Society of Civil Engineers, New York, 1995.

Prevost, R. C., "Flexible Pipe Design Revisited," *Proceedings of the International Conference on Pipeline Design and Installation,* American Society of Civil Engineers, Las Vegas, NV, March 25–27, 1990.

Prevost, R. C. and Kienow, K. K., "Design of Non-Pressure Very Flexible Plastic Pipe," *Advances in Underground Pipeline Engineering,* American Society of Civil Engineers, New York, 1985.

Prevost, R. C. and Kienow, K. K., "Basics of Flexible Pipe Structural Design" *Journal of Transportation Engineering,* Vol. 120, No. 4, 1994.

Roark, R. J., *Formulae for Stress and Strain,* McGraw-Hill, Inc., New York, 1943.

Rogers, C. D. F, "Deformed Shape of Flexible Pipe Related to Surrounding Soil Stiffness," 67th Annual Meeting of the Transportation Research Board, Transportation Research Board, Washington, D.C., January 1988.

Rogers, C. D. F., Fleming, P. R., Loefpky, M. W. J., and Faragher, E., "Structural Performance of Profile-Wall Drainage Pipe—Stiffness Requirements Contrasted with Results of Laboratory Field Tests," *Transportation Research Record 1514,* Transportation Research Board, Washington, D.C., 1995.

Rogers, C. D. F., Fleming, P. R., and Talby, R., "Use of Visual Methods to Investigate Influence of Installation Procedure on Pipe-Soil Interaction," *Transportation Research Record 1541,* Transportation Research Board, Washington, D.C., 1996.

Sargand, S. M., "Structural Performance of an HDPE Leachate Collection Pipe," *Proceedings of the 31st Annual International Solid Waste Exposition,* Solid Waste Association of North America, San Jose, CA, 1993.

Sargand, S. M, Hazen, G. A., Liu, X., Masada, T., and Hurd, J., "Structural Performance of Buried Polyvinyl Chloride Pipes Under Large Distributed Load," *Transportation Research Record 1514,* Transportation Research Board, Washington, D.C., 1995.

Sargand, S. M., Hazen, G. A., and Masada, T., "Structural Evaluation and Performance of Plastic Pipe," FHWA/OH-98/011, Final Report, Ohio Department of Transportation and the Federal Highway Administration, December 1998.

Schluter, J. C., "Large Diameter Plastic Pipe Design," *Advances in Underground Pipeline Engineering,* American Society of Civil Engineers, New York, 1985.

Schluter, J. C. and Capossela, T. A., "The Suitability of Spangler's Iowa Formula for Predicting Deflection in all Flexible Pipes," in *Pipelines in the Constructed Environment,* J. P. Castronovo and J. A. Clark, eds., American Society of Civil Engineers, San Diego, CA, 1998.

Schrock, B. J., "The Pipe/Soil Stiffness Ratio Variable," in *Proceedings Pipeline Infrastructure II,* M. Pickell, ed., American Society of Civil Engineers, San Antonio, TX, 1993.

Selig, E., "Soil Properties for Plastic Pipe Installations" in *Buried Plastic Pipe Technology,* ASTM STP 1093, G. S. Buczala and M. J. Cassady, eds., American Society for Testing and Materials, West Conshohocken, PA, 1990.

Selig, E. T., DiFrancesco, L. C., and McGrath, T. J., "Laboratory Test of Pipe in Hoop Compression," in *Buried Plastic Pipe Technology,* 2nd Vol., STP 1222, D. Eckstien, ed., American Society for Testing and Materials, West Conshohocken, PA, 1994.

Sharff, P. A. and DelloRusso, S. J., "Effects of Acid Environment and Constant Deflection on PVC Sewer Pipe," in *Buried Plastic Pipe Technology,* 2nd Vol., Special Technical Publication 1222, D. Eckstein, ed., American Society for Testing and Materials, West Conshohocken, PA, 1994.

Soini, R., "Interaction between Thermoplastic Pipes and Soft Soil," *Proceedings Europipe '82 Conference,* Access Conferences Limited, Basel, Switzerland, 1982.

Somogy, F. Hutson, R. W., Billione, M. C., and Todres, H. A., "Influence of Depth-of-Cover on Pipe-Soil Interaction" *Advances in Underground Pipeline Engineering,* American Society of Civil Engineers, New York, 1985.

Sonntag, G., "Stabilitat des Elastisch Gebetteren Rohrs unter Aussendruck [Stability of Elastically Embedded Pipe under External Pressure]," *Forsch. Ing. Wes.,* Vol. 32, No. 6, 1966.

Spangler, M. G., "The Structural Design of Flexible Pipe Culverts," *Iowa Engineering Experiment Station Bulletin 153.* Iowa State University, Ames, 1941.

Stevens, G. W. H., "The Stability of a Compressed Elastic Ring and of a Flexible Heavy Structure Spread by a System of Elastic Rings," *Quarterly Journal of Mechanics and Applied Mathematics,* Vol. V, Pt. 2, 1952.

Timoshenko, S., *Theory of Elastic Stability,* McGraw-Hill Book Company, Inc., New York, 1936.

Tohda, J., Hamada, T., Hinobayashi, J., and Inuki, M., "Deformation of HDPE Pipes due to Ground Saturation," *Advances in Underground Pipeline Engineering II,* American Society of Civil Engineers, New York, 1995.

Tohda, J., Yoshimura, H., Morimoto, T., and Seki, H., "Earth Pressure Acting on Buried Flexible Pipes in Centrifuged Models," in *Buried Plastic Pipe Technology,* ASTM STP 1093, G. S. Buczala and M. J. Cassady, eds., American Society for Testing and Materials, West Conshohocken, PA, 1990.

Turkopp, R. C., Torp, S., and Carlstrom, B., "Buried Fiberglass Pipe Performance and Installation Requirements and Design Calculations in International Standardization," *Advances in Underground Pipeline Engineering,* American Society of Civil Engineers, New York, 1985.

Uni-Bell PVC Pipe Association, *Recommended Performance Specifications for Polyvinyl Chloride (PVC) Profile Wall Gravity Sewer Pipe and Fittings Based on Controlled Inside Diameter (Nominal Pipe Sizes 4-48 inch),* Doc. No. UNI-B-9-90, Uni-Bell PVC Pipe Association, Dallas, TX, 1990, http://www.uni-bell.org/pubs/uni-b-9.pdf (accessed April 16, 2008).

Watkins, R. K., "Plastic Pipes under High Landfills," in *Buried Plastic Pipe Technology,* ASTM STP 1093, G. S. Buczala and M. J. Cassady, eds., American Society for Testing and Materials, West Conshohocken, PA, 1990.

Watkins, R. K. and Spangler, M. G., "Some Characteristics of the Modulus of Passive Resistance of Soil, A Study in Similitude," *Highway Research Record 37,* Highway Research Board, Washington, D.C., 1958.

Webb, M. C., McGrath, T. J., and Selig, E. T., "Field Tests of Buried Pipe Installation Procedures," *Transportation Research Record 1541,* Transportation Research Board, Washington, D.C., 1996.

Winter, G. "Strength of Thin Steel Compression Flanges," *Transactions,* ASCE, Vol. 112, 1946.

Zhang, C. and Moore, I. D., "Finite Element Modeling of Non-Linear Time-Dependent Behavior of High Density Polyethylene," *ANTEC'97, Proceedings of the Annual Technical Conference,* The Society of Plastic Engineers, Toronto, ON, Canada, April 1997a.

Zhang, C. and Moore, I. D., "Finite Element Modeling of Inelastic Deformation of Ductile Polymers," *Geosynthetics International,* Vol. 4, No. 2, 1997b.

Zhang, C. and Moore, I. D., "Nonlinear Mechanical Response of High Density Polyethylene, Part I: Experimental Investigation and Model Evaluation," *Polymer Engineering and Science,* Vol. 37, No. 2, 1997c.

Zhang, C. and Moore, I. D., "Nonlinear Mechanical Response of High density Polyethylene, Part II: Uniaxial Constitutive Modeling," *Polymer Engineering and Science,* Vol. 37, No. 2, 1997d.

Zhang, C. and Moore, I. D., "Nonlinear Finite Element Analysis for Thermoplastic Pipes," *Transportation Research Record 1624,* Transportation Research Board, Washington, D.C., 1998.

Zhang, C. and Moore, I. D., unpublished laboratory testing and modelling work on PVC and PP, Geotechnical Research Centre, University of Western Ontario, London, ON, Canada, 1999.

Zoladz, G. V., McGrath, T. J., and Selig, E. T., "Laboratory Tests of Buried Pipe Installation Procedures," *Transportation Research Record 1541,* Transportation Research Board, Washington, D.C., 1996.

APPENDIX B

Laboratory Testing of Finished Pipe

CONTENTS

B.1 Material Tension and Compression Test Behavior

Material tests were conducted to investigate the material properties of representative PVC and HDPE resins used in thermoplastic culvert pipe. The test program was developed with the following objectives:

- Investigate the relative behavior in compression and tension of PVC and HDPE resins used for thermoplastic culvert pipes.
- Investigate strain limits for compression behavior of PVC and PE pipes.

B.1.1 Samples

The tests were, for the most part, conducted on reground pipe resin. Materials used in the tests were supplied by pipe manufacturers. Manufacturer codes and details of the materials supplied are as follows:

- TC-1, PVC, ASTM F949, Cell Class 12454 (for this resin only, tests were conducted on new resin and reground pipe resin),
- TC-2, PVC, ASTM F1803, Cell Class 13364,
- TC-3, PVC Cell Class 13364,
- TC-4, HDPE, AASHTO M294,
- TC-5, HDPE, AASHTO M294, and
- TC-6, HDPE, PE 35430C, B182.6/320kPa.

The PVC resins were characterized for filler content both at Simpson Gumpertz & Heger Inc. (SGH) and the University of Massachusetts (UMass). Both laboratories heated the specimens to approximately 565°C and considered the remaining ash as filler. The results, presented in Table B-1, vary, with UMass finding higher filler contents than SGH. This is likely due to variations in the test method, as SGH used an open muffle furnace to constant weight, while UMass used thermogravimetric analysis.

Compression specimens were produced by reheating ground pipe material and extruding it into a 0.58-in. diameter mold. Specimens were cut to a length of approximately 1.1 in. after cooling. Dimensions of each specimen were measured prior to testing. The compression cylinder specimen height-to-width ratio was kept small to minimize geometric buckling during the tests and ensure true stress-strain behavior.

Table B-1. PVC ignition loss.

Manufacturer	SGH Ash Content (%)	UMass Ash Content (%)
TC-1	4.3	13.7
TC-2	22.4	28.9
TC-3	21.6	31.7

Tension specimens were compression molded in plaques averaging 0.114-in. thickness for the HDPE and 0.123-in. thickness for the PVC. Specimens were cut to the configuration of ASTM D638 Type 1 dog-bone-shaped specimens. Width and thickness of each specimen was measured before testing.

B.1.2 Procedures

Tests were conducted in general accordance with ASTM D638. The test environment was controlled at a temperature of $23 \pm 2°C$ ($73.4 \pm 3.6°F$) and a relative humidity of $50 \pm 5\%$. All tests were conducted on an MTS 133 kN (30,000 lb) capacity universal testing machine. Extensometers were used to monitor strains. The tension tests were conducted with an extensometer on both sides of each specimen to minimize the effect of bending. Due to the small sample size, only one extensometer could be mounted on the compression specimens. As a result, the modulus values are erratic, especially at low strains.

In the compression tests, two Teflon sheets were inserted between the specimen end and the loading platen. This minimized end effects by allowing Poisson expansion during the test.

Tests were run with a constant cross head speed. A total of four speeds were used to achieve strain rates of approximately 100%/min, 10%/min, 1%/min, and 0.1%/min.

B.1.3 Results

The data are summarized in Tables B-2 and B-3 and Figures B-1 and B-2. Results are reported as engineering stress and strain. This results in the compression producing higher strengths and stiffness than the tension tests due to the Poisson effect. Also due to the Poisson effect, the PE materials in compression did not display a true yield point; that is, the stress-strain curve never reached a zero slope. The compression strength reported is the stress at a compression strain of 8%.

Results indicate the following:

- The figures show the known differences between the two resin types; PE stiffness is much more sensitive to strain rate, and PVC is stiffer and stronger than PE.
- Previous assumptions about the compression behavior of PE appear to be appropriate; *NCHRP Report 438* (McGrath and Sagan 2000) concluded that a 4% compression strain limit is appropriate for PE, and the figures show that this is the point where the stress-strain curves deviate significantly to nonlinear behavior; this is consistent with the compression behavior previously reported by Moore and Zhang (1997a, b).
- The PVC stress-strain curves remain reasonably linear to a higher percentage of the yield strength than do the PE curves.

Table B-2. Summary of tension/compression tests.

Compression Tests													
Strength-PVC							Initial Modulus - PVC						
Approx. Rate	TC-1 Regrind	TC-1 New	TC-2	TC-3	Mean	St. Dev.	Approx. Rate	TC-1 Regrind	TC-1 New	TC-2	TC-3	Mean	St. Dev.
(%)	(Mpa)	(Mpa)	(Mpa)	(Mpa)	(Mpa)	(Mpa)	(%)	(MPa)	(MPa)	(MPa)	(MPa)	(MPa)	(MPa)
100	69.3	63.2	67.3	67.8	66.9	2.6	100	2,569	2,422	3,261	2,905	2,789	374
10	59.4	57.7	60.5	63.5	60.3	2.4	10	3,577	2,366	2,630	2,390	2,741	570
1	53.2	50.4	53.4	56.6	53.4	2.6	1	3,420	2,414	2,656	2,484	2,744	463
0.1	49.3	49.4	51.7	52.1	50.6	1.5	0.1	2,601	2,069	3,259	2,051	2,495	570
Strength – PE							Initial Modulus – PE						
Rate	TC-4	TC-5	TC-6		Mean	St. Dev.	Rate	TC-4	TC-5	TC-6		Mean	St. Dev.
100	32.5	32.4	31.8		32.2	0.4	100	2,285		2,233		2,259	37
10	26.9	27.2	26.3		26.8	0.5	10	2,853	1,191	1,081		1,708	993
1	24.3	22.4	23.2		23.3	1.0	1	2,871	1,325	1,327		1,841	892
0.1	20.3	18.9	17.0		18.7	1.7	0.1	1,126	1,043	351		840	425

* No actual strength determined, stress reported at 8% strain

Tension Tests													
Strength – PVC							Initial Modulus – PVC						
Approx. Rate	TC-1 Regrind	TC-2	TC-3		Mean	St. Dev.	Approx. Rate	TC-1 Regrind	TC-2	TC-3		Mean	St. Dev.
(%)	(Mpa)	(Mpa)	(Mpa)		(Mpa)	(Mpa)	(%)	(MPa)	(MPa)	(MPa)		(MPa)	(MPa)
100	48.8	38.0	41.6		42.8	5.5	100	1,817	1,943	2,777		2,179	522
10	42.5	34.4	38.0		38.3	4.0	10	2,175		2,610		2,392	307
1	39.1	33.0	34.7		35.6	3.2	1	2,176	2,158	2,905		2,413	426
0.1	35.1	30.7	30.8		32.2	2.5	0.1	2,152	1,820	2,312		2,095	251
Strength-PE							Initial Modulus – PE						
Rate	TC-4	TC-5	TC-6		Mean	St. Dev.	Rate	TC-4	TC-5	TC-6		Mean	St. Dev.
100	26.4	26.4	24.1		25.6	1.3	100	1,337	1,350	1,267		1,318	45
10	21.7	22.7	20.0		21.5	1.3	10	1,084	1,271	756		1,037	260
1	17.7	17.6	16.0		17.1	0.9	1	680	740	696		705	31
0.1	14.3	14.6	12.5		13.8	1.1	0.1	550	570	433		517	74

Table B-3. Strength and modulus ratios.

Ratio of Compression/Tension Strength – PVC						Ratio of Compression/Tension Modulus – PVC					
Rate (%)	TC-1 Regrind	TC-2	TC-3	Mean	St. Dev.	Rate (%)	TC-1 Regrind	TC-2	TC-3	Mean	St. Dev.
100	1.42	1.77	1.63			100	1.41	1.68	1.05		
10	1.40	1.76	1.67			10	1.64		0.92		
1	1.36	1.62	1.63			1	1.57	1.23	0.86		
0.1	1.41	1.68	1.69			0.1	1.21	1.79	0.89		
Mean	**1.40**	**1.71**	**1.66**	**1.59**			**1.46**	**1.57**	**0.93**	**1.29**	
St. Dev.	**0.03**	**0.07**	**0.03**		**0.15**		**0.19**	**0.30**	**0.08**		**0.34**

Ratio of Compression/Tension Strength – PE						Ratio of Compression/Tension Modulus – PE					
Rate (%)	TC-4	TC-5	TC-6	Mean	St. Dev.	Rate (%)	TC-4	TC-5	TC-6	Mean	St. Dev.
100	1.23	1.23	1.32			100	1.71	0.00	1.76		
10	1.24	1.20	1.31			10	2.63	0.94	1.43		
1	1.37	1.28	1.44			1	4.22	1.79	1.91		
0.1	1.42	1.29	1.36			0.1	2.05	1.83	0.81		
Mean	**1.32**	**1.25**	**1.36**	**1.31**		**Mean**	**2.65**	**1.14**	**1.48**	**1.76**	
St. Dev.	**0.09**	**0.04**	**0.06**		**0.08**	**St. Dev.**	**1.11**	**0.86**	**0.49**		**1.03**

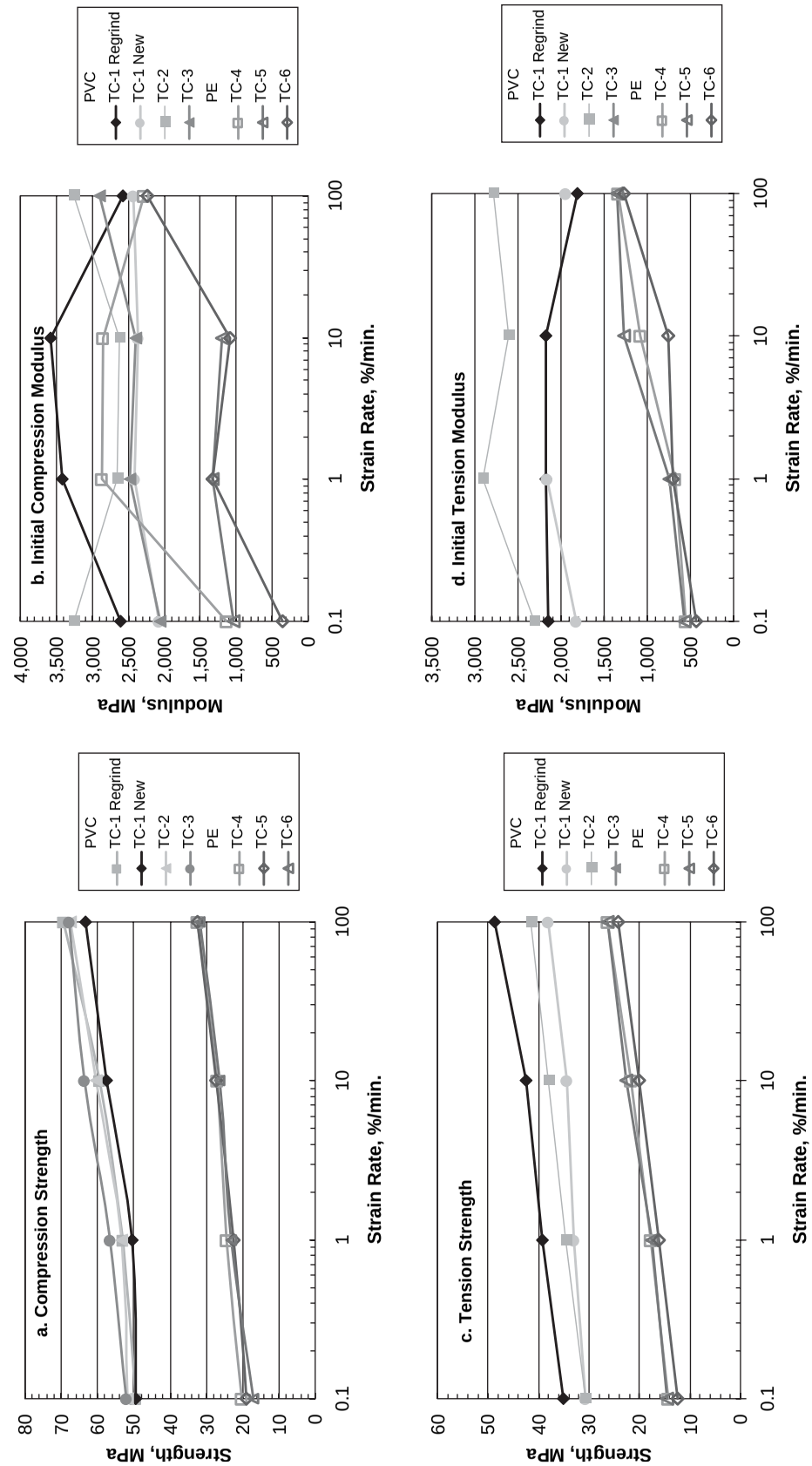

Figure B-1. Comparison of compression and tension parameters.

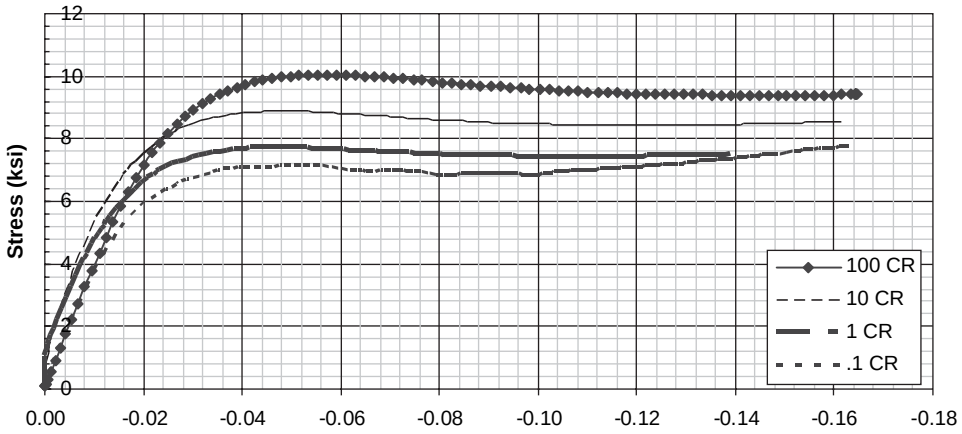

(a) Unfilled resin

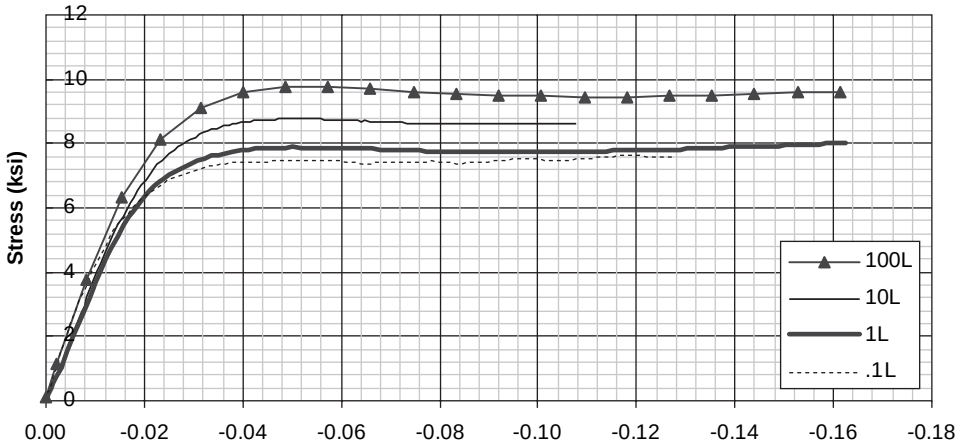

(b) Filled resin

Figure B-2. Compression stress-strain curves for PVC resins.

- For the strain rates considered, the PVC modulus does not change substantially with strain rate. This latter observation is made from the data curves, such as Figure B-2, as the average data in Table B-2 and Table B-3 and Figure B-1 appear more erratic.
- The PVC resins (Cell Class 12454-unfilled and Cell Class 13364-filled) show the known difference in tension strength; however, the compression strengths of these resins are approximately equal, indicating that fillers that disrupt the flow of tensile stresses through the polymer transfer compression stress quite well, much like aggregate in concrete. This suggests that compression strain limits should be set equal for unfilled and filled resins. Stress-strain curves for filled and unfilled PVC resins are shown in Figure B-2.
- The stress-strain curves for both PVC materials remain linear to about 2.5% strain. This suggests a constant limiting compression strain for approved PVC resins.
- The PE moduli, particularly the compression values, are somewhat erratic, likely as a result of having only one extensometer on a small sample.

B.2 Compression Capacity of Profile Wall Pipe

NCHRP Report 438 (McGrath and Sagan 2000) developed a calculation procedure for the capacity of profile wall thermoplastic pipe under compression loads considering local buckling. The proposed procedure was incorporated into the *AASHTO LRFD Bridge Design Specifications* in 2000. During the project, the researchers developed a "stub compression" test to gain an increased understanding of compression behavior and to evaluate the recommended design procedures. The test is shown schematically in Figure B-3. This appendix reports on additional development of the stub compression

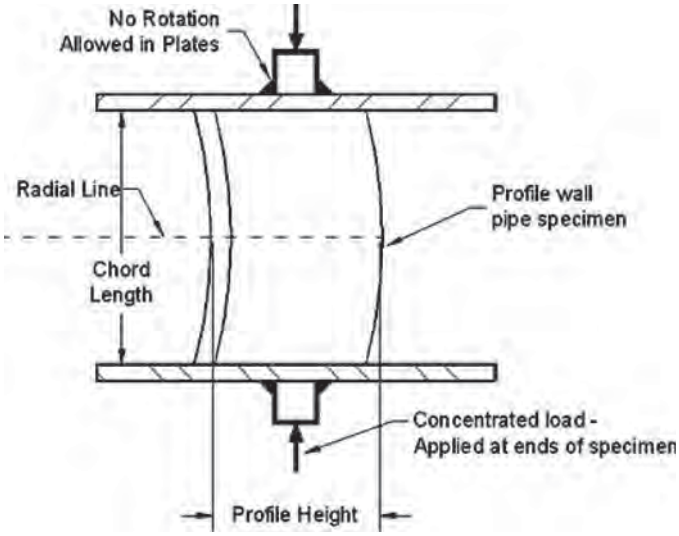

Figure B-3. Schematic of stub compression test.

Figure B-4. Specimen profiles.

test for use as a quality control and/or product qualification test and as a direct determination of the field compression capacity of a profile section. A draft test specification with detailed guidelines on specimen preparation was developed and validated through laboratory round-robin tests (Appendix G).

B.2.1 Phase 1 Stub Compression Tests

Phase 1 stub compression tests were conducted to confirm the findings of *NCHRP Report 438* on a wider range of pipe wall profiles and to further investigate pipe response to stub compression loading. Testing included both a PVC and PE profile wall pipe. This testing was conducted prior to completion of the draft testing specification, and not all parameters reported below are the same as finally recommended in the proposed standard.

B.2.1.1 Specimens

Nineteen profiles were tested, including 13 HDPE and 6 PVC. HDPE specimens were cut from 450-mm to 1,500-mm (18-in. to 60-in.) diameter pipe. The PVC specimens were cut from 350-mm to 900-mm (14-in. to 36-in.) diameter pipe.

Each specimen was given a letter and a number designation. The letter indicates a manufacturer; the number is the nominal inside diameter of the pipe in inches. The HDPE specimens include D18, D24, P24, B24, L24, V24, D30, W30, D36, E42, D48, D60, and E60. The PVC specimens include Z14, X14, J24, C24, Y30, and J36.

Examples of the test specimens are shown in Figure B-4. Cross-sections of the HDPE and PVC specimens are shown in Figure B-5 and Figure B-6 respectively. All specimens were cut to a length that included 15° of the pipe circumference.

Specimens were cut to approximate dimensions from whole sections of pipe. When possible, the specimens were taken from a region approximately 11.25° from a seam, making sure they were free of vent holes, cracks, or other deformations. The specimens were cut to final dimensions using a band saw. After one end of the sample was cut square with the band saw, the end was used as a reference for all other cuts. The section was then cut perpendicular to the corrugations (except for spirally wrapped pipes), taking off approximately ¼ in. from each side until the specimen was the desired length. A recommended procedure for specimen preparation is provided in Appendix G.

B.2.1.2 Test Machine

All tests were conducted using an MTS 133 kN (30,000 lb) capacity universal testing machine with computerized data acquisition, as shown in Figure B-7. The bottom platen of the test fixture was fixed, and the top platen was pinned (in the final draft standard upper and lower platens are both fixed). Load was applied by moving the top platen down at a constant rate of 1.3 mm/min (0.05 in./min). The recorded data included the time, load, crosshead displacement, and tilt (rotation) of the top platen. The stiffness of the test machine and fixtures was determined to be 96.1 MN/m (549,000 lbs/in.) by compressing the platens together and applying a load of 110 kN (25,000 lbs). This stiffness was used to correct the crosshead displacement when determining the specimen deformation.

B.2.1.3 Test Results

A summary of the results of the 19 tests is given in Table B-4.

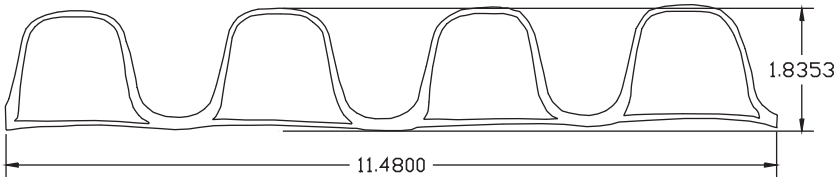

(a) Specimen D18

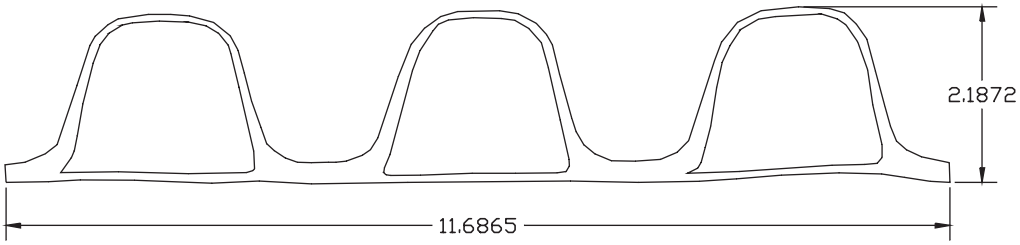

(b) Specimen D24

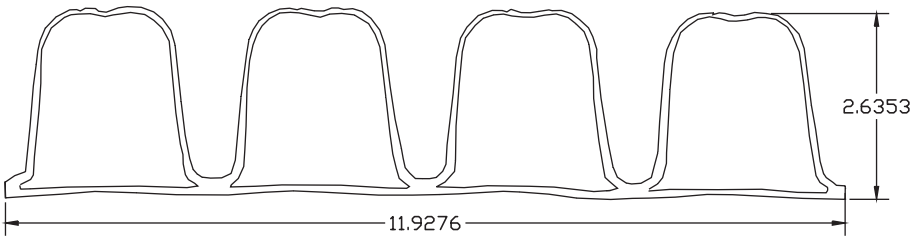

(c) Specimen P24

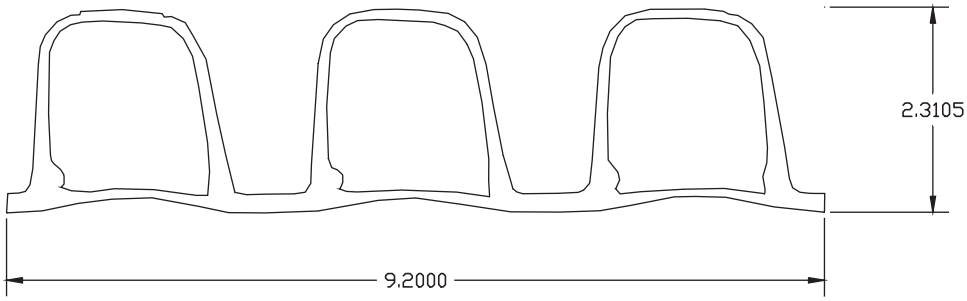

(d) Specimen B24

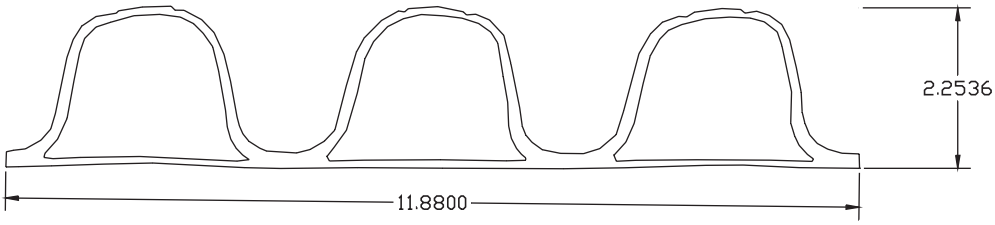

(e) Specimen L24

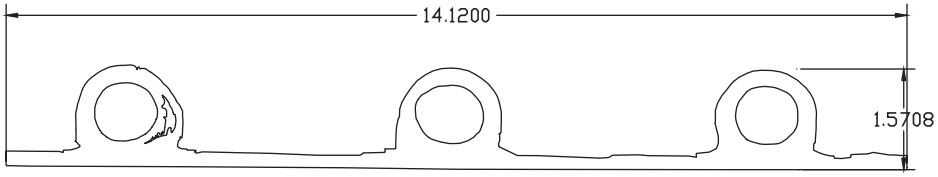

(f) Specimen V24.

Figure B-5. HDPE specimen profiles, in. (1 in. = 25.4 mm).

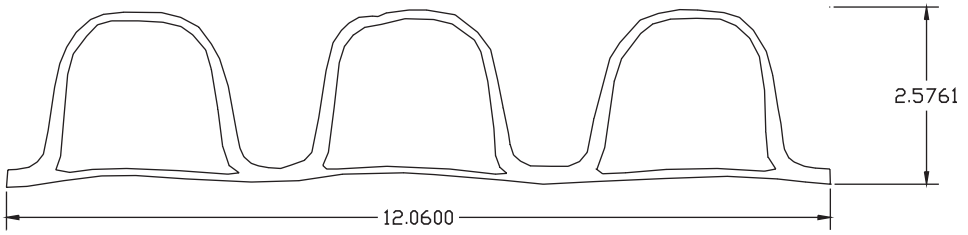

(g) Specimen D30

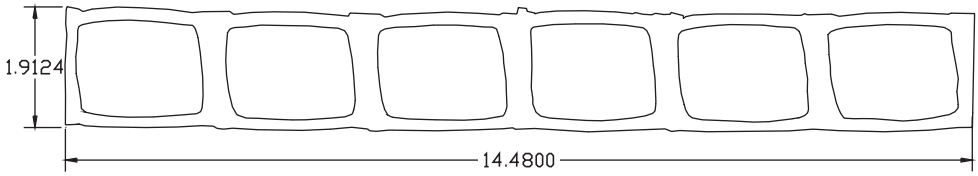

(h) Specimen W30

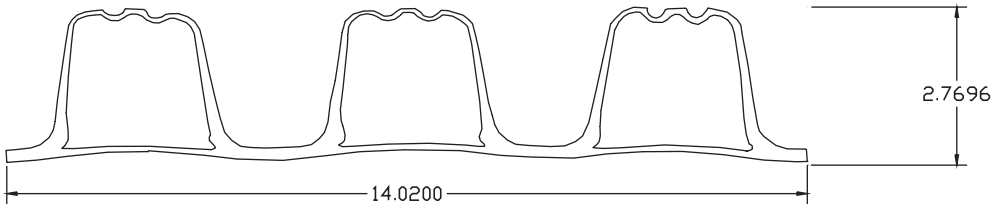

(i) Specimen D36

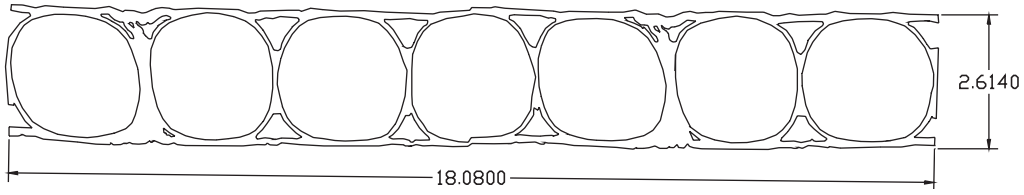

(j) Specimen E42

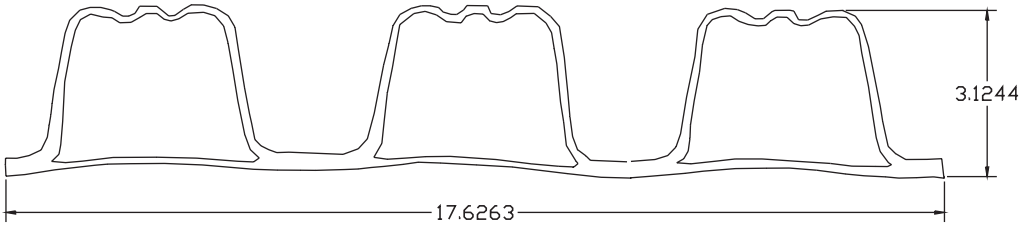

(k) Specimen D48

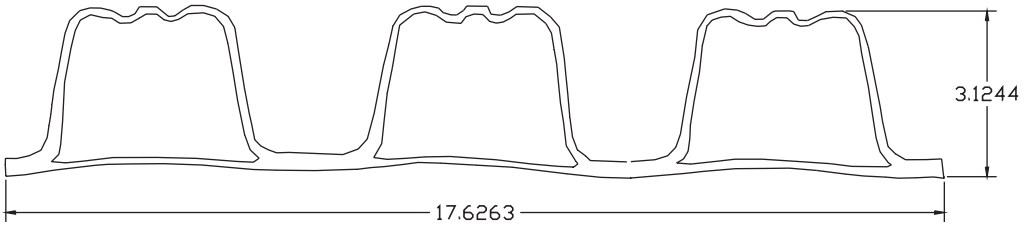

(l) Specimen D60

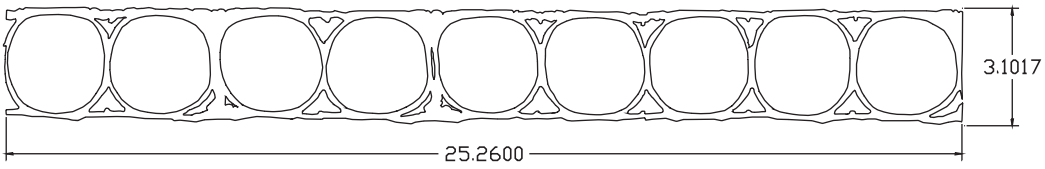

(m) Specimen E60

Figure B-5. (Continued).

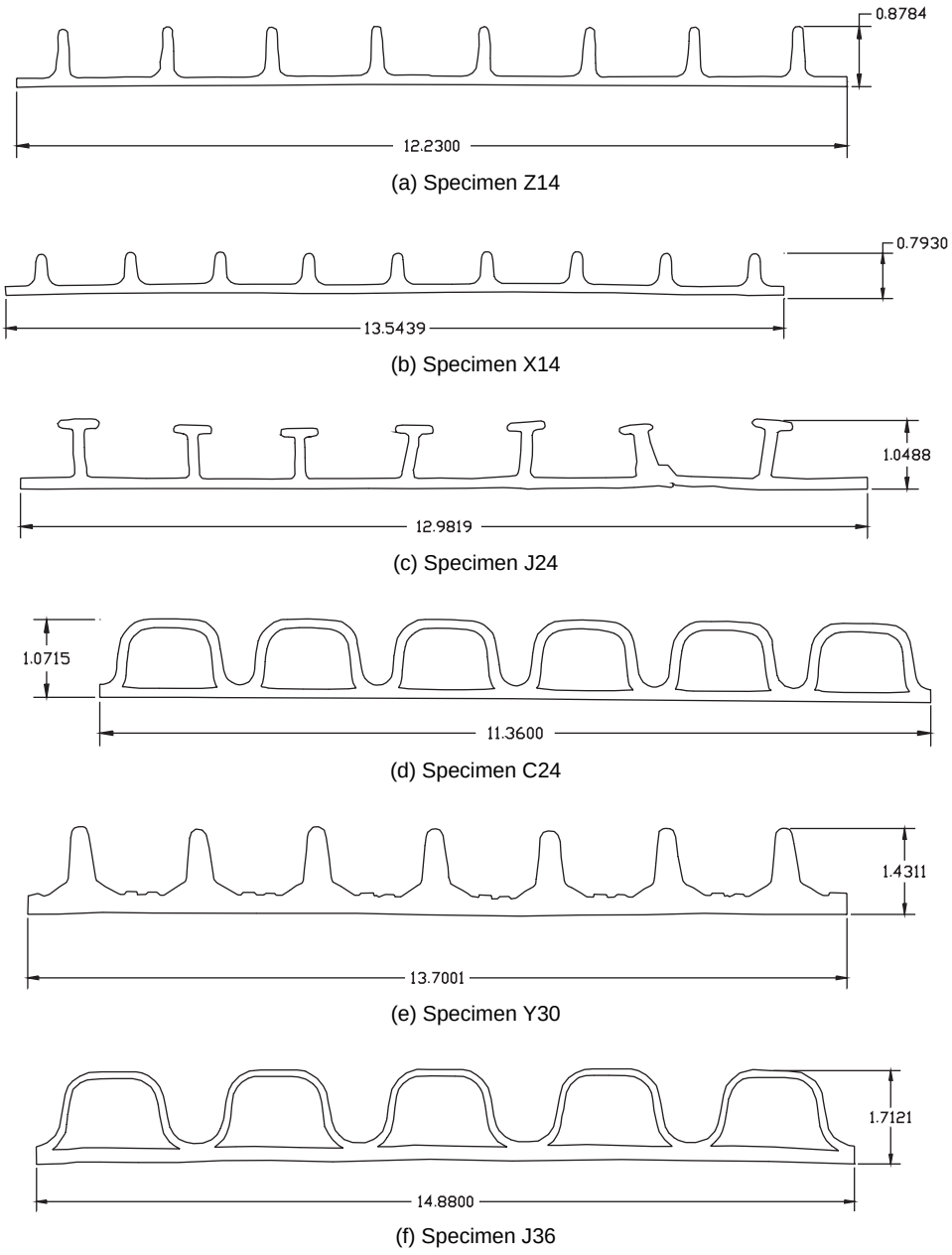

Figure B-6. PVC specimen profiles, in. (1 in. = 25.4 mm).

Typical force versus displacement results are shown in Figure B-8 for PE Specimen D30. Approximately 1.3 mm (0.05 in.) displacement is required to take the slack out of the fixtures, after which the specimen response is initially linear and then transitions to a nonlinear curve, reaches a peak load, and then drops.

The test data are processed by converting units to stress and strain, correcting the toe of the curve for startup variability, and correcting for test machine stiffness. Bending stresses are not calculated, since they are small due to the short specimen height.

B.2.1.4 Test Observations and Discussion

Plots of average stress versus applied strain are provided in Figure B-9 for PE and PVC specimens. The tested HDPE specimens typically reach peak stress between 4% and 6% strain. The tested PVC specimens typically reach peak stress between 3% and 4% strain independently of whether the pipe was manufactured from filled or unfilled resins.

Figure B-10 shows the deformations at failure in Specimens P24, D36, and D60, which formed approximately three buckling half-waves. The entire cross-section, crest, web, and liner,

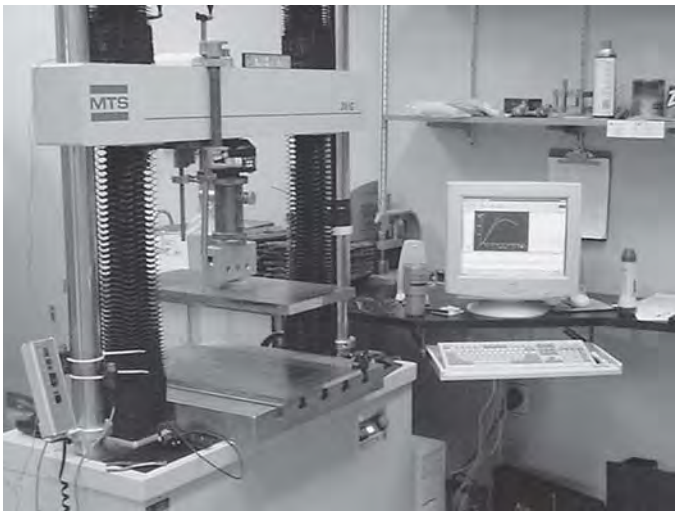

Figure B-7. Test set-up and data acquisition system for stub compression testing.

were engaged in these failures. The most pronounced deformations were observed in the corrugated HDPE profiles.

Figure B-11 shows the deformation in PVC Specimen X14. This specimen has a standing rib, which provides a locally increased capacity, but the portion between the ribs deforms significantly.

Most specimens exhibited some deformation at the crest on the end fixed against rotation. This is consistent with the moment introduced in the specimen by the fixity. However, comparison with calculated capacity, presented later in this appendix, indicates that this local deformation does not significantly affect the overall compression capacity.

B.2.2 Interlaboratory Testing

Following the initial single lab evaluation of the stub compression test, an interlaboratory test program was developed to investigate repeatability within a single lab and for reproducibility across a set of laboratories. Testing was conducted in two stages that included a total of six laboratories. These include one private (P1), two manufacturer (M1 and M2), and three state DOT (DOT1, DOT2, and DOT3) laboratories. Laboratory P1 is the SGH laboratory.

B.2.2.1 Test Procedures and Specimens

Testing complied with the draft standard "Test Method for Determining Compression Capacity of Thermoplastic Profile Wall Pipe by Stub Compression Loading," provided in Appendix G. Two rounds of testing were conducted as follows:

1. SGH prepared all specimens and distributed them to the laboratories, and
2. SGH rough-cut specimens and each laboratory did final preparation and testing.

With this sequence, Round 1 evaluated the equipment procedures and personnel conducting the test, and Round 2 evaluated the ability of the laboratories to produce quality test specimens.

Sample pipes included three HDPE and one PVC pipe. Manufacturer RR1 provided 24-in. diameter pipe, Manufacturer RR2 provided 42-in. diameter pipe, Manufacturer RR3 provided 24-in. and 42-in. diameter pipe, and Manu-

Table B-4. Summary of tested specimens.

Designation	Material	Inside Diameter (in.)	Peak Load (lb/in.)	Average Height (1) (in.)	Time to Peak (s)	Specimen Deflection (in.)	$\varepsilon_{avg.}$ at Peak
D18	PE	18	534	2.570	217.2	0.155	6.0%
D24	PE	24	638	3.405	324.0	0.195	5.7%
P24	PE	24	449	3.322	268.8	0.112	3.4%
B24	PE	24	883	3.415	305.6	0.213	6.2%
L24	PE	24	584	3.329	292.0	0.177	5.3%
V24	PE	24	575	3.304	287.9	0.203	6.1%
D30	PE	30	846	4.196	416.9	0.268	6.4%
W30	PE	30	1311	4.171	409.6	0.236	5.7%
D36	PE	36	786	4.973	380.8	0.236	4.7%
E42	PE	42	1048	5.954	425.6	0.249	4.2%
D48	PE	48	709	6.608	462.4	0.290	4.4%
D60	PE	60	927	8.254	537.5	0.348	4.2%
E60	PE	60	1585	8.121	527.2	0.348	4.3%
Z14	PVC	14	1436	1.940	197.2	0.064	3.3%
X14	PVC	14	1745	1.965	218.0	0.071	3.6%
J24	PVC	24	1600	3.165	218.8	0.097	3.1%
C24	PVC	24	2321	3.249	252.8	0.099	3.1%
Y30	PVC	30	4194	3.987	301.6	0.147	3.7%
J36	PVC	36	3216	4.872	312.8	0.124	2.5%

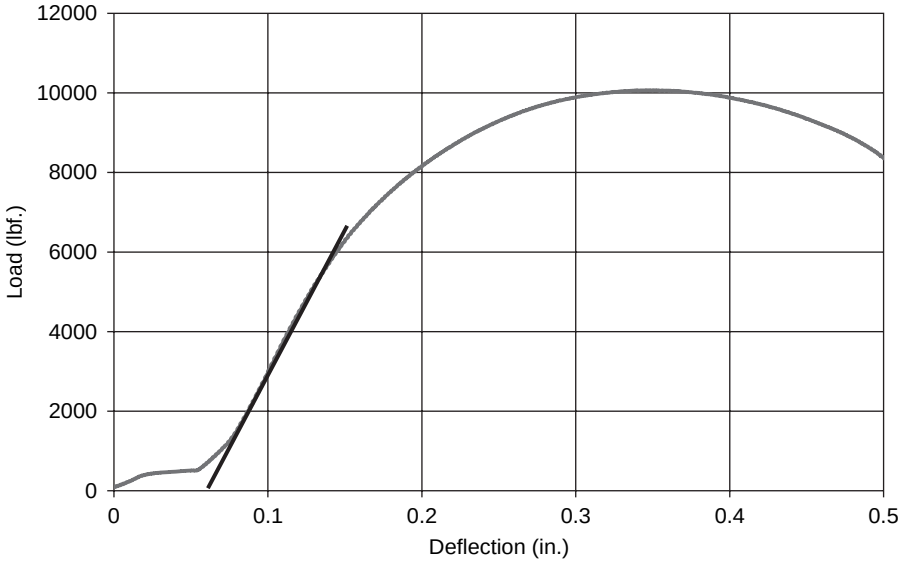

Figure B-8. Specimen D30 unprocessed load versus displacement curve (1 in. = 25.4 mm, 1 lb = 4.45 N, 1 psi = 6.89 kPa).

facturer RR4 provided 24-in. diameter PVC pipe. Figure B-12 shows the four corrugated HDPE profiles considered in the interlaboratory tests, with a scale to give size. Figure B-13 shows the PVC profile.

For Round 1, only HDPE pipe was tested. Each laboratory was supplied with four specimens from each test pipe, cut from locations at 90° intervals around the circumference. In Round 2, the same four pipes, plus the PVC pipe, were tested.

B.2.2.2 Test Results

Tables B-5 and B-6 present results from interlaboratory testing Rounds 1 and 2, respectively. Results include peak load and strain at peak load for each lab and each clock position. The strain at peak load is computed as the crosshead displacement divided by the initial specimen length. Displacement was determined after applying a correction to the toe of the curve. Averages, standard deviations (St. Dev.), and coefficients of variations (COV) are computed for all clock positions for each lab and for all labs at each clock position.

Tables B-2 and B-3 show that all corrugations have a distinct variation in load capacity around the circumference, more pronounced in the HDPE relative to the PVC. This is further illustrated in Figure B-14, which plots the average load for all labs at each clock position divided by the average load for the entire sample set. The figure indicates that the variation for all laboratories at a single clock position is similar to the variation for a single laboratory on a single sample at all clock positions. The figure also illustrates that the variation is not large, with typical values less than 10% from the mean. This observation suggests that testing by multiple laboratories does not introduce any more variation than the inherent variation in the pipe itself.

Results for the two rounds of testing are further summarized in Tables B-7 and B-8 by considering all tests on a pipe as a single dataset.

The tables show that variability of the peak load, measured by the coefficient of variation (COV), is modest. The COV for all tests on a single pipe type has a maximum value of 9.4% in Round 1 and 9.2% in Round 2, indicating no statistical change in the consistency of the results when the labs prepare their own specimens compared to the specimens prepared at SGH. The average loads from both rounds are also substantially the same. The data indicate greater variation in strain at peak load than in the peak load. This is likely due to the variation in specimen heights that results from specimen preparation or due to the load fixtures used at various laboratories and the methods used to account for load fixture stiffness.

Table B-9 presents a summary of the precision of the stub compression tests resulting from the interlaboratory testing.

B.2.3 Repeatability Testing

To evaluate repeatability of the stub compression test, multiple tests were run on specimens from the same sample pipe. Concurrently, tests were conducted (1) to evaluate rotation of the top platen during loading and (2) to determine if a faster load rate might produce more consistent results.

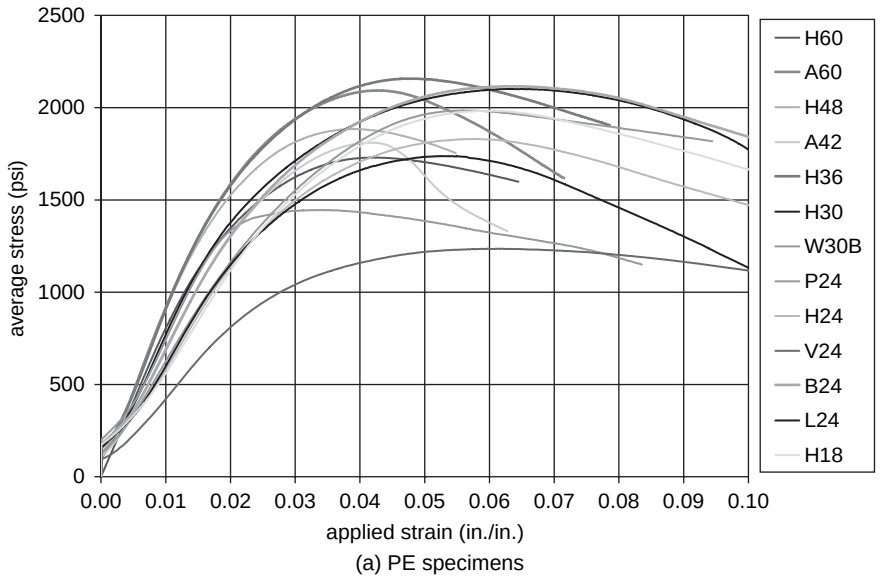

(a) PE specimens

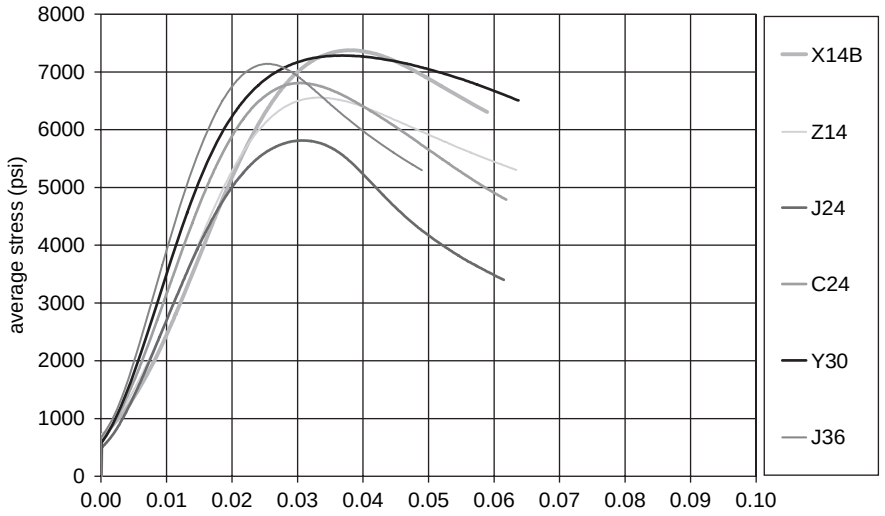

(b) PVC specimens

Figure B-9. Average stress versus applied strain (1 in. = 25.4 mm, 1 lb = 4.45 kN, 1 psi = 6.89 kPa).

B.2.3.1 Test Specimens

Sample pipe was collected in four diameters (36-in., 42-in., 48-in., and 60-in.) from two PE pipe manufacturers and one diameter (24-in.) from one PVC pipe manufacturer. Specimens from one manufacturer are pictured in Figure B-15, including eight from the 36-in. diameter pipe and seven each from 48-in. and 60-in. diameter pipes.

B.2.3.2 Test Procedure

Testing and specimen preparation complied with the "Test Method for Determining Compression Capacity of Thermoplastic Profile Wall Pipe by Stub Compression Loading" in Appendix G. Tests were run past yield to fully characterize the load-deflection behavior. The test start and termination are represented by sample photos in Figure B-16.

In addition to the standard procedure, tests were conducted with the load rate increased to 0.10 in./min from the standard specified rate of 0.05 in./min and with the top platen allowed to rotate to evaluate the effect of end support rotation.

B.2.3.3 Test Results

Results for all tested specimens are provided in Tables B-10 to B-14. Tests on pipe specimens from PE Manufacturer X, 42-in.; PE Manufacturer Y, 36-in.; and PVC Manufacturer Z,

(a) Deformation of P24

(b) Deformation of D36

(c) Deformation of D60

(d) Deformation of D60

Figure B-10. Deformation in stub compression test for HDPE specimens.

Figure B-11. Deformation in stub compression test for a PVC specimen.

24-in.; are used to evaluate rotating versus fixed platen as well as 0.05 in./min versus 0.10 in./min load rate. The tests on specimens from PE Manufacturer Y, 48-in. and 60-in. diameter specimens, were used solely to compare repeatability of the stub compression test.

B.2.3.4 Discussion and Observations

Tables B-15 and B-16 evaluate the consistency of the test with a rotating platen and load rate of 0.05 in./min. The tests were conducted before the natural circumferential variations presented in Figure B-14 had been determined. Considering that variability, the coefficients of variability are relatively small.

Table B-15 provides values for average standard deviation and coefficient of variation for the peak load based on rotating versus fixed platen at the top of the specimen during testing. All specimens in Table B-15 were tested at the specified rate of 0.05 in./min. The results indicate a reduced standard deviation

(a) Sample 24A

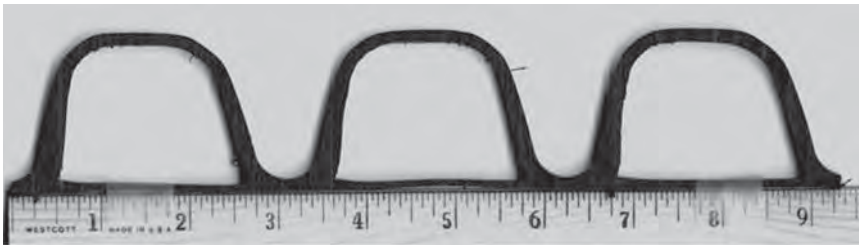

(b) Sample 24C

(c) Sample 42C

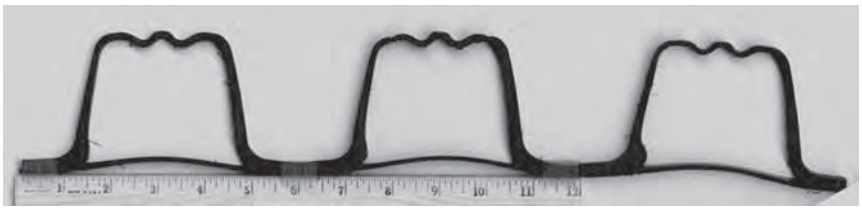

(d) Sample 42B

Figure B-12. Corrugated PE profiles tested in stub compression round-robin.

and coefficient of variation for fixed platen tests, particularly for the PE pipes. The test results also indicate a modestly lower peak load in the tests with fixed top platen.

Based on the increased consistency and uniformity of tests with fixed loading platen, it is recommended that the standard specification include use of fixed platens. The variation in load magnitude is accounted for in the provisions for design using the stub compression test, as discussed in subsequent sections. The fixed-platen configuration is more generally available in testing laboratories.

Figure B-13. PVC profile tested in stub compression round-robin, Sample 24D.

Table B-16 provides values for average standard deviation and coefficient of variation for the peak load rates of 0.05 in./min and 0.10 in./min. All specimens were tested with the top platen fixed against rotation. The results indicate a reduced standard deviation and coefficient of variation for tests conducted at 0.05 in./min. The test results also indicate a lower peak load in the tests with 0.05 in./min that results from the increased creep for the slower load rate and reduced effective modulus. Based on the increased consistency and uniformity of tests conducted with the cross-head rate of 0.05 in./min and

Table B-5. Summary of interlaboratory tests—Round 1.

Peak Load, lb/in.									Strain at Peak Load, %								
Pipe Sample	M1	DOT1	M2	DOT3	P1	All Labs			Pipe Sample	M1	DOT1	M2	DOT3	P1	All Labs		
						Avg.	St. Dev.	COV %							Avg.	St. Dev.	COV %
24A3	793	792	742	691	613	726	76.2	10.5	24A3	8.5	6.1	8.9	6.7	5.4	7.1	1.5	21.3
24A6	805	803	799	724	746	776	37.7	4.9	24A6	8.8	6.6	7.9	6.9	6.4	7.3	1.0	13.5
24A9	670	680	748	682	741	704	37.2	5.3	24A9	8.3	6.1	8.7	6.5	6.0	7.1	1.3	17.9
24A12	708	717	721	661	652	692	32.6	4.7	24A12	7.7	6.2	8.1	6.4	5.5	6.8	1.1	15.9
Average	744	748	753	689	688	724	32.8	4.5	Average	8.3	6.3	8.4	6.6	5.8	7.1	1.2	16.8
St. Dev.	65.6	59.5	33.0	26.3	66.1	Statistics on lab averages			St. Dev.	0.5	0.3	0.4	0.2	0.5	Statistics on lab averages		
COV %	8.8	8.0	4.4	3.8	9.6				COV %	5.5	4.1	5.3	3.3	8.1			
24C3	1,035	1,000	956	854	934	956	69.0	7.2	24C3	12.3	8.1	10.6	8.6	7.8	9.5	1.9	20.4
24C6	1,007	944	904	868	795	903	79.7	8.8	24C6	11.7	7.9	9.6	8.6	6.8	8.9	1.8	20.6
24C9	873	852	861	735	805	825	56.6	6.9	24C9	8.8	6.9	9.7	7.2	6.9	7.9	1.3	16.1
24C12	867	855		787	810	830	37.8	4.6	24C12	10.2	7.0		8.3	6.7	8.0	1.6	19.8
Average	946	913	907	811	836	882	56.5	6.4	Average	10.7	7.5	10.0	8.2	7.1	8.7	1.6	18.5
St. Dev.	88.0	71.9	47.8	61.7	65.8	Statistics on lab averages			St. Dev.	1.6	0.6	0.6	0.7	0.5	Statistics on lab averages		
COV %	9.3	7.9	5.3	7.6	7.9				COV %	14.7	8.2	5.9	8.2	6.9			
42B3	937	960		855	888	910	47.2	5.2	42B3	6.3	4.9		4.8	4.2	5.0	0.9	17.6
42B6	938	955			873	922	43.6	4.7	42B6	6.3	3.9			4.5	4.9	1.2	24.3
42B9	1,049	997		945	901	973	64.1	6.6	42B9	6.7	5.0		5.3	4.3	5.3	1.0	18.9
42B12	1,010	1,023		887	976	974	61.2	6.3	42B12	6.6	4.6		5.6	5.0	5.4	0.9	15.8
Average	984	984		896	909	943	47.2	5.0	Average	6.4	4.6		5.2	4.5	5.2	0.9	17.1
St. Dev.	55.5	32.1		45.2	45.8	Statistics on lab averages			St. Dev.	0.2	0.5		0.4	0.4	Statistics on lab averages		
COV %	5.6	3.3		5.0	5.0				COV %	3.5	10.5		8.4	8.4			
42C3	1,054	1,041		882	950	982	80.8	8.2	42C3	6.3	5.4		5.5	5.7	5.7	0.4	7.1
42C6	962	999		847	1,046	963	84.8	8.8	42C6	7.0	5.2		5.2	5.7	5.8	0.8	14.4
42C9	956	1,040		890	951	959	61.6	6.4	42C9	6.5	5.5		5.5	5.7	5.8	0.5	8.1
42C12	1,156	1,185		1,025	926	1,073	120.0	11.2	42C12	7.8	5.6		5.5	5.9	6.2	1.1	17.5
Average	1,032	1,066		911	968	994	68.7	6.9	Average	6.9	5.4		5.4	5.8	5.9	0.7	11.9
St. Dev.	94.0	81.7		78.3	52.8	Statistics on lab averages			St. Dev.	0.7	0.2		0.1	0.1	Statistics on lab averages		
COV %	9.1	7.7		8.6	5.5				COV %	9.7	2.8		2.8	1.8			

Table B-6. Summary of interlaboratory tests—Round 2.

Peak Load, lb/in.									Strain at Peak Load, %								
Pipe Sample	M1	DOT1	DOT3	DOT2	P1	All Labs			Pipe Sample	M1	DOT1	DOT3	DOT2	P1	All Labs		
						Avg.	St. Dev.	COV %							Avg.	St. Dev.	COV %
24A3	636	663	776	778	613	693	78.73	11.4	24A3	8.2	5.3	5.7	6.3	5.8	6.2	1.1	18.4
24A6	759	853	771	647	746	755	73.78	9.8	24A6	10.1	6.2	5.6	5.9	6.9	6.9	1.8	26.5
24A9	721	817	772	727	741	755	39.52	5.2	24A9	9.2	6.0	6.2	6.8	6.5	7.0	1.3	18.5
24A12	676	698	662	677	652	673	17.31	2.6	24A12	8.7	5.7	5.6	6.9	6.0	6.6	1.3	19.6
Average	698	758	745	707	688	719	30.54	4.2	Average	9.1	5.8	5.8	6.5	6.3	6.7	1.4	20.4
St. Dev.	54	92	55	58	66	Statistics on lab averages			St. Dev.	0.8	0.4	0.3	0.5	0.5	Statistics on lab averages		
COV %	7.7	12.1	7.4	8.2	9.6				COV %	9.0	6.6	5.4	7.3	8.1			
24C3	878	964	881	1,003	934	932	53.97	5.8	24C3	9.9	7.9	7.1	8.7	8.3	8.4	1.0	12.3
24C6	817	897	965		795	869	77.98	9.0	24C6	11.3	7.1	7.0		7.3	8.2	2.1	25.6
24C9	839	853	814	848	805	832	21.05	2.5	24C9	10.1	6.8	6.5	7.8	7.4	7.7	1.4	18.4
24C12	838	1,010	941	995	810	919	90.95	9.9	24C12	9.8	7.8	7.5	8.9	7.2	8.2	1.1	13.1
Average	843	931	900	949	836	892	50.82	5.7	Average	10.3	7.4	7.0	8.5	7.6	8.2	1.3	16.0
St. Dev.	25	70	68	87	66	Statistics on lab averages			St. Dev.	0.7	0.6	0.4	0.6	0.5	Statistics on lab averages		
C.O.V, %	3.0	7.5	7.5	9.2	7.9				COV %	6.8	7.6	5.7	6.8	6.9			
24D3		2,147		2,067	1,957	2,057	95.42	4.6	24D3		5.6		5.3	4.7	5.2	0.5	8.8
24D6		2,118		1,767	1,944	1,943	175.95	9.1	24D6		5.3		6.4	4.7	5.5	0.8	14.9
24D9		2,011		2,126	1,909	2,015	108.56	5.4	24D9		5.5		5.1	4.7	5.1	0.4	7.1
24D12		2,076		1,875	1,898	1,949	109.92	5.6	24D12		6.3		5.1	4.8	5.4	0.8	14.8
Average		2,088		1,959	1,927	1,991	85.36	4.3	Average		5.7		5.5	4.7	5.3	0.5	9.2
St. Dev.		59		167	28	Statistics on lab averages			St. Dev.		0.4		0.6	0.0	Statistics on lab averages		
COV %		2.8		8.5	1.5				C.O.V, %		7.3		11.1	0.6			
42B3		942	957	1,002	888	947	47.22	5.0	42B3		5.9	4.8	7.4	4.8	5.7	1.2	21.7
42B6		876	902	977	873	907	48.55	5.4	42B6		5.9	4.7	6.7	5.2	5.6	0.9	15.4
42B9		856	833	1,087	901	919	115.22	12.5	42B9		5.4	4.5	6.6	4.9	5.3	0.9	16.9
42B12		994	1,009	1,085	976	1,016	47.76	4.7	42B12		6.3	5.4	6.9	5.7	6.1	0.7	11.0
Average		917	925	1,038	909	947	60.60	6.4	Average		5.9	4.9	6.9	5.1	5.7	0.9	16.0
St. Dev.		63	75	56	46	Statistics on lab averages			St. Dev.		0.4	0.4	0.4	0.4	Statistics on lab averages		
COV, %		6.9	8.1	5.4	5.0				COV, %		6.6	8.3	5.5	7.9			
42C3		1,013	933	1,007	950	976	40.06	4.1	42C3		5.8	5.3	5.7	6.3	5.8	0.4	7.0
42C6		1,128		1,066	1,046	1,080	42.68	4.0	42C6		6.4		6.4	6.3	6.4	0.0	0.7
42C9		984		1,021	951	985	35.30	3.6	42C9		5.9		5.9	6.2	6.0	0.2	3.1
42C12		975	940	963	926	951	21.97	2.3	42C12		5.9	5.9	5.4	6.5	5.9	0.4	7.0
Average		1,025	937	1,014	968	986	41.07	4.2	Average		6.0	5.6	5.9	6.3	6.0	0.3	5.0
St. Dev.		70	5	43	53	Statistics on lab averages			St. Dev.		0.3	0.5	0.4	0.1	Statistics on lab averages		
COV %		6.9	0.5	4.2	5.5%				COV %		4.6	8.1	6.9	1.5			

Note: Sample 24D is PVC; all others are HDPE.

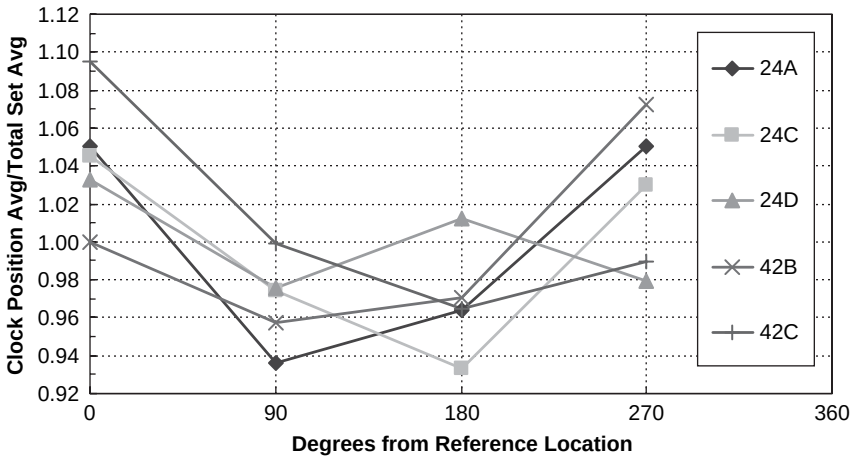

Figure B-14. Variation in stub compression peak load around pipe circumference.

Table B-7. Round-robin results, Round 1, all specimens.

Peak Load, lb/in.				Strain at Peak Load, %			
Sample	Average	St.Dev.	COV, %	Sample	Average	St.Dev.	COV, %
24A	724	55.8	7.7	24A	7.2	1.1	14.7
24C	881	81.0	9.2	24C	8.7	1.6	18.2
42B	946	57.9	6.1	42B	5.4	0.8	14.8
42C	994	93.1	9.4	42C	6.0	0.7	12.0

Table B-8. Round-robin results, Round 2, all specimens.

Peak Load, lb/in.				Strain at Peak Load, %			
Sample	Average	St.Dev.	COV, %	Sample	Average	St.Dev.	COV, %
24A	719	65.3	9.2	24A	6.7	1.3	20.0
24C	889	73.1	8.2	24C	8.1	1.3	16.2
42B	947	77.0	8.1	42B	5.7	0.9	15.6
42C	994	57.7	5.8	42C	6.0	0.4	6.2
24D	1991	118.6	6.0	24D	5.3	0.6	10.7

Table B-9. Test precision for all specimens.

Sample	Material	Average	S_{mean}	S_r	S_R	r	R
24A	HDPE	726	59.1	56.6	49.1	111	96
24C	HDPE	891	76.1	70.8	60.9	139	119
24D	PVC	1991	118.6	84.9	122.5	166	240
42B	HDPE	952	68.8	55.5	59.4	109	116
42C	HDPE	998	80.5	65.1	60.9	128	119

	Standard Deviation of Averages	Repeatability Standard Deviation	Reproducibility Standard Deviation	Repeatability Limit (95%)	Reproducibility Limit (95%)
24A	8.1	7.8	6.8	15.3	13.3
24C	8.5	7.9	6.8	15.6	13.4
24D	6.0	4.3	6.2	8.4	12.1
42B	7.2	5.8	6.2	11.4	12.2
42C	8.1	6.5	6.1	12.8	12.0

Note:
1. Terms are as specified in ASTM E 177-90a – Standard Practice for Use of the Terms Precision and Bias in ASTM Methods, ASTM, West Conshohocken, PA.
2. S_r = standard deviation of repeatability (variation of replicate samples by the same laboratory).
3. S_R = standard deviation of reproducibility (variation between laboratories).
4. Precision statistics as percent of average.

Figure B-15. PE test specimens for intralaboratory repeatability testing.

the higher availability of testing facilities that can test at the slower rate (based on feedback from labs participating in the interlaboratory testing), it is recommended that the standard specification continue to use a test load rate of 0.05 in./min. The variation in load magnitude is accounted for in the provisions for design using the stub compression test, as discussed in subsequent sections.

B.2.4 Calculated Compression Capacity

The procedure for evaluating the capacity of thermoplastic pipe wall sections subject to local buckling was presented in *NCHRP Report 438* and adopted by AASHTO in 2000. The procedures are based on the empirical effective width concept used successfully for many years for design of light-gage steel sections (AISI 1997). The key parameter in this procedure is the ratio of clear width to thickness (w/t) of the individual elements of the profile. Corrugation elements with low w/t ratios are able to develop the full compression capacity of the element; however, as the w/t ratio increases, the element capacity drops. Figure B-17 shows a locally buckled corrugation and schematics to illustrate the section that carries compression loads in the effective width formulation.

The AASHTO LRFD local buckling formulation proceeds through the following steps:

- Quantify the circumferential properties of cross-section area (A), moment of inertia (I), and neutral axis location (c).
- Idealize the cross-section into rectangular elements with length (b) and thickness (t), where the idealized cross-section has A, I, and c of the actual geometry.
- Calculate the peak axial thrust (T) in the pipe wall due to the expected loading.
- Calculate the bending moment (M) in the pipe wall using the maximum allowable deflection.
- Calculate the strain (ε) in the elements of the cross-section based on the idealized rectangular shapes and the calculated thrust and moment.
- Calculate an effective area (A_e) based on the strain and the element width/thickness ratios using the effective width approach for buckling of thin plates.
- Determine a second-order strain in the idealized cross-section elements based on the effective area and the calculated T and M internal force effects.
- Compare the second-order strains to the tension and compression strain limits for the pipe material using load- and resistance-factor design parameters, as appropriate.

The following sections provide design methodologies for thermoplastic pipe that include use of the theoretical local buckling calculation or the stub compression test described in this appendix.

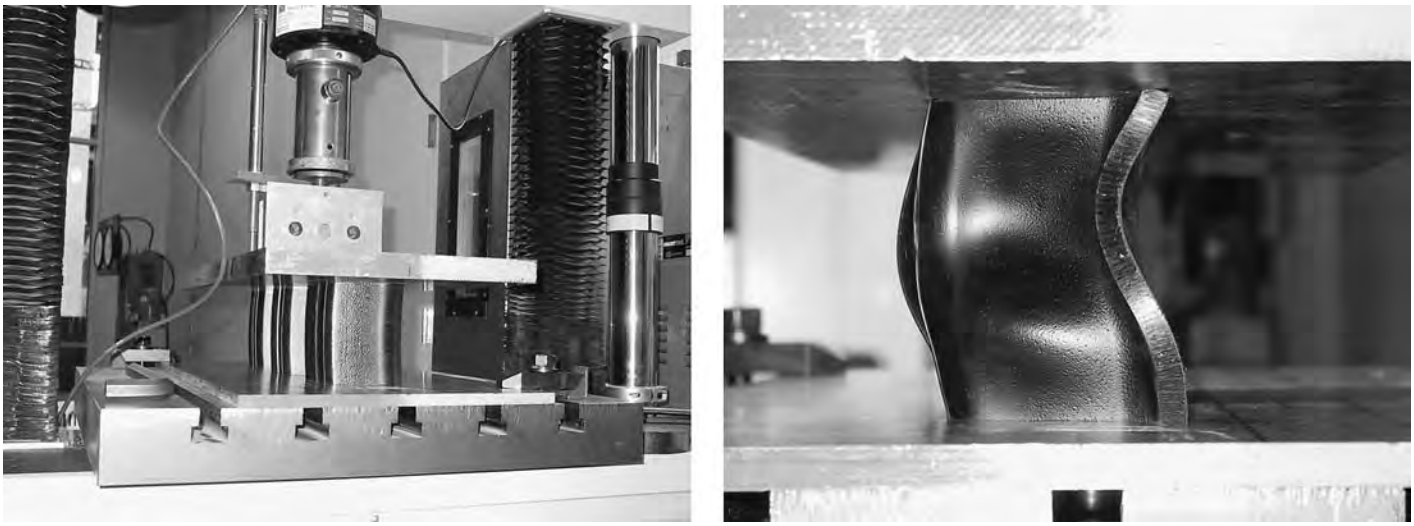

Figure B-16. Typical test start and termination for intralaboratory repeatability testing.

Table B-10. Stub compression—Manufacturer X, 42-in. PE pipe.

Specimen No.	Top Platen Fixity	Crosshead Rate (in./min)	Peak Load (lb)	Peak Load (lb/in.)	Extension at Peak Load (in.)	Extension at Peak Load (in./in.)
1	Fixed	0.05	17,764	1,155	0.264	0.059
2	Fixed	0.05	17,816	1,168	0.280	0.062
3	Rotating	0.05	18,665	1,214	0.329	0.072
4	Rotating	0.05	19,385	1,260	0.352	0.078
5	Fixed	0.10	18,708	1,227	0.282	0.061
6	Fixed	0.10	21,101	1,384	0.300	0.067
7	Fixed	0.10	17,971	1,167	0.236	0.051
Average	Fixed	0.05		1,162		0.060
Std Dev				9		0.002
Average	Rotating	0.05		1,237		0.075
Std Dev				33		0.004
Average	Fixed	0.10		1,259		0.060
Std Dev				112		0.008

Table B-11. Stub compression, test rate 0.05 in./min—Manufacturer Z, 24-in. PVC pipe.

Specimen No.	Top Platen Fixity	Peak Load (lb)	Peak Load (lb/in.)	Extension at Peak Load (in.)	Extension at Peak Load (in./in.)
2	Fixed	22,759	1,889	0.162	0.106
3	Fixed	21,434	1,786	0.143	0.100
4	Fixed	23,526	1,952	0.165	0.109
5	Rotating	23,345	1,945	0.137	0.090
6	Rotating	24,823	2,060	0.152	0.099
7	Rotating	22,306	1,851	0.146	0.094
Fixed	Average		1,876		0.105
	Std. Deviation		84		0.005
Rotating	Average		1,952		0.095
	Std Deviation		105		0.005

Table B-12. Stub compression—Manufacturer Y, 36-in. PE pipe.

Specimen No.	Top Platen Fixity	Crosshead Rate (in./min)	Peak Load (lb)	Peak Load (lb/in.)	Extension at Peak Load (in.)	Extension at Peak Load (in./in.)
1	Rotating	0.05	12,461	878	0.248	0.060
2	Rotating	0.05	11,829	833	0.214	0.052
3	Rotating	0.05	10,333	728	0.225	0.055
4	Rotating	0.05	10,555	743	0.220	0.054
5	Rotating	0.05	11,664	821	0.258	0.063
6	Rotating	0.05	9,991	704	0.224	0.054
7	Rotating	0.05	10,232	721	0.235	0.057
8	Rotating	0.05	9,574	674	0.195	0.048
9	Fixed	0.05	9,993	709	0.217	0.052
10	Fixed	0.05	10,009	710	0.227	0.055
11	Fixed	0.05	10,294	730	0.230	0.056
12	Fixed	0.10	13,320	947	0.178	0.046
13	Fixed	0.10	12,771	907	0.190	0.049
14	Fixed	0.10	13,332	947	0.195	0.051
Average	Fixed	0.05		763		0.055
Std. Deviation				72		0.005
Average	Rotating	0.05		716		0.054
Std Deviation				12		0.002
Average	Fixed	0.10		933		0.048
Std Deviation				23		0.003

Table B-13. Stub compression—Manufacturer Y, 48-in. PE pipe.

Specimen No.	Top Platen Fixity	Crosshead Rate (in./min)	Peak Load (lb)	Peak Load (lb/in.)	Extension at Peak Load (in.)	Extension at Peak Load (in./in.)
1	Rotating	0.05	15,274	878	0.323	0.070
2	Rotating	0.05	14,767	849	0.352	0.075
3	Rotating	0.05	14,924	858	0.360	0.080
4	Rotating	0.05	16,447	945	0.378	0.082
5	Rotating	0.05	14,467	831	0.375	0.081
6	Rotating	0.05	19,675	1,131	0.544	0.119
7	Rotating	0.05	19,323	1,110	0.447	0.096
Average	–	–	16,411	943	0.3967	0.086
Std Deviation	–	–	2,039	117	0.0696	0.015
COV	–	–	12.4%	12.4%	17.5%	17.7%

Table B-14. Stub compression—Manufacturer Y, 60-in. PE pipe.

Specimen No.	Top Platen Fixity	Crosshead Rate (in./min)	Peak Load (lb)	Peak Load (lb/in.)	Extension at Peak Load (in.)	Extension at Peak Load (in./in.)
1	Rotating	0.05	22,113	941	0.282	0.057
2	Rotating	0.05	22,669	965	0.328	0.065
3	Rotating	0.05	23,564	1,003	0.311	0.063
4	Rotating	0.05	21,991	936	0.290	0.059
5	Rotating	0.05	19,343	823	0.276	0.056
6	Rotating	0.05	20,739	883	0.310	0.062
7	Rotating	0.05	21,226	903	0.272	0.055
Average	–	–	21,664	922	0.30	0.059
Std Deviation	–	–	1,376	59	0.02	0.004
C.O.V.	–	–	6.4%	6.4%	7.1%	6.7%

Table B-15. Stub compression tests for comparison of fixed versus rotating top platen.

Specimen Set	Top Platen Fixity	Count	Avg Pk Load lbs	St. Dev. lbs	COV %
Manufacturer X 42-in. PE	Fixed	2	17,790	37	0.2
	Rotating	2	19,025	509	2.7
Manufacturer Z 24-in. PVC	Fixed	3	22,573	1,058	4.7
	Rotating	3	23,492	1,265	5.4
Manufacturer Y 36-in. PE	Fixed	3	10,099	169	1.7
	Rotating	8	10,830	1,022	9.4

Table B-16. Stub compression tests for comparison of load rate.

Specimen Set	Load Rate (in./min)	Count	Avg Pk Ld	Std Dev	COV
Manuf. X, 42-in.	0.05	2	17,790	37	0.2%
	0.10	3	19,260	1,636	8.5%
Manuf. Y, 36-in.	0.05	3	10,099	169	1.7%
	0.10	3	13,141	320	2.4%

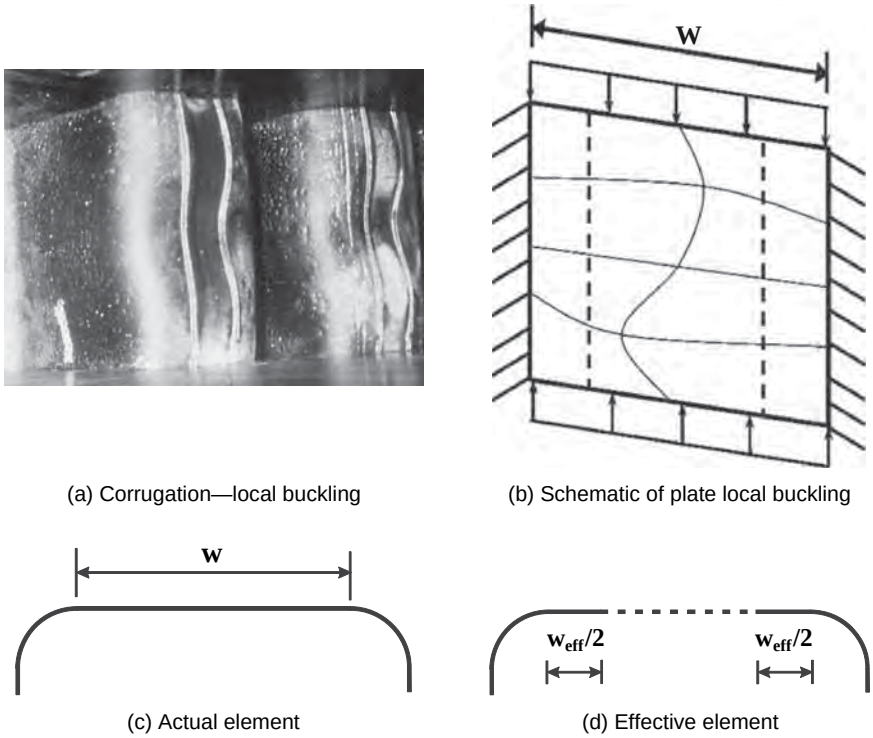

(a) Corrugation—local buckling (b) Schematic of plate local buckling

(c) Actual element (d) Effective element

Figure B-17. Corrugation local buckling (failure mode in stub compression test).

B.2.4.1 Wall Cross-Sectional Properties

Wall cross-sections of corrugated thermoplastic pipes vary around the circumference due to the manufacturing process. This was demonstrated in the stub compression tests reported above (Figure B-14). To evaluate the minimum wall properties, pipe walls should be sectioned at a minimum of three locations spaced uniformly around the circumference. Properties for these sections should be calculated and compared, and the minimum values used for design.

Computer-aided drafting (CAD) and other programs are useful for calculating the section properties from optical scans of pipe sections. Profile sections are cut with a circumferential thickness up to ¼ in. and not less than two corrugations in length. Sections should have an integer number of corrugations and should be cut with the cutting plane radial to the pipe wall. The thin section provides a good visual image for scanning, and the use of multiple corrugations decreases the likelihood of an aberration in the section property measurement by averaging over multiple corrugations.

Figure B-18 shows a section of pipe wall and a specimen for use in obtaining the cross-section properties.

Specimens should be attached to rulers for scanning both to provide scale and a straightening force to restore curling resulting from residual stresses, as evident in Figure B-18**.** The scanned image is imported into the CAD program, scaled by the image of the ruler, and traced using short line segments with visual placement of the line end points around the corrugation shape.

Figure B-19 shows the scanned and CAD tracing images.

The CAD program can then be used to calculate the area, moment of inertia, corrugation depth, period of the corrugation, and section center of gravity location. Figure B-20

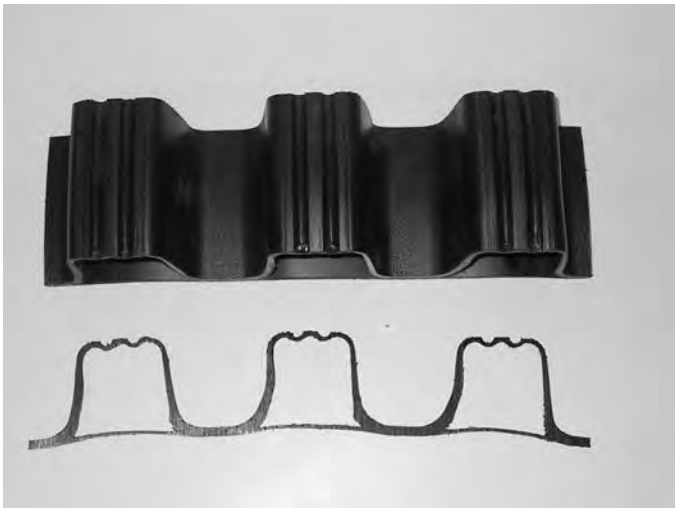

Figure B-18. Specimen cut from pipe wall for section properties.

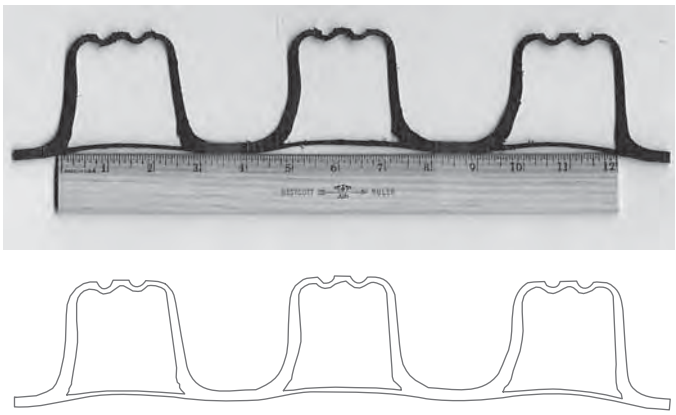

Figure B-19. Scanned specimen for section properties with its CAD tracing.

illustrates this procedure for the center section of the slice in Figure B-19.

B.2.4.2 Corrugation Idealization

General Procedure. After calculating section properties, the corrugation is idealized into rectangular elements that together have the same area, moment of inertia, element widths, element thicknesses, and distances to the inner and outer faces from the center of gravity. This is done by hand or by overlaying rectangular elements on the CAD image of the actual corrugation and calculating section properties. The idealization process includes determination of the unsupported length of each element. This length is combined with the element thickness to quantify the width/thickness ratio for each element. Figure B-21 illustrates idealization of a corrugation.

B.2.4.3 Procedure for Arched Corrugation

Corrugations with curved elements, as shown in Figure B-22a, may not be well represented by the approach described above, and alternate procedures are presented here. The "crest" element of the profile is the curved arch starting where the web elements are no longer primarily straight, as in Figure B-22b. The centroid and area of the arch element are determined for the crest section and a plate with thickness of the crest and length defined by the crest area is placed at the location of the crest centroid. The remainder of the corrugation is idealized as in the general procedure (Figure B-22c). The final idealized shape for the arched corrugation has discontinuous geometry (Figure B-22d). Analysis of the local buckling capacity provides conservative results similar to the general procedure.

B.2.4.4 Typical Idealizations

Figure B-23 provides typical idealized corrugations representing the pipe profiles used for the exploratory stub compression tests in this project.

B.2.4.5 Calculate Design Forces and First Order Strain

The axial thrust at peak load is a direct output of the stub compression test. Bending moment is not included in the calculation, as it is considered minimal for specimens cut as specified in the standard test procedure provided in Appendix G, which have minimal curvature. This has been verified by finite element analysis, as discussed in a subsequent section.

For pipe design for installation, the axial thrust and bending moment are calculated in accordance with simplified design procedures per Appendix E or comprehensive design procedures per Appendix D.

Strain in the cross-section is calculated using the idealized section properties (with gross area), the internal force effects of thrust and bending moment, and the calculated or design secant modulus. This strain is termed the "first order" strain.

B.2.4.6 Determine Effective Area and Second Order Strain

Once the first order strain is determined, sections in compression are evaluated for local buckling. Local buckling is out-of-plane bending of the individual plate elements of a corrugation (crest, web, valley, liner) that reduces the stiffness and strength and eventually leads to section failure.

1 Corrugation - Actual Geometry

Length = 4.8 in.	Period = 4.8 in.
A.g = 2.11 in.^2	A.I = 0.440 in.^2 / in.
I.x = 1.63 in.^4	I.I = 0.340 in.^4 / in.
c.d = 2.7 in.	
y.v = 1.68	

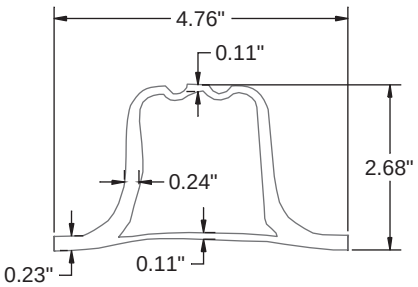

Figure B-20. Section properties for scanned specimen.

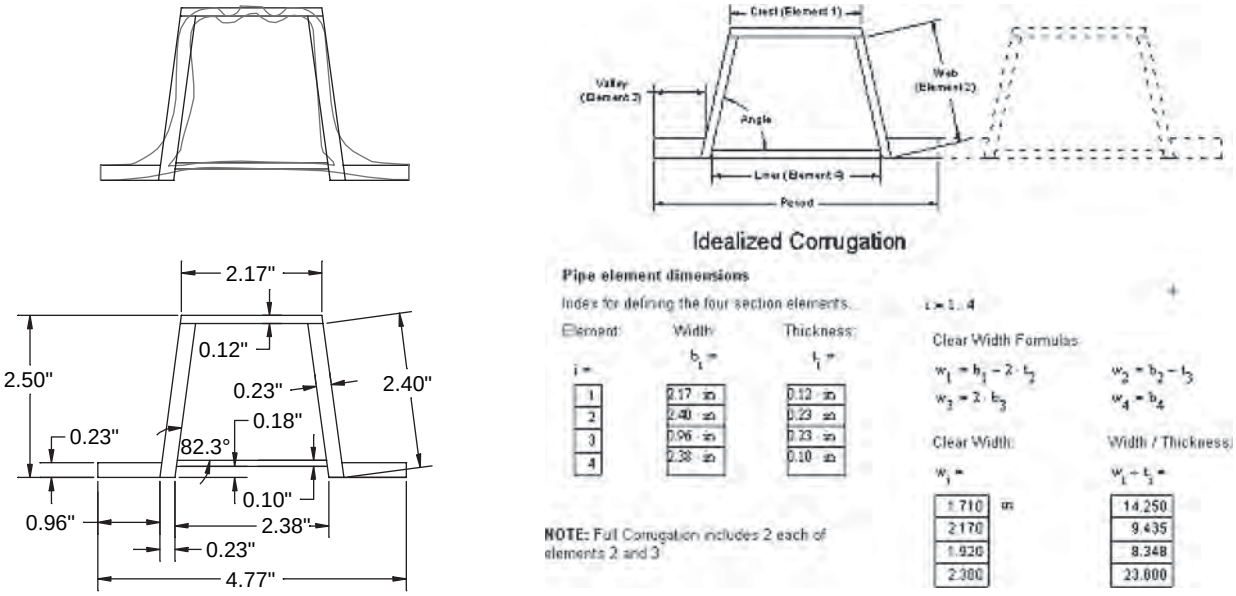

Figure B-21. Idealizing corrugated pipe wall profile.

Section 12.12 of the *AASHTO LRFD Bridge Design Specifications* and the design methodology presented in Appendix E provide simplified equations to calculate the compressive buckling capacity as a function of these parameters that are based on design of cold-formed steel structural members (AISI 1997). The approach assumes that the center portion of elements with high width-to-thickness ratios buckles while the corner, supported sections provide compression strength, as illustrated in Figure B-24.

This procedure is quantified via the following formulas:

$$b_{eff} = \rho b \qquad \text{(Eq. B.1)}$$

$$\lambda = \frac{w}{t}\left(\sqrt{\frac{\varepsilon_y}{k}}\right) \qquad \text{(Eq. B.2)}$$

$$\text{if } \lambda \le 0.673 \text{ then } \rho = 1$$

$$\text{if } \lambda > 0.673 \text{ then } \rho = \left(1 - 0.22/\lambda\right)/\lambda$$

where:

b_{eff} is the effective width of the element,

b is the gross width of the element,

w is the clear width of the element—computed based on the idealized section,

k is the plate buckling coefficient (k = 4 for elements supported on both sides, k = 0.43 for one side support—such as Element 1 in the standing rib and T-rib configurations),

ε_y is the yield strain of the material,

ρ is the effective width reduction factor, and

λ is the slenderness of the element.

B.2.4.7 Effective Area of Specimens in Exploratory Testing

For design of pipe, the ultimate capacity is investigated, so the yield strain is used for all of the elements. Once the ineffective width of each element is determined, it is subtracted from the total cross-sectional area to determine the effective area of the profile.

For the tested specimens, the appropriate idealization from Figure B-23 is used to determine the gross width (b), clear width (w), and thickness (t) of each element. The w/t ratios are determined and given in Table B-17. The plate buckling coefficient (k) is 4 for all of the elements, except Element 1 in the standing rib and the standing "T" sections; in those elements k = 0.43.

Using the formulas for effective width calculation (Equations B.1 and B.2), the predicted average strain in each element is given in Figure B-25 for all of the specimens as a function of the element width-to-thickness ratio and the yield strains from the stub compression tests. The model used for the local buckling reduction predicts lower average strains in the slender elements.

Figure B-25 also suggests that 4% is a reasonable lower strain limit for HDPE pipe in compression and Figure B-26 suggests that 3% is a reasonable bound for PVC pipe in compression.

The gross area, effective area, and ratio of gross to effective area for the tested pipe are summarized in Figures B-27 and B-28, which show that the PVC specimens are typically greater than 90% effective, although two profiles tested between 80% and 90% effective while the PE specimens commonly have

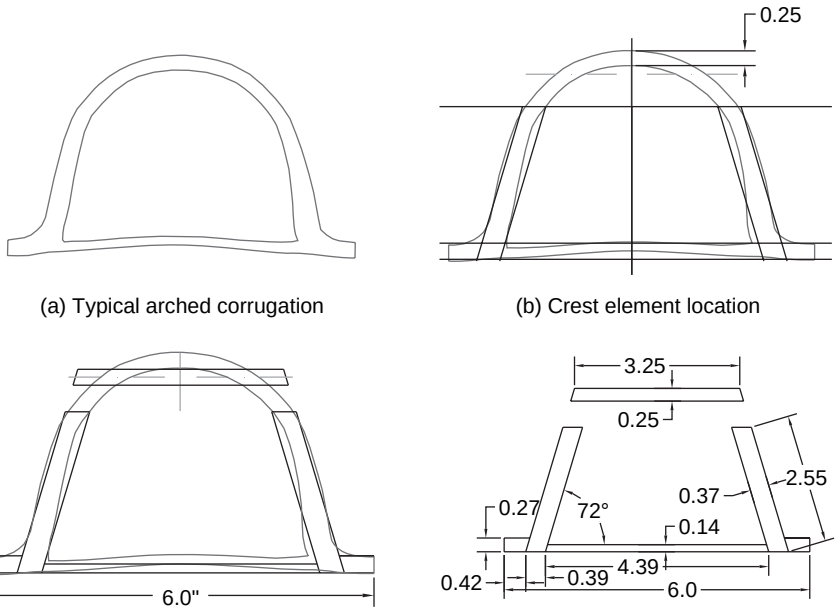

(a) Typical arched corrugation

(b) Crest element location

(c) Idealized crest element

(d) Idealized arched corrugation

Figure B-22. Idealization of arched corrugation.

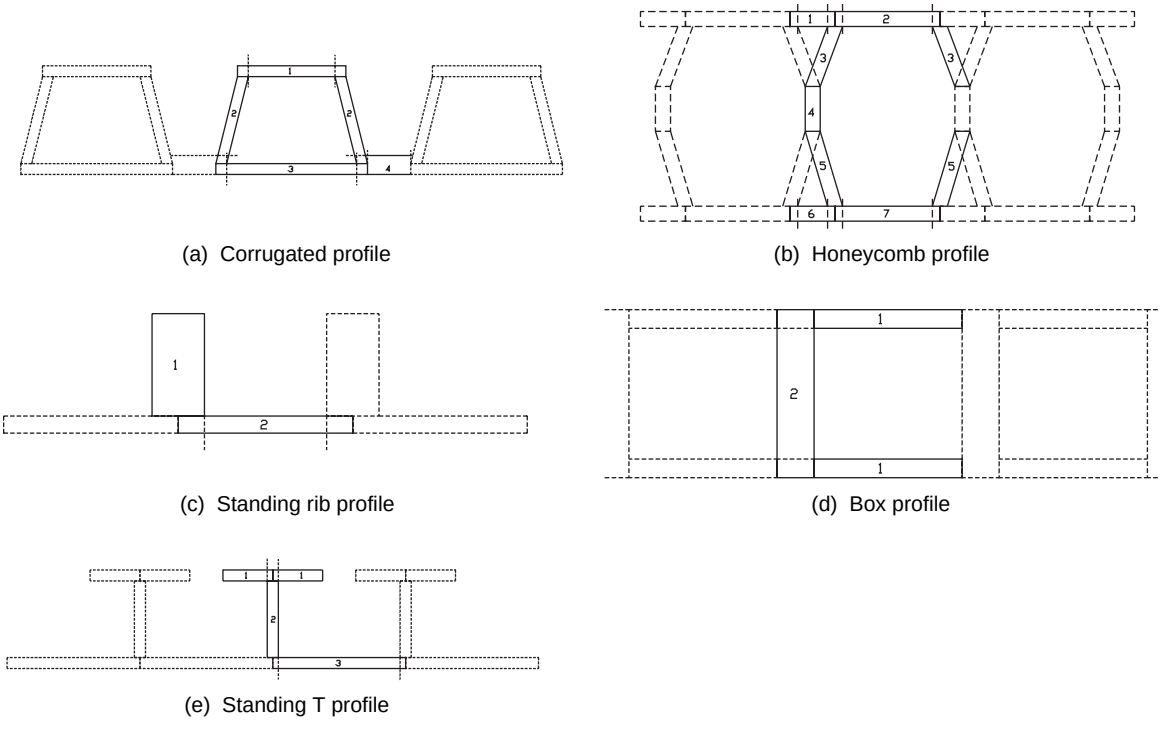

(a) Corrugated profile

(b) Honeycomb profile

(c) Standing rib profile

(d) Box profile

(e) Standing T profile

Figure B-23. Example idealizations of profile wall cross-sections.

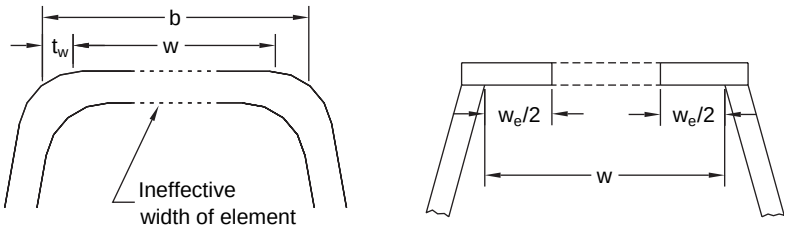

Figure B-24. Illustration of element effective areas for local buckling calculation.

Table B-17. Width/thickness ratios for tested thermoplastic pipe.

Specimen	Material	Profile Type	Inside Diameter (in.)	Element 1 w/t	2 w/t	3 w/t	4 w/t	5 w/t	6 w/t	7 w/t
D18	PE	Corrugated	18	12	14	27	5			
D24	PE	Corrugated	24	14	13	25	4			
P24	PE	Corrugated	24	23	24	26	3			
B24	PE	Corrugated	24	11	12	19	4			
L24	PE	Corrugated	24	13	14	28	5			
V24	PE	Corrugated	24	4	3	3	16			
D30	PE	Corrugated	30	13	11	25	4			
W30	PE	Box	30	10	3					
D36	PE	Corrugated	36	23	14	24	7			
E42	PE	Honeycomb	42	5	13	8	7	7	5	13
D48	PE	Corrugated	48	18	15	28	6			
D60	PE	Corrugated	60	16	12	23	9			
E60	PE	Honeycomb	60	3	9	6	5	5	4	9
Z14	PVC	Standing Rib	14	4	10					
X14	PVC	Standing Rib	14	2	10					
J24	PVC	Standing T	24	1	4	9				
C24	PVC	Corrugated	24	8	6	11	1			
Y30	PVC	Standing Rib	30	2	4					
J36	PVC	Corrugated	36	12	10	8	2			

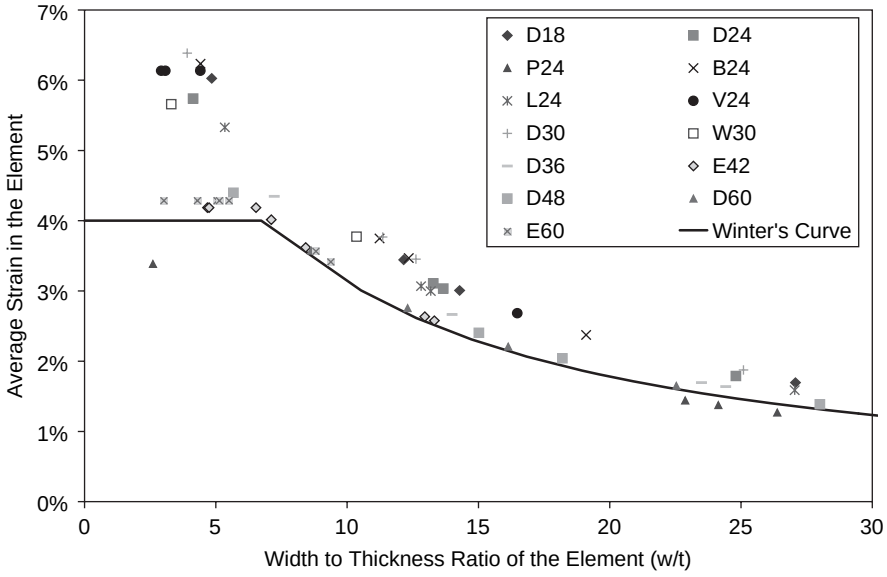

Figure B-25. Predicted average element strain for experimental yield strain, HDPE.

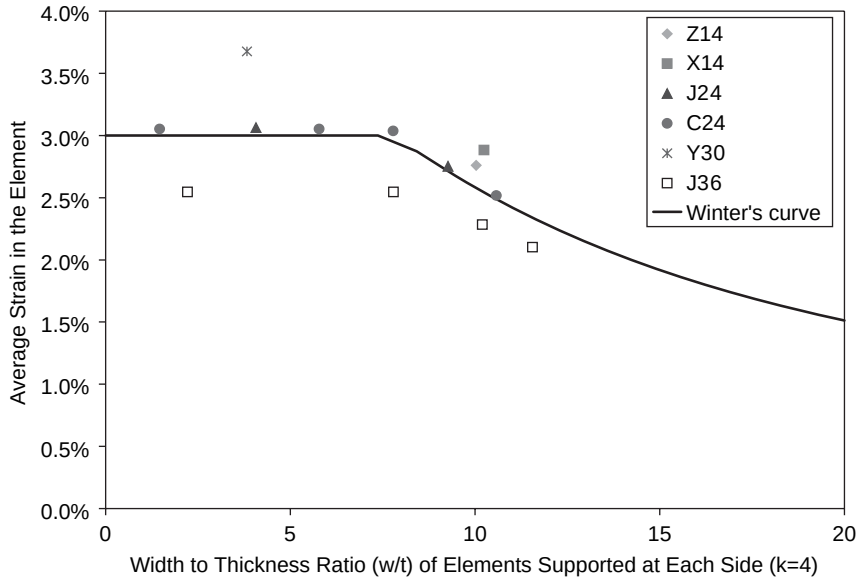

(a) Edge support coefficient, k = 4

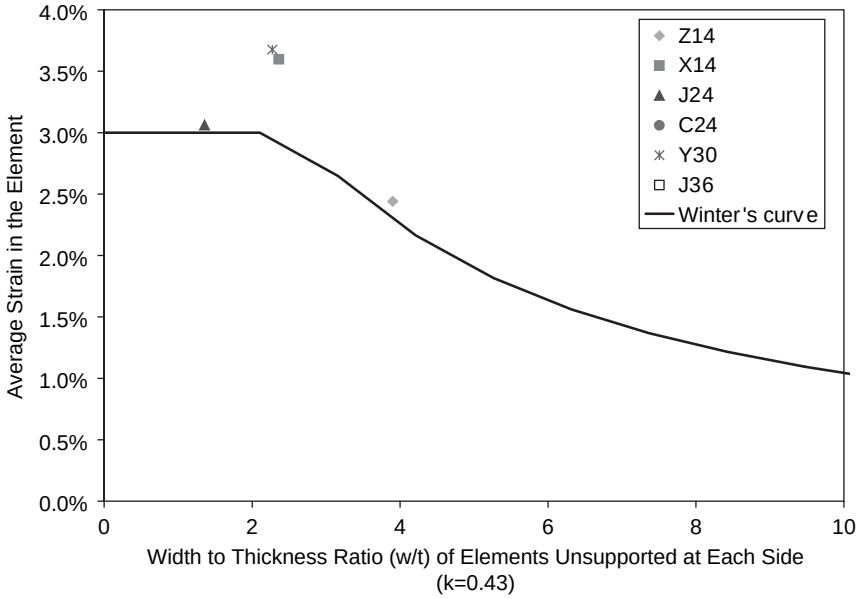

(b) Edge support coefficient, k = 0.43

Figure B-26. Predicted average element strain for experimental yield strain, PVC.

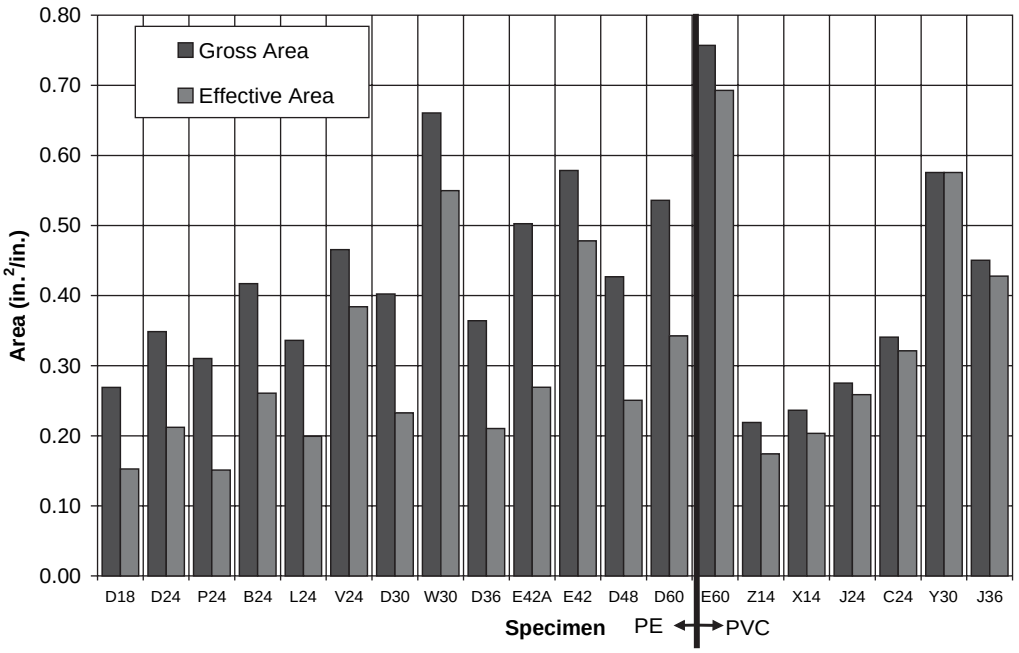

Figure B-27. Specimen gross and effective areas.

effective areas of 60% with some profiles testing up to 90% effective.

B.2.4.8 Experimental Determination of Effective Area

If the secant modulus and the yield strain of the material are known, the effective area of a given cross-section can be determined directly by test, without detailed calculation. This relies on the idea that for a short stub specimen (e.g., 15° or less) only the cross-sectional area, not the moment of inertia, is effective in resisting the applied thrust.

For this case, the effective area can be determined by the following:

$$A_{eff} = \frac{P_{test}}{E_s \varepsilon_y} \leq A_g \qquad \text{(Eq. B.3)}$$

The secant modulus can be determined from appropriate material tests, such as in Zhang and Moore (1997a, 1997b). The yield strain can be the yield strain measured in the test or a specified nominal yield strain (e.g., 4% for HDPE). The effective area would be limited to being less than or equal to the gross area of the specimen.

Such an approach is similar to the methods used for testing in cold-formed steel sections in which the effective area is found by dividing the test capacity by the yield stress. The only complications here are (1) to accurately define the yield stress via correct computation of the secant modulus in the test at the yield strain and time in the test, (2) to determine a methodology for calculation of the effective area when the demands are not at the ultimate level, and (3) to quantify the nonlinear stress-strain behavior.

B.2.4.9 Local Buckling Capacity

The following subsections describe different elements of local buckling capacity.

B.2.4.9.1 Theoretical Capacity. The capacity of thermoplastic culvert pipe in compression is the effective area times the yield stress of the material. The yield stress of the material in the test is the secant modulus in the test times the yield strain. Thus, the capacity is as follows:

$$P_n = A_{eff} E_s \varepsilon_y = A_{eff} f_y \qquad \text{(Eq. B.4)}$$

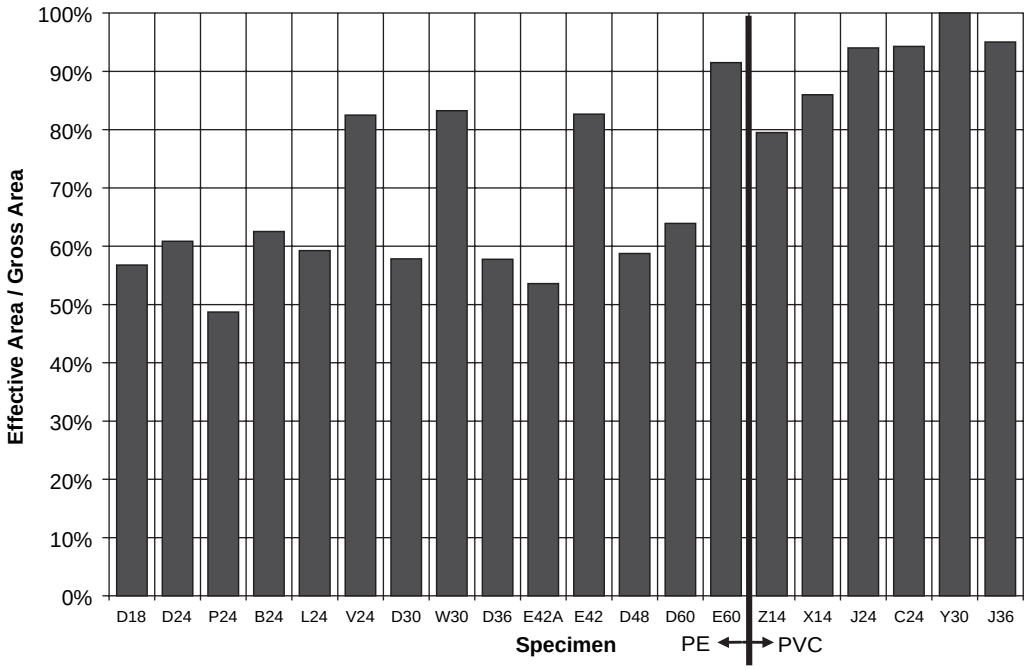

Figure B-28. Percentage of effective cross-section.

The yield strain (ε_y) is determined from material tests and set as a constant value by material. The secant modulus (E_s) is determined from material tests described in this appendix.

B.2.4.9.2 Theoretical Capacity in Exploratory Testing. Figure B-29 and Figure B-30 provide the theoretical capacity for the specimens tested in the exploratory testing. The test strength, predicted strength, and test-to-predicted ratio for the HDPE and PVC specimens are presented in the figures. The mean test-to-predicted ratio for the HDPE specimens is 1.20 with a standard deviation of 0.18 (this statistic is computed with Specimen V24 removed). The mean test-to-predicted ratio for the PVC specimens is 0.64 with a standard deviation of 0.10. The secant modulus for the PVC specimens in these figures is based on *NCHRP Report 438,* and the actual modulus is likely higher, accounting for the discrepancy.

Based on the scatter in the test-to-predicted ratio, no bias is shown for pipe diameters from 450 mm to 1500 mm (18 in. to 60 in.) in HDPE or 350 mm to 900 mm (14 in. to 36 in.) in PVC. Generally, the box and honeycomb profiles have test-to-predicted ratios closer to 1.0 than do the corrugated profiles. Accuracy of the method for the PVC specimens appears to be about the same for the three tested profiles: standing seam, standing T, and corrugated.

B.2.4.9.3 Theoretical Capacity in Interlaboratory Testing. Sample calculations for the compression capacity are provided in the following section. Calculations were completed assuming a strain capacity of 4.09% for short- and long-term loading conditions. Short- and long-term moduli of elasticity were taken at the AASHTO values of 110,000 psi and 22,000 psi respectively. Calculated section capacities are summarized and compared with test capacities in Table B-18.

Table B-18 suggests that the calculated short-term compression capacities are very close to the stub compression test results, while the long-term compression capacities are approximately 30% of the stub compression test capacity. Although Pipe 42C had a lower calculated capacity, it tested to about the same compression capacity as Pipe 42B, suggesting that the shape was not idealized well.

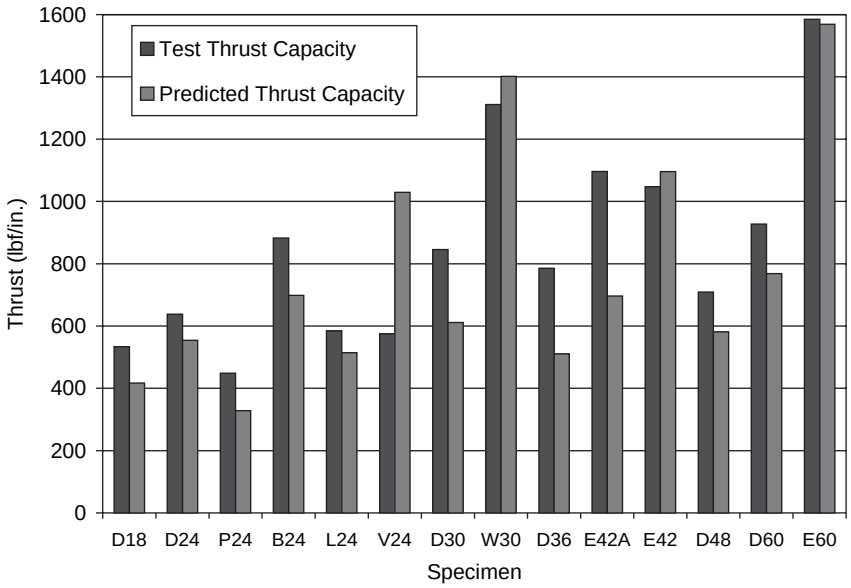

(a) Test and predicted capacity

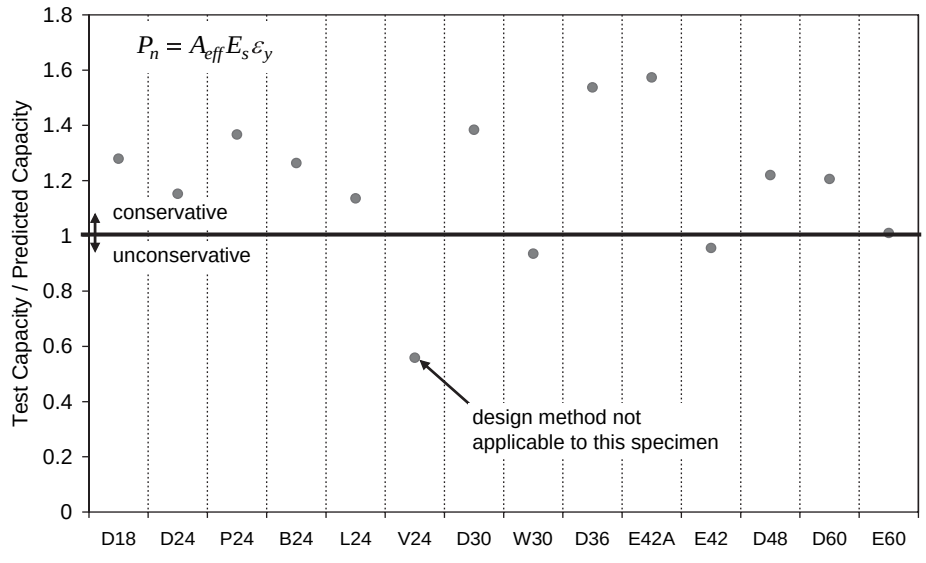

(b) Test-to-predicted ratio

Figure B-29. Theory evaluation for HDPE specimens.

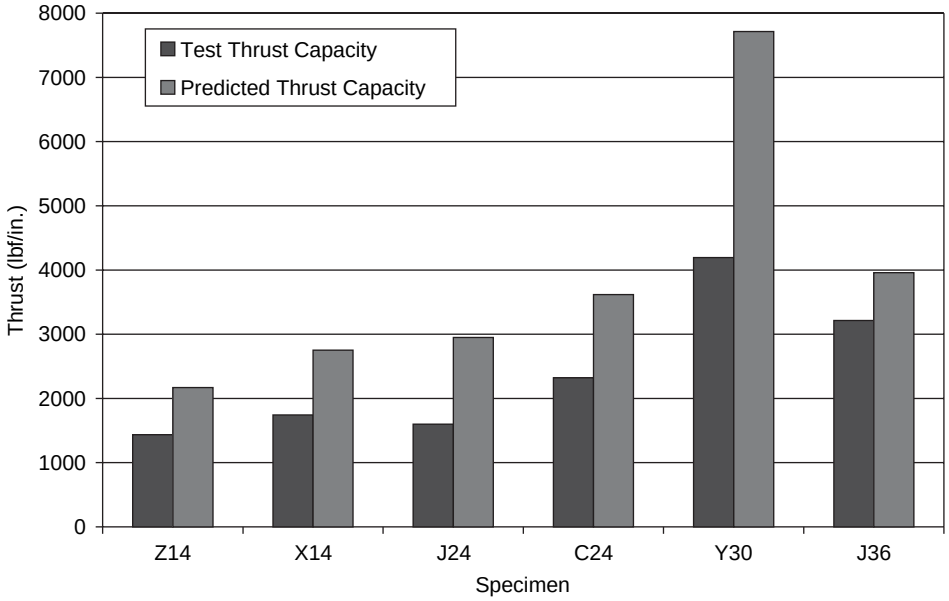

(a) Test and predicted capacity

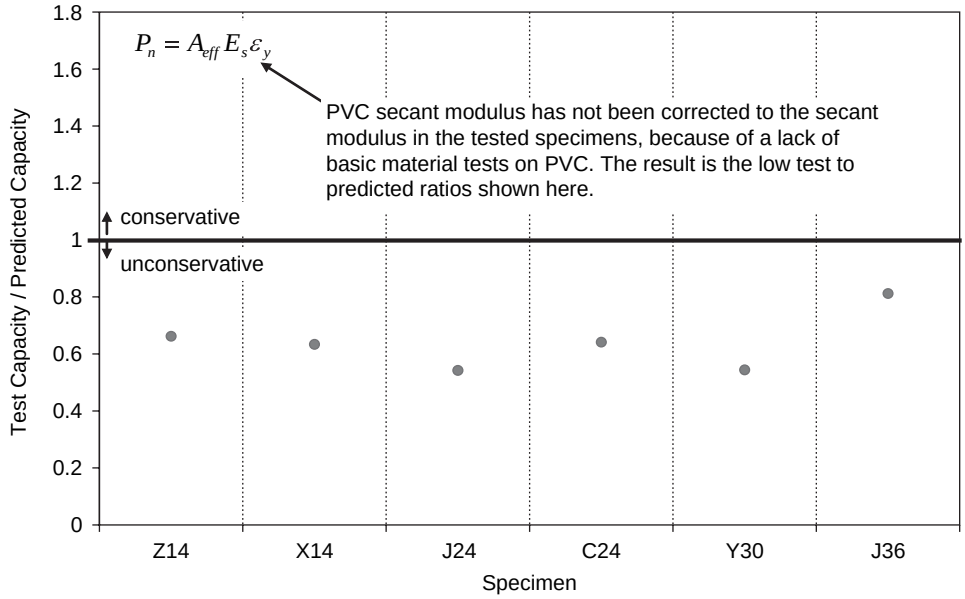

(b) Test-to-predicted ratio

Figure B-30. Theory evaluations for PVC specimens.

Table B-18. Comparison of calculated long-term capacity with stub compression test results.

Pipe	A_l (in.^{2}/in.)	A_{eff} (in.^{2}/in.)	A_{eff} / A_l	T_{stub} (lb/in.)	E = 110,000 psi		E = 22,000 psi	
					T_{calc} (lb/in.)	T_{calc} / T_{stub}	T_{calc} (lb/in.)	T_{calc} / T_{stub}
24A	0.342	0.274	80.2%	726	822	1.13	247	0.34
24C	0.355	0.301	85.0%	891	904	1.01	271	0.30
42C	0.416	0.295	71.0%	998	885	.89	266	0.27
42B	0.414	0.331	79.9%	952	992	1.04	298	0.31
Average						**1.02**		**0.31**
Standard deviation						**0.10**		**0.03**

Note:
A_l = actual profile area per unit length,
A_{eff} = effective profile area based on LRFD Specifications,
T_{stub} = average capacity in stub compression test, and
T_{calc} = calculated compression capacity.

B.2.4.9.4 Calculation for Theoretical Compression Capacity.

Profile Geometry

The profile geometry is idealized as a series of flat elements

Profile type = corrugated

number of elements $n := 6$

element index $i := 1 .. n$

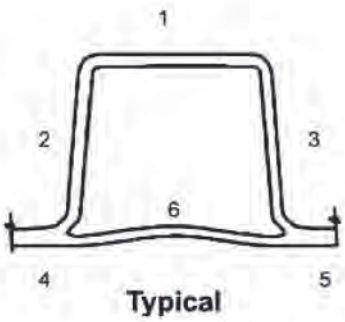

Typical

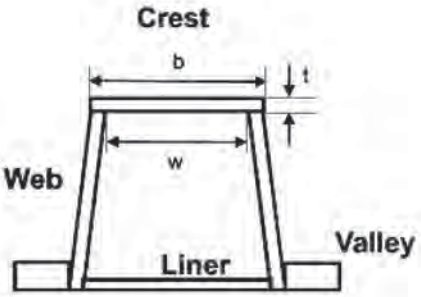

Idealized

Note: In the figure for the idealized section, the valley is shown as two separate elements (Element Nos. 4 and 5 above), symmetric about the corrugation centerline. For calculations which use the term "w," the Valley is treated as a single element (Element No. 4) with two times the width of the half elements.

element number $i =$	gross width, used for Ag $b_i :=$	thickness $t_i :=$	clear width $w_i :=$	$w_i =$		inclination (circumferetial=0 deg radial=90 deg) $\theta_i :=$	vertical distance of element from inside edge $y_i :=$	
1	2.37in	0.160in	$b_1 - t_2 - t_3$	1.936	in	0deg	2.844 · in	Crest
2	2.35in	0.217in	$b_2 - t_4$	1.985		78deg	1.565 · in	Web
3	2.35in	0.217in	$b_2 - t_5$	1.985		78deg	1.565 · in	Web
4	1.00in	0.365in	$b_4 + b_5$	2		0deg	0.182 · in	Valley
5	1.00in	0.365in	0 · in	0		0deg	0.182in	Valley
6	3.45in	0.089in	b_6	3.45		0deg	0.060 · in	Liner

$Period := b_4 + b_5 + b_6 + t_2 + t_3$ $\quad Period = 5.884\,in$

In the above, the following parameters are defined or computed:

- i index that represents the element number
- b_i total width of an idealized element (see figure above)
- t_i thickness of an idealized element (see figure above)
- w_i clear width of an element (see figure above)
- θ_i angle of element relative to inside surface of profile
- y_i distance from inside surface of profile to centroid of element
- Period length of one cylce of the pipe wall profile

Compute cross-sectional area of profile, A_g

gross area of corrugation per unit length of pipe

$$A_g := \frac{\sum_{i=1}^{n} \left(b_i \cdot t_i\right)}{Period} \qquad A_g = 0.414 \frac{in^2}{in}$$

Evaluate local buckling

First compute the slenderness factor, γ_i, for each element of the profile (values for w_i and t_i provided above). Other parameters include:

$\varepsilon_u := 4.09\%$ factored compressive strain in pipe wall

$k := 4$ edge support coefficient, value is for element supported at each end.

Slenderness factors for i = 1 to 6:

slenderness factor
AASHTO Eq. 12.12.3.4-4

$$\lambda_i := \max\left[\left(\frac{w_i}{t_i}\right)\cdot\sqrt{\frac{\varepsilon_u}{k}}, 0.673\right] \qquad \lambda^T = (1.224 \;\; 0.925 \;\; 0.925 \;\; 0.673 \;\; 0.673 \;\; 3.92)$$

Use the slenderness factor to compute effective width factor. The effective width factor is the portion of the element that has not buckled and is still carrying load at the strain level ε_u. Then compute the actual effective width as the product for the effective width, ρ_i, times the clear element widths, $w^T = (1.936 \;\; 1.985 \;\; 1.985 \;\; 2 \;\; 0 \;\; 3.45)\,\text{in}$

Effective width factors for i = 1 to 6:

effective width factor
AASHTO Eq. 12.12.3.4-3

$$\rho_i := \frac{1 - \frac{0.22}{\lambda_i}}{\lambda_i} \qquad \rho^T = (0.67 \;\; 0.824 \;\; 0.824 \;\; 1 \;\; 1 \;\; 0.241)$$

Effective widths for i = 1 to 6:

element effective width

$$w_{e_i} := \rho_i \cdot w_i \qquad w_e^T = (1.298 \;\; 1.636 \;\; 1.636 \;\; 2 \;\; 0 \;\; 0.831)\,\text{in}$$

Compute the net effective area of the element by removing the portion of the elements that have buckled. This is done by subtracting the ineffective area from the gross area. In this calculation:

A_{eff} effective cross-sectional area of profile per unit length after removing areas that have buckled

$A_g = 0.414\,\frac{in^2}{in}$ gross cross-sectional area of profile per unit length

w clear width of individual elements of the profile, provided above

w_e effective width of individual elements of the profile, provided above

Period = 5.884 in length of one cycle of the pipe wall profile

effective unitized area corrugation cross section (subtract ineffective area from total area)

$$A_{eff} := A_g - \frac{\sum_{i=1}^{n}\left[\left(w_i - w_{e_i}\right)\cdot t_i\right]}{\text{Period}} \qquad A_{eff} = 0.331\,\frac{in^2}{in}$$

Summary

Consideration of local buckling reduces the area available to resist load. In this example:

Total cross-sectional area	$A_g = 0.414\,\frac{in^2}{in}$
Effective area	$A_{eff} = 0.331\,\frac{in^2}{in}$
Percentage effective area	$\frac{A_{eff}}{A_g} = 80\%$

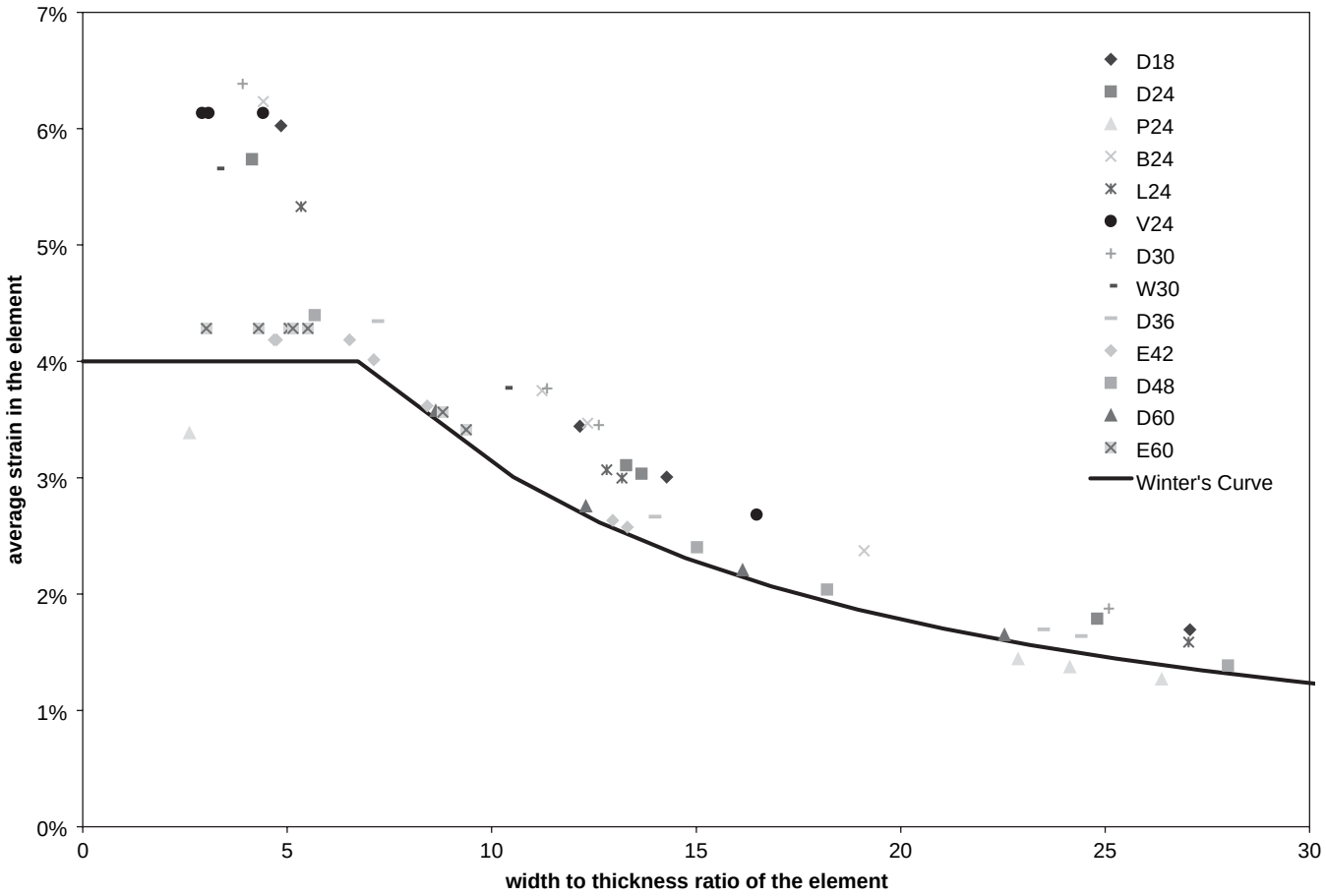

Figure B-31. Predicted average element strain for experimental yield strain, HDPE.

B.2.4.9.5 Local Buckling Strain versus Element Width/Thickness Ratio. The predicted average strain in each element of the PE pipe profiles is given in Figure B-31 as a function of the element width-to-thickness ratio. The model used for the local buckling reduction predicts lower average strains in the slender elements and also suggests that 4% is a reasonable lower strain limit for HDPE pipe in compression. Similar analysis indicates that 3% is a reasonable bound for PVC pipe in compression.

B.2.5 Use of Stub Compression Test for Pipe Design

The current *AASHTO Bridge Design Specifications* are based solely on theoretical capacity with testing used as product QA/QC and verification of safety factors. However, typical AASHTO design does not deal with the variety of corrugation profiles and manufacturing variances inherent in thin-walled profile PE and PVC drainage pipe. For these structures, the approach of combining a test method with the theoretical design improves the design methodology and reduces the difficulty of the theoretical solution without reducing the accuracy of the answer.

As demonstrated in previous sections, the stub compression test provides a compression capacity of the profile wall that allows calculation of the corrugation effective area in the local buckling calculation. This procedure is recommended for inclusion in AASHTO as follows:

1. Calculate the gross area of the profile, A_g (as previously discussed).
2. Run the stub compression test as described in Appendix G and produce the stub compression capacity, P_{sc}, in lbs/in. length as the average of at least three tests from equally spaced locations around the pipe circumference.
3. Calculate the compression capacity, P_{st}, for short-term loading using a multiplier that is applied to the test result for stub compression capacity, $F_{st} = 0.9$.

$$P_{st} = P_{sc} F_{st} \qquad \text{(Eq. B.5)}$$

4. Calculate the effective area using the compression capacity for short-term loading and the short-term material yield strength, F_{us} = 3,000 psi, from Table 1 in *AASHTO LRFD Bridge Design Specifications,* Section 12.12, as follows:

$$A_{eff} = \frac{P_{st}}{F_{us}} \leq A_g \qquad \text{(Eq. B.6)}$$

5. Use the effective area to determine the factored compressive strain due to dead load and live-load-thrust demands for design:

$$\varepsilon_{cu} = \frac{T_{DL.u}}{A_{eff} E_{50}} + \frac{T_{LL.u}}{A_{eff} E_0} \qquad \text{(Eq. B.7)}$$

6. Compare factored compressive strain to the material-dependent strain limits.

Use of this test result as alternative to the theoretical capacity is incorporated into the simplified design method in Appendix E.

B.3 References

American Iron and Steel Institute, "Specification for the Design of Cold-Formed Steel Structural Members, with Commentary," Washington, D.C., 1997.

McGrath, T. J. and Sagan, V. E., *NCHRP Report 438: LRFD Specification for Plastic Pipe and Culvert,* Transportation Research Board, Washington, D.C., 2000.

Zhang, C. and Moore, I. D., "Nonlinear Mechanical Response of High Density Polyethylene—Part I: Experimental Investigation and Model Evaluation," *Polymer Engineering and Science,* Vol. 37, No. 2, 1997a.

Zhang, C. and Moore, I. D., "Nonlinear Mechanical Response of High Density Polyethylene—Part II: Uniaxial Constitutive Modeling," *Polymer Engineering and Science,* Vol. 37, No. 2, 1997b.

APPENDIX C

Computer Modeling and Testing of Pipe-Soil Interaction

CONTENTS

C.1 Thermoplastic Culvert Deformations and Strains: Evaluation Using Two-Dimensional Analyses

C.1.1 Introduction

This section reports on the use of two-dimensional (2D) finite element analysis to develop the limit states design procedures for buried thermoplastic pipes. Tests have been performed on lined, corrugated, high-density polyethylene (HDPE) pipe with annular (axisymmetric) geometry and helically ribbed polyvinyl chloride (PVC) pipe. A second HDPE pipe was also tested; results were similar and are not presented here in the interests of brevity. The laboratory tests were performed in a biaxial pipe test cell, a facility developed to model the biaxial field stresses experienced by pipes deeply buried under embankments (Brachman et al. 2000). Comparisons are made to evaluate the effectiveness of the computer analysis and the simplified method in calculations of pipe behavior under deep burial. The computer analysis is then used to examine one situation involving nonuniform soil support, calculating the magnitudes of deflection and local surface strain for both the HDPE and PVC pipes backfilled with zones of low-stiffness soil beneath the haunches. This appendix concludes with recommendations regarding the strengths and limitations of 2D finite element analysis and with aspects of the analysis that need to be addressed to obtain useful calculations of pipe deflections and circumferential strains. Conclusions also are made regarding the magnitude of local surface strains, and values of strain factor D_f for use in simplified design calculations of circumferential bending strains at the extreme fibers.

C.1.2 Test Instrumentation and Measurements

C.1.2.1 Test Cell Arrangement

The biaxial test cell is a high-strength steel box with dimensions 2 m × 2 m in plan and 1.6 m in height (6.6 ft by 6.6 ft in plan and 5.3 ft in height). Details of the design of the cell are reported in Brachman et al. (2000); the arrangement of the pipe and instrumentation for these tests is described by Dhar and Moore (2001). Pipes of about 600-mm (24-in.) diameter were placed horizontally equidistant from the sidewalls. This leaves backfill of 650 mm (25.6-in.) width on both sides of the pipe. Finite element analysis to study the influence of boundaries has established that at this distance the influence of the sidewall is minimal (McGrath et al. 2001). Soil bedding below the pipe is 340 mm (13.4 in.) thick. Poorly graded sand ($C_u = 3.4$, $C_c = 1.1$) was used as the backfill material. The backfill soil was compacted to a density of about 1,625 kg/m^3, which is 85% of the maximum standard Proctor density. Earth pressure cells were used to measure the vertical and horizontal stresses at the springline and at 200 mm (7.9 in.) below the top surface of the soil. Two settlement plates (A and B) were positioned at the springline level to monitor the vertical soil movements. An air bladder was used to apply uniform pressures on top of the soil. Sidewall friction of the cell was minimized using special sidewall treatment (Tognon et al. 1999).

Tests were conducted in pressure increments of 25 kPa (3.6 psi), with each increment allowed to remain for 20 min, a sufficient period of time to permit the cell pressure to stabilize. Thus, the average rate of loading was 0.021 kPa/sec (0.003 psi/sec). Loading was continued for about 6 hs until limit states, such as local buckling, were observed and a vertical pressure of between 400 kPa (57.6 psi) and 500 kPa (72 psi) was reached.

C.1.2.2 Description of the Profiles

Figure C-1 shows the two pipe profiles considered in this study. The first is a twin walled (lined corrugated) annular HDPE pipe with internal diameter of 610 mm (24 in.). The pipe has 101-mm (4-in.) pitch and 55.2-mm (2.2-in.) corrugation depth. The second pipe is a 605-mm (24-in.) diameter (internal) PVC pipe with helically ribbed profile. The angle of helix of the rib is about 9° with average clear spacing between the ribs of 35.75 mm (1.4 in.).

C.1.2.3 Pipe Instrumentation

Linearly variable differential transducers (LVDTs) were used to measure the changes in horizontal and vertical diameters of the pipes. Wall strains on different components of the profile were measured using resistance strain gages. Biaxial

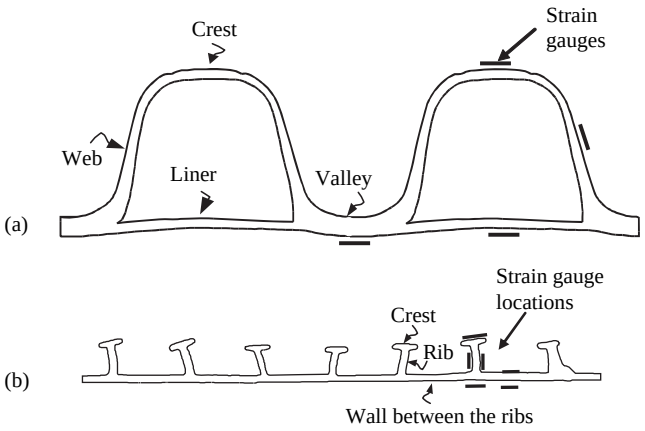

Figure C-1. Pipe profiles and strain gage locations showing (a) lined corrugated HDPE pipe and (b) ribbed PVC profile.

strain gages were used for annular profiles to measure the circumferential and the axial strain. Strain gage rosettes were used for the profile with helically wound ribs. Strain measurements were obtained at the crown, invert, and springline (on both sides) of the pipe. Instrumentation was placed at two sections to check reproducibility of the test results and also to ensure that the data were collected in the event that some of the gages were inoperative. The locations of the strain gages on the profiles are also shown in Figure C-1.

C.1.3 Finite Element Modeling of the Test Cell

The Spangler (1941) equation has been used extensively in design to calculate the deflection of buried flexible pipes, and the closed-form solutions of Burns and Richard (1964) and Hoeg (1968) are also being used to calculate pipe response under deep burial (e.g., Moore 2001). The continuum solutions are based on a number of idealizations, including the modeling of the soil as an infinite, homogeneous, isotropic, and linear elastic material. The 2D finite element method is used when evaluations of the buried pipe response need to consider the materially nonlinear soil behavior or where pipe installation in nonuniform ground is expected to have a significant influence on the pipe response (Chua and Lytton 1987, Hashash and Selig 1990, Katona 1988). Duncan's hyperbolic soil model (Duncan and Chang 1970) and its extension by Selig (1988) have been utilized to characterize the nonlinear elastic behavior of the soil. Time-dependent behavior of thermoplastic material has been represented in most of these 2D analyses using the secant elastic modulus selected to characterize stress divided by strain for the polymer over the time period under consideration, generally focusing specifically on the short-term or long-term values, (e.g., Hashash and Selig [1990], Katona [1988], and Moore [1995]). Brown and Lytton (1984) adopted a simple power law formulation to account for the reduction of HDPE modulus with time, and Moore and Zhang (1998) have developed and used linear viscoelastic, nonlinear viscoelastic, and viscoplastic models for HDPE. These time-dependent material models are not yet available to most pipe designers conducting finite element analysis, so the present study employs 2D finite element analysis based on secant elastic modulus for the polymer (this is discussed in more detail in a subsequent section).

Small strain finite element analysis has been employed to study the interaction of thermoplastic pipe with the backfill soil in the test cell. The vertical cross-section of the test cell model is shown in Figure C-2. Two noded, beam-column elements were used to represent the pipe. The elements are defined along the centerline of the sections. Area (A) and moment of inertia (I) of the sections were calculated by explicit integration of the actual profile geometries. The quantities were expressed per unit length along the pipe axis. Six noded plane-strain-continuum elements were used to model the surrounding backfill.

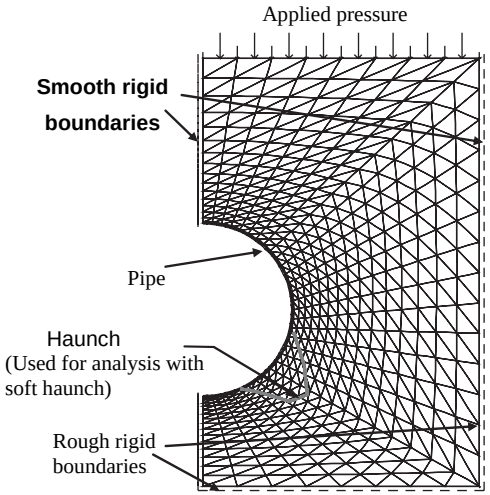

Figure C-2. Finite element mesh.

Using symmetry, only half of the test cell and the pipe within need to be analyzed. A smooth, rigid boundary was used to idealize the line of symmetry, where horizontal displacements were prevented and the crown and the invert of the pipe were restrained against rotation. A smooth, horizontally restrained boundary was used for the sidewalls. The nodal points along the bottom boundary were fixed in both the horizontal and vertical directions.

C.1.4 Model Parameters for Thermoplastic Pipes

Parameters required for the beam-column elements are axial stiffness (EA) and the flexural stiffness (EI), where E is the elastic modulus of the material. The moduli for thermoplastic materials (HDPE and PVC) are dependent on time effects. However, elastic modeling using secant modulus is the simplest and the most widely used approach for thermoplastic pipe analysis with the modulus selected in accordance with the time period over which the response is required. AASHTO provides guidelines for short-term and long-term values of modulus for HDPE as 760 MPa (110 ksi) and 152 MPa (22 ksi), respectively. The values recommended for PVC are 3,030 MPa (440 ksi) and 1,090 MPa (158 ksi) (AASHTO 1998).

Previous analysis of a biaxial test with similar duration and rate of loading showed that the pipe response was successfully calculated using either a nonlinear time-dependent pipe material model or linear elasticity based on secant modulus (Dhar and Moore 2000a). Thus, the modulus of elasticity, E, for the HDPE is taken as 450 MPa (65 ksi), rep-

resenting a secant value for 6 hs, the duration of the experiments, based on the data and viscoplastic modeling of Zhang and Moore (1997). Poisson's ratio ν of 0.46 was used for the HDPE. Modulus, E, and Poisson's ratio, ν, used for the PVC pipe are 2,760 MPa (400 ksi) and 0.3 respectively (Sargand et al. 1995 used similar values in their analysis of PVC pipes). Thus, hoop stiffness (EA) and bending stiffness (EI) of the sections are estimated to be 4,200 N/mm (24 kips/in.) and 1.40×10^6 N-mm^2/mm (12.3 kips in.^{2}/in.), respectively, for the profiled HDPE pipe, and 19,480.1 N/mm (110 kips/in.) and 1.14×10^6 N-mm^2/mm (10 kips in.^{2}/in.), respectively, for the ribbed PVC pipe.

C.1.5 Assessment of Soil Parameters

Stress-strain properties of the soil were determined from the measurements of soil stresses and soil deformation in each of the tests. Coefficient of lateral earth pressure at rest, K_o, of 0.5 was obtained from the measurements of horizontal and vertical stresses for both tests. Typical soil stress measurements in one of the tests are shown in Figure C-3. Poisson's ratio was calculated from the K_o value as $\nu = K_o/(1 + K_o) = 0.33$ to ensure that lateral earth pressures for zero lateral strain like those measured in the test are calculated by the elastoplastic finite element analysis.

The stress-strain relations for the soil appeared to be nonlinear and stress dependent (Figures C-4 and C-5). The nonlinear model of Janbu (1963) was used to characterize the nonlinear stress-dependent soil behavior. Tangent modulus in this power law model is defined as $E = K\sigma^n$, where σ is the mean stress. Parameters (K, n) for the model were estimated from curve fitting to the experimental stress-strain relations.

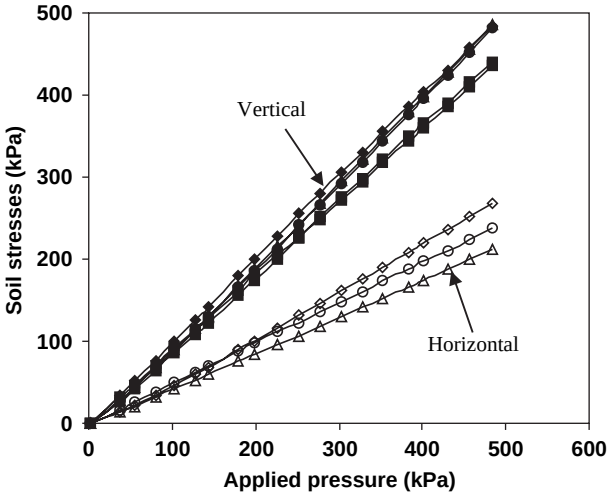

Figure C-3. Soil stresses measured in PVC pipe test (1kPa = 0.144 psi).

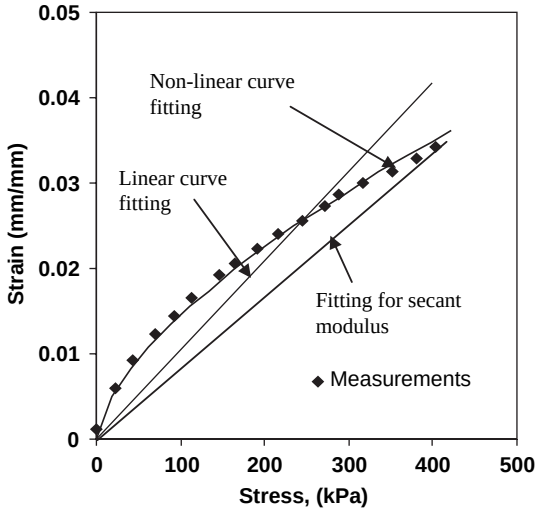

Figure C-4. Stress-strain relation of soil in HDPE pipe test (1kPa = 0.144 psi).

The incremental constitutive equation for the one-dimensional (1D) compression is expressed as

$$d\varepsilon_y = \frac{d\sigma_y}{E} - \frac{\nu}{E}\left(d\sigma_x + d\sigma_z\right) \tag{C.1}$$

where $d\sigma_x = d\sigma_z = K_o(d\sigma_y)$ and K_o is the coefficient of lateral earth pressure at rest. Thus, the relation yields

$$\frac{d\varepsilon_y}{d\sigma_y} = \frac{1 - 2\nu K_o}{E} \tag{C.2}$$

Since $E = K\sigma^n$, and the average stress σ is given by $\sigma = \frac{1+2K_o}{3}\sigma_y$, integration of Equation C.2 gives

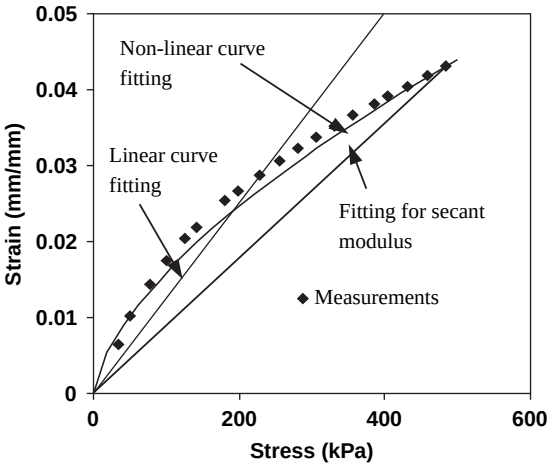

Figure C-5. Stress-strain relation of soil in PVC pipe test (1kPa = 0.144 psi).

$$\varepsilon_y = \frac{3^n\left(1-2\nu K_o\right)}{K\left(1+2K_o\right)^n\left(1-n\right)}\sigma_y^{1-n} \quad \text{(C.3)}$$

Therefore, power-law-type curve fitting (in the form $\varepsilon = A\sigma^{1-n}$) was used to obtain the nonlinear soil parameters. In each case, an equivalent linear modulus (using linear fitting) also has been estimated, since this will be used subsequently to compare solutions based on the linear and nonlinear soil models. Linear and nonlinear curve fits for the tests are shown in Figures C-4 and C-5 above. An elastoplastic model based on the Mohr-Coulomb failure criterion has been used to model the soil plasticity. The angle of internal friction for the backfill soil was estimated as 30° based on the density level and the relation, $K_o = 1 - \sin\phi$. The resulting soil parameters are n = 0.37 and K = 12.5 $(MPa)^n$ in the HDPE pipe test and n = 0.37 and K = 11.7 $(MPa)^n$ in the PVC pipe test (1 MPa = 144 psi). Equivalent linear moduli, E, for the two tests are 6.4 MPa (920 psi) and 5.5 MPa (790 psi), respectively. It is worthwhile to emphasize that all parameters were obtained without back calculation.

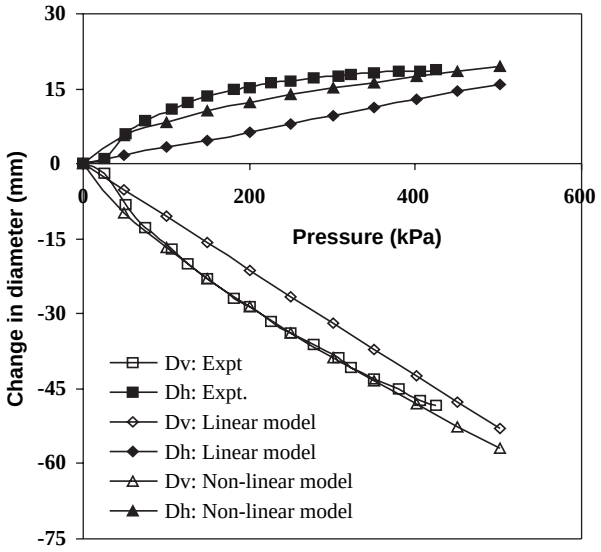

Figure C-6. Comparison of pipe deflection for HDPE pipe (1 mm = 0.042 in.; 1 kPa = 0.144 psi).

C.1.6 Analysis of Test Results

Since the 2D models idealize the problem as plane strain, only the circumferential strain can be calculated. Measurements of the deflection and the circumferential strains are compared in this section with those obtained using the finite element method and the simplified design equations.

C.1.6.1 Comparison of Pipe Deflections

Finite Element Analysis. Measured deflections are compared with the finite element calculation for the two tests in Figures C-6 and C-7, respectively. Analysis with the nonlinear soil model shows good agreement with the measured deflections in both cases. It reveals that accurate modeling of the soil is important in the analysis of pipe-soil interaction, since the soil stiffness largely controls the deformation of buried flexible pipe. The nonlinear model reasonably represents the soil behavior in the tests.

The finite element analyses with linear elastoplastic soil model appear to provide results similar to the nonlinear analyses at the maximum pressure (500 kPa or 72 psi) in Figures C-6 and C-7. The soil moduli for the linear analyses correspond to the values averaged (a line of best fit) over the 0 to 500 kPa (72 psi) stress range, capturing the accumulated effect of the nonlinear modulus on the pipe response at that stress level.

Simplified Methods. Moore (2000) implemented the 2D elastic continuum theory (Hoeg 1968) for design of buried pipes. Continuum theory is rigorous and permits the development of unified design methods that cover metal, concrete, and polymer pipes. However, the continuum theory equations are more complicated than those that can be developed to undertake design for only one class of product, thermoplastic pipes in this case, and they currently cannot assess variable installation conditions, such as poor haunch support. McGrath (1998a) proposed the simplified design equation presented earlier based on the continuum approach (Burns and Richard 1964) to calculate the vertical deflection of flex-

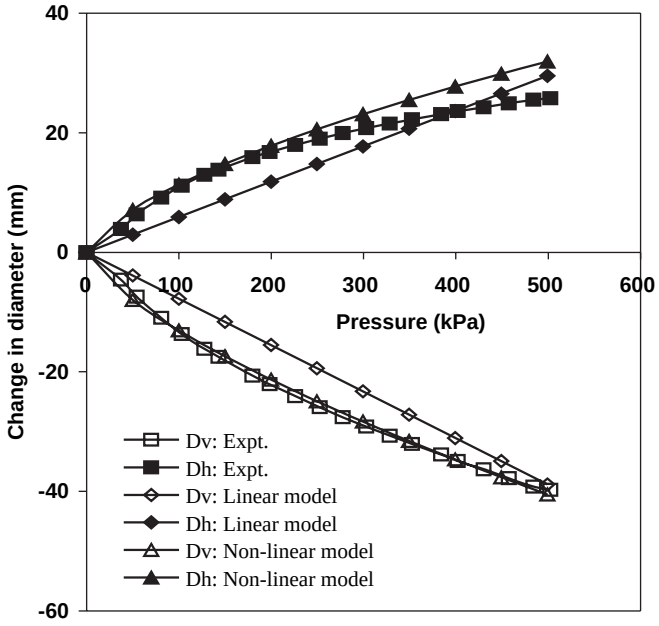

Figure C-7. Comparison of pipe deflection for PVC pipe (1 mm = 0.042 in.; 1 kPa = 0.144 psi).

Table C-1. Soil modulus at 100 and 400 kPa.

Stress kPa	Test Pipe	Constrained Modulus, M, MPa		Elastic Modulus, E, MPa	
		Secant	Average	Secant	Average
100	HDPE	6.8	5.1	4.6	3.4
	PVC	5.7	5.5	3.9	3.7
400	HDPE	11.5	9.6	7.7	6.5
	PVC	10.3	8.7	6.9	5.9

ible thermoplastic pipes. The equation is expressed in similar form to the Iowa equation (Spangler 1941), but incorporates contributions from both the hoop stiffness and the bending stiffness of the pipe-soil system.

The simplified design method is evaluated with the measurements and the finite element analysis in this section. A bedding factor of 0.083 is used in the simplified equation as proposed for 180° bedding, since backfill in the test cell was placed with care to provide good support to the pipe. The constrained modulus, M_s is estimated as either the secant value or the average value (obtained using a line of best fit through the origin over the stress range) using the nonlinear stress-strain relations (Figures C-4 and C-5). Constrained moduli and the corresponding elastic moduli at values of 100 kPa (14.4 psi) and 400 kPa (57.6 psi) of applied stress are summarized in Table C-1.

Calculations of pipe deflections have been obtained using various methods both at 100 kPa (14.4 psi) and 400 kPa (57.6 psi) of vertical earth pressure (Table C-2). Table C-2 shows that the continuum theory gives higher deflection for lined, corrugated, HDPE pipe and lower deflection for ribbed PVC pipe than does the simplified method. The opposite features for the different profiles imply that the structural stiffness of the pipes influences the calculation using the simplified method. The ribbed PVC pipe possesses higher hoop stiffness and lower bending stiffness compared to the corrugated HDPE pipe. It appears that the simplified method provides a conservative estimate of pipe deflection for this pipe with high hoop stiffness.

Calculated deflections obtained using the finite element method at 100 kPa (14.4 psi) and 400 kPa (57.6 psi) also are included in Table C-2. Comparison of measurements with the calculated deflections indicates that the finite element method performs the best in calculating pipe deflections. The method accounts for the soil nonlinearity that controls the behavior of the pipes. The simplified equation appears to render a reasonable estimate, when average modulus is used for the backfill soil. Linear finite element analysis with average soil modulus (Figures C-6 and C-7) also yielded a similar outcome. The simplified method with secant modulus gives somewhat unconservative estimates of deflection. The geometrical nonlinearity, which is predominant at higher stress, cannot be captured by the simplified procedure.

C.1.6.2 Pipe Strains

Simple beam theory has been used to calculate the strains from the thrust and moment values obtained from the finite element analyses. The finite element method calculates the thrust and bending moments at the Gauss (numerical integration) points of the elements. Circumferential strain on a fiber located at a distance Y from the neutral axis of the section is given by

$$\varepsilon = \frac{N}{EA} + \frac{MY}{EI} \qquad \text{(C.4)}$$

Here, N is thrust, M is the bending moment, E is the pipe material modulus, A is the area of the cross-section, and I is the moment of inertia.

Equation C.4 is based on the assumption that strain distribution is linear across the profile so that all fibers located at the same distance from the neutral axis are modeled as responding with the same strain. Linear distribution of strain along the profile depth was measured during the experiments, except on the liner at the springline of the lined corrugated pipe (shown in Figure C-8 at overburden pressure of 200 kPa or 29 psi). Solid marks on Figure C-8a represent the strains on the liner with solid circle at the springline and solid triangle at the crown of the pipe. Circumferential strain on the liner is less due to development of local bending (Moore and

Table C-2. Change in vertical diameter (mm) at 100 and 400 kPa.

Stress kPa	Test Pipe	Expt.	FE	Using Secant Modulus		Using Avg. Modulus	
				(a)*	(b)**	(a)*	(b)**
100	HDPE	–16.8	–16.9	–14.3	–14.7	–17.7	–18.1
	PVC	–13.1	–13.1	–13.8	–12.5	–14.2	–12.9
400	HDPE	–47.2	–48.1	–39.1	–41.0	–44.6	–46.5
	PVC	–34.6	–34.7	–33.5	–30.8	–38.6	–35.4

*Simplified Method (McGrath 1998a)
**Continuum Theory (Hoeg 1968), bonded interface

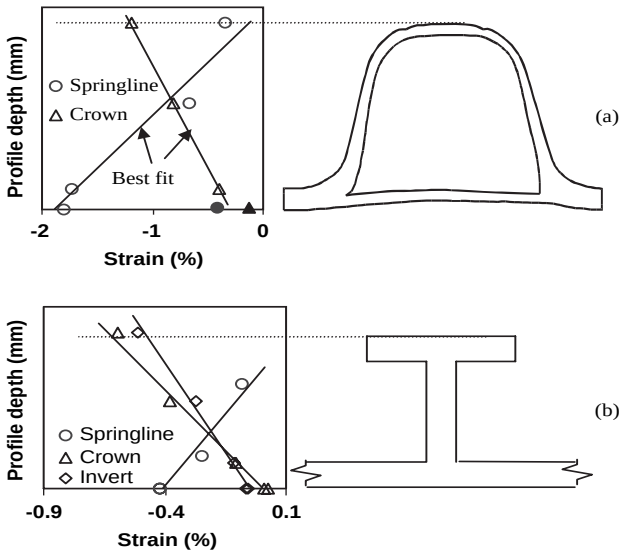

Figure C-8. Distribution of profile circumferential strains shows (a) lined corrugated pipe and (b) ribbed PVC pipe (1 mm = 0.042 in.).

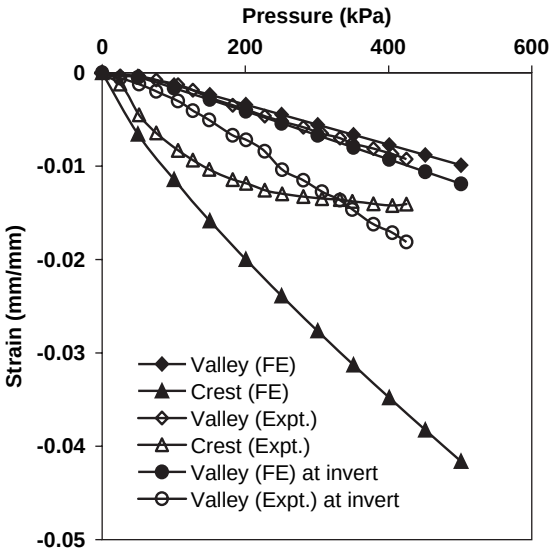

Figure C-10. Comparison of circumferential strains at the crown and invert (HDPE pipe) (1 mm/mm = 1 in./in.; 1 kPa = 0.144 psi).

Hu 1995), a phenomenon that cannot be included in the 2D theory. However, Dhar and Moore (2000b) demonstrated that the 2D theory could be applied to calculate the strains on the elements not subjected to local bending. Strains on two extreme fibers of the section (the valley or the inner wall and the crest) are examined in this appendix.

Comparison of circumferential strain at the springline, crown, and invert of the HDPE pipe are shown in Figures C-9 and C-10, which indicate general agreement between the measured strain and the calculated strain obtained from the 2D finite element analyses. Circumferential strains calculated at the springline (Figure C-9) are similar to the measured values, but are overestimated by about 12% on both the valley and the crest. At the crown, the calculated strain matches the measured strain (Figure C-10), except that the measured strain on the crest is a nonlinear function of overburden pressure and stabilizes to a maximum value of 1.4%. Local buckling is believed to have occurred on the crest of the element at that strain. No strain reading was obtained for crest strain at the invert of the pipe. Measured and calculated strains on the valley are in accord initially (Figure C-10) and deviate at higher stress levels, likely due to the nonlinearity associated with variation of local soil supports at the invert.

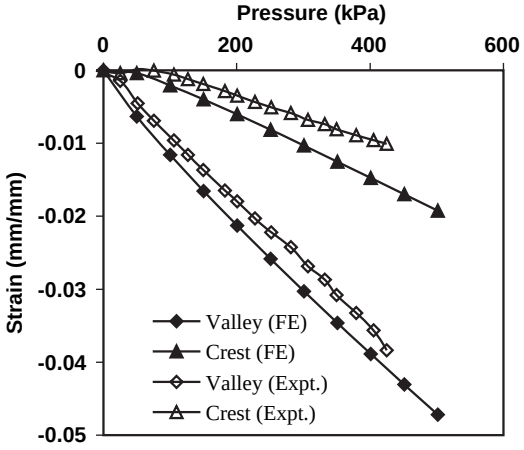

Figure C-9. Comparison of springline circumferential strains in HDPE pipe (1 mm/mm = 1 in./in.; 1 kPa = 0.144 psi).

For the PVC pipe examined, measurements of strains were made at the inner walls, rib web, and the crest of the profile (Figure C-1b). Pipe internal strain under the rib and midway between the ribs was essentially the same at all the locations (crown, springline, and invert). This implies that local bending is not important for the PVC profile. Experimental strains measured at the crown of the pipe are plotted in Figure C-11.

Comparisons of strains (measured and estimated) in the PVC pipe also support the 2D finite element analysis. Figures C-12 through C-14 show general agreement between the strain calculations and the measurements. Strains on the inner surface and the web at the crown are almost coincident. On the crest, the calculated values initially follow the measured values, but deviate at higher stress levels. At the springline, strains on the inner wall are overestimated. Strain at the springline can be reduced on the inner wall and increased on the crest due to insufficient compaction of soil at the haunch or underneath. Finite element estimations of strains are much higher at the invert, perhaps due to local nonuniformity of the soil in that region. Moreover, the trends of the measured

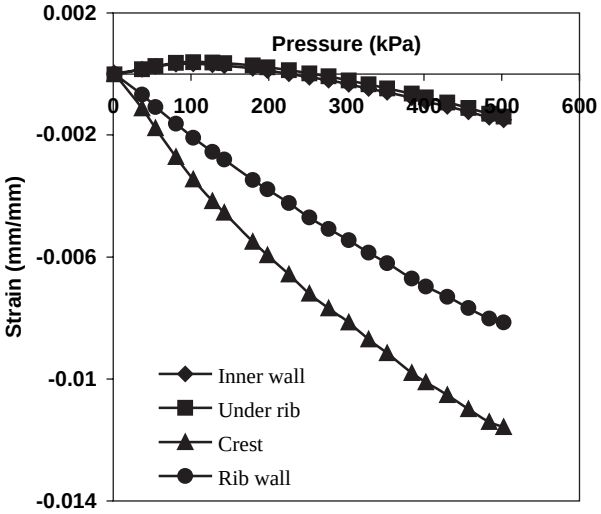

Figure C-11. Strain measurements at the crown (PVC pipe) (1 mm/mm = 1 in./in.; 1 kPa = 0.144 psi).

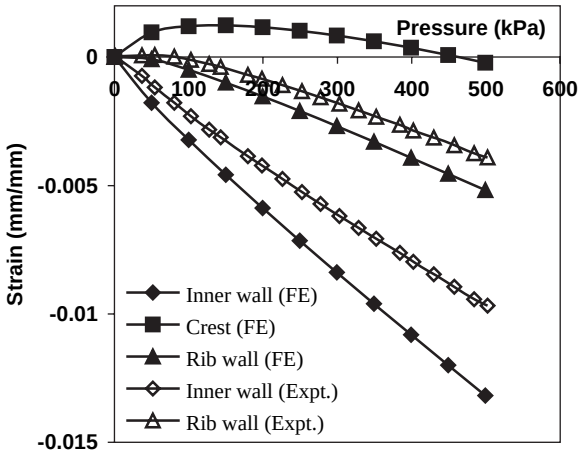

Figure C-13. Comparison of circumferential strain at the springline (PVC pipe) (1 mm/mm = 1 in./in.; 1 kPa = 0.144 psi).

and calculated strains are similar. Effects of different haunch support on the pipe response are studied in the next section of this appendix, where these discrepancies are discussed in more detail. Nevertheless, the 2D finite element method appears to estimate the behavior of the helically wound ribbed PVC pipe successfully.

Strain on the inner surface (under or midway between the ribs) is found to be tensile at low levels of overburden stress as a result of the negative bending moments (compressive outward) at the crown and invert (Figures C-12 and C-14). These strains revert to compressive values at higher stress levels where hoop thrust appears to govern the strains. Due to similar effects, the crest is subjected to tension at the springline (Figure C-13), but the strains remain tensile at that location up to much higher levels of vertical pressure.

C.1.7 Simplified Method for Estimating Peak Bending Strain

The simplified design equation for strain relates the pipe deflection to the peak circumferential bending strain through an empirical strain factor, D_f. For bending of a circular incompressible ring that produces an elliptical deformed shape, the factor is 3 (Roark 1943). For compressible buried pipes, D_f may also depend on the stiffness of the pipe relative to the soil (AWWA 1996). Values of the shape factors for the tests considered are calculated from the bending strains and the

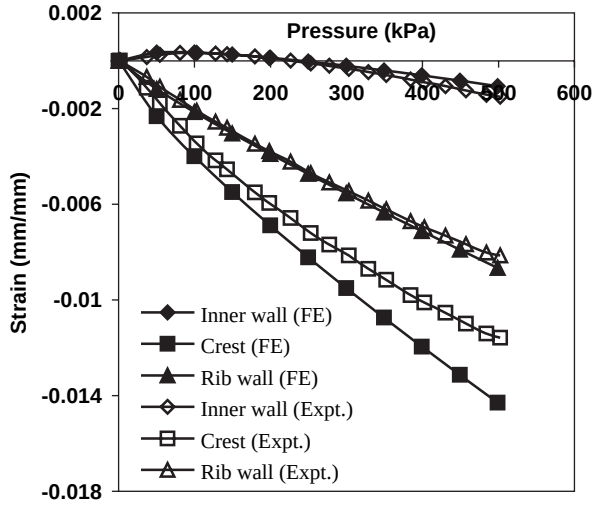

Figure C-12. Comparison of circumferential strain at the crown (PVC pipe) (1 mm/mm = 1 in./in.; 1 kPa = 0.144 psi).

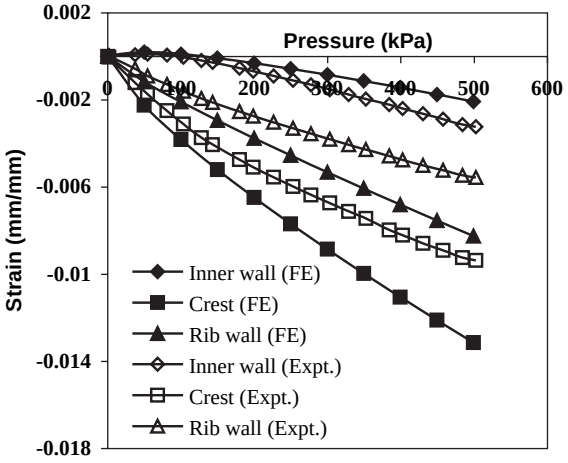

Figure C-14. Comparison of circumferential strains at the invert (PVC pipe) (1 mm/mm = 1 in./in.; 1 kPa = 0.144 psi).

bending deflection, $(D_v - D_h)/2$, given by the finite element method. Analyses in the previous sections indicate that for uniform soil support, the finite element method provides a conservative estimate of the circumferential strain on the profiles of the pipes. For the annular lined corrugated HDPE pipes, the shape factor is between 2.8 and 2.9, which is close to the value for elliptical deformation (i.e., 3). The strain factor is between 2.9 and 3.0 for the helically wound ribbed PVC pipe. Both values are somewhat less than the theoretical value of 3 as a result of factors such as decreases in pipe diameter due to circumferential shortening and the approximate nature of strain gage readings. The PVC pipe possesses considerably higher hoop stiffness compared to the HDPE pipes, but is somewhat more flexible in bending.

C.1.8 Effects of Soft Haunch

Overall performance of buried pipe is strongly influenced by the behavior of the backfill material. Dense backfill generally provides better soil support to the thermoplastic pipe, but it is usually difficult to achieve uniform compaction around the pipe using conventional compaction methods, particularly when working in a pipe trench of limited width. The soil below the pipe haunch cannot be accessed easily to carry out adequate compaction. Rogers et al. (1996) demonstrated that the lack of haunch support might result in strain concentrations and odd-shaped displacement patterns in the pipe. A study was made to develop an understanding of the effects of soft haunch on the pipe behavior. Since the finite element method has been successful in simulating pipe behavior under biaxial loading in the test cell, the analysis is used to investigate the influences of a soft haunch on both lined corrugated HDPE pipe and ribbed PVC pipe. Figure C-2 shows the zone of low-stiffness haunch soil considered in the analysis, a geometry consistent with that considered by McGrath (1998a), but with the side of the low-stiffness zone extended up almost vertically towards the springline. Values of elastic modulus for this zone are reduced relative to the surrounding soil. Linear elastic analysis is performed with a Mohr-Coulomb failure criterion for the backfill to account for the soil plasticity. The pipe material moduli used in the study were 450 MPa (65 ksi) and 3,000 MPa (435 ksi) for the HDPE and PVC, respectively, and the backfill soil modulus was 20 MPa (2.9 ksi). All calculations were performed for an overburden pressure of 300 kPa (43.2 psi).

The deflected shapes of the pipe for different moduli in the haunch region (E_s/E_h = 1 to 100) demonstrate that the stiffness of the surrounding soil influences the pipe deformation (Figure C-15). Here, E_s represents the modulus of backfill soil, and E_h the modulus of the haunch soil. Figure C-15 plots deformed shapes of the lined corrugated HDPE pipe for different soil modulus under the haunches. The invert of the pipe

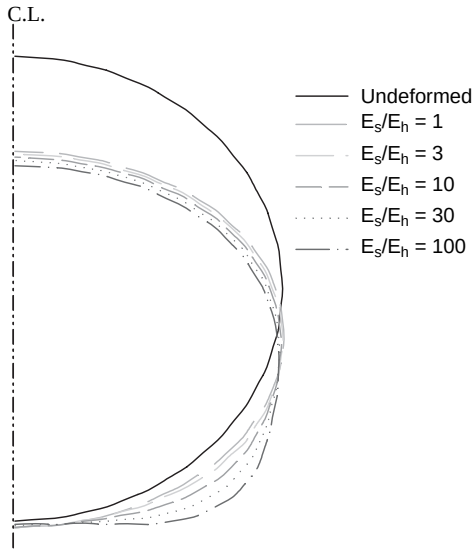

Figure C-15. Deformed shape of the pipe for different soil support (deflection × 5).

flattens when the stiffness of the soil at the haunch is reduced. This is largely consistent with what is denoted as "inverted heart shape" deformation by Rogers (1988), a shape characterized by flattening of the pipe at the invert. Rogers et al. (1996) indicate that the pipe undergoes inverted heart shape deformation when the soil around the haunches is poor while that above it is of good quality. The crown deformation may also be affected if the reductions in stiffness within the soft haunch are substantial.

Distributions of circumferential strains on the extreme fibers (on the valley or the inner wall and the crest) of the sections are plotted for the HDPE and PVC pipes in Figures C-16 and C-17, respectively. The figures illustrate that the weak haunch significantly redistributes the strains around the pipe circumference. Concentration of strains develops at the haunch due to reduction in soil stiffness. Variations of strains around the circumference are similar for the HDPE and the PVC pipes.

For pipes buried in uniform ground, circumferential strain on the valley or the inner surface at the springline represents the maximum value of compression the pipe encounters (as per classical understanding of buried pipe behavior). However, Figures C-16 and C-17 show that the valley (inner surface for PVC pipe) compression decreases at the springline and increases at the haunch with the increase of E_s/E_h ratio. For the reduction of haunch stiffness by a factor of 100, the valley strain or inner wall strain between the ribs increases by 17% (from 2.9% at the springline to 3.4% near the midhaunch) on the HDPE pipe and by 38% (from 0.95% at the springline to 1.3% at the midhaunch) on the ribbed PVC pipe. The maximum compression is located near the middle of the

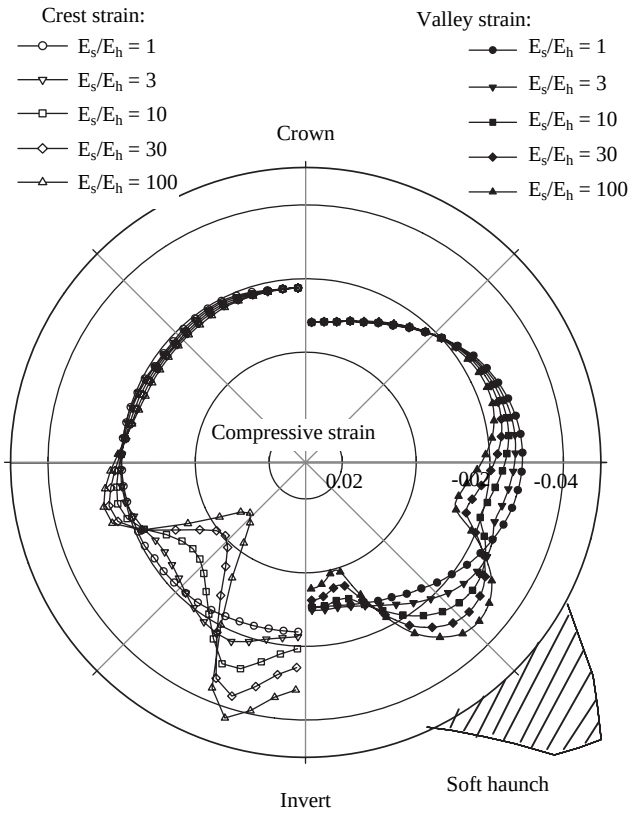

Figure C-16. Distribution of circumferential strains on HDPE pipe.

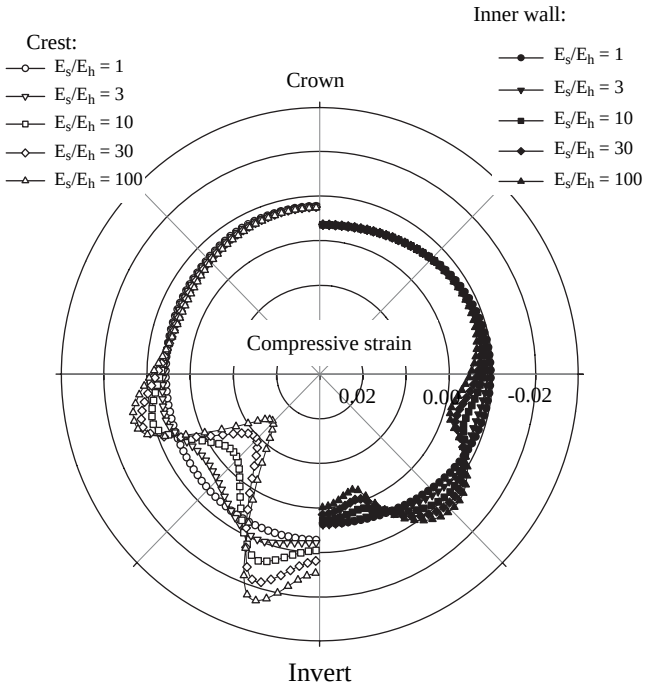

Figure C-17. Distribution of circumferential strains on PVC pipe.

weak haunch in both pipes, although the strain increase is much higher for the PVC pipe.

Strain on the crest of the profile increases even more as a result of the presence of a soft soil under the haunch. At the invert, the crest strain is almost doubled on both the HDPE and the PVC pipe for haunch stiffness of 1/100th of the stiffness of the backfill soil. The strain increase is from 1.6% to 3.2% in the HDPE pipe and 0.72% to 1.46% in the PVC pipe. Maximum compression on the crest occurs near the boundary of the lower stiffness haunch soil. For E_s/E_h beyond 10, the maximum compression of the pipe section is on the crest at the haunch boundary. These large compressions may lead to local buckling or circumferential crushing of the elements.

The strain factors, D_f, for different levels of haunch support are calculated from the maximum bending strain obtained from the finite element method. Table C-3 shows the D_f factors along with the locations (θ) of the maximum bending strains. The θ value is measured in degrees from the crown. Values of D_f for uniform ground support $E_s/E_h = 1$ are up to 20% lower than the theoretical value of 3 for elliptical deformation, since bending moment is reduced somewhat by boundary effects (McGrath et al. 2001). The strain factors increase from 2.4 to about 5.0 for the HDPE pipe and from 2.8 to 10.0 for the PVC pipe due to change of the ratio, E_s/E_h from 1 to 100. This indicates that the influence of the weak haunch is more significant on the PVC pipe than on the lined corrugated HDPE pipe. With the increase of E_s/E_h, the position of the maximum valley strain or inner wall strain moves from the springline toward the middle of the haunch, and the maximum crest strain moves from the invert to the boundary of the lower stiffness soil region under the haunch. This analysis shows the range of shape factors that can arise from a variety of haunch stiffnesses and a large zone of low stiffness material at that location. Final design recommendations would depend on an assessment of appropriate design conditions. Since specifications should always require care in placement of soil under the pipe haunches, the most severe conditions considered here are likely beyond typical design conditions.

Table C-3. Shape factors for weak haunch supports.

E_b/E_h		HDPE Pipe		PVC Pipe	
		Valley	Crest	Inner Wall	Crest
1	D_f	2.7	2.8	2.9	3.1
	θ	90°	0°/180°	90°	0°/180°
3	D_f	2.9	3.1	4.3	4.3
	θ	122°	157°	126°	158°
10	D_f	5.4	5.9	9.7	8.8
	θ	127°	162°	131°	161°
30	D_f	8.8	9.0	14.6	13.3
	θ	132°	162°	134°	164°
100	D_f	11.9	11.3	18.4	17.0
	θ	132°	162°	134°	164°

C.1.9 Conclusion

Analysis of tests on HDPE and PVC pipes reveals that the 2D finite element method can be used effectively to calculate both pipe deflections and circumferential strains. However, performance of the method relies on the appropriateness of the constitutive model used to characterize the material behavior. Janbu's (1963) nonlinear soil model effectively simulated the nonlinear soil behavior. Linear analysis with soil modulus averaged over the stress range provided the best characterization of the accumulated effects of soil nonlinearity for these tests.

Calculation of pipe response by the finite element method matched the measurements within about 10%. Neither local bending nor local buckling can be considered in the 2D analysis (Moore and Hu 1995). However, the method can be used successfully to calculate the response of the elements on which the three-dimensional (3D) effects are not significant. Pipe deflections and the valley strain for the lined corrugated HDPE pipes are not influenced by the local bending or local buckling, and local bending is not important for the ribbed PVC pipe.

Although the finite element method provides a comprehensive design approach that can be used for high-cost or unusual installations, the simplified design equations proposed by McGrath (1998a) are more suitable design tools for standard buried pipe installations. Structural stiffness of the pipes may have an influence on the performance of the simplified method. The method overestimated deflections for pipe with high hoop stiffness (i.e., ribbed PVC pipe) relative to pipe with low hoop stiffness (i.e., corrugated HDPE pipe); however, this may have been the result of a poor match with the actual PVC modulus of elasticity.

Shape factor D_f used in the simplified equations is estimated from the maximum bending strain obtained from the finite element analyses of the tests. Values of D_f were 2.9 for annular lined corrugated HDPE pipe and 2.9 for the helically ribbed PVC pipe, both of which were carefully installed. The values are slightly lower than the value of 3 for elliptical pipe deformation as a result of boundary effects in the test cell.

Nonuniformity of the surrounding soil support has a significant effect on the behavior of buried pipe. Low-stiffness-soil support at the haunch induces "inverted heart shape" deformation of the pipes (Rogers 1988). The weak zone may change the distribution of strain around the pipe circumference considerably. The strains concentrate on the inner surface of the pipe (under the valley of lined corrugated HDPE pipe) towards the middle of the haunch zone and on the crest at the boundary of the zone of low-stiffness haunch soil. For the cases considered, the crest strain appeared to govern the design when the stiffness of the haunch soil was less than one-tenth of the stiffness of the surrounding backfill.

Haunch support appeared to affect the strains on ribbed PVC pipe more significantly than on corrugated HDPE pipe. Strain factor values of approximately 9 and 6 were obtained for PVC and HDPE pipes, respectively, with soil modulus ratio $E_s/E_h = 10$ (corresponding to about a 15% reduction in compaction density under the haunch). Strain factor values rose to over 17 and 11 for PVC and HDPE pipes where $E_s/E_h = 100$. Additional experimental work is reported in Section C.4 to further examine the effect of construction practice on circumferential strain.

C.2 Evaluation of Local Bending in Profile-Wall Polyethylene Pipes

C.2.1 Introduction

Thermoplastic pipes with different wall geometries have been manufactured to achieve effective utilization of pipe materials. A wide variety of wall geometries have been developed by the pipe manufacturing industry over the last decades. However, the shapes of these profiles have led to questions regarding their impact on pipe performance. Hashash (1991) observed liner buckling and circumferential cracking on the inner walls of a lined corrugated pipe under high embankment 100 ft (30.5 m) near Pittsburgh, PA. The localized short-wave deformation and inner-wall tearing was also observed in honeycombed (tubular profile) HDPE pipe under 40 ft (12.2 m) fill in Ohio (Hurd et al. 1997). A recent study on field performance of 45 HDPE culvert pipes at different sites in South Carolina has revealed circumferential cracks in 18% of the pipe, localized bulges in 20% of the pipe, and tears or punctures in 7% of the pipe (Gassman et al. 2005). The study warranted further investigation to sufficiently quantify the problems. Moore and Hu (1996) demonstrated earlier from axisymmetric finite element analysis that localized bending on profile components can produce significant tension at the liner-corrugation junction in lined corrugated HDPE pipe. The circumferential cracking reported by Hashash (1991), Hurd et al. (1997), and Gassman et al. (2005) suggests that high axial (longitudinal) tensile stresses develop in these profiles.

Moore and Hu (1995) used finite element analysis to show that axial tensions arise in lined corrugated HDPE pipes as a result of local bending, a 3D phenomenon that cannot be estimated using conventional 2D shell theory. However, Section C.1 demonstrated that the overall pipe responses (deflections and strains on elements not undergoing local bending) can be predicted effectively using the conventional 2D plane strain idealization.

Section C.3 describes experiments conducted on four different profile-wall pipes under axisymmetric loading (inducing uniform hoop compression). Local bending is investigated here for each of those four profile-wall pipes, with the objective of developing a better understanding of the localized distress encountered in profile-wall pipes in the field. Com-

parisons of strain distributions for the four profiles are made to explore the effects of the profile shape on bending.

First, strain distributions in the walls of the pipes are evaluated using axisymmetric finite element analysis for comparison with strain measurements obtained from laboratory tests. The analysis is then extended to investigate pipe responses in a more realistic biaxial stress field (biaxial stresses develop in the field, since horizontal earth pressures are generally less than the vertical earth pressures). The 3D analysis includes explicit modeling of the profile geometries recorded from various test specimens.

C.2.2 Description of the Profiles and Full-Scale Tests

Sections C.1 and C.3 describe the four different profile-wall pipes studied in the biaxial and/or axisymmetric loading environments using full-scale tests. Two of the pipes investigated were lined corrugated (also known as "twin-wall") profile; one was boxed profile, and the other was tubular (also called "honeycombed") profile. Figure C-18 shows the pipes and profile cross-sections. One of the lined corrugated pipes had a corrugation spacing (pitch) of 80 mm (3.1 in.) and corrugation depth of 58.7 mm (2.3 in.). The other pipe possessed a corrugation spacing of 101 mm (4.0 in.) and corrugation depth of 55.2 mm (2.2 in.). Thus, the spans of the liners were different in these two profiles. Components of each profile are defined in Figure C-18. The box profiled pipe was manufactured by helical winding of the box section so that the central ribs are oriented at an angle of 2° to the pipe circumference. The tubular profiled pipe was manufactured by spirally winding a unit of four tubes. The units were fused together at the ends. The helix angle for the tubular profile was approximately 6° from the pipe circumference. Nominal diameters for the boxed and tubular profiles were 760 mm (29.9 in.) and 1,060 mm (41.7 in.), respectively.

In the axisymmetric loading test, the pipe was placed upright (vertical) concentrically within a steel cylindrical cell (the hoop cell, Moore et al. 1996). The pipe was then backfilled using granular soil (an "SP" material according to Unified Soil Classification System). The backfill soil is placed in approximately 150-mm (6-in.) thick layers, with each layer compacted using a tamper (10 lbs or 4.5 kg in weight). Height of fall of the tamper was 305 mm (12 in.) to achieve a compaction of 80% to 90% of maximum standard Proctor density, established in various trials. Radial pressure was applied to the soil-pipe system using an inflatable air bladder lining the inner surface of the cylinder. The air pressure was measured using a pressure gage and a conventional data acquisition system. The cell was axially restrained along with the pipe to attain a plane-strain condition, and the length of the tested pipe was the same as the length of the cell (1,450 mm or 57 in.). The diameter of the cell was 1,500 mm (59 in.). Figure C-19 shows the arrangement of a pipe in the hoop cell. Pipe deflections and strains on different profile elements were measured during the tests to capture the local bending. Normalized pipe deflections expressed as $\Delta D/D$ (for diameter D) equal the hoop strains assuming that the soil density and stiffness is uniform around the pipe.

C.2.3 Finite Element Model

Axisymmetric finite element analysis was employed to investigate the response of the pipes under axisymmetric loads.

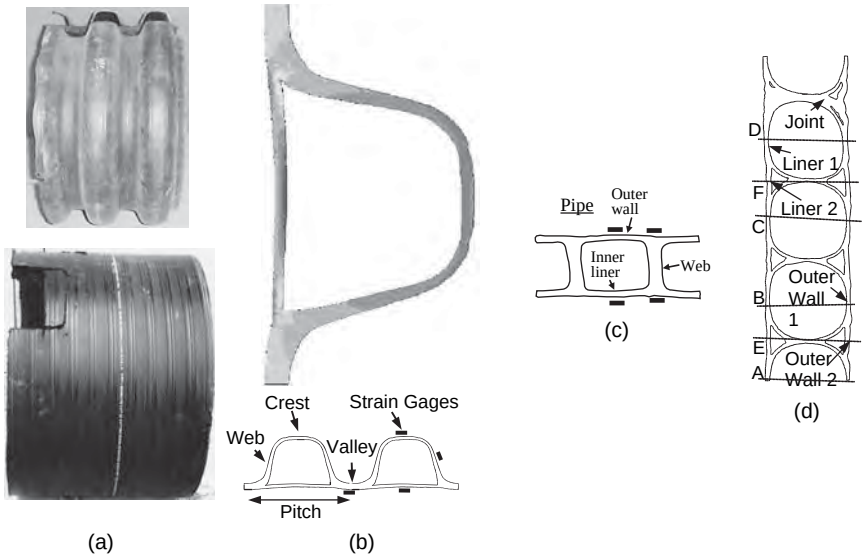

Figure C-18. HDPE pipe profile showing (a) pipes, (b) lined corrugated profile, (c) boxed profile, and (d) tubular profile.

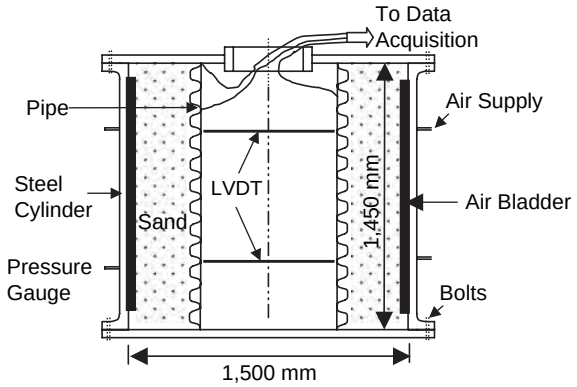

Figure C-19. Arrangement of a pipe in hoop cell test (1,000 mm = 39.4 in.).

Pipes with annular profiles have axisymmetric geometries; therefore, axisymmetric finite element analysis with the finite element mesh defined in the r-z plane can be used to define the problem geometry. Figure C-20 depicts a typical finite element mesh used for an annular pipe with lined corrugated profile (Dimension L is defined as used later in this appendix). The pipes are modeled as being very long, using smooth rigid (axially restrained) boundaries at the top and the bottom of the mesh. The pipes were modeled in the analysis to simulate the test conditions in the hoop cell discussed earlier.

Figure C-20a shows the finite element mesh used for analysis of the lined corrugated pipe in the axisymmetric loading test. The external diameter of the soil region around the pipe corresponds to the inner diameter, 1,500 mm (59 in.), of the steel test cell. This provides a soil ring width of 430 mm (16.9 in.) surrounding the lined corrugated pipes. Finite element meshes for the helically wound boxed and tubular profiles are shown in Figures C-20b and C-20c, respectively. Geometry of the pipe profiles was explicitly modeled in the analysis. Although the geometry of the helical profiles is non-axisymmetric, axisymmetric idealizations were used. This avoids the significant complexities of modeling the true spiral geometry. A comparison of calculated strains and those measured in the tests is used to investigate whether this axisymmetric approximation is reasonable for the helically profiled pipes. A soil ring of 335 mm (13.2 in.) width surrounded the pipe with boxed profile. A 175-mm (6.9-in.) soil ring surrounded the pipe with tubular profile.

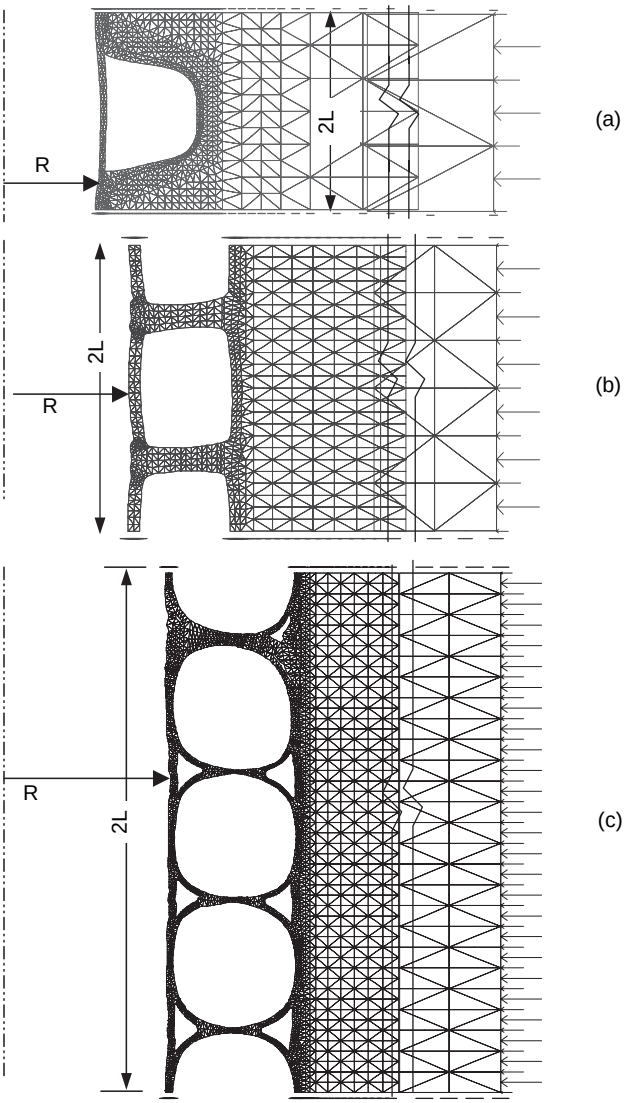

Figure C-20. Finite element mesh for axisymmetric analysis shows (a) lined corrugated pipe, (b) boxed profiled pipe, and (c) tubular profiled pipe.

C.2.4 Material Parameters

C.2.4.1 Pipe Parameters

Use of appropriate constitutive models is necessary to reasonably simulate the physical behavior using finite element analyses. Thermoplastic material exhibits noticeable time-dependent behavior. However, elastic modeling using secant modulus is the most widely used approach for thermoplastic pipe analysis because of its simplicity. Both a linear elastic model based on secant modulus at a particular elapsed time and the viscoplastic model of Zhang and Moore (1997) have been used in this study to analyze the pipes tested in the axisymmetric cell. Zhang and Moore (1997) developed a viscoplastic model for HDPE material after adapting the framework of Bodner's overstress theory (Bodner and Parton 1972). They determined two sets of viscoplastic model parameters for two HDPE pipe materials using uniaxial compression tests on cylindrical specimens (with 12.7-mm or 0.5-in. diameter and 25.4-mm or 1-in. height) cut from pipes obtained from the manufacturers of one of the lined corrugated pipes and the box profile pipe. Moore and Zhang (1998) successfully used

Table C-4. Pipe parameters used in the FE analysis (1 MPa = 144 psi).

Material Model	E (MPa)	ν	C	n	γ (MPa)	β × 10^{-5} (MPa)	d_1 ×10^{-3}	d_2	d_3 ×10^{-2}
Linear Model	450	0.46	–	–	–	–	–	–	–
VP Model-1*	1,350	0.46	0.01	8.0	10^{-4}	7.744	1.055	3.829	2.55
VP Model-2*	1,450	0.46	0.01	8.0	10^{-4}	7.056	1.042	3.829	2.55

*Zhang and Moore (1998)

the model for simulation of HDPE pipe response in a parallel plate test. These parameters are used in this study for simulation of pipe responses in axisymmetric tests. However, it is expected that the quality of the viscoplastic calculations for the profiles presented here could be degraded somewhat because the specific material parameters for each of the test pipes were not available. Parameters used for pipe materials are summarized in Table C-4.

C.2.4.2 Soil Parameters

Stresses and deformations of the soil were not measured during the test in the hoop cell. Soil parameters used for the analysis were those reported by Zhang and Moore (1998), who undertook an analysis of a pipe tested in the same backfill. However, the degree of compaction achieved in each hoop compression test was variable, since compaction was difficult to control in the narrow space between the pipe and the test-cell wall (Dhar and Moore 2004). Zhang and Moore (1998) used modulus of elasticity, E, and Poisson's ratio, ν, for the soil as 30 MPa (or 4.3 ksi) and 0.2, respectively.

An elastoplastic soil model based on the Mohr-Coulomb failure criterion was used in the analysis to capture shear failure during the pipe tests. For the elastic-plastic analysis, an angle of internal friction for the soil, $\phi = 36°$, was selected based on data suggested for material classified as "SW85" by Selig (1990). Angle of dilation was set as equal to the angle of internal friction (i.e., 36°), though one analysis was performed using a smaller dilation angle (i.e., 13°, a typical value for granular material; Skempton 1984), which showed no significant change in the calculated pipe response (less than 1% deviation in calculated deformation).

C.2.5 Comparison of Wall Strains with Measurements

C.2.5.1 Lined Corrugated Pipes

Figure C-21 shows a comparison of the inner-wall strains of a lined corrugated profile. Calculated strains generally provide a reasonable match with the measurements except at high radial stress when local buckling caused the liner strain to be stabilized (Dhar et al. 2004). Other comparisons were similar, but are omitted for brevity. In Figure C-21, calculated circumferential strains on the liner are less than those on the valley, as recorded during the test. Distributions of calculated and measured strains along the interior surface of the two lined corrugated profiles are plotted in Figures C-22 and C-23 at a radial cell pressure of 150 kPa, for hoop and axial strains, respectively. It is evident from the figures that the hoop strains are not uniform along the inner surface of the lined corrugated profiles (even though the distance of the inner wall from

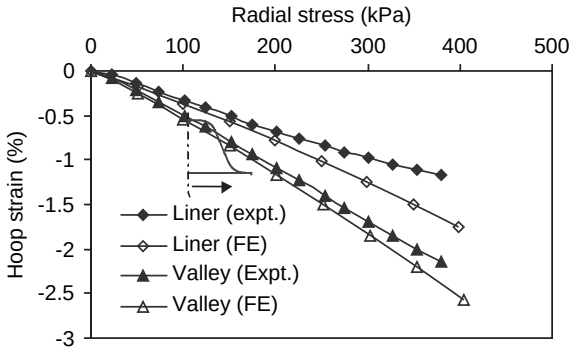

Figure C-21. Comparison of inner-wall strains of lined corrugated profile (1 kPa = 0.144 psi).

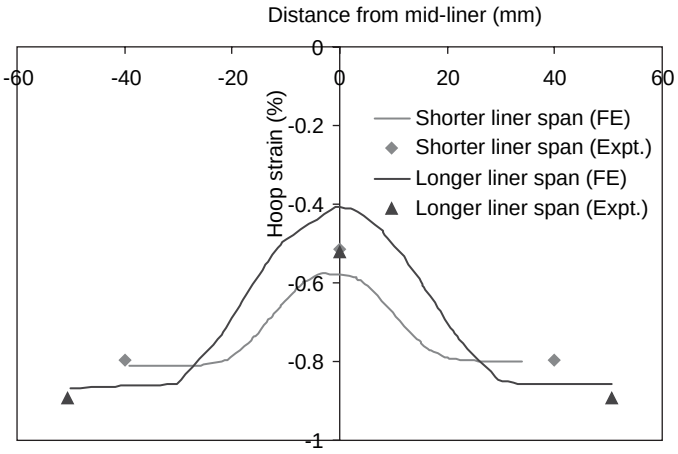

Figure C-22. Distribution of hoop strain on inner wall (150 kPa radial pressure) (1 kPa = 0.144 psi; 10 mm = 0.39 in.).

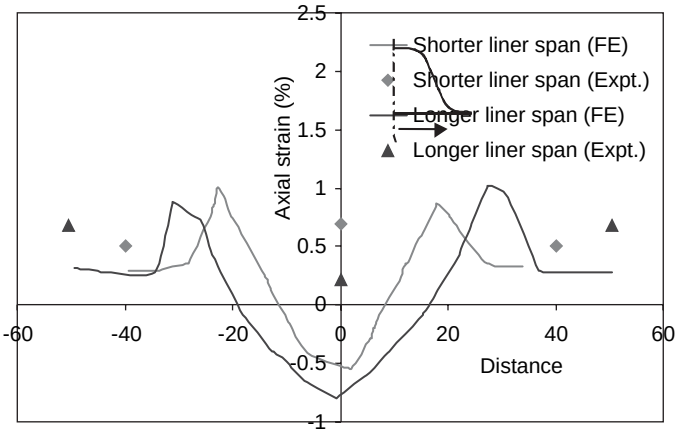

Figure C-23. Axial strain distribution in inner wall (150 kPa radial pressure) (1 kPa = 0.144 psi; 10 mm = 0.39 in.).

the neutral axis of the profile is almost constant). Local bending of the liner has resulted in the compressive hoop strain varying from a maximum at the valley to a minimum at the midposition where the liner spans between the valleys (Figure C-22). The mechanism of the bending can be explained using the deflected shape of the profile under load (Figure C-24). Solid lines in the figure represent the original position, and the dotted lines show the deflected geometry. Local bending develops in the liner because it is forced to deform inwards where it is connected at the valleys and inward movements decrease toward the liner midpoint. This local bending produces peak longitudinal (axial) bending strains in the liner where it connects to the liner and bending strains of opposite sign at the midpoint.

Analysis suggests that the circumferential liner strain is about 70% of the valley strain for the profile with shorter liner span, while the measurement gave this percentage as 65%. The amount of liner-to-valley strain for the longer liner was 50%; the measured value was 60%. The magnitudes of the measured hoop strain at the midliner are somewhat lower than the calculated values, although calculated valley strains match the measurements well. Further details of the analysis of the lined corrugated profiles are available elsewhere (Dhar 2002).

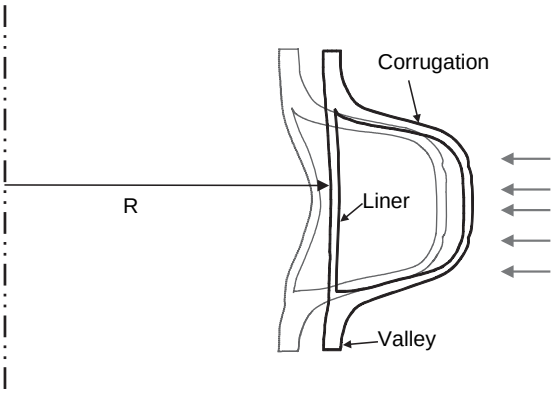

Figure C-24. Mechanism of local bending (after Moore and Hu 1995).

The finite element analysis indicates there is a local increase in tensile axial strain at the liner-corrugation junctions of both profiles (Figure C-23). No measurements of strains were made directly at this position because of the difficulty of attaching gages. Measurements of axial strain at other locations do not match those obtained from the analysis. The most likely explanation for this discrepancy is that the changes in the local strain field occur where a strain gage is adhered to the surface of an HDPE pipe (e.g., Brachman 1999). It appears likely that the effect of strain gage "stiffening" is severe in regions of high strain gradients, particularly through the thickness of the liner element, so that axial strain measurements are poor (circumferential strains feature lower through-thickness gradients, so they are less affected by this phenomenon).

C.2.5.2 Box-Profiled Pipe

Figure C-25 presents axisymmetric finite element calculations and measurements of pipe deflections for the helically wound boxed profile. In Figure C-25, calculations using the viscoplastic HDPE model of Zhang and Moore (1998) better match the measurements than calculations based on linear elastic material modeling. The nonlinear time-dependent effects of the pipe material appear to noticeably influence the behavior. Use of viscoplastic material parameters, which were established for a different HDPE pipe product, may have contributed to the underestimation of the diameter decreases.

Hoop strains at the inner liner and outer walls of the boxed profile match the measurements well (Figure C-25). The measured hoop strain was less than the deflection ratio (Δ/D) (Figure C-25a), although for axisymmetric behavior, the strain is expected to be the same as the deflection ratio. This discrepancy might have resulted because the profile has helical geometry rather than the axisymmetric (annular) configuration modeled in the analysis.

The hoop strains under the web (on the interior surface) and over the web (on the exterior surface) were measured as much less than those on the liner (see Figure C-18 for definition of profile components). Measured strain under the web is about 50% of the liner strain on the interior surface (Figure C-25b), and the outer surface web strain is approximately 70% of the exterior surface value midway between webs (Figure C-25c). The axisymmetric analysis produced almost the same values of strain on the web and liner. The helical winding of the rib may produce localized behavior within the profile which is not captured effectively using the axisymmetric idealization.

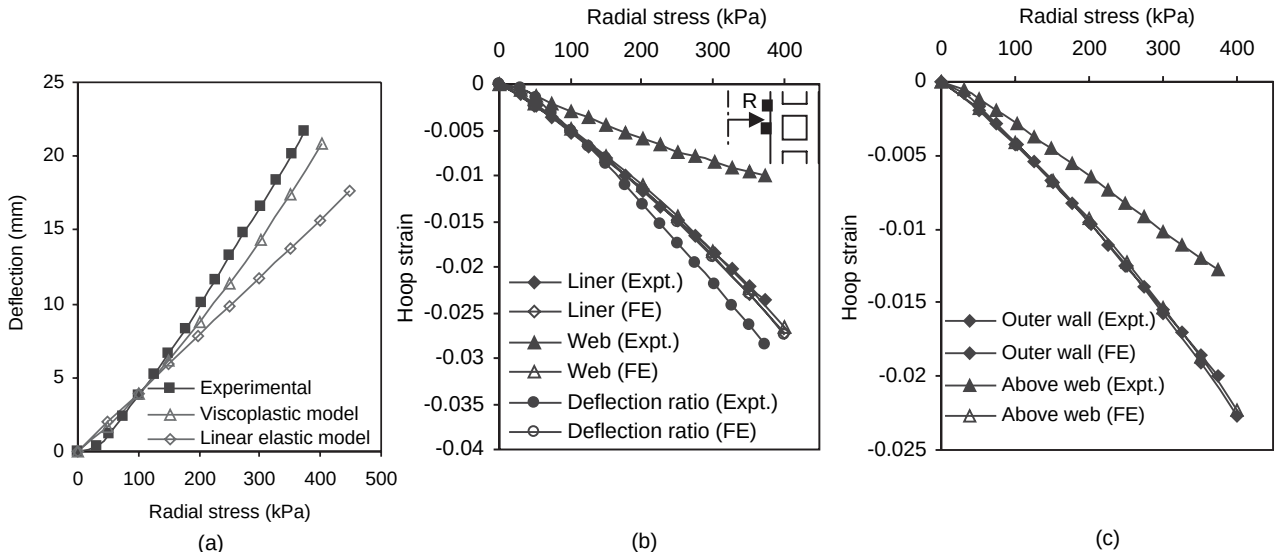

Figure C-25. Response of boxed profiled pipe under hoop compression shows (a) deflection, (b) hoop strains on interior walls, and (c) hoop strains on exterior walls (1 kPa = 0.144 psi; 10 mm = 0.39 in.).

The lateral element (the web) of the profile is very thick, and when analyzed as axisymmetric, it will have high hoop and torsional stiffness. In particular, a rib of helical geometry is likely much easier to twist under torsion, and this may have led to the lower hoop strains at the location of the rib.

The comparison indicates there are limitations associated with the use of an axisymmetric idealization of the profile for calculation of local bending effects (wall strains) in the boxed profile. However, the diameter decrease was successfully estimated, indicating that global response is not affected. The axisymmetric analysis provided upper bounds for the hoop strains in the profile, so use in pipe design should produce conservative estimates of hoop stress and hoop strain.

C.2.5.3 Tubular (Honeycombed) Profile

Figure C-26 shows calculated and measured values of diameter decrease for a pipe with honeycombed (tubular) profile. The axisymmetric finite element procedure appears successful in estimating the pipe deflections for the profile. The viscoplastic model effectively captured the nonlinear nature of the pipe deflections in Figure C-26a.

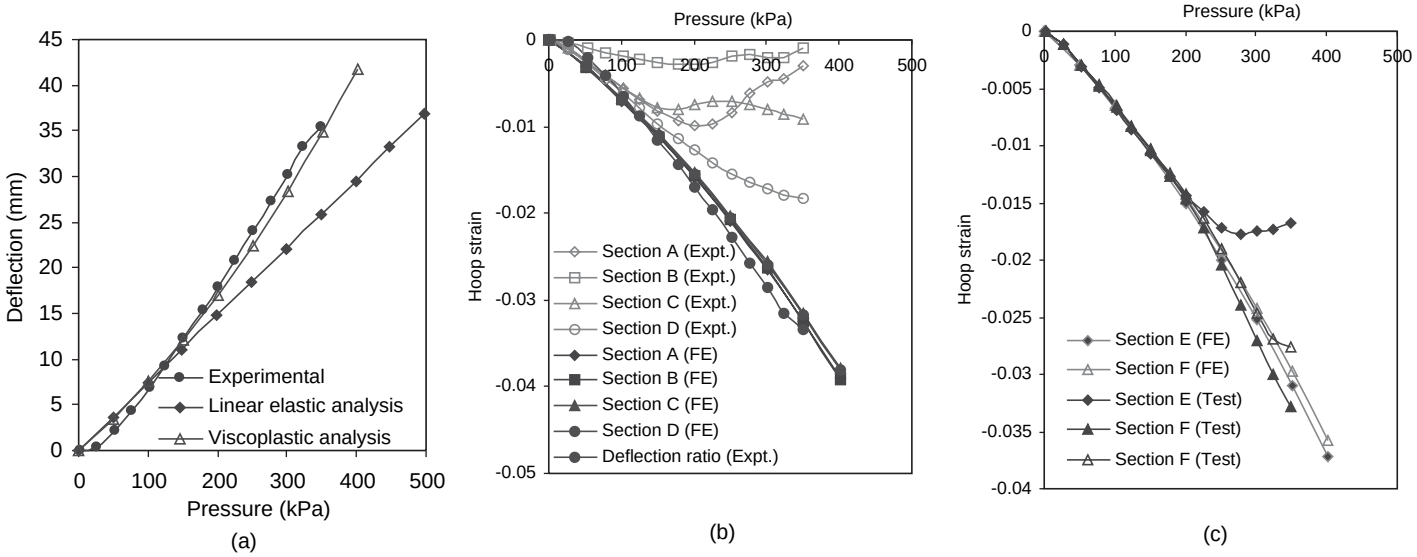

Figure C-26. Responses of tubular profiled pipe shows (a) deflection, (b) hoop strain on Liner 1, and (c) hoop strain on Liner 2 (1 kPa = 0.144 psi; 10 mm = 0.39 in.).

Strains on the tubular profile were measured on the inner liners and the outer walls of all of the tubes of the unit (locations A through F shown in Figure C-18d). This pipe was manufactured by helical winding of a unit of four tubes. Strain estimates at each of these locations show general agreement with the measurements (Figures C-26b and c). With the exception of Point B, which appears to suffer from a gaging problem or a geometric variation not captured in the model, hoop strains at locations of the interior elements (the locations denoted "Liner 1" and "Liner 2" in Figure C-18d) matched well, except at high load levels where certain elements showed the nonlinearity associated with local buckling (Figure C-26c). The geometrically linear finite element model could not capture the buckling, which is a geometrically nonlinear phenomenon. Geometry of the tubular profile was irregular, which significantly affected the local strains and the development of buckling. Hoop strains measured on Outer Wall 2 did not match the calculated values very well (Figure C-27b), while calculation of the strains on Outer Wall 1 performed better (Figure C-27a). In both cases, measured strain was less than the calculated value. In particular, the section connecting the two tubes (that part denoted "Outer Wall 2" in Figure C-18d, the outer segment of the "tubes") provided greatly reduced hoop-strain measurements. This may have resulted from difficulties associated with making the local strain measurements on that outer surface that is in direct contact with the surrounding soil, although in each case, there were repeated measurements that provided similar low values. Axisymmetric idealization of helical profile may also cause the high strain calculation on the elements, as noticed for the box profile discussed earlier.

Figure C-27c shows axial strain on Outer Wall 1 of the tubular profile. Both calculations and measurements indicate that the axial strains at different locations of the profile are inconsistent, clearly the result of local bending associated with the irregular geometry. However, the comparison reveals that the helically wound tubular profile could be modeled more effectively than the boxed profile using an axisymmetric (annular) idealization. Perhaps this is because the walls are very thin for the tubular profile, so they provide little torsional rigidity.

C.2.6 Comparison of Local Strains in Different Profiles

C.2.6.1 Axisymmetric Compression

The study presented here reveals that the finite element analyses with explicit modeling of the profiles can be used to study various aspects of the 3D response of profiled pipes. The 3D profile behavior under uniform radial compression is examined using axisymmetric finite element analysis. Wall strains on different profiles were examined for this comparison of profile performance.

Distributions of hoop strains on the inner surface of the four profiles at a radial cell pressure of 150 kPa are plotted in Figure C-28. Strains are normalized with the deflection ratio so that results for each pipe can be compared (since deformations are not the same on all pipes at a given radial pressure). Strain location is defined using z (the axial distance from the middle of pipe longitudinal segment considered) normalized relative to L (half the axial length of the meshes shown in Figure C-20).

Figure C-28 shows that the box profile has circumferential strains at the surface of the inner wall that are calculated to be almost uniform. The strains for the tubular profile are less

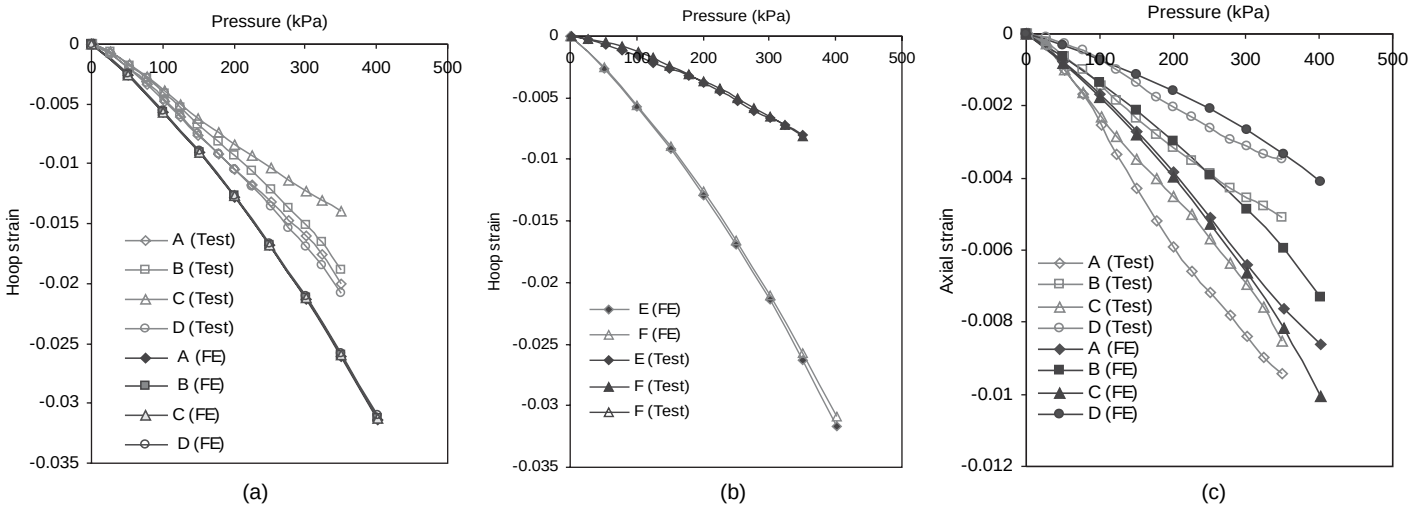

Figure C-27. Outer-wall strains on tubular profiled pipe shows (a) hoop strains on outer wall 1, (b) hoop strains on outer wall 2, and (c) axial strain on wall 1 (1 kPa = 0.144 psi; 10 mm = 0.39 in.).

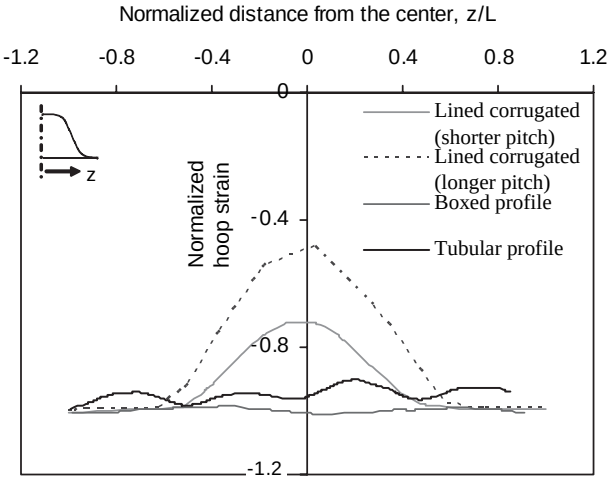

Figure C-28. Comparison of inner-wall hoop strains in different profiles (at 150 kPa, 22 psi).

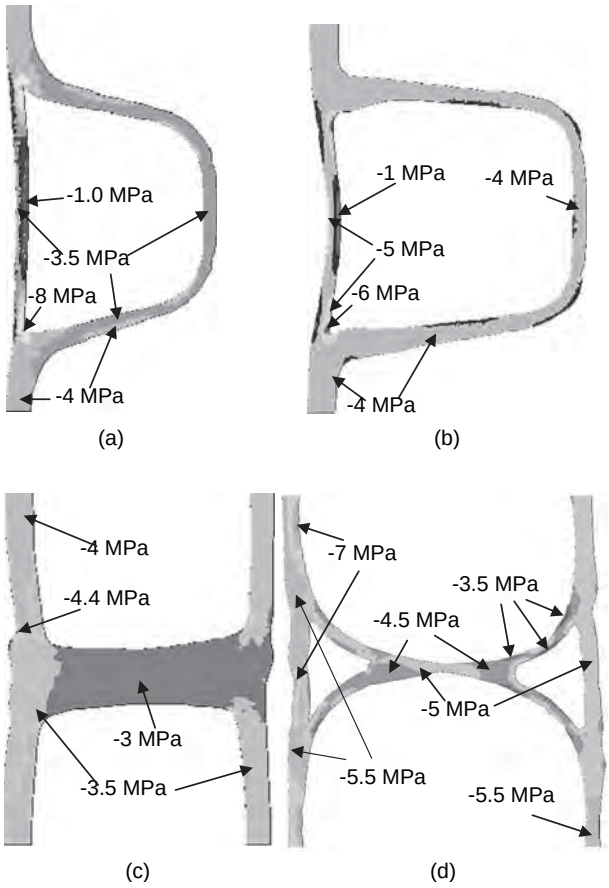

Figure C-29. Contour of circumferential stresses in each of the profiles shows (a) lined corrugated profile with longer liner, (b) lined corrugated profile with shorter liner, (c) boxed profile, and (d) tubular profile (1 MPa = 145 psi).

uniform. However, the hoop strains are not uniform along the inner surface of the two lined corrugated profiles. In the lined corrugated pipes, strain at the center of the liner is a fraction of the valley strain due to the local bending. Between the two lined corrugated profiles, the one with a shorter pitch experiences larger compressive hoop strain in the liner than the profile with longer pitch. Strain at the middle of the liner is about 70% of the valley strain for the pipe with shorter liner, whereas the liner midpoint has about 50% of the valley strain for the profile with longer liner. Clearly, the span of the liner has a significant effect on the strains that develop in it. Not surprisingly, local bending within the liner leads to greater reductions in hoop strain when liner "span" (the distance the liner stretches between corrugation valleys) is increased.

Figure C-29 shows the contours of hoop stresses in each of the profiles plotted at the same radial pressure of 150 kPa. Compressive stress is denoted as negative in the figures. Figure C-29 reveals that local bending develops at the liner-corrugation intersection in the lined corrugated profiles. Hoop stresses on corrugations in both the profiles are approximately the same (−4 MPa, 580 psi), whereas the hoop compression at the intersection is twice as much as the valley stress (−8 MPa, 1.1 ksi) in the profile with the longer liner. The stress at the intersection for the other pipe is 1.5 times the valley stress. The maximum hoop stress on the boxed profile is located where the inner liner is connected to the rib (Figure C-29c). Only a representative portion of the boxed and the tubular profile is shown in Figure C-29. The maximum stress is somewhat higher than the liner hoop stress (liner stress is −4 MPa, 580 psi, and the maximum stress is −4.4 MPa, or 630 psi), with less local bending in the boxed profile. The hoop stress in the tubular profile reaches a maximum (−7 MPa or 1 ksi) at the middle of both inner liners (Figure C-29d), while the average hoop stress within the profile is −5 MPa (720 psi). This indicates that some local bending occurs in the tubular profile. A greater hoop stress is expected in the pipe with tubular profile, since diameter is larger.

Figure C-30 plots the contour of axial stresses in a lined corrugated profile (profile with longer liner). Axial compression at the liner-corrugation connection is of similar magnitude to the hoop compression (−8 MPa or 1.1 ksi), even though axial stress in the valley itself is one-quarter (−1 MPa or 145 psi) of that calculated in the hoop direction. Axial stress contours for the other profiles are not included here due to space restrictions. Figure C-30 again illustrates how axial tension develops on the outer surface of the liner-corrugation junction. The magnitude of the tension is half of the maximum compression on the inner surface (4 MPa or 580 psi). Thus, circumferential compression and axial tension at the junction are the maximum distress the lined corrugated profile undergoes, both of which should be considered when evaluating the performance of the lined corrugated profiles.

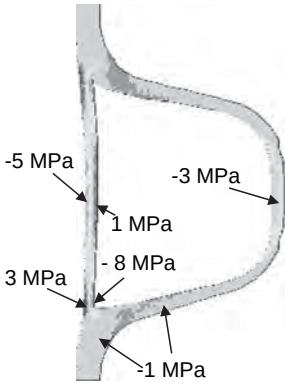

Figure C-30. Contour of axial stresses in a lined corrugated profile (1 MPa = 145 psi).

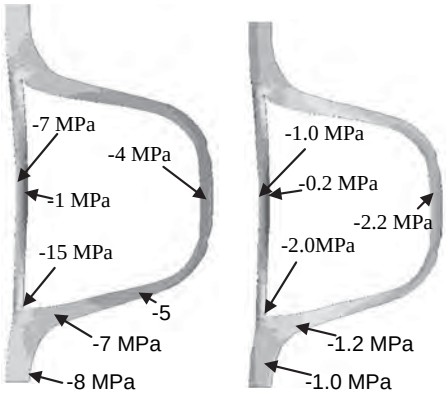

Figure C-31. Circumferential stress contours under biaxial loading (8-m or 26.2-ft burial) (1 MPa = 144 psi).

C.2.6.2 Biaxial Loading

The maximum stresses on each of the four profiles have been examined under more realistic biaxial earth pressures expected in the field. A semi-analytical finite element method (Moore 1995) was used to model the pipe in the biaxial stress field. The semi-analytical method employs a 2D finite element mesh to model the pipe and the surrounding soil in the r-z plane (similar to those shown in Figure C-20), and a Fourier series is used to represent the variations around the pipe circumference. Pipes at two different depths of burial (2 m or 79 in. and 8 m or 315 in.) have been examined for the short-term and long-term profile stresses in the circumferential, axial, and radial directions. Table C-5 shows details of the parameters considered for short-term and long-term simulations. Well-graded sand compacted to 95% of maximum Proctor density (SW95) has been considered as the backfill material. Parameters for the backfill soil at the stress levels corresponding to these depths (2 m and 8 m) are estimated from McGrath et al. (1999).

Contours of circumferential stresses at the springline and crown of a biaxially loaded lined corrugated pipe (profile with longer liner span) buried at a depth of 8 m are plotted in Figure C-31, which shows nonuniform stresses similar to those seen under axisymmetric loading (Figure C-29). Figure C-31 shows that maximum stress develops at the springline of the pipe for this profile. The locations of maximum stresses (within the profile) are the same as those observed under axisymmetric compression. At the crown, circumferential stresses on the outer surface of the pipe wall are greater than those on the inner surface due to increased radius of curvature (outward compression).

Table C-5. Parameters for semi-analytical FE analysis (1 MPa = 145 psi; 1 kPa = 0.145 psi).

Depth (m)	σ_v (kPa)	σ_h (kPa)	Soil (SW95) Parameters		HDPE Modulus, MPa	
			ν	M_s (E) MPa	Short Term	Long Term
2	40	13.3	0.2	18.3 (15.25)	700	150
8	160	53.3	0.2	24.6 (20.5)	700	150

The largest and the smallest values of stress in each profile for the short- and long-term conditions at two different burial depths (79 in., or 2 m, and 315 in., or 8 m) are shown in Tables C-6 and C-7. Only springline stresses are included in the tables, as they are the greatest for a biaxially loaded pipe. Long-term stresses are less than the short-term stresses due to the decrease in pipe modulus, which leads to both additional positive arching and relaxation. For each of the pipes and each burial depth, the long-term stresses are about 40% to 50% of the short-term values.

Tables C-6 and C-7 show that the greatest local bending stresses occur at the liner-corrugation junction of the lined corrugated pipe. Maximum short-term circumferential stresses at 8 m (315 in.) burial are –15 MPa (–2.2 ksi) and –11.5 MPa (–2.65 ksi), respectively, for the pipes with longer and shorter liners. The stresses on the boxed and tubular profile at the same burial depth were –7.8 MPa (–1.1 ksi) and –4.2 MPa (–600 psi), respectively. Using the AASHTO short-term stress limit of HDPE material (i.e., 20.7 MPa or 3.0 ksi), it appears that local short-term stresses on the profiles are less than the short-term allowable stress. However, long-term stress on the corrugated profile with longer liner (i.e., 6 MPa or 863 psi) almost reaches the AASHTO long-term stress limit (i.e., 6.2 MPa 892 psi), indicating that the long-term stress governs the design of this pipe.

Axial tension is also highest in the lined corrugated profiles. The boxed profile and the tubular profiles showed smaller values of tension in the axial direction. However, axial tensile strain was measured on the box profile (Dhar and Moore 2004), which could not be captured using the axisymmetric

Table C-6. Maximum and minimum short-term stress at springline (1 MPa = 145 psi, 1 m = 39.4 in.).

Pipe		Circumferential, σ_θ (MPa)		Axial, σ_a (MPa)		Radial, σ_r (MPa)	
		2 m	8 m	2 m	8 m	2 m	8 m
Twin Wall (longer liner)	Max	–4.2	–15.0	–4.0	–14.0	–1.6	–6.0
	Min	–0.4	–1.0	1.5	6.0	0.6	2.0
Twin Wall (shorter liner)	Max	–3.2	–11.5	–3.0	–11.0	–1.0	–3.4
	Min	–0.6	–2.5	1.4	5.0	0.2	0.6
Boxed	Max	–2.1	–7.8	–1.6	–5.5	–0.45	–1.6
	Min	–0.8	–3.2	0	0	0.15	0.6
Tubular	Max	–1.2	–4.2	–1.0	–3.4	–0.55	–1.8
	Min	–0.3	–1.2	0.1	0.6	0.15	0.4

idealization of this helically wound profile. Maximum compressive radial stresses for all profiles are smaller than the circumferential and axial values. However, the highest tensions in the boxed and tubular profiles appear to develop in the radial direction.

The comparison reveals that the effect of local bending is particularly significant in the lined corrugated pipes. Local bending in the tubular and boxed profiles appeared less significant. Further work using full 3D finite element analysis would be valuable to explore the effects of helical winding in more detail.

C.2.7 Conclusion

The 3D response of profiled pipes has been examined in this appendix to develop an understanding of the 3D issues affecting the behavior of the profile geometries. The pipe profiles were modeled explicitly using geometries recorded from various test specimens. Results of the analysis were compared with the measurements obtained using full-scale laboratory tests reported by Dhar and Moore (2004). Three types of commonly used HDPE pipe profiles (lined corrugated, boxed, and tubular) have been considered in the investigation.

The axisymmetric finite element analysis was effectively used to model the response of the pipe profiles in an axisymmetric stress field. Modeling of the time-dependent nature of the polyethylene influenced the simulation of the laboratory hoop tests, and inclusion of these effects provided improved calculations. This is attributed to the fact that a relatively thin ring of soil is placed around the pipe in the hoop compression test cell, so the contribution of the pipe stiffness rather than the soil stiffness dominates the pipe behavior in this burial condition.

The axisymmetric assumption was less successful for the helically wound box profile, where it provided some values of hoop strain that exceeded measured values. The measurements of hoop strains on the walls were much less than those obtained using the axisymmetric relation, Δ/D. However, calculations of pipe deflection (diameter change) were generally successful, indicating that global response is effectively calculated. Analysis of the helically wound tubular profile revealed that the finite element analysis with the axisymmetric idealization of geometry provides a reasonable first approximation for the 3D profile response, although further work using 3D finite element analysis would be valuable to explore the effects of helical geometry.

The effect of local bending has a substantial effect on the stresses that develop in the lined corrugated profile. The effect was greater on the liner with longer span. Strain distributions in the boxed and tubular profiles are almost uniform along

Table C-7. Maximum and minimum long-term stress at the springline (1 MPa = 145 psi, 1 m = 39.4 in.).

Pipe		Circumferential, σ_θ (MPa)		Axial, σ_a (MPa)		Radial, σ_r (MPa)	
		2 m	8 m	2 m	8 m	2 m	8 m
Twin Wall (longer liner)	Max	–1.9	–6.0	–1.8	–5.5	–0.7	–2.4
	Min	–0.2	–0.5	0.8	2.5	0.2	0.8
Twin Wall (shorter liner)	Max	–1.5	–4.8	–1.4	–4.5	–0.45	–1.4
	Min	–0.3	–1.0	0.6	2.0	0.05	0.2
Boxed	Max	–1.05	–3.6	–0.8	–2.6	–0.18	–0.60
	Min	–1.0	–1.8	0	0	0.08	0.30
Tubular	Max	–0.56	–1.8	–0.45	–1.8	–0.26	–0.90
	Min	–0.22	–0.8	0.05	0.2	0.06	0.20

the pipe axis, though axial stress values indicate that local bending also develops in those profiles. The locations of the maximum stresses were similar under both axisymmetric and biaxial loading for each profile, indicating that both hoop compression testing and axisymmetric finite element analysis are useful means of understanding where zones of tension and compression develop in these structures.

C.3 Liner Buckling in Profiled Polyethylene Pipes

C.3.1 Introduction

Large-diameter thermoplastic pipes are manufactured with a variety of different wall geometries to attain effective utilization of the polymer material in resisting bending. Deeper profiles render higher pipe stiffnesses with reduced use of material. However, high compressive strain across pipe sections, especially in deeply buried pipe, can cause local buckling on various components of the profile that could compromise the pipe's structural integrity. This appendix examines calculations for local buckling of the liner (the inner unsupported wall) of a number of different thermoplastic pipes. Liner buckling can be expected to affect the hydraulic properties of the pipe. Liner buckling may or may not influence the structural integrity of profiles where loss of liner stiffness reduces material providing stiffness on the inner surface of the pipe wall.

Four commonly used profiles for large-diameter HDPE pipes are shown in Figure C-32. The first two (Figure C-32a and C-32b) are twin-walled annular pipes with internal diameter of 610 mm (24 in.), the former with deeper profile and smaller pitch (more closely spaced corrugations). The third (Figure C-32c) and fourth (Figure C-32d) profiles are helically wound profiles with angles of helix of 2° and 6°, respectively. The third has a rectangular boxed profile and a 710-mm (28-in.) internal diameter. The fourth possesses tubular profile, with a 1,060-mm (41.7-in.) internal diameter. Tests have been conducted on each of these pipes using two pipe test vessels modeling deep burial conditions (Moore et al. 1996, Brachman et al. 2000). Tests on pipes have been performed under both biaxial and axisymmetric loading conditions.

The literature on local buckling is reviewed, the pipe testing program is briefly described, and the test data are analyzed using the elastic buckling solutions to predict liner buckling.

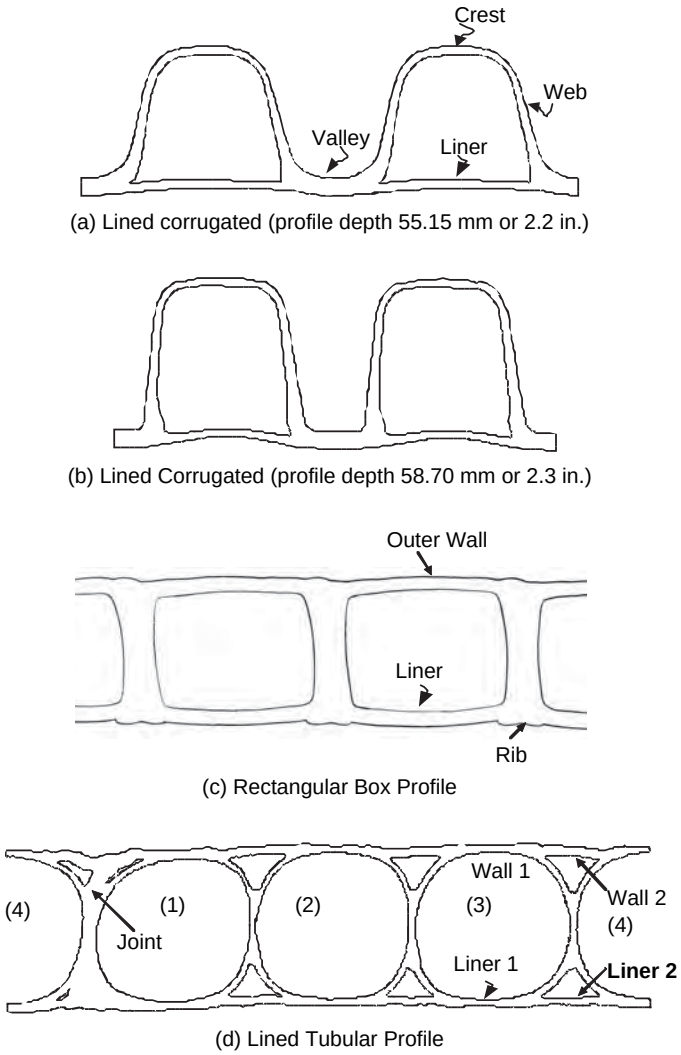

(a) Lined corrugated (profile depth 55.15 mm or 2.2 in.)

(b) Lined Corrugated (profile depth 58.70 mm or 2.3 in.)

(c) Rectangular Box Profile

(d) Lined Tubular Profile

Figure C-32. Types of pipe profiles.

C.3.2 Literature

In the past several decades, a variety of workers have undertaken studies to improve thermoplastic pipe design. Local buckling of individual structural elements in profiled HDPE pipes first received attention by Hashash and Selig (1990) and DiFrancesco (1993), who observed ripples during field and laboratory tests on twin-wall HDPE pipe, respectively. Moore and Hu (1995) demonstrated that these ripples were due to local buckling in the inner wall (the liner). Moore (1996) derived solutions for liner buckling using the linear buckling theory for a stiffened cylindrical shell (Moore 1990). The solution was expressed graphically in terms of critical compressive hoop strain in the liner. Moser (1998) agreed that local buckling is a critical performance limit in tests conducted on profile-wall pipe.

Moore and Laidlaw (1997) examined local buckling elsewhere in the corrugation, utilizing the stiffened plate model from the ASCE (1984) *Structural Plastics Design Manual* for prediction purposes. The manual makes use of the Bryan (1891) equation commonly used to quantify metal plate buckling. The Euler formula for thin plate buckling, as proposed by Bryan (1891), is

$$\sigma_{cr} = \frac{k\pi^2 E}{12(1-\nu^2)(W/t)^2} \qquad \text{(C.5)}$$

where σ_{cr} is the critical buckling stress, k is the edge support coefficient, W is the plate width, t is the plate thickness, E is the elastic modulus, and ν is Poisson's ratio.

Moore and Laidlaw (1997) expressed the critical buckling criterion in the form of critical hoop strain to avoid problems associated with the nonlinear time-dependent material modulus for the polyethylene. They expressed the critical hoop strain as a percentage of the diameter decrease, yielding

$$\varepsilon_{cr} = \left(\frac{\Delta D}{D}\right)_{cr} = \left(\frac{C_b t}{W}\right)^2 \quad \text{(C.6)}$$

where W is the plate width, t is the plate thickness, D is the pipe diameter, ΔD is the diameter decrease, and C_b is the edge restraint factor. Recommendations were made for edge restraint factors C_b for corrugation sidewall, valley, and crest based on the results of laboratory "hoop compression" cell tests. They proposed design values for C_b that account for the potential of the soil to penetrate into the corrugation valley and provide "plate edge" resistance to translation and rotation.

McGrath and Sagan (2000) reviewed the state of the art of local buckling for corrugated polyethylene pipe in a report for NCHRP. The plate-buckling equations for metals (Bryan 1891) were examined for use in estimating the local stability of the corrugated profiles. They used the methodology developed by Winter (1946) to quantify the inelastic behavior of metal plates. Winter proposed an "effective width approach" that takes into account the post-buckling capacity of plate elements. The theory is based on the assumption that the central portion of the plate becomes ineffective when it buckles and that the ultimate capacity is reached when the edge segments reach the yield stress for the material.

C.3.3 Test Program

C.3.3.1 Introduction

Two pipe test cells have been used to study the limit states of buried pipe in the laboratory. The biaxial test cell models the biaxial geostatic stress field expected under deep burial conditions. The hoop cell tests the pipes under axisymmetric loading conditions. Details of the test procedures and measurements are briefly outlined in the following sections. Results of these tests are used throughout Appendix C.

C.3.3.2 Biaxial Cell Test

The test cell (Brachman et al. 2000) is a high-strength steel box with dimensions 2 m × 2 m in plan and 1.6 m in height. Pipes tested within the cell are placed horizontally on a bed of soil and backfilled within the rectangular prism of soil. Uniform pressures are applied at the top surface of the soil using an air bladder placed beneath the stiff lid of the cell, simulating the overburden stresses σ_v. Special sidewall treatment is employed to reduce the sidewall friction and to ensure that most of the surface loads reach the pipe, and the sides of the box are stiff enough to restrain lateral deformation so that close to plane strain (K_o lateral pressure) conditions are attained as follows:

$$\sigma_h = K_o \sigma_v \quad \text{(C.7)}$$

Placement of test pipes in the cell is illustrated in Figure C-33. The pipe is backfilled with poorly graded granular soil (uniformity coefficient C_u of 3.4, curvature coefficient C_c = 1.1). The soil is compacted to a density of 1,600 kg/m^3 (100 pcf) to 1,650 kg/m^3 (103 pcf). The midrange value of 1,625 kg/m^3 (101 pcf) corresponds to 85% of the maximum standard Proctor density.

Instrumentation in the cell measures soil stresses (at the springline level and at the top of the cell) and soil settlements at the springline (Figure C-33).

C.3.3.3 Hoop Cell Test

Although the biaxial test cell is able to simulate the idealized field conditions, the maximum pipe size that can be tested is limited to minimize the influence of the boundaries; however, pipes with larger diameters can be tested under axisymmetric loading conditions in a hoop compression cell. The axisymmetric component of the radial earth pressures $(\sigma_v + \sigma_h)/2$ is important for deeply buried pipe, generating a hoop thrust that leads to circumferential shortening in most profiled thermoplastic pipes.

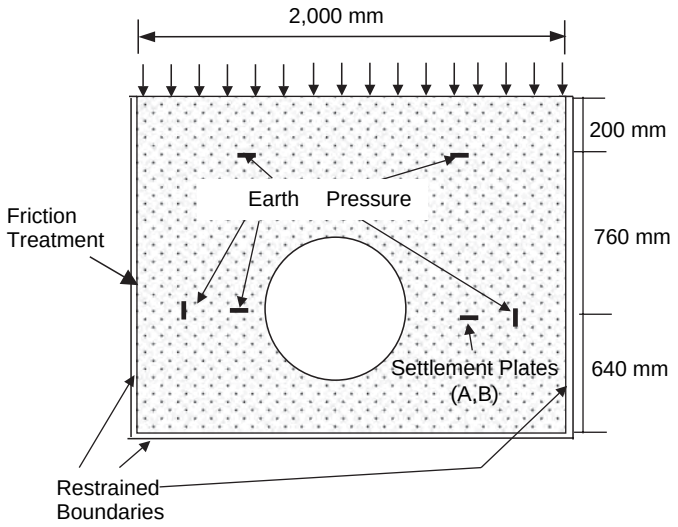

Figure C-33. Schematic of biaxial test cell (1 mm = 0.04 in.).

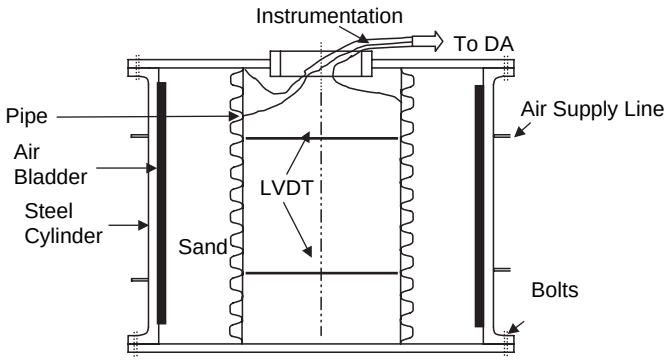

Figure C-34. Schematic of hoop test cell (after Laidlaw 1999).

The hoop test cell (Figure C-34) is a 12.7-mm (0.5-in.) thick vertical steel cylinder of internal diameter 1,500 mm (59 in.) and height 1,450 mm (57 in.). An inflatable polymer bladder is placed on the inside surface of the metal test cylinder. The instrumented pipe is placed upright concentrically within the cylindrical test cell. The space between the pipe and the air bladder is then backfilled to form a ring of soil. Two circular steel plates of 19.5-mm (0.77-in.) thickness cover the ends of the test vessel and are bolted in place using flanges at the end of the steel cylinder. The top plate is fitted with a 390-mm (15.4-in.) diameter sleeve to allow access to instrumentation within the pipe.

The end plates resist the longitudinal (axial) movements during the test as the air bladder is used to apply radial pressures around the outside of the soil annulus. The cylinder located on the inside boundary of that soil ring is thereby placed in a state of axisymmetric hoop compression. The cell was backfilled with the same poorly graded granular backfill as used in the biaxial tests.

C.3.3.4 Pipe Samples

Table C-8 provides a list of the four pipe samples used in the seven pipe loading tests. Samples A (Figure C-32a) and B (Figure C-32b) are lined corrugated pipe, manufactured to have annular geometry. Samples C (Figure C-32c) and D (Figure C-32d) were formed by helically winding a strip of the pipe wall, so that wall elements are oriented at 2° and 6° to the pipe circumference, respectively.

C.3.3.5 Pipe Instrumentation

Pipe instrumentation includes an LVDT to measure the change in pipe diameter and electronic strain gages to measure the wall strains on different components of the profile (Figure C-35). Both the horizontal and the vertical deflections are measured in the biaxial cell tests. Strain gage measurements were taken at the midpoint of each element of the profile (the liner, the web, the crest, and the valley of the corrugation, for example). The circumferential strains at these locations are judged to be the most critical with respect to local buckling. The axial strain is less important, although values at the connection of the different profile elements (e.g., between the liner and the valley) may be important with respect to limit states like local bending.

For profiled pipes manufactured to feature annular geometry, the principal strain directions are known in advance and biaxial strain gages were used to measure the circumferential and the axial strains. Strains on the helically profiled pipes were measured using strain gage rosettes, since the major and minor principal strain directions were unknown. Instrumentation was placed at two sections to check the reproducibility of the test results and to ensure that the data were collected in the event that some of the gauges failed to operate successfully. For samples prepared for testing in the biaxial pipe test cell, strain gages were placed at crown, at invert, and at both springlines. Strain gages were placed on two diametrically opposed sections at each axial (vertical) position for samples prepared for testing in the hoop compression cell.

C.3.3.6 Observations of Local Buckling

A camera capable of moving along the pipe axis was mounted inside each pipe to record the appearance of the

Table C-8. Definition of the tests (1 mm = 0.04 in.).

Sample	Test No.	Pipe	Test Type	Internal Diameter (mm)	Profile Type
AB	1	A (Figure C-32a)	Biaxial	610	Lined corrugated pipe with profile depth of 55.15 mm
BB	2	B (Figure C-32b)	Biaxial	610	Lined corrugated pipe with profile depth of 58.70 mm
AH	3, 4	A (Figure C-32a)	Hoop	610	Lined corrugated pipe with profile depth of 55.15 mm
BH	5	B (Figure C-32b)	Hoop	610	Lined corrugated pipe with profile depth of 58.70 mm
CH	6	C (Figure C-32c)	Hoop	760	Rectangular box profile
DH	7	D (Figure C-32d)	Hoop	1,060	Lined tubular profile

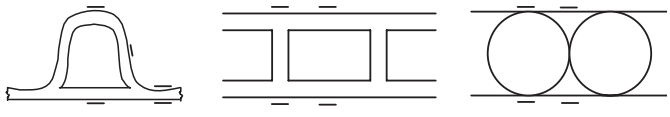

Figure C-35. Location of the strain gages.

inner pipe wall during both hoop compression and biaxial loading tests. The camera was connected to a video system to record and display the image continuously on a television screen. The camera was also free to rotate about its axis, so it could be directed to observe every point around the inner periphery of the pipe. The inside surface of the pipe was marked around the circumference to identify each position being photographed during the test.

Loads were applied with the air bladder system in increments of 25 kPa (3.6 psi). After the application of each incremental load, 20 min were allowed to pass to permit measurements to stabilize. The video images of the inner pipe wall were recorded at each load level. Increments of load were continued until the ripples were observed on the inner wall (the liner) or until the test cell capacity was reached.

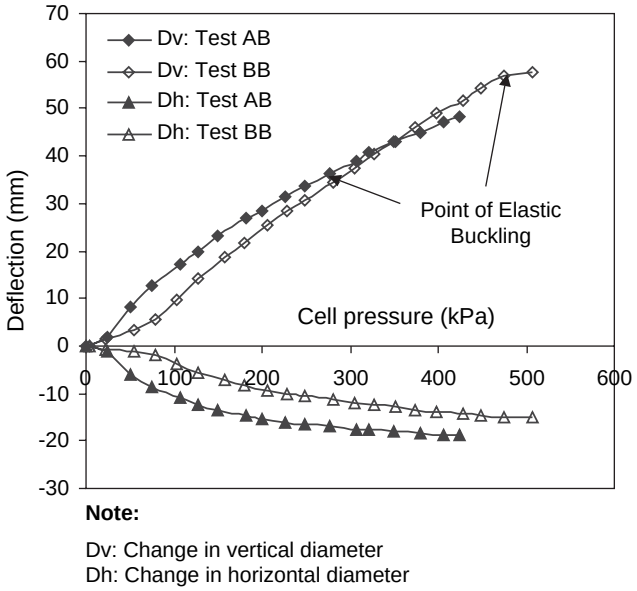

Figure C-36. Vertical and horizontal pipe deflection in Tests AB and BB (1 mm = 0.04 in., 1 kPa = 0.144 psi).

C.3.4 Test Results

C.3.4.1 Introduction

The pipe responses during the biaxial and hoop cell tests are presented in this section. The focus of attention is observations relating to liner buckling. Values of circumferential strain are discussed, since these compressive strains govern the development of pipe-liner buckling.

C.3.4.2 Tests AB and BB

Figure C-36 shows the pipe deflections recorded during the biaxial tests AB and BB. Initiation of a wavelike pattern on the liner was first noticed at a pressure of 275 kPa (39.6 psi) in the test denoted AB. The buckling became more pronounced at higher load levels. Progression of local buckling with different level of load for the test is shown in Figure C-37. White lines in the figure are drawn around the pipe circumference on each liner segment. Liners were numbered from 1 to 10 for identification. Circumferential positions of the pipe are defined as 0° and 180° at the two springlines, 90° at the crown, and 270° at the invert. Notation $C5_{180}$ denotes Liner C5 at 180° (the springline). The vertical and the horizontal diameter changes at the maximum level of load were −48.3 mm or −1.9 in. (−7.9%) and +18.8 mm or +0.74 in. (+3.1%), respectively.

In Test BB, pipe diameter changes at the maximum stress were −57.7 mm or −2.3 in. (−9.4%) and +15.0 mm or +0.6 in. (+2.38%) in the vertical and horizontal directions, respectively. Liner buckling was apparent at a stress level of 425 kPa (61.2 psi) and became more pronounced at higher stresses. Figure C-38 shows liner buckling during Test BB at cell pressure of 500 kPa (72 psi).

The distributions of circumferential wall strain recorded during both tests are illustrated in Figure C-39. Figure C-32 defines the components of the profile. Strains were measured at the center of each of the profile components (liner, corrugation valley, corrugation sidewall, and corrugation crest). The maximum circumferential compression on the midliner develops at the springline of the pipe. Liner buckling initiated at the springline in both the tests. Springline strains are therefore the strain values of interest for the analysis of liner buckling.

Measurements of circumferential springline strains are plotted in Figure C-40. Measured strains have been divided by 0.7 prior to plotting, since the strain gages are known to stiffen the HDPE pipe wall and strain readings must be corrected in this manner to account for that strain gage stiffening (Brachman 1999 provides details of this calibration). Figure C-40 (also Figure C-39) shows that the circumferential strains on the liner are much less (about 20%) than those on the valley (see Section C.2.5.1).

The circumferential strains in both the liner and valley elements are compared in Figure C-40 with those predicted by conventional 2D ring theory (Flugge 1962). The ring theory utilizes the pipe deflections to calculate circumferential strains. The theory significantly overpredicts the strains (likely due to the presence of significant circumferential strain).

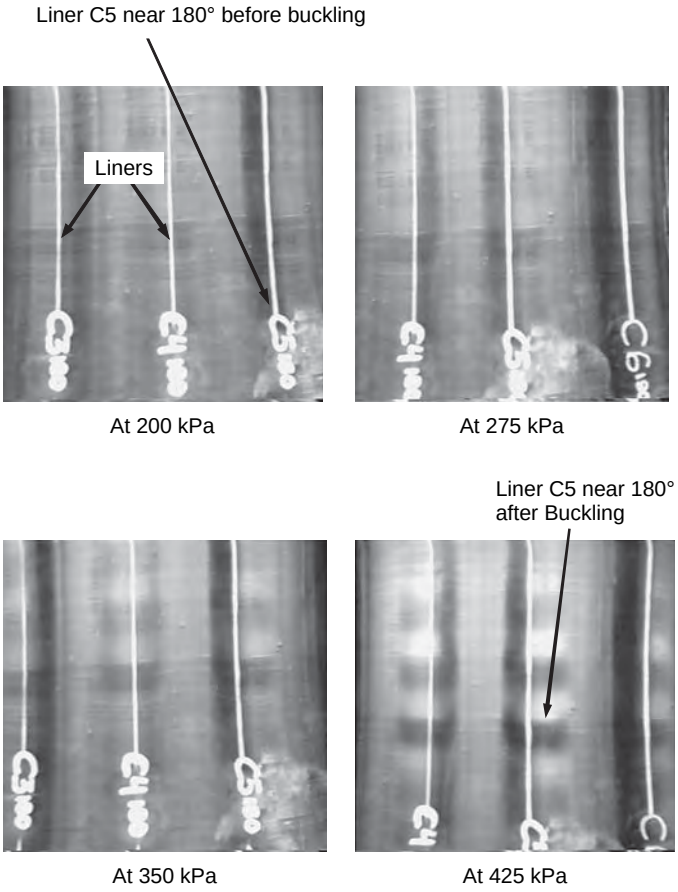

Figure C-37. Development of liner buckling in Test AB (1 kPa = 0.144 psi).

Liner buckling is presumed to be fully developed at the point where the strain level in the liner no longer increases as further increments of load are applied to the system (i.e., the liner reaches its load capacity and further loads are redistributed elsewhere in the pipe profile). Circumferential strains of the liner corresponding to the elastic buckling are 0.76% and 1.05% for Tests AB and BB, respectively.

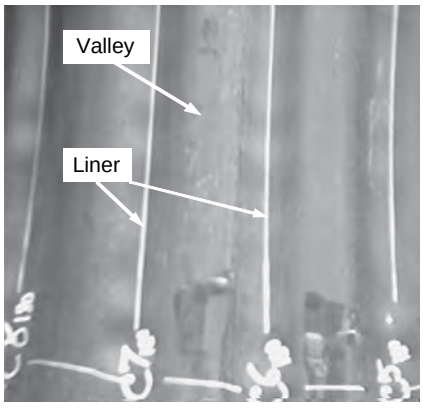

Figure C-38. Liner buckling observed during Test BB.

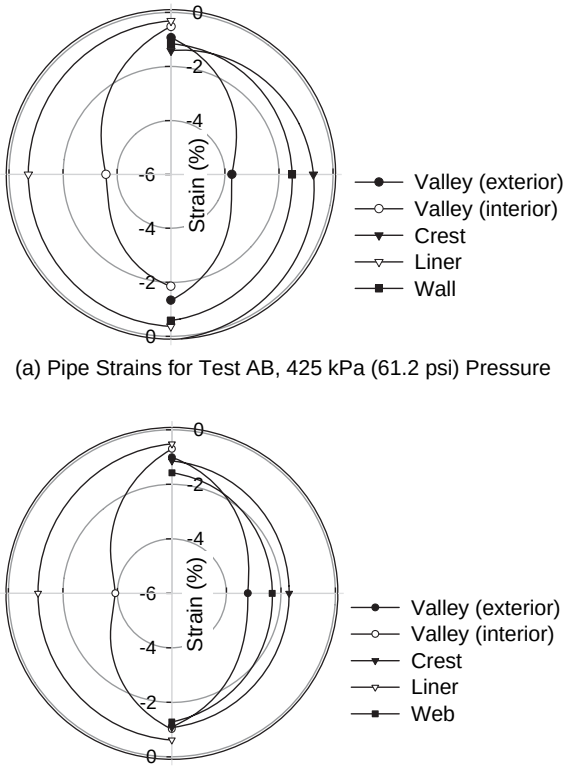

Figure C-39. Circumferential strain distributions.

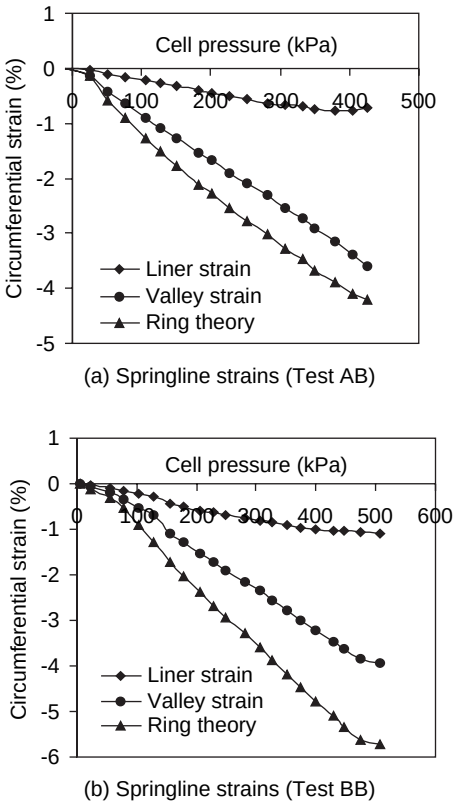

Figure C-40. Circumferential strains on the interior surface at the springline (1 kPa = 0.144 psi).

C.3.4.3 Test AH and BH

Tests AH and BH are the axisymmetric tests on the two lined corrugated pipe profiles. Data from the tests are provided in Figure C-41. Two Type AH tests were performed (Figure C-41a). Two different samples were instrumented and tested, and discrepancies between the two sets of measurements likely result from inconsistencies between the profile geometries.

The liner strains in the hoop tests are found to be about 62% of the interior valley strains. Comparison of this proportion with the biaxial test results implies that the effects of local bending under biaxial loading are more significant than under axisymmetric loading.

Almost identical critical strains were obtained in each type of test (biaxial and axisymmetric): 0.76% and 0.85% for Sample A under biaxial and hoop compression, respectively; the corresponding strains for Sample B are 1.1% and 1.2%. Figure C-42 presents photographs of liner buckling in Tests AH and BH (the image from Test BH shows initiation of local buckling, which is difficult to discern in the printed version of the video image).

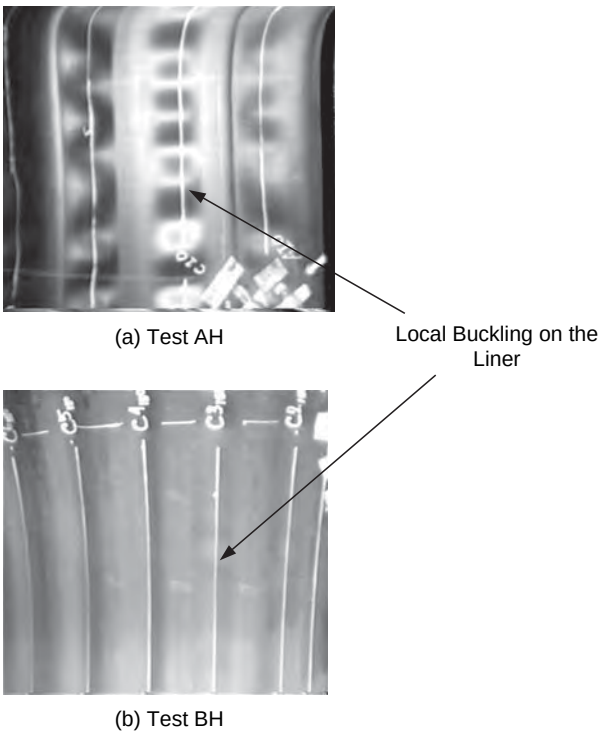

Figure C-42. Liner buckling in Tests AH and BH.

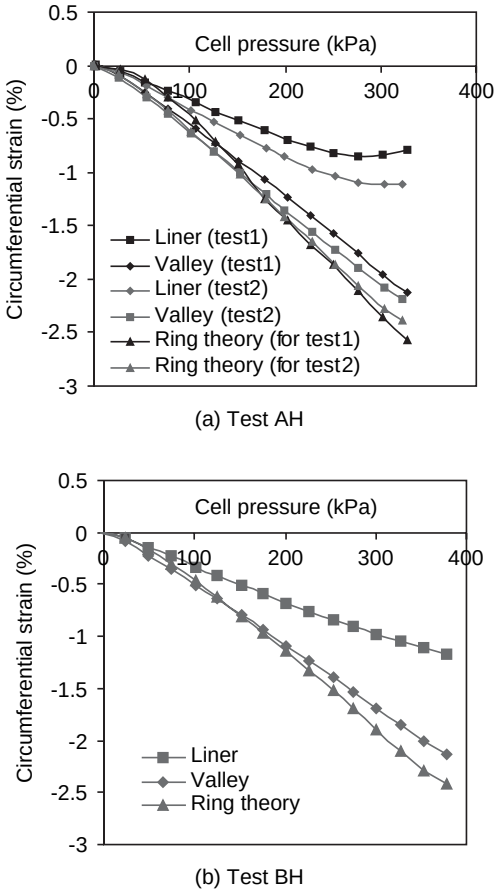

Figure C-41. Axisymmetric response in Tests AH and BH (1 kPa = 0.144 psi).

C.3.4.4 Test CH

Buckling on the liner was apparent in Test CH (Hoop Test) at bladder pressure of 375 kPa (54 psi). Figure C-43 shows the liner buckling obtained during the test. Measurements of strains along with the ratio ΔD/D are plotted in Figure C-44. It shows that the hoop strain in the liner is about 80% of the ΔD/D ratio. For this profile, it is evident from Figures C-44a and C-44b that the circumferential liner strain is much higher than the strain on the rib (rib strain is about 60% of the strain on the liner). This may be caused by the helical geometry. Hoop strain at the initiation of liner buckling is assessed as being 2.4%.

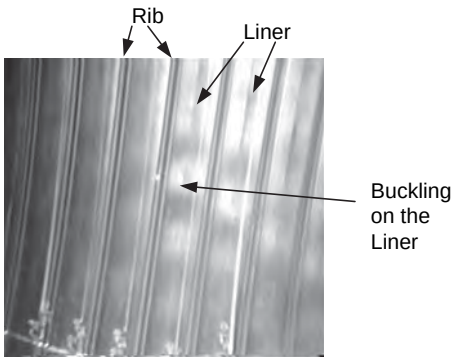

Figure C-43. Local buckling in Test CH.

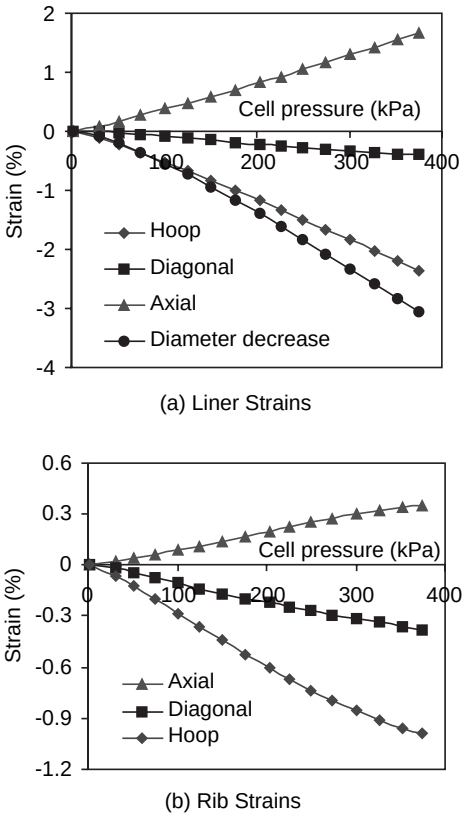

Figure C-44. Interior pipe strains (Test CH).

C.3.4.5 Test DH

This helically wound tubular profiled pipe is manufactured by spirally winding and welding together a succession of units of four tubes. At each welded joint, there is an increase in the material present in the pipe wall and consequently an increase in local stiffness. Strain gages were placed to measure strains on each of the tubes of the unit. Figure C-45 shows the local buckling observed in the middle two tubes (Tube 2 and 3 in Figure C-32d) during Test DH. Circumferential strains on the element that buckled are presented in Figure C-46. Buckling was initiated at a hoop pressure of 180 kPa (25.9 psi). The critical liner strain is assessed as 0.8%.

C.3.5 Evaluation of Plate Buckling Model

Bryan's plate buckling equation (Equation C.5) is evaluated for prediction of liner buckling. The key parameters in the equation are material modulus, E; the width-to-thickness ratio of the "plate" element, W/t; and the edge support coefficient, k. Following the approach of Moore and Laidlaw (1997), the equation is expressed in terms of critical strain for use with thermoplastic pipe. Assuming the liners to be acting under plane-strain conditions,

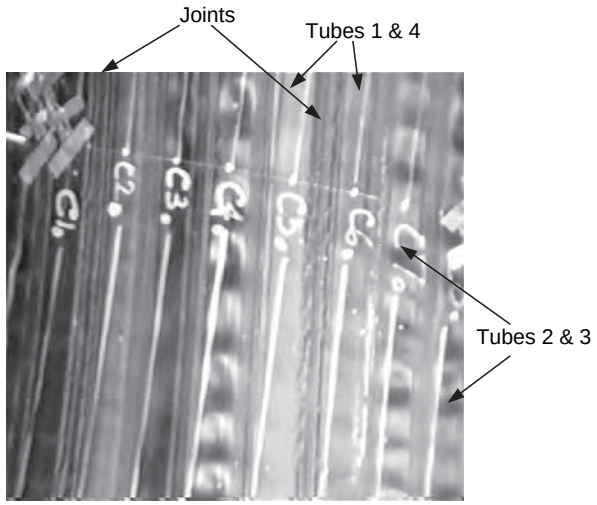

Figure C-45. Local buckling in Test DH.

$\sigma_{cr} = \frac{E}{(1-\nu^2)}\varepsilon_{cr}$, so that Equation C.1 yields

$$\varepsilon_{cr} = \frac{k\pi^2}{12(W/t)^2} \qquad \text{(C.8)}$$

The *Structural Plastics Design Manual* (ASCE 1984) provides guidelines for edge support coefficients for plate buckling. McGrath and Sagan (2000) recommended the use of a value of 4 for elements intersecting approximately at right angles with other elements and 0.43 for freestanding elements. They obtained values by fitting the model to provide a lower bound to results of column compression tests on pipe segments. Simple beam theory was employed to calculate the strains on the pipe wall, since the wall strains were not measured during the tests (likely reasonable for a condition involving simple axial compression along the hoop direction of the pipe wall).

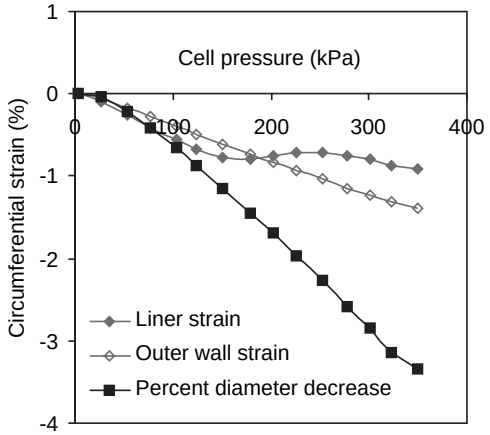

Figure C-46. Internal strain in Test DH.

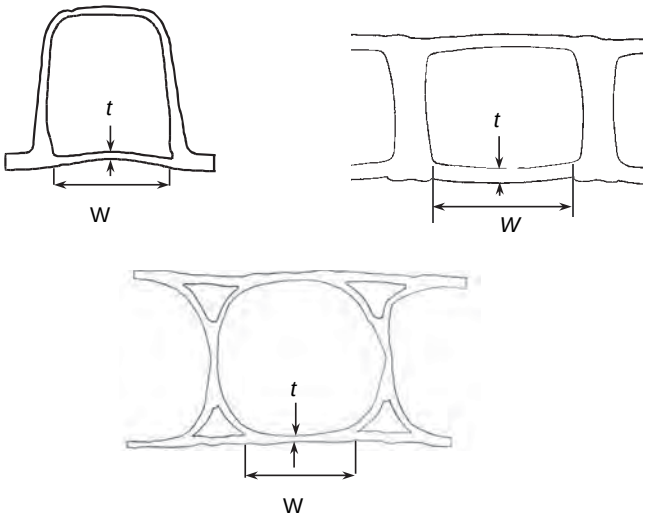

Figure C-47. W and t for the liners.

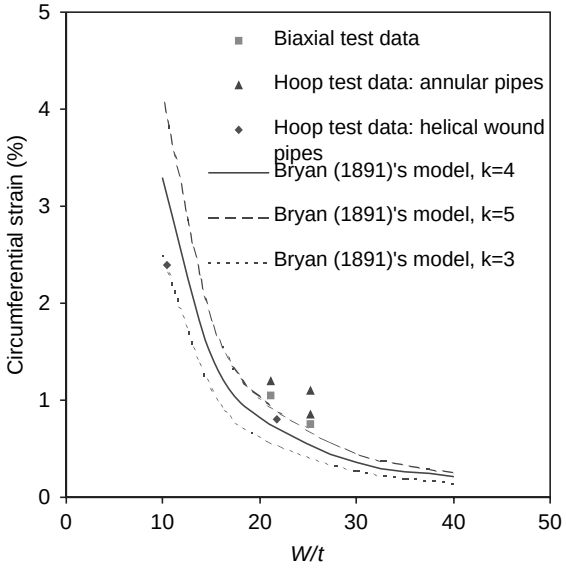

Figure C-48. Buckling model with laboratory test results.

Suitability of the edge support coefficient of 4 for buried pipes is evaluated in this study. Strains measured in the laboratory tests have been utilized in this verification. Width and thickness of the inner wall elements are defined as shown in Figure C-47. Table C-9 summarizes these test results of liner buckling and provides information on the liner geometry (including the ratio of liner span between web elements to average thickness). The buckling solution, Equation C.8, is presented graphically in Figure C-48 together with the test observations by plotting hoop strain versus the W/t ratio. The model results are plotted in Figure C-48 for k = 3, 4, and 5.

With the exception of one data point, it appears that use of the modified form of Bryan's model of elastic buckling with an edge coefficient of 4 forms a lower bound to the test observations of critical strain (Figure C-48). Critical strains for tests under biaxial and hoop compression are largely identical, since the wavelength of the buckling pattern is small enough so that one or more of the buckles fit within the region of maximum hoop strain at the springline.

The single point that lies below the line is one for a relatively thick liner element. It may be that the liner element has reached a material rather than geometrical (i.e., buckling) strength limit for that element (McGrath and Sagan 2000 discusses the implications of material capacity for elements of low slenderness).

C.3.6 Comparison with Other Test Observations

Other buckling observations for lined corrugated pipes have been reported in the literature (Selig et al. 1994, Li and Donovan 1994). Selig et al. (1994) used visual inspection and simple diametral contraction to quantify liner buckling in three hoop compression tests. Load was applied in increments of 35 kPa (5 psi). Liner buckling was perceived to have developed between the third and fourth increments of load. Diameter shortening at the end of the third and fourth increments of pressure was 7 mm (0.28 in.) and 11 mm (0.43 in.), respectively. Pipe deflection corresponding to elastic buckling is assumed here to be 9 mm or 0.35 in (the midvalue). Li and Donovan (1994) reported the pipe deflection corresponding to the initiation of buckling from one further hoop test using Selig's apparatus. Table C-10 provides details of these hoop test conditions and results.

Table C-9. Summary of liner buckling (1 in. = 25.4 mm).

Test Type	Pipe	*W* (mm)	*t* (mm)	W/t	Critical Strain (%)
Biaxial	Lined corrugated	62.0	2.46	25.2	0.76
		50.0	2.36	21.1	1.05
Hoop	Lined corrugated	62.0	2.46	25.2	0.85
		62.0	2.46	25.2	1.1
		50.0	2.36	21.1	1.2
	Box profile	46.0	4.42	10.4	2.4
	Tubular profile	43.5	2.21	19.8	0.80

Table C-10. Observations of liner buckling in lined corrugated pipe (1 in. = 25.4 mm).

Test Type	Size (mm)	Liner Span, *W* (mm)	Thickness, *t* (mm)	ΔD (mm)	ΔD/D %	Corrected Strain, %
Hoop	614*	77.0	2.74	9	1.46	0.73
	614*	78.4	2.72	9	1.46	0.73
	614*	78.1	2.42	9	1.46	0.73
	604+	51.7	2.50	10	1.66	0.83

*Selig et al. (1994)
+Li and Donovan (1994)

Table C-11. Observations of local buckling in lined tubular pipe.

Test Type	Test No.	W/t	$\Delta D_v/D$ %	$\Delta D_h/D$ %	Strain (%) (Ring Theory)	Corrected Strain, %
USU Cell (Moser 1998)	1	27.8	–10.2	+8.0	4.22	0.97
	2	27.8	–4.9	+3.1	2.27	0.52
	3	27.8	–3.5	–0.2	2.42	0.55

Moser (1998) noted liner buckling on tubular profiled pipe under nonaxisymmetric loading. Three tests were conducted on 1,215-mm (47.8-in.) diameter pipes with different densities of soil. The pipes possess a liner span of 47.5 mm (1.9 in.), liner thickness of 1.7 mm (0.066 in.), and a profile depth of 71.5 mm (2.82 in.). Buckling was viewed at the springline of the pipe. Horizontal and vertical deflections of the pipe were measured at the development of liner buckling. Test conditions and results are presented in Table C-11.

One difficulty with using the above-mentioned tests is that the strains on the liner were not measured during the tests. Therefore, ring theory has been used to calculate circumferential strains from the measured pipe deflection. However, it was shown in Section C.3.4 that simple ring theory will overpredict the liner strains. In Figure C-49, the measured liner strains from four of the new hoop tests are plotted against strain estimates based on ring theory. For the point corresponding to liner buckling, the ratio of the measured strain to that obtained from the ring theory is approximately 0.5 (for example, 2% prediction for ring theory corresponds to measured values of 0.8% and 1.1% for Tests AH1 and AH2, respectively). Thus, a correction factor of 0.50 has been selected for the tests referenced in Table C-11, to factor down the estimates of liner strains from those obtained using ring theory. The liner strain is about 70% of the percent diameter decrease for the tubular profiled pipes at liner buckling (Figure C-49). The factor will be less at the springline of a biaxially loaded pipe due to more significant effects of the local bending. As will be discussed in Sections C.4.2 and C.4.3, the liner strain for corrugated pipe was about 62% of the valley strain in the hoop test, whereas the proportion in the biaxial test was about 20% (i.e., one-third of the axisymmetric result). Ring theory does provide a rational estimate of the valley strain. To estimate the liner strain from the ring theory for the biaxially loaded tubular pipe, a correction factor of one-third of the proportion (0.70) of diameter decrease encountered in the hoop test is used (i.e., 0.23).

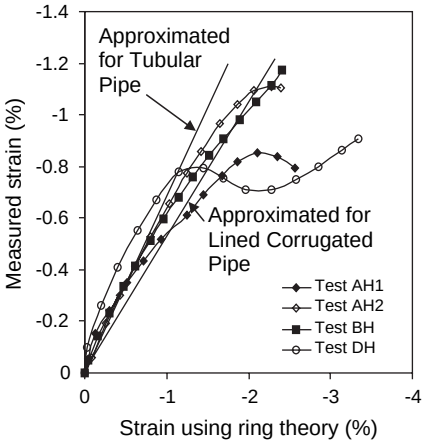

Figure C-49. Liner strain versus ring theory.

The buckling model is compared to the additional liner buckling data (Tables C-10 and C-11) in Figure C-50. The model with the edge support coefficient of 4 is plotted in the figure. The additional data points also indicate that Equation C.8 with k = 4 generally provides a reasonable lower bound estimate of the critical buckling strain.

C.3.7 Discussion and Conclusions

In the past, local buckling, an important limit state for profile-walled thermoplastic pipe, has largely been ignored. Tests have been performed to study the development of local buckling under biaxial and axisymmetric loading conditions.

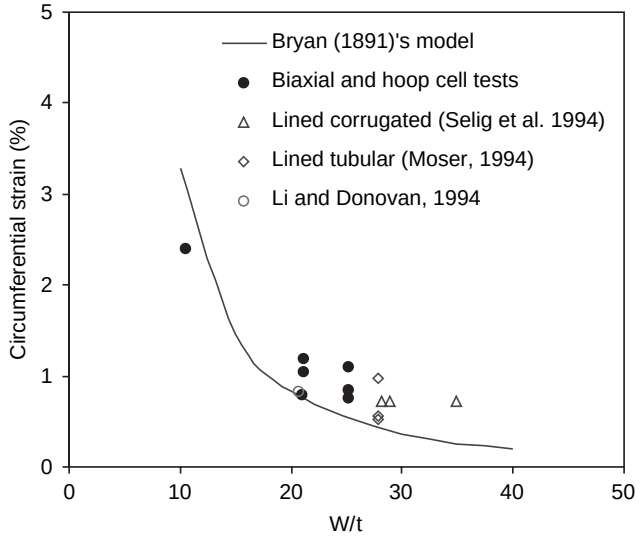

Figure C-50. Comparison of buckling model with other test data.

The Bryan (1891) solution for plate stability has been examined for use in predicting local buckling in profiled HDPE pipes. Comparisons of critical strain have been made between the theory and laboratory observations. Estimates of local buckling using Bryan's equations were undertaken using end support coefficients of 3, 4, and 5 in order to obtain a suitable value to be used in the design for liner buckling.

Observations of liner buckling were recorded using a camera mounted inside the pipe. Strains were measured at the center of the profile components. It appears that the critical buckling strain is not significantly affected by the method of loading. However, local bending within the profile reduces the hoop strains in the critical elements below values that correspond to simple ring theory. These reductions are greater for the biaxial loading condition. The test observations of critical hoop strain reveal that Bryan's model with an edge support coefficient of 4 generally provides a useful lower bound to the critical buckling strains, though less-slender profile elements may have stability influenced by material yield.

Additional data points for liner buckling have been included from the literature. Although these tests did not feature measurements of local strain, estimates of critical strain were made that also appear to be bounded by the modified form of Bryan's equation.

The investigation implies that the plate stability theory of Bryan (1891) provides a useful tool for characterizing the local buckling of profile thermoplastic pipe. Further research would be useful to assess the implications of nonuniform element thickness, the post-buckling behavior of these elements, and the relationship between liner instability and the overall performance of the pipe profile.

C.4 Measured Effects of Compaction and Burial Conditions on Thermoplastic Culverts

C.4.1 Introduction

Various profile geometries have been studied in this project (boxed, tubular, ribbed, and lined corrugated), to define the ability of these buried polymer structures to withstand performance limits such as deflection, wall stress, local and general buckling, and local bending. The circumferential stress and strain resulting from local bending on lined corrugated thermoplastic pipes (see cross-section shown in Figure C-51) has been found to be critical to both cracking and buckling limit states.

The interaction between soil and pipe ultimately controls how the pipe performs, and this depends on the stiffness of the pipe (influenced by its material properties, profile geometry, and diameter) and the stiffness of the backfill soil surrounding the pipe (related to the type of soil, density, confining stress, and strain level). The backfill configuration (type and extent of soil material) and the method of compaction also can impact the nature of loading and support for the pipe.

This project has examined load and resistance factor design procedures involving both material and local buckling limit states that depend on the magnitude of circumferential bending strains that develop in different elements of the profiled wall. Design calculations therefore must include evaluation of the peak circumferential strains and bending strains that can be expected in the field.

Local strain is dependent in part on local bending caused by poor soil support under the haunches of the pipe. Section C.1 described both computational and experimental work to quantify the effect of nonuniform soil support in this area due to either stiff underlying ground (e.g., invert placed directly on a stiff base) or loose backfill filling or partly filling the zone beneath the pipe haunches (see Figure C-51 for location of the haunch). Such nonuniform support may lead to local bending and increases in bending strain in the pipe. The extent of local bending will depend on the stiffness of the pipe and the nature of the nonuniform soil support (influenced by type of backfill, method of construction, extent of construction supervision, etc.).

Section C.1 described finite element analyses conducted to examine the effects of an idealized low-stiffness haunch zone on local bending for two different thermoplastic pipes (PVC and HDPE). The analyses considered a pipe surrounded by a nonuniform backfill support with a soil modulus, E_s, and an area below the haunch modeled with a lower soil modulus, E_h, as shown in Figure C-52. Differing ratios of E_s/E_h from 1 to 100 were applied to examine the effects of a softening haunch relative to the surrounding soil. The finite element analyses show an increase in circumferential strains beneath the haunches of the pipe as E_h decreased relative to E_s. In addition,

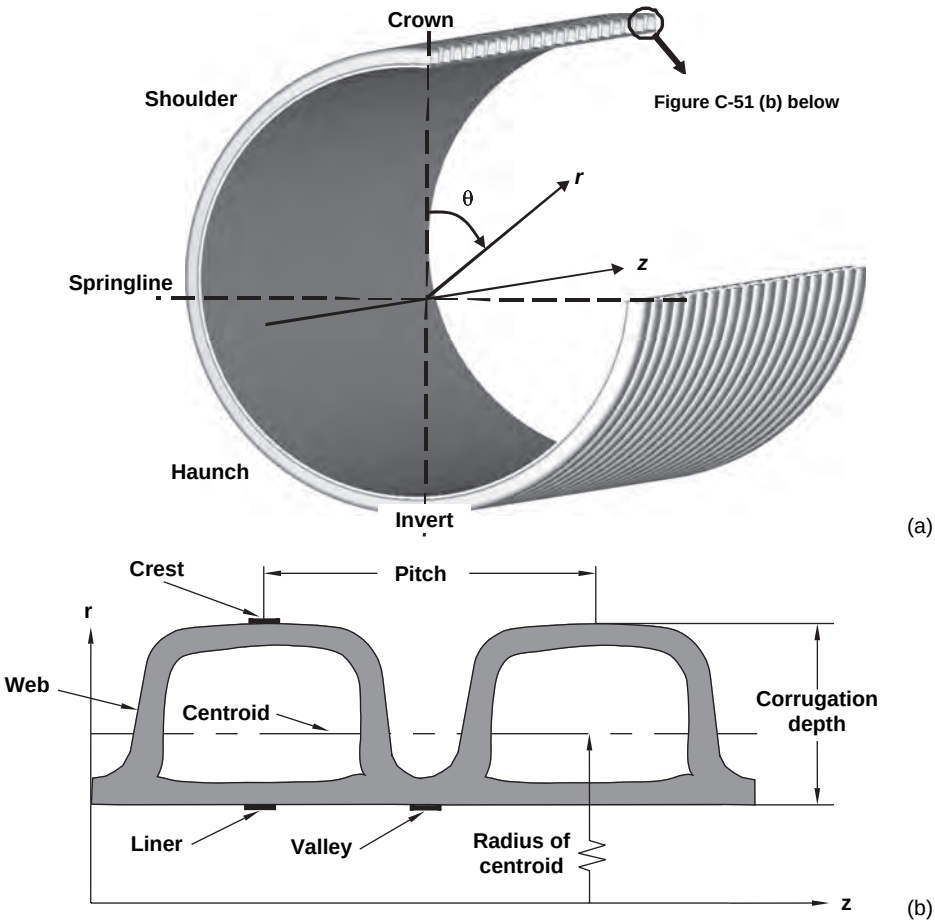

Figure C-51. (a) Sectional view of 600-mm diameter PVC profiled pipe and (b) definition of terms defining profile geometry and showing location of strain gages at crest, valley, and liner.

the ribbed PVC pipe in that study showed greater bending strains than the lined corrugated HDPE pipe.

The objective of the additional experimental work reported here is to provide physical evidence of the effects of backfill condition on pipe performance and its influence on local bending. Measured pipe deflections and strains are reported from six laboratory tests conducted on 600-mm nominal diameter lined corrugated HDPE and PVC pipes. Three different burial conditions were tested to examine the effect of compaction using rammer and vibrating plate compactors as well as a third installation condition involving a stiff base and compaction of only the backfill placed above the pipe springlines. Two different backfills were employed: a uniform sand and a well-graded granular material.

C.4.2 Experimental Details

C.4.2.1 Test Apparatus

The experiments were conducted using the laboratory test cell developed by Brachman et al. (2001). Details of this test cell and its use are provided in Section C.1 and in Figure C-53.

Vertical pressures are applied to the ground surface using a pressurized air bladder. The additional experiments reported here were conducted to a maximum vertical pressure of 200 kPa (equivalent to the vertical stress imposed by the weight of a 10-m deep embankment with a unit weight of 20 kN/m^3). The vertical pressure was applied in successive 25 kPa increments, with each increment held for 10 min to permit measurements to be taken after the soil and pipe responses stabilized.

Once again, friction between the walls and backfill soil was minimized by placing polyethylene sheets lubricated with high-temperature bearing grease along the walls (Tognon et al. 1999). The ends of the pipe were not restrained in the axial direction to avoid interference from the walls of the test cell. A ring cut out of rigid foam board and placed at both ends of the pipe (see Figure C-54) was used to prevent sand from falling into the gap between the ends of the pipe and the test cell.

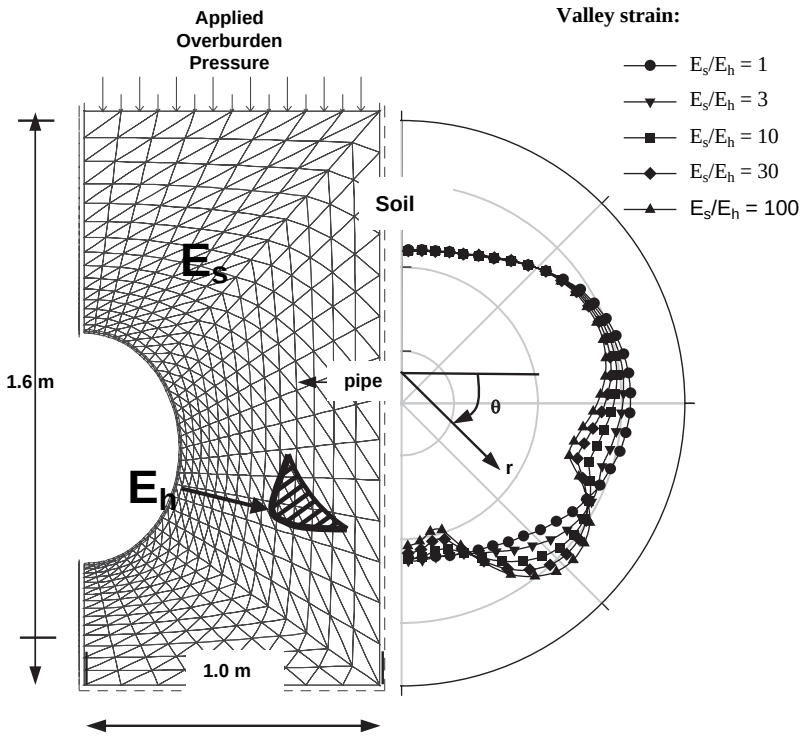

Figure C-52. Circumferential strains on HDPE pipe for different modular ratios at an applied vertical pressure of 70 kPa (from Section C.1).

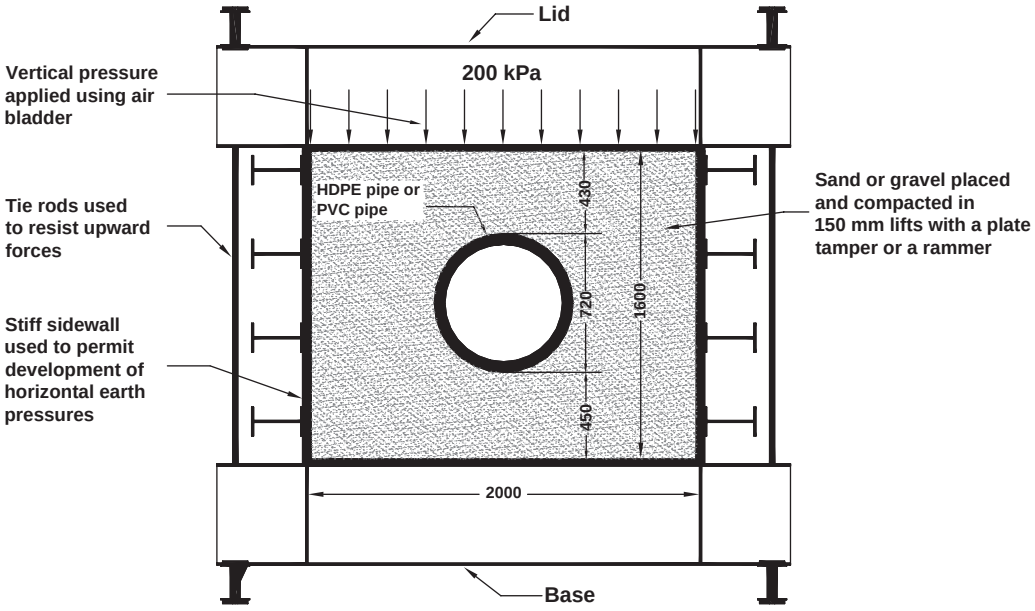

Figure C-53. Cross-section showing biaxial test cell; backfill geometry for Tests T1, T2, T5, and T6 are shown (dimensions in mm).

Figure C-54. Backfilling T2 HDPE pipe with sand up to the pipe shoulders; the rammer and nuclear density gauge are also shown.

C.4.2.2 Materials

Two types of lined corrugated thermoplastic pipe were used in this study, both having nominal internal diameters of 600 mm—an HDPE pipe and a PVC pipe. Profile geometries for both of these pipes are summarized in Table C-12 (the relevant terminology is defined in Figure C-51b).

Two different backfill materials were used. The backfill material used in the first four laboratory tests was synthetic olivine sand, a poorly graded material (Unified Soil Classification—SP) with a mean grain size of 0.5 mm, a uniformity coefficient C_u of 1.46, a curvature coefficient C_c of 0.94, and an angle of internal friction of 44° as reported by Lapos and Moore (2002). Minimum and maximum dry densities are 1,310 kg/m^3 and 1,550 kg/m^3, respectively. For the fifth and sixth tests, a well-graded gravel (Unified Soil Classification—GW) was used. This gravel had a mean grain size of 5.5 mm, a uniformity coefficient C_u of 12.5, a curvature coefficient C_c of 1.62, and a maximum standard Proctor dry density, ρ_{dmax}, of 2,120 kg/m^3. Minimum and maximum dry densities are 1,500 kg/m^3 and 1,980 kg/m^3, respectively.

Table C-12. Sectional properties of the HDPE and PVC pipes tested.

Property	HDPE Pipe	PVC Pipe
Internal diameter (mm)	603	592
Pitch (mm)	101	48
Corrugation depth, t, (mm)	55.2	27.1
Radius of centroid, r, (mm)	323	308

C.4.2.3 Test Conditions

The conditions for each test are summarized in Table C-13. All tests were conducted at a temperature of 22 ± 2°C. For each of the tests, average densities were obtained using a nuclear densometer (MC-1DR-P Portaprobe). Measurements were taken as the soil box was backfilled and also as it was exhumed. Initial (backfill) dry densities with depth can be seen in Figure C-55.

Burial Condition A—T1. Burial Condition A involved placing the sand in 150-mm thick lifts and compacting each lift with two passes of a vibratory plate tamper (M-B-W Model AP2000S). The tamper has a base plate size of 480 mm × 530 mm, and delivers a centrifugal force of 14.35 kN to a depth of 360 mm according to manufacturer specifications (depending on the type of soil). The resulting dry density of the sand was quite uniform with an average dry density of 1,490 kg/m^3 with a range between 1,470 kg/m^3 to 1,510 kg/m^3 as shown in Figure C-55a. For this burial condition, no additional effort was made to compact the soil in the haunches.

Burial Condition B—T2. Burial Condition B involved placing the sand in 150-mm thick lifts and compacting each lift with two passes of a rammer (Wacker Model ES52Y). The rammer had a shoe size of 250 mm × 330 mm, which enabled it to provide greater compaction in the haunch region relative to the plate tamper. It delivers a centrifugal force of 11.5 kN and has a compaction depth of 450 mm according to manufacturer specifications (depending on type of soil). Figure C-54 shows the HDPE pipe in the test cell with sand placed and compacted up to the springline for Condition B (the rammer and nuclear density gage are also visible in the

Table C-13. Description of tests performed.

Test	Description*	Backfill Material	Type of Pipe	Method of Compaction
T1	SP-HDPE-PT	Synthetic Olivine Sand	HDPE	Vibratory plate tamper
T2	SP-HDPE-R	Synthetic Olivine Sand	HDPE	Rammer
T3	SP-HDPE-SB	Synthetic Olivine Sand	HDPE	Stiff base with a loose haunch
T4	SP-PVC-SB	Synthetic Olivine Sand	PVC	Stiff base with a loose haunch
T5	GW-HDPE-PT	Granular "A"	HDPE	Vibratory plate tamper
T6	GW-PVC-PT	Granular "A"	PVC	Vibratory plate tamper

*Notation is as follows: SP = poorly graded sand, GW = well-graded gravel, HDPE = high-density polyethylene; PVC = polyvinyl chloride; PT = plate tamper; R = rammer; SB = stiff base/loose haunch.

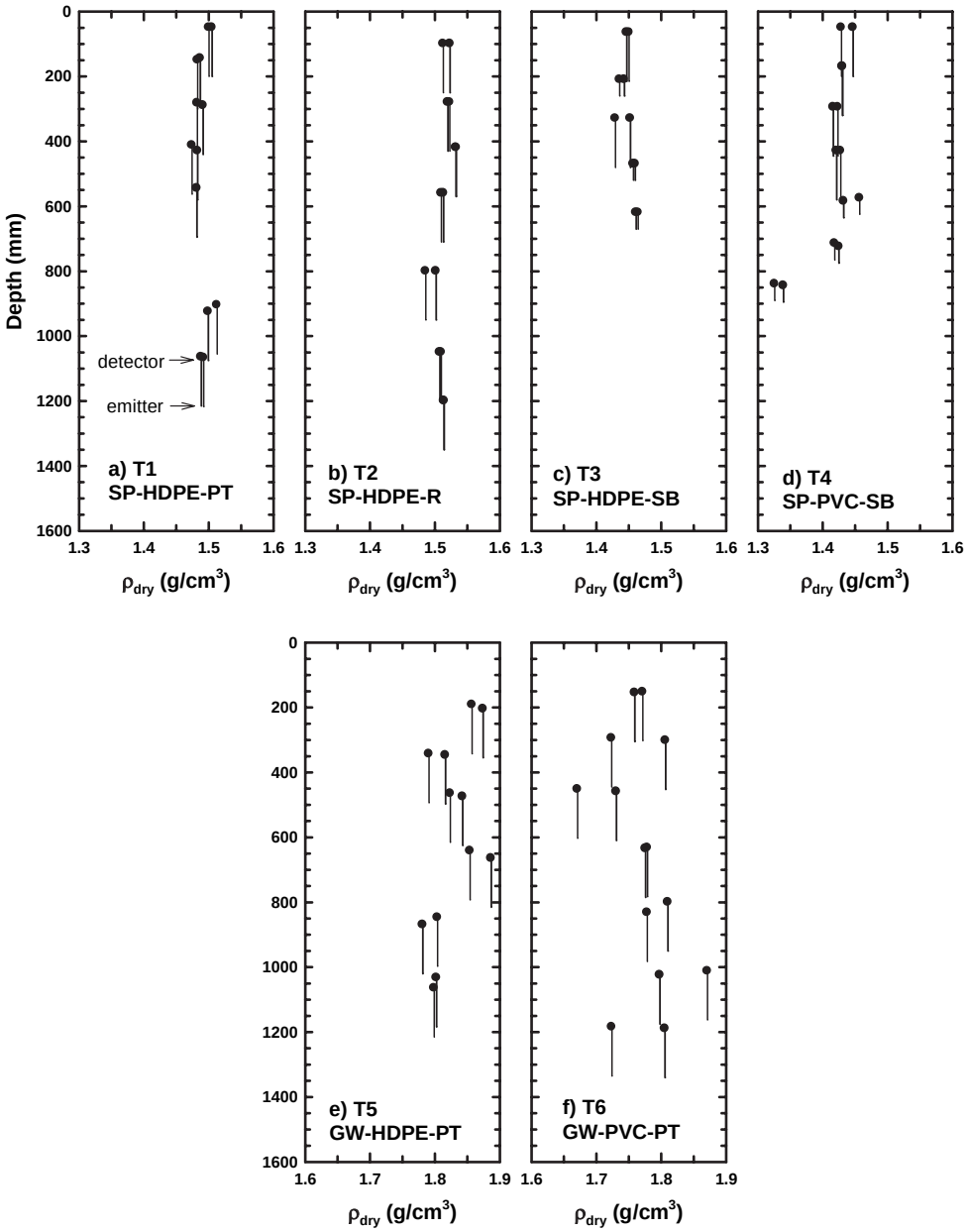

Figure C-55. Local density measurements taken with depth for pipes tested in a poorly graded sand (T1, T2, T3, and T4) and pipes tested in a well-graded gravel (T5 and T6).

photograph). For this installation condition, the average dry density was 1,510 kg/m^3 with a range of 1,480 kg/m^3 to 1,530 kg/m^3, as shown in Figure C-55b. This suggests that the rammer delivered higher compactive effort than the plate tamper since it resulted in higher density measurements.

Burial Condition C—T3 and T4. Burial Condition C involved the case of the pipe placed just above a stiff base surrounded by loose backfill up to the springline and denser backfill above the springline. The geometry for this configuration is shown in Figure C-56. Concrete blocks were first placed at the base of the test cell to simulate a hard foundation for the pipe. A 70-mm thick bedding of compacted sand was then placed over the hard surface. This layer of bedding sand was used below the invert, since it was considered unreasonable to expect the pipes to be subject to direct placement on the rigid base. This layer of bedding sand was also useful for the protection of exterior strain gages located on the invert. The pipe was then positioned on the bedding material and loose sand was placed up to the level of the springline with no effort to compact the soil in the haunches. From the springline to the top of the test cell, sand was placed in 150-mm thick lifts and

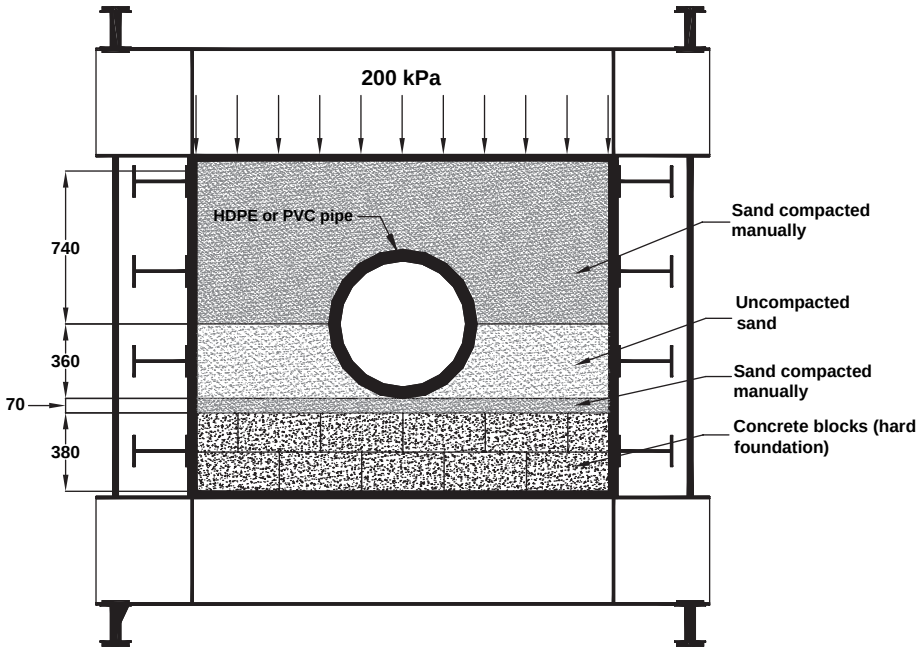

Figure C-56. Cross-section showing biaxial test cell. Backfill geometry of Tests T3 and T4 are shown (measurements in mm).

compacted manually (two passes dropping a 250-mm square plate with 6.8 kg mass a distance of 0.4 m to 0.5 m).

T3 and T4 featured much lower densities (Figure C-55c and C-55d) than the previous two tests, as was expected based on the backfill geometry. The overall dry density for T3 was 1,450 kg/m^3 above the springline and 1,350 kg/m^3 below, while the dry density for T4 was 1,430 kg/m^3 above and 1,340 kg/m^3 below the springline. A photograph of the PVC pipe during compaction of the sand above the springline is shown in Figure C-57.

Burial Condition A—T5 and T6. The last two tests were conducted using Burial Condition A by placing gravel (Figures C-54 and C-58) in 150-mm thick lifts and compacting each lift with two passes of a vibratory plate tamper (Bomag BP 10/36-2). The Bomag vibratory plate tamper has a base plate size of 560 mm × 360 mm; the manufacturer specifications state that it delivers a centrifugal force of 10 kN to the underlying soil.

T5 and T6 (HDPE and PVC pipes buried with granular backfill and compacted with a vibratory plate tamper) contained the largest dry density measurements (Figure C-55e and C-55f) along with the greatest variation of measurements throughout all six tests. The granular backfill is a well-graded material (GW), which explains the increase in densities relative to those obtained with poorly graded sand (SP). The overall dry density obtained during backfilling of T5 was 1,830 kg/m^3 with values ranging from 1,790 kg/m^3 to 1,890 kg/m^3. The overall dry density obtained for T6 was 1,770 kg/m^3 with values ranging from 1,670 kg/m^3 to 1,870 kg/m^3.

Instrumentation. Pipe diameter changes were measured using linear potentiometers (HLP 190, accurate to within ± 0.01 mm). Four potentiometers (one horizontal and one vertical, at two separate axial sections) were used to measure the change in vertical diameter, ΔD_v, and change in horizontal diameter, ΔD_h, of the pipes. All readings were zeroed after installation and backfilling of the pipe.

Surface strains of the pipe were measured using electrical resistance foil gages (Showa, Type N22-FA-2-120-11, accu-

Figure C-57. Photograph taken during backfilling of T4 showing PVC pipe with sand placed above the springline of the pipe; the manual compaction plate and nuclear density gauge are also shown.

Figure C-58. Photograph taken during backfilling of T5 showing HDPE pipe with granular "A" placed just above the springline of the pipe; the nuclear density gage is also shown.

rate to within ± 10 με) with a 2-mm gage length. Biaxial gages were used to measure pipe wall strains in both circumferential, ε_θ, and axial, ε_z, directions. Up to 30 gages were installed on each pipe, and the individual locations of the gages on the HDPE and PVC pipes are shown in Figure C-59. Section A shows the gages on the liner and crest of the profile, while Section B shows those gages placed on the valley interior. No gages were placed on the exterior of the valley, as it was assumed that strains would be larger on the valley interior, which would be more critical with respect to local bending. The close spacing of measurements in one of the lower haunches (between $\theta = 90$ and 180°) was chosen to detect any local bending effects in that zone.

All strains measured on the HDPE pipe were adjusted for local stiffening effects (since the stiffness of the strain gages is similar to that of the HDPE). This was achieved by multiplying the strain readings for each gage by a modification factor unique to that gage. The strain modification factors ranged from 1.13 to 1.45 and were obtained by dividing the hoop strain (change in diameter divided by initial diameter) by the circumferential strain measurements obtained from the strain gages during an unrestrained thermal contraction test from 22 to 0°C. Local strain measurements should equal the average hoop strain (which was calculated from four LP measurements), since under these axisymmetric conditions the pipe experiences uniform radial contraction.

No adjustment of strain measurements was applied for the PVC pipe given its higher modulus relative to the gages. Compressive strains are reported as negative values. As for the deflections, strain readings were zeroed after backfilling.

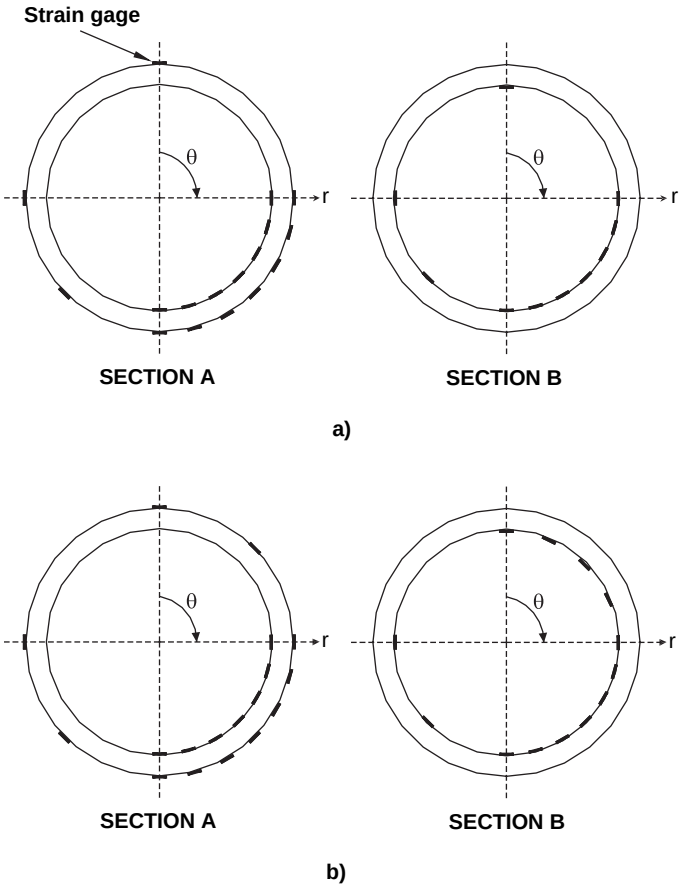

Figure C-59. Locations of strain gages placed at Section A (liner and crest) and Section B (valley) for (a) HDPE pipe and (b) PVC pipe.

C.4.3 Results and Discussion

C.4.3.1 Pipe Deflection

Measured changes in vertical (ΔD_v) and horizontal (ΔD_h) diameter are shown in Figures C-60 through C-63. A summary of ΔD_v, ΔD_h, and the ratio of $\Delta D_v/\Delta D_h$ for an applied vertical pressure of 200 kPa is presented Table C-14. Increases in diameter are represented as positive values, while decreases in diameter are represented as negative values.

Table C-14. Vertical and horizontal deflections at an applied pressure of 200 kPa.

Test	Description	ΔD_v (mm)	ΔD_h (mm)	$\Delta D_v/\Delta D_h$
T1	SP-HDPE-PT	–5.1	0.6	–9
T2	SP-HDPE-R	–4.5	0.1	–44
T3	SP-HDPE-SB	–12.6	3.1	–4
T4	SP-PVC-SB	–7.4	4.2	–2
T5	GW-HDPE-PT	–3.4	1.1	–3
T6	GW-PVC-PT	–0.6	1.3	–1

Figure C-60 shows the influence of three different burial conditions on HDPE pipe deflections when buried in poorly graded sand. Essentially, the decrease in vertical diameter was linearly proportional to the applied overburden over the pressure range tested for T1 and T2 (T3 is discussed later in this section). Similar deflections were obtained for both tests, although the method of compaction differed between these tests (plate tamper versus rammer). The vertical diameter change in Test T2 was 15% less than in Test T1 (at 200 kPa), indicating that the slightly higher density obtained with the rammer led to a higher soil stiffness, resulting in smaller deflections.

Allowable deflection limits for profiled wall HDPE pipe per AASHTO is 5% of the inside pipe diameter. Maximum vertical diameter change in Tests T1 and T2 is 0.85% and 0.74% of the inside pipe diameter, respectively, and is much less than the 5% limit. Also, as expected for the lined corrugated HDPE pipe tested with good soil support, the increase in horizontal diameter is only a small fraction of the vertical diameter change. This results from circumferential shortening of the pipe (i.e., circumferential compression).

When tested with Burial Condition C, the slope of the diameter change versus applied pressure is not linear, but rather decreases, suggesting that the stiffness of the initially uncompacted sand increases over the pressure range tested. The vertical deflections of the HDPE pipe for T3 are nearly 2-½ times larger than those for Condition A (T1). As expected, the close proximity of the hard foundation and uncompacted backfill below the springlines led to larger pipe deflections. However, even the maximum measured deflection is only 2.1% of the internal diameter for this test, which is well below the 5% limit.

Burial condition also has an influence on the horizontal deflection, ΔD_h. The smallest horizontal deflection was seen for T2 (0.1 mm) where soil had highest stiffness, and largest horizontal deflections were seen for T3 (3.1 mm), where soil stiffness was lowest. The ratio of vertical deflection to horizontal deflection, $\Delta D_v/\Delta D_h$, in Table C-14, reflects the nature of the deformed shape of the pipe. The conventional way of viewing this is to attribute the greater springline movements to higher compressions in the loose sand placed beside the pipe in T3 compared to those permitted by the compacted sand used in Tests T1 and T2. An alternate explanation (Moore 2001) comes from consideration of the Fourier decomposition employed in the Hoeg (1968) solution. Stiff backfill leads to much higher levels of circumferential shortening and a uniform component of inward movement of the pipe that cancels out most of the outward movements at the springline that result from ovaling.

The influence of the type of pipe (HDPE versus PVC) for Burial Condition C can be examined by comparing the results from T3 and T4 as shown in Figure C-61. This comparison shows that the vertical deflection of the HDPE pipe is 1.7 times greater than the PVC pipe. As expected for the same initial backfill condition, larger vertical deflections are obtained for the pipe with lower modulus. However, the ratio of vertical deflection to horizontal deflection for the PVC pipe is much smaller than that of HDPE (see Table C-14). This is explained by the fact that PVC experiences less circumferential shortening due to its higher hoop stiffness, and as a result, the hori-

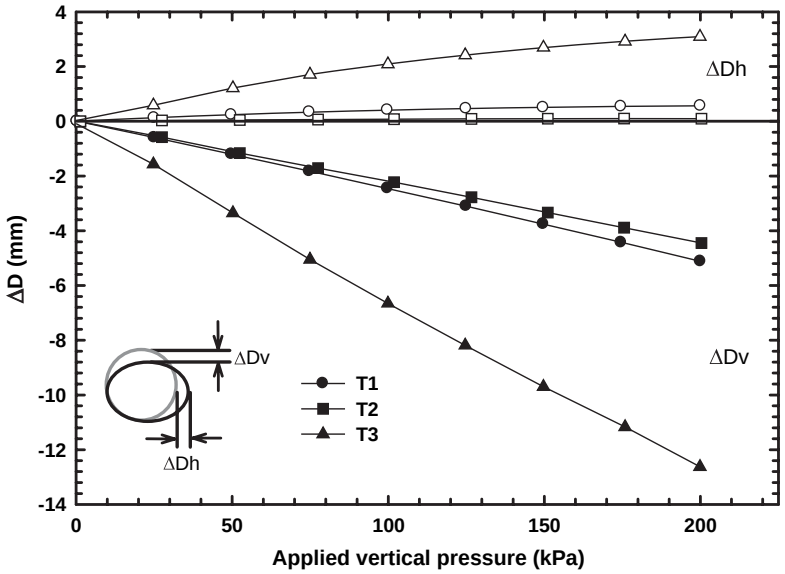

Figure C-60. Vertical and horizontal deflections for T1, T2, and T3 showing influence of installation condition on HDPE pipe deflection when buried in sand.

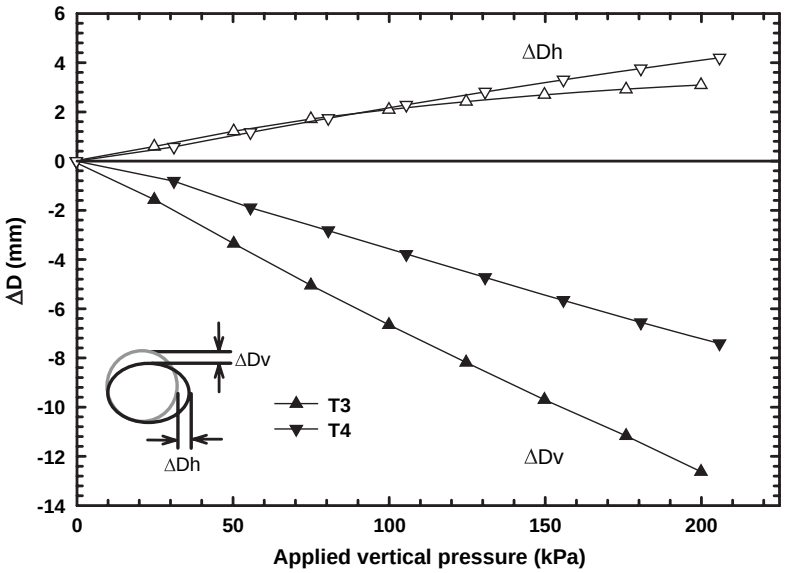

Figure C-61. Vertical and horizontal deflections for T3 and T4 showing differences between HDPE and PVC pipes placed on a rigid base with sand loosely placed in the haunch.

zontal diameter increase is a higher percentage of the vertical diameter decrease than for the HDPE pipe.

The influence of the type of backfill soil on HDPE pipe deflections with plate tamper compaction is shown in Figure C-62. As expected, the well-graded gravel produces smaller vertical deflection, since it is stiffer than the poorly graded sand. However, an interesting response with the gravel was observed. A stiff response was obtained up to vertical pressures of 100 kPa where reductions in apparent stiffness begin to increase the incremental diameter changes at higher applied pressures. This is believed to arise from stresses locked into the well-graded gravel during compaction. It is postulated that once the magnitude of the applied stresses exceeds the compaction induced stresses, the gravel stiffness reduces. The sand does not show the same softening as the gravel, since its poor gradation does not generate the same level of locked-in compaction stresses as the well-graded material. The softening of the gravel may be of practical significance in the selection of

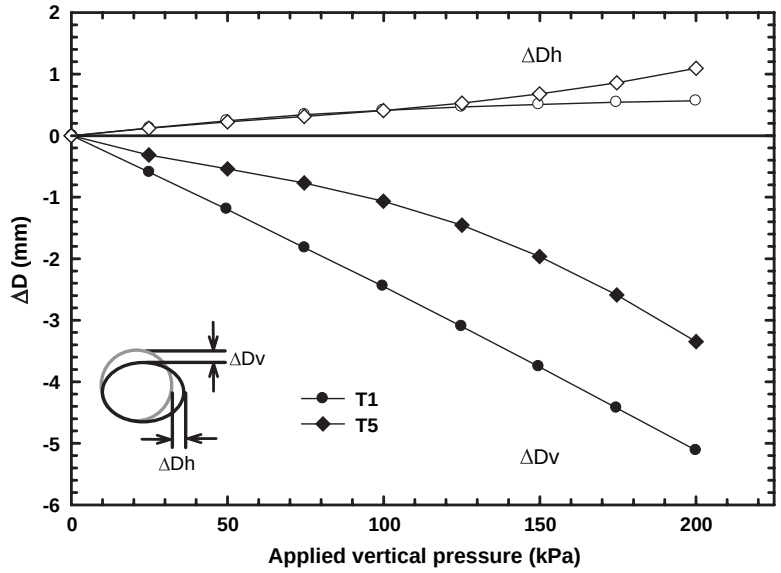

Figure C-62. Vertical and horizontal deflections for T1 and T5 showing the influence of backfill material on the HDPE pipe.

soil modulus during pipe design for burial under vertical pressures larger than 100 kPa. Soil modulus obtained from conventional triaxial compression testing would likely overestimate the modulus active at these high stress levels, since they would not include the effect of the compaction stresses. For higher risk projects, it would be best to infer modulus from a large-scale experiment (like T5), where effects of compaction can be captured and the interaction between the soil and structure can be simulated.

Following T5, a different response was noticed and, as a result, it was decided that for T6 additional monitoring of deflections was needed to interpret the results. This was conducted using digital photographs taken at each increment of pressure. Using digital photography, vector movements can be measured from specific targets (White et al. 2003). Figure C-63 shows the deformed shape of the pipe captured from digital images with 20 times magnification during the load increment from 0 to 200 kPa of applied overburden pressure. This figure also shows how the pipe translates vertically from settlement of the underlying soil and pipe deformation. Figure C-64 presents plots of deflections versus applied pressure for T6.

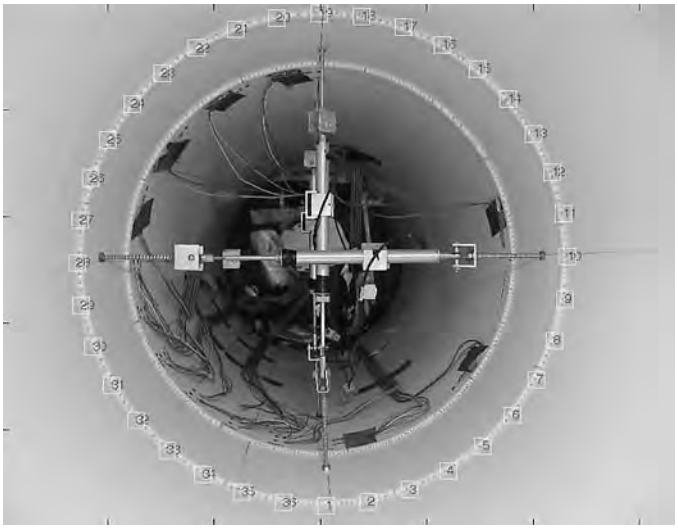

Figure C-63a. Photograph showing locations of tracked changes used to measure changes in pipe diameter.

Overall pipe deflections for T6 are as small as expected and are well below the allowable diameter change of 5%, although the distribution is different from those seen in the previous five tests (visible in the comparison of T6 with T5 in Figure C-64a). Maximum increase and decrease in deflection were recorded in the vertical and horizontal planes similar to the previous tests ($\Delta D_v = -0.6$ mm and $\Delta D_h = 1.3$ mm). However, it appears that there is a change in soil support as the applied vertical pressure is increased. For the first increment in overburden stress, ΔD_v and ΔD_h behave as would be expected. Between 25 and 50 kPa of applied pressure, the pipe starts to exhibit an opposite trend (a diameter decrease at the springlines, and diameter increase between crown and invert). The digital images of the PVC pipe deformations indicate that the pipe is not deforming in a conventional elliptical deformation pattern. Rather, nonelliptical deformations like those described by Rogers, Fleming, and Talby (1996) develop and likely result from the nonuniform distributions of ground support around the pipe circumference that have occurred during installation. In particular, it is likely that the pipe was raised off the bedding during sidefill compaction, leaving a

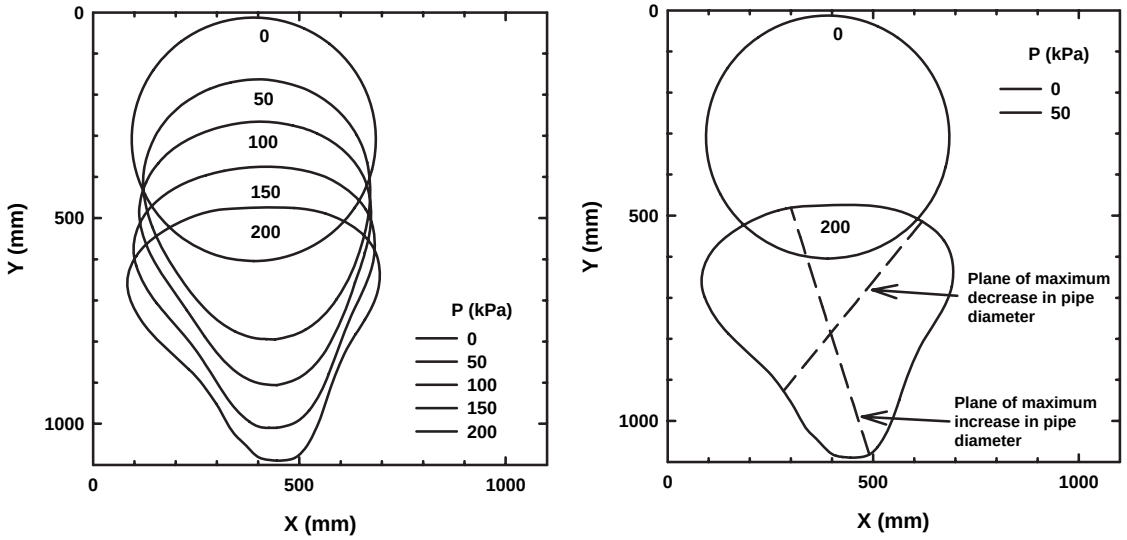

Figure C-63b. Deformed shape of T6 under overburden pressure (× 20 magnification); maximum and minimum diameter changes shown on right.

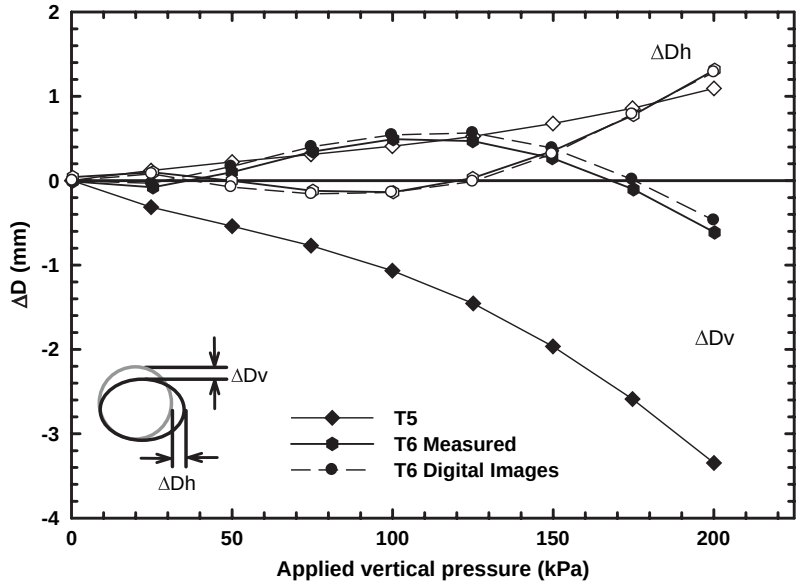

(a)

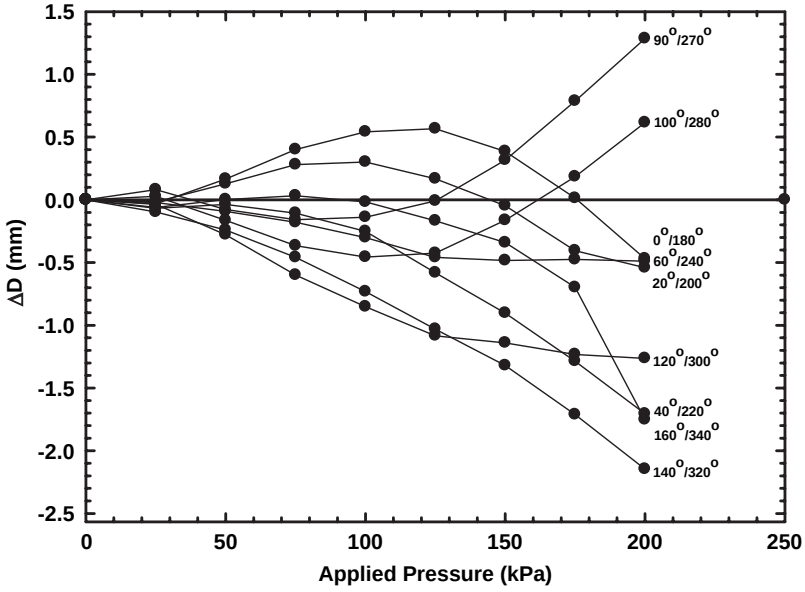

(b)

Figure C-64. (a) vertical and horizontal deflections for T5 and T6 showing differences between HDPE and PVC pipes buried within a well-graded gravel and (b) changes in pipe diameter for T6 with increasing applied overburden pressures.

small void under the invert. Under vertical load, the pipe pushed into the void. Eventually, a more uniform pattern for changes in vertical diameter ΔD_v and horizontal diameter ΔD_h develops.

C.4.3.2 Pipe Strain

Detailed Results for T1. Circumferential strains, ε_θ, and axial strains, ε_z, measured at the corrugation valley and crest are plotted in Figures C-65 and C-66 versus the applied vertical pressure for T1. Valley strains measured on opposing springlines ($\theta = \pm 90°$) are very similar, with a maximum difference of 1% at 200 kPa, indicative of a nearly symmetric pipe response. Crest strains at the two springlines are similar but differ by roughly 12% at 200 kPa. It is possible that these measurements on the exterior of the pipe (i.e., corrugation crest) have a greater sensitivity to local backfill effects.

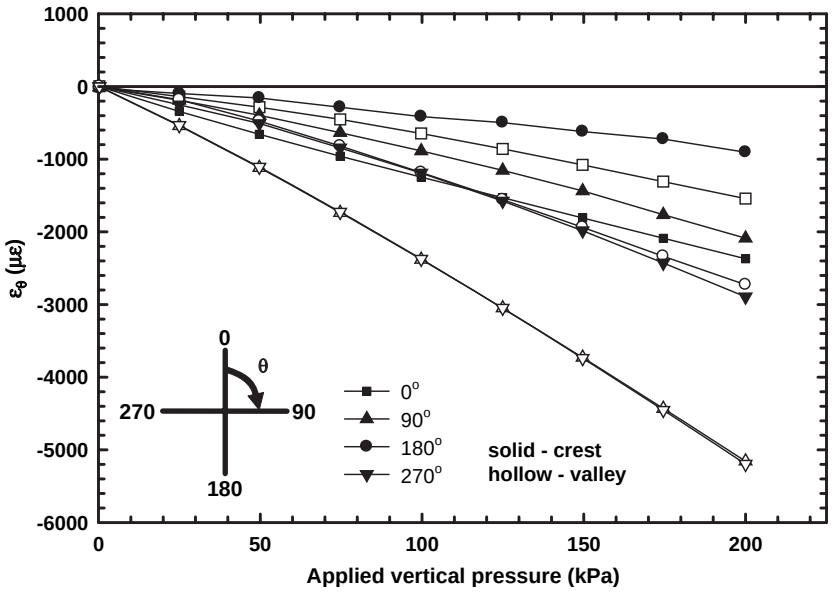

Figure C-65. Circumferential strains at crown, invert, and springlines for T1—SP-HDPE-PT (solid symbols = crest strain; hollow symbols = valley strain).

All axial strains are tensile, except for the value at the exterior invert ($\theta = 180°$ in Figure C-66). While both ε_θ and ε_z are required for any calculations of resulting circumferential and axial stress, only values of ε_θ are reported in the remainder of this section, as they are the major principal strains and are sufficient to quantify the backfill effects being studied and their influence on pipe response. All axial strain measurements are provided in Munro (2006).

The distribution of ε_θ measured around the circumference of the pipe and ε_θ plotted through the profile of the pipe for T1 are given in Figure C-67. The figure reveals the differences between crest and valley compressive strains around the circumference of the pipe at an applied pressure of 200 kPa. Beginning at the crown of the pipe, more compressive strain occurs at the crest, then changes to the valley at the springline, then to the crest at 150°, and then back to the valley at the invert. T2

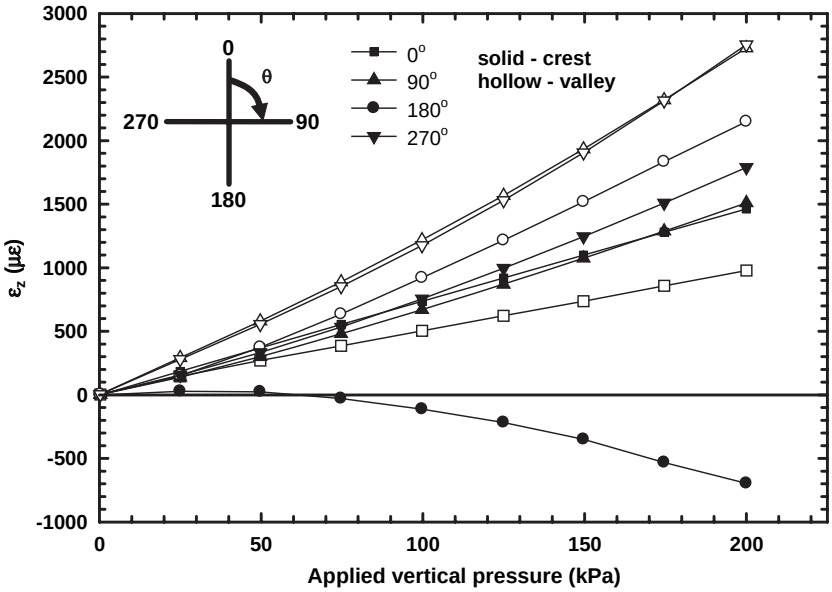

Figure C-66. Axial strains at crown, invert, and springlines for T1—SP-HDPE-PT (solid symbols = crest strain; hollow symbols = valley strain).

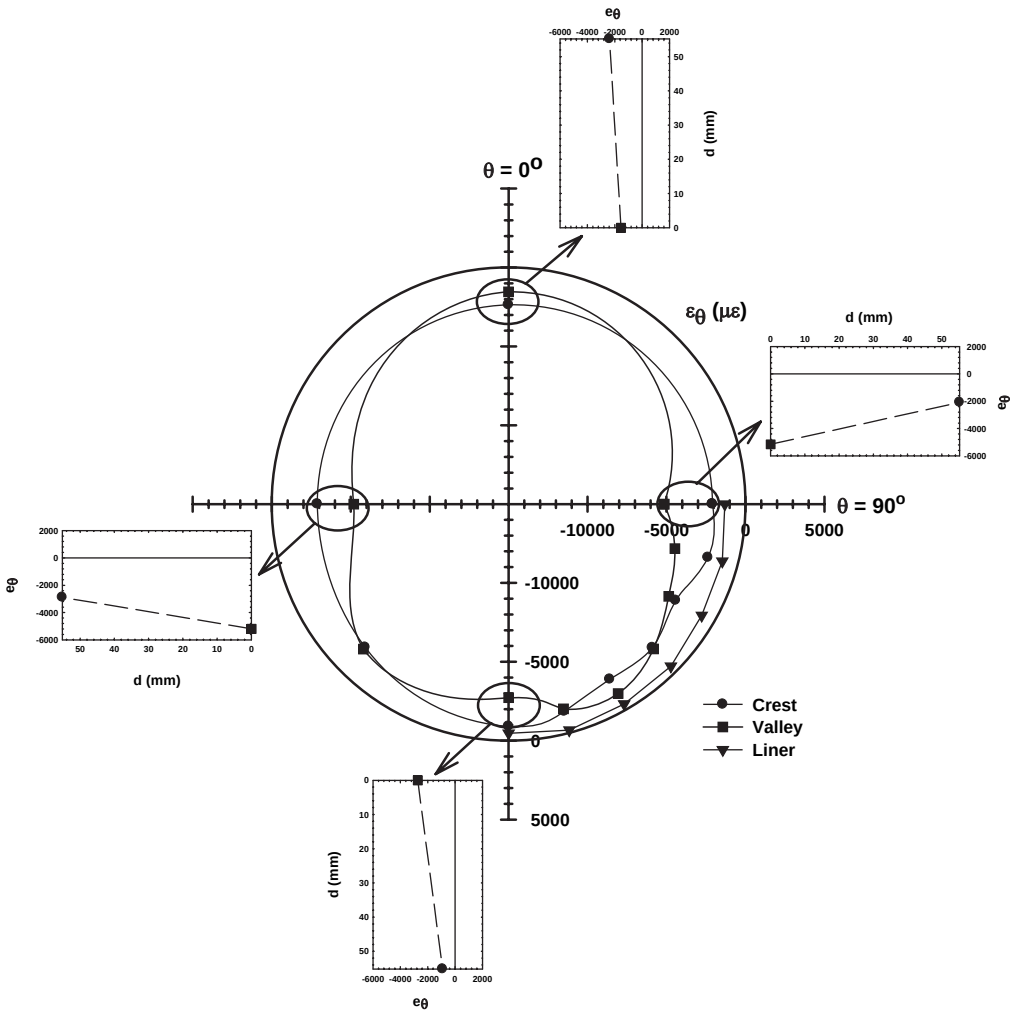

Figure C-67. Distribution of circumferential strains at an applied pressure of 200 kPa for T1.

through T6 experienced the same overall distribution of strain around the circumference of the pipe; illustrations are provided in Munro 2006.

Uniform backfill theory (e.g., Hoeg 1968) suggests that the strain at the crown and invert is more compressive on the exterior surface of the pipe wall. Conversely, springline strain is more compressive on the interior than on the exterior. Although these patterns were observed at the crown and the springlines, the compressive strain at the invert for all tests was larger in the valley than in the crest (contrary to uniform backfill theory). This increase in strain at the valley indicates that local circumferential bending is taking place at or near the invert.

Strains measured in the liner were much less than the crest and valley strains (refer to Figure C-41 for the different corrugation positions), even though they are located at a similar distance from the centroidal axes. The work of Moore and Hu (1995) demonstrated that liner strain is reduced relative to valley strain due to local bending effects in the lined corrugated HDPE pipe (see Section C.2). Due to these findings, subsequent discussion will address strains on the crest and valley only, with measurements of the liner strains provided in Munro (2006).

Influence of Backfill Condition. A summary of maximum compressive strain, ε_θ, for each test is presented in Table C-15. In almost every case (other than T6), the maximum strain was measured in the valley interior, at or near the pipe springlines. T6 (GW-PVC-PT) exhibited maximum strain at the invert of the pipe, suggesting that local bending near the invert is enhanced in that test.

Figures C-68 through C-71 plot measured values of crest and valley strain at an overburden pressure of 200 kPa, to show the influence of backfill condition on strain for the different scenarios examined.

Table C-15. Measured maximum circumferential strains (compressive) located on the valley interior at an applied pressure of 200 kPa for each test.

Test	Description	$\varepsilon_{\theta max}$ ($\mu\varepsilon$)	Location (degrees)
T1	SP-HDPE-PT	–5,200	–90
T2	SP-HDPE-R	–4,460	–90
T3	SP-HDPE-SB	–10,350	–90
T4	SP-PVC-SB	–2,880	–90
T5	GW-HDPE-PT	–4,350	–83
T6	GW-PVC-PT	–3,960	180

T1 versus T2. Strains for the three different burial conditions at an overburden pressure of 200 kPa are plotted in Figure C-68. Circumferential strains on both the crest and valley are provided. Circumferential strains for T2 are slightly smaller than those for T1. This is consistent with the deflections obtained in that the denser sand yields both smaller deflections and smaller strains. By tracking valley strains around the pipe circumference, strain increases at the invert of T1 are approximately 1.6 times the magnitude of those for T2. This increase in strain between θ = 150 and 180° implies slightly greater local bending effects for backfill conditions in T1 relative to those in T2. Greater local bending is consistent with the presence of a softer haunch in T1, which is likely, since the vibrating plate compactor is less able to compact the soil under the haunches. Greater bending also occurs at the springline in T1 relative to T2, corresponding to larger differences between the circumferential strains at valley and crest.

T3. T3 featured much larger pipe deformations and larger crest strains than T1 or T2 (see Figure C-68). The stiff base and uncompacted backfill beneath the springline in this test resulted in large increases in compressive valley strain near the springline and large (relative to T1 and T2) crest strains around the pipe. Since the soil in the haunch was placed in a consistent uncompacted manner, there was no substantial variation in soil stiffness beneath the haunch. This in turn provided essentially uniform, albeit poor, support to the pipe below the springlines. Consequently, no substantial local bending effects were observed in the vicinity of the haunches during T3. For the same reason, only small local bending effects were measured for the PVC pipe (T4) with the same stiff base soil and the same loose soil placed below the springlines (Figure C-69).

T1 versus T5. T5 featured a different backfill material (well-graded gravel) from that used in T1 to T4, and it employed compaction protocols similar to those of T1. Strains measured during T5 were slightly less than those of T1 (Fig-

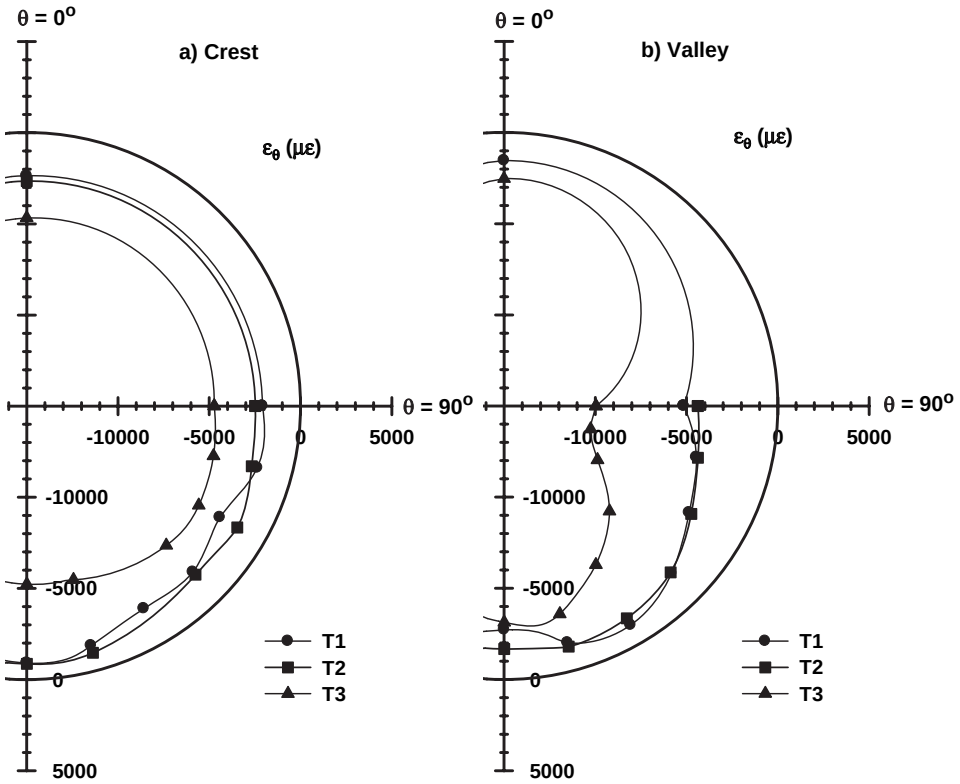

Figure C-68. Crest and valley circumferential strains at an applied pressure of 200 kPa for T1, T2, and T3.

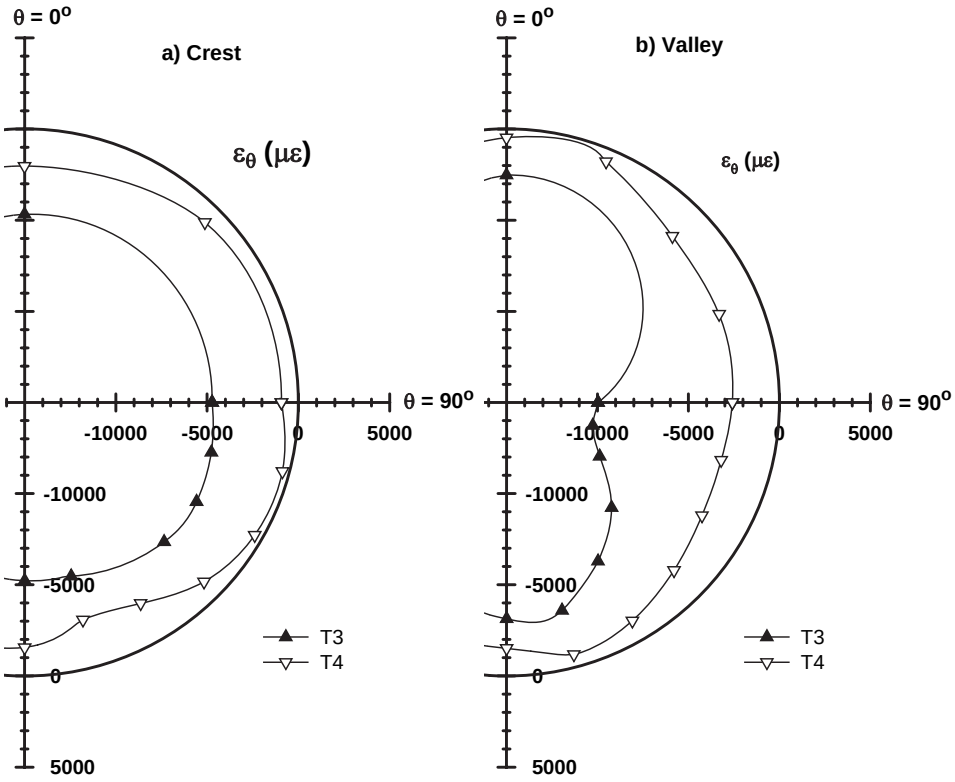

Figure C-69. Crest and valley circumferential strains at an applied pressure of 200 kPa for T3 and T4.

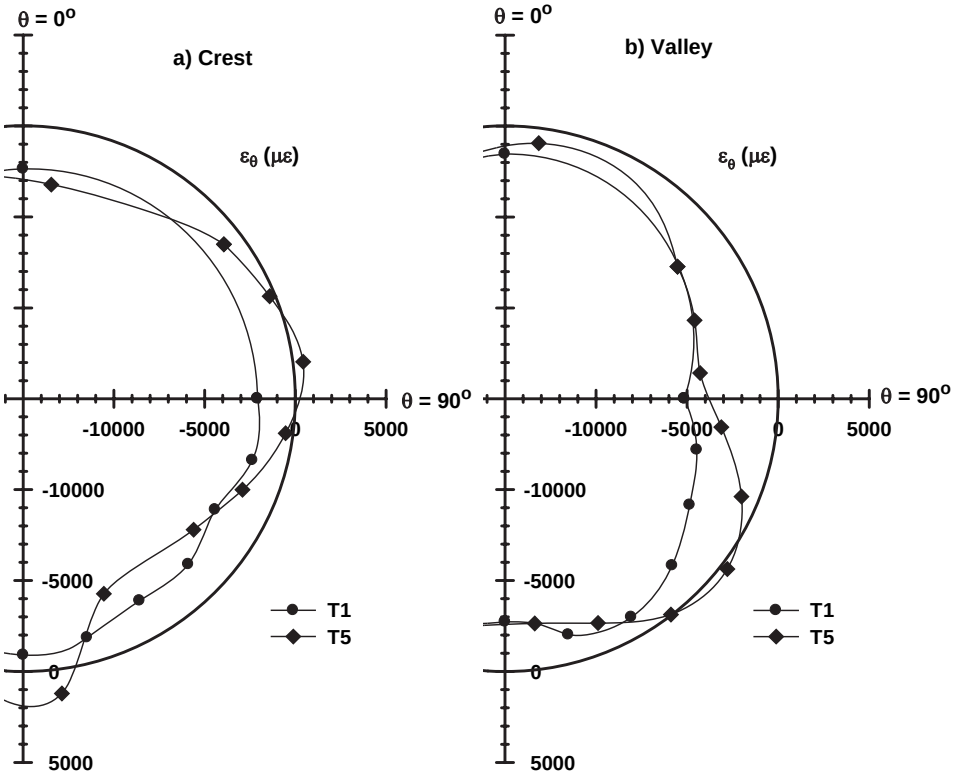

Figure C-70. Crest and valley circumferential strains at an applied pressure of 200 kPa for T1 and T5.

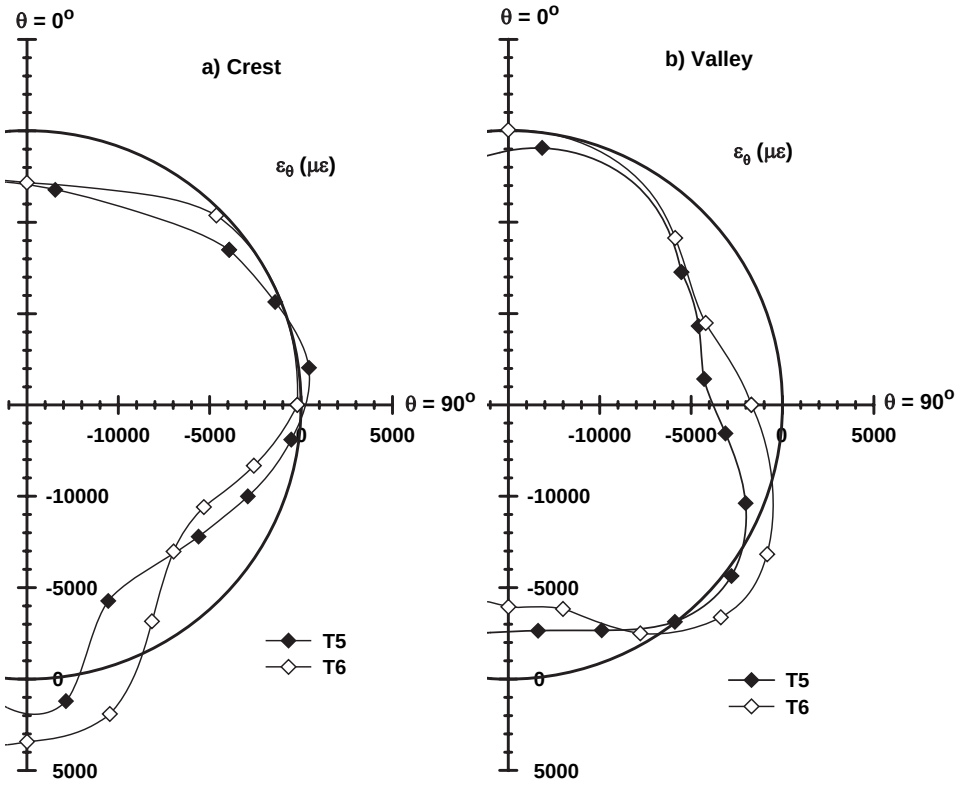

Figure C-71. Crest and valley circumferential strains at an applied pressure of 200 kPa for T5 and T6.

ure C-70), which was expected, since the gravel had a higher stiffness than the sand. Comparisons of circumferential strains on the valley and the crest for both T1 and T5 reveal similar patterns for these two tests, although much greater bending effects are visible from T5.

The largest differences between crest and valley strains occur at the springline and invert of this test. This is consistent with observed pipe deformations, as greater ovaling associated with larger ΔD_h relative to ΔD_v (Table C-14) produces small tensile strains (600 με) just above the springline. Tensile strains can also be seen on the crest, invert (2,000 με), and valley haunch (750 με), which is caused by local bending associated with local variations in backfill stiffness. Such local bending in the haunch region is more prominent for gravel than sand due to a greater contrast in density between the soil in the uncompacted haunch region and the well-compacted soil beyond. Although the maximum tensile strain at 200 kPa is well below the acceptable limits, these results indicate that an HDPE pipe buried in a stiff backfill is more susceptible to the effects of local bending and that backfill condition can lead to strains that deviate from those calculated from a uniform backfill analysis.

T5 versus T6. Measured circumferential strains on the interior (valley) and exterior (crest) surfaces of the pipe in T6 are shown in Figure C-71. Maximum strains occurred at the invert, with maximum tensile strain at the crest and maximum compressive strain in the valley. Furthermore, the strain distribution around the circumference of the pipe in this figure shows that strains for T6 are greater than those of T5, implying that local bending is greater for T6 (seen by the larger differences in crest and valley strains). The locations where bending is seen to be amplified (locations where there are large differences in crest and valley strains) are T5—82°, 165°, and 180° and T6—68°, 120°, and 180°.

C.4.4 Implications for Pipe Design

Circumferential strains can be estimated for pipe design using the design equation proposed by McGrath (1998a). Dhar, Moore, and McGrath (2004) indicate how local bending strains can be calculated from bending deflections and then scaled by the semi-empirical strain factor D_f, of Molin (1971), defined as

$$D_f = \varepsilon_b \left(\frac{R}{c} \right) \left(\frac{D}{\Delta D_b} \right) \tag{C.9}$$

where ε_b is the maximum bending strain in the pipe (taken as ε_θ at the crest minus ε_θ at the valley); R is the radius of the

centroid of the pipe; c, distance from the centroid of the pipe wall to the extreme fiber; D is the diameter of the pipe measured to the corrugation centroid; and ΔD_b is the bending deflection (taken as one-half the difference between ΔD_v and ΔD_h). A negative value of D_f implies that the radius of curvature of the pipe has decreased.

As discussed in Section C.1, D_f equal to 3 corresponds to the elastic pipe-soil interaction solution with uniform soil support. That section reported results from tests on a lined corrugated HDPE pipe and a ribbed PVC pipe in loose, uniform sand backfill. A strain factor D_f equal to 3 was inferred from these tests, which was identical to elastic pipe-soil interaction theory involving uniform soil support (Hoeg 1968).

Strain factor, D_f, has been calculated from measured deflections and pipe wall strains for T1 to T5 and summarized in Table C-16. Values are reported at the crown, springlines, and invert at an applied vertical pressure of 200 kPa. The maximum haunch value between 90° and 180° is also reported. Both the HDPE and PVC pipes tested had D_f values of around 3 for a stiff base at the invert and backfill placement without compaction below the springlines (T3 and T4). Deviations in strain factor from $D_f = 3$ arise from local bending associated with backfill conditions.

Strain factors around the circumference of the pipe for T1 through T5 are presented in Figures C-72 through C-75. The maximum strain factor obtained in T1 was observed to be 4.1, located at the springline of the pipe. The backfill placed under the haunches was not effectively compacted by the plate tamper, and this region of low-stiffness soil support led to enhancement of bending strains. However, the region beyond the sides of the pipe was effectively compacted by the vibrating plate so that a column of denser, higher stiffness backfill formed stretching from the springline down to the level of stiff bedding. This column of material was effective in limiting deflections in the bottom half of the pipe. Since the increases in maximum bending strains exceeded the increases in bending deflections, D_f, a function of the ratio between them was observed to increase.

Despite the considerable differences in burial conditions, T2, T3, and T4 all had maximum measured strain factors of about 3. T3 and T4, which were conducted without compaction of soil placed below the springlines, produced significant increases in both maximum circumferential strains and deflections relative to T2. However, D_f quantifies bending strains normalized relative to bending deflections, and the deflections and strains increased in direct proportion to one another. As a result, T3 and T4 produced similar values of D_f to those of T2.

The maximum strain factor for T5 (see Figure C-74) occurred at an applied pressure of 100 kPa (maximum $D_f = 9.4$ at 83°). Higher D_f values obtained for T5 in relation to T1 are largely attributed to the characteristics of the two different backfill materials and the manner in which these backfills influenced the response of the pipe. The sand has lower soil stiffness in comparison to the gravel and results in greater pipe deflections. Larger bending strains were obtained in T5 along with smaller bending deflections. This implies enhanced local bending and higher D_f values. A comparison was made with the finite element analyses reported in Section C.1 for backfills with different ratio of backfill modulus (E_s) to haunch modulus (E_h). A D_f value of 9.4 corresponds to an E_s/E_h ratio of 30, using the idealized soil modulus distributions employed.

Strain factors for T5 along with T6 also have been determined using calculated vertical deflections from the simplified design equation developed by McGrath (1998a) for thermoplastic pipes. Strain factor, D_f, calculated for T6 using measured deflections produced abnormally high values of strain factor as a result of small bending deflections caused by changes in vertical and horizontal deflections (Figure C-63). During the design process, the vertical diameter decrease, $D\Delta v$, would be calculated as a proportion of the diameter of the pipe, D, from

$$\frac{\Delta v}{D} = \left(\frac{q_v}{\frac{EA}{R} + 0.57 M_s} \right) + \left(\frac{D_l K q_v}{\frac{EI}{R^3} + 0.061 M_s} \right) \qquad \text{(C.10)}$$

where q_v is the applied vertical (overburden) pressure, E is the modulus of the pipe, A is the cross-sectional area of the pipe, I is the moment of inertia of the pipe, R is the radius of the centroid of the pipe cross-section, D_l is the deflection lag factor (equal to 1), K is the bedding coefficient (equal to 0.083 corresponding to 180° bedding), and M_s is the constrained soil modulus. The first term of the equation represents the

Table C-16. Shape factors, D_f, at 200 kPa of applied pressure.

Test	Description	Crown	Springlines		Invert	Haunch	
		(0°)	(90°)	(270°)	(180°)	D_f	(degrees)
T1	SP-HDPE-PT	1.1	–4.1	–3.1	–2.4	–2.9	105
T2	SP-HDPE-R	–	–3.2	–2.7	–1.4	–2.9	105
T3	SP-HDPE-SB	1.0	–2.5	–2.2	1.0	–2.7	105
T4	SP-PVC-SB	1.9	–2.0	–2.4	–	–2.9	105
T5	GW-HDPE-PT	3.9	–4.4	–7.2	–5.9	–6.6	165

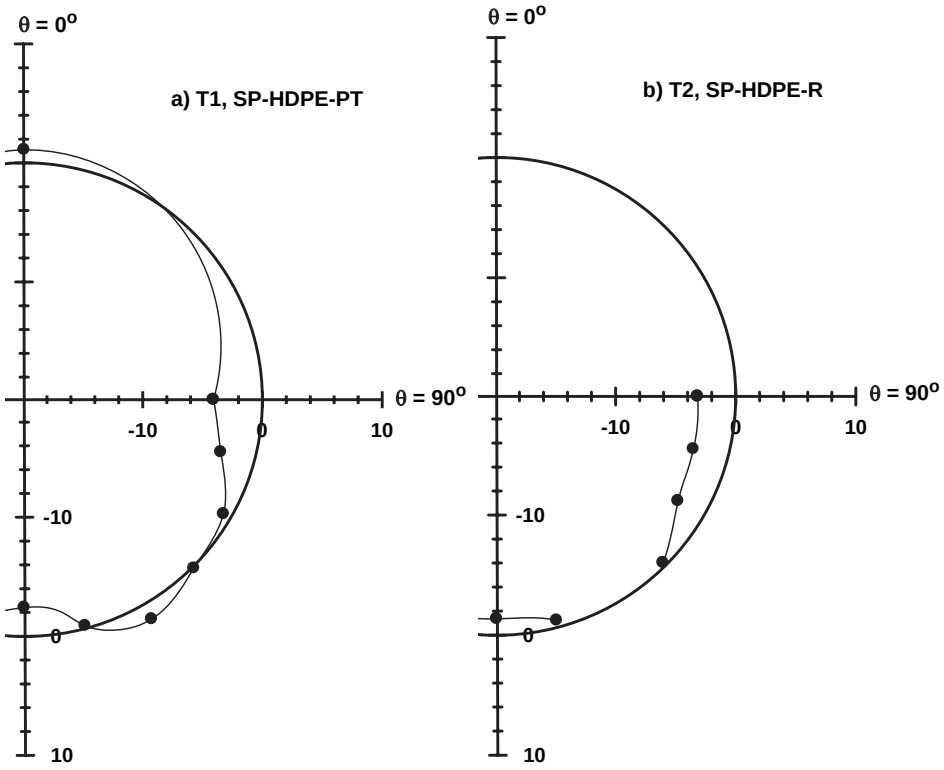

Figure C-72. Strain factor D_f, for T1 and T2 at an applied vertical pressure of 200 kPa.

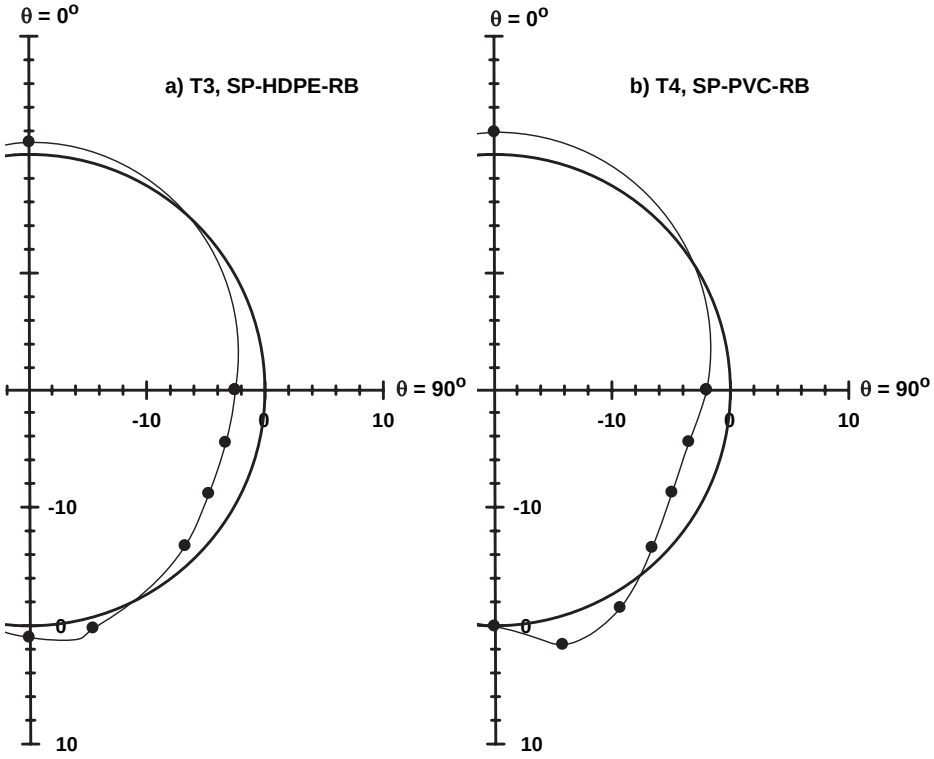

Figure C-73. Strain factor D_f, for T3 and T4 at an applied vertical pressure of 200 kPa.

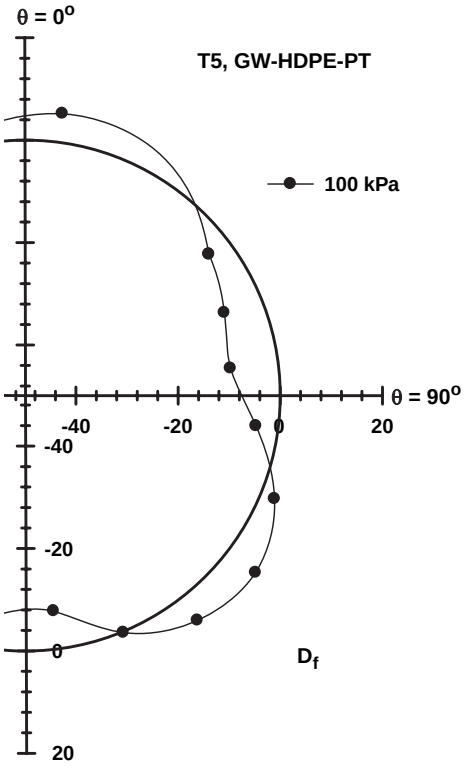

Figure C-74. Strain factor D_f, for T5 at an applied vertical pressure of 100 kPa.

hoop compression, while the second term quantifies bending deformations.

Sectional properties used to calculate vertical deflections of both 600-mm nominal diameter lined corrugated HDPE and PVC pipes for T5 and T6 are given in Table C-17. Using calculated vertical deflections from the simplified design equation and measured strains, D_f values were determined and are shown in Figure C-75a and Tables C-18 and C-19. In the figure, local bending can be seen occurring in three areas of T5 as indicated by higher D_f values around the circumference of the pipe: near the springline ($D_f = -5.2$ at 75°), in the haunch ($D_f = 3.8$ at 120°), and near the invert ($D_f = -4.2$ at 165°).

Maximum D_f values out of all tests were seen in T6 as shown in Figure C-75b. The large values can be attributed to high differences in bending strains coupled with small deflections as a result of high stiffness backfill along with the fact that PVC has a higher pipe modulus than that of HDPE. A similar distribution in D_f values of T6 can be seen relative to that of T5, although less bending is apparent near the springline with more bending in the haunch and invert of the pipe. Strain factors in the haunch and invert are 23 (120°) and 33 (180°), respectively.

T1 and T2 provide measurements for a dense backfill region where geometry is similar to the analyses in Section C.4, T3 and T4 feature a much-more-extensive zone of low-stiffness backfill, and T5 and T6 feature a higher-stiffness backfill than the four previous tests. The differences in strain factor that resulted

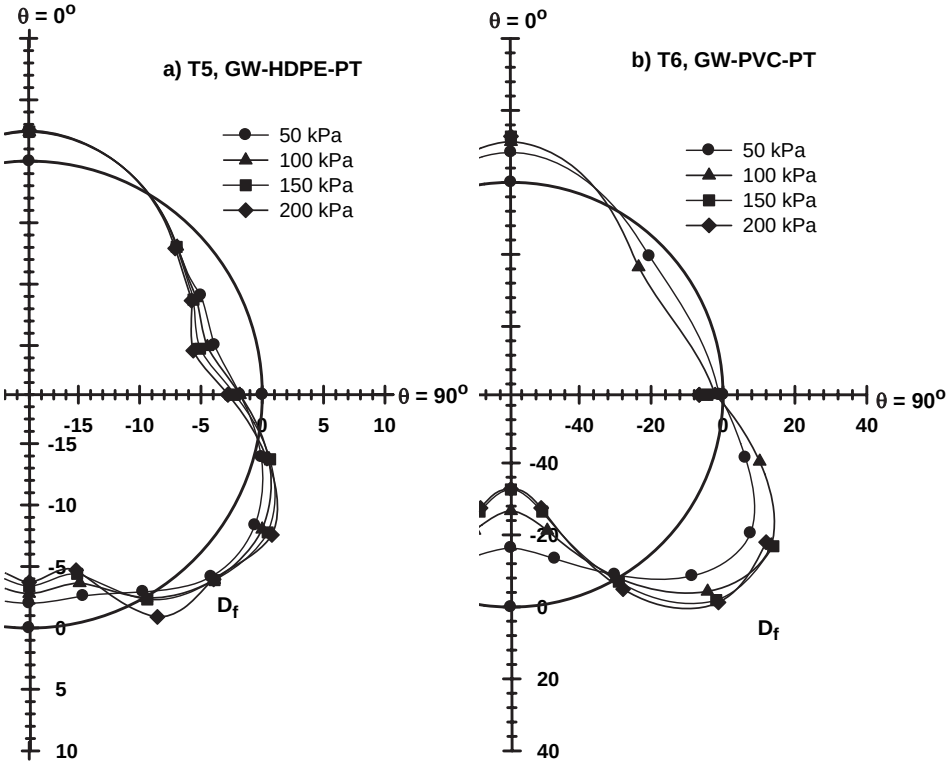

Figure C-75. Strain factor D_f, for T5 and T6 using measured strains and calculated deflections from simplified design equations.

Table C-17. Sectional properties of lined corrugated HDPE and PVC pipes used in simplified design equation.

Property	HDPE Pipe	PVC Pipe
Pipe Sitffness, E_p (MPa)	600	2,760
Area, A (mm^2)	9.3	4,423
Area Moment of Inertia, I (mm^4/mm)	3,104	6,660
Radius of Centroid (mm)	323	308

Table C-18. D_f values for T5 using deflections from simplified design equations.

Theta (degrees)	D_f Values			
	50 kPa	100 kPa	150 kPa	200 kPa
0	2.5	2.4	2.4	2.5
45	–2.0	–1.9	–2.0	–2.2
60	–2.8	–3.3	–3.5	–3.7
75	–3.4	–4.0	–4.6	–5.2
90	–1.8	–1.8	–2.3	–2.8
105	0.6	1.2	1.3	1.0
120	2.2	2.9	3.4	3.8
135	2.0	2.3	2.3	2.3
150	–0.5	0.1	0.3	1.9
165	–2.0	–3.1	–3.9	–4.2
180	–2.0	–2.8	–3.4	–3.7

Table C-19. D_f values for T6 using deflections from simplified design equations.

Theta (degrees)	D_f Values			
	50 kPa	100 kPa	150 kPa	200 kPa
0	8.4	11.3	12.7	12.8
45	–4.6	–8.8		
90	–1.1	–2.2	–4.4	–6.7
105	8.5	12.6		
120	18.0	24.6	25.3	23.0
135	12.3	18.3	21.7	22.6
150	–1.3	–0.5	1.0	3.4
165	–11.9	–19.9	–25.4	–26.4
180	–16.4	–26.8	–32.7	–32.8

from these tests reveal the influences of the burial condition, the type of pipe, and the backfill material. The final choice of strain factor for use in design should be made considering what combinations of soil stiffness and deflection are capable of bringing the pipe to its performance limits (assuming a contractor is permitted to bury the pipe and induce, say, 5% decrease in vertical pipe diameter). The tests reported here imply that it is unnecessarily conservative to use pipe deflections of 5% in strain calculations, where those large deflections are employed together with a high strain factor that is only achieved when using well-compacted, well-graded backfills that feature a restricted zone of loose backfill. This is handled in design by using more modest levels of the shape factor but still assuming 5% deflection.

C.4.5 Conclusions

Results were reported from six additional experiments conducted to examine the influence of pipe type, soil material, and backfill condition on deflections and local bending strains of a lined corrugated HDPE and PVC pipe. As expected, deflections of the HDPE pipe were largest for T3, the test with nonuniform soil support having a rigid base at the invert and loosely placed sand (SP) below the springline. Deflections were smallest for HDPE and PVC pipe Tests T5 and T6, respectively, where a well-graded granular (GW) material was compacted with a plate tamper. Similarly, the largest circumferential strains were measured in T3, while the smallest values of circumferential strain were seen in T5 and T6.

Even when the backfill below the springlines was not compacted and large deflections and strains resulted (T3), a strain factor D_f of 3 was back calculated. Although the backfill conditions were nonuniform in T3, the uniform region of uncompacted material below the springlines produced little local bending. For the six experiments that were conducted, local bending was most prominent for T5 and T6 where burial featured well-graded gravel and the use of a plate compactor with no specific effort to compact soil under the pipe haunches. Strain factor D_f of approximately 9.4 (at 100 kPa)

Table C-20. Description of the tests for local bending analysis.

Test No.	1	2	3	4 & 5	6	7	8
Pipe Profiles	**a**	**b**	**c-1b**	**a**	**b**	**c**	**d**
Test Cell	biaxial	biaxial	biaxial	hoop	hoop	hoop	hoop

Profile type refers to Figure C-32, except as noted.

was calculated for the HDPE pipe, and a factor D_f of 33 was calculated for the PVC pipe. The specific values of D_f reported in this appendix are those for the particular pipe and backfill conditions that were tested.

Experiments performed and reported here imply that pipe deflections of 5% used with high strain factors determined at low deflection levels are overly conservative.

C.5 3D Modeling of Profile Wall Thermoplastic Culverts

C.5.1 Introduction

Thermoplastic pipes with a number of different wall geometries have been manufactured in the search for effective utilization of pipe materials. The 3D geometries of the profiles have led to additional issues requiring consideration during design. Moore and Hu (1996) demonstrated that local bending can produce significant tension at the liner-corrugation junction in lined corrugated HDPE pipe, where sustained high tension can be one of the critical performance limits for thermoplastics. This section examines local bending in thermoplastic pipes with various wall profiles. The starting point of the study was measurement of pipe response in the laboratory under both axisymmetric and biaxial loading conditions as reported in Section C.1.

The finite element method is used here to study the 3D behavior of the profiles investigated in Sections C.1 and C.3 (Figures C-1 and C-3). Axisymmetric analyses were performed to examine the pipes when loaded in hoop compression; a semi-analytic (Moore 1994) method was employed to model the pipes in a biaxial stress field (modeling the geostatic earth pressures simulated in the biaxial pipe test cell).

Laboratory hoop tests and the biaxial tests are modeled, in turn, using the finite element method. Pipe profiles were explicitly modeled with the actual geometry of the tested pipes. Table C-20 shows notations used to describe the profiles in this section. Results of the analysis are compared to the laboratory measurements obtained in the hoop compression and biaxial pipe cell tests to evaluate the effectiveness of the finite element modeling and a number of 3D aspects of profile behavior.

C.5.2 Finite Element Modeling

C.5.2.1 Modeling of the Hoop Cell

Axisymmetric finite element analysis has been employed to investigate the response of the pipes tested in the hoop cell. Pipes with annular profiles have axisymmetric geometries; therefore, axisymmetric finite element analysis with the finite element mesh defined in the r-z plane can be used to define the problem geometry. Figure C-76 depicts a typical finite element mesh used for annular pipe with lined corrugated profile (Dimension L is defined as used later). The pipes are modeled as being very long, using smooth rigid (axially restrained) boundaries at the top and bottom of the mesh. The external diameter of the soil region around the pipe corresponds to the inner diameter, 1,500 mm, of the steel pressure vessel (the axisymmetric pipe test cell developed by Laidlaw [1999]). This provides a soil ring of 430-mm width surrounding the lined corrugated pipes (profiles in Figures C-32a and C-32b), a soil ring of 335-mm width surrounding the boxed profile pipe (profile in Figure C-32c), and a soil ring of 175-mm width surrounding the pipe with tubular profile (Figure C-32d). Finite element meshes for the boxed and tubular profiles are shown in Figures C-77 and C-78. Although the geometry of these helical profiles is nonaxisymmetric, axisymmetric geometry is also assumed. This avoids the significant complexities of modeling the true spiral geometry. A comparison of calculated strains and those measured in the tests is subsequently used to investigate whether this axisymmetric approximation is reasonable for helically shaped pipe. Although it is largely successful, there are certain aspects of the behavior of the boxed profile that are not well captured using this approach.

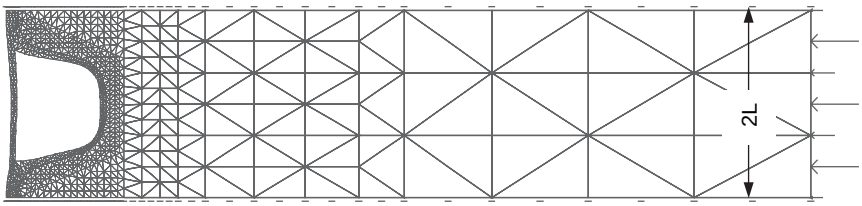

Figure C-76. Finite element mesh for axisymmetric analysis of lined corrugated pipe.

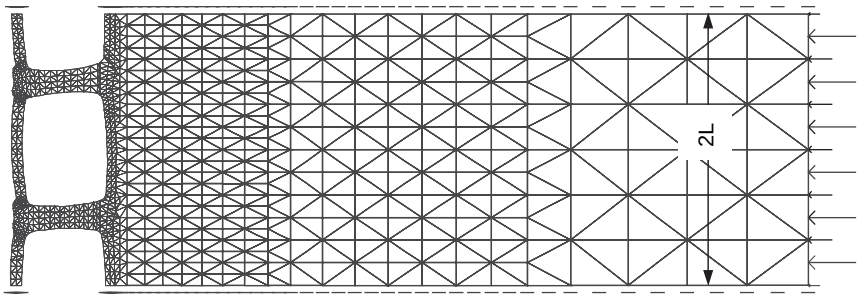

Figure C-77. Finite element mesh for boxed profiled pipe.

C.5.2.2 Modeling of the Biaxial Cell

Moore (1994) employed a simplified finite element model in the analysis of pipes with axisymmetric geometry under biaxial loading. The simplified approach uses a 2D finite element mesh to model the pipe and the surrounding soil in the r-z plane. A Fourier series is used to represent variations around the pipe circumference. The nonaxisymmetric loads are expressed in terms of Fourier harmonics as

$$f(\theta)=\sum_{n=0}^{\alpha}\left(F_n^1 \mathrm{Cos}\, n\theta + F_n^2 \mathrm{Sin}\, n\theta\right) \qquad \text{(C.11)}$$

Pipe response to each harmonic coefficient of the load is then calculated separately, and the combined response is obtained using superposition. Given the dependence on superposition of the semi-analytic method, the analyses are limited to materially and geometrically linear problems.

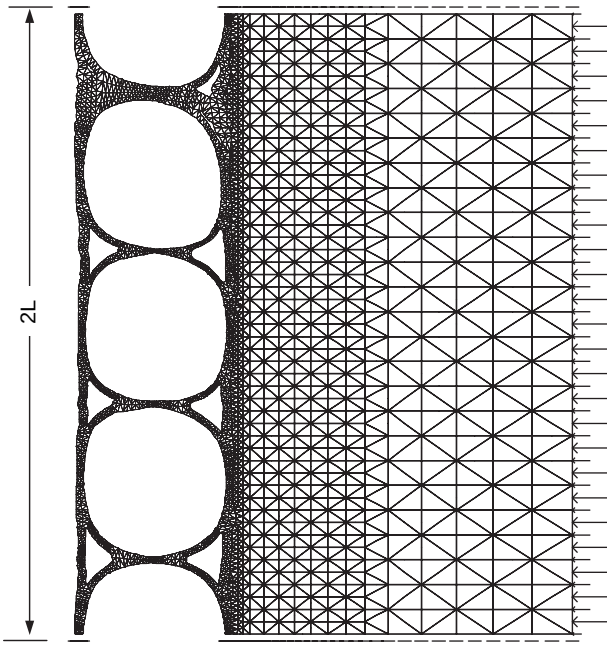

Figure C-78. Finite element mesh for tubular profiled pipe.

The features of the harmonic finite element solution are that displacements, strains, and stresses vary harmonically on the same order as the load. For example, a harmonic load, $F_n \cos n\theta$, produces a displacement field given by

$$\left(u_r, u_\theta, u_z\right)^T = \left\{U_r(n)\cos n\theta, U_\theta(n)\sin n\theta, U_z(n)\cos n\theta\right\}^T \qquad \text{(C.12)}$$

Here u_r, u_θ, u_z are the displacements in r, θ, and z direction, and $U_r(n)$, $U_\theta(n)$, $U_z(n)$ are harmonic coefficients of the displacements.

The biaxial geostatic stress can be imposed using radial stress σ and shear stress τ with two harmonic terms of order 0 and 2 as follows:

$$\left.\begin{aligned}\sigma &= \frac{\sigma_v+\sigma_h}{2}+\frac{\sigma_v-\sigma_h}{2}\cos 2\theta \\ \tau &= \frac{\sigma_v-\sigma_h}{2}\sin 2\theta\end{aligned}\right\} \qquad \text{(C.13)}$$

Harmonic coefficients of pipe response, U(n), to each of the two harmonic load coefficients $\frac{\sigma_v+\sigma_h}{2}$ and $\frac{\sigma_v-\sigma_h}{2}$ with n = 0 and n = 2, respectively, are obtained from the finite element analysis, which, in turn, provides the 3D responses, u(n = 0, 2), of the pipe to each of the loads through Equation C.12. The following combined response is then obtained from superposition:

$$u = u(0)+u(2) \qquad \text{(C.14)}$$

The simplified 3D finite element procedure of Moore (1994) for biaxial loading conditions uses 2D finite element meshes (similar to Figure C-76) for the annular pipes (Tests 1 and 2). The "outer" radial soil boundary is chosen sufficiently distant (8 to 10 times the radius) to minimize the effect of the boundary on the pipe. The helically wound ribbed PVC pipe (Figure C-1b) is also idealized with axisymmetric geometry. Figure C-79 presents the finite element mesh used for the PVC pipe analysis. One cycle of the seven ribs is modeled, including the weld created during the helical winding process. This particular profile has rib size and orientation that is quite variable, and the mesh shown in Figure C-79 represents the specific wall geometry at one of the cross-sections.

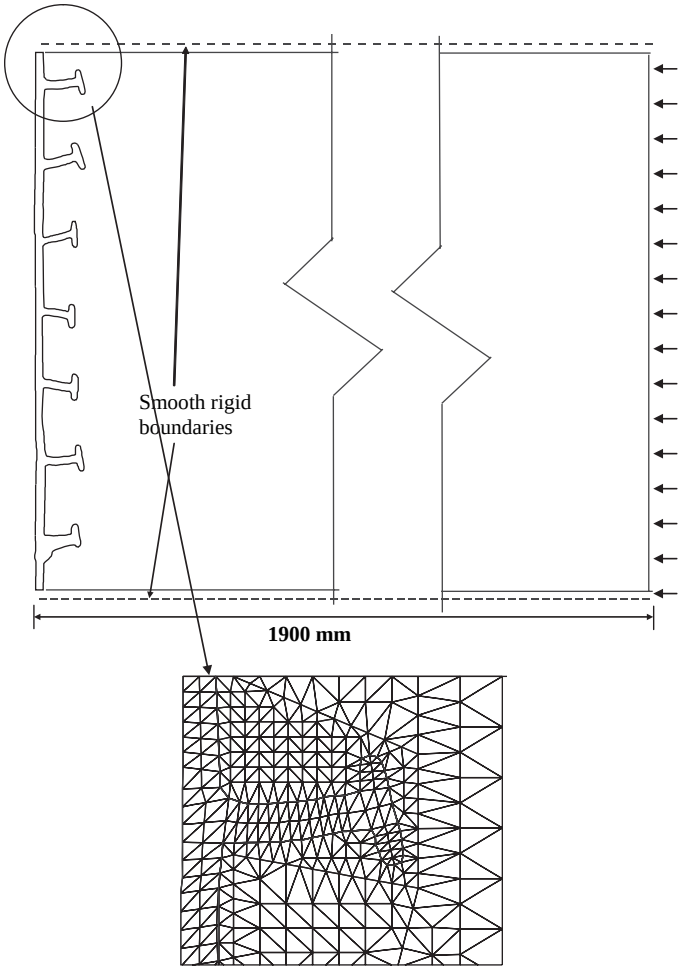

Figure C-79. Finite element mesh for ribbed PVC pipe.

C.5.3 Material Models

C.5.3.1 Pipe Parameters

Use of appropriate constitutive models is necessary to reasonably simulate the physical behavior in finite element analyses. Thermoplastic material exhibits noticeable time-dependent behavior. However, elastic modeling using secant modulus is the most widely used approach for thermoplastic pipe analysis because of its simplicity. Both a linear elastic model based on secant modulus and the viscoplastic model of Zhang and Moore (1997) have been used in this study to analyze the pipes tested in the hoop cell. Zhang and Moore (1998) determined one set of viscoplastic model parameters for the HDPE used to produce corrugated pipe Profile "b" (Figure C-32b) and another set of parameters for pressure-rated HDPE material used by the company that produced boxed Profile "c" shown in Figure C-32c (although material test specimens were extracted from plain, not boxed, profile pipe manufactured by that company). The parameters are used in the analyses of the hoop tests performed using those two pipe profiles.

Since the semi-analytic method utilizes the principle of superposition, linear material properties were needed for analysis of the biaxial tests. The linear model parameters used for HDPE and PVC are summarized in Table C-21.

C.5.3.2 Soil Parameters

Elastic moduli for the soil used in the biaxial test were determined from the measurements made of vertical stress and average vertical strain in a column of soil adjacent to the pipes (where lateral strains are almost zero). Stresses and deformations of the soil were not measured during the hoop cell test. Soil parameters used for the analysis of the hoop test were those reported by Zhang and Moore (1998), who undertook an analysis of a pipe tested in the same backfill. However, the degree of compaction achieved in each hoop compression test is variable, since compaction is difficult to control in the narrow space between the pipe and the test cell wall.

The value of Poisson's ratio of the soil, ν_s, directly influences the lateral earth pressures that are calculated in the finite element analysis of the biaxial test. Measured values of lateral earth pressure coefficient K were therefore used to define ν_s, as discussed in Section C.1.

Table C-21. Pipe parameters used in the 3D analysis.

Test Type	Test No.	Material/Model	Parameter
Biaxial Cell Test	1 and 2	HDPE pipe (linear)	Modulus, E = 450 MPa Poisson's Ratio, ν = 0.46
	3	PVC pipe (linear)	Modulus, E = 2,760 MPa Poisson's Ratio, ν = 0.30
Hoop Cell (Zhang and Moore 1998)	4 and 6	HDPE pipe (VP)	E = 1,350 MPa, ν = 0.46, C=0.01, n = 8.0 $\gamma = 10^{-4}$ MPa β = C744$\times 10^{-5}$ MPa $d_1 = 1.055\times10^{-3}$, $d_2 = 3.829$, $d_3 = 2.55\times10^{-2}$
	7 and 8	HDPE pipe (VP)	E = 1450 MPa, ν = 0.46, C=0.01, n = 8.0 $\gamma = 10^{-4}$ MPa β = C056$\times 10^{-5}$ MPa $d_1 = 1.042\times10^{-3}$, $d_2 = 3.829$, $d_3 = 2.547\times10^{-2}$

Table C-22. Soil parameters for 3D analyses.

Test Type	Test No.	Parameter
Hoop Test	6 and 7	Modulus, E = 30 MPa Poisson's Ratio, ν = 0.2 Cohesion, C = 0 Angle of Internal Friction, ϕ = 36°
Biaxial Test	1	Modulus, E = 6.2 MPa Poisson's Ratio, ν = 0.34
	2	Modulus, E = 6.4MPa Poisson's Ratio, ν = 0.33
	3	Modulus, E = 5.5 MPa Poisson's Ratio, ν = 0.33

The value of Poisson's ratio reported by Zhang and Moore (1998) was used for the soil in the hoop compression test. Angle of internal friction, $\phi = 36°$, for use in the elastic-plastic analysis of soil behavior in the hoop compression test was selected based on the data reported for material classified as "SW85" by Selig (1990). Table C-22 summarizes all the soil parameters used in the finite element analyses of the tests.

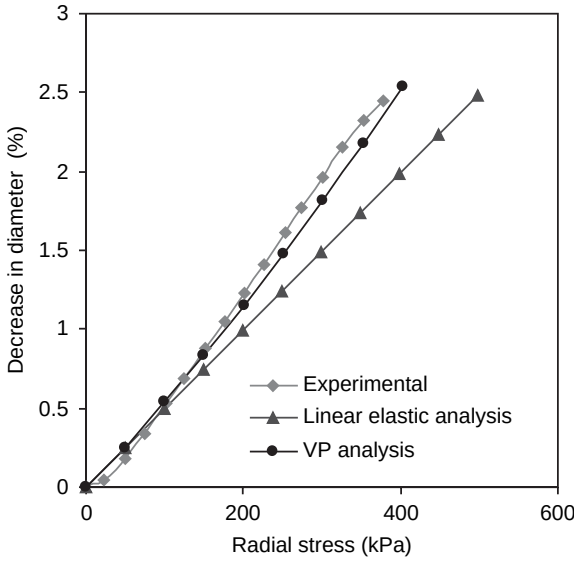

Figure C-80. Pipe deflection in hoop test with axisymmetric FE analysis (Profile "b").

C.5.4 Analysis of the Hoop Test Results

C.5.4.1 Lined Corrugated Pipes (Test 6)

Figure C-80 plots the measurements of pipe deflection in Test 6 together with the finite element calculations. Analysis using the viscoplastic model matched the measurements of pipe deflection well. Since there is only a thin ring of soil surrounding the pipe in the hoop cell, the stiffness of pipe is particularly important (more so than for the same pipe in the field where it lies within an extensive zone of backfill and native soil). True viscoplastic parameters of the pipe material for this test were available. The viscoplastic model simulates the nonlinear time-dependent behavior of the HDPE material very effectively.

Experimental measurements and calculated values of hoop strain on the interior and exterior surfaces of Profile "b" are compared in Figures C-81 and C-82, respectively. The finite element method appears successful in calculating the hoop strains on both the interior and exterior surfaces of the pipe. Calculated strains on the liner are less than those on the valleys (Figure C-81), just as the measured values were found to be. Thus, the analysis captures the localized load distribution that occurs in the liner where it spans between corrugation valleys; however, the analysis is geometrically linear and does not account for local buckling, which is a geometrically nonlinear phenomenon. Measured liner strain stabilizes at high cell loads following the development of local buckling, so calculated strains are greater than the measured values at high cell pressures (Figure C-81). Nonlinear relationships between measured strain and cell pressure are also seen on the web and crest of the exterior walls (Figure C-82)—once again as a result of the local buckling of these elements. Strains on these exterior elements may also be influenced by the local soil support. However, Figure C-82 indicates that the finite element model appears to provide a conservative estimate of hoop strains on these exterior elements.

Figure C-83 shows axial strains on various elements of the lined corrugated Profile "b." Differences in the axial strains on the inner and outer surface of the valley are associated with longitudinal bending. Longitudinal bending on the exterior elements may be influenced by local interaction with the soil, although the analysis still appears to provide reasonable estimates of these strains.

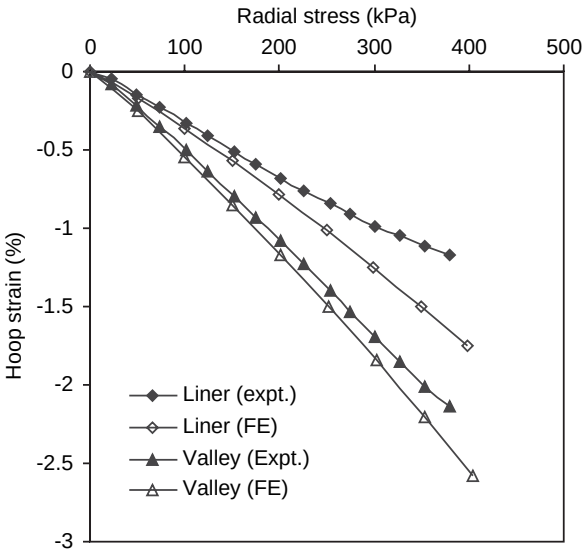

Figure C-81. Hoop strain on the inner walls with axisymmetric FE analysis (Profile "b").

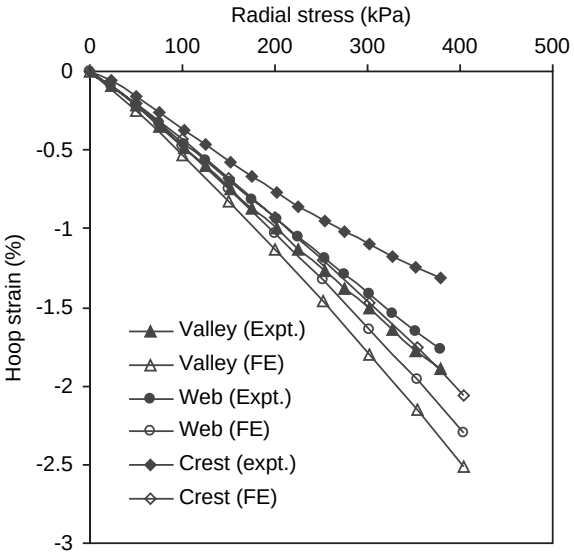

Figure C-82. Hoop strain on the exterior walls (Profile "b").

The axial strains measured on the liner, however, are very different from the calculated values (Figure C-83). The analysis predicts compressive strain on the inner surface at the midpoint of the liner, whereas axial tension was measured during the experiments. This discrepancy likely resulted because plane-strain conditions were not achieved in the test cell, although a plane-strain condition was assumed in the FE analysis. The corrugated element has little axial stiffness, so failure to develop significant axial constraint may have little effect on local stress or strain in that element. The liner, however, forms a continuous cylindrical shell that has substantial axial stiffness. Axial strains will develop in the liner in the absence of full axial restraint on the pipe, although this is associated with axial stretching, not local bending. Measurements of axial strain on the liner show high tensions in Figure C-83. That particular test (Test 6) was performed on a previously tested pipe and only one strain gage for measuring axial strain on the liner was working, so it was not possible to verify the data in the same manner as the other strain measurements where several strain gage readings were obtained.

When profiled pipe is buried in the field, lack of fit at the joints may also reduce axial restraint. However, the soil surrounding the pipe is axially restrained, as opposed to the soil surrounding the pipe in the test cell, which will stretch axially with the pipe as the length of the test cell expands slightly under load. Indeed, local interaction between the backfill and the corrugated exterior of the pipe means that the pipe is "locked into" the soil surrounding it, and it is likely the overall extension of soil surrounding the pipe in the test cell that causes stretching in the pipe sample, not a lack of fit between the ends of the pipe and the cell walls. Local axial strain values in real burial conditions are expected to be much closer to the calculated values than to those measured in the test cell, since axial extensions in the backfill will be suppressed.

Distributions of calculated and measured strain along the interior surface of the profile are plotted in Figures C-84 and C-85 at a radial earth pressure of 150 kPa, where the two figures show hoop and axial strains, respectively. It is evident from the figures that the hoop strains are not uniform along the inner surface of the two lined corrugated profiles (even though the distance of the inner wall from the neutral axis of the profile is almost constant). The local bending results in compressive hoop strain magnitudes that reduce from maxima at the valleys to minima at the midposition where the liner spans between the valleys (Figure C-84). The magnitude of the measured hoop strain at the midliner is somewhat lower

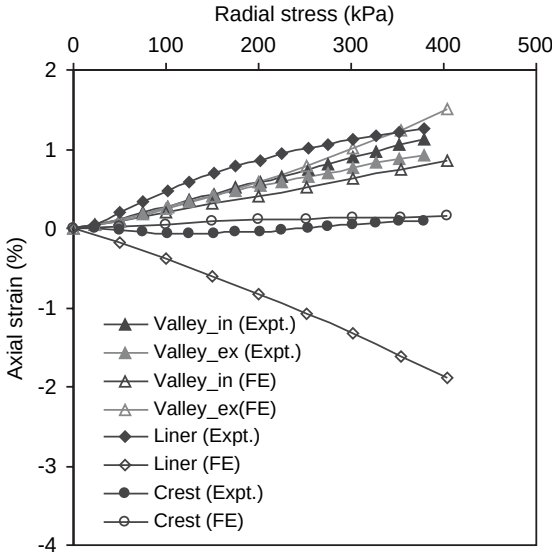

Figure C-83. Axial strain in hoop test (Profile "b").

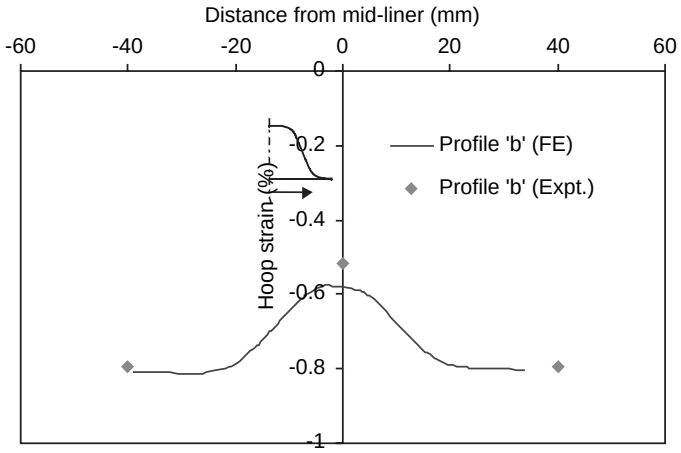

Figure C-84. Distribution of hoop strain on liner (at 150 kPa of cell pressure).

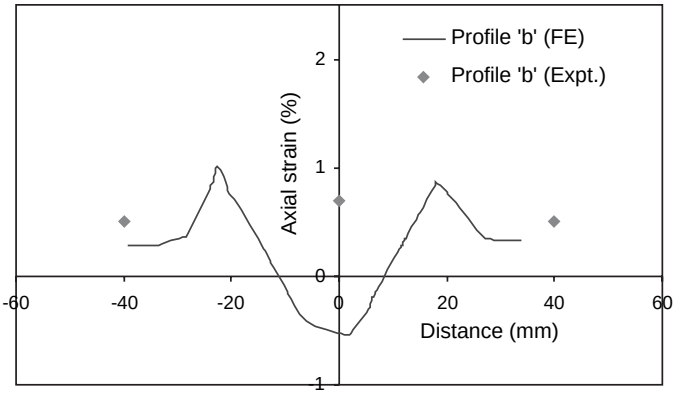

Figure C-85. Axial strain distribution in liner (at 150 kPa of cell pressure).

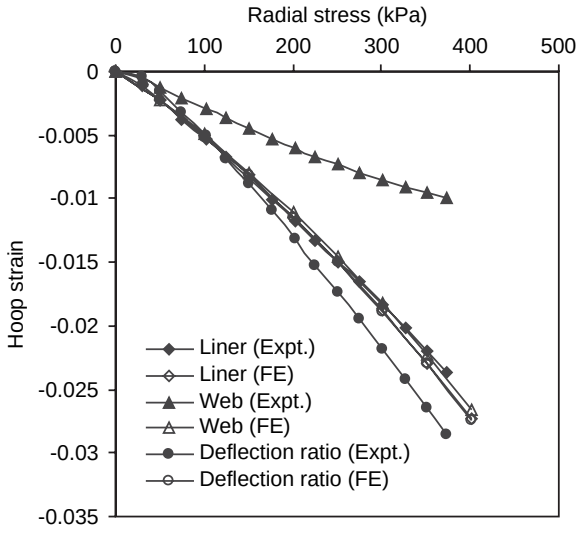

Figure C-87. Interior hoop strains (boxed profile).

than the calculated value, while calculated valley strain matches the measurements well.

The finite element analysis indicates there is a local increase in tensile axial strain at the liner-corrugation junctions of both profiles (Figure C-85). No measurements were made because of the difficulty of attaching gages directly at this position. As discussed earlier, an increase in the overall length of the pipe results in axial strain measurements that are all larger than the corresponding finite element calculations.

C.5.5 Boxed Profile

Figure C-86 presents the axisymmetric finite element calculations and measurements of pipe deflections for the helically wound boxed profile. Calculation using the viscoplastic model rheology for plain pipe manufactured by the same company (Zhang and Moore 1998) better matches the measurements than calculations based on linear elastic material modeling. Once again, the nonlinear time-dependent effects of the pipe material appear to noticeably influence the behavior. Use of viscoplastic material parameters determined for plain, rather than boxed, profile pipe may have contributed to the underestimation of the diameter decreases.

Hoop strains at the inner liner and outer wall of the boxed profile (as defined in Figure C-32c) match the measurements well (Figures C-87 and C-88). The hoop strain was measured as less than the deflection ratio (Δ/D) (Figure C-87), although for axisymmetric behavior the strain would be the same as the

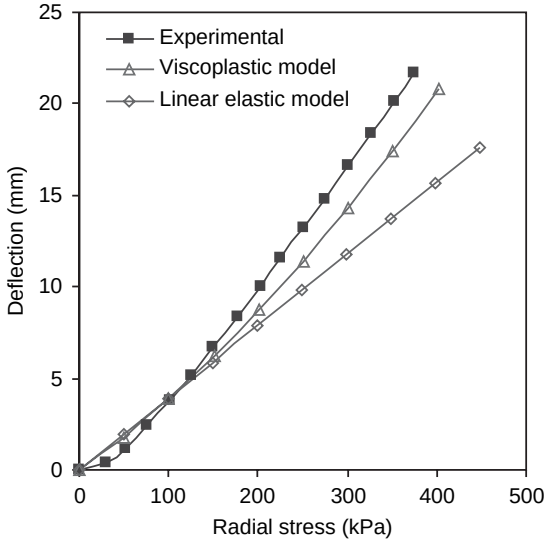

Figure C-86. Deflection of the boxed profile with FE analysis.

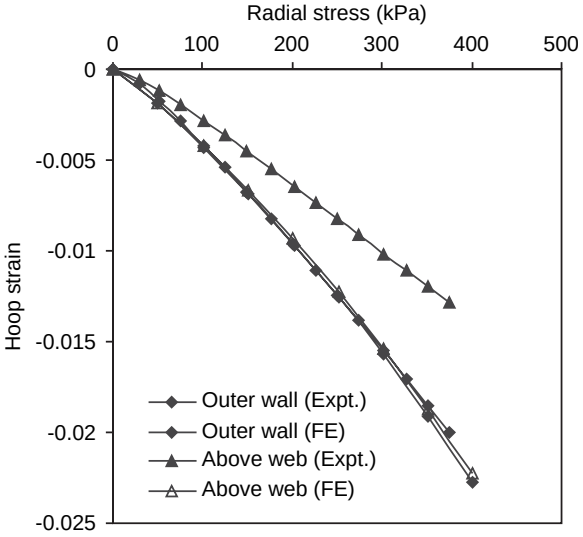

Figure C-88. Hoop strain on the outer surface of the boxed profile.

deflection ratio. This discrepancy might have resulted because the profile is helical rather than axisymmetric (annular).

The hoop strains under and over the webs were measured as much less than those on the liner. Measured strain under the web is about 50% of the liner strain on the interior surface (Figure C-87), and outer surface web strain is approximately 70% of the exterior surface value midway between webs (Figure C-88). The axisymmetric analysis produced almost the same values of strain on the web and liner. The helical winding of the rib appears to produce local bending within the profile. The lateral element (the web) of the profile is very thick, and when analyzed as axisymmetric, it will have high hoop strain and torsional stiffness. In particular, a rib of helical geometry is likely much easier to twist under torsion, and this may have led to the lower hoop strains at the location of the rib. This local bending also appears to have generated much higher axial strain near the rib (Figure C-89).

It appears, then, that there are limits to the use of the axisymmetric idealization of the profile for calculation of local bending effects in the boxed profile. However, the diameter decrease was successfully estimated using the axisymmetric analysis, and the axisymmetric analysis provided upper bounds of the hoop strains in the profile (so use in pipe design should produce conservative estimates of hoop stress and hoop strain). Axisymmetric predictions of hoop and axial strains are shown in Figures C-90 and C-91, shown here using a tension positive sign convention. Contours of hoop strain (Figure C-90) and axial strain (Figure C-91) are almost uniform along any axial line. The significant tensile axial strains within the rib are caused by Poisson's effect associated with radial forces transmitted through the ribs.

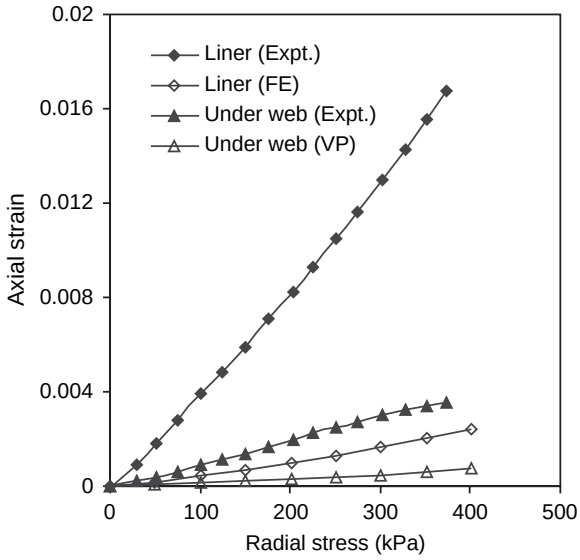

Figure C-89. Comparison of axial strains on the boxed profile.

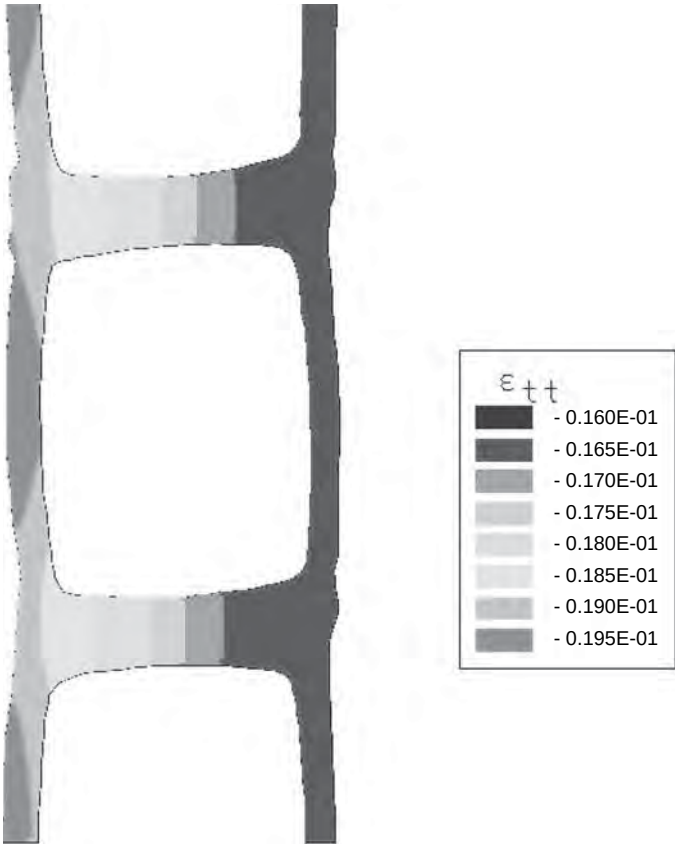

Figure C-90. Contour of hoop strain (tension positive) at 300 kPa (boxed profile).

C.5.6 Analysis of the Biaxial Test Results

C.5.6.1 Introduction

The 3D semi-analytic method of Moore (1994) is evaluated in this section using the measurements of pipe response made in the biaxial test cell. The method involves 3D linear finite element analysis utilizing the axisymmetric pipe geometry and modeling the biaxial geostatic earth loads using two Fourier harmonics. Biaxial tests on two lined corrugated HDPE pipes (Tests 1 and 2) and a helically wound ribbed PVC pipe (Test 3) have been analyzed using this approach. The finite element model approximates the pipes as buried in an infinite region of elastic ground. A study was undertaken to locate the external soil boundary at a sufficient distance from the pipe so that it does not affect pipe behavior.

This section focuses on the response measured at crown and springline, and no comparisons are made with strain values obtained at the inverts of the pipe specimens. Invert strains are greatly influenced by low stiffness soil under the pipe haunches, and this is discussed in considerable detail in Sections C.1 and C.4.

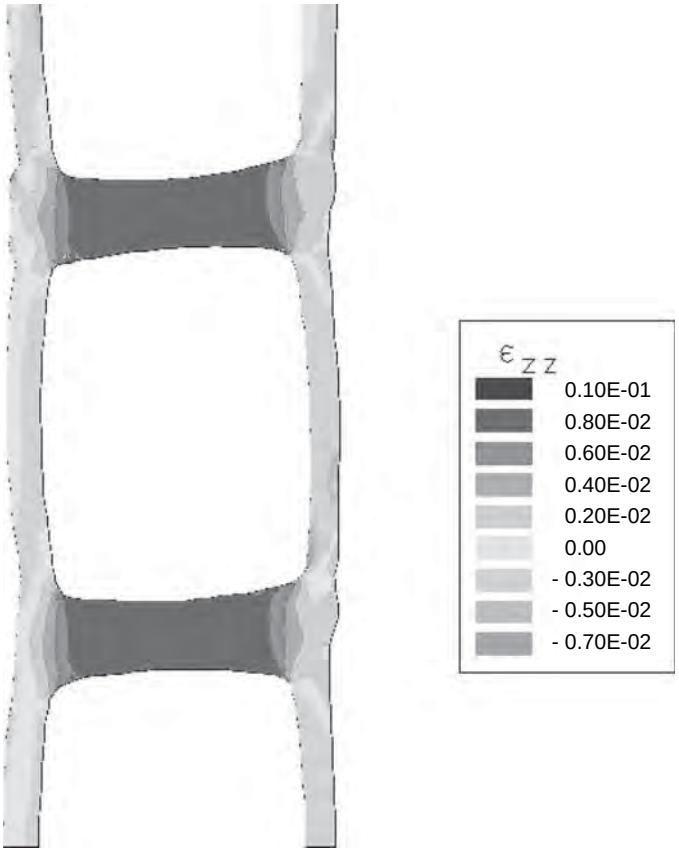

Figure C-91. Contour of axial strain (tension positive) at 300 kPa (boxed profile).

C.5.6.2 Evaluation of the 3D Fourier Semi-Analytic Idealization

The 2D finite element analysis with actual modeling of the test cell is performed to evaluate the assumption of infinite ground in the 3D analysis. The 2D analysis of the pipes has used conventional structural theory based on the section properties area and second moment of area. Results of the 2D and 3D analysis of the same pipe (Profile "b") with the same linear material parameters are compared in Figure C-92. The two analyses provided similar values of changes in pipe diameter (Figure C-92), confirming that the 3D Fourier analysis provides a reasonable simulation of pipe deflection under geostatic stresses.

C.5.6.3 Behavior of Lined Corrugated HDPE Pipes

Figures C-93 and C-94 compare the calculated values of change in pipe diameter in Tests 1 and 2 with the measurements. Deflections are plotted as a function of the vertical cell pressure applied at the surface of the biaxial cell (this vertical pressure is equivalent to the overburden pressure the soil-pipe system would experience when deeply buried in an em-

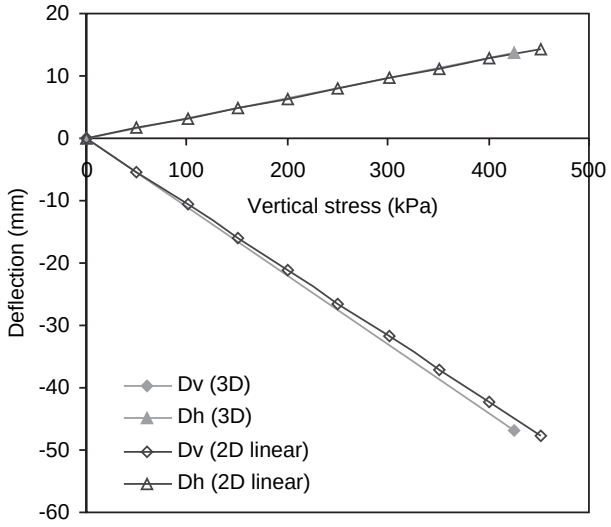

Figure C-92. Comparison between the 2D and 3D FE analysis.

bankment). The figures show that the 3D finite element method is successful in estimating the changes in pipe diameter for this biaxial (geostatic) stress field. Estimated deflections at the maximum vertical pressure match the measurements well (Figures C-93 and C-94), although the nonlinear soil behavior results in a calculated response up to that point that is stiff relative to the measurements. Similar results were obtained using the 2D analysis with a linear elastic soil model (Dhar, Moore, and McGrath 2001). Although nonlinear soil modeling furnishes a better 2D simulation (Dhar, Moore, and McGrath 2001), this nonlinear behavior cannot be con-

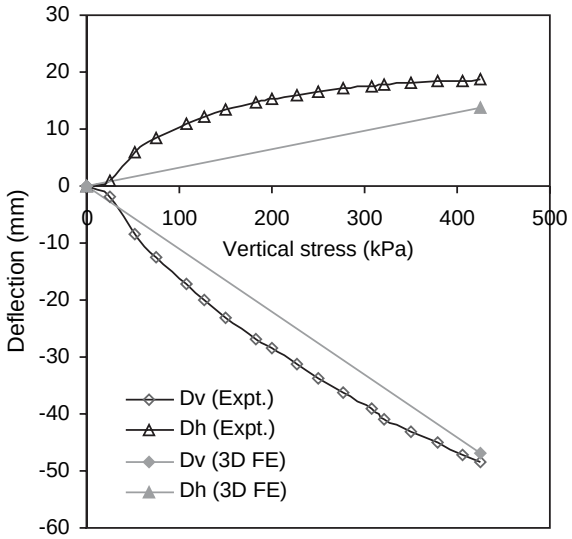

Figure C-93. Deflection in Test 1 with 3D FE calculation.

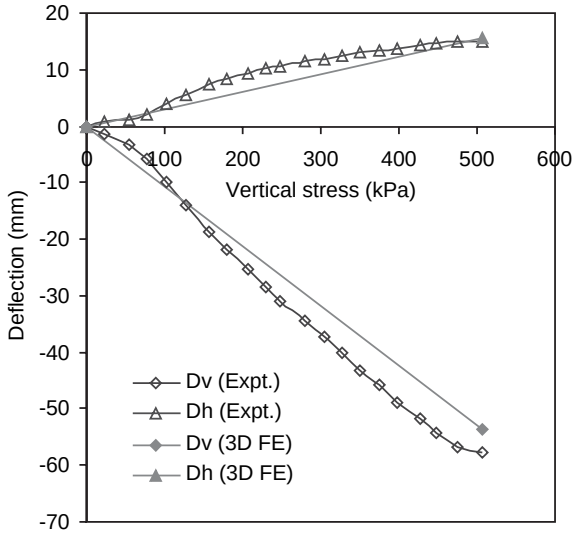

Figure C-94. Deflection in Test 2 with 3D FE calculation.

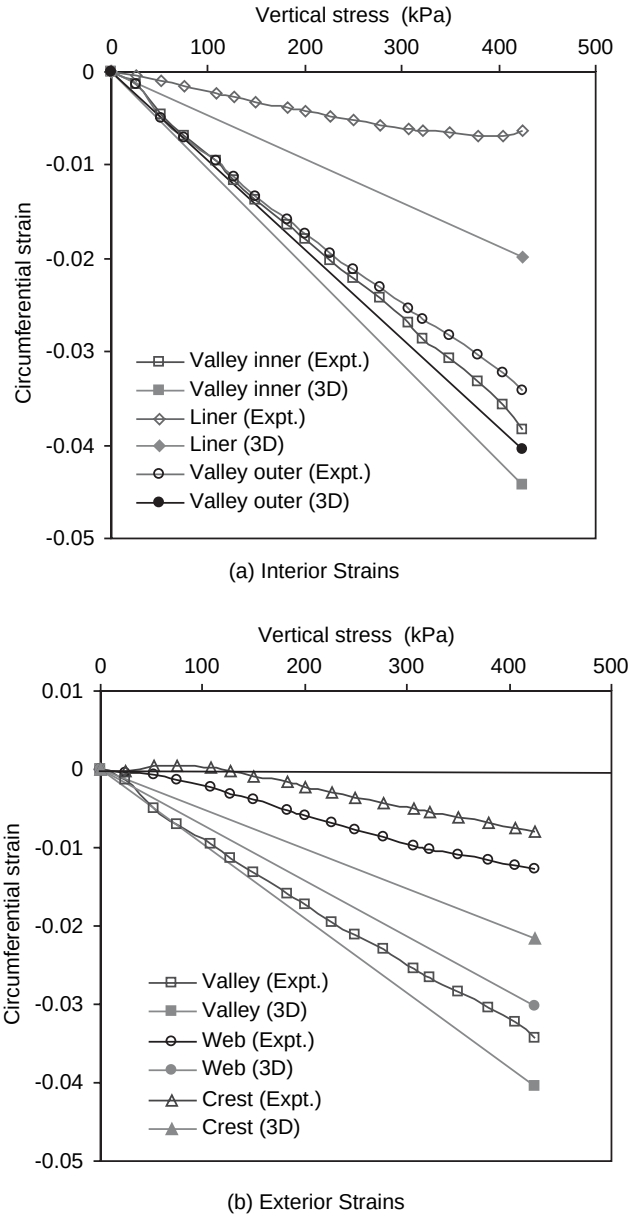

Figure C-95. Comparison of circumferential strains at the springline in Test 1 (Profile "a").

sidered in the semi-analytic finite element analysis, since it is based on superposition of the pipe response to each of the two different Fourier harmonics of applied earth pressure.

Calculated values of circumferential strain are shown in Figures C-95 through C-98. Measurements show a change in curvature of the stress-strain curve for Test 2 (i.e., Figure C-96), which corresponds to the recompression discussed in Section C.3. The 3D analysis provides reasonable estimates of the hoop strain at the springline on both the interior and exterior surfaces of the corrugation valley (Figures C-95 and C-96). The difference of strains between these interior and exterior surfaces is not great (Figure C-95a) because high hoop thrust governs strain at the springline, rather than bending. The finite element procedure overestimates the strains on the exterior elements (Figures C-95b and C-96b), perhaps as a result of the material and geometric nonlinearity. The 2D analysis with a nonlinear soil model (Janbu 1963) was found to provide rational estimates of hoop strain on both the valley and crest of the pipe (Section C.1).

At the crown, the semi-analytic finite element method provides rational estimates of the strain on both the liner and the valley (Figures C-97 and C-98). However, the nonlinear development of wall and crest strain with overburden pressure was not calculated well; again, the method neglects the influence of the local buckling that has developed in these profile elements.

As in the hoop tests, local bending results in hoop strain on the liner that is a fraction of the valley strain. This is seen in the semi-analytic finite element calculations as well as in the measurements (Figures C-95a and C-96a).

The ratio of liner-to-valley strain appears to depend on the circumferential bending of the section. The ratio was measured for Profile "a" as 0.20 at the springline and 0.30 at the crown. However, for the same profile in the hoop test it was 0.60. Analysis of the hoop test with Pipe "a" is discussed in Section C.1. The springline of the pipe is subjected to positive bending (compression inward) and the crown to negative bending (compression outward) for a pipe under biaxial loading. Thus, the section under positive bending has a smaller proportion of the valley strain developing on the liner than the sections with no bending (pure hoop compression) or with negative bending (the crown). The proposed semi-analytic finite element model calculates the liner strains as 45% and 55% of the valley strains, respectively, at the springline and at the crown for Profile "a." Axisymmetric finite element

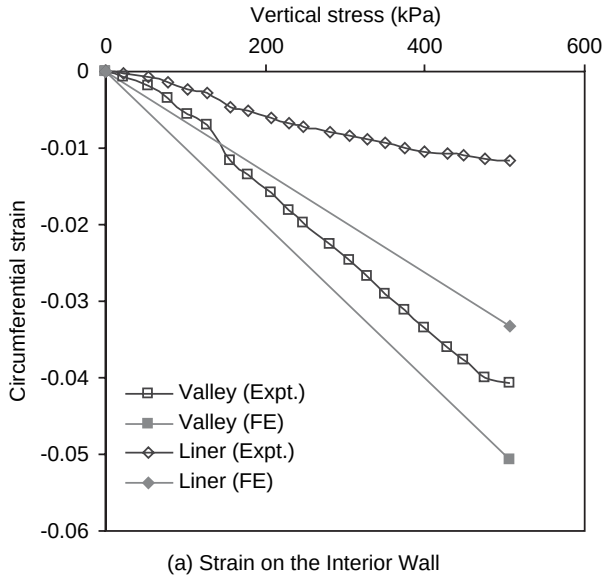

(a) Strain on the Interior Wall

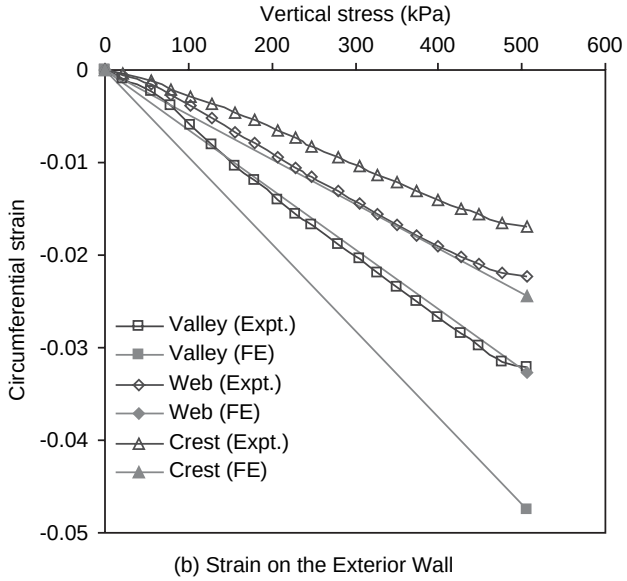

(b) Strain on the Exterior Wall

Figure C-96. Circumferential strains at the springline on Test 2 (Profile "b").

analysis for the profile gives the liner strain as 50% of the valley strain (Appendix C.1). The ratios for Profile "b" pipe were 0.65 (measured 0.30) and 0.85 (measured 0.80) at the springline and crown, respectively.

Figures C-99 through C-102 show comparisons between calculated and measured values of axial strain in the elements of the lined corrugated profile. Strain calculations are reasonable, except those for the liner. Very high axial compressive strain was calculated on the liner both at the springline and at the crown of the pipe, while measurements showed either minimal axial compression (at the springline) or tension (at the crown). As seen earlier, axial strains measured in the liner are

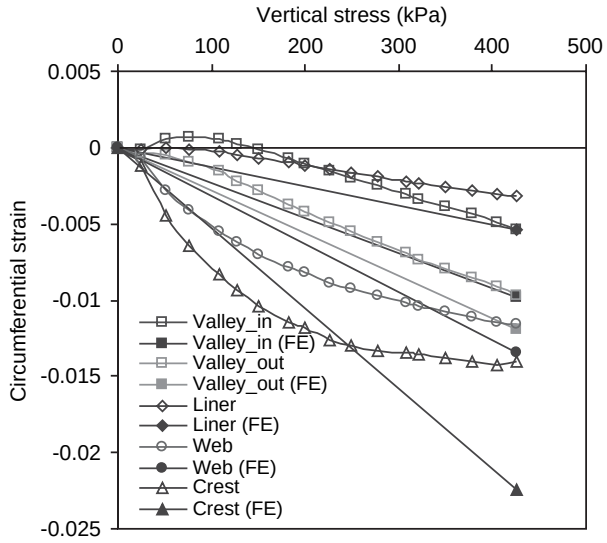

Figure C-97. Strains at the crown in Test 1 (Profile "a").

much more tensile than those calculated using the 3D analysis. This is likely the effect of axial pipe extension, like that discussed earlier in relation to the hoop compression tests.

C.5.6.4 Helically Stiffened Ribbed PVC Pipe

Figure C-103 illustrates the calculated values of ribbed PVC pipe deflection obtained using the semi-analytic 3D finite element model. Once again, the helically wound profile was idealized as axisymmetric in the analysis of the pipe. The deflections again compare well with the measurements, as

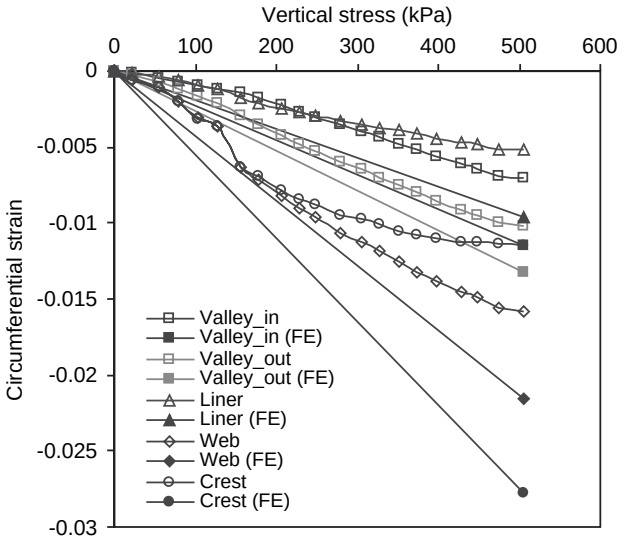

Figure C-98. Strains at the crown in Test 2 (Profile "b").

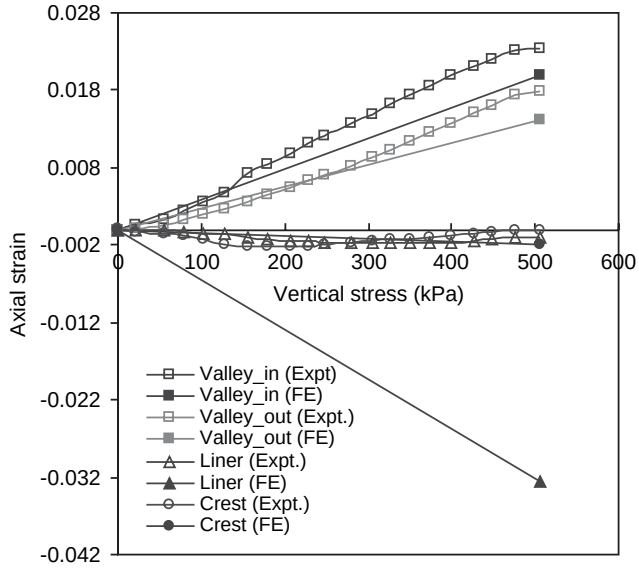

Figure C-99. Axial strain at the springline (Profile "b").

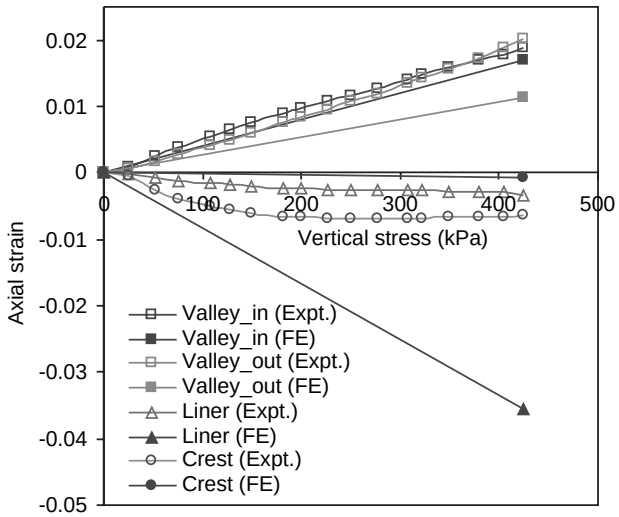

Figure C-101. Axial strain at the springline (Profile "a").

seen elsewhere for 2D analysis (Dhar, Moore, and McGrath 2001). A nonlinear soil response was again measured during the test on the PVC pipe, a response that is not calculated using the elastic finite element procedure based on constant elastic soil modulus.

Hoop strains for the PVC pipe are compared in Figures C-104 and C-105. The finite element calculations of strain are in general agreement with the measured strains in these figures. Almost identical strain values were measured on the valley and the inner surface of the rib, implying that effects of the helix and local bending are not important for this profile.

C.5.7 Effects of Profile Geometry on Pipe Performance

C.5.7.1 Introduction

The laboratory and finite element investigations discussed in Sections C.1 and C.3 revealed that 3D deformation of the profiles may affect the performance of the profiled pipes. The 3D finite element analyses (both axisymmetric and 3D

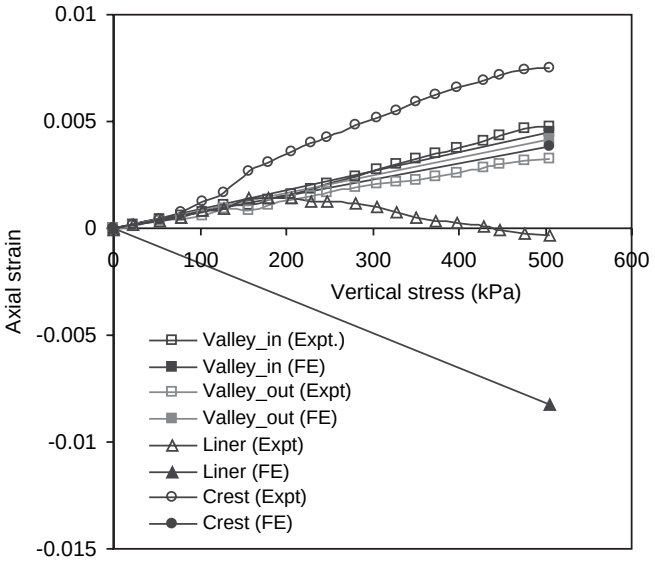

Figure C-100. Axial strain at the crown (Profile "b").

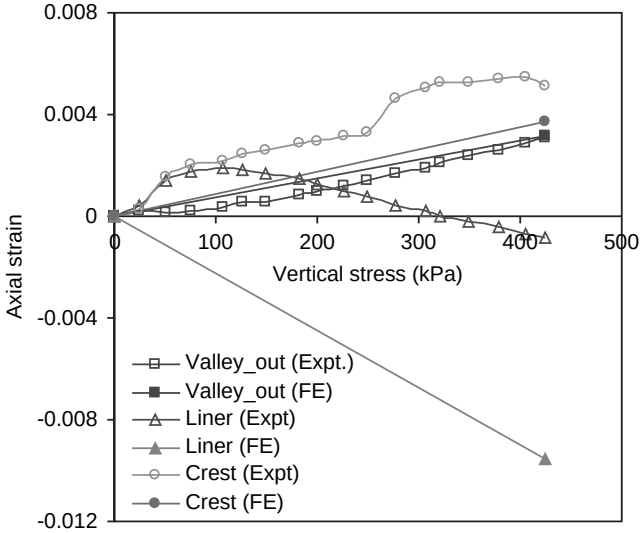

Figure C-102. Axial strain at the crown (Profile "a").

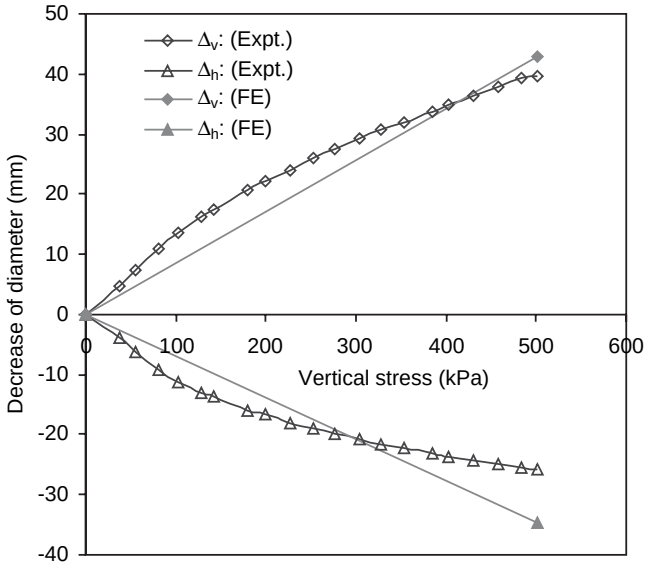

Figure C-103. Comparison of deflections for the PVC pipe.

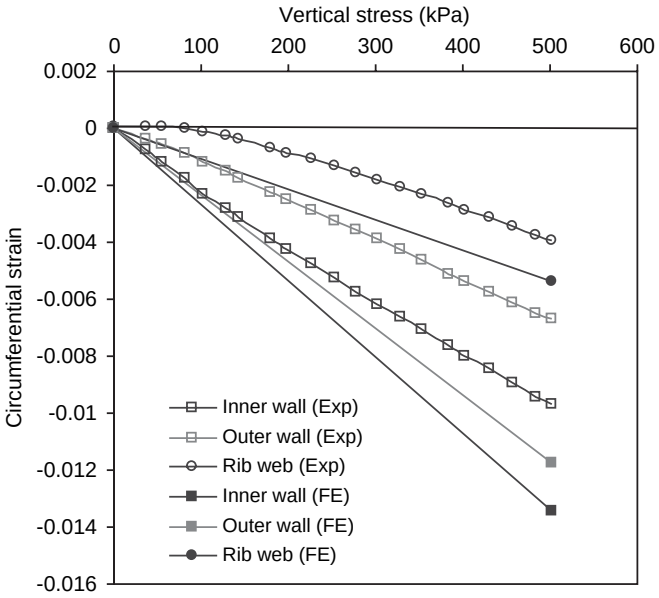

Figure C-105. Prediction of hoop strain at springline (PVC pipe).

semi-analytic) appear to be useful tools for study of the 3D behavior. An investigation of the 3D behavior of four pipe profiles (considered in Section C.3, Figure C-32) is included in this section. The ribbed PVC profile is not considered further in this study, since local bending is not very important for that profile.

Significance of the 3D effects on the profile behavior is first examined under uniform radial compression using axisymmetric finite element analysis, before undertaking a study on more realistic biaxial earth pressure. Pipes are then investigated under biaxial loading at two different burial depths (2 m and 8 m). Short-term and long-term responses are investigated using the short-term and the long-term modulus of the pipe materials. The 3D stress distribution through the profiles is the focus of the study.

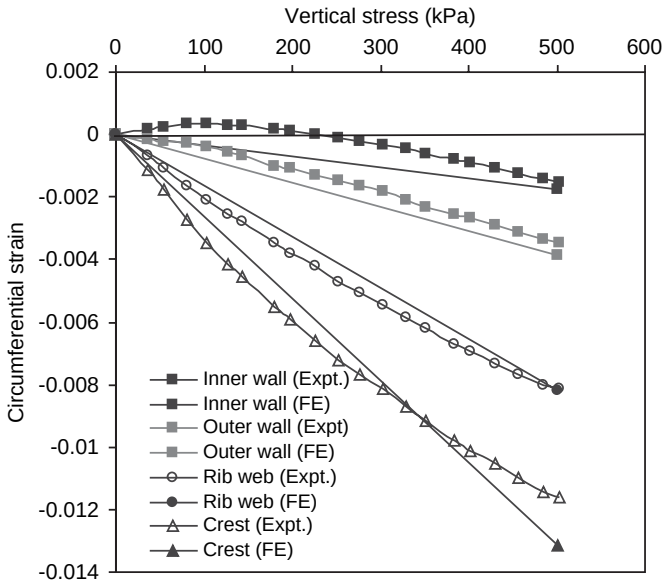

Figure C-104. Prediction of hoop strain at crown (PVC pipe).

C.5.7.2 Axisymmetric Compression

Analysis and measurement of profile strains discussed in Section 3 revealed that strain on the liner of lined corrugated pipe cannot be calculated using conventional 2D theory, since the strains are not uniform (along a line parallel to the pipe axis). Nonuniformity of strain is also evident on the walls of the box profile (Figure C-90) and the tubular profile.

Distributions of hoop strains on the inner surface of the four profiles (Figure C-32) at a radial earth pressure of 150 kPa are plotted in Figure C-106, as obtained from axisymmetric finite element analysis. Strains are normalized with the deflection ratio so results for each pipe can be compared (deformations are not the same at a given radial test cell pressure). Strain location is defined using z (the axial distance from the middle of pipe longitudinal segment considered) normalized relative to L (half the axial length of the meshes shown in Figures C-76 to C-78).

Although the boxed profile and the tubular profile have circumferential strains at the surface of the inner wall that are calculated to be almost uniform (strain measurements for the box profile, however, were not uniform), it is evident (in Figure C-106) that the hoop strains are not uniform along the inner sur-

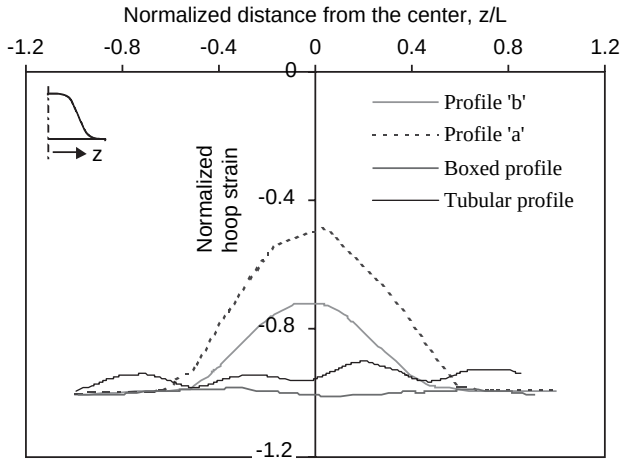

Figure C-106. Interior hoop strains on profiled pipe (at 150 kPa).

face of the two lined corrugated profiles (even though the distance of the inner wall from the neutral axis of the profile is almost constant). In the lined corrugated pipe, strain at the center of the liner is a fraction of the valley strain due to the local bending (Moore and Hu 1995). Between the two lined corrugated profiles (one is discussed in Appendix C.1), Profile "b" (the profile with a deeper corrugation and shorter pitch) experiences larger compressive hoop strains in the liner than does Profile "a." Strain at the middle of the liner is about 70% (measured 55% to 65%) of the valley strain for the pipe with Profile "b," whereas the liner midpoint has about 50% (measured approximately 60%) of the valley strain for Profile "a." Clearly, the span of the liner has a significant effect on the strains that develop in it, and local bending within the liner leads to greater reductions in hoop strain when liner "span" (the distance the liner stretches between corrugation valleys) is increased. Calculated value of axial strain is also less at the midpoint of the liner for Profile "b," indicating more local bending in the liner with longer span (Profile "a").

Figures C-107 and C-108 show the contours of hoop, axial, and radial stresses on the two lined corrugated profiles ("a" and "b") plotted at the same radial pressure of 150 kPa. Compressive stress is denoted as negative in the figures. These figures reveal that a concentration of all of the three stresses develops at the liner-corrugation intersection in both of the profiles. Hoop stresses on corrugations in both the profiles are approximately the same (−4 MPa), whereas the hoop compression at the intersection is twice as much as the valley stress (−8 MPa) in Profile "a" and 1.5 times in Profile "b" (Figures C-107a and C-108a). Axial compression at the intersection is also of similar magnitude as hoop compression (−8 MPa in Profile "a" and −6 MPa in Profile "b"), even though the compression at the valley is one-fourth (−1 MPa) of that

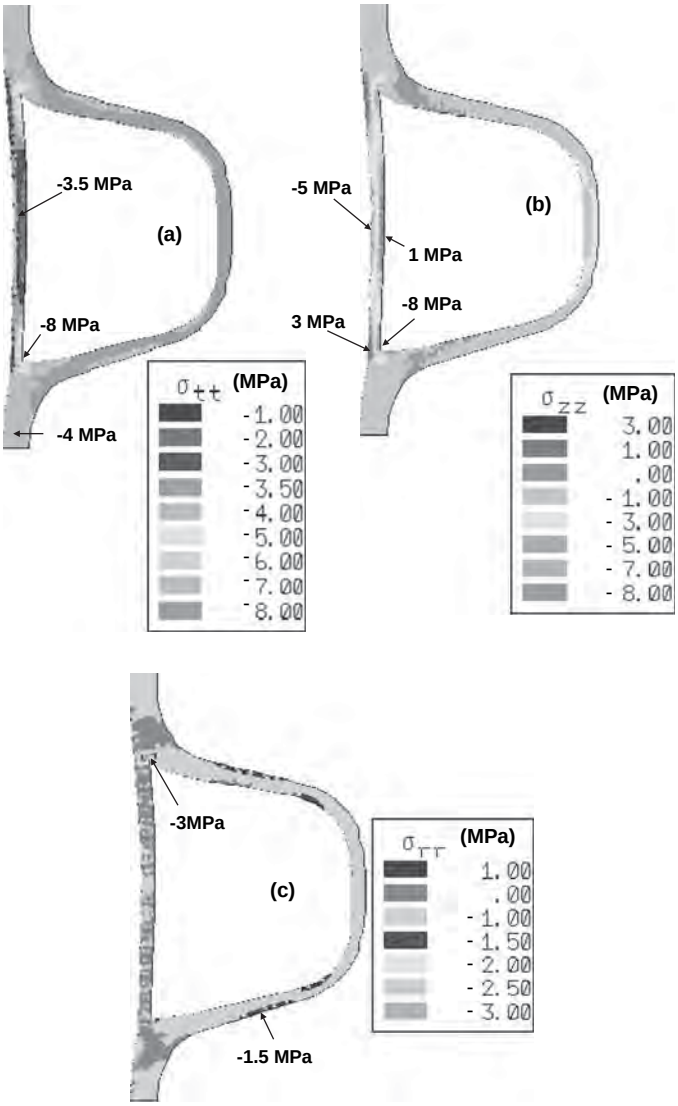

Figure C-107. Stress contours for lined corrugated Profile "a" show (a) hoop, (b) axial, and (c) radial stress (cell pressure 150 kPa).

in hoop direction (in Figures C-107b and C-108b). Axial tension develops on the outer surface of the liner-corrugation junction; the magnitude is half of the maximum compression on the inner surface (3 MPa). The concentration of radial stress (Figures C-107c and C-108c) in the profiles is compressive, and the magnitudes are less than those in the circumferential and axial directions. Thus, circumferential compression and axial tension at the junction are the maximum distress the lined corrugated profile undergoes in axisymmetric compression. Both the maximum tension and the maximum compression should be examined to evaluate the performance of the profiles.

The maximum stress on the boxed profile is the hoop compression, and this is located where the inner liner is connected

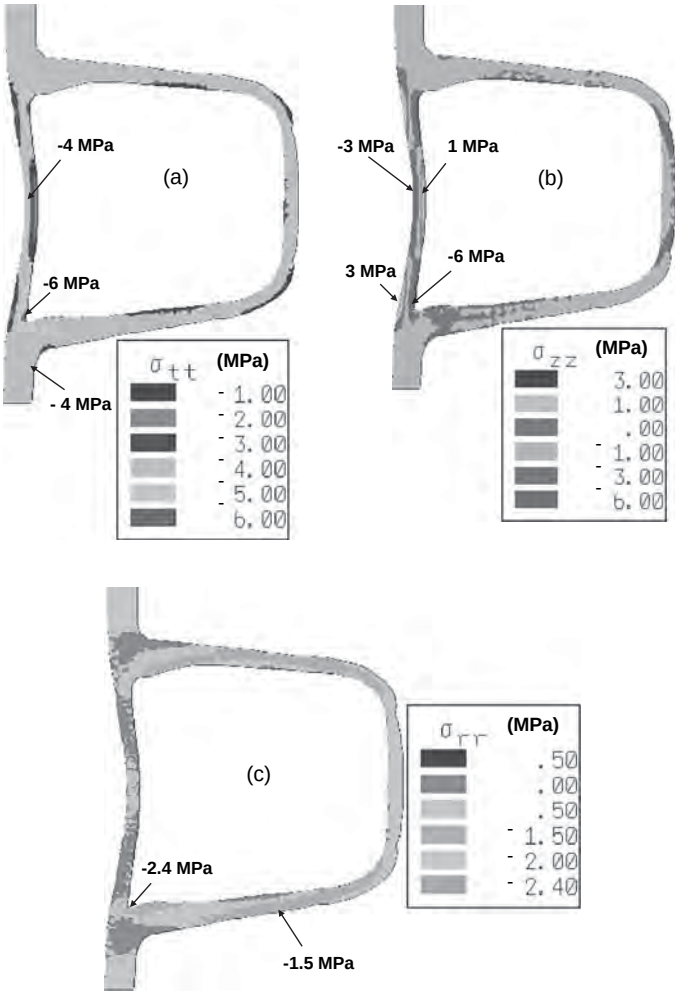

Figure C-108. Stress contours for lined corrugated Profile "b" show (a) hoop, (b) axial, and (c) radial stress.

to the rib (Figure C-109). The maximum stress is somewhat higher than the liner hoop stress (liner stress is –4 MPa and the maximum stress is –4.4 MPa). No tension on the profiles was calculated as seen in Figure C-109. The axial compression on the liner is half of the hoop stress. Radial stress on the profile was found to be insignificant and is therefore not included here.

Stress contours on a section of the tubular profile are drawn in Figure C-110. The hoop stress is seen to reach a maximum (–7 MPa) at the middle of both inner liners (Figure C-110). Axial compression is also higher at those locations, but has less magnitude (–5.5 MPa). Tensile stresses are evident in the profile on segments of the tubes (Figure C-110b and C-110c) in both the axial and radial directions. The tensions are on the inner surface of the tube at the intersection and on the outer surface at the middle of the segment.

C.5.7.3 Biaxial Loading

Locations and magnitude of maximum stresses on each of the four profiles are examined under axisymmetric compression in the previous section. This section provides a study of 3D stresses on the profiles under biaxial loading. Pipes at two different depths of burial (2 m and 8 m) have been examined for the short-term and long-term profile stresses in the circumferential, axial, and radial directions. Table C-23 shows details of the parameters considered in the investigation. Well-graded sand compacted to 95% of maximum Proctor density (SW95) has been taken as the backfill material. Parameters for the backfill soil at the stress levels corresponding to these depths (2 m and 8 m) are estimated from McGrath et al. (1999).

Contours of circumferential stresses at the springline and crown of a biaxially loaded lined corrugated pipe (Profile "a") buried at a depth of 8 m are plotted in Figure C-111. Response of Profile "a" at an 8-m burial depth is considered in some detail to examine the profile stresses at the springline and the crown.

Figure C-111 shows nonuniformity of circumferential stresses on the profile. Springline circumferential stress is –8 MPa (compression negative) at the valley and –4 MPa at the crest of the profile. Crown stresses at the corresponding locations are –1 MPa and –2.2 MPa, respectively. Valley stress is greater than the crest stress at the springline and is smaller at the crown due to opposite bending moments acting on the pipe at those two locations. A concentration of circumferential stress is noticed in Figure C-112 at the interior surface of the liner-corrugation intersection. As noticed in axisymmetric compression (Figure C-107), the maximum stress at the intersection is about twice as much as the valley stress both at the springline and at the crown of the pipe.

A concentration of axial stress at the springline and crown of the biaxially loaded pipe also occurs at the liner-corrugation junction (Figure C-112). As was evident in the analysis of the profile under axisymmetric compression (Section C.5.2), maximum axial compression at the interior surface of the junction (–14 MPa at the springline and –2.2 MPa at crown) is similar in magnitude to circumferential compression (–15 MPa at the springline and –2.0 MPa at the crown). Axial tension on the outer surface is about 45% of the compression on the interior surface. Magnitude of tension at the midliner is less than the tension at the intersection (midliner tension is about 60% of the value at the intersection for Profile "a"). Thus, the liner-corrugation junction of the lined corrugated profile is more likely to reach a stress limit state both in terms of compression and tension.

The study of Profile "a" in biaxial compression reveals that the locations of the largest compression and tension do not change for the two different (axisymmetric or biaxial) loading conditions. The locations of maximum stress under axisymmetric and biaxial loadings were also the same on the other profiles; those locations are shown in Figures C-108 to C-110. Values of the largest and smallest stresses on the different pipe profiles are shown in Tables C-24 and C-25. The stresses at the

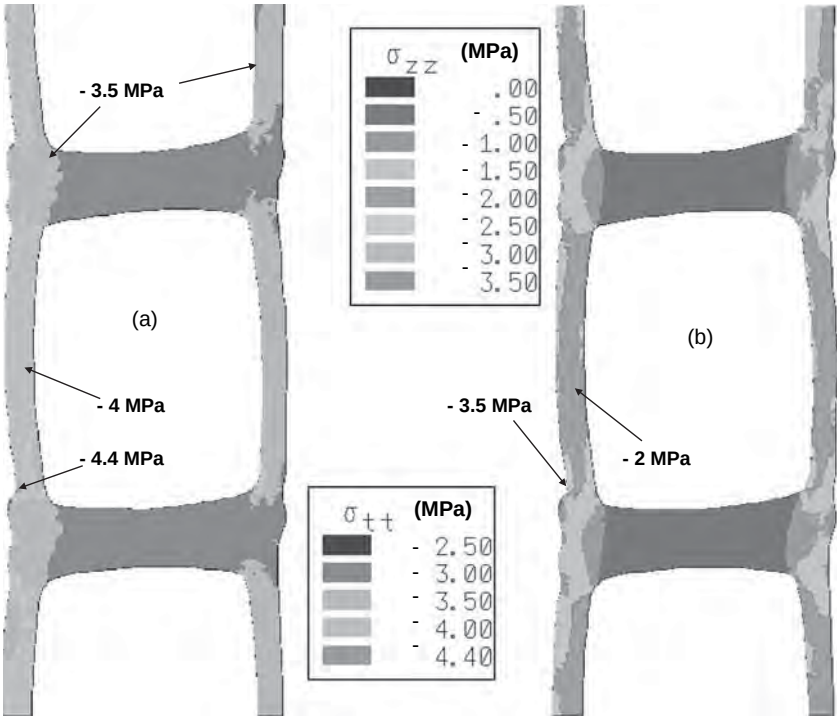

Figure C-109. Stress contours for boxed profile show (a) hoop and (b) axial stress.

springline were greater for all of the profiles, and hence only the springline stresses are included in Tables C-24 and C-25, which show the short-term and long-term stresses, respectively, at the two different burial depths. Long-term stresses are naturally lower than the short-term stresses due to the decrease in pipe modulus, which leads to additional positive arching. For each of the pipes and each burial depth, the long-term stress is 40% to 50% of the short-term stresses.

The comparison of maximum and minimum stresses in Tables C-24 and C-25 reveals that the greatest stress concentration occurs at the liner-corrugation junction. Maximum short-term stresses at an 8-m burial are −15 MPa and −11.5 MPa, respectively, for the twin-wall pipe Profiles "a" and "b." The stresses on the boxed and tubular profile at the same burial depth were −7.8 MPa and −4.2 MPa, respectively. Using the AASHTO short-term stress limit for HDPE material (i.e., 20.7 MPa), it appears that local short-term stresses on the profiles considered in this study are less than the short-term allowable stress. However, long-term stress on the twin-wall Profile "a" (i.e., 6 MPa) almost reaches the AASHTO long-term stress limit (i.e., 6.2 MPa).

Axial tension is also highest in the lined corrugated profiles. The boxed profile does not show any tension in the axial direction, even though axial tensile strain was measured on this helically wound profile. The axisymmetric idealization of the profile may not be suitable for estimating the behavior of this helical structure. Radial stresses in all of the profiles are smaller than the circumferential and axial stresses.

C.5.8 Summary

The 3D response of profiled thermoplastic pipes has been examined to develop an understanding of 3D issues affecting the behavior and design of the profile geometries. The pipe profiles were modeled explicitly, using profile geometry recorded from various test specimens. Results of the analysis were compared with the measurements obtained using laboratory tests. Commonly used HDPE profiles (lined corrugated, boxed, and tubular) and a rib-stiffened PVC profile have been considered in the investigation.

The axisymmetric finite element analysis was successfully used to study the response of the pipe profiles in the axisymmetric stress field. Modeling of the time-dependent nature of the polyethylene influenced the simulation of the laboratory hoop tests, and inclusion of these effects provided improved calculations. This is attributed to the fact that a very thin ring of soil surrounds the pipe in the hoop compression cell, so the contribution of the pipe stiffness rather than the soil stiffness dominates the pipe behavior in this burial condition.

The axisymmetric assumption was less successful for the helically wound box profile, where it provided some values of hoop strain that exceeded measured values and axial strain values that were less than those measured. Although use of the axisymmetric approximation must be undertaken carefully for the boxed profile (in particular, the measurements of hoop strains on the walls were much less than those obtained using the axisymmetric relation, Δ/D), the pipe deflections (diameter changes) were still estimated successfully.

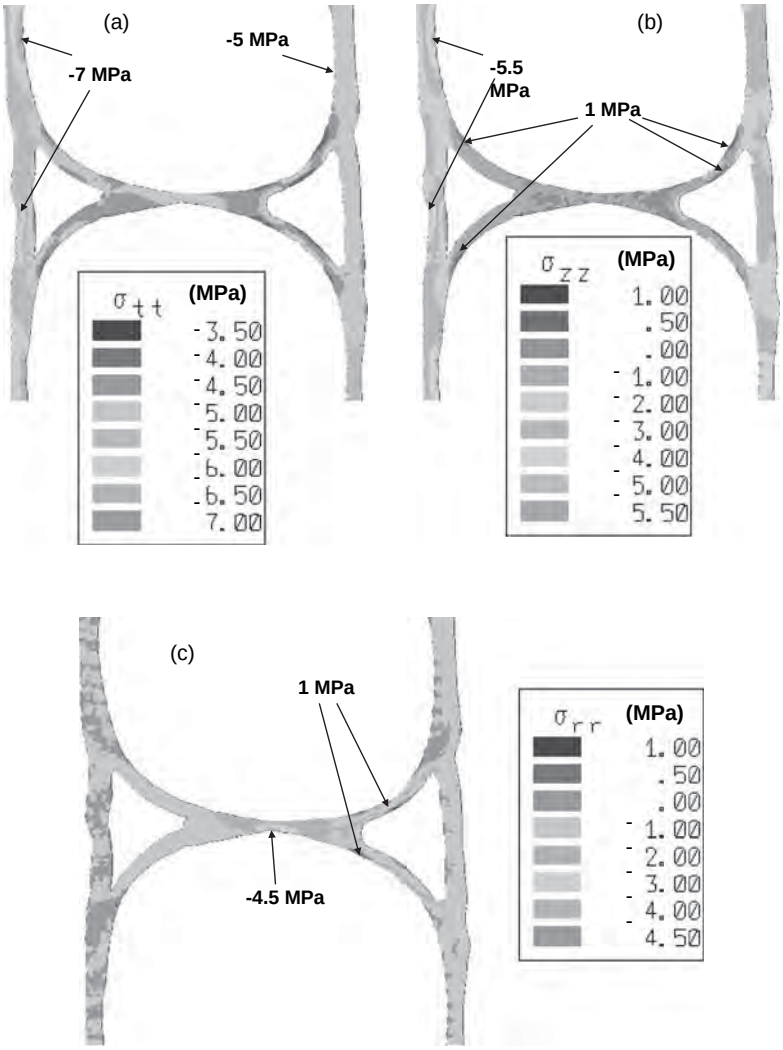

Figure C-110. Stress contours for tubular profile show (a) hoop, (b) axial stress, and (c) radial stress.

The 3D semi-analytic finite element procedure of Moore (1994) provides useful estimates of diameter change and local strain in profiled pipes under the biaxial loading that results from geostatic earth pressures. In particular, it explains variations of hoop strain both around the pipe circumference and across the profile. The method is limited to the modeling of linear soil-pipe interaction, and this may explain why values of hoop strain calculated at the springline or crown are somewhat different from those measured at these locations. Use of that analysis appears to provide conservative values of hoop strain estimates for use in local buckling calculations within the liner at the springline of lined corrugated pipe. Estimates of local liner strain at the crown were found to be unconservative.

Explicit modeling of the profile was used to study the effects of local bending on the four different profiled HDPE pipes. Local bending within the wall of lined corrugated pipe is influenced by the span of the liner (the distance it stretches between corrugation valleys), with greater localized bending for the liner with longer span. The effect of the bending appears less significant on the boxed and tubular profiles.

Table C-23. Parameters used in the study of 3D effects.

Depth	σ_v (kPa)	σ_h (kPa)	Soil (SW95) Parameters		HDPE Modulus, MPa	
			ν	M_s (E), MPa	Short Term	Long Term
2 m	40	13.3	0.25	18.3 (15.25)	700	150
8 m	160	53.3	0.25	24.6 (20.5)	700	150

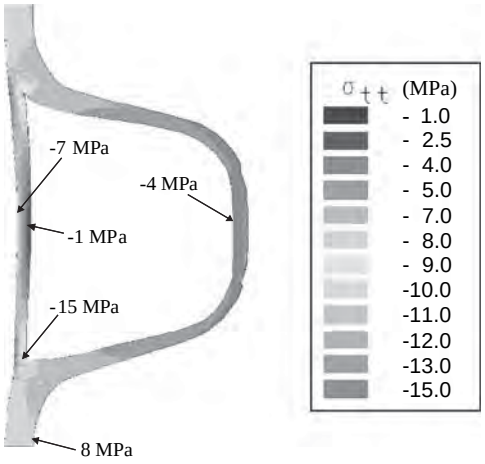

(a) Springline

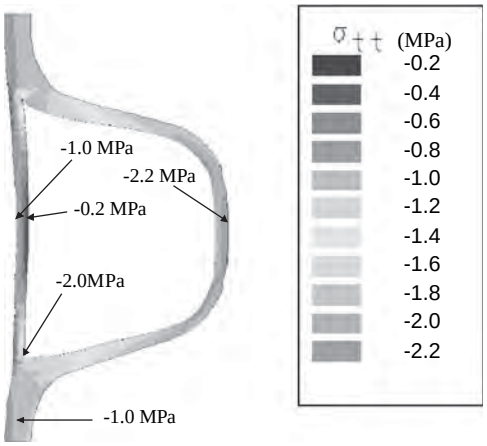

(b) Crown

Figure C-111. Circumferential stress contours under biaxial stress (8-m burial).

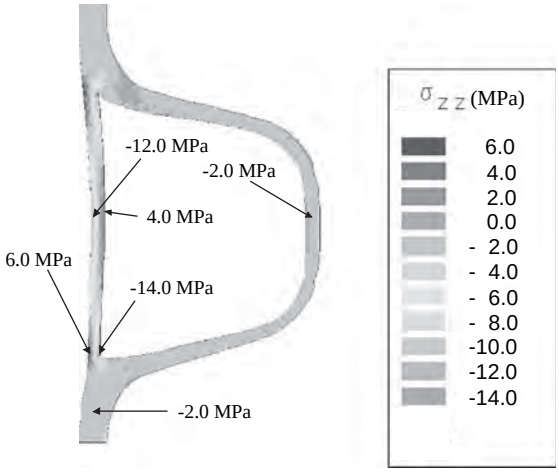

(a) Springline

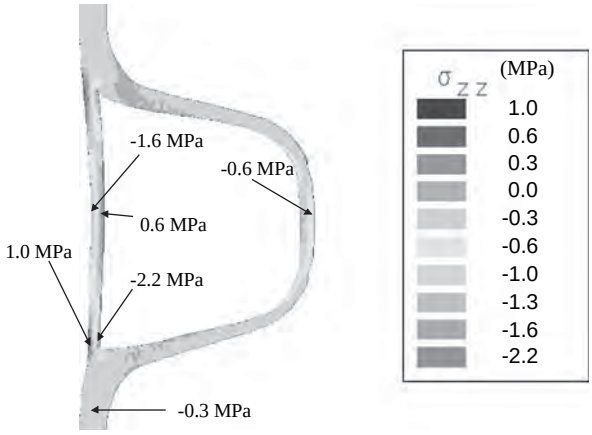

(b) Crown

Figure C-112. Axial stress contours under biaxial stress (8-m burial).

Table C-24. Maximum and minimum short-term stress at the springline (MPa).

Pipe	Circumferential (σ_θ)		Axial (σ_a)		Radial (σ_r)	
	2 m	8 m	2 m	8 m	2 m	8 m
Twin-wall "a"	–4.2	–15.0	–4.0	–14.0	–1.6	–6.0
	–0.4	–1.0	1.5	6.0	0.6	2.0
Twin-wall "b"	–3.2	–11.5	–3.0	–11.0	–1.0	–3.4
	–0.6	–2.5	1.4	5.0	0.2	0.6
Boxed	–2.1	–7.8	–1.6	–5.5	–0.45	–1.6
	–0.8	–3.2	0	0	0.15	0.6
Tubular	–1.2	–4.2	–1.0	–3.4	–0.55	–1.8
	–0.3	–1.2	0.1	0.6	0.15	0.4

Table C-25. Maximum and minimum long-term stress at the springline (MPa).

Pipe	Circumferential (σ_θ)		Axial (σ_a)		Radial (σ_r)	
	2 m	8 m	2 m	8 m	2 m	8 m
Twin-wall "a"	–1.9	–6.0	–1.8	–5.5	–0.7	–2.4
	–0.2	–0.5	0.8	2.5	0.2	0.8
Twin-wall "b"	–1.5	–4.8	–1.4	–4.5	–0.45	–1.4
	–0.3	–1.0	0.6	2.0	0.05	0.2
Boxed	–1.05	–3.6	–0.8	–2.6	–0.18	–0.60
	–1.0	–1.8	0	0	0.08	0.30
Tubular	–0.56	–1.8	–0.45	–1.8	–0.26	–0.90
	–0.22	–0.8	0.05	0.2	0.06	0.20

Calculations for pipes at 8-m burial depth indicate that the long-term value of the maximum stresses on each of the profiles was between 40 and 50% of the short-term stresses.

Design of these profiles should likely include explicit modeling of the profile to study the effects of local bending and to optimize use of material within the profile wall.

C.6 References

American Society of Civil Engineers, *Structural Plastics Design Manual–ASCE Manual for Practice No. 63,* American Society of Civil Engineers, New York, 1984.

American Water Works Association, "Fiberglass Pipe Design," *AWWA Manual of Water Supply Practices M45,* American Water Works Association, Denver, CO, 1996.

Association of State Highway and Transportation Officials, *LRFD Bridge Design Specifications,* 2nd ed., Association of State Highway and Transportation Officials, 1998.

Bodner, S. R. and Parton, Y., "A Large Deformation Elastic-Viscoplastic Analysis of a Thick-Walled Spherical Shell," *Journal of Applied Mechanics,* Vol. 42, No. 2, 1972.

Brachman, R. W. I., "Structural Performance of Leachete Collection Pipes," Ph.D. thesis, Department of Civil and Environmental Engineering, University of Western Ontario, London, ON, Canada, 1999.

Brachman, R. W. I., Moore, I. D., and Rowe, R. K., "The Design of a Laboratory Facility for Evaluating the Structural Response of Small Diameter Buried Pipes," *Canadian Geotechnical Journal,* Vol. 37, No. 2, 2000.

Brachman, R. W. I., Moore, I. D., and Rowe, R. K., "The Performance of a Laboratory Facility for Evaluating the Structural Response of Small-Diameter Buried Pipes," *Canadian Geotechnical Journal,* Vol. 38, 2001.

Brown, F. A. and Lytton, R. L., "Design Criteria for Buried Flexible Pipe," *Pipeline Material and Design,* ASCE National Convention, San Francisco, CA, 1984.

Bryan, G. H., "On the Stability of a Plane Plate under Thrusts in its Own Plane, with Applications to the Buckling of the Sides of a Ship," *Proceedings of the London Mathematical Society,* Vol. 22, London, England, 1891.

Burns, J. Q. and Richard, R. M., "Attenuation of Stresses for Buried Cylinders," *Proceedings of Symposium on Soil-Structure Interaction,* University of Arizona, Tucson, 1964.

Chua, K. M. and Lytton, R. L., "A New Method of Time-Dependent Analysis for Interaction of Soil and Large Diameter Flexible Pipe," Texas Transportation Institute, Texas A&M University System, *Proceedings of the 66th Annual Meeting of the Transportation Research Board,* Transportation Research Board, Washington, D.C., 1987.

Dhar, A., "Limit States of Profiled Thermoplastic Pipes under Deep Burial," Ph.D. thesis, Department of Civil and Environmental Engineering, University of Western Ontario, London, ON, Canada, 2002.

Dhar, A. S. and Moore, I. D., "Non-linear Analysis of Buried HDPE Pipe by the Finite Element Method: Comparison with Laboratory Test," *Proceedings in the International Conference on Geotechnical and Geological Engineering (GeoEng 2000),* Melbourne, Australia, 19–24 Nov. 2000a.

Dhar, A. S. and Moore, I. D., "Local Buckling in Profiled Thermoplastic Pipes," *Proceeding of the 28th Annual Conference of the Canadian Society for Civil Engineer (CSCE2000),* London, ON, Canada, 2000b.

Dhar, A. S. and Moore, I. D., "Sensitivity of Thermoplastic Pipe Behavior to Profile Geometry," International Specialty Conference on Pipelines 2001—Advances in Pipeline Engineering and Construction, San Diego, CA, 2001.

Dhar, A. S. and Moore, I. D., "Laboratory Investigation of Local Bending in Profiled Thermoplastic Pipes," *Advances in Structural Engineering—An International Journal,* Vol. 7, No. 3, 2004.

Dhar, A. S., Moore, I. D., and McGrath, T. J., "Thermoplastic Culvert Deformation and Strain: Evaluation Using Two-Dimensional Analyses," submitted to the *ASCE Journal of Geotechnical & Geoenvironmental Engineering,* 2001.

Dhar, A. S., Moore, I. D. and McGrath, T. J., "Thermoplastic Culvert Deformation and Strain: Evaluation Using Two-Dimensional Analyses," *ASCE Journal of Geotechnical & Geoenvironmental Engineering,* Vol. 130, No. 2, 2004.

DiFrancesco, L. C., "Laboratory Testing of High Density Polyethylene Drainage Pipes," M.Sc. thesis, Department of Civil Engineering, University of Massachusetts, Amherst, 1993.

Duncan, J. M. and Chang, C-Y, "Nonlinear Analysis of Stress and Strain in Soil," *ASCE Journal of the Soil Mechanics and Foundations Division,* Vol. 96, No. SM5, 1970.

Flugge, W., *Stresses in Shells,* Springer-Verlag, Berlin, Federal Republic of Germany, 1962.

Gassman, S. L., Schroeder A. J., and Ray, R. P., "Field Performance of High Density Polyethylene Culvert Pipe," *ASCE Journal of Transportation Engineering,* Vol. 131, No. 2, 2005.

Hashash, N. M. A., "Design and Analysis of Deeply Buried Polyethylene Drainage Pipes," Ph.D. thesis, Department of Civil Engineering, University of Massachusetts, Amherst, 1991.

Hashash, N. M. A. and Selig, E. T., "Analysis of the Performance of a Buried High Density Polyethylene Pipe," *Structural Performance of Flexible Pipe,* Sergand, Mitchell, and Hurd eds., Balkema, Rotterdam, Netherlands, 1990.

Hoeg, K., "Stress against Underground Cylinder," *Journal of Soil Mechanics and Foundation Engineering,* Vol. 94, No. SM4, 1968.

Hurd, J. O., Sargand, S. M., and Masada, T., "Performance of Large Diameter HC-HDPE Pipe under Highway Embankment in Ohio,"

Paper No. 970894, 76th Annual Meeting, Transportation Research Board, Washington, D.C., 1997.

Janbu, N., "Soil Compressibility as Determined by Odometer and Triaxial Tests," *Proceedings of the European Conference on Soil Mechanics and Foundation Engineering, Vol. 1,* Wiesbaden, Federal Republic of Germany, 1963.

Katona, M. G., "Allowable Fill Heights for Corrugated Polyethylene Pipe," Paper No. 87-0012, 67th Annual Meeting, Transportation Research Board, Washington D.C., January 1988.

Laidlaw, T., "Influence of Local Support on Corrugated HDPE Pipe," M.E.Sc. thesis, University of Western Ontario, London, ON, Canada, 1999.

Lapos, B., and Moore, I. D., "Evaluation of the Strength and Deformation Properties of Olimag Synthetic Olivine," *Proceedings of the 55th Canadian Geotechnical Conference,* Niagara Falls, ON, Canada, 2002.

Li, H. and Donovan, J. A., "Ring Bending and Hoop Compression Tests on Big 'O' HDPE Pipe," Department of Civil Engineering, University of Massachusetts, Amherst, 1994.

McGrath, T. J., "Design Method for Flexible Pipe," Polyethylene Pipe Design Task Group of the AASHTO Flexible Culvert Liaison Committee, Simpson Gumpertz & Heger Inc., Arlington, MA, 1998a.

McGrath, T. J., "Replacing E' with the Constrained Modulus in Buried Pipe Design," *Pipelines in the Constructed Environment,* J. P. Castronovo and J. A. Clark, eds., American Society of Civil Engineers, Reston, VA, 1998b.

McGrath, T. J. and Sagan, V. E., *NCHRP Report 438: LRFD Specifications for Plastic Pipe and Culverts,* Transportation Research Board, Washington, D.C., 2000.

McGrath, T. J., Moore, I. D., Lesser, A., and Dhar, A., "Thermoplastic Drainage Pipe, Design and Testing," Second Interim Report, NCHRP Project 4-26 FY '98. Simpson Gumpertz & Heger Inc., Arlington, MA, 2001.

McGrath, T. J., Selig, E. T., Webb, M. C., and Zoladz, G. V., "Pipe Interaction with the Backfill Envelope," Publication No. FHWA-RD-98-191, Federal Highway Administration, U.S. Department of Transportation, McLean, VA, June 1999.

Molin, J., "Calculation Principles for Underground Plastic Pipes," Svenska Vatten-Och Avloppsverksforeningen, VAV P16, January 1971.

Moore, I. D., "Influence of Rib Stiffeners on the Buckling Strength of Elastically Supported Tubes," *International Journal of Solids and Structures,* Vol. 26, No. 5/6, 1990.

Moore, I. D., "Three Dimensional Time-Dependent Models for Buried HDPE Pipe," *Proceedings of the 8th International Conference on Computer Methods and Advances in Geomechanics,* H. J. Siriwardane and M. M. Zaman, eds., A. A. Balkema, Rotterdam, Netherlands, Vol. 2, 1994.

Moore, I. D., "Three Dimensional Response of Deeply Buried Profiled Polyethylene Pipe," Paper No. 950822, 74th Annual Meeting, Transportation Research Board, Washington, D.C., January 1995.

Moore, I. D., "Local Buckling in Profiled HDPE Pipes," *Annual Conference of the Canadian Society for Civil Engineering,* Edmonton, AB, Canada, 1996.

Moore, I. D., "Chapter 18: Culverts and Buried Pipelines," *The Geotechnical and Geoenvironmental Handbook,* R. K. Rowe, ed., Kluwer Academic Publishers, 2000.

Moore, I. D., "Gravity Flow Sewers: Modeling to Capture Limit States for Buried Thermoplastic Pipes," *Proceedings of the 8th International Conference on Computer Methods and Advances in Geomechanics,* H. J. Siriwardane and M. M. Zaman, eds., Balkema, Rotterdam, Netherlands, 2001.

Moore, I. D. and Hu, F., "Response of Profiled High-Density Polyethylene Pipe in Hoop Compression," *Transportation Research Record 1514,* Transportation Research Board, Washington, D.C., 1995.

Moore, I. D. and Hu, F., "Linear Viscoelastic Modelling of Profiled High Density Polyethylene Pipe," *Canadian Journal of Civil Engineering,* Vol. 23, 1996.

Moore, I. D. and Laidlaw, T. C., "Corrugation Buckling in HDPE Pipes—Measurement and Analysis," No. 970565, *Proceedings of the 76th Annual Meeting of the Transportation Research Board,* Transportation Research Board, Washington, D.C., 1997.

Moore, I. D. and Zhang, C., "Nonlinear Predictions for HDPE Pipe Response under Parallel Plate Loading," *Journal of Transportation Engineering,* Vol. 124, No. 3, 1998.

Moser, A. P., "Structural Performance of Buried Profile-Wall High-Density Polyethylene Pipe and Influence of Pipe Wall Geometry," Paper No. 98-0811, *Transportation Research Record 1624,* Transportation Research Board, Washington, D.C., 1998.

Munro, S. M., "Measurement of Backfill Effects on Circumferential Bending in Lined-Corrugated Thermoplastic Pipes and Fiber Reinforced Cement Pipes," M.Sc. thesis, Department of Civil Engineering, Queen's University at Kingston, ON, Canada, 2006.

Roark, R. J., *Formulae for Stress and Strain,* McGraw-Hill, Inc., New York, 1943.

Rogers, C. D., "Some Observations on Flexible Pipe Response to Load," *Transportation Research Record 1191,* Transportation Research Board, Washington, D.C., 1988.

Rogers, C. D. F., Fleming, P. R., and Talby, R., "Use of Visual Methods to Investigate Influence of Installation Procedure on Pipe-Soil Interaction," *Transportation Research Record 1541,* Transportation Research Board, Washington, D.C., 1996.

Sargand, S. M., Hazen, G. A., Liu, X., Masada, T., and Hurd, J., "Structural Performance of Buried Polyvinyl Chloride Pipes under Large Distributed Load," *Transportation Research Record 1514,* Transportation Research Board, Washington, D.C., 1995.

Selig, E. T., "Soil Parameters for Design of Buried Pipelines," *Proceedings, Pipeline Infrastructure Conference,* American Society of Civil Engineers, Boston, MA, 1988.

Selig, E., "Soil Properties for Plastic Pipe Installations," *Buried Plastic Pipe Technology,* ASTM STP 1093, G. S. Buczala and M. J. Cassady, eds., American Society for Testing and Materials, West Conshohocken, PA, 1990.

Selig, E. T., DiFrancesco, L. C., and T. J. McGrath, T. J., "Laboratory Test of Pipe in Hoop Compression," *Buried Plastic Pipe Technology,* 2nd vol., ASTM STP 1222, D. Eckstien, ed., American Society for Testing and Materials, West Conshohocken, PA, 1994.

Skempton, A. "Effective Stress in Soils, Concrete and Rocks," *Selected Papers on Soil Mechanics by Skempton,* A. T. Telford, London, UK, 1984.

Spangler, M. G., "The Structural Design of Flexible Pipe Culverts," *Iowa Engineering Experiment Station Bulletin 153,* Iowa State University, Ames, 1941.

Tognon, A. R. M., Rowe, R. K., and Brachman, R. W. I., "Evaluation of Side Wall Friction for a Buried Pipe Testing Facility," *Geotextiles and Geomembranes,* Vol. 17, 1999.

White, D. J., Take, W. A., and Bolton, M. D., "Soil Deformation Measurement Using Particle Image Velocimetry and Photogrammetry," *Geotechnique,* Vol. 53, No. 7, 2003.

Winter, G., "Strength of Thin Steel Compression Flanges," *Proceedings of the American Society of Civil Engineers,* American Society of Civil Engineers, New York, 1946.

Zhang, C. and Moore, I. D., "Nonlinear Mechanical Response of High Density Polyethylene—Part I: Experimental Investigation and Model Evaluation," *Polymer Engineering and Science,* Vol. 37, No. 2, 1997.

Zhang, C. and Moore, I. D., "Nonlinear Finite Element Analysis for Thermoplastic Pipes," *Transportation Research Record 1624,* Transportation Research Board, Washington, D.C., 1998.

APPENDIX D

Guidelines for Comprehensive Analysis of Thermoplastic Pipe

Comprehensive Design Method

1 Limit States

Service and strength limit states for thermoplastic culverts are those listed with respect to the simplified design method.

The comprehensive design approach provides an alternative means of assessing structural response relative to those same limit states.

Commentary

C1

The range of thermoplastic pipe products that are being manufactured and the range of burial conditions being used, together with the interdependence of the culvert and the soil surrounding it, mean that the process of developing a simplified design procedure may produce significant conservatism for some culverts. The finite element method is capable of capturing the impact of material properties, structure, and soil geometry on the load sharing and load capacity for this soil-structure system. It forms the key to a comprehensive design method that can more effectively treat the limit states of concern for culverts.

The comprehensive design method uses nonlinear finite element analysis to evaluate culvert response. The procedure for evaluating global buckling strength is based on published solutions.

Note that experience has shown that the quality of construction practices when installing culverts can be somewhat variable. Use of a comprehensive design approach requres a commitment to achieving the design assumptions in the field. This includes control of in situ ground conditions and groundwater backfill type and gradation, backfill, placement compaction, and pipe deflections.

Specification	Commentary
2.1 Service Limit States	**C2.1**
Deformations resulting from earth and vehicle live loads are estimated using nonlinear finite element analysis.	
Earth load estimates are for load placed above the structure. Deformations resulting from earth load placed beside and directly over the culvert are managed using the deflection limits specified in the simplified design method. Design issues associated with the burial of thermoplastic culverts are discussed in the simplified design method.	Thermoplastic culvert response to earth load placed beside the culvert (as opposed to earth load placed over the culvert) can be dominated by construction effects such as soil compaction. This response cannot be reliably predicted using finite element analysis.
Estimates of deformation under live load will generally be undertaken using two-dimensional finite element analysis. Three-dimensional analysis may be used when it is available.	Conversion of three-dimensional vehicle loads to line-load equivalents permits use of two-dimensional analysis to predict culvert response under three-dimensional live load. This is discussed in Section 3.4.

Specification	Commentary
2.2 Strength Limit States	
2.2.1 Thrust and Moment	*C2.2.1*
Thrusts and moment are calculated for both earth and live loading. The thrust and moment distributions around the full structure can be estimated.	Estimates of thrust are not expected to be significantly influenced by construction effects. Moment is significantly influenced by • soil properties, • culvert and soil geometry, • live-load position, and • construction effects.
The thrust limit associated with global buckling is estimated using the procedure outlined in Section 2.2.2. Maximum expected thrust obtained from finite element analysis is then compared with the thrust capacity associated with buckling.	Construction practices in particular can influence bending moment. The effect of local variations in soil support under the pipe can be very important. Techniques for modeling these variations are discussed in Section 3.2.1.
Thrusts and moments are used to evaluate circumferential strains at the extreme fibers as described in Section 2.2.3. Strain limits are those associated with the material itself, as well as the strain limits relating to local instability in the profile wall. These strain limits are treated in the same manner as in the simplified design method.	

Specification

2.2.2 Global Buckling Procedure

A procedure is available for calculating the correction factor for backfill soil geometry R_h. This R_h factor is then used in the buckling equation outlined in the simplified design method. Typical problem geometry is shown in Figure 2.2a.

Factor R_h is a function of

- H = depth of fill over top of culvert, m, in.
- S = culvert diameter, m, in.
- M_s = constrained modulus of select backfill soil, kN/m^2, lb/in.^{2}
- M_o = constrained modulus for the soil beyond the select backfill material of modulus M_s, kN/m^2, lb/in.^{2}
- W = minimum width of the backfill soil (that with modulus M_s), m, in.
- E = long-term Young's modulus of the thermoplastic, kN/m^2, lb/in.^{2}
- I = second moment of area of the pipe wall per unit length, m^4/m, in.^{4}/in.

Values of W/S, H/S, and EI/M_sS^3 are used to determine R_h based on interpolation from Figures 2.2.2b to 2.2.2h.

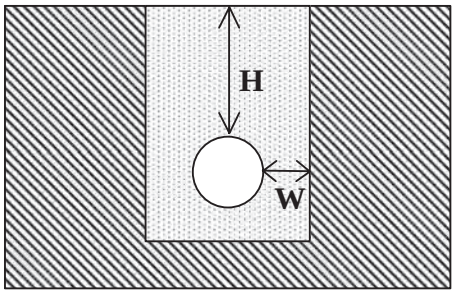

Figure 2.2a. Definition of backfill geometry.

Commentary

C2.2.2

This procedure provides an alternative method of calculating factor R_h to replace the expressions given in the simplified design method. Finite element analysis of culvert buckling capacity is not currently possible using the public domain software CANDE (it is being incorporated in CANDE 2007), but can be undertaken using some proprietary codes.[1] Such calculations should be undertaken by analysts with appropriate specialized expertise.

Structural properties and soil properties often vary around the culvert perimeter. Lowest values are used in design calculations for buckling strength, since in some cases buckling mode can extend around a considerable proportion of the perimeter and may not be concentrated at the zone of maximum thrust.

R_h values are read from the figures[2] that have W/S and M_0/M_s values that bound those for the culvert being evaluated. Each figure is examined to determine the value of R_h for the specific values of H/S and EI/M_sS^3. Interpolation is then used to estimate the correction factor for the intermediate W/S and M_0/M_s values.

This solution permits the influence of the native soil material modulus M_o, the burial depth H, and the width of the zone of select backfill to be examined, in addition to the effect of relative flexural stiffness EI/M_sS^3 on factor R_h.

[1] Example, I.D. Moore, "The Elastic Stability of Shallow Buried Tubes," *Geotechnique*, Vol. 37, No. 2, 1987, 151-161.
[2] Adapted from I.D. Moore, A. Haggag, and E.T. Selig, "Buckling Strength of Flexible Cylinders with Nonuniform Elastic Support," *International. Journal of Solids and Structures*, Vol. 31, No. 22, 1994, 3041-3058.

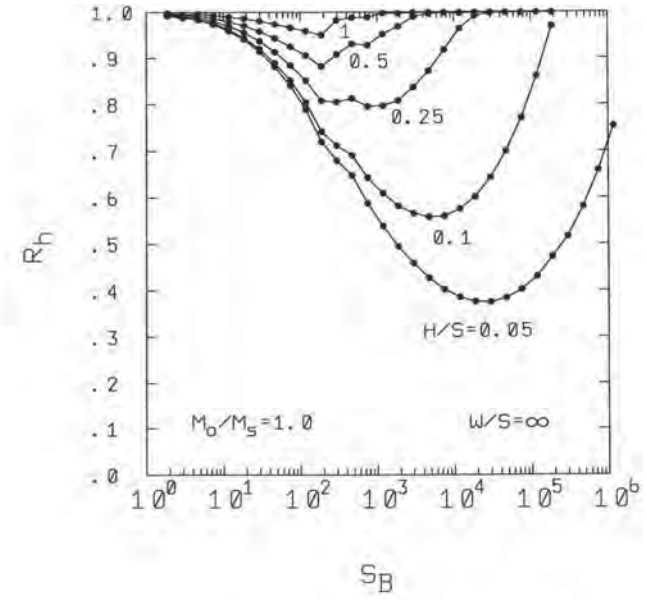

Figure 2.2b. Correction factor for M_o/M_s=1 and/or W/S>2.

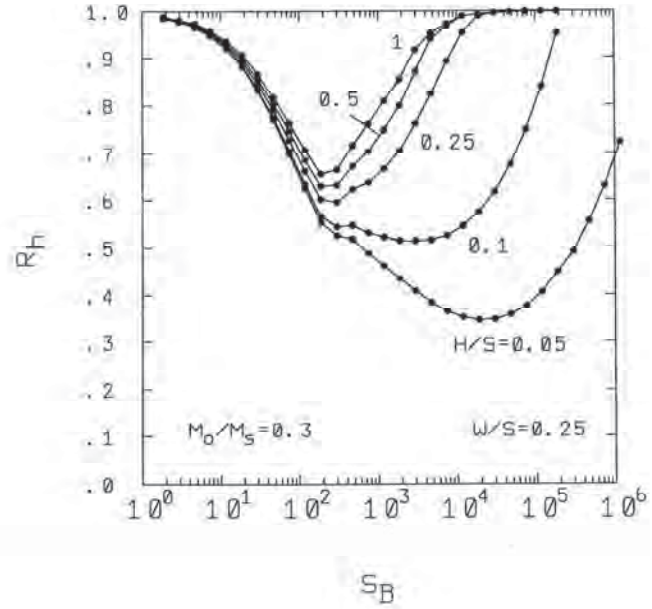

Figure 2.2d. Correction factor for M_o/M_s=0.3 and W/S=0.25.

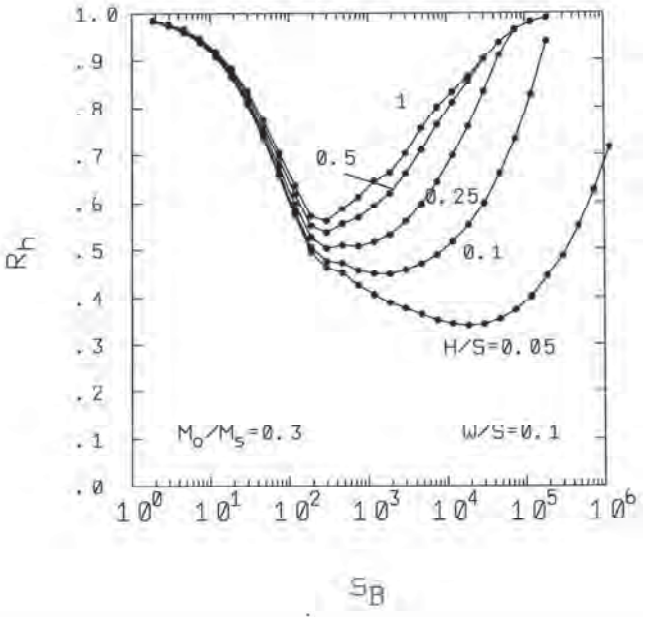

Figure 2.2c. Correction factor for M_o/M_s=0.3 and W/S=0.1.

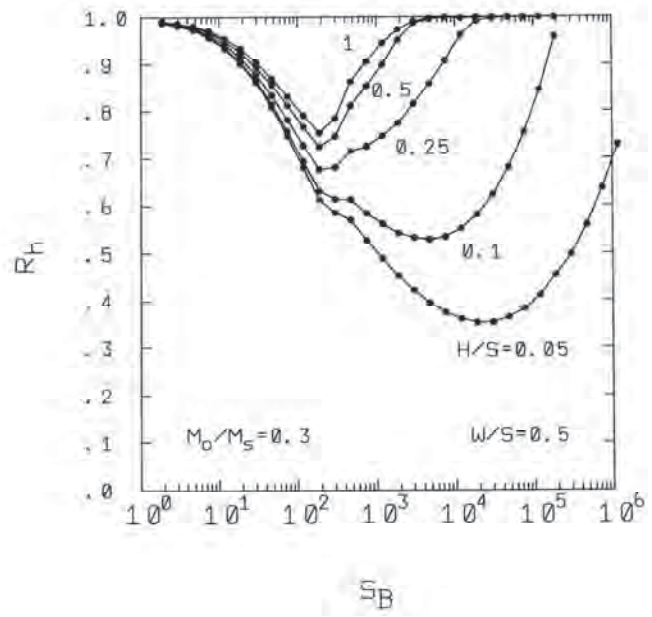

Figure 2.2e. Correction factor for M_o/M_s=0.3 and W/S=0.5.

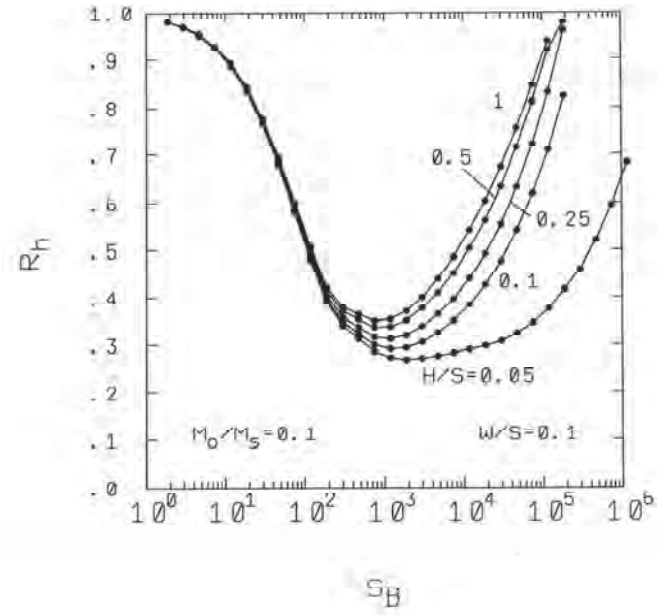

Figure 2.2f. Correction factor for M_o/M_s=0.1 and W/S=0.1.

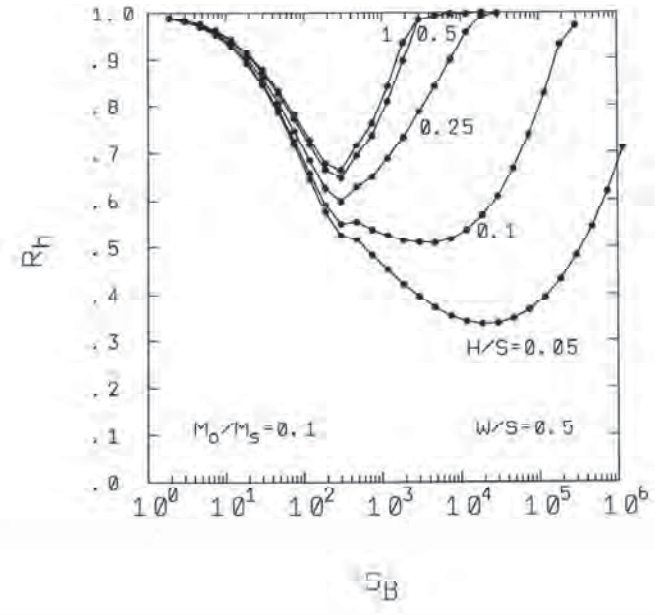

Figure 2.2h. Correction factor for M_o/M_s=0.1 and W/S=0.

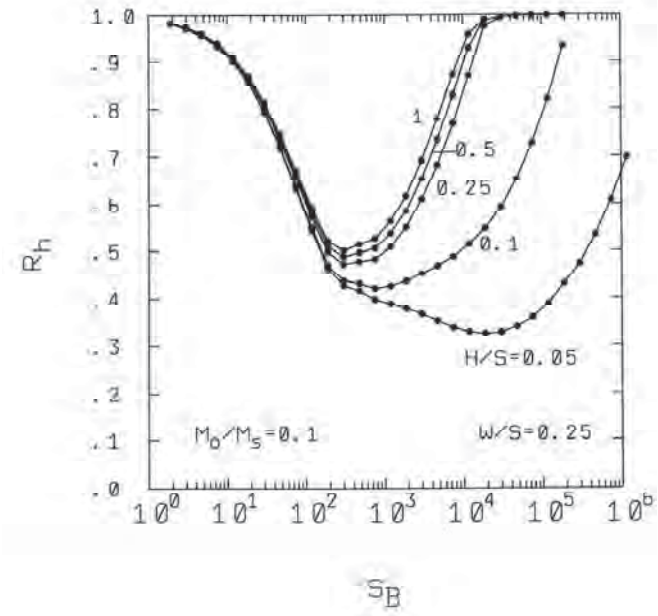

Figure 2.2g. Correction factor for M_o/M_s=0.1 and W/S=0.25.

Specification

2.2.3

Simple beam theory has been used to calculate the strains from the thrust and moment values obtained from the finite element analyses. The finite element method calculates the thrust and bending moments at the Gauss (numerical integration) points of the elements. Circumferential strain at a distance Y from the neutral axis of the section is given by

$$\varepsilon = \frac{N}{EA} + \frac{MY}{EI} \qquad (2.2.3)$$

where

N = thrust,

M = bending moment,

E = pipe material modulus,

A = area of the cross-section,

I = moment of inertia, and

Y = distance of the extreme fiber from the profile centroid.

The strain distribution can be calculated around the culvert. The maximum values that develop on each particular element of the profile wall can then be used in assessments of local buckling strength.

Commentary

C2.2.3

Equation 2.2.3 is based on the assumption that strain distribution is linear across the profile so that all fibers located at the same distance from the neutral axis are modeled as responding with the same strain. Linear distribution of strain along the profile depth was observed during experiments,[3] except on the liner of pipe with corrugated profiles, where strains are typically substantially smaller. Liner strain can be estimated using either three-dimensional finite element analysis featuring explicit modeling of the wall geometry or empirical measures of liner strain versus corrugation strain.[4]

[3] A.S. Dhar and I.D. Moore, "Corrugated High-Density Polyethylene Pipe: Laboratory Testing and Two-Dimensional Analysis to Develop Limit States Design," *Transportation Research Record 1814*, Transportation Research Board, Washington D.C., 2002.

[4] A.S. Dhar and I.D. Moore, "Liner Buckling in Profiled Polyethylene Pipes," *Geosynthetics International*, Vol. 8, No. 4, 2001, 303-326.

Specification

Commentary

3 Analysis

C3

This section reviews issues associated with undertaking the two-dimensional finite element analysis that is key to culvert design using the comprehensive method.

3.1 Choice of Soil Parameters

C3.1

Three alternatives can be used for parameter selection.

A. Use of values of M_S recommended for use in simplified design. These can be fitted to either a stress-dependent nonlinear elastic modulus function or a modulus function which varies with depth.

B. Use of standard values like those in CANDE.

C. Use of data derived from laboratory tests.

Performance limits such as deflection and moment are strongly linked to choice of soil moduli. Parameters are available in CANDE. The CANDE soil model recommended for culvert analysis is the Duncan hyperbolic Young's modulus with the Selig hyperbolic bulk modulus. Properties from this model were developed by Selig and were used by AASHTO for development of the current reinforced concrete design procedures and for thermoplastic pipe. The properties are available in the appendix of the CANDE User Manual. Note that the modified Selig properties are about twice as stiff as the recommended second set of properties in the appendix. Use of the non-modified properties is recommended for design.

If soil properties are determined by laboratory test, the results should be interpreted by a geotechnical expert familiar with parameter selection for culvert design.

3.2 Nonlinear Modeling

C3.2

Many choices can be made regarding the modeling of nonlinearity. This section provides some guidance on which issues must be considered.

3.2.1 Soil

C3.2.1

The two most-common approaches to modeling the nonlinear material response of the soil are
A) Nonlinear elasticity: the hyperbolic model and
B) Elastoplasticity.
Either is acceptable. The second method may be used in conjuction with a stress-dependent function for initial elastic modulus, like that of Janbu.[5]

A. The hyperbolic model is used widely in North America and is the basis of various public-domain and proprietary programs. The model approximates the increases in soil stiffness that occur as confining pressure is increased, and the decreases in stiffness that occur as shear stresses increase.

[5] N. Janbu, "Soil Compressibility as Determined by Oedometer and Triaxial Tests," *Proceedings of the European Conference on Soil Mechanics and Foundation Engineering*, Wiesbaden, Vol.1, 1963, 19-25.

Specification

Commentary

B. Many multipurpose proprietary codes available for use in soil engineering incorporate elastoplastic constitutive models. These characterize the fundamental change in soil response that occurs once shear failure has developed. Such modeling is required if bearing capacity and other phenomena involving extensive plastic response are to be calculated.

CANDE employs the hyperbolic model. This has been used successfully in many predictions of culvert deformation, thrust, and moment at working loads. It is not expected that elastoplastic finite element programs will be commonly used in comprehensive culvert design (although such use is not prohibited). Such programs are best classified as research tools and their use requires appropriate technical expertise.

Strains arising from bending moments are significantly influenced by the zone of lower-modulus soil that develops under the haunches of the pipe (Figure 3.2a). A zone of reduced modulus representing a soft area in the haunch must be included even though haunching is specified.

Elastic modulus in the haunch zone is expected to be between from 5% to 20% of the backfill modulus. The lowest of these values should be used for backfill soils that are very loose when dumped without compaction and when haunching is not specified. If poor construction is envisaged, the size of the zone of low-modulus material should be expanded.

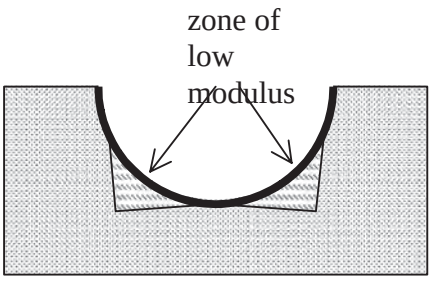

Figure 3.2a. Zone of low-modulus backfill under the pipe haunches.

Specification

3.2.2 Structure

Linear elastic structural modeling is used to predict thrust and moment for comparison with strength limits. Four choices can be made to model the culvert modulus.

A. Short-term modulus as recommended in the simplified design method.

B. Long-term modulus as recommended in the simplified design method.

C. Secant elastic modulus for some other time interval, based on explicit test data.

D. Linear or nonlinear viscoelastic or viscoplastic modeling using parameters evaluated from tests undertaken on the specific pipe material.

The first two choices can be used to obtain short-term and long-term response, respectively. The third and fourth choices are used when test data are available and permit response to be calculated at any specific time.

3.2.3 Interfaces

There are two interfaces that need consideration in finite element analysis of buried structures.

A. The interface between the culvert and the backfill soil.

B. The walls of the trench when one is used for culvert burial (the interface between the trench backfill and the soil beside the trench).

Shear strength of these interfaces should be no more than the angle of internal friction, ϕ, of the soil. Typical interface shear strength values would be from 50% to 70% of tan(ϕ).

Commentary

C3.2.2

Linear elastic modeling of the pipe material can be undertaken using secant elastic moduli, and these can be used to obtain estimates of structural response at short-term, long-term, or intermediate time periods. More sophisticated nonlinear and/or time-dependent modeling is permitted, but programs featuring these models are best classified as research tools, and their use requires appropriate technical expertise.

Generally, when the culvert response to soil load only is required, the long-term modulus can be used. The use of a long-term modulus will cause deflections to increase only slightly and will provide an appropriate estimate of long-term thrust. Response to live load should always be modeled with the short-term modulus.

Geometrically nonlinear structural response must be modeled if precise modeling of culvert response at deflection levels exceeding a 5% change in vertical pipe diameter is required. This is not available at present in the public-domain program CANDE (soon available in CANDE 2007), but is available in a number of multipurpose proprietary codes available for use in analysis of soil-structure interaction.

C3.2.3

The interface can play an important role in controlling the shear stresses and normal stresses that pass from soil to culvert. These influence the development of both thrust and moment in the culvert.

Nonlinear elastic finite element procedures must include an explicit interface model to limit shear stress transfer between culvert and backfill. Elastoplastic finite element procedures will implicitly limit the shear strength of the soil-structure interface to the angle of internal friction, ϕ, of the soil.

Specification	Commentary
	Simplified analysis using either a fully bonded or smooth interface condition between the backfill and the pipe may be acceptable, provided the implications for thrust, moment, and deflection are properly assessed. The use of a smooth interface condition between the culvert and the backfill will lead to almost uniform thrust distributions; in particular, the thrust at the springline will be lower than would otherwise be calculated. Bending moments and deflections will be close to those calculated for frictional interface.

Specification

3.2.4 Modeling Construction

The finite element solution must simulate the placement of soil layers beside and over the culvert.

Soil layer thickness should be set to realistic values (thickness similar to lift thickness to be used during construction).

3.3 Modeling Earth Load

Earth loads are modeled using elements that have strength, stiffness, and unit weight. These elements should be used until a cover depth, H, of at least three culvert diameters, or at least up to the top of the trench where one is used for culvert burial and trench depth to the pipe crown is greater than three diameters. Above that position, soil can be represented merely as applied vertical load equivalent to ground self-weight.

Fluid loads need to be considered when the culvert is located below the groundwater level.

Commentary

C3.2.4

Nonlinear soil and structural behavior leads to system response that is load-path dependent. The modeling of culvert construction is normally necessary if reasonable finite element predictions are to be obtained. Most finite element procedures incorporate this capability, although care must be taken to ensure numerical stability.

C3.3

Modeling the earth placed far above the culvert crown as a static distributed load effectively ignores the strength and stiffness of the soil, while considering its load. It will generally provide conservative solutions.

Buoyant unit weight can be used down below the water table and total unit weight above the water table. External fluid loading can be modeled as an inward acting pressure around the pipe surface.

The finite element analysis of trench installations must feature explicit treatment of the shear strength of the trench walls (limiting the shear stresses that develop between the backfill and the soil beside the trench). Very unconservative estimates of pipe response can result if these shear stress limits are neglected. However, caution must be used when using finite element calculations for trench burial, since it is uncertain whether the benefits of trench arching remain over long periods of time.

Specification	Commentary
3.4 Modeling Live Load	**C3.4**
Separate live-load distribution factors may be defined and used in separate calculations for deflection, thrust, and moment. The response of large-diameter culverts should be examined with live loads located at different positions over the culvert (over the crown and over the shoulder, for example).	Successful prediction of culvert response (deflection, thrust, and moment) using two-dimensional finite element procedures can be accomplished provided that three-dimensional live-vehicle loading is modeled as a line load (as in the AASHTO procedures for large-span culverts). Live-load distribution widths may be different for deflection, moment, and thrust, since three-dimensional load spreading may affect each of these differently. Further work is needed to improve the selection of equivalent line loads.

APPENDIX E

Simplified Design of Thermoplastic Pipe

CONTENTS

E.1 Simplified Design Equations

Based on review of previously available simplified design procedures, and through testing conducted as part of this project, the simplified design procedure presented in this appendix is proposed for use in AASHTO.

The proposed method was developed on the philosophy that most culvert installations do not challenge the capacity of a typical pipe, and thus, the simplified method should provide a relatively simple procedure to verify that any given installation is within known bounds that will provide good performance. Comprehensive procedures for analysis are presented in Appendix D.

It has been well established by much previous research that many pipes installed carefully and in complete conformance to good installation requirements will perform much better than predicted by the equations presented herein. A 24-in. (0.6 m) diameter pipe north of Pittsburgh, PA, was installed under 100 ft (30 m) of fill, and except for some material issues, it has performed well. The equations presented herein indicate that under the same installation conditions (SW soil at 100% of maximum standard Proctor density), this same pipe can only be buried 26 ft (8 m) and still meet all applicable factors of safety and would fail at 70 ft (21 m) of fill. To allow designers to take advantage of this dichotomy between typical installations and properly built and inspected installations, we propose decreasing the earth-load factor to 1.3 as used for reinforced concrete culverts and introducing a new factor, $K_E = 1.5$, to restore the typical design safety to historic values. This factor can be held at a value of 1.5 for most installations. For some instances, primarily where pipe would be deeply buried, designers may consider reducing the value of K_E provided that quality control and inspection procedures are at levels to ensure that the installation will meet specifications. Such installations, being deep, expensive, and with severe consequences if they fail, should receive high levels of inspection.

The procedures proposed largely draw on the efforts of past research. In our work in culvert research, we have often found that the original research by people such as Marston and Spangler often showed great insights. As a result, much of this work is still applicable. We give much credit to these past giants of buried pipe research.

E.1.1 Design Procedure

The following design procedure is proposed for thermoplastic culvert pipe. A design example is attached at the end of this appendix in Section E.4.

E.1.1.1 Design for Thrust

Design for thrust requires determining the thrust force, followed by evaluation of the limit states related to hoop compression.

E.1.1.1.1 Thrust-Load Calculation (Factored and Service-Load Calculation). Thrust in the pipe wall should be evaluated for short- and long-term loading conditions. Live loads need not be considered for the long-term condition. The proposed procedure was adopted into AASHTO in 2000 based on work by McGrath (1998a).

Thrust in the pipe wall is computed as

$$T = P\left(\frac{D_o}{2}\right)(\text{lb/ft}) \tag{E.1}$$

where

- T = wall thrust – T_u for factored load and T_s for service load (lb/ft),
- P = the design load – P_u for factored load and P_s for service load (psf), and
- D_o = outside diameter of pipe (ft).

The factored load P_u and the service load P_s are computed as

$$P_u = \gamma_E K_{\gamma E}\,\text{VAF}(P_{sp})T_{rf} + \gamma_L P_L C_L + \gamma_h P_w, \quad (\text{psf}) \tag{E.2}$$

$$P_s = \text{VAF}(P_{sp})T_{rf} + P_L C_L + P_w, \quad (\text{psf}) \tag{E.3}$$

$$\text{VAF} = 0.76 - 0.71\left(\frac{S_H - 1.17}{S_H + 2.92}\right)(\text{dimensionless}) \tag{E.4}$$

$$S_H = \frac{\phi_s M_s R}{E_p A_g}(\text{dimensionless}) \tag{E.5}$$

where

- VAF = vertical arching factor (dimensionless),
- T_{rf} = factor to account for design location,
  - = 0.6 for crown,
  - = 1.0 for springline,
- P_{sp} = soil prism pressure, evaluated at springline (psf),
- H = depth of fill over top of pipe (ft),
- P_L = live-load pressure computed in accordance with AASHTO LRFD Specifications (psf),
- C_L = live-load distribution coefficient = $L_w/D_o \le 1.0$ (dimensionless),
- L_w = live-load distribution width in the parallel to the span of the pipe at the elevation of the crown (ft),
- P_w = hydrostatic water pressure at the springline of the pipe (psf),
  - = $\gamma_w H_w$,
- γ_w = unit weight of water (lb/ft^3),
- H_w = depth of groundwater above springline of pipe (ft),
- γ_E = load factor for earth pressure (dimensionless),
- $K_{\gamma E}$ = installation factor for earth load, 1.0 to 1.5 (use 1.5 unless special construction control is implemented),
- γ_L = load factor for live load (dimensionless),
- γ_h = load factor for hydrostatic pressure (dimensionless),

ϕ_s = resistance factor for soil stiffness (dimensionless),
M_s = secant constrained soil modulus (psi),
R = radius from center of pipe to centroid of pipe profile (in.),
E_p = modulus of elasticity of pipe wall material (psi), and
A_g = gross area of pipe wall per unit length of pipe (in.^{2}/in.); note that a reduced area, A_{eff}, is introduced later. In theory, the design procedure could be iterated using A_{eff}. This is not recommended at this time. This is partly due to the fact that it is a relatively new design procedure and partly to keep the overall procedure within the goads of a "simplified" method.

Use the initial modulus of elasticity to evaluate short-term loading conditions and the long-term modulus for long-term loading conditions. For live-load conditions, the thrust due to live load can be computed with the initial modulus and the thrust due to earth load should be computed using the modulus that represents the specified design life of the installation. For current AASHTO specifications this should be the 75-year modulus. Since the design basis is in strain, the strains due to each load can be added.

Note that the VAF approach is only developed for the embankment load case. No guidance is currently available to predict the reduced loads on pipe in trench conditions. The only trench load theory proposed for flexible pipe was that by Spangler, which does not have good guidance on which input parameters to select. However, traditionally flexible pipe are designed for embankment loads whether placed in embankment or trench conditions, and applying the VAF approach to trench installations is conservative.

The soil prism pressure can be calculated for three conditions, as follows:

1. Water table is above the top of the pipe.

$$P_{sp} = \left[H - \left(H_w - \tfrac{1}{2}D_o\right)\right]\gamma_s + \left(H_w - 0.39D_o\right)\gamma_b \quad (\text{psf}); \quad \text{(E.6)}$$

where
H = depth of fill over top of pipe (ft),
H_w = depth of water above the springline (ft),
D_o = outside diameter of pipe (ft),
γ_s = wet soil density (lb/ft^3), and
γ_b = buoyant soil density (lb/ft^3).

2. Water table is below the top of the pipe.

$$P_{sp} = \left(H + 0.11D_o\right)\gamma_s \quad (\text{psf}) \quad \text{(E.7)}$$

where
H = depth of fill over top of pipe (ft),
D_o = outside diameter of pipe (ft), and
γ_s = wet soil density (lb/ft^3).

3. Water table is at or above the ground surface.

$$P_{sp} = \left(H + 0.11D_o\right)\gamma_b \quad (\text{psf}) \quad \text{(E.8)}$$

The secant constrained soil modulus, M_s, may be selected from Table E-1 based on the backfill type and density and the soil prism pressure, P_{sp}. If the structural backfill material is compacted crushed stone, then the modulus values for Sn-100 may be used. If the backfill is uncompacted crushed stone, use the modulus values for Sn-90. An approximate correlation of the USCS and AASHTO soil classification systems is presented in Table E-2. The width of structural backfill is an important consideration when the in situ soils are soft. Currently, only "Fiberglass Pipe Design," in the *AWWA Manual of Water Supply Practices M45* (AWWA 2005) addresses this issue. In general, if the native soils stand without support, the designer can safely assume they will provide adequate lateral support. This evaluation is based on the structural stability of the trench wall and is unrelated to requirements for bracing the wall for personnel safety.

The secant constrained modulus may also be determined experimentally using the stress-strain curve resulting from a uniaxial strain test on a sample of soil compacted to the field-specified density. The constrained modulus is the slope of the secant from the origin of the curve to a point on the curve corresponding to the soil prism pressure, P_{sp}. Some expert experience is required to conduct this test.

The constrained soil modulus values in Table E-1 are known to be somewhat conservative. McGrath (1998b) noted that the values correlate reasonably closely to Howard's (1977) values for E′, the traditional parameter for deflection. Howard's values were back calculated from field measurements, which mean they likely include the effect of variable construction practices. This provides some conservatism in the deflection predictions.

Thrust due to live load is calculated in accordance with AASHTO procedures, except that two values of live-load thrust can be calculated. Typically, live load is calculated at a depth of the crown. Recent research for NCHRP Project 15-29, Design Specifications for Live Load Distribution to Buried Structures, has shown that this provides a reasonable estimate of peak thrust, but that using the depth to the springline (distributing the load in both directions) also provides a reasonable estimate of springline thrust.

The maximum thrust, crown earth load plus peak live load or springline earth load plus springline live load (plus any water loading in either case) condition, should be evaluated for design. This is demonstrated in the design example.

E.1.1.1.2 Compressive Capacity Considering Local Buckling (Factored and Service-Load Calculation). The factored compressive strain due to factored thrust, incorporating local buckling effects, is

Table E-1. Design values for constrained soil modulus, M_s.

Stress Level, P_{sp} (psi)	Soil Type and Compaction Condition			
	Sn-100 (psi)	Sn-95 (psi)	Sn-90 (psi)	Sn-85 (psi)
1	2,350	2,000	1,275	470
5	3,450	2,600	1,500	520
10	4,200	3,000	1,625	570
20	5,500	3,450	1,800	650
40	7,500	4,251	2,100	825
60	9,300	5,000	2,500	1,000
Stress Level, P_{sp} (psi)		**Si-95 (psi)**	**Si-90 (psi)**	**Si-85 (psi)**
1		1,415	670	360
5		1,670	740	390
10		1,770	750	400
20		1,880	790	430
40		2,090	900	510
60		2,380	1,120	700
Stress Level, P_{sp} (psi)		**Cl-95 (psi)**	**Cl-90 (psi)**	**Cl-85 (psi)**
1		533	255	130
5		625	320	175
10		690	355	200
20		740	395	230
40		815	460	285
60		895	525	345

Notes

1. The soil types are defined by a two-letter designation that indicates general soil classification, Sn for sands and gravels, Si for silts, and Cl for clays. Specific soil groups that fall into these categories, based on ASTM D2487 and AASHTO M145, are listed in Table E-2.
2. The numerical suffix to the soil type indicates the compaction level of the soil as a percentage of maximum dry density determined in accordance with AASHTO T-99.

$$\varepsilon_c^u = \frac{T_u}{A_{eff} E_p} (\text{dimensionless}) \quad \text{(E.9)}$$

The service compressive strain due to service thrust, incorporating local buckling effects, is

$$\varepsilon_c^s = \frac{T_s}{A_{eff} E_p} (\text{dimensionless}) \quad \text{(E.10)}$$

where

T_u = ultimate thrust (lb/ft),
T_s = service thrust (lb/ft),
A_{eff} = effective area of the cross-section, per unit length of pipe; see below (sq in./in.), and
E_p = short- or long-term modulus of pipe material as appropriate (psi).

To evaluate local buckling, the profile is idealized into a series of flat plate elements (Figure E-1; also see Appendix B). The following equations compute the expected widths of each element that will be ineffective due to buckling. The effective area of the profile is determined by subtracting the ineffective area of each element from the gross section area. Although it seems simpler to add the effective areas, the area in the corners

Table E-2. Equivalent ASTM and AASHTO soil classifications.

Basic Soil Type (1)	ASTM D2487	AASHTO M145
Sn (Gravelly sand, SW)	SW, SP GW, GP	A1, A3
Si (Sandy silt, ML)	GM, SM, ML also GC and SC with less than 20% passing #200 sieve	A-2-4, A-2-5, A4
Cl (Silty clay, CL)	CL, MH, GC, SC also GC, and SC with more than 20% passing #200 sieve	A-2-6, A-2-7, A5, A6

Note: The soil classification listed in parentheses is the type that was tested to develop the constrained soil modulus values in Table E-1. The correlations to other soil types are approximate.

of the elements (i.e., (b – w) t) would be neglected. See Figure E-1. The entire process is explained in more detail in Appendix B.

$$A_{eff} = A_g - \sum (b - b_e)t \,(\text{in.}^2/\text{in.}) \tag{E.11}$$

where

$$b_e = \rho b \,(\text{in.}) \tag{E.12}$$

$$\rho = \frac{(1 - 0.22/\lambda)}{\lambda} \,(\text{dimensionless}) \tag{E.13}$$

$$\lambda = \frac{w}{t}\sqrt{\frac{\varepsilon}{k}} \geq 0.673 \,(\text{dimensionless}) \tag{E.14}$$

b_e = element effective width (in.),
ρ = effective width factor (dimensionless),
b = total gross width of element between supporting elements (in.),
w = total clear width of element between supporting elements (in.),
λ = slenderness factor (dimensionless),
t = thickness of element (in.),
ε = strain in element (iteration is not required),
$= \frac{T_u}{A_g E_p}$ (dimensionless), and
k = plate buckling coefficient (k = 4 for supported elements, k = 0.43 for unsupported elements).

An alternative to calculating the effective area based on the profile geometry is to use the results of the proposed stub compression test (see Appendix B for more details). This procedure is completed as follows:

1. Calculate the gross area of the profile, A_g.
2. Run the stub compression test as described in Appendix G and produce the stub compression capacity, P_{sc}, in lb/in. of length as the average of at least three tests on specimens from locations equally spaced around the pipe circumference.

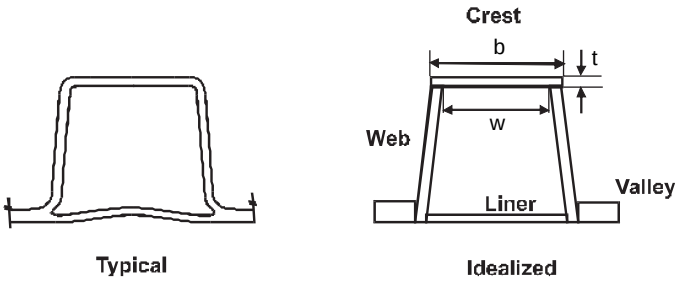

Figure E-1. Idealization of pipe wall profile.

3. Calculate the compression capacity, P_{st}, for short-term loading using a multiplier that is applied to the test result for stub compression capacity, $F_{st} = 0.9$.

$$P_{st} = P_{sc} F_{st} \tag{E.15}$$

4. Calculate the effective area using the compression capacity for short-term loading and the short-term material yield strength, F_{us} (3,000 psi for HDPE), from *AASHTO LRFD Bridge Design Specifications,* Section 12.12, as follows:

$$A_{eff} = \frac{P_{st}}{F_{us}} \leq A_g \tag{E.16}$$

5. Use the effective area to determine the factored compressive strain due to dead-load and live-load thrust demands for design as

$$\varepsilon_{cu} = \frac{T_{DL \cdot u}}{A_{eff} E_{50}} + \frac{T_{LL \cdot u}}{A_{eff} E_0} \tag{E.17}$$

6. Compare factored compressive strain to the material-dependent strain limits.
7. For long-term use $F_{lt} = 0.3$ for HDPE.

The factored compression strain due to thrust, incorporating local buckling effects, ε_c^u, should not exceed the limiting compressive strain of the material.

$$\varepsilon_c^u \leq \phi_T \varepsilon_{yc} \,(\text{dimensionless}) \tag{E.18}$$

where
ε_c^u = factored compressive strain due to thrust (dimensionless),
ϕ_T = resistance factor for thrust effects (dimensionless), and
ε_{yc} = limiting compressive strain of the pipe wall material (dimensionless).

E.1.1.1.3 Global Buckling (Strength Limit State Check). The equations for global resistance presented here are a conservative simplification of the continuum buckling theory proposed by Moore (1990). Detailed analyses using the full theory may be applied in lieu of the method presented here (see Appendix D).

The following strength limit state check provides for safety against local buckling:

$$\varepsilon_c^u \leq \phi_{bck} \varepsilon_{bck} \,(\text{dimensionless}) \tag{E.19}$$

where
ε_c^u = factored compressive strain in the pipe (dimensionless),

ϕ_{bck} = resistance factor for global buckling (dimensionless), and
ε_{bck} = nominal strain capacity for global buckling (dimensionless).

The nominal strain capacity for global buckling of the pipe can be computed as:

$$\varepsilon_{bck} = \frac{1.2C_n\left(E_pI_p\right)^{1/3}}{A_{eff}E_p}\left(\frac{\phi_s M_s\left(1-2\nu\right)}{\left(1-\nu\right)^2}\right)^{2/3} R_h \qquad \text{(E.20)}$$

where
C_n = calibration factor to account for nonlinear effects = 0.55 (dimensionless),
E_p = modulus of elasticity of pipe wall material (psi),
I_p = moment of inertia of pipe profile per unit length of pipe (in.^{4}/in.),
A_{eff} = effective area of pipe profile per unit length of pipe (in.^{2}/in.),
ϕ_s = resistance factor for soil pressure (non-dimensional),
M_s = secant constrained soil modulus (psi),
ν = Poisson's ratio of soil (dimensionless), and
R_h = correction factor for backfill soil geometry, see below (dimensionless).

The term ϕ_s appears in this expression for ε_{bck} to account for backfills that are compacted to levels below that specified in the design. A lower level of compaction ultimately decreases the thrust that can be developed. This phenomenon results from an increase in the vertical arching effect, which is brought on by low compaction levels. For designs meeting all other requirements of these specifications and the *AASHTO LRFD Bridge Construction Specifications*

$$R_h = \frac{11.4}{11+D/H} \qquad \text{(E.21)}$$

where
D = centroidal diameter of pipe (ft) and
H = depth of fill over top of culvert (ft).

The complete theory proposed by Moore (see Appendix D) provides variations in R_h that consider nonuniform backfill support. In the extreme case where the width of structural backfill at the side of the culvert is 0.1 times the span and the modulus of the soil outside of the structural backfill is 0.1 times the modulus of the backfill, then

$$R_h = \frac{20}{56+D/H} \qquad \text{(E.22)}$$

E.1.1.2 Design for Flexure (Strength Limit State Check)

To ensure adequate flexural capacity, the combined strains at the extreme fibers of the pipe profile must be evaluated at the allowable deflection limits against the limiting strain values.

Check the following at the extreme fiber where flexure causes tension:

$$\varepsilon_f - \varepsilon_c^u < \phi_f\left(1.5\varepsilon_{yt}\right)\left(\text{dimensionless}\right) \qquad \text{(E.23)}$$

Check the following at the extreme fiber where flexure causes compression:

$$\varepsilon_f + \varepsilon_c^u < \phi_f\left(1.5\varepsilon_{yc}\right)\left(\text{dimensionless}\right) \qquad \text{(E.24)}$$

A 50% increase in strain limit is allowed for combined strain where
ε_f = flexural strain,
ε_c^u = the factored compressive strain due to factored thrust, incorporating local buckling effects,
ε_{yt} = service limiting tensile strain of the pipe wall material (dimensionless),
ε_{yc} = factored limiting compressive strain of the pipe wall material (dimensionless),
ϕ_f = resistance factor for flexure (dimensionless), and
ε_f = factored strains due to flexure.

In the absence of a more detailed analysis, the flexural strain may be computed based on the empirical relationship between strain and deflection as follows:

$$\varepsilon_f = \gamma_E D_f\left(\frac{c}{R}\right)\left(\frac{\Delta_f}{D}\right)\left(\text{dimensionless}\right) \qquad \text{(E.25)}$$

where
ε_f = factored flexural strain (dimensionless),
D_f = shape factor from Table E-3 (dimensionless),
c = the larger of the distance from neutral axis of profile to the extreme innermost or outermost fiber (in.),
R = radius from center of pipe to centroid of pipe profile (in.),
Δ_f = reduction of vertical diameter due to flexure (in.),
$= \Delta_A - \varepsilon_c^s D$ (the service compressive strain is used, as this is a service condition),
Δ_A = total allowable deflection of pipe, reduction of vertical diameter (in.),
D = diameter to centroid of pipe profile (in.), and
γ_E = load factor for earth pressures (dimensionless).

The expression for ε_f excludes the load factors for live load, γ_L, and hydrostatic pressure, γ_h. This is a simplification justified

Table E-3. Shape factors based on pipe stiffness, backfill, and compaction level.

Pipe Stiffness kPa, (psi)	Pipe Zone Embedment Material and Compaction Level			
	Gravel[1]		Sand[2]	
	Dumped to Slight[3]	Moderate to High[4]	Dumped to Slight[3]	Moderate to High[4]
62 (9)	5.5	7.0	6.0	8.0
124 (18)	4.5	5.5	5.0	6.5
248 (36)	3.8	4.5	4.0	5.5
496 (72)	3.3	3.8	3.5	4.5

[1]GW, GP, GW-GC, GW-GM, GP-GC, and GP-GM per ASTM D2487 (includes crushed rock).
[2]SW, SP, SM, SC, GM, and GC or mixtures per ASTM D2487.
[3]< 85% of maximum dry density per AASHTO T-99, < 40% relative density (ASTM D4253 and D4254).
[4]≥ 85% of maximum dry density per AASHTO T-99, 40% relative density (ASTM D4253 and D4254).

on the basis that live-load levels are low enough to play a minor role in flexural behavior. Additionally, hydrostatic pressure is nearly uniform, and therefore, it causes only a small flexural response. More detailed analyses must consider the likelihood of inconsistent soil support to the pipe in the haunch zone and local deformations during placement and compaction of backfill.

The empirical shape factor is used in the design of fiberglass pipe and is presented in *AWWA Manual of Water Supply Practices* (1996). It demonstrates that flexural strains are highest in low-stiffness pipe backfilled in soils that require substantial compactive effort (silts and clays) and lowest in high-stiffness pipe backfilled in soils that require little compactive effort (sands and gravels). Table E-3 does not cover all possible backfills and density levels. Designers should interpolate or extrapolate the table as necessary for specific projects.

Shape factors for PE can be reduced by 1.0 for PE pipe to account for the significant circumferential shortening.

E.1.1.3 Installation Design: Deflection Check (Service Limit Check)

Deflection is actually controlled through proper construction in the field, and construction contracts should be sure to place responsibility for control of deflections on the contractor. However, feasibility of a specified installation should be checked prior to writing the project specifications.

McGrath (1998a) showed that the Spangler Iowa formula, solved for a 180° bedding angle and the soil prism load, predicts deflections virtually identical to those of the Burns and Richard elasticity theory, which assumes a perfectly bedded pipe. This suggests that, although the Spangler equation has been much discussed and often maligned for inaccuracy, it treats the basic elements of pipe-soil interaction properly in a very simple equation. No other simplified methods are available that offer any improved prediction capability.

Therefore, Spangler's expression for predicting the flexural deflection combined with the deflection due to circumferential shortening provides the best method currently available to predict total field deflection, as follows:

$$\Delta_t \le \Delta_A \tag{E.26}$$

where

Δ_A = total allowable deflection of pipe, reduction of vertical diameter (in.).

The flexural deflection is calculated as

$$\Delta_t = \frac{\left(D_L K_B P_{sp} + C_L P_L\right) D_o}{E_p I_p / R^3 + 0.061 M_s} + \varepsilon_c^s D_i \tag{E.27}$$

where

D_L = deflection lag factor (dimensionless),
K_B = bedding coefficient (dimensionless),
P_{sp} = soil prism pressure (psi),
P_L = live-load pressure computed in accordance with AASHTO specifications (psi),
C_L = live-load distribution coefficient = $L_w/D_o \le 1.0$ (dimensionless),
M_s = secant constrained soil modulus (psi),
E_p = modulus of elasticity of pipe wall material (psi),
I_p = moment of inertia of pipe profile per unit length of pipe (in.^{4}/in.),
D_o = outside diameter of the pipe (in.),
D_i = inside diameter of the pipe (in.),
R = radius from center of pipe to centroid of pipe profile = $D/2$ (in.), and
ε_c^s = compressive strain due to service thrust, incorporating local buckling effects.

This equation uses the constrained modulus, M_s, as the soil property; however, note that the soil prism load is used as input rather than the reduced load used to compute thrust.

This check should be completed to determine that the expected field deflection, computed above, based on thrust and flexure, is lower than the maximum allowable specified deflection limit.

E.1.2 Calculations with the Simplified Design Equations

The proposed design method was exercised on a 48-in. diameter PE pipe to determine allowable fill heights. The calculations for the pipe embedded in Sn95 soil at 100% standard Proctor density are presented in Section E.3. Standard load factors were used, and K_{gE} was set to 1.5 to provide the traditional level of safety. Live load was the LRFD Design Truck (HS20), and groundwater was assumed below the top of the pipe. Results are presented in Table E-3a, which also includes calculations with all load and resistance factors set to 1.0.

Table E-3a shows maximum depths of fill comparable to current AASHTO specifications, but reduces the minimum depth of fill controlled by strength parameters. This is consistent with field observations and the recently completed shallow burial study of 60-in. diameter PE by the Minnesota Department of Transportation (McGrath and Beaver 2005). In all cases, the shallow depths of fill are controlled by the deflection criterion. The deflection equation is conservative, as the soil properties used in the model are known to consider field variations. Good construction practices could likely limit the deflection to less than the allowed value in these cases, and the limits would be less conservative. However, in the case of shallow burial, performance will be limited by road surface performance. The Minnesota study showed significant pavement deterioration at a depth of 1 ft and moderate effects at a depth of 2 ft for 60-in. diameter pipes. That study recommended minimum depths of cover of the larger of 2 ft or one-half pipe diameter.

The maximum depths of fill with all load factors set to 1.0 show a substantial increase for pipe in dense, high-quality backfills. This demonstrates that there is substantial capacity in a buried thermoplastic pipe if construction procedures are followed. This is the basis for introducing the K_{gE} factor.

E.2 Evaluation of Simplified Design Methods

E.2.1 Introduction

A number of limit states are important to the design of buried thermoplastic pipes. Pipe deflections have traditionally been the prime focus of attention when designing to maintain the serviceability of a culvert structure, with deflection limits between 5% and 7.5% specified in various codes of practice (e.g., AASHTO, AS/NZS 2566.1, ASTM F894-95, AWWA M45, CSA B182). Pipe deformations are also associated with the development of circumferential strains in the pipe wall, strains that can induce other limit states.

A study has been undertaken here toward developing limit states design methods for buried thermoplastic pipes. Appendix C described the two-dimensional (2D) finite element analysis and demonstrates that it is an effective tool in calculating pipe deflections and wall strains. Finite element analysis requires both specialized computational facilities and user expertise to apply the method effectively. Although the finite element method is still important for specific high-cost culverts, a procedure based on simplified design equations will be useful for engineers to analyze standard pipeline structures. The simplified equations are suitable for hand calculation or inclusion in a spreadsheet.

This section focuses on the simplified design equations proposed to calculate deflections and wall strains of buried thermoplastic pipe. Performance of the equations is evaluated using the pipe deflections and strains measured in the three biaxial tests described in Appendix C.

E.2.2 Pipe Deflections

Moore (2000) describes the use of the 2D elastic continuum theory (Hoeg 1968) in the design of buried pipes. Continuum theory is rigorous and permits the development of unified design methods that cover metal, concrete, and polymer pipes. However, the equations derived from the theory likely are too complicated for use in codified design procedures and are currently unable to assess the impacts of variable installation

Table E-3a. Results of design calculations: 48-in. diameter corrugated PE pipe.

Soil Type	Minimum Depth of Fill		Maximum Depth of Fill		Maximum Depth of Fill, Factor of Safety = 1	
	Depth (ft)	Limit State	Depth (ft)	Limit State	Depth (ft)	Limit State
Sn100	< 1		26	Compr.	70	Compr.
Sn95	< 1		18	Compr	38	Compr
Sn90	< 1		12	Compr	21	Compr
Sn85	3	Defl.	7	Defl.	9	Defl.
Si95	< 1		12	Compr.	22	Compr.
Si90	2	Defl.	8	Compr./Defl	11	Compr./Defl.
Si85	NG	Defl.	NG	Defl.	6	Defl.

conditions of pipes, such as poor haunch support. Instead, simplified design equations can be developed to use for only each specific class of pipe product (i.e., thermoplastic pipes in this case).

McGrath (1998a) proposed a simplified design equation based on the continuum approach (Burns and Richard 1964) to calculate the vertical deflection of flexible thermoplastic pipes. The equation is expressed in similar form to the Iowa equation (Spangler 1941), but incorporates contributions from both the hoop stiffness and the bending stiffness of the pipe-soil system. McGrath's simplified equation is

$$\frac{\Delta_v}{D} = \left(\frac{q_v}{\frac{EA}{R} + 0.57 M_s} \right) + \left(\frac{D_l K_b q_v}{\frac{EI}{R^3} + 0.061 M_s} \right) \quad \text{(E.28)}$$

The first term in Equation E.28 represents the average circumferential shortening, while the second is the conventional term similar to one Spangler proposed for quantifying bending deformations. However, the constrained modulus, M_s, is used instead of the semi-empirical soil stiffness parameter E′ employed by Spangler. Other parameters of the equations are defined as follows:

Δ_v = vertical deflection,
D = pipe diameter,
q_v = overburden pressure at springline,
E = pipe material modulus,
R = radius of the centroid of the pipe section,
M_s = one-dimensional soil modulus,
K_b = bedding coefficient, and
D_l = deflection lag factor.

E.2.3 Wall Strains

The circumferential wall strain for a buried pipe is composed of its hoop component, ε_h, and bending component, ε_b, so that, $\varepsilon = \varepsilon_h + \varepsilon_b$. The hoop strain is caused by the thrust, and the bending strain is that caused by the bending moment at any pipe section. Simplified equations can be developed to calculate these two components of strains separately.

E.2.3.1 Hoop Strain

Hoop strain at any pipe section can be calculated from thrust acting on the section. When a unit length of the pipe is considered as in plane stress condition, the hoop strain at any section is given by

$$\varepsilon_h = \frac{N}{EA} \qquad \text{for plane stress condition} \quad \text{(E.29)}$$

Here N is hoop thrust at the section, EA is hoop stiffness, both expressed per unit length of the pipe, and ν is Poisson's ratio of pipe material.

The hoop thrust is nonuniform around the circumference for pipes in biaxially stressed ground ($K \neq 1$). McGrath (1998a) proposed a simplified equation to calculate the maximum thrust at the springline of pipes in the biaxial stress field. The equation is expressed in terms of a vertical arching factor (VAF) to account for the interaction of pipe with the surrounding soil, as follows:

$$N = PR_o(VAF) \quad \text{(E.30)}$$

where

N = the maximum thrust at the springline (per unit length),
P = vertical geostatic soil stress, and
R_o = outside radius of pipe.

The vertical arching factor (VAF) in Equation E.30 gives the proportion of the weight of the soil column over the pipe (the prism load) that reaches the pipe. McGrath (1998a) proposed an approximate design solution for the VAF on the basis of his study using the fundamental elasticity solution (Burns and Richard 1964), solutions obtained using the finite element analysis, and experimental evidence. The solution is expressed as

$$VAF = 0.76 - 0.71\left(\frac{S_H - 1.17}{S_H + 2.92} \right) \quad \text{(E.31)}$$

where

S_H = Hoop Stiffness Factor $= \frac{M_s R}{EA}$ and M_s is the constrained modulus of soil.

This section evaluates the approximate equation for VAF using the finite element analyses of the three biaxial tests (with HDPE Pipe 1, HDPE Pipe 2, and PVC pipe) considered in this study. The VAF is calculated using the simplified equation (Equation E.31) for the test pipes and the results are compared with the N/PR_o values obtained from the finite element analysis. Both the measured and the design soil parameters (McGrath et al. 1999) were used in Equation E.31 to calculate the VAF. McGrath et al. (1999) proposed the design values of backfill soil modulus (Table E-4) for three general classes of soil (SW, ML, and CL) at different levels of vertical stress. Soil moduli at any other stresses were interpolated from the values in Table E-4. The digit following the soil class name in Table E-4 designates the percent of maximum standard Proctor density. The backfill material used in the tests was represented by SP85.

Table E-5 compares the VAF given by the various methods. The finite element method provided upper bound values of

Table E-4. Suggested design values for constrained soil modulus, M_s (MPa) (after McGrath et al. 1999).

Stress Level (kPa)	Soil Type and Compaction Condition*								
	SW95	SW90	SW85	ML95	ML90	ML85	CL95	CL90	CL85
7	13.8	8.8	2.24	9.8	4.6	2.5	3.7	1.8	0.9
35	17.9	10.3	3.59	11.5	5.1	2.7	4.3	2.2	1.2
70	20.7	11.2	3.93	12.2	5.2	2.8	4.8	2.5	1.4
140	23.8	12.4	4.48	13.0	5.5	3.0	5.1	2.7	1.6
275	29.3	14.5	5.69	14.4	6.2	3.5	5.6	3.1	2.0
410	34.5	17.2	6.9	15.9	7.1	4.1	6.2	3.6	2.4

*SW: well-graded sand; ML: low plastic silt; and CL: low plastic clay

the VAF as evident in the table. Finite element calculations were approximately 10% higher than those obtained from the simplified equation. The simplified equation with design soil modulus (McGrath et al. 1999) also provided higher values of the factor. Table E-5 includes experimental measurements of VAF, calculated from measured hoop strain and the relation $VAF = EA\varepsilon_h/PR_o$. These indicate that measured values are less than the calculated values of the vertical arching factors. The particular lowest measured value for the HDPE Pipe 2 (Test 2) at 100 kPa represents the reloading path (discussed in Appendix C) for the test. However, Equation E.31 with measured soil modulus provides a VAF close to the measured values for the HDPE pipes, even though the calculated values are somewhat higher for the PVC pipe.

The approximate model (Equation E.31) for the vertical arching factor appeared most effective in estimating the fraction of vertical earth load reaching the pipe. For PVC pipe, the calculated VAF is greater than 1, indicating that the pipe is stiffer than the surrounding soil. All the factors for the HDPE pipe were less than unity.

E.2.3.2 Bending Strain

A semi-empirical formula can be used to calculate the peak circumferential bending strain on a deformed pipe, as follows:

$$\varepsilon_b = D_f\left(\frac{c}{R}\right)\left(\frac{\Delta D_b}{D}\right) \tag{E.32}$$

where

c is the distance to the extreme fiber from the neutral axis and
D is the pipe diameter.

Equation E.32 relates the bending deflection (ΔD_b) of pipe to the peak circumferential bending strain through an empirical strain factor D_f. The bending component of the pipe deflection can be obtained from the second part of Equation E.28, that is

$$\frac{\Delta D_b}{D} = \frac{D_l K_b q_v}{\frac{EI}{R^3} + 0.061 M_s} \tag{E.33}$$

The magnitude of the strain factor is 3 for pure bending of a circular incompressible ring when deformed into an elliptical shape. The maximum bending strain is located at the springline for the elliptically deformed ring. Elliptical deformation is also expected for the buried pipe when the backfill soil is uniform. However, if the backfill soil is nonuniform, the pipe may deflect to a shape different from the elliptical. As

Table E-5. Vertical arching factor.

Tests	Stress Level	Soil Modulus, MPa		VAF			
		Measured	Design	FE	Measured Soil Modulus	Design Soil Modulus	Test
HDPE 1	100	6.87	4.17	0.98	0.89	0.95	0.84
	200	8.88	5.02	0.94	0.86	0.93	0.83
	300	10.31	5.91	0.92	0.83	0.91	0.84
	400	11.47	6.81	0.90	0.81	0.89	0.86
HDPE 2	100	11.3	4.17	0.89	0.83	0.95	0.65
	200	11.3	5.02	0.89	0.83	0.94	0.82
	300	11.3	5.91	0.89	0.83	0.92	0.83
	400	11.3	6.81	0.89	0.83	0.90	0.84
PVC	100	5.28	4.17	1.17	1.02	1.02	0.80
	200	7.42	5.02	1.16	1.01	1.02	0.85
	300	8.97	5.91	1.15	1.00	1.01	0.90
	400	10.25	6.81	1.14	0.99	1.01	0.92

Table E-6. Soil modulus at 100 and 400 kPa.

Stress kPa	Test Pipe	Constrained Modulus, M, MPa		Elastic Modulus E, MPa		Design Constrained Modulus, MPa
		Secant	Average	Secant	Average	
100	HDPE 1	6.8	5.1	4.6	3.4	4.2
	HDPE 2	11.3	11.3	6.4	6.4	
	PVC	5.7	5.5	3.9	3.7	
400	HDPE 1	11.5	9.6	7.7	6.5	6.8
	HDPE 2	11.3	11.3	6.4	6.4	
	PVC	10.3	8.7	6.9	5.9	

a result, the maximum bending strain can be located at locations other than the springline, depending upon the conditions of ground support. The strain factor, D_f, for the maximum bending strain will also be different.

E.2.4 Evaluation of the Simplified Equations

Measurements of the deflection and the circumferential strains are compared with those obtained using the simplified design equations in this section. Results of nonlinear finite element analyses, discussed in Appendix C, and the continuum solution are also included in the comparison.

E.2.4.1 Comparison of Pipe Deflections

The simplified design equation for deflection (Equation E.28) involves a bedding factor and a constrained modulus for the soil. Spangler and Handy (1973) recommended the values of the bedding factor for various bedding angles from 0° (no bedding) to 180° (bedding up to the springline). The bedding angle is defined as the angle subtended by the bedding at the pipe axis. A factor of 0.083 is used in this study as suggested for 180° bedding (Spangler and Handy 1973), since backfill in the test cell was placed with care to provide good support to the pipe. The maximum recommended value is 0.110. The secant value of the constrained modulus, M_s, was used for one set of calculations, and the average value of constrained modulus estimated from the measured stress-strain relations was used for a second set of calculations of deflection. Table E-6 shows the two sets of constrained moduli and the corresponding elastic moduli at 100 kPa and 400 kPa of vertical stresses. The secant and the average modulus are the same for the test with HDPE Pipe 2 (Test 2), since the stress-strain response was essentially linear for the test.

Table E-7 presents the calculated values of pipe deflection obtained using various methods both at 100 kPa and 400 kPa of vertical earth pressure. The continuum theory gave greater deflection values than the simplified method for the lined corrugated HDPE pipes, and lower deflection for the ribbed PVC pipe. The lower deflection for the HDPE pipe and greater deflection for the PVC pipe by the simplified method imply that the structural stiffness of the pipes may affect the performance of the method. The ribbed PVC pipe possessed higher hoop stiffness and less bending stiffness relative to the corrugated HDPE pipe. The simplified method provided higher deflection than the continuum theory for the pipe with high hoop stiffness.

The nonlinear finite element (FE) method generally provided the best estimates of pipe deflection (Table E-7). The FE method accounts for the soil nonlinearity that controls the behavior of the pipes in the biaxial cell. The simplified equation also appears to render a reasonable estimate of pipe deflection. The method with secant modulus provides estimates of the deflections that are unconservative. However, when the average modulus was used, the simplified equation provided higher deflections than the measurements except for HDPE Pipe 2 (in Test 2). Soil response for Test 2 was linear,

Table E-7. Change in vertical diameter (mm) at 100 and 400 kPa.

Stress kPa	Test No.	Expt.	FE	Using Secant Modulus		Using Avg. Modulus		Using Design Modulus	
				(a)*	(b)**	(a)*	(b)**	(a)*	(b)**
100	HDPE 1	–16.8	–16.9	–15.5	–16.1	–19.3	–20.0	–22.4	–22.8
	HDPE 2	–9.9	–10.5	–14.2	–11.1	–14.2	–11.1	–21.7	–19.2
	PVC	–13.1	–13.1	–14.2	–12.9	–14.7	–13.4	–18.5	–16.7
400	HDPE 1	–47.2	–48.1	–42.3	–44.6	–48.3	–50.4	–62.4	–64.4
	HDPE 2	–48.8	–45.1	–34.5	–44.3	–34.5	–44.3	–61.0	–55.5
	PVC	–34.6	–34.7	–34.5	–31.7	–39.7	–36.3	–49.0	–44.7

*(a) Simplified method (McGrath 1998a)
**(b) Continuum theory (Hoeg 1968): bonded interface

Table E-8. Springline strains: comparison with measurements.

		Hoop Strain, %				Bending Strain, %			
			FE:	Simplified				Simplified	
	Stress	Measured	N/EA	M_{meas}	M_{Design}	Measured	FE	M_{meas}	M_{Design}
HDPE 1	100	–0.65	–0.84	–0.69	–0.73	–0.31	–0.32	–0.31	–0.48
	200	–1.27	–1.62	–1.32	–1.43	–0.52	–0.51	–0.48	–0.81
	300	–1.94	–2.37	–1.93	–2.11	–0.74	–0.66	–0.63	–1.05
	400	–2.34	–3.09	–2.51	–2.76	–0.91	–0.80	–0.76	–1.23
HDPE 2	100	–0.47	–0.71	–0.59	–0.68	–0.08	–0.20	–0.22	–0.53
	200	–1.17	–1.42	–1.19	–1.34	–0.35	–0.43	–0.44	–0.91
	300	–1.78	–2.12	–1.78	–1.97	–0.58	–0.68	–0.66	–1.18
	400	–2.39	–2.83	–2.37	–2.58	–0.84	–0.98	–0.88	–1.39
PVC	100	–0.12	–0.19	–0.16	–0.16	–0.11	–0.13	–0.16	–0.20
	200	–0.25	–0.38	–0.32	–0.32	–0.18	–0.20	–0.24	–0.34
	300	–0.39	–0.57	–0.48	–0.48	–0.23	–0.27	–0.30	–0.44
	400	–0.53	–0.76	–0.63	–0.64	–0.27	–0.32	–0.36	–0.52

and therefore, the secant and average modulus are the same. The level of error for the two HDPE pipes increased at 400 kPa by up to 30% (for HDPE Pipe 2), since the geometrical nonlinearity, which occurs at this higher stress, is not captured by the simplified procedure. The simplified equation with design values of soil modulus provides conservative estimates of deflection for all of the pipes.

E.2.4.2 Strains

Hoop strains and bending strains were calculated separately using both the simplified model and the finite element method for comparison. Data are presented in tabular form in Table E-8. Hoop strains from the measurements were estimated as the values at the neutral axis of the profile sections, assuming a linear best-fit distribution of strains through the profile. Hoop strains were then subtracted from the total strain to obtain the bending strains. Figure E-2 illustrates how the hoop and bending strains were estimated from the strain measurements. The dashed line represents the location of the centroidal axis. Strains at the springline of the pipe were considered, since the springline strain on the interior pipe surface corresponds to the maximum value of compression

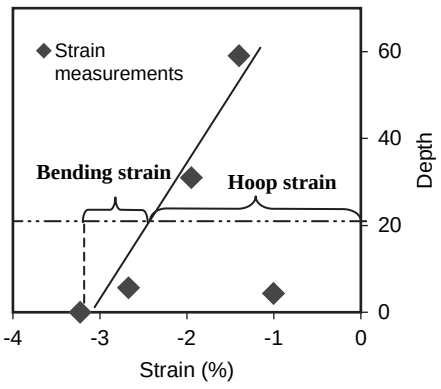

Figure E-2. Components of strains.

for biaxially loaded pipes and therefore is a design limit state. Springline strains on the interior surface of pipes were compared in this study.

Equation E.33 is used to calculate the bending component of deflection for use in bending strain Equation E.32. Values of the empirical factors in Equation E.33 were $D_l = 1$ and $K_b = 0.083$. A strain factor of 3 was used in Equation E.32, assuming an elliptical deformation shape for the pipe in the test cell. Measured values of constrained modulus were used in the simplified equations to calculate the pipe strains.

Figures E-3a and E-3b compare the measurements of hoop and bending strains with the design estimates for HDPE Pipe 1. The finite element method overestimated the hoop strain by about 15% for this profile (Figure E-3a). However, the finite element value of bending strain matches the measurements well (Figure E-3b). Finite element estimates of hoop strains also exceed the measured values for the other profiles (Figures E-4 and E-5), while the bending strains were calculated reasonably. This reveals that the overestimations of strain provided by the FE method seen earlier in Appendix C were due to the excessive hoop strains. Assumption of a bonded interface between the pipe and the surrounding soil may have caused these excessive hoop strains, since this will increase thrusts calculated at the springline. The high hoop strains may also result from plane stress idealization of the pipe in the analysis, which neglects the restraint provided by axial stiffness to the circumferential strains. The VAFs calculated by the finite element method seen earlier in Table E-5 were also higher.

The simplified equations for hoop and bending strains appear to work very well (Figures E-3 and E-4). The equations provided upper bound values of the strains on the PVC pipe. Neglect of the Poisson's effect (restraint provided by axial stiffness) might have contributed to this overestimation. Axial stiffness for the helically wound PVC pipe was high. Large values of bending strains on the second HDPE pipe were also obtained using the simplified method. Performance of

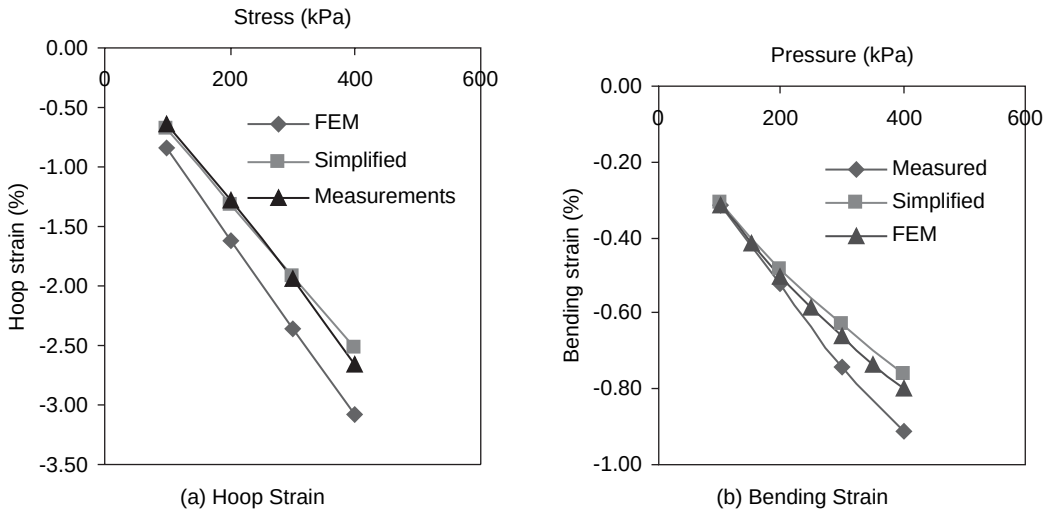

Figure E-3. Comparison of strains on HDPE Pipe 1.

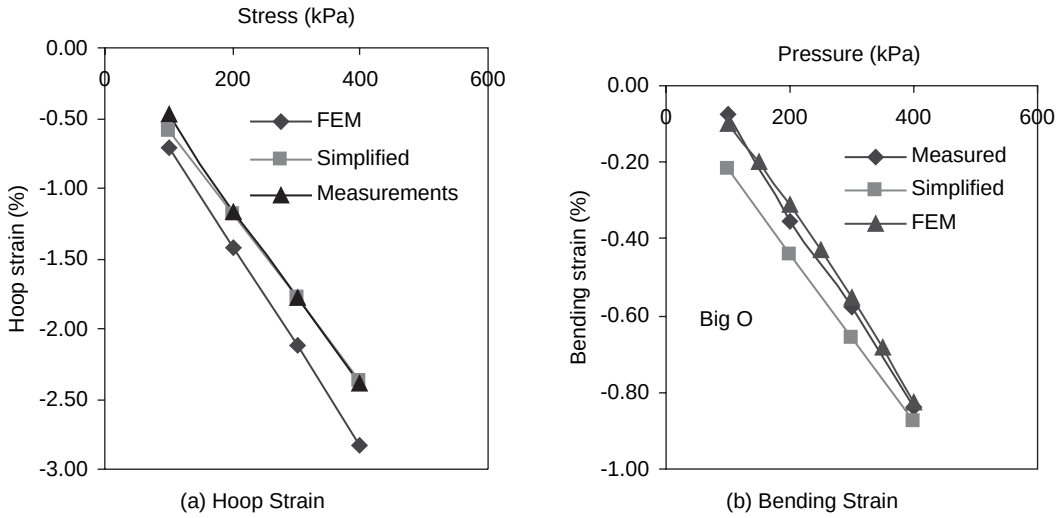

Figure E-4. Comparison of strains on HDPE Pipe 2.

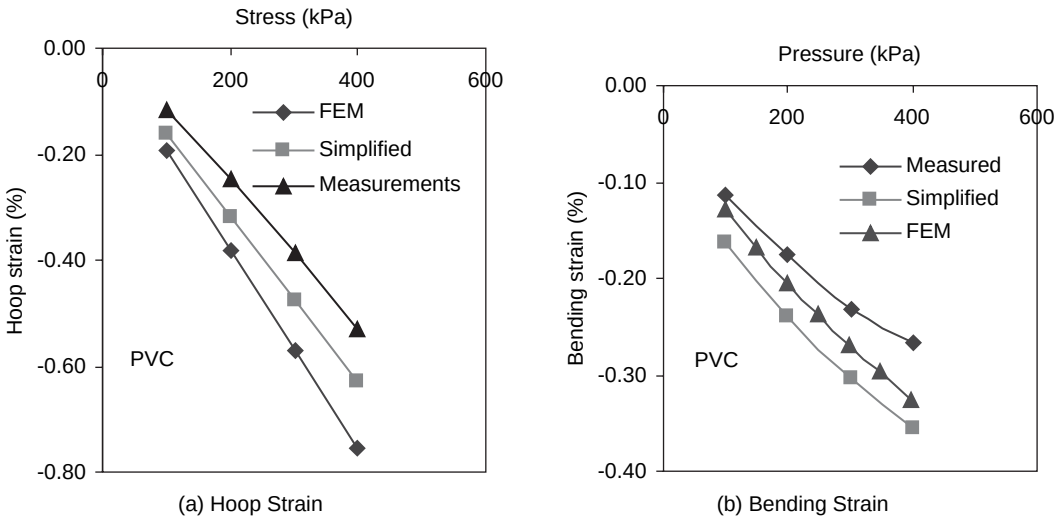

Figure E-5. Hoop and bending strain comparison for PVC pipe.

Table E-9. Shape factor for peak bending strain.

Tests		HDPE 1	HDPE 2	PVC
D_f	FE	2.8-2.9	2.9-3.2	2.9-3.0
	Expt.	2.6-3.0	2.0-2.7	2.4

the equation for bending strain depends on choice of the parameters like D_f and K_b. The D_f value of 3 used in the calculation is applicable for elliptical shape of deformation, an idealized pattern that will not be achieved in any experiments. For nonelliptical deformation, the strain factor for the springline bending strain is less (Dhar and Moore 2001). The factor is back calculated using the bending strains, and the bending deflection $(D_v - D_h)/2$ given by the finite element analysis and the measurements as shown in Table E-9. The finite element method provided D_f values close to 3 (for a carefully installed pipe), which is for elliptical deformation given that backfill soil was assumed uniform in the FE analysis. The experimental values of the D_f factor are somewhat less than 3 as a result of factors like nonuniform ground supports and/or the approximate nature of strain gage readings.

The simplified models with design soil parameters (McGrath 1998a) furnished conservative estimates (greater values) of strains, since the design soil moduli are less than the measured values (Table E-8).

E.2.5 Summary

Analysis reveals that although the finite element method is suitable for comprehensive design calculations for high-cost or unusual installation, the simplified design equations proposed by McGrath (1998a) are more suitable design tools for standard buried pipe installations. The simplified equation for deflection incorporates both of the hoop and bending stiffness components of the pipe-soil response, where the first of these terms is very important for compressible pipe like thermoplastic culverts. The structural stiffness of the pipes may have an influence on the performance of the equation, since the method was found to overestimate deflections for pipe with high hoop stiffness (e.g., ribbed PVC pipe) relative to pipe with low hoop stiffness (e.g., corrugated HDPE pipe).

The calculation method proposed for hoop and bending strains can be used to estimate the circumferential strains at the springline of the pipe. The vertical arching factor (VAF) provides a reasonable approximation of the effects of soil-pipe interaction on the springline thrust.

However, the performance of any method relies on the appropriateness of the constitutive model used to characterize the material behavior. The nonlinear soil model used in finite element calculations effectively simulates the nonlinear soil response, but this is difficult to include in simplified design models. Instead, a linear soil model with modulus averaged over the stress range provided the best characterization of the accumulated effects of soil nonlinearity for the tests considered in this research.

Shape factor D_f used in the simplified equations is estimated from the maximum bending strain obtained from the measurements and the finite element analyses of the tests. Finite element values of the factor were close to 3 for well-installed pipe, which is for elliptical deformed shape, since the finite element solution employed uniform properties for the soil surrounding the pipe. Measure values of the D_f were less than 3, indicating nonuniformity of the backfill soil modulus.

E.3 Simplified Design Example

This design example presents example calculations to demonstrate the proposed simplified design method for thermoplastic pipe. In this example a colon followed by an equal sign, := , indicates a calculation. The equal sign alone indicates the result of a calculation, or the statement of a previously defined term.

INPUTS

Load factors

earth	$\gamma_E := 1.3$
earth load coefficient to provide historical safety	$K_{\gamma E} := 1.5$
live	$\gamma_L := 1.75$
water	$\gamma_w := 1.0$

Resistance factors

thrust	$\phi_T := 1.00$
soil stiffness	$\phi_s := 0.90$
global buckling	$\phi_{bck} := 0.70$
flexure	$\phi_f := 1.00$

Material properties: pipe

Initial modulus of elasticity	$E_{ps} := 110ksi$
long term modulus of elasticity	$E_{pl} := 21ksi$
tensile limiting strain (assumes load factor of 1.5 on service tensile strain limit in LRFD Specifications)	$\varepsilon_{yt} := -0.075$
compressive limiting strain	$\varepsilon_{yc} := 0.041$

Geometric properties

Pipe material	Pipe := "PE"
outside diameter	$D_o := 54.26in$
inside diameter	$D_i := 48in$
total allowable deflection of pipe, reduction of vertical diameter, as percentage of D_i	AllowableDeflectionRatio := 5%

Material properties: soil

soil type for constrained modulus of elasticity	"Sn" for sand, "Si" for silt, or "Cl" for clay	SoilType := "Sn"
compaction condition - % of maximum standard Proctor density	100, (only avail for Sn) 95, 90, or 85	CompactionCondition := 100
soil type to determine shape factor	"G" for gravel or "S" for sand	GravelOrSand := "S"
wet soil unit weight	$\gamma_s := 120pcf$	
water unit weight	$\gamma_{wa} := 62.4pcf$	
buoyant soil unit weight	$\gamma_{buo} := 75pcf$	
Poisson's ratio of soil	$\upsilon := 0.3$	

Miscellaneous Factors

calibration factor for non-linear effects in the global buckling equation $C_n := 0.55$

deflection lag factor $D_L := 1.5$

deflection bedding coefficient $K_B := 0.1$

plate buckling coefficient $k := 4.0$

factor to account for uncertainty in water level $K_{wa} := 1.3$

earth load factor for crown thrust $T_{rf} := 0.6$

Applied loads

depth of fill above top of pipe $H_f := 25ft$

depth of water above pipe springline $H_w := 0ft$

live load (wheel load) $LL := 16kips$

wheel spacing on axle $wh_{sp} := 6ft$

axle spacing $ax_{sp} := 14ft$

live load distribution factor $LLDF := 1.15$

multiple presence factor $mp := 1.2$

impact - varies linearly from 1.33 at 0 ft depth of fill to 1.00 at 8.0 ft depth of fill. 1.00 for depths of fill greater than 8.0 ft.

$$Imp := \begin{cases} 1.0 + 0.33 \cdot \dfrac{8 \cdot ft - H_f}{8 \cdot ft} & \text{if } H_f \le 8 \cdot ft \\ 1.0 & \text{otherwise} \end{cases} \qquad Imp = 1$$

length of wheel contact area $L_0 := 10in$

width of wheel contact area $W_0 := 20in$

DEFINE PROFILE GEOMETRY AND COMPUTE SECTION PROPERTIES

The profile geometry is idealized as a series of flat elements

Profile type = corrugated

number of elements $n := 6$

element index $i := 1..n$

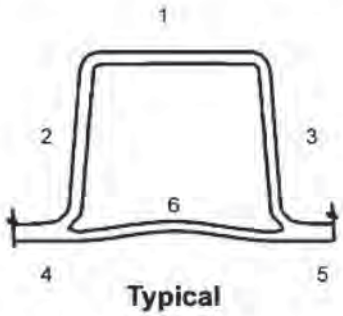

Typical

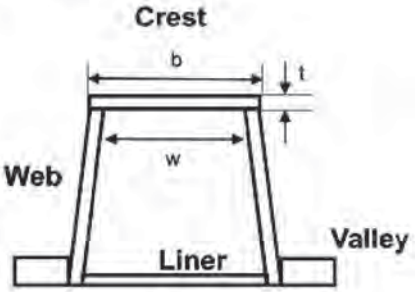

Idealized

Note: In the figure for the idealized section, the valley is shown as two separate elements (Element Nos. 4 and 5 above), symmetric about the corrugation centerline. For calculations which use the term "w," the Valley is treated as a single element (Element No. 4) with two times the width of the half elements

element number $i =$	gross width, used for Aα $b_i :=$	thickness $t_i :=$	clear width $w_i :=$	$w_i =$		inclination (circumferetial=0 deg radial=90 deg) $\theta_i :=$	vertical distance of element from inside edge $y_i :=$	
1	3.204 · in	0.16in	$b_1 - t_2 - t_3$	2.841	in	0deg	3.049 · in	Crest
2	2.991in	0.1815in	$b_2 - t_4$	2.7		83deg	1.484 · in	Web
3	2.991in	0.1815in	$b_2 - t_5$	2.7		83deg	1.484 · in	Web
4	0.942in	0.291in	$b_4 + b_5$	1.884		0deg	0.1450 · in	Valley
5	0.942in	0.291in	0 · in	0		0deg	0.1450in	Valley
6	3.604in	0.12in	b_6	3.604		0deg	0.06 · in	Liner

$Period := b_4 + b_5 + b_6 + t_2 + t_3$ $\quad Period = 5.851\ in$

In the above, the following parameters are defined or computed:

i	index that represents the element number
b_i	total width of an idealized element (see figure above)
t_i	thickness of an idealized element (see figure above)
w_i	clear width of an element (see figure above)
θ_i	angle of element relative to inside surface of profile
y_i	distance from inside surface of profile to centroid of element
Period	length of one cylce of the pipe wall profile

Compute Area and moment of inertia of profile

Variables used in the following sections include the profile terminology defined above and the following. Values for previously defined variables are provided:

A_g	area of pipe wall profile per unit length of pipe
y_c	distance from inside surface of profile to the centroid of the corrugation
I_p	moment of inertia of the pipe profile per unit length of pipe
D	diameter of pipe to centroid of profile
$D_i = 4\,ft$	inside diameter of pipe
R_m	radius of pipe to centroid of profile
PS	pipe stiffness
$E_{ps} = 110000\,psi$	short term modulus of elasticity

gross area of corrugation per unit length of pipe

$$A_g := \frac{\sum_{i=1}^{n} \left(b_i \cdot t_i\right)}{Period} \qquad A_g = 0.441 \frac{in^2}{in}$$

distance of profile centroid from inside surface

$$y_c := \frac{\sum_{i=1}^{n} \left(b_i \cdot t_i \cdot y_i\right)}{\sum_{i=1}^{n} \left(b_i \cdot t_i\right)} \qquad y_c = 1.272\,in$$

moment of inertia of corrugation per unit length of pipe

$$I_p := \frac{1}{Period} \cdot \sum_{i=1}^{n} \left[b_i \cdot t_i \cdot \left(y_i - y_c\right)^2 + \frac{b_i \cdot t_i \cdot \left[\left(t_i\right)^2 \cdot \sin\left(\frac{\pi}{2} - \theta_i\right)^2 + \left(b_i\right)^2 \cdot \cos\left(\frac{\pi}{2} - \theta_i\right)^2 \right]}{12} \right] \qquad I_p = 0.650 \frac{in^4}{in}$$

diameter to centroid of pipe wall profile

$$D := D_i + 2y_c \qquad D = 50.54\,in$$

radius to centroid of pipe wall profile

$$R_m := \frac{D}{2} \qquad R_m = 25.27\,in$$

Calculated Pipe stiffness

$$PS := E_{ps} \cdot I_p \div \left(0.149 \cdot {R_m}^3\right) \qquad PS = 30 \frac{lbf}{in \cdot in}$$

Note: Calculated pipe stiffness is typically higher than the stiffness determined in the parallel plate test due to geometric effects. The calculated properties are used in design.

LOAD CALCULATIONS

Live load

Live load spreads with increasing depth of fill as a function of the live load distribution factor, LLDF. Compute the depth at which load spreading from individual wheels on the same axle interact, $H_{int.wh}$, and the depth at which wheels on adjacent axles, $H_{int.ax}$, interact:

In these equations:

$wh_{sp} = 6\,ft$	center to center spacing of wheels on one axle
$W_0 = 1.667\,ft$	width of wheel footprint at surface
$ax_{sp} = 14\,ft$	center to center spacing of wheels on adjacent axles
$L_0 = 0.833\,ft$	length of wheel footprint at surface
$LLDF = 1.15$	live load distribution factor, rate of increase of wheel load spread with depth of fill

Determine depth at which wheels and axles interact

$$H_{int.wh} := \frac{wh_{sp} - W_0}{LLDF} \qquad H_{int.wh} = 3.77\,ft$$

$$H_{int.ax} := \frac{ax_{sp} - L_0}{LLDF} \qquad H_{int.ax} = 11.45\,ft$$

Compute thrust at top of pipe and springline - thus, evaluate live load at both depths

LL @ Top of pipe - Compute distribution length and width of live load at top of pipe as a function of the depth of fill and whether or not the depth is less than or greater than the interaction depths, $H_{int.ax}, H_{int.wh}$:

In these equations:

$H_f = 7.62\,m$	depth of fill to top of pipe
L_L	live load distribution legnth parallel to pipe diameter as a function of depth
L_w	live load distribution width parallel to flow in pipe as a function of depth
P_{LL}	total live load of all overlapping wheels

live load application length - parallel to pipe diameter $L_L := \begin{cases} L_0 + LLDF \cdot H_f & \text{if } H_f < H_{int.ax} \\ L_0 + LLDF \cdot H_f + ax_{sp} & \text{otherwise} \end{cases}$ $L_L = 43.6\,ft$

live load application width - parallel to flow in pipe $L_w := \begin{cases} W_0 + LLDF \cdot H_f & \text{if } H_f < H_{int.wh} \\ W_0 + LLDF \cdot H_f + wh_{sp} & \text{otherwise} \end{cases}$ $L_w = 36.4\,ft$

total surface live load considered in design $P_{LL} := \begin{cases} LL & \text{if } H_f < H_{int.ax} \wedge H_f < H_{int.wh} \\ 2 \cdot LL & \text{if } H_f < H_{int.ax} \wedge H_f \geq H_{int.wh} \\ 2 \cdot LL & \text{if } H_f \geq H_{int.ax} \wedge H_f < H_{int.wh} \\ 4 \cdot LL & \text{otherwise} \end{cases}$ $P_{LL} = 64\,kips$

Determine if live load length exceeds the pipe diameter. Compute the ratio of L_w to D_o. If this is less than one, the load spread is less than the diameter and the ratio should be used as the live load distribution coefficient. If the ratio is greater than one, set the live load coefficient to 1.0. This coefficient is used later to determine the total load on the culvert.

live load distribution coefficient $C_L := \min\left(\frac{L_w}{D_o}, 1.0\right)$ $C_L = 1$

Calculate the live load pressure at the top of the pipe:

In these equations:

P_{Ltop}	live load magnitude at the depth of the top of the pipe:
$P_{LL} = 64\,kips$	total live load applied to the loaded area
$Imp = 1.0$	factor to account for impact
$mp = 1.2$	multiple presence factor
$L_w = 36.4\,ft$	live load distribution width parallel to flow in pipe at depth of top of pipe
$L_L = 43.6\,ft$	live load distribution length parallel to pipe diameter at depth of top of pipe

live load pressure $P_{Ltop} := \frac{P_{LL} \cdot Imp \cdot mp}{L_w \cdot L_L}$ $P_{Ltop} = 48\,psf$

Calculate live load pressure at the springline (Assumes that live load spreads along length of pipe as it attenuates from the crown to the springline). Calculation and terms are the same as above for top of pipe except that the distribution width is computed at the depth of the springline by adding 0.5 times the outside diameter to the depth of fill.

live load application width - parallel to pipe diameter $L_{w.sp} := \begin{cases} W_0 + LLDF \cdot (H_f + 0.5 \cdot D_o) & \text{if } H_f + 0.5 \cdot D_o < H_{int.ax} \\ W_0 + LLDF \cdot (H_f + 0.5 \cdot D_o) + wh_{sp} & \text{otherwise} \end{cases}$ $L_{w.sp} = 39.0\,ft$

live load pressure at springline $P_{Lsl} := \frac{P_{LL} \cdot Imp \cdot mp}{L_{w.sp} \cdot L_L}$ $P_{Lsl} = 45\,psf$

Hydrostatic pressure - calculate based on depth to springline of pipe. If water level is below springline set to 0 psf.

In this calculation:

P_w	hydrostatic pressure at springline level of pipe
$H_w = 0\,ft$	depth of water above pipe springline
$\gamma_{wa} = 62.4\,pcf$	unit weight of water

$$P_w := \begin{cases} \gamma_{wa} \cdot H_w & \text{if } H_w > 0 \cdot ft \\ 0 \cdot psf & \text{otherwise} \end{cases} \qquad P_w = 0.0\,psf$$

Vertical soil pressure - compute vertical soil pressure on pipe. First compute soil prism load.

In the following calculation:

P_{sp}	soil pressure due to the soil prism load
$H_f = 25\,ft$	depth of fill to top of pipe
$D_o = 4.52\,ft$	outside diameter of pipe
$H_w = 0\,ft$	depth of water above pipe springline
$\gamma_s = 120\,pcf$	wet unit weight of soil
$\gamma_{buo} = 75\,pcf$	buoyant unit weight of soil

$$P_{sp} := \begin{cases} \left(H_f + 0.11 \cdot D_o\right) \cdot \gamma_s & \text{if } H_w < 0.5 \cdot D_o \\ \left[H_f - \left(H_w - 0.5 \cdot D_o\right)\right] \cdot \gamma_s + \left(H_w - 0.5 \cdot D_o + 0.11 \cdot D_o\right) \cdot \gamma_{buo} & \text{if } H_w \geq 0.5 \cdot D_o \wedge H_w \leq H_f + 0.5 \cdot D_o \\ \left(H_f + 0.11 \cdot D_o\right) \cdot \gamma_{buo} & \text{otherwise} \end{cases}$$

1st line: water table below top of pipe
2nd line: water table above pipe
3rd line: water table at or above ground surface

$P_{sp} = 3060\,psf$

Compute the Vertical arching factor, VAF, to determine the portion of the soil prism load that is actually applied to the pipe.

In this calculation:

M_s	soil secant constrained modulus
$\phi_s = 0.9$	resistance factor to account for variability in soil stiffness
$R_m = 2.11\,ft$	radius to centroid of pipe wall
$E_{pl} = 21000\,psi$	long-term modulus of elasticity of pipe wall material, in this case the 75 year modulus is used.
$A_g = 0.441\,\frac{in^2}{in}$	gross area of pipe wall per unit length of pipe
S_H	hoop stiffness factor (ratio of soil stiffness to pipe hoop stiffness
VAF	vertical arching factor - ratio of load on pipe to total weight of soil prism load

secant constrained modulus — interpolated from LRFD Table 12.12.3.4-1 — $M_s = 5.62\,ksi$

hoop stiffness factor — $S_H := \frac{\phi_s \cdot M_s \cdot R_m}{E_{pl} \cdot A_g}$ — $S_H = 13.8$

vertical arching factor $VAF := 0.76 - 0.71\left(\frac{S_H - 1.17}{S_H + 2.92}\right)$ $VAF = 0.22$

Total pressure on pipe - earth plus water plus live load. Check crown and springline thrust conditions:

In these calculations:

P_{usl}	factored thrust at pipe springline
$\gamma_E = 1.30$	earth load factor
$\gamma_L = 1.75$	live load factor
$\gamma_w = 1.00$	water load factor
$K_{\gamma E} = 1.5$	installation factor
$VAF = 0.223$	vertical arching factor computed above
$P_{sp} = 21.2\,psi$	soil prism pressure
$C_L = 1.00$	live load distribution factor, value of 1.0 indicates load over entire pipe diameter
$P_{Lsl} = 0.31\,psi$	live load pressure at springline
$P_{Ltop} = 0.336\,psi$	live load pressure at crown
$K_{wa} = 1.3$	factor to account for variability in water load
$P_w = 0\,psi$	hydrostatic pressure
P_{utop}	factored thrust at pipe crown
T_{rf}	factor to reduce earth load thrust at crown of pipe

Springline

factored $P_{uSL} := \gamma_E \cdot K_{\gamma E} \cdot VAF \cdot P_{sp} + \gamma_L \cdot C_L \cdot P_{Lsl} + \gamma_w \cdot K_{wa} \cdot P_w$ $P_{uSL} = 1412\,psf$

Top of pipe

factored $P_{utop} := \gamma_E \cdot K_{\gamma E} \cdot VAF \cdot P_{sp} \cdot T_{rf} + \gamma_L \cdot C_L \cdot P_{Ltop} + \gamma_w \cdot K_{wa} \cdot P_w$ $P_{utop} = 885\,psf$

Determine if load is controlled at the crown or the springline. Calculate the controlling value, P_u, as the maximum of the two values just computed.

$P_u := \max(P_{uSL}, P_{utop})$ $P_u = 1412\,psf$

Compute the maximum factored thrust, T_u, as the total load pressure time 0.5 of the pipe diameter:

Factored thrust $T_u := P_u \cdot \frac{D_o}{2}$ $T_u = 3193\,plf$

Compressive strain calculation considering local buckling (Use long-term E for earth and water and short-term E for live loads

Compute the compressive strain in the pipe wall. The calculation for strain is identical to the computation of thrust force above exept that thrust force is divided by modulus of elasticity, E_{pl}, or E_{ps}, depending on the duration of the load under consideration and by the gross cross-sectional area per unit length, A_g.

In these calculations, in addition to the variables defined above:

ε_u factored compressive strain in pipe wall

$E_{pl} = 21000\,psi$ long-term modulus of elasticity (75 year modulus in this case)

$E_{ps} = 110000\,psi$ initial modulus of elasticity

$A_g = 0.441\,\frac{in^2}{in}$ gross area of pipe wall profile per unit length.

factored compressive strain

$$\varepsilon_u := \left(\begin{cases} \dfrac{\gamma_E \cdot K_{\gamma E} \cdot VAF \cdot P_{sp}}{E_{pl}} + \dfrac{\gamma_L \cdot C_L \cdot P_{Lsl}}{E_{ps}} + \dfrac{\gamma_w \cdot K_{wa} \cdot P_w}{E_{pl}} & \text{if } P_{uSL} > P_{utop} \\ \dfrac{\gamma_E \cdot K_{\gamma E} \cdot VAF \cdot P_{sp} \cdot T_{rf}}{E_{pl}} + \dfrac{\gamma_L \cdot C_L \cdot P_{Ltop}}{E_{ps}} + \dfrac{\gamma_w \cdot K_{wa} \cdot P_w}{E_{pl}} & \text{otherwise} \end{cases} \right) \cdot \frac{D_o}{2 \cdot A_g}$$

$\varepsilon_u = 2.74\,\%$

Evaluate local buckling - first compute the slenderness factor, γ_i, for each element of the profile (values for w_i and t_i) provided above. Other parameters include:

$\varepsilon_u = 2.74\,\%$ factored compressive strain in pipe wall

$k = 4$ edge support coefficient, value is for element supported at each end.

Slenderness factors for i = 1 to 6:

slenderness factor
AASHTO Eq. 12.12.3.4-4

$$\lambda_i := \max\left[\left(\frac{w_i}{t_i}\right) \cdot \sqrt{\frac{\varepsilon_u}{k}}, 0.673\right]$$

$\lambda^T = (1.471 \quad 1.232 \quad 1.232 \quad 0.673 \quad 0.673 \quad 2.488)$

Use the slenderness factor to compute effective width factor. The effective width factor is the portion of the element that has not buckled and is still carrying load at the strain level ε_u. Then compute the actual effective width as the product for the effective width, ρ_i, times the clear element widths, $w^T = (2.841 \quad 2.7 \quad 2.7 \quad 1.884 \quad 0 \quad 3.604)\,in$

Effective width factors for i = 1 to 6:

effective width factor
AASHTO Eq. 12.12.3.4-3

$$\rho_i := \frac{1 - \frac{0.22}{\lambda_i}}{\lambda_i}$$

$\rho^T = (0.578 \quad 0.667 \quad 0.667 \quad 1 \quad 1 \quad 0.366)$

Effective widths for i = 1 to 6:

element effective width

$$w_{e_i} := \rho_i \cdot w_i$$

$w_e^T = (1.643 \quad 1.8 \quad 1.8 \quad 1.884 \quad 0 \quad 1.321)\,in$

Compute the net effective area of the element by removing the portion of the elements that have buckled. This is done by subtracting the ineffective area from the gross area. In this calculation:

A_{eff} effective cross-sectional area of profile per unit length after removing areas that have buckled

$A_g = 0.441 \frac{in^2}{in}$ gross cross-sectional area of profile per unit length

w clear width of individual elements of the profile, provided above

w_e effective width of individual elements of the profile, provided above

$Period = 5.851\ in$ length of one cycle of the pipe wall profile

effective unitized area corrugation cross section (subtract ineffective area from total area)

$$A_{eff} := A_g - \frac{\sum_{i=1}^{n} \left[\left(w_i - w_{e_i}\right) \cdot t_i\right]}{Period} \qquad A_{eff} = 0.305 \frac{in^2}{in}$$

Percentage effective area

$$\frac{A_{eff}}{A_g} = 69\%$$

Compute the increased compressive strain in the pipe based on the effective area. In this calculation:

$\varepsilon_{c.u}$ factored compressive strain considering net effective area

$\varepsilon_u = 2.74\%$ factored compressive strain considering gross area

$A_g = 0.441 \frac{in^2}{in}$ gross area of pipe profile per unit length

$A_{eff} = 0.305 \frac{in^2}{in}$ net effective area of pipe profile per unit length

factored compressive strain in pipe

$$\varepsilon_{c.u} := \varepsilon_u \cdot \frac{A_g}{A_{eff}} \qquad \varepsilon_{c.u} = 3.96\%$$

For use later in service load deflection calculation, compute the service compression strain in the pipe. This calculation is the same as completed above for the factored strain, ε_u, except that no load factors are applied and the net effective area, A_{eff} is used.

service strain on reduced cross-section

$$\varepsilon_{c.s} := \begin{cases} \left(\frac{VAF \cdot P_{sp}}{E_{pl}} + \frac{C_L \cdot P_{Lsl}}{E_{ps}} + \frac{K_{wa} \cdot P_w}{E_{pl}}\right) \cdot \frac{D_o}{2 \cdot A_{eff}} & \text{if } P_{uSL} > P_u \\ \left(\frac{VAF \cdot P_{sp} \cdot T_{rf}}{E_{pl}} + \frac{C_L \cdot P_{Ltop}}{E_{ps}} + \frac{K_{wa} \cdot P_w}{E_{pl}}\right) \cdot \frac{D_o}{2 \cdot A_{eff}} & \text{otherwise} \end{cases} \qquad \varepsilon_{c.s} = 2.03\%$$

Summary of compression strain levels in pipe computed based on net area:

Factored compression strain based on net pipe wall area $\varepsilon_{c.u} = 3.96\%$

Service compression strain based on net pipe wall area $\varepsilon_{c.s} = 2.03\%$

CAPACITY CALCULATIONS AND CHECKS

Compression capacity considering net pipe wall area

Factored compression strain: $\varepsilon_{c.u} = 3.96\%$

Factored capacity (Input strain limit times resistance factor): $\phi_T \cdot \varepsilon_{yc} = 4.10\%$

Capacity check

$$\text{CompressionCheck} := \begin{cases} \text{"OK"} & \text{if } \varepsilon_{c.u} \le \phi_T \cdot \varepsilon_{yc} \\ \text{"Not OK"} & \text{otherwise} \end{cases} \qquad \text{CompressionCheck} = \text{"OK"}$$

Determine total used capactiy: $\dfrac{\varepsilon_{c.u}}{\phi_T \cdot \varepsilon_{yc}} = 96.6\%$ of capacity is used

Global buckling (strength limit state)

Global buckling capacity is determined using the continuum theory. In these calculations:

R_h	correction factor for backfill soil geometry and depth of fill
$D = 4.21\ \text{ft}$	diameter to centroid of pipe wall
$H_f = 25\ \text{ft}$	depth of fill to top of pipe
ε_{bck}	critical buckling strain
C_n	calibration factor for non-linear effects
$E_{pl} = 21000\ \text{psi}$	long-term modulus of elasticity (75 year used in this problem)
$I_p = 0.65\ \frac{\text{in}^4}{\text{in}}$	moment of inertia of pipe wall profile
$A_{eff} = 0.305\ \frac{\text{in}^2}{\text{in}}$	effective area of pipe wall after reduction for local buckling
$\phi_s = 0.9$	resistance factor for soil
$M_s = 5625\ \text{psi}$	constrained modulus of soil, AASHTO Table 12.12.3.4-1
$\upsilon = 0.3$	Poisson's ratio of soil
$\phi_{bck} = 0.7$	resistance factor for buckling capacity

correction factor for backfill soil geometry

$$R_h := \frac{11.4}{11 + \frac{D}{H_f}} \qquad R_h = 1.021$$

strain for global buckling calculation

$$\varepsilon_{bck} := \frac{1.2 \cdot C_n \left(E_{pl} \cdot I_p\right)^{\frac{1}{3}}}{A_{eff} \cdot E_{pl}} \cdot \left[\frac{\phi_s \cdot M_s \cdot (1 - 2 \cdot \upsilon)}{(1 - \upsilon)^2}\right]^{\frac{2}{3}} \cdot R_h \qquad \varepsilon_{bck} = 64.6\%$$

Factored strain (Load): $\varepsilon_{c.u} = 4.0\%$

Factored capacity: $\phi_{bck} \cdot \varepsilon_{bck} = 45.3\%$

Capacity check

$$\text{GlobalBucklingCheck} := \begin{cases} \text{"OK"} & \text{if } \varepsilon_{c.u} \le \phi_{bck} \cdot \varepsilon_{bc} \\ \text{"Not OK"} & \text{otherwise} \end{cases} \qquad \text{GlobalBucklingCheck} = \text{"OK"}$$

Determine total capacity used

$$\frac{\varepsilon_{c.u}}{\phi_{bck} \cdot \varepsilon_{bck}} = 8.8\%$$

Flexure (strength limit state)

Evaluate flexural capacity assuming pipe is deflected to service limit. The available flexural capacity is determined based on the pipe deflection available after subtracting the service deflection due to hoop compression, $\varepsilon_{c.s} = 2\%$, from the specified service deflection limit, $\text{AllowableDeflectionRatio} = 5\%$. In these calculations:

$PS = 29.7$ psi	Pipe stiffness, computed above - short term pipe stiffness is used in deflection calculation
$D_{f.init}$	Initial shape factor interpolated from AASHTO Table 12.12.3.5.4b-1
$D_{f.des}$	shape factor after correcting for type of thermoplastic and checking against minimum value
Δ_A	allowable total deflection, inches
Δ_f	allowable deflection due to flexure, inches
$D = 4.21$ ft	diameter to centroid of pipe wall
$D_i = 4$ ft	inside pipe diameter
$D_o = 4.52$ ft	outside pipe diameter
$R_m = 2.11$ ft	radius to centroid of pipe wall
c_{max}	maximum distance from pipe wall centroid to extreme fiber
$\gamma_E = 1.3$	earth load factor

Allowable deflection

$$\Delta_A := \text{AllowableDeflectionRatio} \cdot D_i \qquad \Delta_A = 2.4\,\text{in}$$

Determine deflection capacity available for flexure by subtracting deflection due to hoop compression from allowable deflection:

$$\Delta_f := \Delta_A - \varepsilon_{c.s} \cdot D \qquad \Delta_f = 1.372\,\text{in}$$

Determine maximum distance from centroidal axis of profile to extreme fiber

$$c_{max} := \max\left(\frac{D_o - D}{2}, \frac{D - D_i}{2}\right) \qquad c_{max} = 1.858\,\text{in}$$

Initial shape factor interpolated from AASHTO Table 12.12.3.5.4b-1 $\qquad D_{f.init} = 3.98$

If pipe material is PE, reduce D_f for PE material

$$D_{f.1} := \begin{cases} D_{f.init} - 1 & \text{if Pipe} = \text{"PE"} \\ D_{f.init} & \text{otherwise} \end{cases}$$

Check that reduced value of D_f is not less than 3.5. Set result to design value of D_f

$$D_{f.des} := \text{if}\left(D_{f.1} < 3.5, 3.5, D_{f.1}\right) \qquad D_{f.des} = 3.5$$

Calclulate maximum available factored bending strain:

$$\varepsilon_f := \gamma_E \cdot D_{f.des} \cdot \left(\frac{c_{max}}{R_m}\right) \cdot \left(\frac{\Delta_f}{D}\right) \qquad \varepsilon_f = 0.91\%$$

Check combined bending tension and compression strain limits

Tension - computed as factored flexural strain minus hoop compression strain

factored tensile strain (load) $\varepsilon_f - \varepsilon_{c.u} = -3.1\,\%$

Factored capacity (input capacity times resistance factor) $\phi_f \cdot \varepsilon_{yt} = -7.5\,\%$

capacity check

$$\text{FlexuralTensionCheck} := \begin{cases} \text{"OK"} & \text{if } \varepsilon_f - \varepsilon_{c.u} \geq \phi_f \cdot \varepsilon_{yt} \\ \text{"Not OK"} & \text{otherwise} \end{cases}$$

$\text{FlexuralTensionCheck} = \text{"OK"}$

Determine total capacity used (0% indicates no tension in pipe wall:

$$\varepsilon_{used.tension} := \begin{cases} 0 & \text{if } \varepsilon_{yt} < 0.0 \\ \dfrac{\varepsilon_f - \varepsilon_{c.u}}{\phi_f \cdot \varepsilon_{yt}} & \text{otherwise} \end{cases}$$

$\varepsilon_{used.tension} = 0\,\%$

Compression - computed as sum of factored flexural strain and hoop compression strain:

factored compression strain (load): $\varepsilon_f + \varepsilon_{c.u} = 4.9\,\%$

Factored capacity (50% increase is allowed for capacity due to combined strain):

$$\phi_f \cdot \left(1.5 \cdot \varepsilon_{yc}\right) = 6.15\,\%$$

capacity check

$$\text{FlexuralCompressionCheck} := \begin{cases} \text{"OK"} & \text{if } \varepsilon_f + \varepsilon_{c.u} \leq \phi_f \cdot \left(1.5 \cdot \varepsilon_{yc}\right) \\ \text{"Not OK"} & \text{otherwise} \end{cases}$$

$\text{FlexuralCompressionCheck} = \text{"OK"}$

Determine total capacity used

$$\frac{\varepsilon_f + \varepsilon_{c.u}}{\phi_f \cdot \left(1.5 \cdot \varepsilon_{yc}\right)} = 79.2\,\%$$

Deflection (service limit state)

The pipe design is now complete as controlling deflection in the field is a contractor responsibility.

This check ensures that the expected deflection after installation is reasonable and should be achievable in the field. The calculation is made using the short term modulus of elasticity. In these calculations:

Δ_t	total service field deflection
$K_B = 0.1$	bedding coefficient, accounts for inconsistent bedding support
$D_L = 1.5$	deflection lag coefficient, accounts for time dependent increase in load
$P_{sp} = 21.248\,psi$	soil prism load
$C_L = 1.0$	live load coefficient - portion of diameter over which live load is applied
$P_{Ltop} = 0.336\,psi$	live load at top of pipe
$D_o = 4.522\,ft$	outside pipe diameter
$E_{ps} = 110000\,psi$	initial modulus of elasticity of pipe
$I_p = 0.65\,\frac{in^4}{in}$	moment of inertia of pipe wall
$R = 1.823\,K \cdot m^{-1}\,ft$	radius to centroid of pipe wall profile
$M_s = 5625\,psi$	constrained modulus of soil
$\varepsilon_{c.s} = 2.03\,\%$	service hoop compresion strain in pipe
$D_i = 4\,ft$	inside pipe diameter

total field deflection add bending deflection to hoop compression deflection:

$$\Delta_t := \frac{K_B \cdot \left(D_L \cdot P_{sp} + C_L \cdot P_{Ltop}\right) \cdot D_o}{\frac{E_{ps} \cdot I_p}{R_m^{\,3}} + 0.061 \cdot M_s} + \varepsilon_{c.s} \cdot D_i \qquad \Delta_t = 1.48\,in$$

deflection as a percentage of diameter $\frac{\Delta_t}{D_i} = 3.082\,\%$

specified limiting deflection — Allowable deflection $\Delta_A = 2.40\,in$

capacity check

$$DeflectionCheck := \begin{cases} \text{"OK"} & \text{if } \Delta_t \le \Delta_A \\ \text{"Not OK"} & \text{otherwise} \end{cases} \qquad DeflectionCheck = \text{"OK"}$$

Determine total capcity used: $\frac{\Delta_t}{\Delta_A} = 61.6\,\%$

CALCULATION SUMMARY

Inputs

Depth/Backfill

Depth of fill over top of pipe	$H_f = 25$ ft	Soil type	SoilType = "Sn"
Depth of water over springline	$H_w = 0$ ft	Compaction level	CompactionCondition = 100

Load Factors

Earth	$\gamma_E = 1.30$	Earth load Installaction factor	$K_{\gamma E} = 1.50$
Live	$\gamma_L = 1.75$		
Water	$\gamma_w = 1.00$	Water load design factor	$K_{wa} = 1.3$

Resistance Factors

Tension	$\phi_T = 1.00$	Soil	$\phi_s = 0.90$
Flexure	$\phi_f = 1.00$	Buckling	$\phi_{bck} = 0.70$

Misc. Factors

Deflection lag factor	$D_L = 1.5$	Pipe Material	Pipe = "PE"
Design shape factor	$D_{f.des} = 3.5$	Crown thrust reduction factor	$T_{rf} = 0.6$

Outputs - Capacity Checks

Condition	*Strain or Deflection level*	*Fraction of capacity used*
Hoop Compression		
CompressionCheck = "OK"	$\varepsilon_{c.u} = 3.96\%$	$\frac{\varepsilon_{c.u}}{\phi_T \cdot \varepsilon_{yc}} = 96.6\%$
GlobalBucklingCheck = "OK"	$\varepsilon_{c.u} = 3.96\%$	$\frac{\varepsilon_{c.u}}{\phi_{bck} \cdot \varepsilon_{bck}} = 8.8\%$
Combined strain - tension		
FlexuralTensionCheck = "OK"	$\varepsilon_f - \varepsilon_{c.u} = -3.1\%$ (negative value indicates no tension)	$\frac{\varepsilon_f - \varepsilon_{c.u}}{\phi_f \cdot (\varepsilon_{yt})} = 40.7\%$
Combined strain - compression		
FlexuralCompressionCheck = "OK"	$\varepsilon_f + \varepsilon_{c.u} = 4.9\%$	$\frac{\varepsilon_f + \varepsilon_{c.u}}{\phi_f \cdot (1.5 \cdot \varepsilon_{yc})} = 79.2\%$
Deflection		
DeflectionCheck = "OK"	$\frac{\Delta_f}{D_i} = 3.08\%$	$\frac{\Delta_f}{\Delta_A} = 61.6\%$

E.4 References

American Water Works Association, "Fiberglass Pipe Design," in *AWWA Manual of Water Supply Practices M45,* 2nd ed., American Water Works Association, Denver, CO, 2005.

ASTM International, *ASTM F894-98a–Standard Specification for Polyethylene (PE) Large Diameter Profile Wall Sewer and Drain Pipe.* ASTM International, West Conshohocken, PA, 1998.

Burns, J. Q. and Richard, R. M., "Attenuation of Stresses for Buried Cylinders," *Proceedings of Symposium on Soil-Structure Interaction,* University of Arizona, Tucson,1964.

Dhar, A. S., Moore, I. D., and McGrath, T. J., "Thermoplastic Culvert Deformation and Strain: Evaluation Using Two-Dimensional Analyses," submitted to the ASCE *Journal of Geotechnical & Geoenvironmental Engineering,* 2001.

Hoeg, K., "Stress against Underground Cylinder," *Journal of Soil Mechanics and Foundation Engineering,* Vol. 94, No. SM4, 1968.

Howard, A. K., "Modulus of Soil Reaction Values for Buried Flexible Pipe," *ASCE Journal of the Geotechnical Engineering Division,* Vol. 103, No. GT1, 1977.

McGrath, T. J., "Design Method for Flexible Pipe," a report prepared for the Polyethylene Pipe Design Task Group of the AASHTO Flexible Culvert Liaison Committee, Simpson Gumpertz & Heger Inc., Arlington, MA, 1998a.

McGrath, T. J., "Replacing E′ with the Constrained Modulus in Buried Pipe Design," in *Pipelines in the Constructed Environment,* J. P. Castronovo and J. A. Clark, eds., American Society of Civil Engineers, Reston, VA, 1998b.

McGrath, T. J. and Beaver, J. L., *Performance of Thermoplastic Pipe under Highway Vehicle Loading,* Research Report to Minnesota DOT, Oakdale, MN, Simpson Gumpertz & Heger Inc., 2005.

McGrath, T. J., Selig, E. T., Webb, M. C., and Zoladz, G. V., "Pipe Interaction with the Backfill Envelope," Publication No. FHWA-RD-98-191, Federal Highway Administration, U.S. Department of Transportation, McLean, VA, June 1999.

Moore, I. D., "Three-Dimensional Response of Elastic Tubes," *International Journal of Solids and Structures,* Vol. 26, No. 4, 1990.

Moore, I. D., "Culverts and Buried Pipelines," in *The Geotechnical and Geoenvironmental Handbook,* R. K. Rowe, ed., Kluwer Academic Publishers, 2000.

Spangler, M. G., "The Structural Design of Flexible Pipe Culverts," *Iowa Engineering Experiment Station Bulletin 153.* Iowa State University, Ames, 1941.

Spangler, M. G. and Handy, R. L., *Soil Engineering,* Intext Educational Publishers, New York, 1973.

APPENDIX F

HDPE Resin Studies

CONTENTS

F.1 Introduction

An investigation was conducted to evaluate the effects of carbon black with carrier resin and percentage of regrind material on the properties of corrugated HDPE pipe. Twenty-four specimens of corrugated HDPE pipe resins from five different manufacturers were investigated. Table F-1 lists the sample compositions. To simplify the overall presentation, the statistical method of analysis and the raw data are presented in Sections F.1 and F.7 at the end of this appendix.

F.2 Material Tests

The types of tests are focused on material characterization to identify effects of carbon black, regrind materials, and manufacturing process. Table F-2 shows the tests performed on the pipe samples. Table F-3 shows the summary of the test data.

F.2.1 Density

The density tests were performed according to ASTM D792, Procedure B, using isopropanol. Three replicates were tested for each material. The resin densities of pipe plaque and pipe liner were calculated by subtracting the carbon black content in the materials, as shown in Section F.6.1. The amount of carbon black in the pipe and pipe plaque was determined according to ASTM D4218. A minimum of two replicates were tested on each material. The average carbon black value was used in the calculation to obtain the resin density in the pipe plaque and pipe liner, as shown in Section F.7.1.

The average resin density values that were obtained by either direct measurement or calculation are summarized in Table F-4. The calculated density of the pipe plaque is slightly different from the measured density of the corresponding resin plaque as indicated by the ratio between pipe plaque (PP) and resin plaque (RP). The range of their differences is within ± 0.002 g/cc. In contrast, the density of the pipe liner is lower than the corresponding plaque for pipes less than 60 in. in diameter; such difference could be caused by the faster cooling used in the pipe manufacturing process. For 60-in. pipes, the thickness of the liner is significantly greater than pipes with smaller diameters, slowing down the cooling rate to that similar to 15°C/min.

F.2.2 Melt Index

The melt index (MI) of resin and pipe was evaluated according to ASTM D1238 using a condition of 2.16 kg/190°C. The effects of carbon black with carrier resin on MI were evaluated by comparing MI value between virgin resin and pipe, as shown in Table F-5. The individual MI data are included

Table F-1. HDPE corrugated pipe samples.

Company	Pipe Diameter (in.)	Pure Resin Type	Pure Resin (%)	Regrind (%)	Carbon Black (Estimated) (%)
I	24	A	100	0	2 – 2.5
			90	10	2 – 2.5
			80	20	2 – 2.5
	36	B	100	0	2 – 2.5
			90	10	2 – 2.5
			80	20	2 – 2.5
	48	C	100	0	2 – 2.5
	60	D	100	0	2 – 2.5
II	24	E	100	0	2 – 2.5
			90	10	2 – 2.5
			80	20	2 – 2.5
	36	F	100	0	2 – 2.5
	48	G	100	0	2 – 2.5
			90	10	2 – 2.5
			80	20	2 – 2.5
	60	F	100	0	2 – 2.5
III	24	I	100	0	2 – 2.5
	30	J	100	0	2 – 2.5
			80	20	2 – 2.5
IV	24	K	100	0	2 – 2.5
V	24	L	100	0	2 – 2.5
			90	10	2 – 2.5
			80	20	2 – 2.5
	36	M	100	0	2 – 2.5

Table F-2. Type of tests and test material.

Test	ASTM	Test Material
Density	D792	Resin plaque, pipe plaque, and pipe liner
Melt Index	D1238	Resin and pipe
Carbon Black	D4218	Pipe
Oxidative Induction Time (OIT)	D3895	Resin and pipe
Notched Constant Ligament Stress (NCLS)	F2136	Resin plaque, pipe plaque, and pipe liner

Table F-3. Summary of HDPE test results.

Code	Diameter (inch)	Pure Resin (%)	Test										
			Density			C.B.	M.I.		NCLS			OIT	
			Resin	Pipe plq	Pipe liner	Pipe	Resin	Pipe	Resin plq	Pipe plq	Pipe Liner	Resin	Pipe
I	24	100%	0.950	0.948	0.944	3.3	0.24	0.20	41.1	36.4	29.2	17.4	24.3
		90%		0.948	0.944	3.4		0.20		26.3	24.0		18.6
		80%		0.949	0.944	3.4		0.21		24.3	21.5		21.3
	36	100%	0.951	0.948	0.944	3.1	0.32	0.28	32.9	34.6	24.5	66.3	44.6
		90%		0.949	0.944	3.0		0.29		32.3	23.6		42.9
		80%		0.949	0.944	3.0		0.28		36.1	28.3		39.9
	48	100%	0.950	0.950	0.948	2.5	0.10	0.13	39.7	29.4	13.0	16.3	24.6
	60	100%	0.948	0.946	0.945	3.0	0.09	0.13	30.2	15.2	9.7	15.4	10.4
II	24	100%	0.949	0.949	0.943	2.5	0.20	0.20	24.3	19.6	11.8	28.2	30.7
		90%		0.948	0.944	2.5		0.18		29.7	18.5		30.4
		80%		0.949	0.944	2.5		0.17		31.1	17.9		28.5
	36	100%	0.951	0.952	0.947	2.5	0.18	0.16	28.5	28.2	20.6	26.3	25.9
	48	100%	0.951	0.950	0.944	2.5	0.20	0.19	21.3	18.5	12.1	19.8	23.1
		90%		0.950	0.945	2.7		0.15		30.6	13.7		26.6
		80%		0.950	0.945	2.7		0.15		28.7	13.4		27.1
	60	100%	0.947	0.949	0.948	2.4	0.18	0.16	32.5	25	22.8	39.9	34.2
III	24	100%	0.952	0.951	0.945	2.1	0.22	0.20	56	53.9	32.1	12.9	24.5
	30	100%	0.952	0.951	0.945	2.4	0.20	0.17	12.5	14.5	9.1	25.7	30.5
		80%		0.952	0.947	3.3		0.18		16.9	9.7		33.7
IV	24	100%	0.951				0.34		25.7			6.8	
	Crown	95%						0.29		21.2			10.7
	Liner	75%		0.9516	0.947	2.5		0.38		16.6	8.9		8.3
V	24	100%	0.951	0.951	0.944	2.2	0.27	0.25	34.1	24.8	12.1	11.1	8.3
		90%		0.950	0.946	2.1		0.25		21.6	10.2		7.9
		80%		0.950	0.946	2.1		0.25		22.7	10.8		8.6
	36	100%	0.951	0.951	0.949	2.0	0.37	0.28	37.7	26.3	14.4	7.5	8.8

Table F-4. Average density values of resin plaque, pipe plaque, and pipe liner.

Type	Density (g/cc)			Density Ratio	
	Resin Plaque (RP)	Pipe Plaque (PP)	Pipe Liner (PL)	PP/RP	PL/RP
I-24"	0.950	0.948	0.944	0.998	0.996
I-36"	0.951	0.948	0.944	0.997	0.996
I-48"	0.950	0.950	0.948	1.000	0.998
I-60"	0.948	0.946	0.945	0.998	0.999
II-24"	0.949	0.949	0.943	1.000	0.994
II-36"	0.951	0.952	0.947	1.001	0.995
II-48"	0.951	0.950	0.944	1.001	0.993
II-60"	0.947	0.949	0.948	1.002	0.999
III-24"	0.952	0.951	0.945	1.001	0.993
III-30"	0.952	0.951	0.945	1.001	0.993
V-24"	0.951	0.951	0.944	1.000	0.993
V-36"	0.951	0.951	0.949	1.000	0.998

Table F-5. Average MI values between resin and pipe (100% virgin).

Type	MI (g/10 min)		MI Ratio
	Resin	Pipe	P/R
I-24"	0.24	0.20	0.83
I-36"	0.32	0.28	0.88
I-48"	0.10	0.13	1.30
I-60"	0.09	0.13	1.44
II-24"	0.20	0.20	1.00
II-36"	0.18	0.16	0.89
II-48"	0.20	0.19	0.95
II-60"	0.18	0.16	0.89
III-24"	0.22	0.20	0.92
III-30"	0.20	0.17	0.85
V-24"	0.27	0.25	0.93
V-36"	0.37	0.28	0.76

as Section F.7.2 of this report. A majority of the pipe samples exhibited a slightly lower MI value than the corresponding resin due to the addition of carbon black. The carbon black particles changed the rheology by increasing the viscosity of the molten polymer. However, two pipe samples (I-48″ and I-60″) exhibited an opposite behavior; the MI values of these pipes are higher than the corresponding resins. A possible reason causing such difference may be the carrier resin that was used in blending carbon black to form the master batch. (A master batch typically contains 50% of carbon black and is blended with a carrier resin.) The proportionate master batch and virgin resin are mixed in the extruder to obtain a pipe with desired carbon black content. If the carrier resin in the master batch has significantly higher MI value than the virgin pipe resin, the MI of the final pipe product would be affected accordingly.

Table F-6 shows the MI of the pipes with different percentages of regrind. The test data indicate that MI is not affected by the regrind in the majority of the pipes. However, in Pipes II-24″ and II-48″, the regrind material lowers the MI value. It is possible that this is due to the regrind material coming from different pipes with lower MI values.

Table F-6. Effects of quantity of regrind on MI.

Pipe	MI (g/10 min)		
	0% Regrind	10% Regrind	20% Regrind
I-24"	0.20	0.20	0.21
I-36"	0.28	0.29	0.28
II-24"	0.20	0.18	0.17
II-48"	0.19	0.15	0.15
III-30"	0.17	NA	0.18
V-24"	0.25	0.25	0.25

NA = Not available

F.2.3 Stress Crack Resistance Evaluation

The stress crack resistance (SCR) properties were evaluated on resin plaque, pipe plaque, and pipe liner using the NCLS test, ASTM F2136. For pipe liner tests, the test specimens were taken from the orientation parallel to the longitudinal axis of the pipe, and the notch was introduced on the outer surface of the liner, as shown in Figures F-1a and F-1b. The notch depth was 20% of the thickness of the specimen. The average test values are shown in Table F-3, and individual data are included in Section F.7.3. The average coefficient variation for the resin plaque, pipe plaque, and pipe liner are 9.6%, 6.1%, and 8.0%, respectively. These values are less than 15%, which is the average repeatability value listed in the precision statement of the test. Thus, the tests exhibited acceptable consistency within a single laboratory.

F.3 Evaluation of Test Results

F.3.1 Effects of Carbon Black

Table F-7 shows the average NCLS failure times of resin plaques, pipe plaques, and pipe liners from 100% virgin materials. For a majority of the resins, the addition of carbon black with carrier resin decreased the SCR of the resin, as indicated by the PP/RP ratio. The reduction factors range from 0.50 to 0.99. For Pipes I-36″ and III-30″, the failure time of PP is slightly higher than the corresponding RP.

F.3.2 Effects of Manufacturing Process

The effects of manufacturing process on SCR are obtained by comparing the NCLS failure time of pipe liner with the corresponding pipe plaque, as shown in Table F-8. In each set of pipe samples, which includes 100% virgin, 10% regrind, and 20% regrind pipes, the pipe liner to pipe plaque (PL/PP) ratio is relatively similar, since these pipes were produced from the same machine. However, the processing effects vary significantly from machine to machine. The average reduction factors range from 0.44 to 0.91. Table F-9 shows the reduction factors based on the diameter of the pipes and shows no trend. It seems that for pipes with diameters of 36 in. and 48 in., the reduction factors are very similar regardless of the manufacturers, while large differences are observed for pipes with diameters of 24 in. and 60 in.

F.3.3 Combined Effects of Carbon Black and Pipe Processing

The combined effects of carbon black and manufacturing process on SCR of the resin are reflected by the ratio between pipe liner (PL) and resin plaque (RP) and can also be obtained by multiplying the reduction factors from carbon black (PP/RP)

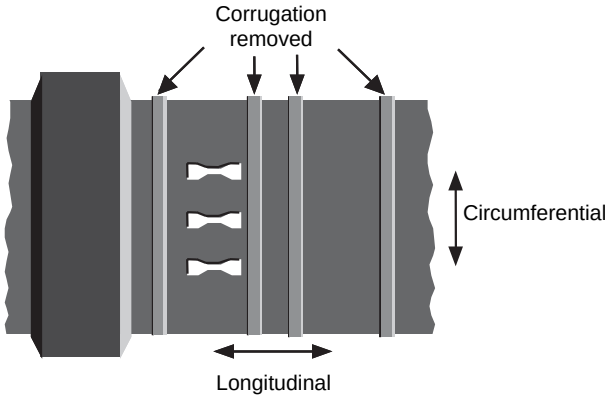

(a) Orientation of the NCLS test specimen taken from the pipe liner

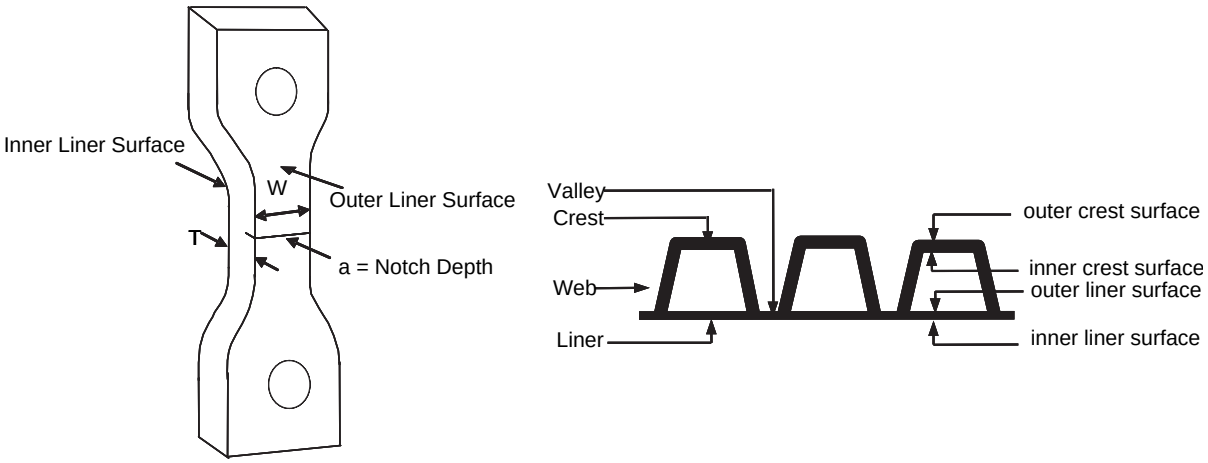

Front view of the notched specimen

(b) Location of the notch with respect to the pipe liner surfaces

Figure F-1. NCLS test specimens from pipe liner.

Table F-7. Average NCLS test value on 100% virgin pipe materials.

Type	NCLS (hour)			NCLS Ratio	
	Resin Plaque (RP)	Pipe Plaque (PP)	Pipe Liner (PL)	PP/RP	PL/RP
I-24"	41.1	36.4	29.2	0.89	0.71
I-36"	32.9	34.6	24.5	1.05	0.74
I-48"	39.7	29.4	13.0	0.74	0.33
I-60"	30.2	15.2	9.7	0.50	0.32
II-24"	24.3	19.6	11.8	0.81	0.49
II-36"	28.5	28.2	20.6	0.99	0.72
II-48"	21.3	18.5	12.1	0.87	0.57
II-60"	32.5	25.0	22.8	0.77	0.70
III-24"	56.0	53.9	32.1	0.96	0.57
III-30"	12.5	14.5	9.1	1.16	0.73
V-24"	34.1	24.8	12.1	0.73	0.35
V-36"	37.7	26.3	14.4	0.70	0.38
Average				**0.85**	**0.51**
Standard Deviation				0.18	0.17
Coefficient Variation				0.21	0.33

Table F-8. Effect of pipe manufacturing processing on SCR.

Pipe	NCLS (hour)						NCLS Ratio			Average Ratio Value
	100% Virgin		10% Regrind		20% Regrind		PL/PP			
	Pipe Plaque	Pipe Liner	Pipe Plaque	Pipe Liner	Pipe Plaque	Pipe Liner	100% Virgin	10% Regrind	20% Regrind	
I-24"	36.4	29.2	26.3	24.0	24.3	21.5	0.80	0.91	0.88	0.87
I-36"	34.6	24.5	32.2	23.6	36.1	28.3	0.71	0.73	0.78	0.74
I-48"	29.4	13.0	NA	NA	NA	NA	0.44	NA	NA	0.44
I-60"	15.2	9.7	NA	NA	NA	NA	0.64	NA	NA	0.64
II-24"	19.6	11.8	29.7	24.7	31.1	17.9	0.60	0.62	0.58	0.60
II-36"	28.2	20.6	NA	NA	NA	NA	0.74	NA	NA	0.74
II-48"	18.5	12.1	30.6	13.7	28.7	13.4	0.65	0.45	0.47	0.52
II-60"	25.0	22.8	NA	NA	NA	NA	0.91	NA	NA	0.91
III-24"	53.9	32.1	NA	NA	NA	NA	0.60	NA	NA	0.60
III-30"	14.5	9.1	NA	NA	16.9	9.7	0.63	NA	0.57	0.60
IV-24"	NA	NA	NA	NA	16.6	8.9	NA	NA	0.54	0.54
V-24"	24.8	12.1	21.6	10.2	22.7	10.8	0.49	0.47	0.48	0.48
V-36"	26.3	14.4	NA	NA	NA	NA	0.55	NA	NA	0.55
Average										**0.63**
Standard Deviation										0.14
Coefficient Variation										0.22

Note: IV-24" consists of 25% regrind.
NA = Not Available.

Table F-9. Effect of manufacturing process based on different pipe diameters.

Pipe Diameter (in.)	Average PL/PP	Average
24	0.87, 0.62, 0.66, 0.54, 0.48	0.63
30	0.60	0.60
36	0.74, 0.74, 0.77	0.75
48	0.44, 0.52	0.48
60	0.64, 0.91	0.78

and pipe processing (PL/PP). As expected, the reduction factors are greater than carbon black alone, ranging from 0.32 to 0.74, shown in Table F-7.

F.3.4 Effects of Regrind Materials

The effects of regrind materials on the SCR were evaluated on both pipe plaque and pipe liner materials, as shown in Table F-10. For the same pipe sample, the ratio values are relatively similar between plaque and liner, except for Sam-

Table F-10. Effect of regrind materials on SCR.

NCLS Test on Pipe Plaque					
Pipe	NCLS (hour)			Ratio	
	0% Regrind	10% Regrind	20% Regrind	10%/0% Ratio	20%/0% Ratio
I-24"	36.4	26.3	24.3	0.72	0.67
I-36"	34.6	32.3	36.1	0.93	1.04
II-24"	19.6	29.7	31.1	1.52	1.59
II-48"	18.5	30.6	28.7	1.65	1.55
III-30"	14.5	NA	16.9	NA	1.17
V-24"	24.8	21.6	22.7	0.87	0.92
Average				**1.15**	
NCLS Test on Pipe Liner					
Pipe	NCLS (hour)			Ratio	
	0% Regrind	10% Regrind	20% Regrind	10%/0% Ratio	20%/0% Ratio
I-24"	29.2	24.0	21.5	0.82	0.74
I-36"	24.5	23.6	28.3	0.96	1.16
II-24"	11.8	18.5	17.9	1.57	1.52
II-48"	12.1	13.7	13.4	1.13	1.11
III-30"	9.1	NA	9.7	NA	1.01
V-24"	12.1	10.2	10.8	0.84	0.89
Average				**1.07**	

ple II-48″. However, large differences are detected among pipes. The uncertainty is the type of regrind being added to these pipes. For Pipes II-24″ and II-48″, the regrind material enhances the SCR of the pipes more than 50%, as indicated in the data obtained from the pipe plaques. Such a large increase suggests that the regrind materials used in these two pipes probably came from materials with better SCR properties (i.e., not the same regrind material from the corresponding pipe containing 100% virgin resin). This hypothesis seems consistent with the MI results of these two pipes, which have lower MI values as regrind is added. The high ratio value of 1.17 for Pipe III-30″ may be contributed by the high carbon black content in the 20% regrind material.

Nevertheless, regardless of the regrind material used, increasing the regrind amount from 10% to 20% does not show significant change in the SCR.

F.3.5 Oxidation Resistance Evaluation

The long-term oxidation resistance of the corrugated pipe was assessed using the OIT test, ASTM D3895. The OIT tests were performed on both resin and finished pipe. Two replicates were tested for each material. The test data are included in Section F.7.4. The OIT value reflects the amount of antioxidant remaining in the material, a higher OIT value indicates a greater amount of antioxidants. Table F-11 presents the average OIT values of resins and pipes, and shows a large variation. In addition, the pipe processing does not seem to decrease the amount of antioxidants in all 12 tested samples, since 7 of the 12 samples exhibit a P/R ratio value greater than 1. (Note that the ASTM standard indicates the repeatability of the test being ± 5% for a HDPE material with OIT value of 163 min.)

Antioxidants can be introduced into a pipe in two ways. One is from the resin support in the virgin resin and the other is from the master batch of carbon black with carrier resin. If antioxidants are included in the virgin resin only, the OIT value of the finished pipe should be lower than the corresponding resin, since some of the antioxidants have been consumed during the pipe extrusion. For example, Pipe I-36″ may fall into this case. On the other hand, if antioxidants are added to the virgin resin as well as the carbon black master batch, the OIT of the finished pipe should exhibit a higher OIT value than the corresponding resin, or small difference in OIT values between resin and pipe. Of the 12 samples, 5 exhibited a 10% or higher increase in the OIT value in the finished pipe relative to the corresponding virgin resin.

Table F-11. OIT value between resin and pipe without regrind.

Type	OIT (min)		OIT Ratio
	Resin	Pipe	P/R Ratio
I-24"	17.4	24.3	1.40
I-36"	66.3	44.6	0.67
I-48"	16.3	24.6	1.51
I-60"	15.4	10.4	0.68
II-24"	28.2	30.7	1.09
II-36"	26.3	25.9	0.98
II-48"	19.8	23.1	1.17
II-60"	39.9	34.2	0.86
III-24"	12.9	24.5	1.90
III-30"	25.7	30.5	1.19
V-24"	11.1	8.3	0.75
V-36"	7.5	8.8	1.17

Due to the uncertainty in the properties of the carbon black master batch, the oxidation resistance of the pipe should be evaluated instead of the virgin resin.

The effects of regrind materials on OIT are shown in Table F-12. In general, the OIT does not change significantly by the amount of regrind. The only exception is I-24″ with 10% regrind.

F.4 Discussion

The effects of carbon black, regrind materials, and manufacturing processing on pipe properties are evaluated by density, MI, NCLS, and OIT tests. The lower density measured in the pipe liner indicates that the pipe was formed at a cooling rate faster than 15°C/min, which is used to prepare the molded plaque. The carbon black in the pipe tends to lower the MI value as the melt viscosity increases, while blending 10% to 20% of regrind to the virgin resin generally does not affect the MI value.

For the SCR property, the addition of carbon black decreases the resistance of the pure resin by an average factor of 0.85

Table F-12. Effect of regrind material in OIT value.

OIT Test On Pipe					
Pipe	OIT (min)			Ratio	
	0% Regrind	10% Regrind	20% Regrind	10%/0% Ratio	20%/0% Ratio
I-24"	24.3	18.6	21.3	0.77	0.88
I-36"	44.6	42.9	39.9	0.96	0.89
II-24"	30.7	30.4	28.5	0.99	0.93
II-48"	23.1	26.6	27.1	1.15	1.17
III-30"	30.5	NA	33.7	NA	1.10
V-24"	8.3	7.9	8.6	0.95	1.04

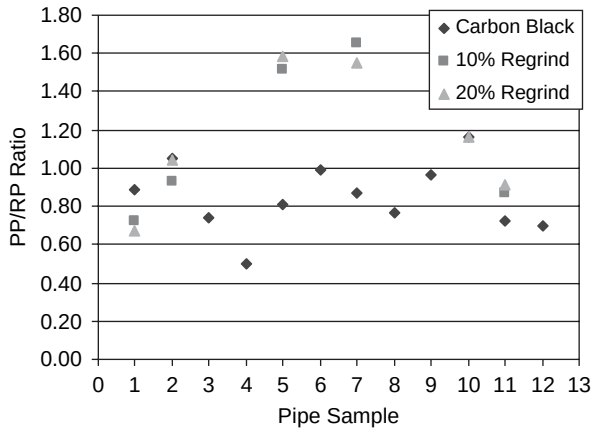

Figure F-2. Effects of carbon black and regrind on the SCR of virgin resin.

(Table F-7 under PP/RP column), while the effect of regrind is strongly dependent on the SCR of the added regrind material. The effects of carbon black and two different levels of regrind in SCR are shown in Figure F-2. Pipes containing 10% and 20% regrind material exhibit similar SCR properties. Note that regrind materials are limited to materials generated from manufacturer's own production, and properties of regrind material are required to meet the same cell classification as new material. In practice, no tests are conducted to determine whether the properties were changed during the initial manufacturing cycle. The proposed finished pipe tests will control properties of pipes that contain regrind material. In summary, blending carbon black and regrind generally decreases the SCR of the virgin resin.

The combined effect of adding 2% to 3% carbon black and up to 20% of regrind material on the SCR of virgin resins is determined by including all 25 PP/RP values. As shown in Table F-13, the overall average of the PP/RP ratio is 0.92. In order to estimate the standard deviation and the 95% single-side confidence interval of each ratio value, the Delta Method is used to analyze the NCLS test data. Furthermore, the 95% single-side confidence interval of the mean ratio value is calculated. (The details of the calculation are presented in Section F.6.) The results are shown in Figure F-3. The 95% single-side confidence interval of the mean is from 0.72 to 1.06.

The appropriate PP/RP value that should be applied to determine the failure time of virgin resin plaque (RP) is evaluated based on the 24-h value set in *NCHRP Report 429* from 19 field-cracked pipes. From a conservative approach, the lower limit of

Table F-13. NCLS test data from resin plaques, pipe plaques, and pipe liners.

Type	Pure Resin (%)	NCLS Test					
		Resin Plaque (RP)	Pipe Plaque (PP)	Pipe Liner (PL)	PP/RP Ratio	PL/PP Ratio	PL/RP Ratio
I-24"	100%	41.1	36.4	29.2	0.89	0.80	0.71
	90%		26.3	24.0	0.64	0.91	0.58
	80%		24.3	21.5	0.59	0.88	0.52
I-36"	100%	32.9	34.6	24.5	1.05	0.71	0.74
	90%		32.3	23.6	0.98	0.73	0.72
	80%		36.1	28.3	1.10	0.78	0.86
I-48"	100%	39.7	29.4	13.0	0.74	0.44	0.33
I-60"	100%	30.2	15.2	9.7	0.50	0.64	0.32
II-24"	100%	24.3	19.6	11.8	0.81	0.60	0.49
	90%		29.7	18.5	1.22	0.62	0.76
	80%		31.1	17.9	1.28	0.58	0.74
II-36"	100%	28.5	28.2	20.6	0.99	0.73	0.72
II-48"	100%	21.3	18.5	12.1	0.87	0.65	0.57
	90%		30.6	13.7	1.44	0.45	0.64
	80%		28.7	13.4	1.35	0.47	0.63
II-60"	100%	32.5	25	22.8	0.77	0.91	0.70
III-24"	100%	56	53.9	32.1	0.96	0.60	0.57
III-30"	100%	12.5	14.5	9.1	1.16	0.63	0.73
	80%		16.9	9.7	1.35	0.57	0.78
IV-24"	95%	25.7	21.2		0.82		
	70%		16.6	8.9	0.65	0.54	0.78
V-24"	100%	34.1	24.8	12.1	0.73	0.49	0.35
	90%		21.6	10.2	0.63	0.47	0.30
	80%		22.7	10.8	0.67	0.48	0.32
V-36"	100%	37.7	26.3	14.4	0.70	0.55	0.38
				Average	**0.92**	**0.63**	**0.59**
				Standard Deviation	**0.27**	**0.15**	**0.18**

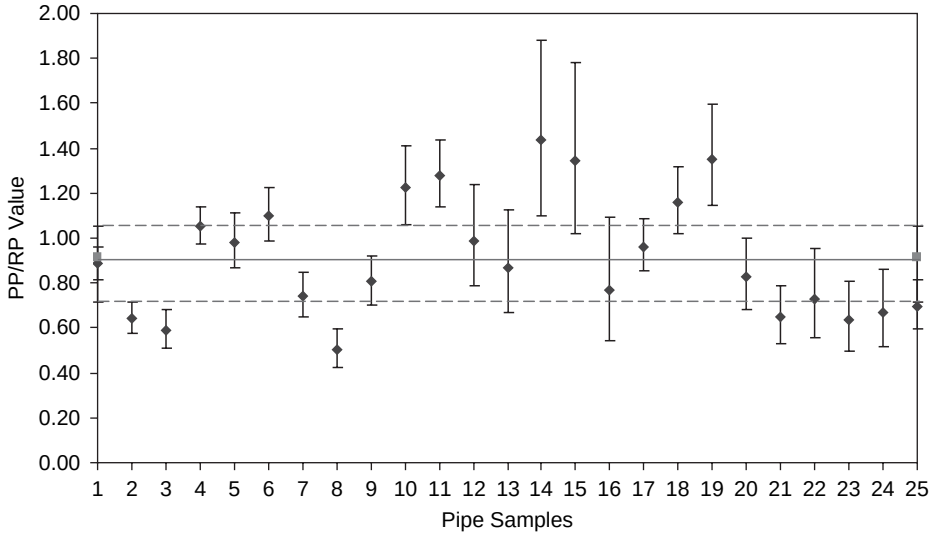

Figure F-3. PP/RP values together with the 95% confidence interval.

the mean is selected ($\sigma_{5\%} = 0.72$). The failure time of the virgin resin should increase by to 33 hs (calculated as 24 h/0.72).

The manufacturing processing of the pipe can affect the SCR of the virgin resin significantly due to residual stress and processing orientation. The processing effects are identified by comparing the failure time of the pipe liner (PL) to the corresponding pipe plaque (PP). In Figure F-4, the reduction factors caused by the addition of carbon black (PP/RP) and the pipe processing (PL/PP) are compared with the combined effects (PL/RP) for pipes made from 100% virgin resins. Except for Pipe Samples 4 and 6 (I-60″ and II-60″), the combined reduction factor is mainly affected by the processing effect.

The quantitative evaluation of processing effects is presented in the PL/PP ratio column of Table F-13. For each set of pipe samples, which includes 100% virgin resin pipes containing 10% and 20% regrind materials, their PL/PP ratios are relatively similar, since these pipes were manufactured from the same machine. However, processing effects change greatly from machine to machine. The PL/PP ratio values range from 0.44 to 0.91 for 13 sets of pipe samples. In addition, the processing reduction factor does not correlate to the diameter of the pipes, as indicated in Table F-9.

The reduction factor of manufacturing processing is evaluated by comparing the failure time of the pipe liner to the corresponding pipe plaque. The average combined reduction factor is 0.66, as shown in the PL/PP column of Table F-13. The same method used to calculate the standard deviation and the 95% single-side confidence interval of the mean for PP/RP is applied to analyze the PL/PP data. The results are shown in Figure F-5 and the calculation is shown in Section F.6. The 95% confidence interval of the mean is from 0.55 to 0.76.

The pipe liner is expected to have a lower failure time than the corresponding pipe plaque due to processing effects. The failure time of the pipe liner is determined from the 24-h

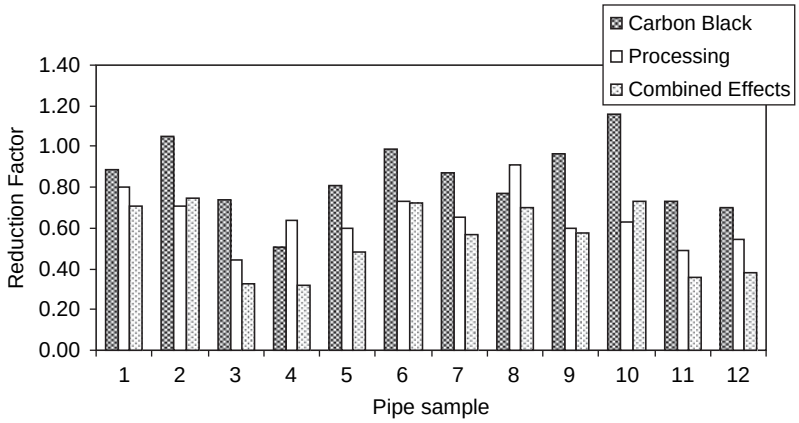

Figure F-4. Influence factor on pipes made from 100% virgin resins.

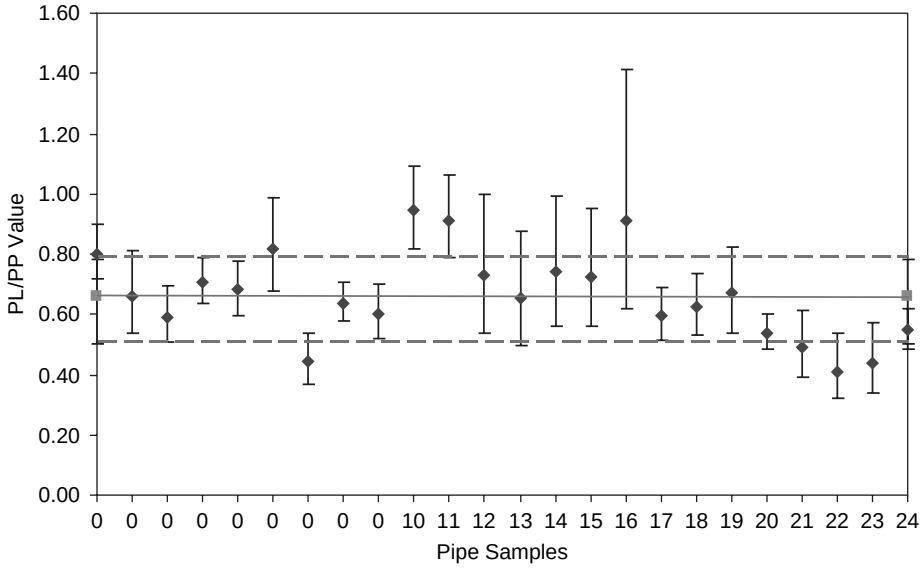

Figure F-5. PL/PP values together with the 95% confidence interval.

recommendation for a pipe plaque from *NCHRP Report 429*. Conservatively, we would like to have the least possible reduction due to processing, which would be 18 h (calculated as 0.76 * 24 h).

For the oxidation resistance, the OIT test was used to assess the amount of antioxidants in each of the pipe resins and finished pipes. A large variation is observed among tested materials. The OIT values range from 7.5 min to 66.3 min for virgin resins and from 8.8 min to 44.6 min for finished pipes containing no regrind material (Table F-11). Five of the twelve pipes showed OIT values higher than the corresponding virgin resins, indicating that the carbon black master batch can influence the OIT value. On the other hand, the regrind materials have no significant effect on the OIT value; less than 10% reduction in the OIT value is obtained after adding regrind. Due to the unknown impact of the carbon black master batch, the OIT test should be performed on the finished pipe instead of the virgin resin. Although the focus of this part of the project does not include establishing the appropriate OIT value for corrugated HDPE pipes due to the long required testing time, Florida Department of Transportation (FDOT) did set a minimum OIT value of 25 min for 100-year design life. This value was developed based on aging data obtained from HDPE geomembranes.

F.5 Proposed Specification Failure Times for NCLS Test

In summary, the following three specified values are proposed to evaluate the SCR of the corrugated HDPE pipes:

1. Minimum average failure time of virgin resin should be 33 h.
2. Minimum average failure time of a pipe plaque should be 24 h.
3. Minimum average failure time of the pipe liner should be 18 h.

Based on the above proposed specifications, 7 of the 13 virgin resins tested in the project passed the 33-h value, 16 of the 24 pipes passed the 24-h pipe plaque value, and 11 of the 24 pipe samples passed the 18-h pipe liner value. In Table F-14, samples passing the proposed specified value are highlighted. The data indicate that pipes with qualified virgin resin might not necessarily pass the pipe liner proposed value due to the large variation in the pipe processing effect. Of the pipes that were made from qualified resins, 5 failed the pipe liner requirements, and 8 of the 24 pipes qualify under all three proposed values. The importance of a pipe liner specification is clearly demonstrated in this study, and it is even more critical than the virgin resin specification.

F.6 Method of Statistical Analysis

The statistical method used in this analysis is taken from M. G. Morgan and M. Henrion, *Uncertainty: A Guide to Dealing with Uncertainty in Quantitative Risk and Policy Analysis,* Cambridge University Press, Cambridge, UK, 1990.

F.6.1 Determine Mean and Standard Deviation of Individual PP/RP Value Using Lognormal Distribution

The PP/RP ratio is expressed as follows:

$$R = \frac{A}{B} \qquad \text{(F.1)}$$

$$\ln R = \ln A - \ln B$$

Table F-14. Highlighting samples passed proposed specified values.

Pipe Sample	Pure Resin (%)	NCLS Test Results (hours)		
		Resin Plaque (RP)	Pipe Plaque (PP)	Pipe Liner (PL)
I-24"	100%	41	36	29
I-24"	90%		26	24
I-24"	80%		24	22
I-36"	100%	33	35	25
I-36"	90%		32	24
I-36"	80%		36	28
I-48"	100%	40	29	13
I-60"	100%	30	15	10
II-24"	100%	24	20	12
II-24"	90%		30	19
II-24"	80%		31	18
II-36"	100%	29	28	21
II-48"	100%	21	19	12
II-48"	90%		31	14
II-48"	80%		29	13
II-60"	100%	33	25	23
III-24"	100%	56	54	32
III-30"	100%	13	15	9
III-30"	80%		17	10
IV-24"	70%	26	17	9
V-24"	100%	34	25	12
V-24"	90%		22	10
V-24"	80%		23	11
V-36"	100%	38	26	14

where

R = PP/RP failure time ratio,
A = PP failure time, and
B = RP failure time.

The Delta Method is used to determine the variance of PP and RP.

$$Var[ln(R_i)] = Var[ln(A_i)] - Var[ln(B_i)] \quad \text{(F.2)}$$

$$ln(R_i) \approx (ln(R_i), \sigma_{R_i}) \quad \text{(F.3)}$$

$$ln(A_i) \approx (ln(PP_i), \sigma_{PP_i}) \quad \text{(F.4)}$$

$$ln(B_i) \approx (ln(RP_i), \sigma_{RP_i}) \quad \text{(F.5)}$$

where

PP_i = the mean failure time of a given pipe plaque sample,
RP_i = the mean failure time of a given resin plaque sample, and
σ = standard deviation of the NCLS test (a set of five specimens) on PP or RP plaque.

F.6.2 Mean Ratio Value (R)

$$ln(R_i) = ln(PP_i) - ln(RP_i) \quad \text{(F.6)}$$

For example, Pipe Sample I-24″ (100% virgin):

$PP_1 = 36.4$hr
$RP_1 = 41.1$
$\ln(R_1) = \ln(36.4) - \ln(41.1)$
$= 3.59 - 3.71$
$= -0.12$
$R_1 = \underline{0.89}$

F.6.3 Log Standard Deviation for R

$$(\sigma_{R_i})^2 = (\sigma_{PP_i})^2 + (\sigma_{RP_i})^2 \quad \text{(F.7)}$$

or

$$(ln(\sigma_{R_i}))^2 = (ln(1 + COV_{PP_i}))^2 + (ln(1 + COV_{RP_i}))^2 \quad \text{(F.8)}$$

where COV is coefficient of variation of the NCLS test (a set of five specimens) on PP or RP plaque.

For example, Pipe Sample I-24″ (100% virgin):

$COV_{PP1} = 0.0357$
$COV_{RP1} = 0.0341$
$(ln(\sigma_{R1}))^2 = (\ln(1 + 0.0357))^2 + (\ln(1 + 0.0341))^2$
$= 0.00123 + 0.00112$
$ln(\sigma) = \underline{0.0485}$

F.6.4 Determine the Single-Side 95% Confidence Interval for Individual PP/RP Value

$$95\%\ \text{C.I. of } R = \exp[\ln(R) + 1.65(\ln\sigma)] \text{ to } \exp[\ln(R) - 1.65(\ln\sigma)] \quad \text{(F.9)}$$

Tables F-15 and F-16 show the NCLS test results on RP and PP materials, respectively. Table F-17 shows the calculation of the mean and 95% confidence interval (CI) of each PP/RP value.

F.6.5 Determine the Mean and 95% Confidence Interval of 25 Pipe Samples

The mean ($\bar{R}$) of the 25 PP/RP value is 0.92.

The 95% CI is defined by the following equation (using the equation in ASTM E691 for repeatability standard deviation):

$$S_r = \sqrt{\sum_1^p \left(\frac{S^2}{p}\right)} \quad \text{(F.10)}$$

Table F-15. NCLS test data on resin plaque.

Resin Plq (RP)	Mean	Std	COV
I-24"	41.1	1.4	0.0341
I-36"	32.9	1.5	0.0456
I-48"	39.7	2	0.0504
I-60"	30.2	2.8	0.0927
II-24"	24.3	1.4	0.0576
II-36"	28.5	4.1	0.1439
II-48"	21.3	3.4	0.1596
II-60"	32.5	7.6	0.2338
III-24"	56	3.5	0.0625
III-30"	12.5	0.8	0.0640
IV-24"	25.7	2	0.0778
V-24	34.1	5.1	0.1496
V-36	37.7	2.7	0.0716

Table F-16. NCLS test data on pipe plaque (PP).

Pipe Plq (PP)	Mean	Std	COV
I-24"-100%	36.4	1.3	0.0357
I-24"-90%	26.3	1.5	0.0570
I-24"-80%	24.3	2.1	0.0864
I-36"-100%	34.6	0.6	0.0173
I-36"-90%	32.3	2.1	0.0650
I-36"-80%	36.1	1.8	0.0499
I-48"-100%	29.4	2	0.0680
I-60"-100%	15.2	0.9	0.0592
II-24"-100%	19.6	1.2	0.0612
II-24"-90%	29.7	2	0.0673
II-24"-80%	31.1	1.4	0.0450
II-36"-100%	28.2	0.8	0.0284
II-48"-100%	18.5	1	0.0541
II-48"-90%	30.6	2.1	0.0686
II-48"-80%	28.7	2.5	0.0871
II-60"-100%	25	0.9	0.0360
III-24"-100%	53.9	2.3	0.0427
III-30"-100%	14.5	0.7	0.0483
III-30"-80%	16.9	1.4	0.0828
IV-24"-95%	21.2	2	0.0943
IV-24"-75%	16.6	1.6	0.0964
V-24"-100%	24.8	2.2	0.0887
V-24"-90%	21.6	1	0.0463
V-24"-80%	22.7	1.6	0.0705
V-36"-100%	26.3	1.8	0.0684

Table F-17. Calculated data for PP/RP ratio.

Material	$\sigma_{(lnRP)}$ $(ln(1+CV))^2$	$\sigma_{(lnPP)}$ $(ln(1+CV))^2$	$\sigma_{(lnR)}$	ln(R)	R	R (95%)	R (5%)
I-24"-100%	0.00112	0.00123	0.0485	-0.1214	**0.89**	**0.96**	**0.82**
I-24"-90%		0.00308	0.0648	-0.4464	**0.64**	**0.71**	**0.58**
I-24"-80%		0.00687	0.0894	-0.5255	**0.59**	**0.69**	**0.51**
I-36"-100%	0.00199	0.00030	0.0478	0.0504	**1.05**	**1.14**	**0.97**
I-36"-90%		0.00397	0.0772	-0.0184	**0.98**	**1.12**	**0.86**
I-36"-80%		0.00237	0.0660	0.0928	**1.10**	**1.22**	**0.98**
I-48"-100%	0.00242	0.00433	0.0821	-0.3004	**0.74**	**0.85**	**0.65**
I-60"-100%	0.00786	0.00331	0.1057	-0.6865	**0.50**	**0.60**	**0.42**
II-24"-100%	0.00314	0.00353	0.0817	-0.2149	**0.81**	**0.92**	**0.70**
II-24"-90%		0.00425	0.0859	0.2007	**1.22**	**1.41**	**1.06**
II-24"-80%		0.00194	0.0712	0.2467	**1.28**	**1.44**	**1.14**
II-36"-100%	0.01807	0.00078	0.1373	-0.0106	**0.99**	**1.24**	**0.79**
II-48"-100%	0.02193	0.00277	0.1572	-0.1409	**0.87**	**1.13**	**0.67**
II-48"-90%		0.00441	0.1623	0.3623	**1.44**	**1.88**	**1.10**
II-48"-80%		0.00698	0.1700	0.2982	**1.35**	**1.78**	**1.02**
II-60"-100%	0.04416	0.00125	0.2131	-0.2624	**0.77**	**1.09**	**0.54**
III-24"-100%	0.00368	0.00175	0.0736	-0.0382	**0.96**	**1.09**	**0.85**
III-30"-100%	0.00385	0.00222	0.0779	0.1484	**1.16**	**1.32**	**1.02**
III-30"-80%		0.00633	0.1009	0.3016	**1.35**	**1.60**	**1.14**
IV-24"-95%	0.00562	0.00813	0.1172	-0.1925	**0.82**	**1.00**	**0.68**
IV-24"-75%		0.00847	0.1187	-0.4371	**0.65**	**0.79**	**0.53**
V-24"-100%	0.01943	0.00722	0.1632	-0.3185	**0.73**	**0.95**	**0.56**
V-24"-90%		0.00205	0.1465	-0.4566	**0.63**	**0.81**	**0.50**
V-24"-80%		0.00464	0.1551	-0.4069	**0.67**	**0.86**	**0.52**
V-36"-100%	0.00478	0.00438	0.0957	-0.3601	**0.70**	**0.82**	**0.60**

Table F-18. Overall mean value of PP/RP and 95% confidence interval.

Pipe	R	ln(R)	ln(σ)	Average ln(R)	Average of ln(σ)
I-24"-100%	0.89	-0.12	0.049		
I-24"-90%	0.64	-0.45	0.065		
I-24"-80%	0.59	-0.53	0.089		
I-36"-100%	1.05	0.05	0.048		
I-36"-90%	0.98	-0.02	0.077		
I-36"-80%	1.10	0.09	0.066		
I-48"-100%	0.74	-0.30	0.082		
I-60"-100%	0.50	-0.69	0.106		
II-24"-100%	0.81	-0.21	0.082		
II-24"-90%	1.22	0.20	0.086		
II-24"-80%	1.28	0.25	0.071		
II-36"-100%	0.99	-0.01	0.137		
II-48"-100%	0.87	-0.14	0.157	-0.13	0.116
II-48"-90%	1.44	0.36	0.162		
II-48"-80%	1.35	0.30	0.170		
II-60"-100%	0.77	-0.26	0.213		
III-24"-100%	0.96	-0.04	0.074		
III-30"-100%	1.16	0.15	0.078		
III-30"-80%	1.35	0.30	0.101		
IV-24"-95%	0.82	-0.19	0.117		
IV-24"-75%	0.65	-0.44	0.119		
V-24"-100%	0.73	-0.32	0.163		
V-24"-90%	0.63	-0.46	0.147		
V-24"-80%	0.67	-0.41	0.155		
V-36"-100%	0.70	-0.36	0.096		

where

S_r = repeatability standard deviation,

p = number of laboratories (in our case, number of samples), and

S = standard deviation of each sample.

Table F-18 shows the 25 PP/RP values used to obtain $\ln(\bar{R})$, and $\ln(\bar{\sigma})$. The single-side 95% confidence interval of the average is calculated using the equation below:

$$95\%\ \text{C.I. of}\ \bar{R} = \exp\left\lfloor \ln(\bar{R}) \pm 1.65(\ln\bar{\sigma}) \right\rfloor \qquad \text{(F.11)}$$

The lower and upper limits are 0.72 and 1.06, respectively.

F.6.6 Determine Mean and Standard Deviation of Individual Values of PL/PP

The same calculation procedure used for PP/RP is applied onto the PL/PP data. Table F-19 shows the NCLS test results on PL material. Table F-20 shows the mean and 95% CI of each PL/RP value.

Table F-21 shows the 24 PL/RP values used to obtain $\ln(\bar{R})$, and $\ln(\bar{\sigma})$. The 95% confidence interval of the average is calculated from these two values, and the lower and upper limits are 0.55 to 0.76, respectively.

Table F-19. NCLS test data on pipe liner (PL).

Pipe Liner (PL)	Mean	Std	COV
I-24"-100%	29.2	1.7	0.058
I-24"-90%	24	2.9	0.121
I-24"-80%	21.5	1.9	0.088
I-36"-100%	24.5	0.6	0.024
I-36"-90%	23.6	1.1	0.047
I-36"-80%	28.3	2.4	0.085
I-48"-100%	13	1.7	0.131
I-60"-100%	9.7	0.5	0.052
II-24"-100%	11.8	0.9	0.076
II-24"-90%	18.5	1.4	0.076
II-24"-80%	17.9	1.4	0.078
II-36"-100%	20.6	1.9	0.092
II-48"-100%	12.1	1	0.083
II-48"-90%	13.7	1.2	0.088
II-48"-80%	13.4	0.7	0.052
II-60"-100%	22.8	4.4	0.193
III-24"-100%	32.1	1.5	0.047
III-30"-100%	9.1	0.3	0.033
III-30"-80%	9.7	0.7	0.072
IV-24"-75%	8.9	0.4	0.045
V-24"-100%	12.1	0.9	0.074
V-24"-90%	10.2	1.2	0.118
V-24"-80%	10.8	1.4	0.130
V-36"-100%	14.4	0.8	0.056

Table F-20. Calculated data for PL/PP ratio.

Material	σ(lnPP) $(\ln(1+CV))^2$	σ(lnPL) $(\ln(1+CV))^2$	σ(lnR)	Mean ln(R)	R	R (95%)	R (5%)
I-24"-100%	0.00123	0.00320	0.0666	-0.2204	**0.80**	**0.90**	**0.72**
I-24"-90%	0.00308	0.01301	0.1193	-0.4165	**0.66**	**0.80**	**0.54**
I-24"-80%	0.00687	0.00717	0.0917	-0.5265	**0.59**	**0.69**	**0.51**
I-36"-100%	0.00030	0.00059	0.0297	-0.3452	**0.71**	**0.74**	**0.67**
I-36"-90%	0.00397	0.00208	0.0487	-0.3826	**0.68**	**0.74**	**0.63**
I-36"-80%	0.00237	0.00663	0.0832	-0.2010	**0.82**	**0.94**	**0.71**
I-48"-100%	0.00433	0.01510	0.1394	-0.8160	**0.44**	**0.56**	**0.35**
I-60"-100%	0.00331	0.00253	0.0764	-0.4492	**0.64**	**0.72**	**0.56**
II-24"-100%	0.00353	0.00540	0.0945	-0.5074	**0.60**	**0.70**	**0.52**
II-24"-90%	0.00425	0.00532	0.0941	-0.0578	**0.94**	**1.10**	**0.81**
II-24"-80%	0.00194	0.00567	0.0959	-0.0907	**0.91**	**1.07**	**0.78**
II-36"-100%	0.00078	0.00778	0.0926	-0.3140	**0.73**	**0.85**	**0.63**
II-48"-100%	0.00277	0.00631	0.0953	-0.4246	**0.65**	**0.77**	**0.56**
II-48"-90%	0.00441	0.00705	0.0991	-0.3004	**0.74**	**0.87**	**0.63**
II-48"-80%	0.00698	0.00259	0.0732	-0.3225	**0.72**	**0.82**	**0.64**
II-60"-100%	0.00125	0.03114	0.1800	-0.0921	**0.91**	**1.23**	**0.68**
III-24"-100%	0.00175	0.00209	0.0619	-0.5183	**0.60**	**0.66**	**0.54**
III-30"-100%	0.00222	0.00105	0.0572	-0.4659	**0.63**	**0.69**	**0.57**
III-30"-80%	0.00633	0.00486	0.0841	-0.4020	**0.67**	**0.77**	**0.58**
IV-24"-75%	0.00847	0.00193	0.1020	-0.6234	**0.54**	**0.63**	**0.45**
V-24"-100%	0.00722	0.00515	0.1112	-0.7176	**0.49**	**0.59**	**0.41**
V-24"-90%	0.00205	0.01237	0.1400	-0.8885	**0.41**	**0.52**	**0.33**
V-24"-80%	0.00464	0.01486	0.1486	-0.8313	**0.44**	**0.56**	**0.34**
V-36"-100%	0.00438	0.00292	0.0855	-0.6023	**0.55**	**0.63**	**0.48**

Table F-21. Overall mean value of PL/PP and 95% confidence interval.

Pipe	R	ln(R)	ln(σ)	Average ln(R)	Average of ln(σ)
I-24"-100%	0.80	-0.2204	0.0666		
I-24"-90%	0.66	-0.4165	0.1193		
I-24"-80%	0.59	-0.5265	0.0917		
I-36"-100%	0.71	-0.3452	0.0297		
I-36"-90%	0.68	-0.3826	0.0487		
I-36"-80%	0.82	-0.2010	0.0832		
I-48"-100%	0.44	-0.8160	0.1394		
I-60"-100%	0.64	-0.4492	0.0764		
II-24"-100%	0.60	-0.5074	0.0945		
II-24"-90%	0.94	-0.0578	0.0941		
II-24"-80%	0.91	-0.0907	0.0959		
II-36"-100%	0.73	-0.3140	0.0926		
II-48"-100%	0.65	-0.4246	0.0953	-0.44	0.100
II-48"-90%	0.74	-0.3004	0.0991		
II-48"-80%	0.72	-0.3225	0.0732		
II-60"-100%	0.91	-0.0921	0.1800		
III-24"-100%	0.60	-0.5183	0.0619		
III-30"-100%	0.63	-0.4659	0.0572		
III-30"-80%	0.67	-0.4020	0.0841		
IV-24"-75%	0.54	-0.6234	0.1020		
V-24"-100%	0.49	-0.7176	0.1112		
V-24"-90%	0.41	-0.8885	0.1400		
V-24"-80%	0.44	-0.8313	0.1486		
V-36"-100%	0.55	-0.6023	0.0855		

F.7 Data for Individual Specimens

F.7.1 Density Data (ASTM D792, Procedure B)

Measured density value on resin plaque, pipe plaque (with carbon black) and pipe liner (with carbon black).

Company	Diameter (in.)	Pure Resin (%)	Test Material	Density (g/cc)			
				1	2	3	Average
I	24	100	Resin Plaque	0.950	0.950	0.950	**0.950**
			Pipe Plaque	0.963	0.963	0.963	**0.963**
			Pipe Liner	0.958	0.958	0.958	**0.958**
		90	Pipe Plaque	0.963	0.963	0.963	**0.963**
			Pipe Liner	0.959	0.959	0.959	**0.959**
		80	Pipe Plaque	0.964	0.964	0.964	**0.964**
			Pipe Liner	0.959	0.959	0.959	**0.959**
	36	100	Resin Plaque	0.951	0.951	0.951	**0.951**
			Pipe Plaque	0.962	0.962	0.962	**0.962**
			Pipe Liner	0.958	0.958	0.958	**0.958**
		90	Pipe Plaque	0.962	0.962	0.961	**0.962**
			Pipe Liner	0.958	0.957	0.958	**0.958**
		80	Pipe Plaque	0.963	0.963	0.964	**0.963**
			Pipe Liner	0.957	0.958	0.957	**0.957**
	48	100	Resin Plaque	0.950	0.950	0.949	**0.950**
			Pipe Plaque	0.962	0.962	0.962	**0.962**
			Pipe Liner	0.959	0.959	0.960	**0.959**
	60	100	Resin Plaque	0.948	0.947	0.948	**0.948**
			Pipe Plaque	0.960	0.960	0.961	**0.960**
			Pipe Liner	0.958	0.958	0.957	**0.958**

Calculated density value for pipe plaque and pipe liner.

Calculate the Density of the Resin based on equation provided in ASTM D3350
$\rho_{(resin)} = \rho_{(product)} - 0.0044C$, C = % carbon black

Company	Diameter (in.)	Pure Resin (%)	Test Material	Density (g/cc)	Carbon Black (%)	Calculated Density (g/cc)
I	24	100	Pipe Plaque	0.963	3.4	**0.9480**
			Pipe Liner	0.958	3.3	**0.9435**
		90	Pipe Plaque	0.963	3.4	**0.9480**
			Pipe Liner	0.959	3.4	**0.9440**
		80	Pipe Plaque	0.964	3.4	**0.9490**
			Pipe Liner	0.959	3.4	**0.9440**
	36	100	Pipe Plaque	0.962	3.1	**0.9484**
			Pipe Liner	0.958	3.1	**0.9444**
		90	Pipe Plaque	0.962	2.9	**0.9492**
			Pipe Liner	0.958	3.2	**0.9439**
		80	Pipe Plaque	0.963	3.2	**0.9489**
			Pipe Liner	0.957	3.0	**0.9438**
	48	100	Pipe Plaque	0.962	2.5	**0.9500**
			Pipe Liner	0.959	2.5	**0.9480**
	60	100	Pipe Plaque	0.960	3.1	**0.9464**
			Pipe Liner	0.958	3.0	**0.9448**

Measured density value on resin plaque, pipe plaque (with carbon black) and pipe liner (with carbon black).

Company	Diameter (in)	Pure Resin (%)	Test Material	Density (g/cc)			
				1	2	3	**Average**
II	24	100	Resin Plaque	0.949	0.949	0.949	**0.949**
			Pipe Plaque	0.959	0.960	0.960	**0.960**
			Pipe Liner	0.954	0.953	0.954	**0.954**
		90	Pipe Plaque	0.960	0.959	0.959	**0.959**
			Pipe Liner	0.955	0.956	0.955	**0.955**
		80	Pipe Plaque	0.959	0.960	0.960	**0.960**
			Pipe Liner	0.956	0.955	0.955	**0.955**
	36	100	Resin Plaque	0.951	0.951	0.951	**0.951**
			Pipe Plaque	0.963	0.962	0.963	**0.963**
			Pipe Liner	0.958	0.958	0.958	**0.958**
	48	100	Resin Plaque	0.951	0.951	0.951	**0.951**
			Pipe Plaque	0.961	0.961	0.962	**0.961**
			Pipe Liner	0.956	0.955	0.955	**0.955**
		90	Pipe Plaque	0.961	0.962	0.962	**0.962**
			Pipe Liner	0.956	0.957	0.957	**0.957**
		80	Pipe Plaque	0.961	0.962	0.962	**0.962**
			Pipe Liner	0.958	0.956	0.957	**0.957**
	60	100	Resin Plaque	0.947	0.948	0.947	**0.947**
			Pipe Plaque	0.960	0.960	0.960	**0.960**
			Pipe Liner	0.959	0.959	0.959	**0.959**

Calculated density value for pipe plaque and pipe liner.

Calculate the Density of the Resin based on Equation provided in ASTM D3350 $\rho_{(resin)} = \rho_{(product)} - 0.0044C$, **C = % carbon black**						
Company	Diameter (in)	Pure Resin (%)	Test Material	Density (g/cc)	Carbon Black (%)	Calculated Density (g/cc)
II	24	100	Pipe Plaque	0.960	2.5	**0.9490**
			Pipe Liner	0.954	2.5	**0.9430**
		90	Pipe Plaque	0.959	2.4	**0.9484**
			Pipe Liner	0.955	2.5	**0.9440**
		80	Pipe Plaque	0.960	2.5	**0.9490**
			Pipe Liner	0.955	2.5	**0.9440**
	36	100	Pipe Plaque	0.963	2.6	**0.9516**
			Pipe Liner	0.958	2.5	**0.9470**
	48	100	Pipe Plaque	0.961	2.5	**0.9500**
			Pipe Liner	0.955	2.5	**0.9440**
		90	Pipe Plaque	0.962	2.8	**0.9497**
			Pipe Liner	0.957	2.7	**0.9451**
		80	Pipe Plaque	0.962	2.7	**0.9501**
			Pipe Liner	0.957	2.7	**0.9451**
	60	100	Pipe Plaque	0.960	2.5	**0.9490**
			Pipe Liner	0.959	2.4	**0.9484**

Measured density value on resin plaque, pipe plaque (with carbon black), and pipe liner (with carbon black).

Company	Diameter (in)	Pure Resin (%)	Test Material	Density (g/cc)			
				1	2	3	**Average**
III	24	100	Resin Plaque	0.952	0.952	0.951	**0.952**
			Pipe Plaque	0.961	0.960	0.961	**0.961**
			Pipe Liner	0.954	0.955	0.955	**0.955**
	30	100	Resin Plaque	0.952	0.952	0.952	**0.952**
			Pipe Plaque	0.961	0.961	0.961	**0.961**
			Pipe Liner	0.956	0.956	0.957	**0.956**
		80	Pipe Plaque	0.967	0.966	0.965	**0.966**
			Pipe Liner	0.962	0.961	0.960	**0.961**
IV	24	100	Resin Plaque	0.952	0.950	0.951	**0.951**
		75	Pipe Plaque	0.963	0.962	0.963	**0.963**
		75	Pipe Liner	0.958	0.957	0.957	**0.957**
V	24	100	Resin Plaque	0.951	0.951	0.951	**0.951**
			Pipe Plaque	0.960	0.959	0.959	**0.959**
			Pipe Liner	0.954	0.954	0.955	**0.954**
		90	Pipe Plaque	0.959	0.958	0.959	**0.959**
			Pipe Liner	0.955	0.955	0.955	**0.955**
		80	Pipe Plaque	0.959	0.959	0.959	**0.959**
			Pipe Liner	0.955	0.955	0.955	**0.955**
	36	100	Resin Plaque	0.951	0.951	0.952	**0.951**
			Pipe Plaque	0.961	0.961	0.961	**0.961**
			Pipe Liner	0.958	0.958	0.958	**0.958**

Calculated density value for pipe plaque and pipe liner.

Calculate the Density of the Resin based on Equation provided in ASTM D3350 $\rho_{(resin)} = \rho_{(product)} - 0.0044C$, **C = % carbon black**						
Company	Diameter (in)	Pure Resin (%)	Test Material	Density (g/cc)	Carbon Black (%)	Calculated Density (g/cc)
III	24	100	Pipe Plaque	0.961	2.2	**0.9513**
			Pipe Liner	0.954	2.1	**0.9448**
	30	100	Pipe Plaque	0.961	2.3	**0.9509**
			Pipe Liner	0.956	2.4	**0.9454**
		80	Pipe Plaque	0.966	3.2	**0.9519**
			Pipe Liner	0.961	3.3	**0.9465**
IV	24	75	Pipe Liner Plaque	0.963	2.6	**0.9516**
		75	Pipe Liner	0.958	2.5	**0.9470**
V	24	100	Pipe Plaque	0.960	2.0	**0.9512**
			Pipe Liner	0.954	2.2	**0.9443**
		90	Pipe Plaque	0.959	2.0	**0.9502**
			Pipe Liner	0.955	2.1	**0.9458**
		80	Pipe Plaque	0.959	2.0	**0.9502**
			Pipe Liner	0.955	2.1	**0.9458**
	36	100	Pipe Plaque	0.961	2.2	**0.9513**
			Pipe Liner	0.958	2.0	**0.9492**

F.7.2 Melt Index Data

Company	Diameter (in.)	Pure Resin (%)	Test Material	Melt Index (g/10min)				
				1	2	3	4	Average
I	24	100	Resin	0.24	0.23	0.24	0.24	**0.24**
			Pipe	0.20	0.21	0.20	0.20	**0.20**
		90	Pipe	0.20	0.20	0.20	0.20	**0.20**
		80	Pipe Plaque	0.20	0.21	0.21	0.21	**0.21**
	36	100	Resin	0.32	0.32	0.32	0.32	**0.32**
			Pipe	0.28	0.28	0.28	0.27	**0.28**
		90	Pipe	0.29	0.28	0.29	0.29	**0.29**
		80	Pipe	0.27	0.27	0.27	0.27	**0.27**
	48	100	Resin	0.10	0.10	0.10	0.10	**0.10**
			Pipe	0.13	0.13	0.13	0.13	**0.13**
	60	100	Resin	0.10	0.08	0.10	0.09	**0.09**
			Pipe	0.13	0.13	0.13	0.12	**0.13**
II	24	100	Resin	0.20	0.20	0.22	0.20	**0.20**
			Pipe	0.20	0.20	0.20	0.20	**0.20**
		90	Pipe	0.17	0.17	0.18	0.18	**0.18**
		80	Pipe	0.17	0.17	0.17	0.17	**0.17**
	36	100	Resin	0.18	0.19	0.18	0.18	**0.18**
			Pipe	0.16	0.17	0.16	0.16	**0.16**
	48	100	Resin	0.20	0.20	0.20	0.20	**0.20**
			Pipe	0.18	0.20	0.18	0.20	**0.19**
		90	Pipe	0.15	0.15	0.15	0.15	**0.15**
		80	Pipe	0.15	0.15	0.15	0.15	**0.15**
	60	100	Resin	0.18	0.19	0.18	0.19	**0.19**
			Pipe	0.17	0.17	0.17	0.15	**0.16**
III	24	100	Resin	0.22	0.23	0.22	0.22	**0.22**
			Pipe	0.20	0.21	0.20	0.20	**0.20**
	30	100	Resin	0.20	0.20	0.20	0.20	**0.20**
			Pipe	0.17	0.17	0.17	0.17	**0.17**
		80	Pipe	0.18	0.18	0.18	0.18	**0.18**
IV	24	100	Resin	0.35	0.34	0.34	0.34	**0.34**
		90	Pipe Crown	0.28	0.29	0.29	0.30	**0.29**
		75	Pipe Liner	0.38	0.38	0.37	0.38	**0.38**
V	24	100	Resin	0.27	0.26	0.27	0.27	**0.27**
			Pipe	0.23	0.25	0.25	0.25	**0.25**
		90	Pipe	0.25	0.25	0.23	0.25	**0.25**
		80	Pipe	0.23	0.25	0.25	0.25	**0.25**
	36	100	Resin	0.36	0.37	0.37	0.37	**0.37**
			Pipe	0.27	0.27	0.28	0.28	**0.28**

F.7.3 Notched Constant Ligament Stress Test Data

Sample - I-24 inch Resin plaque (100% Virgin)				
Applied Stress (psi)	Thickness (in)	Ligament Thickness (in)	Applied Load (g)	Failure Time (hr.)
600	0.075	0.061	691.7	38.90
	0.075	0.061	691.7	42.2
	0.075	0.061	691.7	42.1
	0.076	0.062	703.1	42.1
	0.076	0.062	703.1	41.6
			Average Failure Time	41.4
			Standard Deviation	1.4
			Coefficient Variation	3%

Sample - I-24 inch Pipe liner plaque (100% Virgin)				
Applied Stress (psi)	Thickness (in)	Ligament Thickness (in)	Applied Load (g)	Failure Time (hr.)
600	0.075	0.061	691.7	38.5
	0.075	0.061	691.7	35.5
	0.076	0.062	703.1	36.7
	0.076	0.062	703.1	36.2
	0.076	0.062	703.1	35.2
			Average Failure Time	36.4
			Standard Deviation	1.3
			Coefficient Variation	4%

Sample - I-24 inch Pipe liner (100% Virgin)				
Applied Stress (psi)	Thickness (in)	Ligament Thickness (in)	Applied Load (g)	Failure Time (hr.)
600	0.075	0.060	680.4	28.1
	0.078	0.063	714.4	28.7
	0.083	0.067	759.8	30.0
	0.085	0.068	771.1	27.6
	0.087	0.070	793.8	31.7
			Average Failure Time	29.2
			Standard Deviation	1.7
			Coefficient Variation	6%

Sample - I-24 inch Pipe Plaque (10% Regrind)				
Applied Stress (psi)	Thickness (in)	Ligament Thickness (in)	Applied Load (g)	Failure Time (hr.)
600	0.074	0.06	680.4	27.5
	0.074	0.06	680.4	23.7
	0.075	0.061	691.7	26.5
	0.075	0.061	691.7	26.7
	0.075	0.061	691.7	27.3
			Average Failure Time	26.3
			Standard Deviation	1.5
			Coefficient Variation	6%

Sample - I-24 inch Pipe Liner (10% Regrind)				
Applied Stress (psi)	Thickness (in)	Ligament Thickness (in)	Applied Load (g)	Failure Time (hr.)
600	0.083	0.066	753.0	26.3
	0.084	0.067	762.0	27.5
	0.079	0.063	716.7	22.2
	0.080	0.064	725.8	23.6
	0.085	0.068	771.1	20.5
			Average Failure Time	24.0
			Standard Deviation	2.9
			Coefficient Variation	12%

Sample - I-24 inch Pipe Plaque (20% Regrind)				
Applied Stress (psi)	Thickness (in)	Ligament Thickness (in)	Applied Load (g)	Failure Time (hr.)
600	0.075	0.061	691.7	27.6
	0.076	0.062	703.1	23.9
	0.076	0.062	703.1	23.5
	0.076	0.062	703.1	21.9
	0.076	0.062	703.1	24.6
			Average Failure Time	24.3
			Standard Deviation	2.1
			Coefficient Variation	9%

Sample - I-24 inch Pipe Liner (20% Regrind)				
Applied Stress (psi)	Thickness (in)	Ligament Thickness (in)	Applied Load (g)	Failure Time (hr.)
600	0.083	0.066	753.0	22.5
	0.083	0.066	753.0	20.4
	0.077	0.062	698.5	24.3
	0.078	0.062	707.6	20.2
	0.087	0.070	789.3	19.9
			Average Failure Time	21.5
			Standard Deviation	1.9
			Coefficient Variation	9%

Sample - I-36 inch Resin plaque (100% Virgin)				
Applied Stress (psi)	Thickness (in)	Ligament Thickness (in)	Applied Load (g)	Failure Time (hr.)
600	0.074	0.060	680.4	35.2
	0.074	0.060	680.4	31.8
	0.074	0.060	680.4	33.7
	0.074	0.060	680.4	32.6
	0.075	0.061	691.7	31.4
			Average Failure Time	32.9
			Standard Deviation	1.5
			Coefficient Variation	5%

Sample - I-36 inch Pipe Plaque (100% Virgin)				
Applied Stress (psi)	Thickness (in)	Ligament Thickness (in)	Applied Load (g)	Failure Time (hr.)
600	0.073	0.059	669.1	35.0
	0.073	0.059	669.1	34.4
	0.073	0.059	669.1	35.2
	0.073	0.059	669.1	34.7
	0.074	0.06	680.4	33.6
			Average Failure Time	34.6
			Standard Deviation	0.6
			Coefficient Variation	2%

Sample - I-36 inch Pipe Liner (100% Virgin)				
Applied Stress (psi)	Thickness (in)	Ligament Thickness (in)	Applied Load (g)	Failure Time (hr.)
600	0.096	0.077	873.2	25.4
	0.099	0.08	907.2	24.1
	0.101	0.081	918.5	24.8
	0.104	0.084	952.6	24.0
	0.106	0.085	963.9	24.2
			Average Failure Time	24.5
			Standard Deviation	0.6
			Coefficient Variation	2%

Sample - I-36 inch Pipe Plaque (10% Regrind)				
Applied Stress (psi)	Thickness (in)	Ligament Thickness (in)	Applied Load (g)	Failure Time (hr.)
600	0.076	0.062	703.1	34.1
	0.076	0.062	703.1	34.1
	0.077	0.063	714.4	32.2
	0.077	0.063	714.4	29
	0.078	0.064	725.8	32.2
			Average Failure Time	32.3
			Standard Deviation	2.1
			Coefficient Variation	6%

Sample - I-36 inch Pipe Liner (10% Regrind)				
Applied Stress (psi)	Thickness (in)	Ligament Thickness (in)	Applied Load (g)	Failure Time (hr.)
600	0.11	0.088	997.9	22.2
	0.110	0.088	997.9	24.1
	0.104	0.083	941.2	24.8
	0.099	0.079	895.9	22.7
	0.099	0.079	895.9	24.2
			Average Failure Time	23.6
			Standard Deviation	1.1
			Coefficient Variation	5%

Sample - I-36 inch Pipe Plaque (20% Regrind)				
Applied Stress (psi)	Thickness (in)	Ligament Thickness (in)	Applied Load (g)	Failure Time (hr.)
600	0.076	0.062	703.1	33.5
	0.076	0.062	703.1	38.3
	0.076	0.062	703.1	36.8
	0.077	0.063	714.4	35.2
	0.077	0.063	714.4	36.8
			Average Failure Time	36.1
			Standard Deviation	1.8
			Coefficient Variation	5%

Sample - I-36 inch Pipe Liner (20% Regrind)				
Applied Stress (psi)	Thickness (in)	Ligament Thickness (in)	Applied Load (g)	Failure Time (hr.)
600	0.095	0.076	861.8	26.4
	0.101	0.081	918.5	30.0
	0.101	0.081	918.5	28.2
	0.109	0.087	986.6	25.7
	0.111	0.089	1009.3	31.3
			Average Failure Time	28.3
			Standard Deviation	2.4
			Coefficient Variation	8%

Sample - I-48 inch Resin Plaque (100% Virgin)				
Applied Stress (psi)	Thickness (in)	Ligament Thickness (in)	Applied Load (g)	Failure Time (hr.)
600	0.072	0.058	657.7	42.40
	0.073	0.059	669.1	38.2
	0.073	0.059	669.1	41.3
	0.073	0.059	669.1	38.1
	0.073	0.059	669.1	38.4
			Average Failure Time	39.7
			Standard Deviation	2.0
			Coefficient Variation	5%

Sample - I-48 inch Pipe Plaque (100% Virgin)				
Applied Stress (psi)	Thickness (in)	Ligament Thickness (in)	Applied Load (g)	Failure Time (hr.)
600	0.076	0.062	703.1	32.9
	0.077	0.063	714.4	28.4
	0.077	0.063	714.4	29.3
	0.078	0.064	725.8	27.9
	0.078	0.064	725.8	28.5
			Average Failure Time	29.4
			Standard Deviation	2.0
			Coefficient Variation	7%

Sample - I-48 inch Pipe Liner (100% Virgin)				
Applied Stress (psi)	Thickness (in)	Ligament Thickness (in)	Applied Load (g)	Failure Time (hr.)
600	0.109	0.088	997.9	14.0
	0.111	0.089	1009.3	13.2
	0.112	0.09	1020.6	13.8
	0.112	0.09	1020.6	13.9
	0.120	0.096	1088.6	10.1
			Average Failure Time	13.0
			Standard Deviation	1.7
			Coefficient Variation	13%

Sample - I-60 inch Resin Plaque (100% Virgin)				
Applied Stress (psi)	Thickness (in)	Ligament Thickness (in)	Applied Load (g)	Failure Time (hr.)
600	0.075	0.061	691.7	33.8
	0.075	0.061	691.7	27.5
	0.076	0.062	703.1	32.3
	0.076	0.062	703.1	27.5
	0.076	0.062	703.1	29.9
			Average Failure Time	30.2
			Standard Deviation	2.8
			Coefficient Variation	9%

Sample - I-60 inch Pipe Plaque (100% Virgin)				
Applied Stress (psi)	Thickness (in)	Ligament Thickness (in)	Applied Load (g)	Failure Time (hr.)
600	0.075	0.061	0.0	14.4
	0.076	0.062	703.1	15.2
	0.077	0.063	714.4	14.5
	0.077	0.063	714.4	15.6
	0.077	0.063	714.4	16.5
			Average Failure Time	15.2
			Standard Deviation	0.9
			Coefficient Variation	6%

Sample - I-60 inch Pipe Liner (100% Virgin)				
Applied Stress (psi)	Thickness (in)	Ligament Thickness (in)	Applied Load (g)	Failure Time (hr.)
600	0.132	0.106	1202.0	9.9
	0.134	0.108	1224.7	10.4
	0.127	0.102	1156.7	9.7
	0.108	0.087	986.6	9.1
	0.113	0.091	1031.9	9.4
			Average Failure Time	9.7
			Standard Deviation	0.5
			Coefficient Variation	5%

Sample - II-24 inch Resin Plaque (100% Virgin)				
Applied Stress (psi)	Thickness (in)	Ligament Thickness (in)	Applied Load (g)	Failure Time (hr.)
600	0.075	0.061	691.7	25.4
	0.075	0.061	691.7	25.2
	0.076	0.062	703.1	22.7
	0.076	0.062	703.1	22.9
	0.077	0.063	714.4	25.2
			Average Failure Time	24.3
			Standard Deviation	1.4
			Coefficient Variation	6%

Sample - II-24 inch Pipe Plaque (100% Virgin)				
Applied Stress (psi)	Thickness (in)	Ligament Thickness (in)	Applied Load (g)	Failure Time (hr.)
600	0.076	0.062	703.1	17.9
	0.076	0.062	703.1	18.9
	0.076	0.062	703.1	21.2
	0.076	0.062	703.1	19.9
	0.077	0.063	714.4	19.9
			Average Failure Time	19.6
			Standard Deviation	1.2
			Coefficient Variation	6%

Sample - II-24 inch Pipe Liner (100% Virgin)				
Applied Stress (psi)	Thickness (in)	Ligament Thickness (in)	Applied Load (g)	Failure Time (hr.)
600	0.092	0.074	834.6	13.3
	0.092	0.074	834.6	11.5
	0.091	0.073	825.6	11.2
	0.087	0.070	789.3	11.5
	0.086	0.069	780.2	11.3
			Average Failure Time	11.8
			Standard Deviation	0.9
			Coefficient Variation	7%

Sample - II-24 inch Pipe Plaque (10% Regrind)				
Applied Stress (psi)	Thickness (in)	Ligament Thickness (in)	Applied Load (g)	Failure Time (hr.)
600	0.075	0.061	691.7	32.8
	0.076	0.062	703.1	28.2
	0.076	0.062	703.1	30.2
	0.076	0.062	703.1	27.9
	0.076	0.062	703.1	29.5
			Average Failure Time	29.7
			Standard Deviation	2.0
			Coefficient Variation	7%

Sample - II-24 inch Pipe Liner (10% Regrind)				
Applied Stress (psi)	Thickness (in)	Ligament Thickness (in)	Applied Load (g)	Failure Time (hr.)
600	0.117	0.094	1061.4	17.5
	0.119	0.095	1079.6	18.2
	0.115	0.092	1043.3	17.5
	0.117	0.094	1061.4	18.3
	0.124	0.099	1124.9	20.9
			Average Failure Time	18.5
			Standard Deviation	1.4
			Coefficient Variation	8%

Sample - II-24 inch Pipe Plaque (20% Regrind)				
Applied Stress (psi)	Thickness (in)	Ligament Thickness (in)	Applied Load (g)	Failure Time (hr.)
600	0.075	0.061	691.7	30.7
	0.075	0.061	691.7	31.5
	0.075	0.061	691.7	29.9
	0.076	0.062	703.1	30
	0.076	0.062	703.1	33.2
			Average Failure Time	31.1
			Standard Deviation	1.4
			Coefficient Variation	4%

Sample - II-24 inch Pipe Liner (20% Regrind)				
Applied Stress (psi)	Thickness (in)	Ligament Thickness (in)	Applied Load (g)	Failure Time (hr.)
600	0.122	0.098	1106.8	18.8
	0.116	0.093	1052.4	16.7
	0.120	0.096	1088.6	19.9
	0.115	0.092	1043.3	17.1
	0.117	0.094	1061.4	17
			Average Failure Time	17.9
			Standard Deviation	1.4
			Coefficient Variation	8%

Sample - II-36 inch Resin Plaque (100% Virgin)				
Applied Stress (psi)	Thickness (in)	Ligament Thickness (in)	Applied Load (g)	Failure Time (hr.)
600	0.075	0.061	691.7	34.9
	0.076	0.062	703.1	24.1
	0.076	0.062	703.1	29.7
	0.076	0.062	703.1	26.4
	0.076	0.062	703.1	27.4
			Average Failure Time	28.5
			Standard Deviation	4.1
			Coefficient Variation	14%

Sample - II-36 inch Pipe Plaque (100% Virgin)				
Applied Stress (psi)	Thickness (in)	Ligament Thickness (in)	Applied Load (g)	Failure Time (hr.)
600	0.075	0.061	691.7	27.8
	0.075	0.061	691.7	28.3
	0.075	0.061	691.7	27.7
	0.075	0.061	691.7	27.7
	0.076	0.062	703.1	29.5
			Average Failure Time	28.2
			Standard Deviation	0.8
			Coefficient Variation	3%

Sample - II-36 inch Pipe Liner (100% Virgin)				
Applied Stress (psi)	Thickness (in)	Ligament Thickness (in)	Applied Load (g)	Failure Time (hr.)
600	0.077	0.062	703.1	19.8
	0.078	0.063	714.4	20.7
	0.08	0.064	725.8	23.8
	0.083	0.067	759.8	18.9
	0.092	0.074	839.2	19.7
			Average Failure Time	20.6
			Standard Deviation	1.9
			Coefficient Variation	9%

Sample - II-48 inch Resin Plaque (100% Virgin)				
Applied Stress (psi)	Thickness (in)	Ligament Thickness (in)	Applied Load (g)	Failure Time (hr.)
600	0.075	0.061	691.7	27.2
	0.075	0.061	691.7	18.4
	0.075	0.061	691.7	20.7
	0.075	0.061	691.7	20.1
	0.076	0.062	703.1	20.1
			Average Failure Time	21.3
			Standard Deviation	3.4
			Coefficient Variation	16%

Sample - II-48 inch Pipe Plaque (100% Virgin)				
Applied Stress (psi)	Thickness (in)	Ligament Thickness (in)	Applied Load (g)	Failure Time (hr.)
600	0.074	0.060	680.4	19.2
	0.075	0.061	691.7	18.4
	0.075	0.061	691.7	17.4
	0.075	0.061	691.7	19.9
	0.077	0.063	714.4	17.8
			Average Failure Time	18.5
			Standard Deviation	1.0
			Coefficient Variation	5%

Sample - II-48 inch Pipe Liner (100% Virgin)				
Applied Stress (psi)	Thickness (in)	Ligament Thickness (in)	Applied Load (g)	Failure Time (hr.)
600	0.085	0.068	771.1	13.3
	0.101	0.081	916.3	12.2
	0.087	0.070	789.3	10.5
	0.079	0.063	716.7	12.6
	0.104	0.083	943.5	11.8
			Average Failure Time	12.1
			Standard Deviation	1.0
			Coefficient Variation	9%

Sample - II-48 inch Pipe Plaque (10% Regrind)				
Applied Stress (psi)	Thickness (in)	Ligament Thickness (in)	Applied Load (g)	Failure Time (hr.)
600	0.075	0.061	691.7	32.0
	0.075	0.061	691.7	28.4
	0.075	0.061	691.7	33.2
	0.075	0.061	691.7	30.5
	0.075	0.061	691.7	28.7
			Average Failure Time	30.6
			Standard Deviation	2.1
			Coefficient Variation	7%

Sample - II-48 inch Pipe Liner (10% Regrind)				
Applied Stress (psi)	Thickness (in)	Ligament Thickness (in)	Applied Load (g)	Failure Time (hr.)
600	0.088	0.070	798.3	14.9
	0.091	0.073	825.6	13.3
	0.090	0.072	816.5	13.3
	0.084	0.067	762.0	12.0
	0.075	0.060	680.4	14.9
			Average Failure Time	13.7
			Standard Deviation	1.2
			Coefficient Variation	9%

Sample - II-48 inch Pipe Plaque (20% Regrind)				
Applied Stress (psi)	Thickness (in)	Ligament Thickness (in)	Applied Load (g)	Failure Time (hr.)
600	0.076	0.062	703.1	33.0
	0.076	0.062	703.1	27
	0.076	0.062	703.1	27.1
	0.076	0.062	703.1	27.9
	0.076	0.062	703.1	28.7
			Average Failure Time	28.7
			Standard Deviation	2.5
			Coefficient Variation	9%
Applied Stress (psi)	Thickness (in)	Ligament Thickness (in)	Applied Load (g)	Failure Time (hr.)
600	0.081	0.065	734.8	12.4
	0.107	0.086	970.7	14.1
	0.105	0.084	952.6	13.8
	0.101	0.081	916.3	13.5
	0.106	0.085	961.6	13.1
			Average Failure Time	13.4
			Standard Deviation	0.7
			Coefficient Variation	5%

Sample - II-60 inch Resin Plaque (100% Virgin)				
Applied Stress (psi)	Thickness (in)	Ligament Thickness (in)	Applied Load (g)	Failure Time (hr.)
600	0.074	0.06	680.4	30.2
	0.075	0.061	691.7	42.5
	0.075	0.061	691.7	33.1
	0.075	0.061	691.7	21.7
	0.076	0.062	703.1	35.0
			Average Failure Time	32.5
			Standard Deviation	7.6
			Coefficient Variation	23%
Sample - II-60 inch Pipe Plaque (100% Virgin)				
Applied Stress (psi)	Thickness (in)	Ligament Thickness (in)	Applied Load (g)	Failure Time (hr.)
600	0.074	0.06	680.4	24.3
	0.074	0.06	680.4	23.8
	0.075	0.061	691.7	25.1
	0.075	0.061	691.7	26.1
	0.075	0.061	691.7	25.5
			Average Failure Time	25.0
			Standard Deviation	0.9
			Coefficient Variation	4%
Sample - II-60 inch Pipe Liner (100% Virgin)				
Applied Stress (psi)	Thickness (in)	Ligament Thickness (in)	Applied Load (g)	Failure Time (hr.)
600	0.171	0.137	1553.6	25.1
	0.163	0.130	1474.2	29.1
	0.162	0.130	1474.2	22.1
	0.147	0.118	1338.1	18.8
	0.142	0.114	1292.8	18.8
			Average Failure Time	22.8
			Standard Deviation	4.4
			Coefficient Variation	19%

Sample - III-24 inch Resin Plaque (100% Virgin)				
Applied Stress (psi)	Thickness (in)	Ligament Thickness (in)	Applied Load (g)	Failure Time (hr.)
600	0.075	0.061	691.7	55.7
	0.075	0.061	691.7	54.5
	0.075	0.061	691.7	58.8
	0.076	0.062	703.1	59.8
	0.076	0.062	703.1	51.2
			Average Failure Time	56.0
			Standard Deviation	3.5
			Coefficient Variation	6%
Sample - III-24 inch Pipe Plaque (100% Virgin)				
Applied Stress (psi)	Thickness (in)	Ligament Thickness (in)	Applied Load (g)	Failure Time (hr.)
600	0.074	0.06	680.4	55.2
	0.074	0.06	680.4	49.8
	0.075	0.061	691.7	55.1
	0.075	0.061	691.7	54.3
	0.075	0.061	691.7	54.9
			Average Failure Time	53.9
			Standard Deviation	2.3
			Coefficient Variation	4%
Sample - III-24 inch Pipe Liner (100% Virgin)				
Applied Stress (psi)	Thickness (in)	Ligament Thickness (in)	Applied Load (g)	Failure Time (hr.)
600	0.087	0.070	789.3	31.2
	0.093	0.074	843.7	31.2
	0.093	0.074	843.7	30.8
	0.09	0.072	816.5	33.9
	0.096	0.077	870.9	33.6
			Average Failure Time	32.1
			Standard Deviation	1.5
			Coefficient Variation	5%

Sample - III-30 inch Resin Plaque (100% Virgin)				
Applied Stress (psi)	Thickness (in)	Ligament Thickness (in)	Applied Load (g)	Failure Time (hr.)
600	0.075	0.061	691.7	12.2
	0.075	0.061	691.7	11.5
	0.075	0.061	691.7	12.7
	0.075	0.061	691.7	13.6
	0.075	0.061	691.7	12.3
			Average Failure Time	12.5
			Standard Deviation	0.8
			Coefficient Variation	6%

Sample - III-30 inch Pipe Plaque (100% Virgin)				
Applied Stress (psi)	Thickness (in)	Ligament Thickness (in)	Applied Load (g)	Failure Time (hr.)
600	0.076	0.062	703.1	13.8
	0.075	0.061	691.7	15
	0.075	0.061	691.7	15
	0.075	0.061	691.7	15
	0.074	0.06	680.4	13.8
			Average Failure Time	14.5
			Standard Deviation	0.7
			Coefficient Variation	5%

Sample - III-30 inch Pipe Liner (100% Virgin)				
Applied Stress (psi)	Thickness (in)	Ligament Thickness (in)	Applied Load (g)	Failure Time (hr.)
600	0.096	0.077	873.2	9.2
	0.095	0.076	861.8	8.9
	0.087	0.07	793.8	9.1
	0.08	0.064	725.8	9.5
	0.081	0.065	737.1	8.7
			Average Failure Time	9.1
			Standard Deviation	0.3
			Coefficient Variation	3%

Sample - III-30 inch Pipe Plaque (20% Regrind)				
Applied Stress (psi)	Thickness (in)	Ligament Thickness (in)	Applied Load (g)	Failure Time (hr.)
600	0.076	0.062	703.1	18.8
	0.076	0.062	703.1	15.8
	0.075	0.061	691.7	17.3
	0.074	0.06	680.4	15.1
	0.074	0.06	680.4	17.3
			Average Failure Time	16.9
			Standard Deviation	1.4
			Coefficient Variation	9%

Sample - III-30 inch Pipe Liner (20% Regrind)				
Applied Stress (psi)	Thickness (in)	Ligament Thickness (in)	Applied Load (g)	Failure Time (hr.)
600	0.091	0.073	825.6	9.5
	0.091	0.073	825.6	9.6
	0.101	0.081	916.3	9.1
	0.093	0.074	843.7	10.9
	0.094	0.075	852.8	9.5
			Average Failure Time	9.7
			Standard Deviation	0.7
			Coefficient Variation	7%

Sample - IV-24 inch Resin Plaque (100% Virgin)				
Applied Stress (psi)	Thickness (in)	Ligament Thickness (in)	Applied Load (g)	Failure Time (hr.)
600	0.076	0.062	703.1	23.30
	0.076	0.062	703.1	25.5
	0.076	0.062	703.1	28.6
	0.075	0.061	691.7	26.6
	0.075	0.061	691.7	24.6
			Average Failure Time	25.7
			Standard Deviation	2.0
			Coefficient Variation	8%

Sample - IV-24 inch Pipe Liner Plaque (75% Regrind)				
Applied Stress (psi)	Thickness (in)	Ligament Thickness (in)	Applied Load (g)	Failure Time (hr.)
600	0.073	0.059	669.1	18.2
	0.073	0.059	669.1	16.3
	0.073	0.059	669.1	18.0
	0.070	0.056	635.0	16.0
	0.070	0.056	635.0	14.3
			Average Failure Time	16.6
			Standard Deviation	1.6
			Coefficient Variation	10%

Sample - IV-24 inch Pipe Liner (75% Regrind)				
Applied Stress (psi)	Thickness (in)	Ligament Thickness (in)	Applied Load (g)	Failure Time (hr.)
600	0.071	0.057	646.4	8.9
	0.074	0.059	669.1	9.7
	0.082	0.066	748.4	8.7
	0.080	0.064	725.8	8.8
	0.080	0.064	725.8	8.6
			Average Failure Time	8.9
			Standard Deviation	0.4
			Coefficient Variation	5%

Sample - IV-24 inch Pipe Crown Plaque (5% Regrind)				
Applied Stress (psi)	Thickness (in)	Ligament Thickness (in)	Applied Load (g)	Failure Time (hr.)
600	0.074	0.06	680.4	19.9
	0.074	0.06	680.4	21.5
	0.074	0.06	680.4	18.9
	0.074	0.06	680.4	24.2
	0.074	0.06	680.4	21.5
			Average Failure Time	21.2
			Standard Deviation	2.0
			Coefficient Variation	9%

Sample - V-24 inch Resin Plaque (100% Virgin)				
Applied Stress (psi)	Thickness (in)	Ligament Thickness (in)	Applied Load (g)	Failure Time (hr.)
600	0.078	0.064	725.8	37.1
	0.078	0.064	725.8	33.6
	0.078	0.064	725.8	25.4
	0.080	0.066	748.4	37.1
	0.080	0.066	748.4	37.1
			Average Failure Time	34.1
			Standard Deviation	5.1
			Coefficient Variation	15%

Sample - V-24 inch Pipe Plaque (100% Virgin)				
Applied Stress (psi)	Thickness (in)	Ligament Thickness (in)	Applied Load (g)	Failure Time (hr.)
600	0.075	0.061	691.7	21.9
	0.075	0.061	691.7	23.6
	0.075	0.061	691.7	27.1
	0.076	0.062	703.1	24.7
	0.077	0.063	714.4	26.7
			Average Failure Time	24.8
			Standard Deviation	2.2
			Coefficient Variation	9%

Sample - V-24 inch Pipe Liner (100% Virgin)				
Applied Stress (psi)	Thickness (in)	Ligament Thickness (in)	Applied Load (g)	Failure Time (hr.)
600	0.08	0.064	725.8	11.8
	0.076	0.0608	689.5	13.7
	0.086	0.0688	780.2	11.7
	0.09	0.072	816.5	12.2
	0.084	0.0672	762.0	11.3
			Average Failure Time	12.1
			Standard Deviation	0.9
			Coefficient Variation	8%

Sample - V-24 inch Pipe Plaque (10% Regrind)				
Applied Stress (psi)	Thickness (in)	Ligament Thickness (in)	Applied Load (g)	Failure Time (hr.)
600	0.075	0.061	691.7	22.6
	0.075	0.061	691.7	20.8
	0.076	0.062	703.1	22.6
	0.076	0.062	703.1	21.3
	0.076	0.062	703.1	20.5
			Average Failure Time	21.6
			Standard Deviation	1.0
			Coefficient Variation	5%

Sample - V-24 inch Pipe Liner (10% Regrind)				
Applied Stress (psi)	Thickness (in)	Ligament Thickness (in)	Applied Load (g)	Failure Time (hr.)
600	0.075	0.060	680.4	11.0
	0.082	0.066	743.9	11.8
	0.08	0.064	725.8	9.0
	0.085	0.068	771.1	9.5
	0.087	0.070	789.3	9.7
			Average Failure Time	10.2
			Standard Deviation	1.2
			Coefficient Variation	11%

Sample - V-24 inch Pipe Plaque (20% Regrind)				
Applied Stress (psi)	Thickness (in)	Ligament Thickness (in)	Applied Load (g)	Failure Time (hr.)
600	0.075	0.061	691.7	25.4
	0.075	0.061	691.7	22.1
	0.075	0.061	691.7	21
	0.076	0.062	703.1	22.6
	0.076	0.062	703.1	22.3
			Average Failure Time	22.7
			Standard Deviation	1.6
			Coefficient Variation	7%

Sample - V-24 inch Pipe Liner (20% Regrind)				
Applied Stress (psi)	Thickness (in)	Ligament Thickness (in)	Applied Load (g)	Failure Time (hr.)
600	0.094	0.075	852.8	13.2
	0.075	0.060	680.4	9.7
	0.076	0.061	689.5	10.1
	0.086	0.069	780.2	10.4
	0.09	0.072	816.5	10.5
			Average Failure Time	10.8
			Standard Deviation	1.4
			Coefficient Variation	13%

Sample - V-36 inch Resin Plaque (100% Virgin)				
Applied Stress (psi)	Thickness (in)	Ligament Thickness (in)	Applied Load (g)	Failure Time (hr.)
600	0.074	0.06	680.4	35.8
	0.074	0.06	680.4	42.5
	0.075	0.061	691.7	36.2
	0.075	0.061	691.7	36.7
	0.075	0.061	691.7	37.5
			Average Failure Time	37.7
			Standard Deviation	2.7
			Coefficient Variation	7%

Sample - V-36 inch Pipe Plaque (100% Virgin)				
Applied Stress (psi)	Thickness (in)	Ligament Thickness (in)	Applied Load (g)	Failure Time (hr.)
600	0.074	0.060	680.4	28.6
	0.075	0.061	691.7	26.5
	0.075	0.061	691.7	26.6
	0.075	0.061	691.7	25.9
	0.076	0.062	703.1	23.7
			Average Failure Time	26.3
			Standard Deviation	1.8
			Coefficient Variation	7%

Sample - V-36 inch Pipe Liner (100% Virgin)				
Applied Stress (psi)	Thickness (in)	Ligament Thickness (in)	Applied Load (g)	Failure Time (hr.)
600	0.115	0.092	1043.3	13.9
	0.119	0.095	1079.6	13.3
	0.129	0.103	1170.3	14.7
	0.128	0.102	1161.2	15.1
	0.117	0.094	1061.4	14.9
			Average Failure Time	14.4
			Standard Deviation	0.8
			Coefficient Variation	5%

F.7.4 Oxidative Induction Time Test Data

Company	Diameter (in.)	Pure Resin (%)	Resin Std-OIT (min)			Pipe Std-OIT (min)		
			Test 1	Test 2	Average	Test 1	Test 2	Average
I	24	100	17.0	17.8	**17.4**	24.3	24.4	**24.3**
		90				18.3	19.0	**18.6**
		80				21.3	21.3	**21.3**
	36	100	64.4	68.1	**66.3**	43.3	45.8	**44.6**
		90				43.0	42.7	**42.9**
		80				39.7	40.1	**39.9**
	48	100	17.5	15.1	**16.3**	24.7	24.5	**24.6**
	60	100	15.8	15.0	**15.4**	10.5	10.3	**10.4**
II	24	100	31.3	25.1	**28.2**	30.5	30.9	**30.7**
		90				31.0	29.8	**30.4**
		80				32.2	24.8	**28.5**
	36	100	27.2	25.4	**26.3**	26.4	25.4	**25.9**
	48	100	20.9	18.8	**19.8**	23.7	22.5	**23.1**
		90				26.7	26.5	**26.6**
		80				27.4	26.8	**27.1**
	60	100	40.0	39.8	**39.9**	33.9	34.6	**34.2**
III	24	100	5.3	8.4	**6.8**			
	24 (crown)	95				11.3	10.1	**10.7**
	24 (liner)	75				8.5	8.2	**8.3**
IV	24	100	12.2	9.9	**11.1**	8.8	7.8	**8.3**
		90				8.1	7.7	**7.9**
		80				9.3	7.9	**8.6**
	36	100	8.4	6.7	**7.5**	8.6	8.9	**8.8**
V	24	100	14.5	11.3	**12.9**	25.1	24.0	**24.5**
	36	100	27.6	23.7	**25.7**	29.9	31.0	**30.5**
		80				35.0	32.3	**33.7**

APPENDIX G

Proposed Standard for Stub Compression Test

Test Method for Determination of Compression Capacity for Profile Wall Plastic Pipe by Stub Compression Loading

1. Scope

1.1 This test method covers determination of compression capacity of profile wall plastic pipe in the stub compression test.

1.2 This test method covers thermoplastic resin pipe.

1.3 *This standard does not purport to address all of the safety concerns, if any, associated with its use. It is the responsibility of the user of this standard to establish appropriate safety and health practices and to determine the applicability of regulatory limitations prior to use.*

2. Referenced Documents

2.1 ASTM Standards:

D695—Test Method for Compressive Properties of Rigid Plastic[1]

D1600—Terminology for Abbreviated Terms Relating to Plastics[1]

D2122—Test Method for Determining Dimensions of Thermoplastic Pipe and Fittings[2]

F412—Terminology Relating to Plastic Piping Systems[2]

3. Terminology

3.1 *Definitions:* Definitions are in accordance with Terminology F412, and abbreviations are in accordance with Terminology D1600, unless otherwise specified.

3.2 *Definitions of Terms Specific to This Standard:*

3.2.1 *Local Buckling*—local wrinkling resulting from compressive load in one or more elements of the wall section visible to the eye. When advanced, it may result in failure of the entire profile.

3.2.2 *Period*—the length of a single repetition of the corrugation or rib pattern, defined as the distance from the centerline of a valley or liner element to the centerline of the adjacent valley or liner element (see Figure G-1).

3.2.3 *Profile Height*—the distance from the surface of the inside wall of the pipe (inner surface of the valley or liner element) to the surface of the outside wall of the pipe (outer surface of the crest or rib element in Figure G-1). May also be determined as (OD-ID)/2.

3.2.4 *Profile Wall*—thin-walled pipe with corrugated or ribbed geometry.

4. Summary of Test Method

4.1 A small sample of pipe wall is compressed between two rigid plates at a controlled rate. Both plates are fixed with respect to rotation. The sample has a longitudinal length of three periods and a chord (circumferential) length of 1.5 times the profile height. Load, displacement (of the load plates), and time data are obtained. The test ends when the ultimate load is exceeded and the level of load begins to decrease. The ultimate load, cross-head displacement at ultimate load, and test time at ultimate load are recorded.

5. Significance and Use

5.1 The maximum load achieved in this test may be used for the following:

5.1.1 To evaluate compression load capacity of profile wall thermoplastic pipe.

5.1.2 To evaluate the manufactured consistency of pipe wall cross-section thickness distribution.

6. Apparatus

6.1 *Testing Machine*—A properly calibrated compression testing machine of the constant-rate-of-cross-head-movement type meeting the requirements of ASTM

[1] *Annual Book of ASTM Standards,* Vol 08.01.

[2] *Annual Book of ASTM Standards,* Vol 08.04.

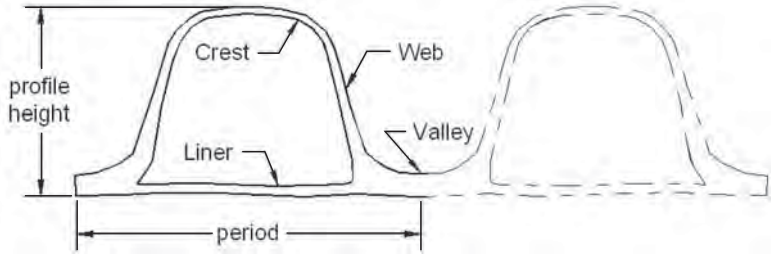

Figure G-1. Typical lined profile wall.

Test Method D695 shall be used to conduct the test. The rate of head approach shall be 0.05 ± 0.01 in./min (1.27 ± 0.25 mm/min). The testing machine shall be capable of compressing the sample to its capacity. The testing machine shall monitor the applied load to accuracy of ± 25 lbs (110 N).

6.2 *Loading Plates*—The load shall be applied to the specimen through two parallel steel bearing plates. The plates shall be flat, smooth, and clean. The thickness of the plates shall be sufficient so that no bending or deformation occurs during the test, but shall not be less than 0.25 in. (6.0 mm). The plate length shall equal or exceed the specimen longitudinal length and the plate width shall not be less than the profile height plus 6.0 in. (150mm).

6.3 *Deflection Indicator*—The cross-head displacement shall be measured with a suitable instrument meeting the requirements of Test Method D695, except that the instrument shall be accurate to 0.001 in. (0.025 mm).

7. Sampling, Test Specimens, and Test Units

7.1 The test specimen shall be a wall section cut from a finished pipe product.

7.2 The specimen longitudinal length shall be three periods.

7.3 The specimen chord (circumferential) length shall be 1.5 times the profile height with tolerance of ¼ in.

7.4 Specimen ends shall be cut flat and parallel to each other and to the radial line through the center of the sample. The cut ends are not radial.

Note 1—The most important aspect of specimen preparation is cutting the ends to a plane surface. This is complicated by the thin flexible elements of many profile wall pipes. Guidance for specimen preparation is provided in Annex A.

8. Conditioning

8.1 Condition pipe for at least 4 h in air, at a temperature of 73.4 ± 3.6°F (23 ± 2°C), and conduct the test in a room maintained at the same temperature.

9. Procedure

9.1 Record the pipe nominal diameter, pipe model/classification, profile type, manufacturer, conditioning temperature, and date of test.

9.2 Make and record the following measurements for each specimen:

9.2.1 Determine the longitudinal length of each specimen to the nearest 1/16 in. (1.5 mm), by making and averaging three measurements equally spaced over the chord length.

9.2.2 Determine the chord length of each specimen to the nearest 1/16 in. (1.5 mm), by making and averaging three measurements equally spaced along the longitudinal length.

9.2.3 Determine the profile height of each specimen to the nearest 1/16 in. (1.5 mm), by making and averaging three measurements equally spaced along the longitudinal length.

9.3 Place the specimen on the lower plate, centering the specimen under the testing machine cross-head vertical axis, as illustrated in Figure G-2.

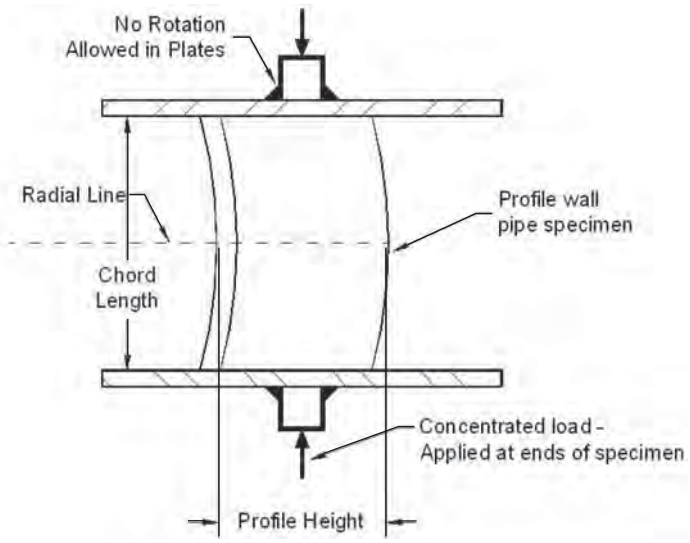

Figure G-2. Stub compression test setup.

Table G-1. Stub Compression Test—Precision Statistics.[A]

Material	Sample	Average	S_{mean}	S_r[B]	S_R[C]	r	R	Standard Deviation of Averages[D]	Repeatability Standard Deviation[D]	Reproducibility Standard Deviation[D]	Repeatability Limit (95%)[D]	Reproducibility Limit (95%)[D]
HDPE	24A	726	59.1	56.6	49.1	111	96	8.1	7.8	6.8	15.3	13.3
HDPE	24C	891	76.1	70.8	60.9	139	119	8.5	7.9	6.8	15.6	13.4
PVC	24D	1991	118.6	84.9	122.5	166	240	6.0	4.3	6.2	8.4	12.1
HDPE	42B	952	68.8	55.5	59.4	109	116	7.2	5.8	6.2	11.4	12.2
HDPE	42C	998	80.5	65.1	60.9	128	119	8.1	6.5	6.1	12.8	12.0

[A]Terms are as specified in ASTM Practice E177.
[B]S_r = standard deviation of repeatability (variation of replicate samples by the same laboratory).
[C]S_R = standard deviation of reproducibility (variation between laboratories).
[D]Precision statistics as percent of average.

9.4 With the displacement indicator in place, bring the upper plate into contact with the specimen with no more than 50 lbs (220 N) seating force.

9.5 Compress the sample at a constant rate of 0.05 ± 0.01 in./min (1.27 ± 0.25 mm/min).

9.6 Record the load, displacement, and time measurements continuously or intermittently with reference to the relative movement of the bearing plates. If measurements are made intermittently, make and record such measurements at increments of not more than 1% of the original specimen chord length.

9.7 Note the ultimate load carried by the sample.

9.8 Discontinue the test when the load on the specimen fails to increase with increasing deflection.

10. Calculation or Interpretation of Results

10.1 Calculate the ultimate compressive load capacity per unit length of pipe wall as the ultimate load (lbs) divided by the average longitudinal length (in.).

11. Report

11.1 Report the following information:

11.1.1 Agency conducting test.

11.1.2 Date of test.

11.1.3 Complete identification of the material tested, including type, source, manufacturer's code, previous history (if any), product identification by standard number, and pipe nominal diameter.

11.1.4 Specimen dimensions, including longitudinal length, chord length, and profile height.

11.1.5 Conditioning temperature, time, and environment.

11.1.6 The ultimate load carried by the specimen.

11.1.7 The ultimate compressive load capacity of the pipe wall.

11.1.8 The average load rate throughout the test duration.

12. Precision and Bias

12.1 *Precision*—An interlaboratory study of stub-compression-test ultimate loads was conducted with six laboratories participating. The pipe samples were 24A = 24-in. PE corrugated pipe, 24C = 24-in. PE corrugated pipe, 24D = 24-in. PVC ribbed pipe, 42B = 42-in. PE corrugated pipe, and 42C = 42-in. PE corrugated pipe. Information regarding the precision is found in Table G-1.

13. Keywords

13.1 Stub compression, thermoplastic pipe, compression, local buckle

ANNEX

(Nonmandatory Information)
A. Specimen Preparation

A.1 This annex provides a detailed procedure for preparing specimens for the stub compression test. Specimens are composed of thin elements and are very flexible; therefore, clamping and care are required to produce parallel ends for loading between the parallel plates. Suggested tools are those found to work best during the research to develop this standard. Other labs may use different procedures or equipment.

A.2 The detailed specimen cutting procedure follows:

A.2.1 Rough-cut specimens from the pipe to a chord length approximately 2 in. longer than the final chord length of 1.5 times the corrugation depth using a reciprocating saw.

A.2.2 Square the longitudinal ends to be parallel to the circumference of the pipe. Use a band saw or belt sander to ensure that the ends are square and evaluate with a carpenter's square (Figure G-A-1a).

A.2.3 Cut the circumferential ends of each specimen square and parallel with a band saw. Use a wood cutting sled to slide along the saw table (Figure G-A-1b). Align the specimen with the longitudinal axis of the cutting sled and use the centerline of the cutting sled to center the specimen (Figure G-A-1c). Tighten the wing nuts on both ends of the cutting sled so the specimen will not move during cutting, but not so tight as to flatten the specimen against the cutting sled.

A.2.4 To ensure a square cut, place a wooden board flush against the band saw fence and place the cutting sled flush against the wooden board. Align the specimen with the band saw blade and run the specimen through the saw several times, holding the cutting sled flat on the band saw platform with the end tight to the wooden board (Figure G-A-1d). Each time the specimen is cut, take smaller and smaller slices from opposite sides of the specimen until the specimen chord length is within the specified tolerance of 1.5 times the profile height, and the ends are parallel. Experience shows that the end surface is flatter with each cut.

A.2.5 Place the specimen on a flat, level surface to check that the ends are plane, parallel, and square. Place a 6-in. level on the specimen in several locations to check that ends are plane along the specimen length and across the corrugation depth. Use a carpenter's square to check that the specimen center is parallel with a radial line from the center of the pipe from which the specimen was removed. Flip the specimen so that the opposing end is flat against the table and repeat these checks (Figure G-A-1a).

A.2.6 If necessary, make small adjustments to the ends of the sample using a belt sander. Following any adjustments, repeat checks for plane, parallel, and square ends described in the previous step.

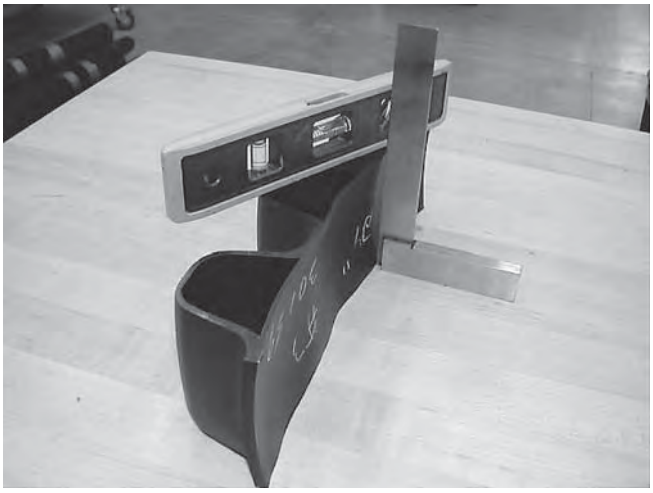

a. Check for Quality of Specimen Cuts

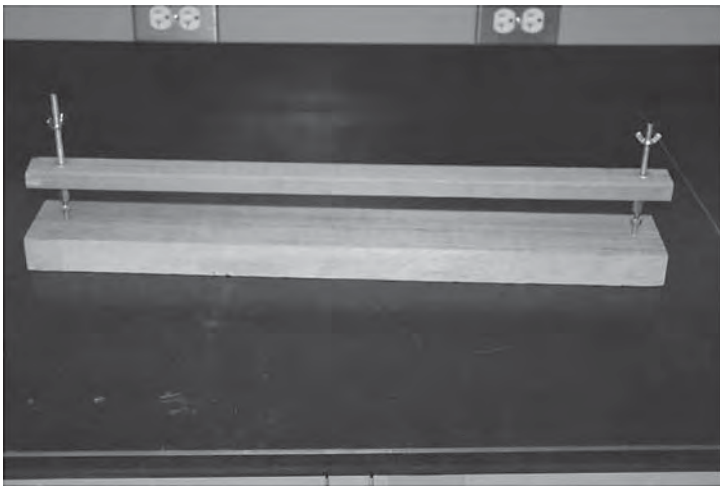

b. Cutting Sled

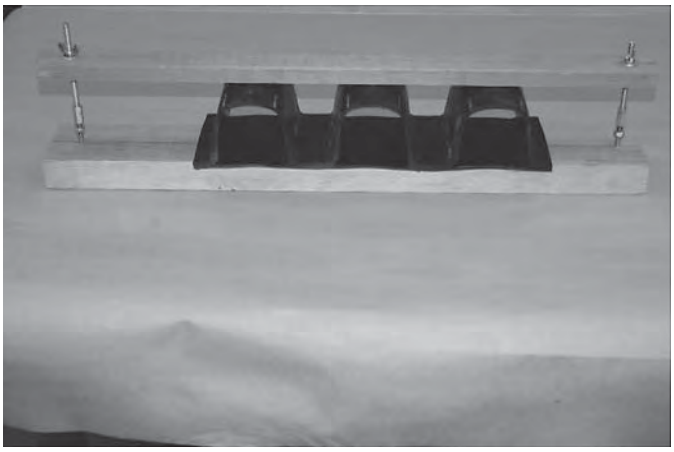

c. Cutting Sled with Specimen

d. Cutting Specimen

Figure G-A-1. Specimen cutting procedure.

APPENDIX H

Proposed Design Specifications for Buried Thermoplastic Pipe

SPECIFICATIONS	COMMENTARY
3.4.1 Load Factors and Load Combinations	**C.3.4.1**
Table 3.4.1-2 Load Factors for Permanent Loads, γ_p : Insert new load factors for earth load for thermoplastic culverts. Thermoplastic culverts: Maximum 1.3 Minimum: 0.9	Load factors for earth loads have traditionally been set at about 2.0 for flexible culverts and 1.3 for rigid culverts. Since the uncertainty of earth load magnitude for flexible and rigid culverts should be similar, the earth load factor is set to 1.3; however, to preserve the overall safety at the same levels as historical specifications, an earth-load-installation factor is introduced later in these specifications. This factor may be adjusted based on field control of construction practices.
3.6.1.2.6 Distribution of Wheel Loads Through Earth Fills	**C3.6.1.2.6**
Waiting for results of NCHRP Project 15-29, Design Specifications for Live Load Distribution to Buried Structures.	
12.4.1.3 Envelope Backfill Soils	**C12.4.1.3**
As a minimum, bedding and backfill materials shall meet the requirements of AASHTO M145 for A-1, A-2-4, A-2-5, or A-3 soils. A maximum of 50% of the particle sizes may pass the 0.150 mm (No. 100).	The restriction on materials passing the 0.150-mm (No. 100) sieve is intended to eliminate uniform fine sands for use as pipe embedment. Such materials are difficult to work with, are sensitive to moisture content, and do not provide support comparable to coarser or more broadly graded materials at the same percentage of maximum density. Restricted materials include some A-1-b, A-3, A-2-4, and A-2-5 soils. The engineer may permit exceptions to these restrictions in special cases. If so, a suitable plan should be submitted for control of moisture content and compaction procedures. These silty and clayey materials should never be used in a wet site. Increased inspection levels should be considered if such a plan is approved.
12.5.5 Resistance Factors	**C12.5.5**
Table 12.5.5-1 Resistance Factors for Buried Structures PE and PVC Pipe: Thrust $\phi_T = 1.00$ Soil stiffness $\phi_s = 0.90$ Global buckling $\phi_{bck} = 0.70$ Flexure $\phi_f = 1.00$	The new design methods evaluate more load conditions than prior specifications. Separate resistance factors are provided for each mode of behavior.

SPECIFICATIONS	COMMENTARY
12.5.6.3 Flexibility Limits and Construction Stiffness – Thermoplastic Pipe	
No changes proposed.	
12.6.6.3 Minimum Soil Cover	**C12.6.6.3**
Revise provisions for thermoplastic pipe: General ID/8 ≥ 12 in. Under pavement ID/2 ≥ 24 in.	McGrath and Beaver (2005) have shown that the significant thermal expansion in thermoplastic pipe can affect pavement performance under shallow fills.
12.12 THERMOPLASTIC PIPES	
12.12.1 General	**C12.12.1**
No changes proposed.	No changes proposed.
12.12.2 Service Limit States	**C12.12.2**
No changes proposed.	No changes proposed.
12.12.2.1 Deflection Requirement	**C12.12.2.1**
Total deflection, Δ_t, shall be less than the allowable deflection, Δ_A, as follows: $\Delta_t \leq \Delta_A$ where: Δ_t = total deflection of pipe expressed as a reduction of the vertical diameter (mm, in.) Δ_A = total allowable deflection of pipe, reduction of vertical diameter (mm, in.)	Deflection is controlled through proper construction in the field, and construction contracts should place responsibility for control of deflections on the contractor. However, feasibility of a specified installation needs to be checked prior to writing the project specifications. Pipe deflection is defined positive for reduction of the vertical diameter and expansion of horizontal diameter. The construction specifications set the allowable deflection, Δ_A, for thermoplastic pipe at 5% as a generally appropriate limit. The Engineer may accept alternate deflection limits for specific projects if calculations using the design method in this section show that the pipe meets all of the strength-limit-state requirements.

SPECIFICATIONS

Total deflection shall be calculated using Spangler's expression for predicting flexural deflection in combination with the expression for circumferential shortening.

$$\Delta_t = \frac{\left(D_L\ K_B\ P_{sp} + C_L P_L\right) D_o}{E_p I_p / R^3 + 0.061\, M_s} + \varepsilon_{sc} D \qquad (12.12.1)$$

in which:

$$\varepsilon_{sc} = T_s / \left(A_{eff} E_p\right) \qquad (12.12.2)$$

$$T_s = P_s \left(\frac{D_o}{2}\right) \qquad (12.12.3)$$

where:

ε_{sc} = service compressive strain due to thrust, as specified in 12.12.4.1.3 (dimensionless)

T_s = service thrust per unit length (N/mm)

D_L = deflection lag factor (dimensionless)

K_B = bedding coefficient (dimensionless)

P_{sp} = soil prism pressure (EV), evaluated at pipe springline (MPa, psf)

C_L = live-load distribution coefficient (dimensionless)

P_L = design live-load pressure including vehicle, dynamic load allowance, and multiple presence effect (MPa, psf)

D_o = outside diameter of pipe (mm, in.)

E_p = short- or long-term modulus of pipe material, as specified in Table 12.12.3.3-1 (MPa, psf)

I_p = moment of inertia of pipe profile per unit length of pipe (mm^4/mm, $in.^4$/in.)

R = radius from center of pipe to centroid of pipe profile (mm, in.)

COMMENTARY

This equation uses the constrained soil modulus, M_s, as the soil property. Note that the soil prism load is used as input, rather than the reduced load used to compute thrust.

This check should be completed to determine that the expected field deflection based on thrust and flexure is lower than the maximum allowable deflection for the project.

Thrust and hoop strain in the pipe wall are defined positive for compression.

There are no standard values for the deflection lag factor. It should be taken greater than 1.0. A value of 1.5 is typical.

The bedding coefficient, K, varies from 0.083 for full support to 0.110 for line support at the invert. Haunching is always specified to provide good support; however, it is still common to use a value of K equal to 0.10 to account for inconsistent haunch support.

SPECIFICATIONS | **COMMENTARY**

= D/2

D = diameter to centroid of pipe profile (mm, in.)

M_s = secant constrained soil modulus, as specified in 12.12.3.4-1 (MPa, psf)

P_s = design service load (MPa, psf)

A_{eff} = effective area of pipe wall per unit length of pipe in Article 12.12.4.1.2.2 (mm^2/mm, $in.^2$/in.)

12.12.3 Safety Against Structural Failure

12.12.3.1 General

Buried thermoplastic culverts shall be investigated at the strength limit state for thrust, general and local buckling, and combined strain.

C12.12.3.1

Total compressive strain in a thermoplastic pipe can cause yielding or buckling, and total tensile strain can cause cracking.

12.12.3.2 Section Properties

Section properties for thermoplastic pipe should be determined from cut sections of pipe or obtained from the pipe manufacturer. These include wall area, moment of inertia, and profile geometry.

C12.12.3.2

Historically, the AASHTO specifications have contained minimum values for the moment of inertia and wall area of thermoplastic pipe; however, these values have been minimum values and are not meaningful for design. This is particularly so since provisions to evaluate local buckling were introduced in 2001. These provisions require detailed profile geometry that varies with manufacturer. Thus, there is no way to provide meaningful generic information on section properties. A convenient method for determining section properties for profile wall pipe is to make optical scans of pipe wall cross-sections and determine the properties with a computer drafting program.

SPECIFICATIONS	COMMENTARY
12.12.3.3 Chemical and Mechanical Requirements Mechanical properties for design shall be as specified in Table 1. Except for buckling, the choice of either initial or long-term mechanical property requirements, as appropriate for a specific application, shall be determined by the Engineer. Investigation of general buckling shall be based on the value of modulus of elasticity that represents the design life of the project.	**C12.12.3.3** Properties in Table 1 include “initial” and “50-year” values. No product standard requires determining the actual long-term properties; thus, there is some uncertainty in the actual values. However, pipe designed with the Table 1 values for 50-year modulus of elasticity have performed well, and the properties are assumed to be reasonably conservative. Estimated values for a modulus of elasticity for a 75-year design life have been estimated from relaxation tests on PVC and PE in parallel plate tests. The tests were conducted for over two years and show that the modulus of elasticity reduces approximately linearly with the logarithm of time. Further, with a log-linear extrapolation, the differences between 50-year and 75-year modulus values are very small. These values should be reasonably conservative, with the same reliability as the 50-year values. Pipe and thermoplastic resin suppliers should be asked to provide confirmation of long-term moduli values for any particular product.

Table 12.12.3.3-1. Mechanical Properties of Thermoplastic Pipe

Type of Pipe	Minimum Cell Class	Service Long-Term Tension Strain (%)	Factored Compr. Strain Limit (%)	Initial		50-Year		75-Year	
				F_u min	E min	F_u min	E min	F_u min	E min
Solid Wall PE Pipe – ASTM F714	ASTM D3350, 335434C	5.0	4.1	3.0	110.0	1.44	22.0	1.4	21
Corrugated PE Pipe – AASHTO M294	ASTM D3350, 435400C	5.0	4.1	3.0	110.0	0.90	22.0	0.9	21
Profile PE Pipe – ASTMF894	ASTM D3350, 334433C	5.0	4.1	3.0	80.0	1.12	20.0	1.1	19
	ASTM D3350, 335434C	5.0	4.1	3.0	110.0	1.44	22.0	1.4	21
Solid Wall PVC Pipe –AASHTO M278, ASTM F679	ASTM D1784, 12454C	5.0	2.6	7.0	400.0	3.70	140.0	3.6	137
	ASTM D1784, 12364C	3.5	2.6	6.0	440.0	2.60	158.4	2.5	156
Profile PVC Pipe – AASHTO M304	ASTM D1784, 12454C	5.0	2.6	7.0	400.0	3.70	140.0	3.6	137
	ASTM D1784, 12364C	3.5	2.6	6.0	440.0	2.60	158.4	2.5	156

SPECIFICATIONS

COMMENTARY

12.12.3.4 Thrust

Loads on buried thermoplastic pipe are based on the soil prism load, modified as necessary to consider the effects of pipe-soil interaction. Because of the time-dependent nature of thermoplastic pipe properties, the load will vary with time. Calculations must consider the duration of a load when selecting pipe properties to be used in design. Live loads need not be considered for the long-term loading condition.

C12.12.3.4

Time of loading is an important consideration for some types of thermoplastic pipe. Live loads and occasional flood conditions are normally considered short-term loads. Earth loads or permanent high groundwater are normally considered long-term loads.

12.12.3.5 Factored and Service Load

The factored load, P_u, shall be taken as:

$$P_u = \eta_{EV}\left(\gamma_{EV} K_{gE} K_2 VAF\, P_{sp} + \gamma_{WA}\, P_W\right) + \eta_{LL}\gamma_{LL}\, P_L\, C_L \qquad (12.12.4)$$

$$P_s = K_2 VAF\, P_{sp} + P_L\, C_L + P_W \qquad (12.12.5)$$

in which:

$$VAF = 0.76 - 0.71\left(\frac{S_H - 1.17}{S_H + 2.92}\right) \qquad (12.12.6)$$

$$S_H = \frac{\varphi_s M_s R}{E_p A_g} \qquad (12.12.7)$$

$$C_L = \frac{L_W}{D_o} \le 1.0 \qquad (12.12.8)$$

$$L_W = W_0 + LLDF(H) \qquad (12.12.9)$$

where:

P_u = factored load (MPa, psf)

K_{gE} = 1.5; installation factor to provide traditional safety. Use of a value less than 1.5 requires additional monitoring of the installation during construction, and provisions for such monitoring must be provided on the contract documents.

K_2 = coefficient to account for variation of

C12.12.3.5

For η factors, refer to Article 12.5.4 regarding assumptions about redundancy for earth loads and live loads.

The factor K_2 is introduced to consider variation in thrust around the circumference, which is necessary when combining thrust with moment or thrust due to earth and live load under shallow fill. K_2 is set at 1.0 to determine thrust at the springline and 0.6 to determine thrust at the crown. The term P_L is also modified for this reason in later sections.

Figure C3.11.3-1 shows the effect of groundwater on the earth pressure. P_{sp} does not include the hydrostatic pressure. P_{sp} is the pressure due to the weight of soil above the pipe and should be calculated based on the wet density for soil above the water table and based on the buoyant density for soil below the water table. See Table 3.5.1-1 for common unit weights.

In computing L_W, add axle spacing (and increase total live load) if depth is sufficient for axle loads to interact.

The factor K_{gE} is introduced to provide the same safety level as traditionally used for thermoplastic culverts. Designers may consider the use values of K_{gE} as low as 1.0 provided that procedures are implemented to ensure compliance with construction specifications. Provisions to

SPECIFICATIONS

thrust around the circumference
= 1.0 for thrust at the springline
= 0.6 for thrust at the crown or haunch region

VAF = vertical arching factor (dimensionless)

S_H = hoop stiffness factor (dimensionless)

P_W = hydrostatic water pressure at the springline of the pipe (MPa, psf)

C_L = live-load distribution coefficient (dimensionless)

L_W = live-load distribution width in the circumferential direction at the elevation of the crown (mm, in.)

η_{EV} = load modifier as specified in Article 1.3.2, as they apply to vertical earth loads on culverts (dimensionless)

γ_{EV} = load factor for vertical pressure from dead load of earth fill, as specified in Article 3.4.1 (dimensionless)

P_{sp} = soil prism pressure (EV), evaluated at pipe springline (MPa, psf)

γ_{WA} = load factor for hydrostatic pressure, as specified in Article 3.4.1 (dimensionless)

η_{LL} = load modifier as specified in Article 1.3.2, as they apply to live loads on culverts (dimensionless)

γ_{LL} = load factor for live load, specified in Article 3.4.1 (dimensionless)

P_L = live-load pressure (LL) with dynamic load allowance (MPa, psf)

ϕ_s = resistance factor for soil stiffness

M_s = secant constrained soil modulus, as specified in Table 2 (MPa, psf)

COMMENTARY

provide such assurance include active monitoring of the backfill gradation and compaction levels at the side of the culvert and measurement of change in vertical pipe diameter when the backfill reaches the top of the pipe. At this point in the construction process the vertical pipe diameter should be greater than the vertical diameter prior to backfilling but not more than 3% greater than the vertical diameter prior to backfilling.

The use of the vertical arching factor is based on the behavior, demonstrated by Burns and Richard (1964), that pipe with high hoop-stiffness ratios (S_H, ratio of soil stiffness to pipe hoop stiffness) carry substantially less load than the weight of the prism of soil directly over the pipe. This behavior was demonstrated experimentally by Hashash and Selig (1990) and analytically by Moore (1995). McGrath (1999) developed the simplified form of the equation presented in this section.

The VAF approach is only developed for the embankment load case. No guidance is currently available to predict the reduced loads on pipe in trench conditions. The only trench load theory proposed for flexible pipe was that by Spangler, which does not have good guidance on selection of input parameters. It is conservative to use the VAF approach as presented for embankments.

The term ϕ_s appears in Equation 7 to account for variability in backfill compaction. A lower level of compaction increases the applied thrust force on the pipe.

SPECIFICATIONS	COMMENTARY
R = radius from center of pipe to centroid of pipe profile (mm, in.)	For selecting values of the constrained soil modulus, M_s, prior editions of the specifications contained the commentary "Suggested practice is to design for a standard Proctor backfill density five percent less than specified by the contract documents." This statement is not considered necessary with the addition of post-construction inspection guidelines to the LRFD Construction Specifications, which should provide reasonable assurance that the design condition is achieved.
E_p = short- or long-term modulus of pipe material, as specified in Table 1 (MPa, psf)	If evaluating the short-term load condition, then use the initial modulus of elasticity to compute S_H. Similarly, if evaluating the long-term loading condition, then use the long-term modulus of elasticity to compute S_H.
A_g = gross area of pipe wall per unit length of pipe (mm^2/mm, $in.^2/in.$)	
D_o = outside diameter of pipe (mm, in.)	
W_0 = width of live-load ground-surface contact area parallel to flow in pipe in Article 3.6.1.2.5 (mm, in.)	
LLDF = live-load-distribution factor	

SPECIFICATIONS

In the absence of site-specific data, the secant constrained soil modulus, M_s, may be selected from Table 1 based on the backfill type and density and the geostatic earth pressure, P_{sp}. Linear interpolation between soil stress levels may be used for the determination of M_s.

For culverts under depths of fill up to 3 m (10 ft), the soil type and density selected from Table 1 shall be representative of the conditions for a width of one-half diameter each side of the culvert, but never less than 0.5 m (18 in.) on each side of the culvert. For culverts under depths of fill greater than 3 m (10.0 ft), the soil type and density selected shall be representative of the conditions for a width of one diameter on each side of the culvert.

The constrained modulus may also be determined experimentally using the stress-strain curve resulting from a uniaxial strain test on a sample of soil compacted to the field-specified density. The constrained modulus is the slope of the secant from the origin of the curve to a point on the curve corresponding to the soil prism pressure, P_{sp}.

Insert current Table 12.12.3.4-1 as Table 1 (M_s values).

Insert current Table 12.12.3.4-2 as Table 1 (soil group descriptions).

12.12.3.7 Soil Prism

The soil-prism load shall be calculated as a pressure representing the weight of soil above the pipe springline. The pressure can be calculated for three conditions.

If the water table is above the top of the pipe and at or above the ground surface:

$$P_{sp} = (H + 0.11D_o)\gamma_b \qquad (12.12.10)$$

COMMENTARY

If the structural backfill material is compacted crushed stone, then the secant constrained soil modulus, M_s, values for Sn-100 may be used. If the backfill is uncompacted (dumped) crushed stone, use the modulus values for Sn-90. Although it is not common practice to monitor density of crushed stone backfills, experience has found that a modest compaction effort improves culvert performance and allows the use of the compacted values.

The width of structural backfill is an important consideration when the in situ soil in the trench wall or the embankment fill at the side of the structural backfill is soft. Currently, only AWWA's, *Fiberglass Pipe Design (M45)*, addresses this issue.

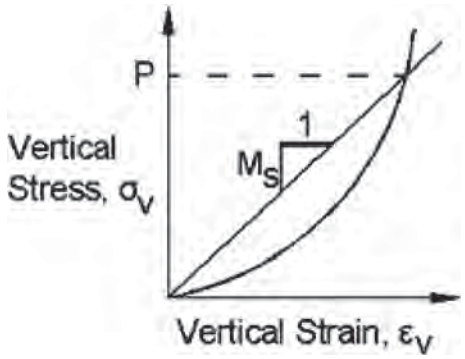

Figure C12.12.3.4.2-1. Schematic one-dimensional stress-strain curve of soil backfill.

C12.12.3.7

The soil prism load and vertical arching factor (VAF) serve as a common reference for the load on all types of pipe.

The soil prism calculation needs to consider the unit weight of the backfill over the pipe. Use the wet unit weight above the water table and the buoyant unit weight below the water table. In cases where the water table fluctuates, multiple conditions may need to be evaluated.

SPECIFICATIONS

COMMENTARY

If the water table is above the top of the pipe and below the ground surface:

$$P_{sp} = \left((H_W - 0.5D_o) + 0.11D_o\right)\gamma_b + \left((H - 0.5D_o) - H_W\right)\gamma_s \quad (12.12.11)$$

If the water table is below the top of the pipe:

$$P_{sp} = \left(H + 0.11D_o\right)\gamma_s \quad (12.12.12)$$

where:

P_{sp} = soil-prism pressure (EV), evaluated at pipe springline (MPa, psf),

D_o = outside diameter of pipe (mm, in.),

γ_b = unit weight of buoyant soil (N/m^3, lb/ft^3),

H = depth of fill over top of pipe (mm, in.),

H_w = depth of water table above springline of pipe (mm, in.), and

γ_s = wet unit weight of soil (N/m^3, lb/ft^3).

Figure C3.11.3-1 shows the effect of groundwater on the earth pressure. See Table 3.5.1-1 for common unit weights.

12.12.3.87 Hydrostatic Pressure

C12.12.3.87

The pressure due to ground water shall be calculated as:

$$P_W = \gamma_w \, K_{wa} \, H_w \quad (12.12.13)$$

where:

P_W = hydrostatic water pressure at the springline of the pipe (MPa, psf),

γ_W = unit weight of water (N/m^3, lb/ft^3), and

K_{wa} = factor for uncertainty in level of groundwater table.

Hydrostatic loading due to external water pressure should be calculated in all cases where the water table may be above the pipe springline at any time. This load contributes to hoop thrust but does not affect deflection.

There is often uncertainty in the level of the groundwater table and its annual variations. The designer may use the factor K_{wa} with values up to 1.3 to account for this uncertainty or may select conservative values of H_w.

SPECIFICATIONS

COMMENTARY

12.12.3.9 Live Load

The live load shall be determined as a pressure applied at the pipe crown. The live-load magnitude shall be based on the design vehicular live load in Article 3.6.1.2 and shall include modifiers for multiple presence/overload, dynamic load allowance, and distribution through cover soils.

The live-load pressure, P_L, shall be taken as

$$P_L = \frac{P\,(1 + IM/100)\,m}{(L_0 + (H + K_1)\,LLDF)(W_0 + (H + K_1)\,LLDF)} \quad (12.12.14)$$

where:

P_L = service live load on culvert (MPa, psf),

P = design wheel load in Article 3.6.1.2.2 (N, kip),

IM = dynamic load allowance in Article 3.6.2.2 (%),

m = multiple presence factor in Table 3.6.1.1.2-1 (dimensionless),

L_0 = length of live-load contact area parallel to pipe diameter in Article 3.6.1.2.5 (mm, in.),

H = depth of fill over top of pipe (mm, in.),

LLDF = factor for distribution of live load through earth fills in Article 3.6.1.2.6 (dimensionless),
= 1.15, 1.00

W_0 = width of live-load ground surface contact area parallel to flow in pipe in Article 3.6.1.2.5 (mm, in.),

K_1 = coefficient to consider design location,
= 0 for live load at the crown of the pipe, and
= $D_0/2$ for live load at the springline.

C12.12.3.9

Live-load calculations are included here to demonstrate the computation of live-load thrust at the crown and springline in accordance with current AASHTO. NCHRP Project 15-29 to revise this is nearing completion. This project is proposing no changes to the live-load distribution.

Increase as necessary if depth is sufficient for wheels and/or axles to interact.

Add axle spacing if depth is sufficient for axles to interact.

Add wheel spacing if depth is sufficient for wheels to interact.

Setting the term K_1 to 0 is the normal assumption in distributing live loads to the pipe and accounts for the load attenuating to the top of the pipe; however, the load continues to spread longitudinally along the pipe as it attenuates from the crown to the springline. Using the term $K_1 = D_0/2$ provides a means to account for this.

SPECIFICATIONS

COMMENTARY

12.12.4 Safety Against Structural Failure

12.12.4.1 Resistance to Axial Thrust

12.12.4.1.1 General

Elements of profile wall pipe shall be designed to resist local buckling. To determine local buckling resistance, profile-wall pipe geometry must be idealized and an effective area determined in accordance with the following provisions.

12.12.4.1.2 Local Buckling Effective Area

12.12.4.1.2.1 Idealized Wall Profile

No change from current 12.12.3.5.3b

12.12.4.1.2.2 Slenderness and Effective Width

To evaluate the resistance to axial thrust, the area of the profile is reduced to an effective area, A_{eff}, for local buckling effects. The effective area of the profile is determined by subtracting the ineffective area of each element from the gross section area, as follows:

$$A_{eff} = A_g - \sum (b - b_e)t \qquad (12.12.15)$$

in which:

$$b_e = \rho w \qquad (12.12.16)$$

$$\rho = \frac{\left(1 - 0.22/\lambda\right)}{\lambda} \qquad (12.12.17)$$

$$\lambda = \left(\frac{w}{t}\right)\sqrt{\frac{\varepsilon}{k}} \geq 0.673 \qquad (12.12.18)$$

$$\varepsilon = \frac{T_u}{A_g E_p} \qquad (12.12.19)$$

C12.12.4.1.2.2

Insert text from current C12.12.3.5.3c on p 12-74.4.

Insert text from current C12.12.3.5 on the bottom section of p 12-74.2.

The calculations in Equations 15 to 20 must be repeated for each element in the idealized profile.

$$T_u = P_u \left(\frac{D_o}{2} \right) \qquad (12.12.20)$$

Commentary: To complete the local buckling calculations, the profile is idealized into a group of rectangular elements. To complete the idealization, it should include (see NCHRP Project 4-26 final report for guidance on other profile types):

- Maintain the correct total area.
- If the crest element is curved, it should be idealized at the centroid of the curvature. The idealized element need not touch the idealized webs.

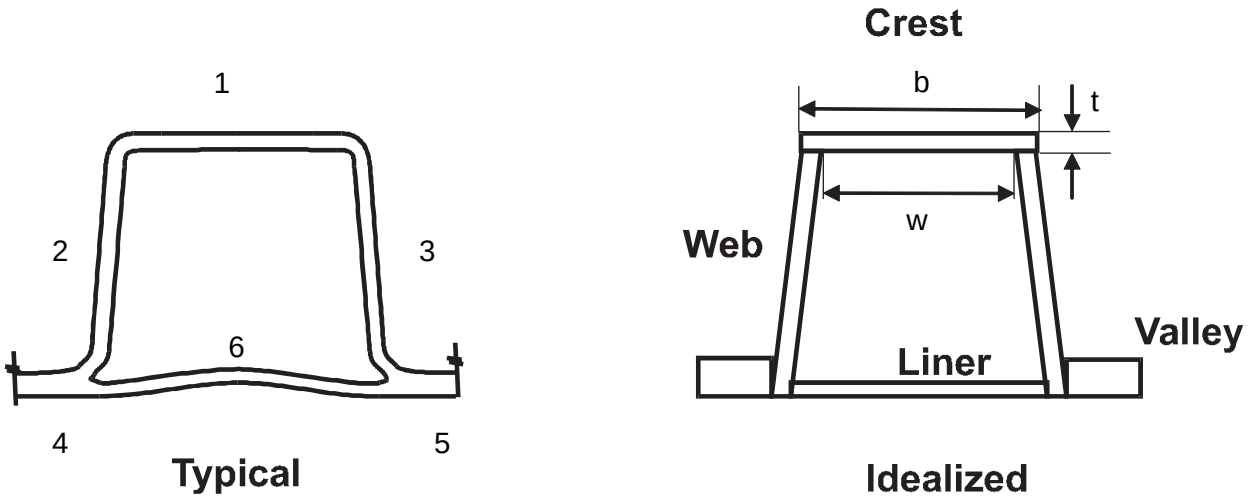

Figure C.12.12.4.1.2.2-1. Idealization of profile wall pipe into rectangular elements.

where:

A_{eff} = effective area of pipe wall per unit length of pipe (mm^2/mm, $in.^2$/in.),

b_e = element effective width (mm, in.),

ρ = effective width factor (dimensionless),

λ = slenderness factor (dimensionless),

ε = strain in element, iteration is not required (dimensionless),

T_u = factored thrust per unit length (N/mm),

A_g = gross area of pipe wall per unit length of pipe (mm^2/mm),

SPECIFICATIONS

COMMENTARY

b = total width of element (mm, in.),

t = thickness of element (mm, in.),

w = total clear width of element between supporting elements (mm, in.),

k = plate buckling coefficient, k=4 for supported elements, k=0.43 for unsupported elements, such as free standing ribs (dimensionless),

T_u = factored thrust per unit length (N/mm),

E_p = short- or long-term modulus of pipe material, as specified in Table 1 (MPa, psf),

P_u = design factored load (MPa, psf), and

D_o = outside diameter of pipe (mm, in.).

The plate buckling coefficient is analogous to the effective length factor, k, in column buckling.

12.12.4.1.2.3 Alternate Procedure for Determining Effective Area

C12.12.4.1.2.3

As an alternate to determining the effective area by the calculation procedure presented below, the results of the stub compression test, AASHTO T-XXX, may be used. The procedure is as follows:

The stub compression test has been incorporated as a requirement into AASHTO product standards M294 and M304. The test data should be readily available from manufacturers and quality control tests.

$$A_{eff} = \frac{P_{st} K_t}{F_u} \leq A_g \qquad (12.12.21)$$

in which:

P_{st} = stub compression capacity from T-XXX, lb/in. (N/mm),

K_t = time factor, from Table 1, and

F_u = material yield strength for design load duration, psi, MPa.

Time Period	PE	PVC
Initial	0.9	0.95
50-year	0.3	0.6
75-year (est.)	0.25	0.5

SPECIFICATIONS **COMMENTARY**

12.12.4.1.3 Compression Strain

The factored compressive strain due to factored thrust, ε_{uc}, and the service compressive strain due to service thrust, ε_{sc}, shall be taken as

$$\varepsilon_{uc} = T_u/\left(A_{eff} E_p\right) \quad (12.12.22)$$

$$\varepsilon_{sc} = T_s/\left(A_{eff} E_p\right) \quad (12.12.23)$$

where:

ε_{uc} = factored compressive strain due to thrust (dimensionless),

ε_{sc} = service compressive strain due to thrust (dimensionless),

T_u = factored thrust per unit length (N/mm),

T_s = service thrust per unit length (N/mm),

A_{eff} = effective area of pipe wall per unit length of pipe (mm^2/mm, $in.^2/in.$), and

E_p = short- or long-term modulus of pipe material, as specified in Table 1 (MPa, psf).

12.12.4.1.4 Compression Strain

The factored compression strain due to thrust, incorporating local buckling effects, ε_{uc}, shall not exceed the limiting compressive strain of the material.

$$\varepsilon_{uc} \leq \phi_T \varepsilon_{yc} \quad (12.12.24)$$

where:

ε_{uc} = factored compressive strain due to thrust (dimensionless),

ϕ_T = resistance factor for thrust effects (dimensionless), and

ε_{yc} = factored compression strain limit of the pipe wall material, Table 1 (dimensionless).

SPECIFICATIONS

COMMENTARY

12.12.4.1.5 General Buckling Requirement

The factored compression strain due to thrust, incorporating local buckling effects, ε_{uc}, shall not exceed the factored general buckling capacity of the pipe wall.

$$\varepsilon_{uc} \le \phi_{bck}\varepsilon_{bck} \qquad (12.12.25)$$

where:

ε_{uc} = factored compressive strain due to thrust (dimensionless),

ϕ_{bck} = resistance factor for global buckling (dimensionless), and

ε_{bck} = nominal strain capacity for general buckling (dimensionless).

The nominal strain capacity for general buckling of the pipe can be computed as:

$$\varepsilon_{bck} = \frac{1.2C_n\left(E_pI_p\right)^{1/3}}{A_{eff}E_p}\left(\frac{\phi_s M_s\left(1-2\nu\right)}{\left(1-\nu\right)^2}\right)^{2/3} R_h \qquad (12.12.26)$$

in which:

$$R_h = \frac{11.4}{11+D/H} \qquad (12.12.27)$$

where:

ε_{bck}= factored compressive strain due to thrust (dimensionless),

R_h = correction factor for backfill soil geometry (dimensionless),

C_n = calibration factor to account for non-linear effects = 0.55 (dimensionless),

E_p = short or long term modulus of pipe material, as specified in Table 12.12.3.3-1 (MPa, psf),

I_p = moment of inertia of pipe profile per unit length of pipe (mm^4/mm, $in.^4/in.$),

C12.12.4.1.5

The equations for global resistance presented here are a conservative simplification of the continuum buckling theory presented by Moore (1990). Detailed analysis using the full theory may be applied in lieu of the calculations in this section.

The term ϕ_s appears in this expression for ε_{bck} to account for backfills compacted to levels below that specified in the design. Lower levels of compaction increase the thrust force in the pipe.

For designs meeting all other requirements of these specifications and the AASHTO *LRFD Bridge Construction Specifications*, the correction for backfill soil geometry, R_h, is equal to value at left.

The complete theory proposed by Moore et al. provides variations in R_h that consider nonuniform backfill support. In the extreme case where the width of structural backfill at the side of the culvert is 0.1 times the span and the modulus of the soil outside of the structural backfill is 0.1 times the modulus of the backfill, then

$$R_h = \frac{20}{56+D/H} \qquad (C1)$$

SPECIFICATIONS

COMMENTARY

A_{eff} = effective area of pipe profile per unit length of pipe (mm^2/mm, $in.^2$/in.),

ϕ_s = resistance factor for soil pressure (dimensionless),

M_s = secant constrained soil modulus, as specified in Table 2 (MPa, psf),

ν = Poisson's ratio of soil (dimensionless),

Poisson's ratio is used to convert the constrained modulus of elasticity to the plane-strain modulus.

D = diameter to centroid of pipe profile (mm, in.), and

H = depth of fill over top of pipe (mm, in.).

12.12.4.2 Combined Bending and Thrust

12.12.4.2.1 General

To ensure adequate flexural capacity the combined strain at the extreme fibers of the pipe profile must be evaluated at the allowable deflection limits against the limiting strain values.

12.12.4.2.2 Combined Strain

C12.12.4.2.2

If summation of axial strain, ε_{uc}, and bending strain, ε_f, produces tensile strain in the pipe wall, check the combined strain at the extreme fiber where flexure causes tension:

$$\varepsilon_f - \varepsilon_{uc} < \phi_f \varepsilon_y \qquad (12.12.4.2.2\text{-}28)$$

Check the combined strain at the extreme fiber where flexure causes compression:

$$\varepsilon_f + \varepsilon_{uc} < \phi_f \left(1.5\varepsilon_{yc}\right) \qquad (12.12.4.2.2\text{-}29)$$

where:

ε_f = factored strain due to flexure (dimensionless),

ε_{uc} = factored compressive strain due to thrust (dimensionless),

ϕ_f = resistance factor for flexure

Insert text from current C12.12.3.5.4a on pp. 12-74.5 to 12-74.6.

Past practice has used service tensile strain limits specified in Table 12.12.3.3-1, with no guidance on ultimate strain limits. For purposes of design calculations, assume that ultimate tensile strain capacity is 50% greater than the service capacities provided in Table 12.12.3.3-1.

A higher strain limit is allowed under combined bending and compression. This increase is permitted because the web element under flexure has a low stress at the center of the element, reducing the likelihood of buckling, and allowing it to provide more stability to the crest and valley elements.

Flexural strains are always taken as positive.

SPECIFICATIONS

(dimensionless), and

ε_{yc} = ultimate tension strain of the pipe wall material, specified as 50% greater than the allowable long-term strain in Table 1 (dimensionless).

In the absence of a more-detailed analysis, the flexural strain may be computed based on the empirical relationship between strain and deflection as follows:

$$\varepsilon_f = \gamma_{EV} D_f \left(\frac{c}{R}\right)\left(\frac{\Delta_f}{D}\right) \qquad (12.12..4.2.2\text{-}30)$$

in which:

$$\Delta_f = \Delta_A - \varepsilon_{sc} D \qquad (12.12.4.2.2\text{-}31)$$

where:

ε_f = factored strain due to flexure (dimensionless)

Δ_f = reduction of vertical diameter due to flexure (mm, in.)

γ_{EV} = load factor for vertical pressure from dead load of earth fill, as specified in Article 3.4.1 (dimensionless)

D_f = shape factor from Table 12.12.4.5.2-1 (dimensionless) The shape factors for corrugated PE pipe can be reduced 1.0 from the table values to account for the effect of the low hoop stiffness ratio.

c = The larger of the distance from neutral axis of profile to the extreme innermost or outermost fiber (mm, in.)

R = radius from center of pipe to centroid of pipe profile (mm, in.)
= D/2

D = diameter to centroid of pipe profile (mm, in.)

Δ_A = total allowable deflection of pipe,

COMMENTARY

Peak flexural stress occurs near the crown for live-load conditions and near the haunch/invert region for deep burial cases. The factors K_1 and K_2 should be used in the thrust computations to determine the thrust strains used in Equations 1 and 2.

The service compressive strain is used for determination of the factored strain due to flexure instead of the ultimate compressive strain. The use of the ultimate compressive strain would result in an unconservative flexural strain demand.

Insert text from current C12.12.3.5.4b on p. 12-74.6.

The AASHTO Construction Specifications currently restrict the allowable total vertical deflection to 5%.

SPECIFICATIONS **COMMENTARY**

reduction of vertical diameter (mm, in.)

ε_{sc} = service compressive strain due to thrust (dimensionless)

No change from current Table 12.12.3.5.4b-1.

12.12.5 Handling

No change from current 12.12.3.6 text.

12.12.6 Construction and Installation

The contract documents shall require that the construction and installation conform to Section 30, "Thermoplastic Culverts," *AASHTO LRFD Bridge Construction Specifications*.

References

Burns, J.Q. and Richard, R.M., “Attenuation of Stresses for Buried Cylinders,” *Proceedings of Symposium on Soil-Structure Interaction*, University of Arizona, Tucson, 1964.

Hashash, N. and Selig, E.T., *Analysis of the Performance of Buried High Density Polyethylene Pipe.* Structural Performance of Flexible Pipes. Balkema, Rotterdam, Netherlands,1990.

McGrath, T.J., “Calculating Loads on Buried Culverts Based on Pipe Hoop Stiffness*,” Transportation Research Record 1656*, Transportation Research Board, Washington, D.C., 1999.

McGrath, T.J. and Beaver, J.L., *Performance of Thermoplastic Pipe Under Highway Vehicle Loading*, Research Report to Minnesota DOT, Oakdale, MN, Simpson Gumpertz & Heger Inc., 2005.

Moore, I.D., “Three-Dimensional Response of Elastic Tubes,” *International Journal of Solids and Structures*, Vol. 26, No. 4, 1990.

Moore, I.D., “Three Dimensional Response of Deeply Buried Profiled Polyethylene Pipe,” Paper No. 950822, 74th Annual Meeting, Transportation Research Board, Washington, D.C., 1995.

APPENDIX I

Proposed Construction Specifications for Buried Thermoplastic Pipe

SPECIFICATIONS **COMMENTARY**

SECTION 30 – THERMOPLASTIC CULVERTS

30.1 GENERAL

30.1.1 Description

This work shall consist of furnishing, installing, and inspecting buried thermoplastic pipe in conformance with these specifications and the contract documents.

C30.1.1

Plastic pipe is manufactured by a variety of methods with a variety of wall profiles. Common profiles are solid cylindrical wall with or without a standing rib, corrugated, and corrugated with a smooth liner.

As used in this specification, thermoplastic pipe is defined in the AASHTO *LRFD Bridge Design Specification*, Section 12, "Buried Structures and Tunnel Liners."

30.1.2 Importance of Construction Procedures

Satisfactory performance of culverts requires proper control of construction procedures at all times. The embedment material placed around a culvert provides a significant support that is relied upon in the culvert structural design. Together, the culvert and embedment form an integral soil-structure system. Therefore, selection of suitable quality backfill materials, which are then properly placed and compacted, is essential.

C30.1.2

In general, as the quality of backfill (represented primarily by the particle size and the portion of the backfill passing the No. 200 sieve) decreases, higher compaction levels (e.g., percentage of maximum density per AASHTO T99 or T190) are required to achieve equivalent culvert performance.

30.1.3 Terminology

Terminology used in this Specification is illustrated in Figure 1 and defined below:

Bedding is the material on which the structure is seated. It may be in situ soil, if such soil meets all necessary requirements, or imported backfill material. The bedding may be specified as a different material than the structural backfill.

Culvert bottom is the lowest point on the outside of the culvert for closed shapes.

Culvert crown is the highest point on the inside of the culvert.

SPECIFICATIONS	COMMENTARY

Culvert invert is the lowest point on the inside of the culvert for closed shapes.

Culvert top is the highest point on the outside of the culvert.

Embankment is the soil already placed and compacted in layers at the sides of and above the embedment zone.

Embedment zone is the zone of structural backfill around the culvert. It consists of bedding, haunch material, sidefill, and initial topfill.

Foundation soil is the soil that supports the bedding, culvert, and structural backfill. It must provide a firm stable surface and may be undisturbed, existing (in situ) soil, replaced and compacted in situ soil, or an imported material.

Haunch is the portion of the culvert between the culvert bottom and the springline.

Haunch zone is the region of the backfill between the bedding or foundation soil and the culvert surface from the culvert bottom to near the springline. It is a region where hand placement and compaction methods are normally required for the backfill. Backfill in the haunch zone is usually the same material as the structural backfill.

In situ soil is the native, undisturbed soil existing at the site of the culvert installation.

Shoulder is the portion of the culvert between the culvert top and the springline.

Sidefill is the embedment zone between the haunch and the shoulders of the culvert supporting the sides of the culvert.

Springline is the line along the side of the culvert where the tangent to the culvert wall is vertical. It occurs at the widest point in the culvert.

SPECIFICATIONS **COMMENTARY**

Structural backfill is all the material placed and compacted around the culvert to help support the culvert.

Topfill is the embedment zone over the top of the culvert beginning at the shoulders and extending upward to the limit of the structural backfill zone. The topfill is generally the same material as the structural backfill. For long-span culverts, it must be the same as the structural backfill.

30.2 WORKING DRAWINGS

When complete drawings are not provided in the contract documents, the Contractor shall provide to the Engineer, Manufacturer's installation instructions or working drawings and substantiating calculations in sufficient detail to permit a structural review. Sufficient copies shall be furnished to meet the needs of the Engineer and other entities with review authority. The working drawings shall be submitted sufficiently in advance of proposed installation and use to allow for their review, revision if needed, and approval without delay of the work. The Contractor shall not start construction of any thermoplastic pipe installations for which working drawings are required until the drawings have been approved by the Engineer. Such approval will not relieve the Contractor of responsibility for results obtained by use of these drawings or any of the other responsibilities under the contract.

30.3 MATERIALS

30.3.1 Thermoplastic Pipes

Polyethylene pipe (PE) shall conform to the material workmanship and inspection requirements of AASHTO M294, or ASTM F714 or F894.

Polyvinylchloride (PVC) pipe shall conform to the material workmanship and inspection requirements of AASHTO M278 or M304.

SPECIFICATIONS	COMMENTARY

30.3.2 Bedding Materials and Backfill

30.3.2.1 General

Bedding shall be granular material with a maximum particle size of 25 mm (1 in.). Backfill shall be granular materials as specified in the contract documents; shall be free of organic material, rock fragments larger than 38 mm (1.5 in.) in the greatest dimension, and frozen lumps; shall have a moisture content within the limits required for compaction.

As a minimum, bedding and backfill materials shall meet the requirements of AASHTO M 145 for A-1, A-2-4, A-2-5, or A-3 soils. A maximum of 50% of the particle sizes may pass the 0.150-mm (No. 100) sieve and a maximum of 20% may pass the 0.075-mm (No. 200) sieve.

C30.3.2.1

Granular backfill has 35% or less material by weight finer than the 0.075-mm (No. 200) sieve as defined in AASHTO M 145.

While it is economical to use in situ material for bedding culverts, the Engineer must verify that the in situ material meets the requirements stated in Section 30.3.2.1. This is often difficult, since in situ soils are highly variable. If use of in situ material is allowed, the Engineer should include provisions for assessing it during construction and importing new bedding material if necessary.

Construction of culverts during the winter months may pose potential problems when frozen soils are included in the backfill zone or when frost-susceptible soils are used as backfill material. Frozen soil will not compact effectively and may result in points of concentrated loads when frozen and regions of inadequate support upon thawing.

Frost-susceptible soils should not be used in the embedment zone within the frost penetration depth. This will exclude the use of silty sand or silty gravel where freezing temperatures occur.

The restriction on materials passing the 0.150-mm (No. 100) sieve and the 0.075-mm (No. 200) sieve is intended to eliminate soils composed of significant amounts of fine sands and silts. Such materials are difficult to work with, are sensitive to moisture content, and do not provide support comparable to coarser or more broadly graded materials at the same percentage of maximum density. Restricted materials include some A-1-b, A-3, A-2-4, and A-2-5 soils. All A-2-6 and A-2-7 soils display similar characteristics and are eliminated from use as backfill materials. The Engineer may permit exceptions to these restrictions in special cases. If so, a suitable plan should be submitted for control of moisture content and compaction procedures.

SPECIFICATIONS	COMMENTARY
	These silty and clayey materials should never be used in a wet site or if significant live loads will be imposed on the pipe. Increased inspection levels should be considered if such a plan is approved.
30.3.2.2 Control of Particle Migration	**C30.3.2.2**
The gradation of bedding and backfill materials shall be selected to prevent particle migration between adjacent materials. Gradations of in situ bedding, backfill, and embankment materials shall be evaluated for compliance with this requirement. Alternatively, a suitable geotextile may be used to maintain separation of incompatible materials.	Control of migration is based on the relative gradations of adjacent materials. Acceptable criteria include the following: $D_{15}/d_{85} < 5$ where D_{15} is the sieve-opening size passing 15% by weight of the coarser material and d85 is the sieve-opening size passing 85% by weight of the finer material. $D_{50}/d_{50} < 25$ where D_{50} is the sieve-opening size passing 50% by weight of the coarser material and d_{50} is the sieve-opening size passing 50% by weight of the finer material. This criterion need not apply if the coarser material is well graded as defined in ASTM D2487.
30.3.2.3 Controlled Low-Strength Material	**C30.3.2.3**
Controlled low-strength material (CLSM), also known as flowable fill, may be used as structural backfill. If not specified in the contract documents, a mix design and complete construction details must be submitted. Minimum construction details include methods for control of flotation forces, and waiting time between placing CLSM and backfilling over the structure.	FHWA Report FHWA-RD-98-191 (McGrath et al. 1998) indicates that CLSM can be an effective backfill material for thermoplastic culverts. Other research has been conducted on this subject, including *NCHRP Report 597—Development of a Recommended Practice for Use of Controlled Low-Strength Material in Highway Construction* (Folliard et al. 2008).
30.4 ASSEMBLY	
30.4.1 General	
Thermoplastic pipe units shall be assembled in accordance with the Manufacturer's instructions and as specified in the contract documents. Copies of the Manufacturer's assembly instructions shall be furnished to the installation crew. All pipes shall be unloaded and handled with reasonable care. Pipe and fittings shall not be rolled or dragged over gravel or rock. Care shall be taken	

SPECIFICATIONS	COMMENTARY

to prevent the units from striking rock or other hard objects during placement.

Damaged pipe or fittings shall not be incorporated into the project.

30.4.2 Joints

Joints for thermoplastic pipe shall comply with the details shown in the contract documents and on the approved working drawings. Each joint shall be sealed to prevent infiltration of soil (soiltight), fines (silttight), or water (watertight) as required by the contract documents. Field tests may be required by the Engineer whenever there is a question regarding compliance with the contract requirements.

Joints shall be installed so that the connection of pipe sections will form a continuous surface, free from irregularities in the flow line.

C30.4.2

Currently available joint types include corrugated bands, bell-and-spigot pipe ends, and double-bell couplings. All of these joint types can be supplied with or without gaskets. Other joint types may be used provided that documentation is provided to demonstrate that the joint meets the project requirements.

Joints are often provided as soiltight or watertight. Definitions of soiltight and silttight joints are vague. Examples can be found in AASHTO *LRFD Bridge Construction Specifications*, Section 26, "Metal Culverts." Watertight joints are normally specified to meet ASTM D3212. Pressure capability of joint shall be based on project requirements. Commonly available pressure capabilities are 0.015, 0.035, and 0.075 MPa (2, 5, and 10 psi). The AASHTO Materials Engineers are currently working on joint definition issues.

30.5 INSTALLATION

30.5.1 General

Space shall be provided at the site for storage of the culvert pipes unless they are installed as delivered.

Unanticipated ground conditions shall be reported to the Engineer. Water conditions shall be controlled so that pipes are laid in dry conditions.

All pipe laying, joining, and backfilling shall be in accordance with the stricter of the Manufacturer's instructions or these specifications.

C30.5.1

Controlling groundwater without violating the assumptions of the pipe design is important. It is often necessary to consult with a Geotechnical Engineer to address drainage issues.

SPECIFICATIONS	COMMENTARY
30.5.2 Excavation and Groundwater Control	**C30.5.2**
Excavation shall be to the width, depth, and grade shown in the contract documents. Trenches shall be excavated in such a manner as to ensure that the sides will be stable under all working conditions. All construction shall be in conformance to all applicable safety standards.	Since trench width has an impact on the performance of the pipe, the AASHTO *LRFD Bridge Design Specifications* also provided guidance on trench width.
Open only as much trench as can be safely maintained and backfill as soon as practicable, but not later than the end of each working day.	If possible, the trench walls below the top of the pipe should be vertical. The Engineer may allow trenches to be left open overnight provided that the excavation is secured in accordance with all applicable safety standards and prevented from accumulating water from rain.
Trench walls shall be sloped, benched, braced, or otherwise supported to ensure their stability throughout construction in conformance to all applicable safety standards. Remove large stones, rocks, and any debris falling into the trench.	Trench walls should be undisturbed in situ soil at least up to the top of the culvert at the time of backfilling.
Sloped walls may be benched to facilitate compaction of backfill against them. If horizontal trench bracing is use, it shall be removed as backfill progresses upward. Unless otherwise directed by the Engineer, sheeting driven below the top of the pipe elevation shall be left in place and cut off not less than 460 mm (1.5 ft) above the top of the pipe after backfill has been installed to this elevation.	
When seepage is present, use sheeting with soiltight joints to prevent washing out of soil behind the sheeting. Take necessary action to prevent surface runoff from entering the trench.	
An alternative to sheeting and bracing to provide a safe working condition in the bottom of a trench is to use a movable trench shield. The trench shield shall be used in a manner that will not leave voids in the backfill or disrupt compacted backfill when advanced.	
For installations where the top of the culvert extends above or within the rise of the existing ground, and the existing ground will be covered with an embankment, remove vegetation, organic, or frozen material, and any soft materials that do not meet the stiffness requirements of the structural	In instances where the depth of fill over the culvert will be significant, the replacement material above the existing ground may need to be structural backfill to provide a suitable embedment zone. The AASHTO *LRFD Bridge Design Specifications* provide guidance.

SPECIFICATIONS	COMMENTARY

backfill for a distance at least equal to the culvert diameter each side of the culvert springline. Replace with embankment material.

30.5.3 Groundwater Control

Water conditions shall be controlled. Remove water seeping into the trench from the sides or top. If continuous seepage occurs, install a sump pump. When the water table is above the bottom of the trench, quick conditions or instability of the trench bottom can occur. Lower the groundwater level to below the trench bottom. Maintain this water level until the pipe and sufficient backfill are placed to compensate for the uplift forces.

Sites requiring excavation below the groundwater table shall be dewatered to at least 300 mm (12 in.) below the deepest portion of the excavation, or when the culvert is installed in a stream or river bed, the water shall be diverted or separated by cofferdams. Obtain advance approval of the Engineer if construction must continue in water. Under these conditions, free-draining gravels shall be used as foundation and bedding.

30.5.4 Trench Width

Trench width shall be sufficient to ensure working room to properly and safely place and compact haunching and other backfill materials. If not specified in the contract documents, the space between the pipe and trench wall shall be wider than the compaction equipment used in the pipe zone, but not less than 1.5 times the outside pipe diameter plus 300 mm (12 in.). Determination of trench width in soils that are unsupported and unstable shall include consideration of the size of the pipe, the stiffness of the backfill and in situ soil, the depth of cover, and other site specific conditions as applicable.

If in situ materials are inadequate to provide support to the pipe, increase the width of excavation to provide 300 mm (12 in.) or one-half the span, whichever is larger, on each side of the culvert.

C30.5.4

Narrower trenches may be allowed if culverts are backfilled with CLSM. CLSM readily flows under and around the culvert to provide good haunch and sidefill support, thus reducing the needed working room at the side of the culvert.

The AASHTO *LRFD Bridge Design Specifications* provide additional guidance on the width of trench backfill in wet native soil conditions. Generally, native soils are adequate if they will stand without support (unrelated to support requirements for worker safety).

SPECIFICATIONS	COMMENTARY

30.5.5 Foundation

The foundation under the culvert shall be investigated for its adequacy to support the loads. The foundation soil shall be investigated for the full width of the trench, or for wide trench or embankment installations, a width of 300 mm (12 in.) or one-half the span of the culvert, whichever is larger, on each side of the culvert springline. The remedies for soft or inadequate foundation soils noted below shall apply to the same widths as investigated (see Figure 2). The foundation depths specified include the combined foundation and bedding depth.

- For rock and boulders, use b = culvert diameter 1D, and use a minimum d = 150 mm (6 in.) but not less than twice the corrugation.
- For soft spots, use b = 2D or the trench width, whichever is smaller, and use a minimum d = 100 mm (4 in.), but not less than the corrugation depth or less than a depth sufficient to reduce the stress on the soft soil to its allowable bearing value.

If the in situ soil is suitable to support the culvert, it may serve as the foundation. The bottom of the excavation shall be undisturbed in situ material. If boulders, rock, vegetation, organic, or frozen material, or any soft materials that do not meet the stiffness requirements of the structural backfill are present, they shall be removed for a width of at least one-half diameter on either side of the culvert to a depth specified by the Engineer and replaced with specified bedding material. If the foundation is loose, it shall be compacted as specified, but to not less than 90% of maximum density per AASHTO T99 for A-1 or A-3 soils or 95% of maximum density for A-2 soils, before placing the culvert. After compaction, the foundation shall be uniformly firm and level to support the culvert along its length.

C30.5.5

A foundation should be provided such that the structure backfill does not settle more than the pipe to avoid downdrag loads on the culvert and to maintain specified pipe invert elevations. If the foundation is firm under the pipe but soft at the sides, compression of the soft material can cause increased load on the pipe due to downdrag. Thus, the foundation quality must be evaluated for a width greater than the pipe.

SPECIFICATIONS	COMMENTARY

When the natural foundation soil is judged by the Engineer to be unsatisfactory to support the pipe, or structural backfill, the soil shall be excavated to the depth “d” and width “b” prescribed in the contract documents. The excavation shall be backfilled with bedding material compacted as specified, but to not less than 90% of maximum dry density per AASHTO T99 for A-1 or A-3 soils or 95% of maximum dry density for A-2 soils.

30.5.6 Bedding

C30.5.6

A bedding layer shall be provided to the thickness specified. Unless indicated otherwise in the contract documents, the bedding shall be compacted to a minimum density equal to 90% of the maximum dry density per AASHTO T99, except that the portion of the bedding layer under the center third of the culvert diameter shall be left uncompacted.

The bedding surface shall conform to the specified elevation, grade, and alignment and shall be straight and flat over the length of the pipe section so that unacceptable longitudinal bending does not occur, and the pipe drains as designed.

The maximum desired loose bedding layer thickness for compaction is 150 mm (6 in.).

Leaving the center third of the bedding uncompacted provides a soft cushion for the pipe, minimizing hard support on the invert. In addition, the compacted bedding at the sides of the culvert provides a path for soil to arch over the top of the culvert.

The tolerance of the culvert to longitudinal bending depends on the culvert material and geometric properties.

30.5.7 Placing Culvert Sections

C30.5.7

The culvert shall be placed after the foundation soil and bedding are prepared. Pipes shall be placed on the bedding starting at the downstream end. If less than a full length of pipe is needed to meet the plan specified length, the partial piece shall not be the terminal piece.

While it is preferable to lay pipe starting at the downstream end, the Engineer may grant permission to begin at other locations.

30.5.8 Structural Backfill

30.5.8.1 General

C30.5.8.1

Equipment and construction procedures used to backfill culverts shall be selected such that requirements for backfill density and control of culvert deflection and shape will be met. Sufficient inspection and testing should be undertaken to

AASHTO *LRFD Bridge Design Specifications* provide guidance on the suitability of in situ soils for use in the structural backfill zone.

Once a backfilling procedure is established, the primary inspection effort should be to ensure that

SPECIFICATIONS	COMMENTARY
verify that the quality of the soil and the compactive effort are as specified.	the established procedure is followed. Only occasional checks of soil density may then be required, as long as the material and procedures are unchanged. A good construction control plan will improve efficiency of installation effort and help ensure proper performance without having to rely on time-consuming testing, particularly in the haunch area, which is difficult to access.
Placing and compacting backfill to the top of the culvert shall be completed in such a manner that the culvert shape is not distorted and that the vertical diameter does not increase more than 3%.	Culvert wall stress caused by deformation during compaction can be more severe than the wall stress caused by ovaling deformation due to earth load over the culvert, so the deflection requirement during backfilling is more restrictive.
When trench wall supports are used, they shall be left in place below the top of the culvert or removed in a manner that avoids disturbing compacted backfill. Remove all foreign material falling into the trench during placement and compacting of the backfill. The three basic stages of construction (backfilling) are haunch, sidefill, and topfill. For each of these stages, procedures shall be established that will achieve the specified degree of compaction without damaging or excessively distorting the culvert.	
30.5.8.2 Backfilling under the Haunch	**C30.5.8.2**
Material shall be carefully placed in the haunches using mechanical tampers, manual tampers, or other means that fill all voids and meet the specified compaction levels. Adjacent sidefill zones shall be placed along with the haunch zones to provide lateral support for the haunch material. Installation of haunch fill shall be carried out on both sides simultaneously to avoid rolling the culvert, and the compaction force shall be controlled so that the culvert is not lifted off grade, and the bottom of the culvert is not damaged. If the culvert is to be backfilled with CLSM, follow all requirements of the project specifications or the submitted detailed work plan. Provide means to prevent culvert flotation.	It is important that the selected tamping procedures will meet the design assumptions. In general, a minimum compaction level exceeding 85% T99 is needed to prevent a collapsing soil structure upon saturation. The effort required to achieve a particular degree of compaction varies with the backfill material type. Investigation of various means of achieving compaction in the haunch zone, and the effect of haunch support on buried pipe performance is reported in FHWA Report FHWA-RD-98-191, *Pipe Interaction with the Backfill Envelope* (McGrath et al. 1998). These studies showed that large void spaces result underneath culverts without good compaction in the haunch area. Loose layers

SPECIFICATIONS	COMMENTARY
	should generally not exceed 150 mm (6 in.) in thickness to permit the backfill material to be worked into the haunch zone. Shovel slicing was shown to be effective in providing haunch support. Different-sized tampers were shown to be effective for different backfill soils. A large-faced tamper (75 x 150 mm or 3 x 6 in.) was effective for silty sand, while a small-faced tamper (25 x 75 mm or 1 x 3 in.) was effective for crushed stone backfill. Haunching is best accomplished by placing part of the first layer of backfill, working it into the haunches and then placing the remainder of the lift. Thick layers prevent material from being worked into the haunches.
Water jetting to densify the backfill is not allowed unless approved in advance by the Engineer.	Water jetting has been found to be an effective procedure for compacting backfill and developing uniform support with clean coarse-grained backfills and good drainage; however, problems have been encountered in achieving consistent results, and verification is difficult.
30.5.8.3 Sidefill	**C30.5.8.3**
Structural backfill material in the sidefill zone shall be placed in horizontal, uniform layers not exceeding 150 mm (6 in.) loose thickness unless a larger thickness is specified. The layers shall be compacted with appropriate equipment to the specified density. The maximum density shall be as specified, but not less than 90% T99 for A-1 and A-3 soils and 95% for A-2 soils.	For equal performance, the compaction requirements should be a function of soil type. Performance will vary widely among the acceptable soils when compacted to the same density specification. Also, design soil stiffness is very sensitive to the level of compaction (McGrath et al. 1998).
The maximum difference in the sidefill surface elevations between the two sides of the culvert at any time shall not exceed one-quarter of the diameter, or 600 mm (24 in.) whichever is smaller. For pipe less than 600 mm (24 in.) in diameter, this difference need not be less than one-half the diameter.	Generally, compaction of fill material to the required density is dependent on the thickness of the layer of fill being compacted, soil type, amount of compactive force, and length of time the force is applied. Experience with compaction indicates that 150-mm (6-in.) thick loose layers using two coverages with a given compactor will give better uniformity and higher average level of compaction than one 300-mm (12-in.) thick loose layer with four coverages of the same compactor. Alternatively, a 300-mm (12-in.) loose layer will require larger compactors to produce the same average compaction as achieved by a smaller compactor with a 150-mm (6-in.) thick layer.
The sidefill surface elevation shall be kept at or below the level of adjacent soil or embankment. Placement and compaction of the sidefill layers adjacent to the haunch zone shall be carried out concurrently with backfilling under the haunch.	
Sidefill material shall be placed, spread, and	

SPECIFICATIONS	COMMENTARY
compacted working parallel to the culvert to avoid creating areas of unequal support. Equipment used to compact sidefill within 1 m (3 ft) from each side of the culvert shall not impose excessive force on the culvert that results in distorting the culvert shape. Thermoplastic culverts are flexible, thus sidefill material must be placed and compacted to avoid excessive and unsymmetrical deformations. The shape must be monitored to ensure satisfactory results.	Larger compactors must be evaluated for possible induced structural distortions. Unequal support may result when compacting perpendicular to the culvert long axis.
30.5.8.4 Topfill	**C30.5.8.4**
When the sidefill elevation reaches the shoulders, placement of structural topfill begins. Procedures, as approved by the Engineer, shall be used for placing and compacting topfill. Topfill need not extend above the top of the pipe more than 6 in. unless otherwise specified. Additional material over the topfill shall be provided to protect all culverts before permitting heavy construction equipment to pass over them. Construction loads may require additional cover beyond that required for the final condition to which the design loads apply.	See design specifications for guidance on minimum cover depths. Specifying a depth of 6 in. above the top of the pipe provides protection for the pipe as less controlled materials are placed and compacted to complete the trench backfill. This dimension is unrelated to the depth of fill required to prevent damage from vehicles passing over the pipe.
30.6 Minimum Cover	
Per current Section 30.5.5.	
30.7 INSPECTION REQUIREMENTS	
30.7.1 Visual Inspection	
Per current Section 30.5.6.1.	Per current Section C30.5.6.1.
30.7.2 Installation Deflection	
Per current Section 30.5.6.2.	Per current Section C30.5.6.2.
30.7.3 Compaction Control	**C30.7.3**
Field compaction shall be evaluated based on compacted density and moisture content obtained from acceptable methods, such as the cone replacement (AASHTO T191, ASTM D1556) or the	The best approach to compaction control is to conduct frequent tests early in the project to establish the critical control parameters that achieve the specified compaction level, such as

SPECIFICATIONS	COMMENTARY

nuclear gage (AASHTO T238 and T239, ASTM D2922). A reference density test shall be performed on a representative sample to obtain a value of maximum dry density (MDD) and optimum moisture content (OMC). This test shall be repeated for each new soil type encountered and for composition variations within the same soil type. Thus, samples should be taken periodically during construction to provide an appropriate series of reference tests.

The contract documents shall determine the number and location of field tests to ensure that the quality of the soil and the compaction obtained is as specified and shall stipulate acceptance criteria for the compacted soil.

type of equipment, number of passes, and moisture content. Once the parameters are established, the test frequency can be reduced as long as the identified parameters are monitored.

30.7.4 Use of Reduced Installation Factor

If the culvert design was completed with an installation factor less than 1.5, additional deflection checks are required during construction.

C30.7.4

Specific requirements should be called out on the contract documents. They should include provisions for actively monitoring backfill gradation and compaction levels at the side of the culvert throughout the construction process and measurement of change in vertical pipe diameter when the backfill reaches the top of the pipe. At this point in the construction process, the vertical pipe diameter should be greater than the vertical diameter prior to backfilling but not more than 3% greater than the vertical diameter prior to backfilling.

30.8 MEASUREMENT

Culverts shall be measured in meters installed in place, completed, and accepted. The number of meters shall be the average of the top and bottom centerline lengths of pipe.

SPECIFICATIONS	COMMENTARY

30.9 PAYMENT

Per current Section 30.7.

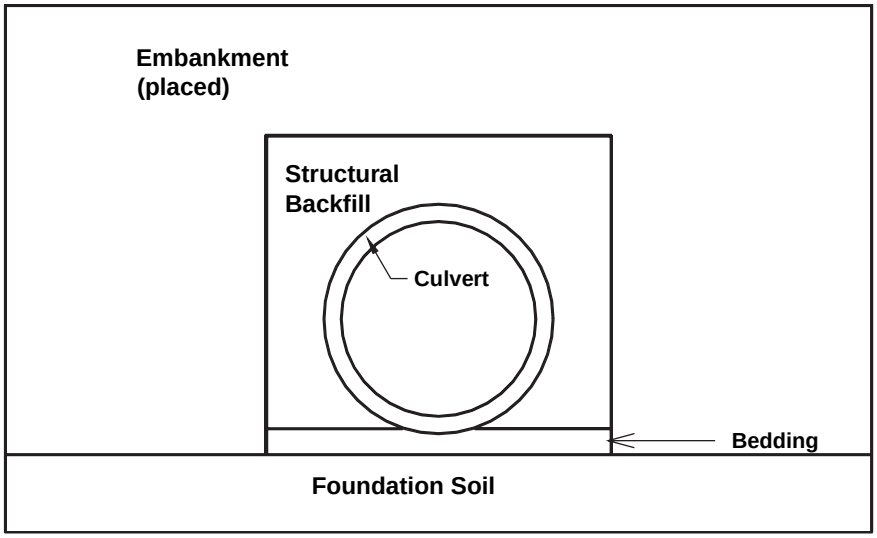

a) Embankment Installation

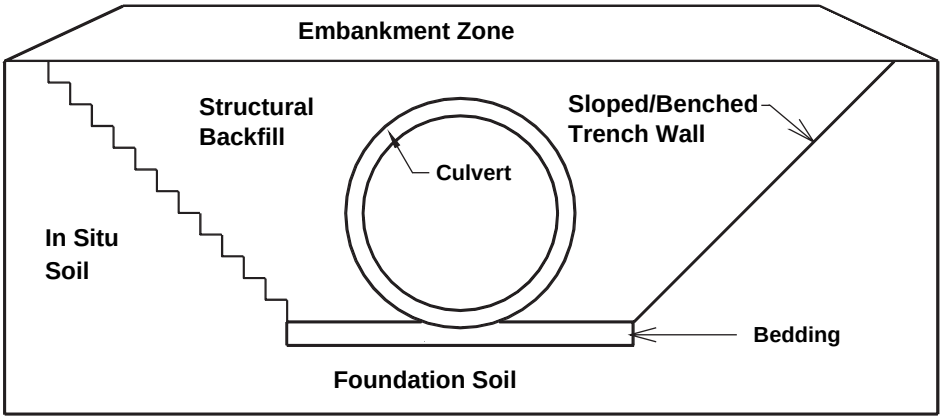

b) Trench Installation

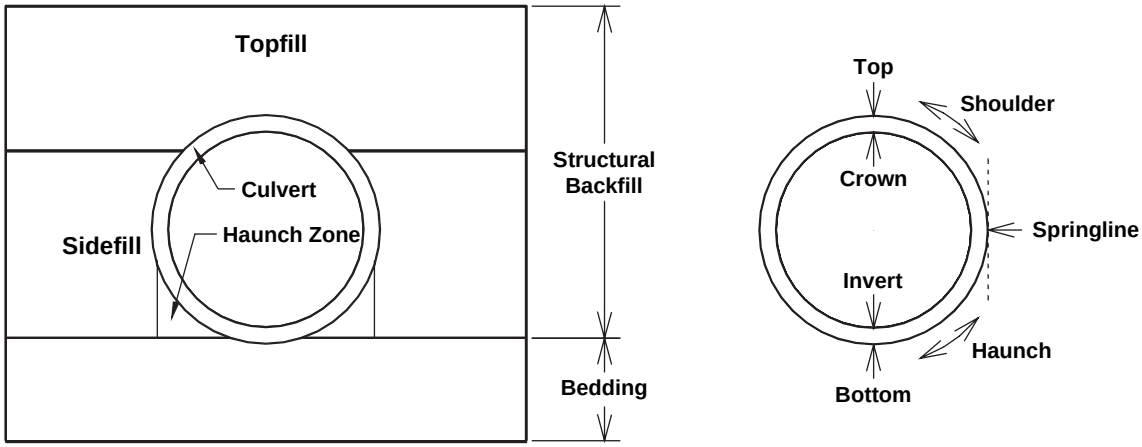

c) Embedment Zone

d) Culvert

Figure 1. Terminology for culvert installation.

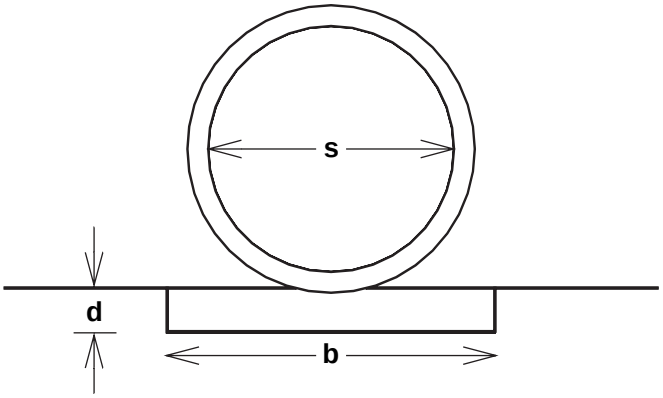

Figure 2. Foundation treatment with placed bedding.

References

Folliard, K.J., Lianxiang, D., Trejo, D., Halmen, C., Sabol, S., and Leshchinsky, D., *NCHRP Report 597—Development of a Recommended Practice for Use of Controlled Low-Strength Material in Highway Construction,* Transportation Research Board, Washington, D.C., 2008.

McGrath, T.J., Selig, E.T., Webb, M.C., and Zoladz, G.V., Pipe Interaction with the Backfill Envelope, FHWA-RD-98-191, Federal Highway Administration, U.S. Department of Transportation, McLean, VA, June 1998.

APPENDIX J

Proposed Revisions to Product Standards for Thermoplastic Pipe

Proposed CHANGES to M 294-07	JUSTIFICATION

6.1.1 NCLS Test for Finished Pipe

Delete last sentence and replace with:
For slow crack growth resistance, acceptance of pipe shall be determined by tests on finished pipe using the notched constant ligament-stress (NCLS) test according to the procedure described in Section 9.5. The average failure time of the pipe liner shall not be less than 18 hours.

Note: If alternate profile geometries do not have a "liner" element, conduct exploratory tests on all profile elements to determine the element with the shortest NCLS failure time. Use that element as the standard for subsequent tests.

The proposed standard applies research that demonstrates the need to test the finished pipe product rather than the virgin resin. The proposed standard is more conservative than the prior requirement on the virgin resin. For product acceptance, a requirement is set only on the finished product. To meet this requirement, data show that virgin resin should have an NCLS time of approximately 33 hours and a remolded pipe plaque should have a failure time of approximately 24 hours; however, depending on additives and production methods, these times will vary.

Modify Section 7.4 Pipe Stiffness

Modify the required pipe stiffness for pipe with diameters larger than 675 mm as follows:

Diameter, mm	Pipe Stiffness, kPa
750	200
900	155
1,050	145
1,200	135
1,350	120
1,500	105

The increase in the crosshead speed for the parallel plate test, proposed under Section 9.1, results in a faster test and a higher apparent stiffness due to the time-dependent modulus of elasticity of polyethylene. The proposed pipe stiffness values account for this effect. Pipe meeting the current pipe stiffness requirements at the current crosshead speed should meet the requirements at the proposed crosshead speed.

Proposed CHANGES to M 294-07	JUSTIFICATION
New Section 7.7 Stub Compression Test for Finished Pipe Profile compression capacity in any specimen in the stub compression test shall not be less than 50% of the gross section area times the minimum specified yield strength when tested in accordance with Section 9.9. **Notes:** 1. Computing the minimum capacity requires determining the cross-sectional area of the pipe wall. This can be accomplished conveniently by optically scanning the profile and determining the section properties using a computer drafting program. 2. Frequency of the stub compression test shall be determined by AASHTO during approval of this recommendation. Including the test in the NTPEP program, or establishing a test frequency that would be similar to the NTPEP cycle, should be adequate to provide assurance of conformance to this requirement.	No current test evaluates the compression capacity of a thermoplastic pipe, yet design calculations show that compression stresses are more critical to capacity than tension stresses. The new test ensures a minimum compression capacity.
Add Item 7.9. to Requirements: **"**7.9. *Manufacturer Records*—Manufacturers shall keep records of the following: (1) resin manufacturer's data sheets and certification that the base resin meets cell class requirements of the product specification; (2) manufacturer's data sheets and quantities for all additives; (3) test results to demonstrate that if resins of two different cell classifications are blended, the resulting mixture meets the requirements of the specified cell class; (4) correlation of resin shipment source with pipe markings.**"**	Raw materials are specified through a cell classification system that identifies and sets limits on parameters deemed important for strength, stiffness, processing, durability, and slow crack growth. Finished product tests evaluate strength, stiffness, and aspects of durability. However, finished product tests cannot evaluate all aspects of pipe durability and performance. To ensure that current requirements are met for the finished product, the purchaser of pipe certified by AASHTO should be provided an accurate record of the materials used in manufacture. Additionally, current practice does not require all manufacturers to correlate the source of resins used in manufacture with markings on the pipe. This is desirable and should be required in manufacturer records.

Proposed CHANGES to M 294-07	JUSTIFICATION
Add exception (5) to Test Methods, Item 9.1:	
"(5) the crosshead speed shall be the faster of 12.7 mm per minute (0.5 in. per minute) or 2% of the nominal inside diameter per minute.**"**	The change increases test speed for larger-diameter pipe. This reduces the test time and results in a relatively consistent strain rate for all pipe diameters. Testing to 20% deflection at the current speed can take up to 20 minutes with no benefit derived. The proposed test speed also results in a relatively constant strain rate for the larger pipe sizes, meaning the effective modulus will be the same; this is technically desirable.
New Section 9.9 Stub Compression Capacity	
Determine the stub compression capacity of the pipe section in accordance with Standard T-XXX (Appendix G). Conduct four tests on specimens cut from the same ring of pipe at 90° intervals around the circumference.	Testing has shown that profile wall capacity varies around the circumference due to geometric variations. Testing at 90° intervals provides reasonable assurance that one specimen will be near the location with minimum capacity.

SUGGESTED CHANGES to M 304-01	JUSTIFICATION
Modify Requirements, Item 7.4., as follows: currently states **"**7.4. *Pipe Flattening*—There shall be no evidence of splitting, cracking, breaking, or separation of ribs or seams, when pipe is tested in accordance with Section 8.4.**"** change to **"**7.4. *Pipe Flattening*—There shall be no evidence of splitting, cracking, breaking, or separation of ribs or seams when pipe is tested in accordance with Section 8.4, and the load on the pipe shall not decrease until the pipe inside diameter is reduced by 20 percent of its original dimension.**"**	
Modify Requirements, Item 7.9., as follows: currently states **"**7.9. *Acetone Immersion*—The pipe shall meet the requirements as defined in ASTM D2152 when tested in accordance with Section 8.7. **NOTE 5**—This is intended only for use as a quality control test and not for use as a simulated service test.**"** change to **"**7.9. *Extrusion Quality*: 7.9.1. *Acetone Immersion*—The pipe shall meet the requirements as defined in ASTM D2152 when tested in accordance with Section 8.7.1. **NOTE 5**—This is intended only for use as a quality control test and not for use as a simulated service test. 7.9.2. *Heat Reversion*—The pipe shall not exhibit any of the effects listed in the suggested interpretation of results of ASTM Practice F1057 when tested in accordance with Section 8.7.2.**"**	Some PVC pipe specifications (ASTM F949 for profile-wall sewer pipe) include the heat reversion test outlined in ASTM F1057. This test exposes the pipe specimens to 180°C for 30 minutes and reveals incomplete exsiccation and the presence of stress, infused areas, or contamination. The heat reversion test is understood to be a more demanding test of extrusion quality than the acetone immersion test. This test should be incorporated to augment the acetone immersion test at this time.

SUGGESTED CHANGES to M 304-01	JUSTIFICATION
Add Item 7.12. to Requirements	
"7.12. *Manufacturer Records*—Manufacturers shall keep records of the following: (1) resin manufacturer's data sheets and certification that the base resin meets cell class requirements of the product specification; (2) manufacturer's data sheets and quantities for all additives; (3) test results to demonstrate that if resins of two different cell classifications are blended, the resulting mixture meets the requirements of the specified cell class; (4) correlation of resin shipment source with pipe markings.**"**	Raw materials are specified through a cell classification system that identifies and sets limits on parameters deemed important for strength, stiffness, processing, durability, and resistance to crack growth. Finished product tests evaluate strength, stiffness, and aspects of durability. However, finished product tests cannot evaluate all aspects of pipe durability and performance. To ensure that current requirements are met for the finished product, the purchaser of pipe certified by AASHTO should be provided with an accurate record of the materials used in manufacture. Additionally, current practice does not require all manufacturers to correlate the source of resins used in manufacture with markings on the pipe. This is desirable and should be required in manufacturer records.
Add New Section 7.12	
Profile compression capacity in any specimen in the stub compression test shall not be less than 95% of the gross section area times the minimum specified yield strength when tested in accordance with Section 8.10. **Note:** Computing the minimum capacity requires determining the cross-sectional area of the pipe wall. This can be conveniently accomplished by optically scanning the profile and determining the section properties using a computer drafting program.	No current test evaluates the compression capacity of a thermoplastic pipe, yet design calculations show that compression stresses are more critical to capacity than tension stresses. The new requirement ensures a minimum compression capacity.
Modify Test Methods, Item 8.4, as follows:	
<u>append the following sentence</u> **"**Record the deflection at which the peak load occurs.**"**	

SUGGESTED CHANGES to M 304-01	JUSTIFICATION
Modify Test Methods, Item 8.6. as follows:	
currently states **"**8.6. *Pipe Stiffness*—Determine the pipe stiffness at 5 percent deflection in accordance with ASTM D2412. Test three specimens, each with a length equal to one pipe diameter (but not less than 300 mm nor greater than 900 mm) and determine the average pipe stiffness.**"**	The increase in the crosshead speed for the parallel plate test, proposed under Section 9.1, results in a faster test and a higher apparent stiffness due to the time-dependent modulus of polyethylene. The proposed pipe stiffness values account only for this effect. Pipe meeting the current pipe stiffness requirements at the current crosshead speed should meet the requirements at the proposed crosshead speed.
change to **"**8.6. *Pipe Stiffness*—Determine the pipe stiffness at 5 percent deflection in accordance with ASTM D2412, except that the crosshead speed shall be the faster of 12.7 mm per minute (0.5 in. per minute) or 2% of the nominal inside diameter per minute. Test three specimens, each with a length equal to one pipe diameter (but neither less than 300 mm nor greater than 900 mm) and determine the average pipe stiffness.**"**	

SUGGESTED CHANGES to M 304-01	JUSTIFICATION
Modify Test Methods, Item 8.7. as follows:	
currently states **"**8.7. *Acetone Immersion*—Conduct this test in accordance with ASTM D2152. This procedure is used for determining the degree of fusion of extruded PVC plastic pipe as indicated by reaction to immersion in anhydrous acetone. It is applicable only for distinguishing between unfused and properly fused PVC.**"**	
change to **"**8.7. *Extrusion Quality*: 8.7.1. *Acetone Immersion*—Conduct this test in accordance with ASTM D2152. This procedure is used for determining the degree of fusion of extruded PVC plastic pipe as indicated by reaction to immersion in anhydrous acetone. It is applicable only for distinguishing between unfused and properly fused PVC. 8.7.2. *Heat Reversion*—Conduct this test in accordance with ASTM Practice F1057. This procedure is used for estimating the quality of extruded PVC plastic pipes by observing the reaction of pipe specimens after exposure to heat.**"**	
New Section 8.10 Stub Compression Test for Finished Pipe Determine the stub compression capacity of the pipe section in accordance with Standard T-XXX (Appendix G). Conduct four tests on specimens cut from the same ring of pipe at 90° intervals around the circumference.	Testing has shown that profile-wall capacity varies around the circumference due to geometric variations. Testing at 90° intervals provides reasonable assurance that one specimen will be near the location with minimum capacity.

Abbreviations and acronyms used without definitions in TRB publications:

AAAE	American Association of Airport Executives
AASHO	American Association of State Highway Officials
AASHTO	American Association of State Highway and Transportation Officials
ACI–NA	Airports Council International–North America
ACRP	Airport Cooperative Research Program
ADA	Americans with Disabilities Act
APTA	American Public Transportation Association
ASCE	American Society of Civil Engineers
ASME	American Society of Mechanical Engineers
ASTM	American Society for Testing and Materials
ATA	Air Transport Association
ATA	American Trucking Associations
CTAA	Community Transportation Association of America
CTBSSP	Commercial Truck and Bus Safety Synthesis Program
DHS	Department of Homeland Security
DOE	Department of Energy
EPA	Environmental Protection Agency
FAA	Federal Aviation Administration
FHWA	Federal Highway Administration
FMCSA	Federal Motor Carrier Safety Administration
FRA	Federal Railroad Administration
FTA	Federal Transit Administration
IEEE	Institute of Electrical and Electronics Engineers
ISTEA	Intermodal Surface Transportation Efficiency Act of 1991
ITE	Institute of Transportation Engineers
NASA	National Aeronautics and Space Administration
NASAO	National Association of State Aviation Officials
NCFRP	National Cooperative Freight Research Program
NCHRP	National Cooperative Highway Research Program
NHTSA	National Highway Traffic Safety Administration
NTSB	National Transportation Safety Board
SAE	Society of Automotive Engineers
SAFETEA-LU	Safe, Accountable, Flexible, Efficient Transportation Equity Act: A Legacy for Users (2005)
TCRP	Transit Cooperative Research Program
TEA-21	Transportation Equity Act for the 21st Century (1998)
TRB	Transportation Research Board
TSA	Transportation Security Administration
U.S.DOT	United States Department of Transportation